MATHEMATICAL MODELING OF CHEMICAL SLUG INJECTION DRIVEN BY WATER IN ENHANCED OIL RECOVERY PROCESSES

FELIPE DE OLIVEIRA APOLINÁRIO

UNIVERSIDADE ESTADUAL DO NORTE FLUMINENSE - UENF
LABORATÓRIO DE ENGENHARIA E EXPLORAÇÃO DE PETRÓLEO - LENEP
MACAÉ - RJ
APRIL - 2022

MATHEMATICAL MODELING OF CHEMICAL SLUG INJECTION DRIVEN BY WATER IN ENHANCED OIL RECOVERY PROCESSES

FELIPE DE OLIVEIRA APOLINÁRIO

Dissertation presented to the Science and Technology Center of Universidade Estadual do Norte Fluminense in partial fulfillment of the requirements for the degree of Doctor in Reservoir and Exploration Engineering.

Advisor: Adolfo Puime Pires

MACAÉ - RJ
ABRIL - 2022

MATHEMATICAL MODELING OF CHEMICAL SLUG INJECTION DRIVEN BY WATER IN ENHANCED OIL RECOVERY PROCESSES

FELIPE DE OLIVEIRA APOLINARIO

Tese apresentada ao Centro de Ciência e Tecnologia da Universidade Estadual do Norte Fluminense Darcy Ribeiro, como parte das exigências para obtenção do título de Doutor em Engenharia de Reservatório e de Exploração.

Aprovada em 01 de abril de 2022.

Comissão Examinadora:

Adriano dos Santos, (D.Sc., Engenharia Civil / Geotécnica) – PUC-Rio

Carlos Enrique Pico O.

Carlos Enrique Pico Ortiz (D.Sc., Engenharia Mecânica) – LENEP/CCT/UENF

Fernando Diogo de Siqueira

Fernando Diogo de Siqueira (D.Sc., Engenharia de Reservatório e de Exploração) – LENEP/CCT/UENF

Adolfo Puime Pires (D.Sc., Engenharia de Reservatório e de Exploração) – LENEP/CCT/UENF
(Orientador)

FICHA CATALOGRÁFICA
UENF - Bibliotecas
Elaborada com os dados fornecidos pelo autor.

A643 Apolinario, Felipe de Oliveira.

Mathematical Modeling of Chemical Slug Injection Driven by Water in Enhanced Oil Recovery Processes / Felipe de Oliveira Apolinario. - Campos dos Goytacazes, RJ, 2022.

297 f. : il.
Inclui bibliografia.

Tese (Doutorado em Engenharia de Reservatório e de Exploração) - Universidade Estadual do Norte Fluminense Darcy Ribeiro, Centro de Ciência e Tecnologia, 2022.
Orientador: Adolfo Puime Pires.

1. Métodos químicos de recuperação avançada de petróleo. 2. Injeção de polímeros. 3. Injeção de água de baixa salinidade. 4. Leis de conservação. 5. Sistemas de equações diferenciais parciais hiperbólicas. I. Universidade Estadual do Norte Fluminense Darcy Ribeiro. II. Título.

CDD - 622.3382

Agradecimentos

Aos meus pais, Elioneide e Roberto,por todo o suporte familiar dado ao longo de todo o desenvolvimento desse trabalho, sempre me dando forças para seguir em frente independente da situação. Sem eles nada disso seria possível.

À minha esposa, Anna Radovanovic, por todo o suporte emocional, amor, paciência nos momentos de turbulência, e auxílio intelectual principalmente nas fases iniciais desse trabalho.

Ao meu orientador e amigo, Adolfo Puime, por todos os ensinamentos e dedicação ao longo desses anos de doutorado.

Aos amigos do LDSC, por tornarem sempre o ambiente de trabalho mais leve, por todos os cafés com conversas sempre (ou quase sempre) produtivas.

À CAPES pelo suporte financeiro desse trabalho.

Resumo

A injeção de polímeros é o método químico de recuperação avançada mais utilizado. A adição de polímeros aumenta a viscosidade da água de injeção, o que resulta em um aumento da eficiência de varrido. Recentemente, observou-se que a injeção de água de baixa salinidade e com concentração controlada de cátions e pH poderia ser utilizada para aumentar a recuperação de petróleo. A inversão de molhabilidade resultante da substituição de um cátion bivalente por um cátion monovalente na rocha é o principal fenômeno físico responsável pela mobilização de óleo residual na injeção de água de baixa salinidade. Usualmente, a injeção de produtos químicos é feita na forma de um banco com os produtos dissolvidos e deslocado por água. Matematicamente, esse cenário significa que a condição de contorno é descontínua. Neste trabalho apresentamos a solução para a injeção unidimensional de um banco contendo n produtos químicos dissolvidos e deslocado por água em reservatórios de petróleo. Como exemplos apresentamos os casos de um banco contendo dois e três polímeros dissolvidos, e ainda o caso da injeção de água de baixa salinidade considerando três cátions dissolvidos e os efeitos do pH. Os componentes químicos adsorvem no meio poroso segundo uma isoterma do tipo Langmuir multicomponente. A solução desses problemas é construída a partir do desacoplamento do sistema original de equações hiperbólicas em um sistema auxiliar e em uma equação de levantamento. O sistema auxiliar inclui apenas as propriedades termodinâmicas do sistema, e a equação de levantamento depende das propriedades hidrodinâmicas. O sistema auxiliar foi resolvido utilizando a teoria da cromatografia multicomponente, e sua solução é utilizada para resolver a equação de levantamento pelo método das características. Em seguida, a solução do sistema auxiliar e da equação de levantamento é mapeada para o plano espaço-tempo. Na solução de concentração é possível observar o desenvolvimento completo de um ciclo cromatográfico no meio poroso. As diferentes distribuições de concentração de componentes químicos no reservatório resultam no surgimento de bancos de água e de óleo na solução de saturação de água. A formulação matemática apresentada na solução do problema de injeção de água de baixa salinidade expande a teoria da cromatografia multicomponente para o caso em que os coeficientes da isoterma de adsorção dependem do pH.

Palavras-chave: Métodos Químicos de Recuperação Avançada de Petróleo, Injeção de Polímeros, Injeção de Água de Baixa Salinidade, Leis de Conservação, Sistemas de Equações Diferenciais Parciais Hiperbólicas.

Abstract

Polymer flooding is the most important chemical method of enhanced oil recovery. Adding polymer to injection water increases water viscosity and optimize the sweep efficiency. Recently, it was observed that injection of controlled water salinity, cation concentration and pH improve oil recovery. The cation exchange on clay surfaces results in wettability alteration, which is the main physical phenomenon related to mobilization of residual oil in low salinity waterflooding. Usually, a chemical slug is displaced by pure water, leading to a discontinuity in the boundary condition of the mathematical problem. In this work we present the solution for the one-dimensional multicomponent chemical slug injection driven by water in oil reservoirs. The solution for the cases of slugs containing two or three dissolved polymers and for the low salinity waterflooding considering three dissolved cations and pH effect are presented. The chemical components adsorb on the rock following a multicomponent Langmuir-type adsorption isotherm. The introduction of a potential function replacing time in the original system of equations decouples the system of conservation laws into an auxiliary system and a lifting equation. The auxiliary system depends on the thermodynamic equilibrium conditions, and the lifting equation depends on the solution of the auxiliary system and on the hydrodynamic properties of the flow. The auxiliary system was solved applying the theory of the multicomponent chromatography, and its solution is used to solve the lifting equation applying the method of characteristics. Next, the solution is mapped onto the space-time plane. In the concentration solution it is possible to observe the development of a full chromatographic cycle. The different concentration distributions in the reservoir results on the appearance of water and oil banks in the water saturation solution. The mathematical formulation presented in the low salinity waterflooding problem extends the theory of multicomponent chromatography to the case where the adsorption coefficients depend on pH.

Keywords: Chemical Methods of Enhanced Oil Recovery, Polymer Flooding, Low Salinity Waterflooding, Conservation Laws, Hyperbolic Systems of Partial Differential Equations.

Chapter 1 – Water Slug Injection Containing *n* Polymers in Porous Media

Received: 28 January 2019 | Revised: 10 June 2019 | Accepted: 18 July 2019
DOI: 10.1002/aic.16735

TRANSPORT PHENOMENA AND FLUID MECHANICS

AIChE JOURNAL

Water slug injection containing *n* polymers in porous media

Anália S. de Paula[1] | **Felipe de O. Apolinário**[2] | **Adolfo P. Pires**[2]

[1]Reservoir Engineering Department-Macaé/RJ, Petróleo Brasileiro S.A., Rio de Janeiro, Brazil

[2]Laboratório de Engenharia e Exploração de Petróleo, Universidade Estadual do Norte Fluminense Darcy Ribeiro, Macaé, Rio de Janeiro, Brazil

Correspondence
Felipe de O. Apolinário, Universidade Estadual do Norte Fluminense Darcy Ribeiro, Laboratório de Engenharia e Exploração de Petróleo, Av. Brennand, s/n Imboassica, Macaé, Rio de Janeiro 27925-535, Brazil.
Email: felipe_apolinario03@hotmail.com

Funding information
Coordenação de Aperfeiçoamento de Pessoal de Nível Superior

Abstract

Injection of water containing dissolved chemicals is an efficient oil recovery technique. One of the problems of this method is the loss of the chemical components due to interactions between rock and fluid. In polymer injection, adsorption may happen and lead to low process efficiency. The interaction between rock and fluid is governed by the adsorption isotherm, which relates the polymer concentration in water with the adsorbed amount on the rock. In this paper the problem of oil displacement by a water slug containing *n* chemical components that may be adsorbed is analyzed. The system of conservation laws is solved and the structure of the solution for the case of Henry´s adsorption isotherm is completely described. The concentration profile of each component and the chromatographic cycle is calculated through simple expressions. The complete and detailed solution for the case of slug injection containing three chemical components is presented. The general solution developed can be used to model several Enhanced Oil Recovery techniques, in which the chemical components adsorb in porous media following Henry's adsorption isotherm.

KEYWORDS
chemical enhanced oil recovery, conservation laws, enhanced oil recovery, hyperbolic systems of partial differential equations, polymer flooding

1 | INTRODUCTION

Different techniques can be employed to improve recovery in oil fields. Water injection is the most used and the one-dimensional mathematical problem was solved analytically.[1] It was considered immiscible and incompressible phases (oil and water). Adding polymer to the injection water reduces water mobility and modifies the fractional flow curve, hence increasing the sweep efficiency.

Chemical enhanced oil recovery (EOR) has been applied in onshore and offshore petroleum fields. The most used chemical components dissolved in the injected water are polymer, surfactants, and alkalis. This technique recovers part of the remaining oil mainly due to a favorable mobility ratio change.

One of the first offshore chemical EOR projects took place at West Bay and Quarantine Bay Field, in Louisiana shallow waters, in 1981. Later, other chemical EOR projects were applied in Cuadras field in California, Bohai Bay in China, Dalia in Angola and Captain in North Sea, among others.[2]

Laboratory, analytical and numerical analyses must be performed before field application of enhanced oil recovery methods. Injection of one dissolved chemical component causes thermodynamic and hydrodynamic interactions between porous media and reservoir fluids (original oil and injected water) and can be mathematically modeled by a *2x2* nonlinear mass conservation system. One-dimensional multiphase flow in porous media with constant initial and boundary conditions can be solved by the method of characteristics and the solution consists of a combination of shocks and rarefaction waves, and constant states.

The different enhanced recovery methods can lead to multicomponent multiphase flow problems in porous media. In general, it may be considered that the components are distributed among *n* phases in thermodynamics equilibrium, and the phase composition affects its physical properties (density, viscosity, surface tension, etc.). Some problems may be solved analytically depending on the physical approach. One of the approaches is the theory of multicomponent chromatography, which describes the behavior of a two-phase system, one mobile and the other stationary, composed of *n* components, and each component concentration affects the distribution of all others. The second case is based on immiscible fluid flow in porous media considering two mobile phases, however, this theory does not include the distribution of the components between the phases.

Helfferich[3] solved a general problem consisting of *n* phases and *n* components using the coherence conditions showing the composition paths. The system of hyperbolic partial differential equations was solved by the method of characteristics and the consistency condition already adopted for modeling chromatography was also used. This theory was subsequently applied by Hirasaki[4] in a three-component system which simulates surfactant injection in a two-phase system. Johansen and Winther[5] developed the Riemann problem solution for a hyperbolic system composed by *n* equations using an *"S"* fractional flow curve.

In general, the continuous injection of aqueous solutions containing chemicals is not economically feasible; a more attractive alternative is the slug injection. In this case, the boundary conditions are functions of time and lead to interactions between waves in the mathematical solution. Therefore, in slug injection problems only part of the solution is self-similar. This part of the solution is identical to the case of continuous injection and was applied to three adsorption isotherms.[6]

The introduction of a potential function associated with the aqueous phase volume conservation can be used to solve the system of hyperbolic equations that represents the two-phase multicomponent flow in porous media. This variable is used to replace the variable time and splits the original system into an auxiliary system and a lifting equation. In the case of polymer injection considering adsorption, the parameters of the flow function of the auxiliary system are related only to the thermodynamic properties and are defined by the adsorption isotherms, that is, independent of hydrodynamic properties such as relative permeabilities and viscosities.[7]

This methodology was later applied to solve the problem of water injection containing a polymer in the presence of salt that does not adsorb nor alter the fractional flow curve,[8] and to the injection of one and *n* polymers.[9] In the last case, it was only considered continuous injection of aqueous solutions containing chemicals, leading to self-similar solutions. Ribeiro and Pires[10] developed an analytical solution using the same model for the case of water slug injection containing one polymer, considering linear (Henry), convex (Langmuir) and concave isotherms for an *"S"* shape fractional flow function. For convex fractional flow function, it was also presented a solution for the injection of slugs containing two polymers that adsorb according to Henry´s isotherm; a solution for the injection of a slug containing a polymer and a surfactant which does not adsorb but changes residual oil saturation; and the solution for the injection of a water slug containing one polymer in the presence of salt that changes the polymer adsorption.

Borazjani et al.[11] solved the problem of water slug injection containing one polymer in the presence of salt, considering an *"S"* shape fractional flow function and the linear Henry adsorption isotherm. De Paula and Pires[12] presented the solution to the problem of oil displacement by water slugs containing one polymer in the presence of salt, considering Langmuir's isotherm to model the adsorption phenomena and an *"S"* shape fraction flow curve. They used the splitting method developed by Pires et al.[7] to build the solution, which is composed by concentration discontinuities (jumps) and rarefactions waves. A sensitivity analysis was performed considering different parameters and slug sizes showing that a smaller adsorption leads to a more homogeneous profile and more effective oil displacement.

The splitting technique can also be applied to EOR problems considering advective transport, parabolic terms and relaxation non-equilibrium equations. In cases where the auxiliary system allows the development of an analytical solution, the complete exact solution can be constructed.[13]

Borazjani et al.[14] presented an analytical solution for a nonself-similar, two-phase, one dimensional problem of displacement of oil by a polymer slug with changing salinity, showing that the low salinity front moves faster than the polymer due to adsorption. It was also presented the solution to the injection of a polymer slug in a low salinity system displaced by a low salinity or high salinity water drive. Compared to the low salinity case, the high salinity increases the velocity of water front, causing an early water breakthrough time and increase of water-cut after water breakthrough. It was considered an *"S"* fractional flow function and Henry isotherm.

Khorsandi et al.[15] showed the analytical solution for low salinity polymer flood using the splitting method. Wettability alteration based on cation exchange reactions was considered in the problem, and the results were compared to numerical and experimental data.

Hamid and Muggeridge[16] developed the analytical solution to the problem of polymer slug injection in porous media considering viscous fingering effects. The solution was built using the method of characteristics and the splitting technique. The results were compared to numerical simulation and were used to estimate the minimum polymer slug size needed to avoid an early breakthrough due to the viscous fingering.

Despite of the advances in the development of solutions to enhanced oil recovery problems, a general solution that considers a variable boundary condition has not been presented in the literature. Therefore, in this paper the 1D two-phase problem of water slug injection containing *n* polymers whose adsorption is governed by Henry´s isotherm is analyzed. We consider that the polymer does not dissolve in the oil phase and changes only the water viscosity. Next section presents the mathematical model, followed by the detailed solution for the case of three dissolved components. After that, the general solution for any number of polymers is shown. The developed solution can be applied to several problems that arise in enhanced oil recovery, like polymer and surfactant flooding, and low salinity waterflooding with polymers.

2 | MATHEMATICAL DERIVATION

In this section the mathematical model for one-dimensional oil displacement by the injection of a water slug containing *n* polymers in porous media is presented.

The following assumptions are considered:

- one dimensional and isothermal flow;
- homogeneous porous media;
- incompressible system;
- no dispersive and diffusive effects;
- gravity and capillary effects negligible;
- chemicals are dissolved only in the aqueous phase;
- water density is independent of the concentration of chemical additives.

The system that represents the physical process of oil displacement by water slug containing n dissolved polymers is composed of (n + 1) equations derived from volume conservation of water and mass of each dissolved component:

$$\begin{cases} \phi\dfrac{\partial s}{\partial t}+u_T\dfrac{\partial f\left(s,\vec{c}\right)}{\partial x}=0 \\ \phi\dfrac{\partial (c_1 s+a_1(c_1))}{\partial t}+u_T\dfrac{\partial\left(c_1 f\left(s,\vec{c}\right)\right)}{\partial x}=0 \\ \phi\dfrac{\partial (c_2 s+a_2(c_2))}{\partial t}+u_T\dfrac{\partial\left(c_2 f\left(s,\vec{c}\right)\right)}{\partial x}=0 \\ \vdots \\ \phi\dfrac{\partial (c_n s+a_n(c_n))}{\partial t}+u_T\dfrac{\partial\left(c_n f\left(s,\vec{c}\right)\right)}{\partial x}=0 \end{cases} \tag{1}$$

where $\vec{c}$ is the concentration vector of the chemical components dissolved in water, $\vec{a}$ is the vector of the amount adsorbed on the rock surface, $f\left(s,\vec{c}\right)$ is the water fractional flow function, s is the saturation of the aqueous phase, ϕ is the porosity of the reservoir and u_T is the total flow velocity. Using the following dimensionless variables:

$$X=\frac{x}{\frac{\Omega_s}{A}} \tag{2}$$

$$T=\frac{\int_0^t u_T(\tau)d\tau}{\varphi\frac{\Omega_s}{A}} \tag{3}$$

we can rewrite Equations 1 in its dimensionless form:

$$\begin{cases} \dfrac{\partial s}{\partial T}+\dfrac{\partial f\left(s,\vec{c}\right)}{\partial X}=0 \\ \dfrac{\partial (c_1 s+a_1(c_1))}{\partial T}+\dfrac{\partial\left(c_1 f\left(s,\vec{c}\right)\right)}{\partial X}=0 \\ \dfrac{\partial (c_2 s+a_2(c_2))}{\partial T}+\dfrac{\partial\left(c_2 f\left(s,\vec{c}\right)\right)}{\partial X}=0 \\ \vdots \\ \dfrac{\partial (c_n s+a_n(c_n))}{\partial T}+\dfrac{\partial\left(c_n f\left(s,\vec{c}\right)\right)}{\partial X}=0 \end{cases} \tag{4}$$

where T is the number of slug volumes injected, X is the dimensionless position related to the length of the slug, Ω_s is the volume of the injected slug and A is the cross-sectional area of the porous media. Moreover, we will normalize the saturation by:

$$s=\frac{s(X,T)-s^{(I)}}{s^{(J)}-s^{(I)}} \tag{5}$$

where $s^{(I)}$ is the initial water saturation and $s^{(J)}$ is the water saturation at the porous media inlet (injection point).

From now on, we use Henry´s adsorption isotherm, which states that the adsorbed amount of each component is a function of the concentration of the component itself:

$$a_i(c_i)=\Gamma_i c_i \tag{6}$$

In the case of slug injection containing dissolved chemicals, we consider that when the slug injection begins, the reservoir water saturation is irreducible, and no polymers are present in the reservoir. During the injection of the slug, water fractional flow and polymers concentration are specified. At the end of the slug injection (T = 1), the water drive begins (injection of pure water, no chemicals dissolved). Thus, we have the following initial and boundary conditions:

$$\begin{cases} s(X,0)=0, \\ \vec{c}(X,0)=\vec{c}^{(I)}, \end{cases} X>0 \tag{7}$$

$$\begin{cases} f(0,T)=f^{(J)}=1 & T>0 \\ \vec{c}(0,T)=\begin{cases} \vec{c}^{(J)}, & 0<T<1 \\ 0, & T>1 \end{cases} \end{cases} \tag{8}$$

To solve the system of Equations 4 subject to the initial and boundary conditions given in Equations 7 and 8, we introduce the following potential function, associated with volume conservation of water[7]:

$$d\varphi=f\left(s,\vec{c}\right)dT-sdX \tag{9}$$

Replacing this potential function as an independent variable splits the original (n + 1) × (n + 1) system into an $n \times n$ system, that depends only on the adsorption isotherm (thermodynamics properties), and a lifting equation that is a function of the transport properties and of the solution of the auxiliary system. Thus, this technique separates thermodynamics equilibrium and transport properties. Applying the splitting technique in Equations 4 gives:

$$\begin{cases} \dfrac{\partial}{\partial\varphi}\left(\dfrac{s}{f\left(s,\vec{c}\right)}\right)-\dfrac{\partial}{\partial X}\left(\dfrac{1}{f\left(s,\vec{c}\right)}\right)=0 \\ \dfrac{\partial a_i(c_i)}{\partial\varphi}+\dfrac{\partial c_i}{\partial X}=0, i=1,2,\ldots,n \end{cases} \tag{10}$$

In the space (X, φ), the initial and boundary conditions given by Equations 7 and 8 become:

$$\begin{cases} s(X,0)=0, X>0 \\ \vec{c}(X,0)=\vec{c}^{(I)}, X>0 \end{cases} \tag{11}$$

$$\begin{cases} f(0,\varphi)=f^{(J)}(\varphi)=1,\ \varphi>0 \\ \vec{c}(0,\varphi)=\begin{cases} \vec{c}^{(J)},\ 0<\varphi<1 \\ 0,\ \varphi>1 \end{cases} \end{cases} \tag{12}$$

Defining $\frac{1}{f\left(s,\vec{c}\right)}$ as $U\left(s,\vec{c}\right)$ and $-\frac{s}{f\left(s,\vec{c}\right)}$ as $F\left(U,\vec{c}\right)$, the system of Equations (10) becomes:

$$\begin{cases} \dfrac{\partial F\left(U,\vec{c}\right)}{\partial\varphi}+\dfrac{\partial U\left(s,\vec{c}\right)}{\partial X}=0 \\ \dfrac{\partial a_i(c_i)}{\partial\varphi}+\dfrac{\partial c_i}{\partial X}=0,\ i=1,2,\ldots,n \end{cases} \tag{13}$$

Applying the initial and boundary conditions (Equations 11 and 12) in the definitions of $U\left(s,\vec{c}\right)$ and $F\left(U,\vec{c}\right)$ we obtain the initial and boundary conditions for the new independent variables of the lifting equation:

$$\begin{cases} U\rightarrow+\infty \\ F\rightarrow-\infty \end{cases},\ \varphi=0 \tag{14}$$

$$\begin{cases} U=1 \\ F=-1 \end{cases},\ X=0 \tag{15}$$

After the solution is found in space (X, φ), the inversion mapping to time domain is obtained from the following expression:

$$dT=\frac{d\varphi}{f\left(s(X,\varphi)\vec{c}(X,\varphi)\right)}+\frac{s}{f\left(s(X,\varphi)\vec{c}(X,\varphi)\right)}dX \tag{16}$$

3 | RESULTS AND DISCUSSIONS

Now we will present the solution for the case of oil displacement by a water slug containing three dissolved polymers. In such case, the system of Equations 4 becomes:

$$\begin{cases} \dfrac{\partial s}{\partial T}+\dfrac{\partial f\left(s,\vec{c}\right)}{\partial X}=0 \\ \dfrac{\partial(c_1s+a_1(c_1))}{\partial T}+\dfrac{\partial\left(c_1f\left(s,\vec{c}\right)\right)}{\partial X}=0 \\ \dfrac{\partial(c_2s+a_2(c_2))}{\partial T}+\dfrac{\partial\left(c_2f\left(s,\vec{c}\right)\right)}{\partial X}=0 \\ \dfrac{\partial(c_3s+a_3(c_3))}{\partial T}+\dfrac{\partial\left(c_3f\left(s,\vec{c}\right)\right)}{\partial X}=0 \end{cases} \tag{17}$$

Applying the potential function (9) in (17), the system of equations is splitted in two parts: a lifting equation and an auxiliary system, given by:

$$\frac{\partial F\left(U,\vec{c}\right)}{\partial\varphi}+\frac{\partial U\left(s,\vec{c}\right)}{\partial X}=0 \tag{18}$$

$$\begin{cases} \dfrac{\partial a_1(c_1)}{\partial\varphi}+\dfrac{\partial c_1}{\partial X}=0 \\ \dfrac{\partial a_2(c_2)}{\partial\varphi}+\dfrac{\partial c_2}{\partial X}=0 \\ \dfrac{\partial a_3(c_3)}{\partial\varphi}+\dfrac{\partial c_3}{\partial X}=0 \end{cases} \tag{19}$$

Considering the thermodynamic behavior ruled by Henry´s adsorption isotherm, where the amount adsorbed is proportional to the chemical component concentration in the aqueous phase, we have:

$$a_1(c_1)=\Gamma_1c_1 \tag{20}$$

$$a_2(c_2)=\Gamma_2c_2 \tag{21}$$

$$a_3(c_3)=\Gamma_3c_3 \tag{22}$$

The components will be ordered according to the value of its adsorption constant (Γ_i), so that $\Gamma_1>\Gamma_2>\Gamma_3$. The water viscosity without chemical additives will be named μ_w^0, and α_i is a parameter related to the contribution of component i to the solution viscosity. It will be also considered that the polymer solution viscosity is described by the expression:

$$\mu_w\left(\vec{c}\right)=\mu_w^0(1+\alpha_1c_1+\alpha_2c_2+\alpha_3c_3) \tag{23}$$

According to Henry's law, the viscosity of the aqueous solution is proportional to the polymer concentration in the water phase. We will also consider that, the smaller the polymer adsorption, the smaller the solution viscosity. Therefore, we have $\alpha_1>\alpha_2>\alpha_3$ and we will choose α_i terms so that $\alpha_1+\alpha_2>\alpha_1+\alpha_3>\alpha_2+\alpha_3$.

Rewriting the auxiliary system (19) in matrix form we find:

$$\begin{bmatrix}1&0&0\\0&1&0\\0&0&1\end{bmatrix}\begin{bmatrix}c_1\\c_2\\c_3\end{bmatrix}_X+\begin{bmatrix}\dfrac{da_1(c_1)}{dc_1}&0&0\\0&\dfrac{da_2(c_2)}{dc_2}&0\\0&0&\dfrac{da_3(c_3)}{dc_3}\end{bmatrix}\begin{bmatrix}c_1\\c_2\\c_3\end{bmatrix}_\varphi=\begin{bmatrix}0\\0\\0\end{bmatrix} \tag{24}$$

The eigenvalues λ_i of this system of equations are real and distinct: $\lambda_1=a_1'(c_1)$; $\lambda_2=a_2'(c_2)$ and $\lambda_3=a_3'(c_3)$. Moreover, the corresponding eigenvectors are linearly independent, and therefore, the system is strictly hyperbolic. Recalling that the adsorption of the components is governed by Henry's isotherm and the assumption that the component $(n-1)$ adsorbs less than the component n, we can write the eigenvalues in terms of adsorption isotherm's constants: $\lambda_1=\Gamma_1$; $\lambda_2=\Gamma_2$ and $\lambda_3=\Gamma_3$. So, the solution of the auxiliary system (19) subject to initial and boundary conditions (11)–(12), which is composed by jumps of concentration, is given by:

$$c_1(X,\varphi)=\begin{cases}0, & 0\le\varphi\le\Gamma_1X\\ c_1^{(J)}, & \Gamma_1X\le\varphi\le\Gamma_1X+1\\ 0, & \Gamma_1X+1\le\varphi\le+\infty\end{cases}\tag{25}$$

$$c_2(X,\varphi)=\begin{cases}0, & 0\le\varphi\le\Gamma_2X\\ c_2^{(J)}, & \Gamma_2X\le\varphi\le\Gamma_2X+1\\ 0, & \Gamma_2X+1\le\varphi\le+\infty\end{cases}\tag{26}$$

$$c_3(X,\varphi)=\begin{cases}0, & 0\le\varphi\le\Gamma_3X\\ c_3^{(J)}, & \Gamma_3X\le\varphi\le\Gamma_3X+1\\ 0, & \Gamma_3X+1\le\varphi\le+\infty\end{cases}\tag{27}$$

The solution of the auxiliary system divides the plan (X, φ) into 10 regions (Figure 1). It can be observed the development of the chromatographic cycle, where all the injected components are completely separated. The distribution of the components within each region is given by:

- Regions 1; 7; 9 and 10: $c_1 = 0$, $c_2 = 0$ and $c_3 = 0$;
- Region 2: $c_1 = 0$, $c_2 = 0$ and $c_3 = 1$;
- Region 3: $c_1 = 0$, $c_2 = 1$ and $c_3 = 1$;
- Region 4: $c_1 = 1$, $c_2 = 1$ and $c_3 = 1$;
- Region 5: $c_1 = 0$, $c_2 = 1$ and $c_3 = 1$;
- Region 6: $c_1 = 0$, $c_2 = 0$ and $c_3 = 1$;
- Region 8: $c_1 = 0$, $c_2 = 1$ and $c_3 = 0$.

The coordinates of the points that separate the regions (shock curves intersection) can be written as functions of isotherm constants Γ_i:

- Point A:

$$X_A=\frac{1}{\Gamma_1-\Gamma_3};\quad \varphi_A=\frac{\Gamma_1}{\Gamma_1-\Gamma_3}\tag{28}$$

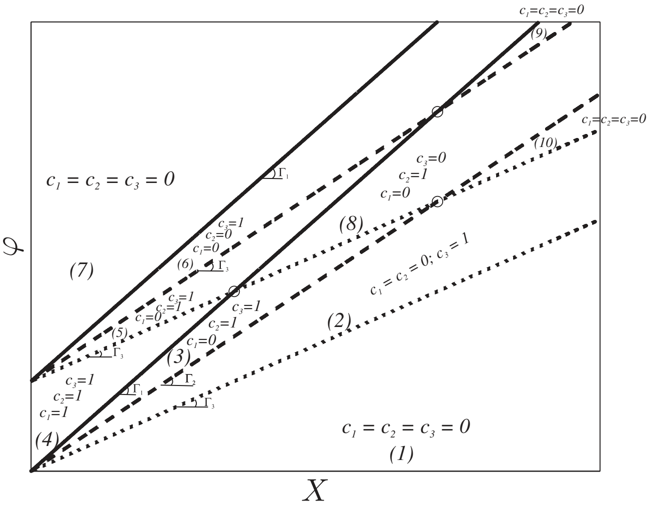

FIGURE 1 Solution of the auxiliary problem

- Point B:

$$X_B=\frac{1}{\Gamma_2-\Gamma_3};\ \varphi_B=\frac{\Gamma_2}{\Gamma_2-\Gamma_3}\tag{29}$$

- Point C:

$$X_C=\frac{1}{\Gamma_1-\Gamma_2};\ \varphi_C=\frac{\Gamma_1}{\Gamma_1-\Gamma_2}\tag{30}$$

The concentration profile is calculated from the auxiliary problem solution (Equations 25–27). During the slug injection, all three components are present in the reservoir, and component 3 travels ahead of components 1 and 2 due to its smaller adsorption rate (Figure 2a). Figure 2b presents the slug displacement by pure water injection (no dissolved components). Figure 2c shows the splitting of the components in the porous media and no longer exists a region where all three components coexist. When $\varphi_B < \varphi < \varphi_C$, component 3 is completely separated from components 1 and 2 (Figure 2d). For $\varphi > \varphi_C$, all components are separated, and the chromatographic cycle is completed (Figure 2e).

Once the solution of the auxiliary problem is found and the concentration profile in the auxiliary plane is known, the next step is to solve the lifting equation to calculate the saturation. Recalling that the concentration of each component remains constant in each of the different regions, applying the chain rule in Equation (18), leads to:

$$\frac{\partial F}{\partial U}\frac{\partial U}{\partial\varphi}+\frac{\partial U}{\partial X}=0\tag{31}$$

The solution of Equation 31 is found by the method of characteristics. The characteristic speed is given by:

$$\frac{d\varphi}{dX}=\frac{\partial F}{\partial U}\tag{32}$$

On each characteristic curve the value of U is constant. The solution $U(X, \varphi)$ of Equation 31 (Figure 3) is composed by five different regions limited by the crossing points of the shock waves of the auxiliary system solution:

$$U(X,\varphi)=\begin{cases}U_I, & 0<\varphi<1\\ U_{II}, & 1<\varphi<\varphi_A\\ U_{III}, & \varphi_A<\varphi<\varphi_B\\ U_{IV}, & \varphi_B<\varphi<\varphi_C\\ U_V, & \varphi_C<\varphi\end{cases}\tag{33}$$

The solution path in ($F \times U$) plane is presented in Figures 4–8. The superscript (n) indicates the value of U at point n and corresponds to a constant state region, and the subscript (n) represents a rarefaction wave in region n. Values of U before a shock are defined as U^+, and U^- corresponds to the value of the variable after the shock. Each part of the solution of $U(X, \varphi)$ (Equation 33) is given by:

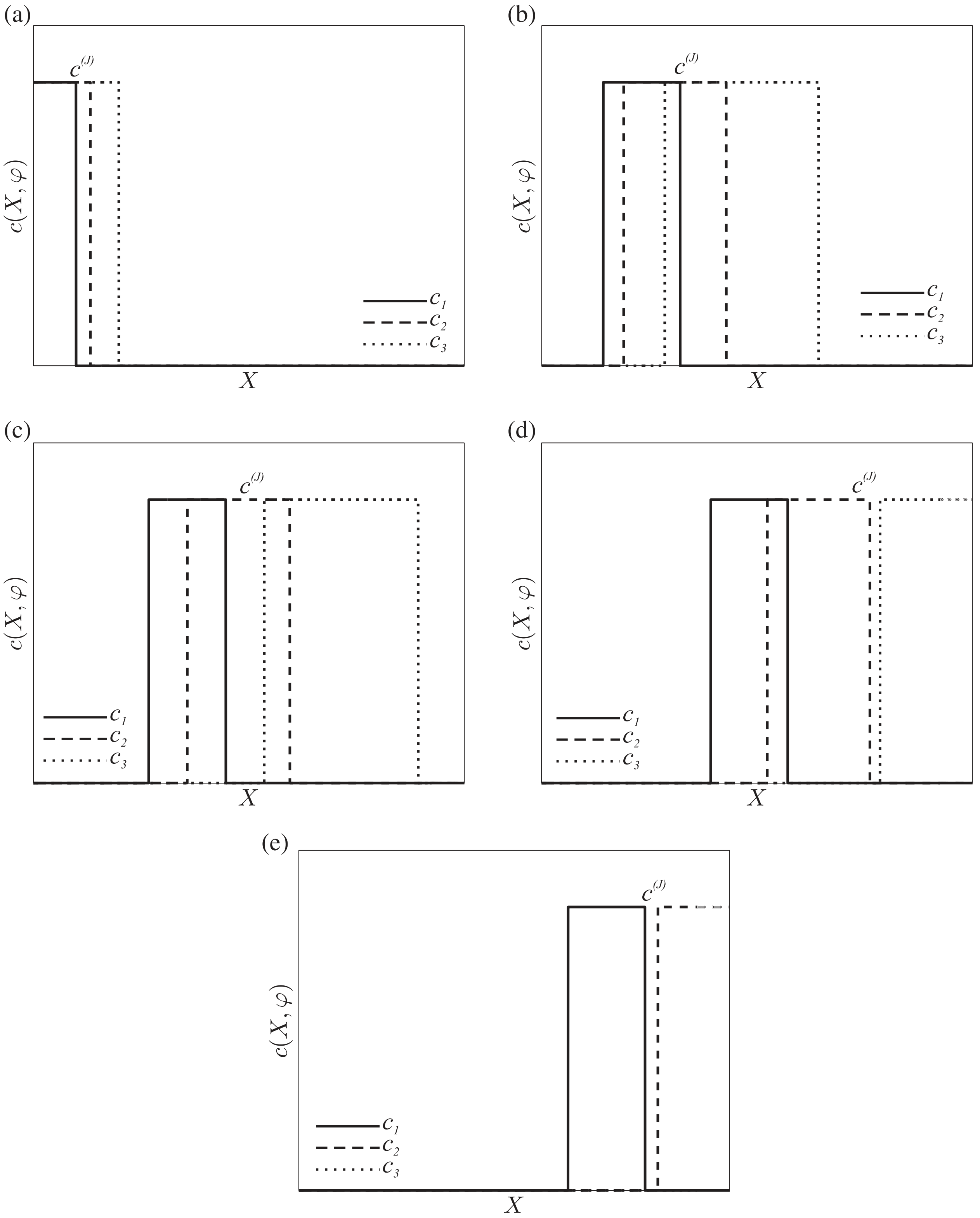

FIGURE 2 (a) Polymer concentration profile during slug injection; (b) polymer concentration profile: $1 < \varphi < \varphi_A$; (c) polymer concentration profile: $\varphi_A < \varphi < \varphi_B$; (d) polymer concentration profile: $\varphi_B < \varphi < \varphi_C$; (e) polymer concentration profile: $\varphi > \varphi_C$

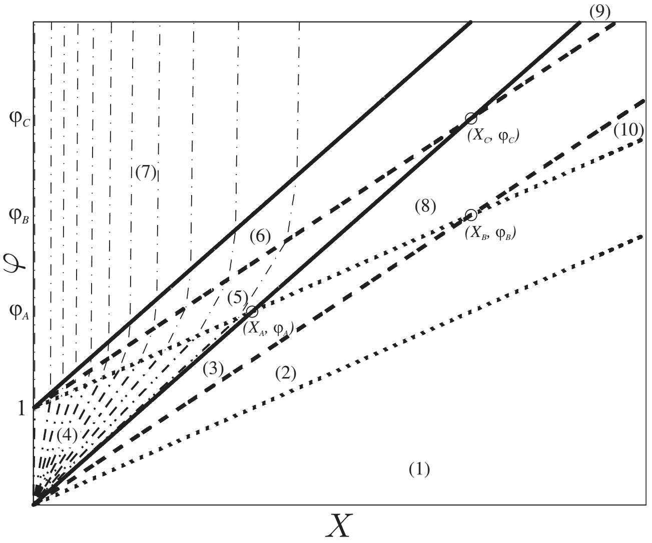

FIGURE 3 *U*-characteristics in plane (X, φ)

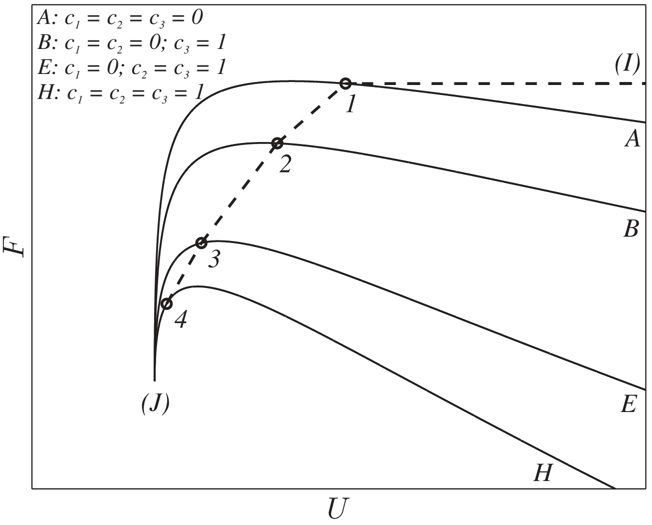

FIGURE 4 Solution of U_I in plane ($F \times U$)

- For $\varphi < 1$:

$$U_I = \begin{cases} U^{(J)}, & X = 0 \\ U_4(X,\varphi), & \dfrac{\varphi}{\dfrac{\partial F\left(U = 1, \vec{c} = \vec{c}^{(J)}\right)}{\partial U}} < X < \dfrac{\varphi}{\Gamma_1} \\ U^{(3)}, & \dfrac{\varphi}{\Gamma_1} < X < \dfrac{\varphi}{\Gamma_2} \\ U^{(2)}, & \dfrac{\varphi}{\Gamma_2} < X < \dfrac{\varphi}{\Gamma_3} \\ U^{(1)}, & \dfrac{\varphi}{\Gamma_3} < X < +\infty \\ U^{(I)}, & \varphi = 0 \end{cases} \tag{34}$$

- For $1 < \varphi < \varphi_A$:

$$U_{II} = \begin{cases} U^{(J)}, & X = 0 \\ U_7^{+}(X,\varphi), & \dfrac{\varphi}{\dfrac{\partial F\left(U = 1, \vec{c} = 0\right)}{\partial U}} < X < \dfrac{(\varphi - 1)}{\Gamma_1} \\ U_6^{-}(X,\varphi), & \dfrac{(\varphi - 1)}{\Gamma_1} < X < \dfrac{(\varphi - 1)}{\Gamma_2} \\ U_5^{-}(X,\varphi), & \dfrac{(\varphi - 1)}{\Gamma_2} < X < \dfrac{(\varphi - 1)}{\Gamma_3} \\ U_4^{-}(X,\varphi), & \dfrac{(\varphi - 1)}{\Gamma_3} < X < \dfrac{\varphi}{\Gamma_1} \\ U^{(3)}, & \dfrac{\varphi}{\Gamma_1} < X < \dfrac{\varphi}{\Gamma_2} \\ U^{(2)}, & \dfrac{\varphi}{\Gamma_2} < X < \dfrac{\varphi}{\Gamma_3} \\ U^{(1)}, & \dfrac{\varphi}{\Gamma_3} < X < +\infty \\ U^{(I)}, & \varphi = 0 \end{cases} \tag{35}$$

- For $\varphi_A < \varphi < \varphi_B$:

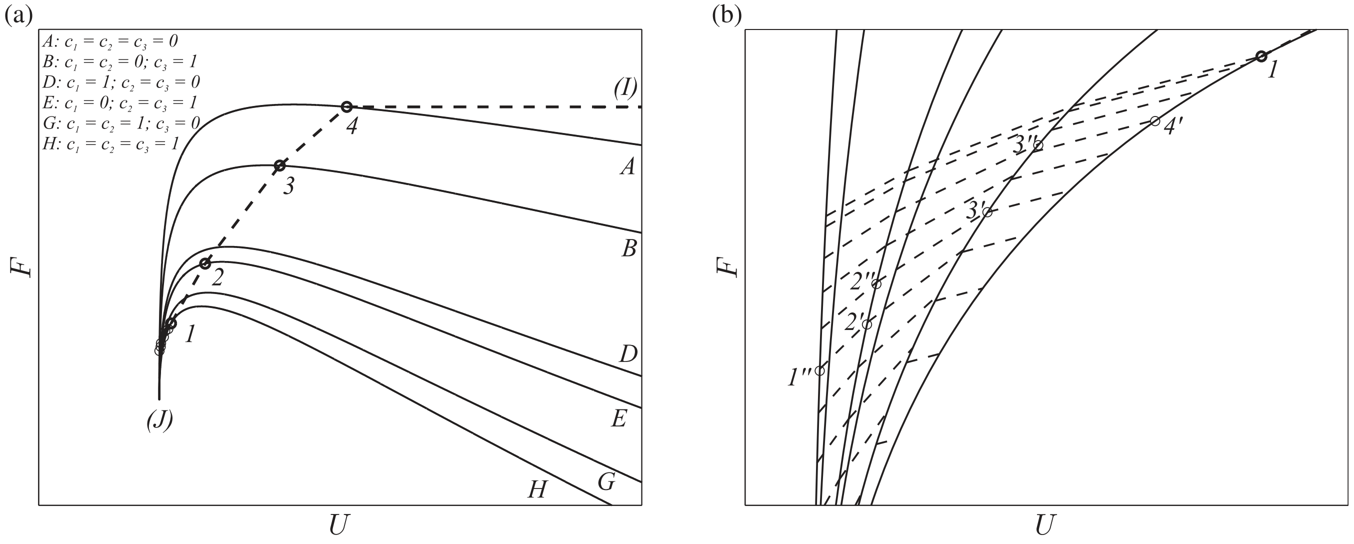

FIGURE 5 (a) Solution of U_{II} in plane ($F \times U$); (b) zoom in solution U_{II}

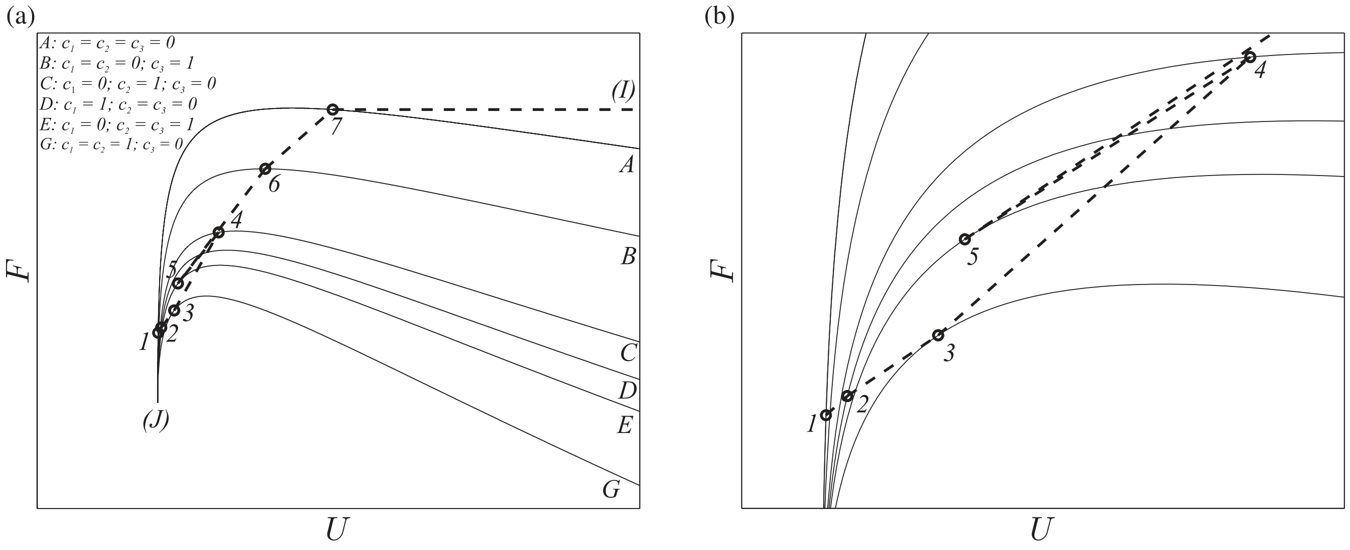

FIGURE 6 (a) Solution of U_{III} in plane ($F \times U$); (b) zoom in solution U_{III}

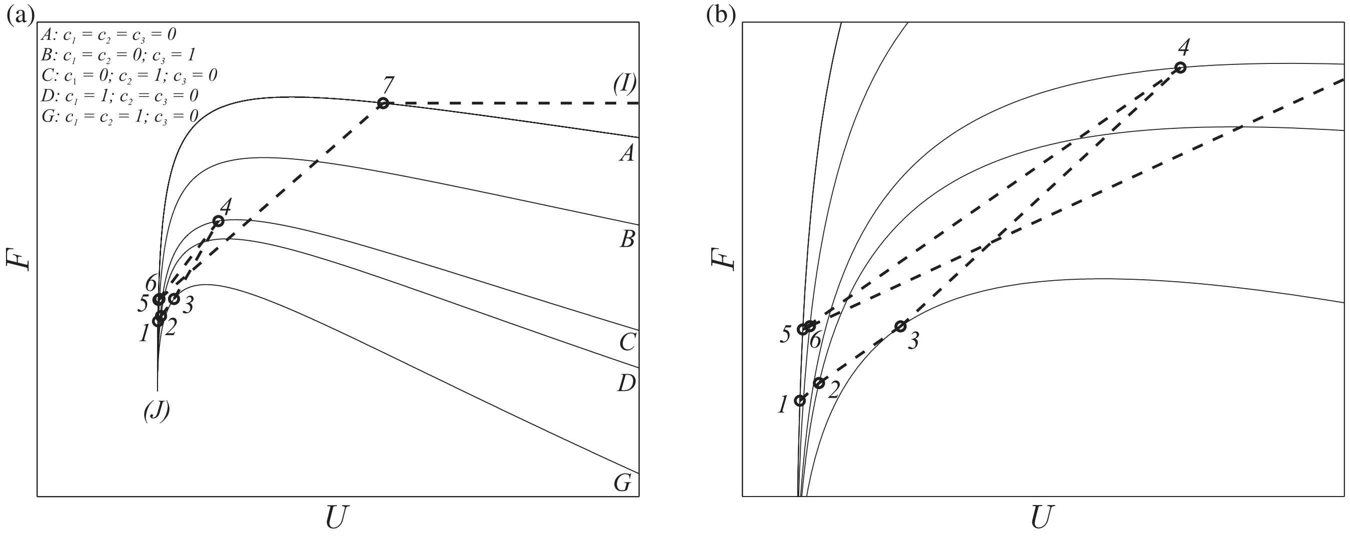

FIGURE 7 (a) Solution of U_{IV} in plane ($F \times U$); (b) zoom in solution U_{IV}

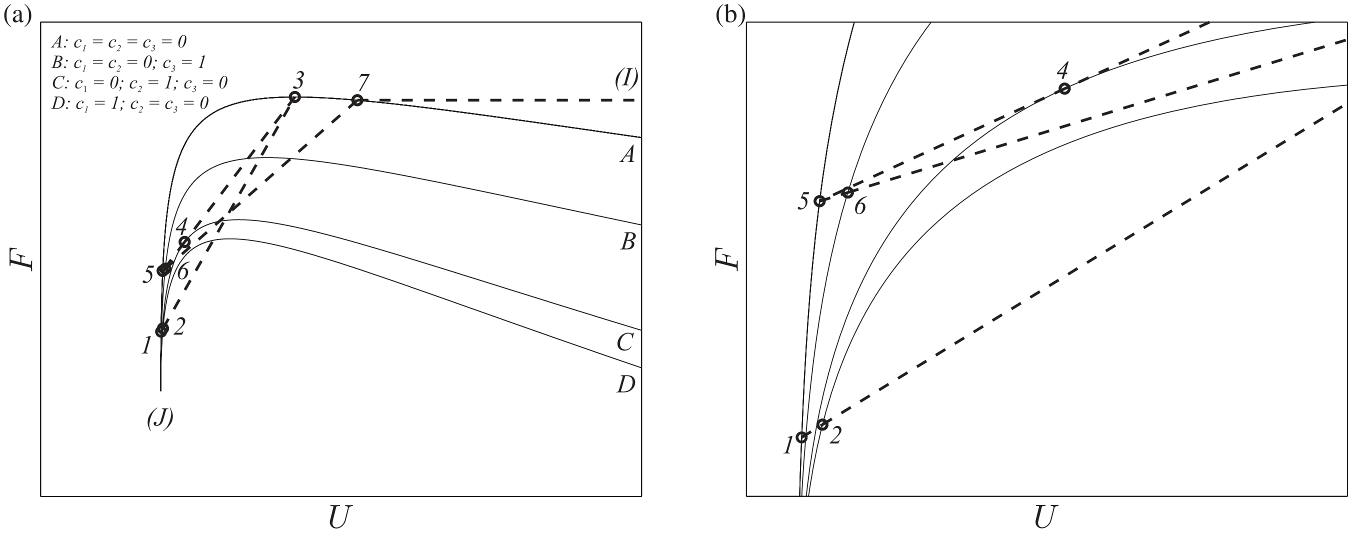

FIGURE 8 (a) Solution of U_V in plane ($F \times U$); (b) zoom in solution U_V

$$U_{III} = \begin{cases} U^{(J)}, & X = 0 \\ U_7^{+}(X,\varphi), & \dfrac{\varphi}{\dfrac{\partial F\left(U=1,\vec{c}=0\right)}{\partial U}} < X < \dfrac{(\varphi-1)}{\Gamma_1} \\ U_6^{-}(X,\varphi), & \dfrac{(\varphi-1)}{\Gamma_1} < X < \dfrac{(\varphi-1)}{\Gamma_2} \\ U_5^{-}(X,\varphi), & \dfrac{(\varphi-1)}{\Gamma_2} < X < \dfrac{\varphi}{\dfrac{\partial F\left(U^{(5-)},c_1=c_2=1,c_3=0\right)}{\partial U}} \\ U^{(5-)}, & \dfrac{\varphi}{\dfrac{\partial F\left(U^{(5-)},c_1=c_2=1,c_3=0\right)}{\partial U}} < X < \dfrac{\varphi}{\Gamma_1} \\ U^{(8)}, & \dfrac{\varphi}{\Gamma_1} < X < \dfrac{\varphi-1}{\Gamma_3} \\ U^{(3)}, & \dfrac{\varphi-1}{\Gamma_3} < X < \dfrac{\varphi}{\Gamma_2} \\ U^{(2)}, & \dfrac{\varphi}{\Gamma_2} < X < \dfrac{\varphi}{\Gamma_3} \\ U^{(1)}, & \dfrac{\varphi}{\Gamma_3} < X < +\infty \\ U^{(I)}, & \varphi = 0 \end{cases} \tag{36}$$

- For $\varphi_B < \varphi < \varphi_C$:

$$U_{IV} = \begin{cases} U^{(J)}, & X = 0 \\ U_7^{+}(X,\varphi), & \dfrac{\varphi}{\dfrac{\partial F\left(U=1,\vec{c}=0\right)}{\partial U}} < X < \dfrac{(\varphi-1)}{\Gamma_1} \\ U_6^{-}(X,\varphi), & \dfrac{(\varphi-1)}{\Gamma_1} < X < \dfrac{\varphi}{\dfrac{\partial F\left(U^{(6-)},c_1=1,c_2=c_3=0\right)}{\partial U}} \\ U^{(6-)}, & \dfrac{\varphi}{\dfrac{\partial F\left(U^{(6-)},c_1=1,c_2=c_3=0\right)}{\partial U}} < X < \dfrac{(\varphi-1)}{\Gamma_2} \\ U^{(5-)}, & \dfrac{(\varphi-1)}{\Gamma_2} < X < \dfrac{\varphi}{\Gamma_1} \\ U^{(8)}, & \dfrac{\varphi}{\Gamma_1} < X < \dfrac{\varphi}{\Gamma_2} \\ U^{(10)} & \dfrac{\varphi}{\Gamma_2} < X < \dfrac{\varphi-1}{\Gamma_3} \\ U^{(2)}, & \dfrac{\varphi-1}{\Gamma_3} < X < \dfrac{\varphi}{\Gamma_3} \\ U^{(1)}, & \dfrac{\varphi}{\Gamma_3} < X < +\infty \\ U^{(I)}, & \varphi = 0 \end{cases} \tag{37}$$

- For $\varphi > \varphi_C$:

$$U_{V} = \begin{cases} U^{(J)}, & X = 0 \\ U_7^{+}(X,\varphi), & \dfrac{\varphi}{\dfrac{\partial F\left(U=1,\vec{c}=0\right)}{\partial U}} < X < \dfrac{\varphi}{\dfrac{\partial F\left(U^{(7+)}\vec{c}=0\right)}{\partial U}} \\ U^{(7+)}, & \dfrac{\varphi}{\dfrac{\partial F\left(U^{(7+)},\vec{c}=0\right)}{\partial U}} < X < \dfrac{(\varphi-1)}{\Gamma_1} \\ U^{(6-)}, & \dfrac{(\varphi-1)}{\Gamma_1} < X < \dfrac{\varphi}{\Gamma_1} \\ U^{(9)}, & \dfrac{\varphi}{\Gamma_1} < X < \dfrac{(\varphi-1)}{\Gamma_2} \\ U^{(8)}, & \dfrac{(\varphi-1)}{\Gamma_2} < X < \dfrac{\varphi}{\Gamma_2} \\ U^{(10)} & \dfrac{\varphi}{\Gamma_2} < X < \dfrac{\varphi-1}{\Gamma_3} \\ U^{(2)}, & \dfrac{\varphi-1}{\Gamma_3} < X < \dfrac{\varphi}{\Gamma_3} \\ U^{(1)}, & \dfrac{\varphi}{\Gamma_3} < X < +\infty \\ U^{(I)}, & \varphi = 0 \end{cases} \tag{38}$$

The path of $U_I(X, \varphi)$ is shown in Figure 4 and is given by $J - 4 \rightarrow 3 \rightarrow 2 \rightarrow 1 \rightarrow I$, where the symbol ($\rightarrow$) indicates a shock and (–) a rarefaction. This solution starts with a rarefaction wave from the injection condition $U^{(J)}$ to the point $U^{(4)}$ on the curve $F(U, c_1 = c_2 = c_3 = 1)$. At this point, there is a jump with velocity Γ_1 up to the point $U^{(3)}$ on the curve $F(U; c_1 = 0, c_2 = c_3 = 1)$. Subsequently, there is a jump with velocity Γ_2 to the point $U^{(2)}$ on $F(U; c_1 = c_2 = 0, c_3 = 1)$, and finally a new jump to $U^{(1)}$ on $F(U; c_1 = c_2 = c_3 = 0)$ with velocity Γ_3. Note that through each jump with velocity Γ_i, the component i disappears. The Buckley-Leverett jump is achieved only when $X \rightarrow +\infty$.

The rarefaction waves can be calculated by:

$$\frac{\partial F(U,c_1=c_2=c_3=1)}{\partial U} = \frac{\varphi}{X} \tag{39}$$

The jump that connects $U^{(4)}$ and $U^{(3)}$ begins in $F(U, c_1 = c_2 = c_3 = 1)$ where:

$$\frac{\partial F\left(U=U^{(4)},c_1=c_2=c_3=1\right)}{\partial U} = \Gamma_1 \tag{40}$$

From the Rankine–Hugoniot conditions we find the constant states $U^{(3)}$, $U^{(2)}$, and $U^{(1)}$:

$$\frac{[F]}{[U]} = \frac{F\left(U^{(4)};c_1=c_2=c_3=1\right) - F\left(U^{(3)};c_1=0,c_2=c_3=1\right)}{U^{(4)}-U^{(3)}} = \Gamma_1 \tag{41}$$

$$\frac{F\left(U^{(3)};c_1=0,c_2=c_3=1\right) - F\left(U^{(2)};c_1=c_2=0,c_3=1\right)}{U^{(3)}-U^{(2)}} = \Gamma_2 \tag{42}$$

$$\frac{F\left(U^{(2)};c_1=c_2=0,c_3=1\right) - F\left(U^{(1)};c_1=c_2=c_3=0\right)}{U^{(2)}-U^{(1)}} = \Gamma_3 \tag{43}$$

The shock path given by $\varphi = \Gamma_3 X + 1$ separates the self-similar region (regions 1–4 in Figure 3, which corresponds to solution $U_I(X, \varphi)$), from regions where the pure water injected interacts with the polymer slug (regions 5, 6 and 7 in Figure 3). The rarefaction waves resulting from these interactions ($U_7^{+}(X,\varphi)$, $U_6^{-}(X,\varphi)$, and $U_5^{-}(X,\varphi)$) are calculated through the solution of the following system of transcendental equations:

$$\varphi^{*} = \Gamma_i X^{*} + 1 \tag{44}$$

$$\frac{\partial F\left(U^{+},\vec{c}^{\,+}\right)}{\partial U} = \frac{\varphi^{*}}{X^{*}} \tag{45}$$

$$\frac{F\left(U^{+},\vec{c}^{\,+}\right) - F\left(U^{-},\vec{c}^{\,-}\right)}{U^{+}-U^{-}} = \Gamma_i \tag{46}$$

$$\frac{\partial F\left(U^{-},\vec{c}^{\,-}\right)}{\partial U} = \frac{\varphi-\varphi^{*}}{X-X^{*}} \tag{47}$$

Therefore, for $U_5^{-}(X\varphi)$, we have:

$$\varphi^* = \Gamma_3 X^* + 1 \tag{48}$$

$$\frac{\partial F\left(U^+, c_1 = c_2 = c_3 = 1\right)}{\partial U} = \frac{\varphi^*}{X^*} \tag{49}$$

$$\frac{F\left(U^+, c_1 = c_2 = c_3 = 1\right) - F\left(U_5^-; c_1 = c_2 = 1, c_3 = 0\right)}{U^+ - U_5^-} = \Gamma_3 \tag{50}$$

$$\frac{\partial F\left(U_5^-, c_1 = c_2 = 1, c_3 = 0\right)}{\partial U} = \frac{\varphi - \varphi^*}{X - X^*} \tag{51}$$

For the calculation of $U_6^-(X,\varphi)$ we recall that $U_6^+(X,\varphi) = U_5^-(X,\varphi)$. Thus,

$$\varphi^* = \Gamma_2 X^* + 1 \tag{52}$$

$$\frac{\partial F\left(U_6^+ = U_5^-; c_1 = c_2 = 1, c_3 = 0\right)}{\partial U} = \frac{\varphi^*}{X^*} \tag{53}$$

$$\frac{F\left(U_6^+ = U_5^-, c_1 = c_2 = 1, c_3 = 0\right) - F\left(U_6^-; c_1 = 1, c_2 = c_3 = 0\right)}{U_6^- - U_5^-} = \Gamma_2 \tag{54}$$

$$\frac{\partial F\left(U_6^-, c_1 = 1, c_2 = c_3 = 0\right)}{\partial U} = \frac{\varphi - \varphi^*}{X - X^*} \tag{55}$$

Similarly, for $U_7^-(X,\varphi)$, we know that $U_7^+(X,\varphi) = U_6^-(X,\varphi)$:

$$\varphi^* = \Gamma_1 X^* + 1 \tag{56}$$

$$\frac{\partial F\left(U_7^+ = U_6^-; c_1 = 1, c_2 = c_3 = 0\right)}{\partial U} = \frac{\varphi^*}{X^*} \tag{57}$$

$$\frac{F\left(U_7^+ = U_6^-, c_1 = 1, c_2 = c_3 = 0\right) - F\left(U_7^-; c_1 = c_2 = c_3 = 0\right)}{U_6^- - U_7^-} = \Gamma_1 \tag{58}$$

$$\frac{\partial F\left(U_7^-; c_1 = c_2 = c_3 = 0\right)}{\partial U} = \frac{\varphi - \varphi^*}{X - X^*} \tag{59}$$

So, the solution $U_{II}(X, \varphi)$ is given by (Figures 3 and 5):

- Injection condition: U constant and equal to $U^{(J)}$ with $c_1 = c_2 = c_3 = 0$;
- Region (7): U-rarefaction where $c_1 = c_2 = c_3 = 0$, and U varies from $U^{(J)}$ to $U_7^+(X,\varphi)$;
- Region (6): U-shock with velocity Γ_1 from the end of the rarefaction $U_7^+(X,\varphi)$ where $c_1 = c_2 = c_3 = 0$ to $U_6^-{}'(X,\varphi)$ where $c_1 = 1$, $c_2 = c_3 = 0$, followed by a rarefaction wave from $U_6^-{}'(X,\varphi)$ to $U_6^-{}''(X,\varphi)$;
- Region (5): U-shock with velocity Γ_2 from the end of the rarefaction $U_6^-{}''(X,\varphi)$ with $c_1 = 1$, $c_2 = c_3 = 0$ to $U_5^-{}'(X,\varphi)$ with $c_1 = c_2 = 1$, $c_3 = 0$, followed by a rarefaction wave from $U_5^-{}'(X,\varphi)$ to $U_5^-{}''(X,\varphi)$;
- Region (4): U-shock with velocity Γ_3 from the end of the rarefaction $U_5^-{}''(X,\varphi)$ where $c_1 = 1$, $c_2 = c_3 = 0$ to $U_4^-{}'(X,\varphi)$ where $c_1 = c_2 = c_3 = 1$, followed by a rarefaction wave from $U_4^-{}'(X,\varphi)$ to $U_4^-{}''(X,\varphi)$;
- Region (3): U-shock with velocity Γ_3 from the end of rarefaction $U_4^-{}''(X,\varphi)$ where $c_1 = c_2 = c_3 = 1$ to $U^{(3)}$ in which $c_1 = 0$, $c_2 = c_3 = 1$, followed by a constant state $U^{(3)}$;
- Region (2): jump from $U^{(3)}$ to $U^{(2)}$ with velocity Γ_2, followed by a constant state $U^{(2)}$ where $c_1 = c_2 = 0$, $c_3 = 1$;
- Region (1): jump from $U^{(2)}$ to $U^{(1)}$ with velocity Γ_3, followed by a constant state $U^{(1)}$ where $c_1 = c_2 = c_3 = 0$;
- For $\varphi = 0$: jump from $U^{(1)}$ to initial condition $U^{(I)}$.

The superscripts ′ and ″ indicate, respectively, the values of U at the beginning and at the end of each rarefaction wave resulting from the interaction between waves of different families. For example, $6'$ in solution U_{II} (Figure 5b) is the point where the solution jumps from region 7 to region 6, and $6''$ is the end of rarefaction in region 6 where the solution jumps from region 6 to region 5. Note that for different values of φ, the beginning, the end and the length of the rarefaction will also be different.

Analogously to the solution $U_{II}(X, \varphi)$, we can write the solution path for $U_{III}(X, \varphi)$, $U_{IV}(X, \varphi)$, and $U_V(X, \varphi)$. These solutions are given by:

$$U_{III}(X,\varphi) : (J) - 7^{+''} \rightarrow 6^{-'} - 6^{-''} \rightarrow 5^{-'} - 5^- \rightarrow 8 \rightarrow 3 \rightarrow 2 \rightarrow 1 \rightarrow I$$

$$U_{IV}(X,\varphi) : (J) - 7^{+''} \rightarrow 6^{-'} - 6^{-''} \rightarrow 5^- \rightarrow 8 \rightarrow 10 \rightarrow 2 \rightarrow 1 \rightarrow I$$

$$U_V(X,\varphi) : (J) - 7^{+''} - 7^{+'} \rightarrow 6^- \rightarrow 9 \rightarrow 8 \rightarrow 10 \rightarrow 2 \rightarrow 1 \rightarrow I$$

The rarefaction and shock waves in each region are calculated following the same procedures already described to the solution $U_{II}(X, \varphi)$.

Once the solution of the problem in the auxiliary plane is found we can determine $f\left(s(X, \varphi)\vec{c}\right)$ and $s(X, \varphi)$ from the definitions of F and U:

$$f = \frac{1}{U(X,\varphi)} \tag{60}$$

$$s = -\frac{F\left(U, \vec{c}\right)}{U(X,\varphi)} \tag{61}$$

At this point both lifting equation and auxiliary system have already been solved. The next step is the inverse mapping from the plane ($X \times \varphi$) to plane ($X \times T$), calculated from Equation (16), and determining $s(X, T)$ and $c(X, T)$. As the adsorption is modeled by Henry´s isotherm, U rarefactions are straight lines carrying constant saturations. This condition is also applied to shocks at the front of the slug (D_i, $i = 1, 2, 3$). However, shocks at the rear of the slug ($\varphi_A = \Gamma_1 X + 1$, $\varphi_B = \Gamma_2 X + 1$, and $\varphi_C = \Gamma_3 X + 1$) are not straight lines in ($X \times T$)

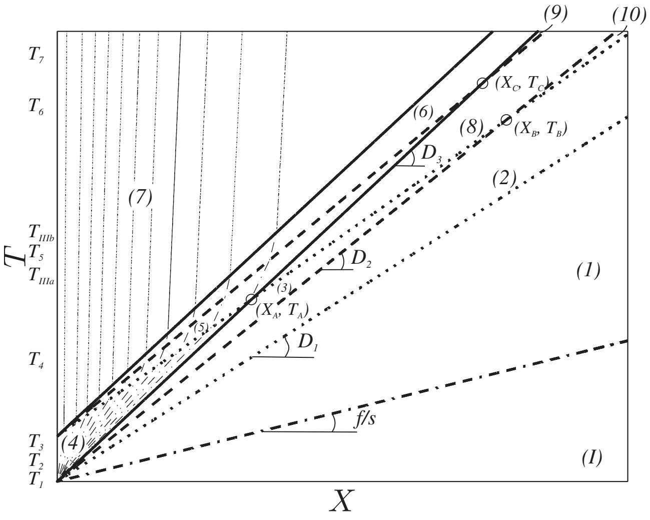

FIGURE 9 Solution in $(X \times T)$ plane

domain due to interactions between water injection waves ($\varphi > 1$) and polymers slug waves (Figure 9).

The relations between shock waves in $(X \times T)$ plane (D_j) and $(X \times \varphi)$ (V_i) are[7]:

$$D_j = \frac{f^{\pm}}{s^{\pm} + \frac{1}{V_i}}; \quad i = 1,2,3; \quad j = A,B,C \tag{62}$$

where V_i is found from the Rankine–Hugoniot conditions of the auxiliary system:

$$V_i = \frac{[c_i]}{[a_i]} \tag{63}$$

In the solution of the auxiliary system, there is a jump from a constant state in region 1 ($U^{(1)}$) to the initial condition ($U^{(I)}$) when $\varphi = 0$. This shock is similar to a Buckley–Leverett shock (Buckley and Leverett, 1942) in $(X \times \varphi)$ plane. Therefore,

$$V_{BL} = \frac{\varphi}{X} = 0 \tag{64}$$

Thus, the Buckley–Leverett shock in the $(X \times \varphi)$ plane is a straight line on the axis $\varphi = 0$. Applying Equation 64 in Equation 62, we find this shock in $(X \times T)$ plane:

$$D_{BL} = \frac{f^+}{s^+} \tag{65}$$

Rarefaction waves slopes in space $(X \times \varphi)$, carrying constant saturation and concentration, are used to determine the characteristic waves slopes in $(X \times T)$ using Equation 16.

So, the solution of $s(X, T)$ in plane $(X \times T)$ is also divided in five parts (Figure 9):

$$s(X,T) = \begin{cases} s_I, & 0 < T < 1 \\ s_{II}, & 1 < T < T_A \\ s_{III}, & T_A < T < T_B \\ s_{IV}, & T_B < T < T_C \\ s_V, & T > T_C \end{cases} \tag{66}$$

The solution $s_I(X, T)$ is:

$$s_I(X,T) = \begin{cases} s^{(J)}, & X < \dfrac{\partial f\left(s^{(J)}, c_1 = c_2 = c_3 = 1\right)}{\partial s} T \\ s_4(X,T), & \dfrac{\partial f\left(s^{(J)}, c_1 = c_2 = c_3 = 1\right)}{\partial s} T < X < D_1 T \\ s^{(3)}, & D_1 T < X < D_2 T \\ s^{(2)}, & D_2 T < X < D_3 T \\ s^{(1)}, & D_3 T < X < D_{BL} T \\ s^{(I)}, & D_{BL} T < X \end{cases} \tag{67}$$

The solution $s_{II}(X, T)$ is given by:

$$s_{II}(X,T) = \begin{cases} s^{(J)}, & X < \dfrac{\partial f\left(s^{(J)}, c_1 = c_2 = c_3 = 0\right)}{\partial s} T \\ s_7^+(X,T), & \dfrac{\partial f\left(s^{(J)}, c_1 = c_2 = c_3 = 0\right)}{\partial s} T < X < D_A(T-1) \\ s_6^-(X,T), & D_A(T-1) < X < D_B(T-1) \\ s_5^-(X,T), & D_B(T-1) < X < D_C(T-1) \\ s_4^-(X,T), & D_C(T-1) < X < D_1 T \\ s^{(3)}, & D_1 T < X < D_2 T \\ s^{(2)}, & D_2 T < X < D_3 T \\ s^{(1)}, & D_3 T < X < D_{BL} T \\ s^{(I)}, & D_{BL} T < X \end{cases} \tag{68}$$

The solution to $s_{III}(X, T)$ is divided in three parts, separated by T_{IIIa} and T_{IIIb}. Therefore, we have for $T_A < T < T_{IIIa}$:

$$s_{IIIa}(X,T) = \begin{cases} s^{(J)}, & X < \dfrac{\partial f\left(s^{(J)}, \vec{c} = 0\right)}{\partial s} T \\ s_7^+(X,T), & \dfrac{\partial f\left(s^{(J)}, \vec{c} = 0\right)}{\partial s} T < X < D_A(T-1) \\ s_6^-(X,T), & D_A(T-1) < X < D_B(T-1) \\ s_5^-(X,T), & D_B(T-1) < X < \dfrac{\partial f\left(s^{(5-)}, c_1 = c_2 = 1, c_3 = 0\right)}{\partial s} \\ s^{(5-)}, & \dfrac{\partial f\left(s^{(5-)}, c_1 = c_2 = 1, c_3 = 0\right)}{\partial s} T < X < D_1 T \\ s^{(8)}, & D_1 T < X < D_C(T-1) \\ s^{(3)}, & D_C(T-1) < X < D_2 T \\ s^{(2)}, & D_2 T < X < D_3 T \\ s^{(1)}, & D_3 T < X < D_{BL} T \\ s^{(I)} & D_{BL} T < X \end{cases} \tag{69}$$

For $T_{IIIa} < T < T_{IIIb}$ we have:

$$s_{IIIb}(X,T)=\begin{cases} s^{(J)}, & X<\dfrac{\partial f\left(s^{(J)},\vec{c}=0\right)}{\partial s}T \\ s_7^{+}(X,T), & \dfrac{\partial f\left(s^{(J)},\vec{c}=0\right)}{\partial s}T<X<D_A(T-1) \\ s_6^{-}(X,T), & D_A(T-1)<X<\dfrac{\partial f\left(s^{(6-)},c_1=1,c_2=c_3=0\right)}{\partial s}T \\ s^{(6-)}, & \dfrac{\partial f\left(s^{(6-)},c_1=1,c_2=c_3=0\right)}{\partial s}T<X<D_B(T-1) \\ s^{(5-)}, & D_B(T-1)<X<D_1T \\ s^{(8)}, & D_1T<X<D_C(T-1) \\ s^{(3)}, & D_C(T-1)<X<D_2T \\ s^{(2)}, & D_2T<X<D_3T \\ s^{(1)}, & D_3T<X<D_{BL}T \\ s^{(I)} & D_{BL}T<X \end{cases} \tag{70}$$

and for $T_{IIIb} < T < T_B$:

$$s_{IIIc}(X,T)=\begin{cases} s^{(J)}, & X<\dfrac{\partial f\left(s^{(J)},\vec{c}=0\right)}{\partial s}T \\ s_7^{+}(X,T), & \dfrac{\partial f\left(s^{(J)},\vec{c}=0\right)}{\partial s}T<X<\dfrac{\partial f\left(s^{(7+)},\vec{c}=0\right)}{\partial s} \\ s^{(7+)}, & \dfrac{\partial f\left(s^{(7+)},\vec{c}=0\right)}{\partial s}<X<D_A(T-1) \\ s^{(6-)}, & D_A(T-1)<X<D_B(T-1) \\ s^{(5-)}, & D_B(T-1)<X<D_1T \\ s^{(8)}, & D_1T<X<D_C(T-1) \\ s^{(3)}, & D_C(T-1)<X<D_2T \\ s^{(2)}, & D_2T<X<D_3T \\ s^{(1)}, & D_3T<X<D_{BL}T \\ s^{(I)} & D_{BL}T<X \end{cases} \tag{71}$$

The solution to $s_{IV}(X, T)$ is:

$$s_{IV}(X,T)=\begin{cases} s^{(J)}, & X<\dfrac{\partial f\left(s^{(J)},\vec{c}=0\right)}{\partial s}T \\ s_7^{+}(X,T), & \dfrac{\partial f\left(s^{(J)},\vec{c}=0\right)}{\partial s}T<X<\dfrac{\partial f\left(s^{(7+)},\vec{c}=0\right)}{\partial s}T \\ s^{(7+)}, & \dfrac{\partial f\left(s^{(7+)},\vec{c}=0\right)}{\partial s}T<X<D_A(T-1) \\ s^{(6-)}, & D_A(T-1)<X<D_1T \\ s^{(5-)}, & D_1T<X<D_B(T-1) \\ s^{(8)}, & D_B(T-1)<X<D_C(T-1) \\ s^{(10)}, & D_C(T-1)<X<D_2T \\ s^{(2)}, & D_2T<X<D_3T \\ s^{(1)}, & D_3T<X<D_{BL}T \\ s^{(I)} & D_{BL}T<X \end{cases} \tag{72}$$

For $s_V(X, T)$ we have the solution:

$$s_{V}(X,T)=\begin{cases} s^{(J)}, & X<\dfrac{\partial f\left(s^{(J)},\vec{c}=0\right)}{\partial s}T \\ s_7^{+}(X,T), & \dfrac{\partial f\left(s^{(J)},\vec{c}=0\right)}{\partial s}T<X<\dfrac{\partial f\left(s^{(7+)},\vec{c}=0\right)}{\partial s}T \\ s^{(7+)}, & \dfrac{\partial f\left(s^{(7+)},\vec{c}=0\right)}{\partial s}T<X<D_A(T-1) \\ s^{(6-)}, & D_A(T-1)<X<D_1T \\ s^{(9)}, & D_1T<X<D_B(T-1) \\ s^{(8)}, & D_B(T-1)<X<D_2T \\ s^{(10)}, & D_2T<X<D_C(T-1) \\ s^{(2)}, & D_C(T-1)<X<D_3T \\ s^{(1)}, & D_3T<X<D_{BL}T \\ s^{(I)} & D_{BL}T<X \end{cases} \tag{73}$$

The solution of $c(X, T)$ for $T < 1$ is:

$$c_1(X,T)=\begin{cases} c_1^{(J)}, & X<D_1T \\ c_1^{(I)}, & D_1T<X \end{cases} \tag{74}$$

$$c_2(X,T)=\begin{cases} c_2^{(J)}, & X<D_2T \\ c_2^{(I)}, & D_2T<X \end{cases} \tag{75}$$

$$c_3(X,T)=\begin{cases} c_3^{(J)}, & X<D_3T \\ c_3^{(I)}, & D_3T<X \end{cases} \tag{76}$$

And for $T > 1$ we find:

$$c_1(X,T)=\begin{cases} 0, & 0<X<D_A(T-1) \\ c_1^{(J)}, & D_A(T-1)<X<D_1T \\ c_1^{(I)}, & D_1T<X \end{cases} \tag{77}$$

$$c_2(X,T)=\begin{cases} 0, & 0<X<D_B(T-1) \\ c_2^{(J)}, & D_B(T-1)<X<D_2T \\ c_2^{(I)}, & D_2T<X \end{cases} \tag{78}$$

$$c_3(X,T)=\begin{cases} 0, & 0<X<D_C(T-1) \\ c_3^{(J)}, & D_C(T-1)<X<D_3T \\ c_3^{(I)}, & D_3T<X \end{cases} \tag{79}$$

Figure 10 shows the saturation profile for the different regions of solutions of $s(X, T)$. When $T < 1$, the self-similar solution is composed by a saturation rarefaction from the injection condition to the first concentration shock, followed by three concentration and one saturation shocks, and the initial condition. Note that this part of the solution is similar to the case of continuous injection of water containing three dissolved polymers. Figure 10a presents saturation profiles for three different slug volumes injected, where $T_1 < T_2 < T_3 < 1$ (Figure 9). It is important to point out that, for $T < 1$, the number of slug volumes injected is equal to the number of porous volumes injected.

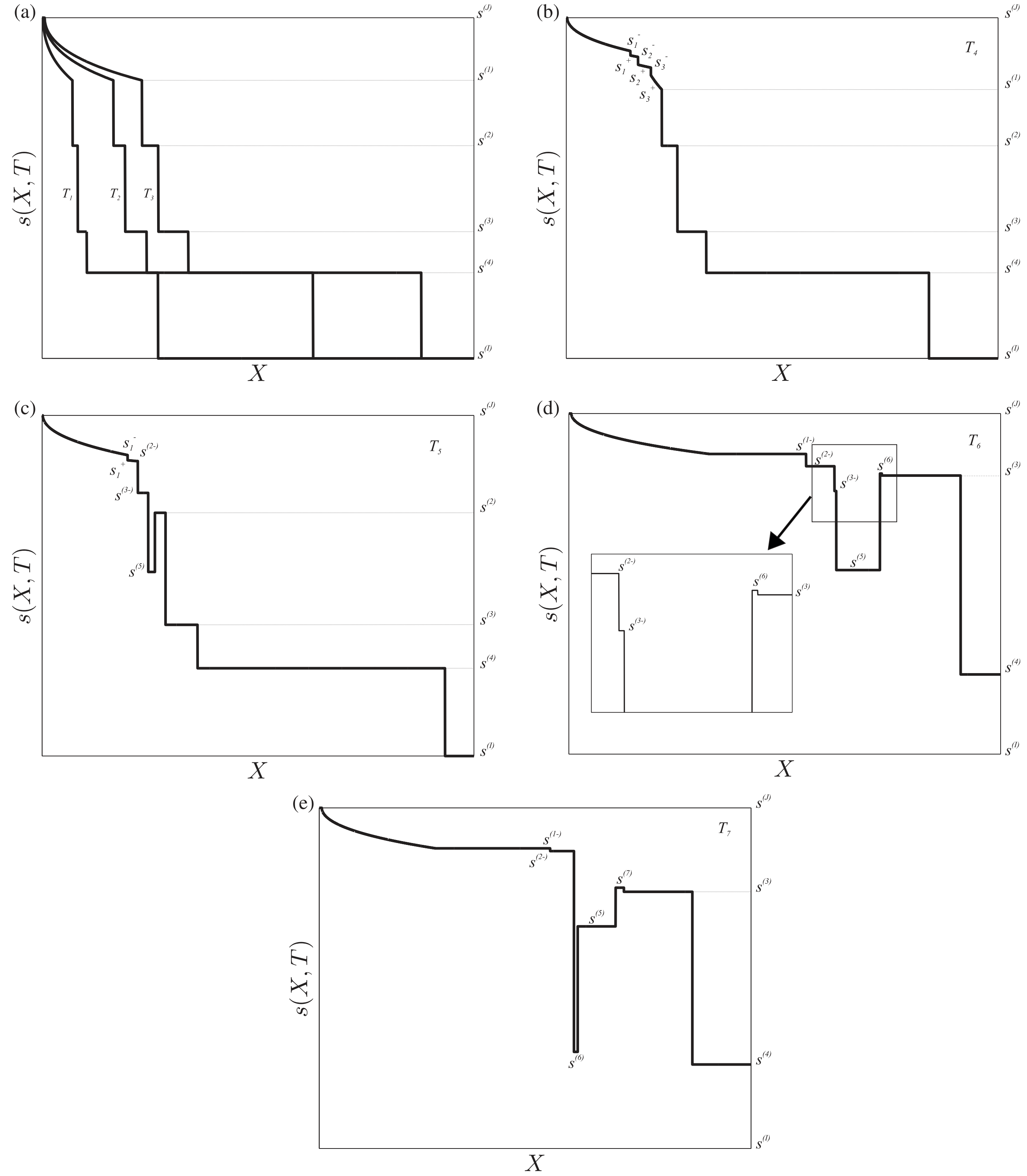

FIGURE 10 (a) Saturation profile for $T < 1$; (b) saturation profile when $1 < T < T_A$; (c) saturation profile when $T_A < T < T_B$; (d) saturation profile when $T_B < T < T_C$; (e) saturation profile when $T > T_C$

When $1 < T < T_A$, the injection of pure water leads to waves interactions with the polymer slug waves, and three rarefaction waves appear: one without chemical components, one with only component 1 and a third one with components 1 and 2 dissolved. In this region, at the beginning of water drive (pure water, no chemical components dissolved), the initial part of the chromatographic cycle can be observed, in which the polymer with the lowest adsorption rate travels slightly ahead of the others. The profile for this part of the solution is calculated at T_4 (Figure 9) and is shown in Figure 10b.

For $T_A < T < T_B$, the separation of the chemical components of the polymer slug can be observed. It can be noted that component 3 is completely separated from component 1, and no longer exists a region where all the components are present. In other words, there is no region in porous media where the water viscosity is equal to the viscosity when all the components are dissolved (slug viscosity). The solution profile is determined at T_5 (Figure 10c).

In the case where $T_B < T < T_C$, component 2 separates from component 3, and after T_B, component 3 is completely separated from the other chemicals in porous media (Figure 10d).

Finally, for $T > T_C$, the chromatographic cycle is completed, and all components injected in porous media are separated (Figure 10e).

It can be also observed in the solution profiles several regions of higher water saturation surrounded by lower saturations ($T > T_A$). This is a feature present in the non-self-similar parts of solutions of multicomponent slug injection problems due to the separation of the components in the porous media.

In the case of polymer slug injection, the appearance of higher water saturation regions occurs whenever there is a decreasing in concentration (which leads to a lower value of solution viscosity) followed by an increasing in concentration, which results in a higher value of solution viscosity. In other words, high water saturation regions can be formed in multicomponent polymer slug injection when a lower viscosity solution is surrounded by higher viscosity solution (see Figures 10c-10e).

The different solution paths in ($f \times s$) plane are presented in Figures 11–15. Note that the solution paths are related to the solution presented in Figure 10.

The solution for three components can be generalized to solve the displacement of oil by water slug containing n chemicals dissolved. This problem is modeled by the following system of equations:

$$\begin{cases} \dfrac{\partial s}{\partial T} + \dfrac{\partial f\left(s, \vec{c}\right)}{\partial X} = 0 \\ \dfrac{\partial (c_1 s + a_1(c_1))}{\partial T} + \dfrac{\partial \left(c_1 f\left(s, \vec{c}\right)\right)}{\partial X} = 0 \\ \dfrac{\partial (c_2 s + a_2(c_2))}{\partial T} + \dfrac{\partial \left(c_2 f\left(s, \vec{c}\right)\right)}{\partial X} = 0 \\ \vdots \\ \dfrac{\partial (c_n s + a_n(c_n))}{\partial T} + \dfrac{\partial \left(c_n f\left(s, \vec{c}\right)\right)}{\partial X} = 0 \end{cases} \tag{80}$$

Introducing the potential function (Equation 9) into the system of Equations 80, the auxiliary system is rewritten as:

$$\begin{cases} \dfrac{\partial a_1(c_1)}{\partial T} + \dfrac{\partial c_1}{\partial X} = 0 \\ \dfrac{\partial a_2(c_2)}{\partial T} + \dfrac{\partial c_2}{\partial X} = 0 \\ \vdots \\ \dfrac{\partial a_n(c_n)}{\partial T} + \dfrac{\partial c_n}{\partial X} = 0 \end{cases} \tag{81}$$

In this case, there is also the independent lifting equation:

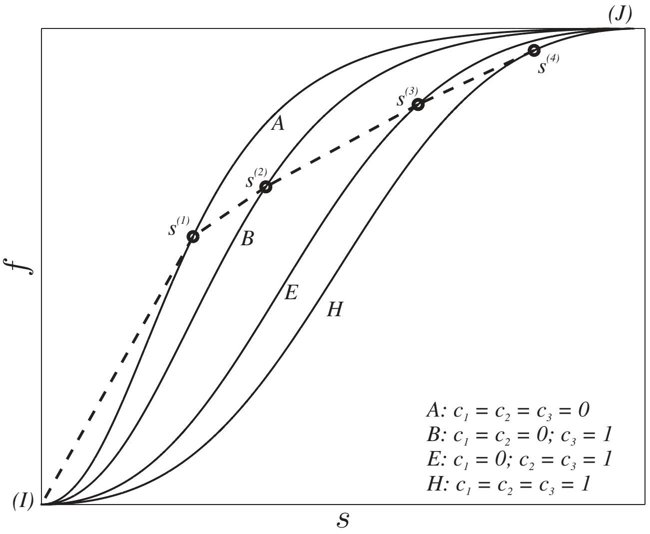

FIGURE 11 Solution path in plane ($f \times s$) for region s_I

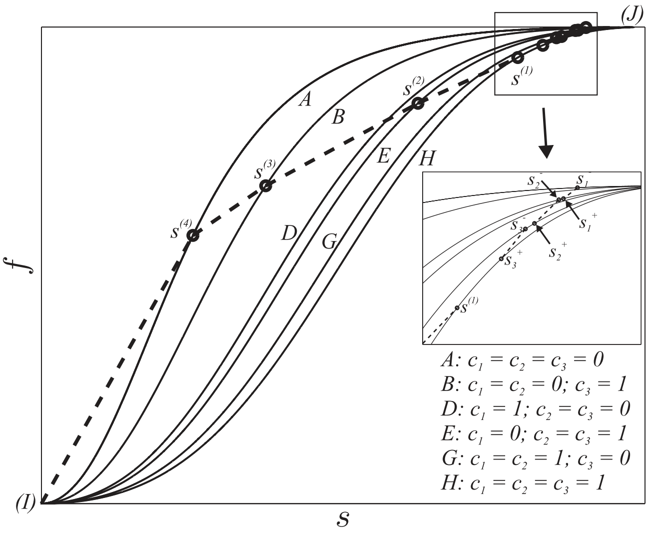

FIGURE 12 Solution path in plane ($f \times s$) for region s_{II}

$$\frac{\partial F\left(U, \vec{c}\right)}{\partial \varphi} + \frac{\partial U\left(s, \vec{c}\right)}{\partial X} = 0 \tag{82}$$

The initial and boundary conditions for this problem are given by:

$$\begin{cases} s(X,0) = 0, \\ \vec{c}(X,0) = \vec{c}^{(I)}, \end{cases} X > 0 \tag{83}$$

$$\begin{cases} f(0,T) = f^{(J)} & T > 0 \\ \vec{c}(0,T) = \begin{cases} \vec{c}^{(J)}, & 0 < T < 1 \\ 0, & T > 1 \end{cases} \end{cases} \tag{84}$$

where, $\vec{c} = (c_1, c_2, \ldots, c_n)$.

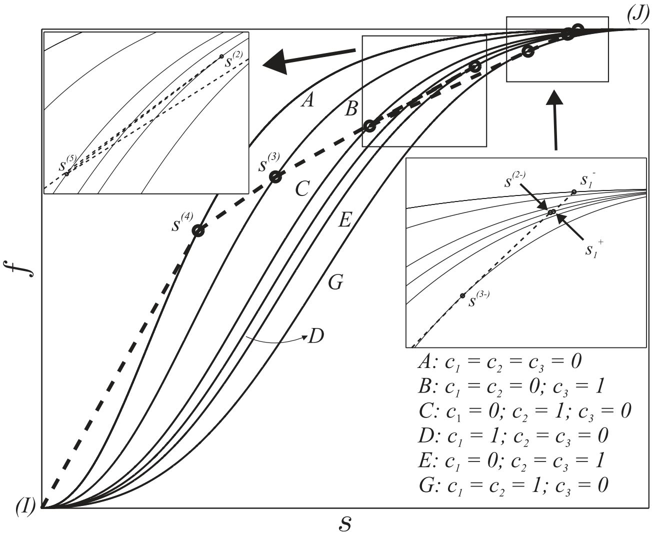

FIGURE 13 Solution path in plane ($f \times s$) for region s_{III}

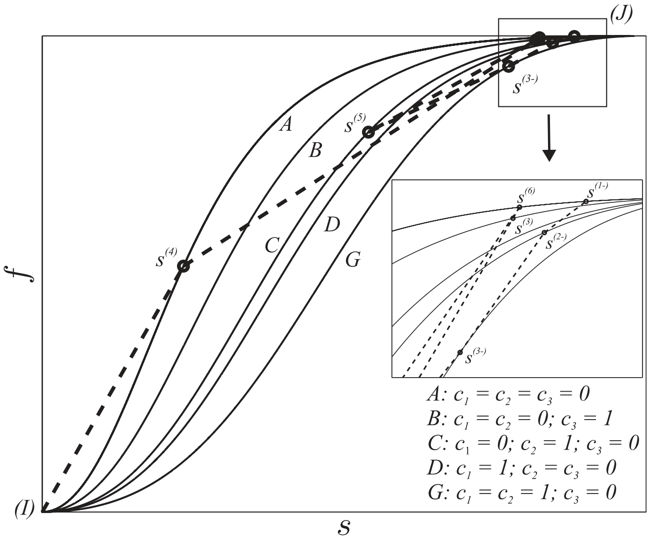

FIGURE 14 Solution path in plane ($f \times s$) for region s_{IV}

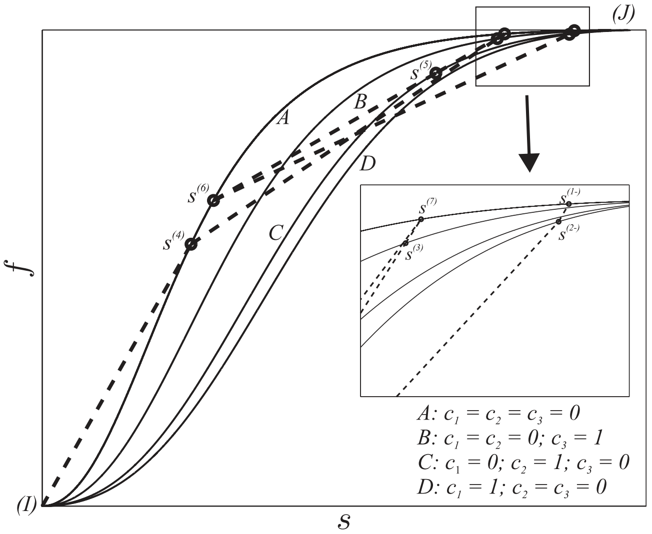

FIGURE 15 Solution path in plane ($f \times s$) for region s_V

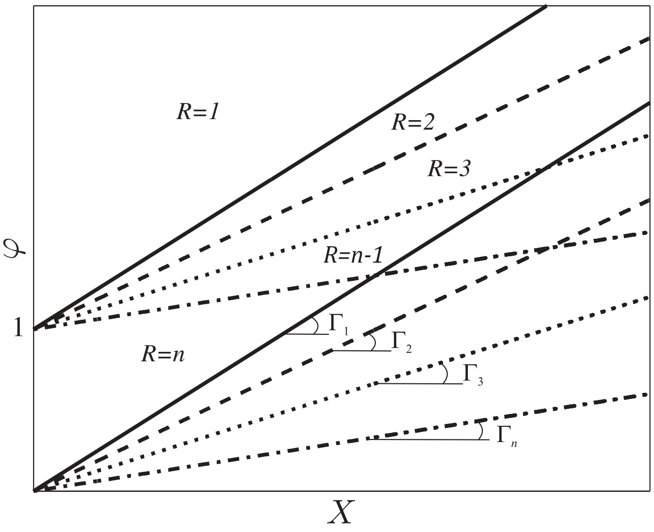

FIGURE 16 Solution of the slug injection containing n polymers in plane ($X \times \varphi$)

In this work, we consider that the fractional flow function depends on the concentration of the n components dissolved in the water, given by the vector $\vec{c}$, while the component adsorption, modeled by Henry's isotherm, depends only on its dissolved concentration. The components are numbered in order of decreasing adsorption, so that $\Gamma_1 > \Gamma_2 > \ldots > \Gamma_n$.

To solve the thermodynamic part of the problem we write the auxiliary system in matrix form (see Equation 24), and the eigenvalues are $\lambda_1 = \Gamma_1 > \lambda_2 = \Gamma_2 > \ldots > \lambda_n = \Gamma_n$. These eigenvalues are the characteristic velocities of the auxiliary problem solution. So, the solution to the problem of oil displacement by a water slug containing n dissolved components in the auxiliary plane is composed by $2n$ concentration shocks:

$$\vec{c}(X,\varphi) = \begin{cases} c_1(X,\varphi) = \begin{cases} 0, & 0 \le \varphi \le \Gamma_1 X \\ c_1^{(J)}, & \Gamma_1 X \le \varphi \le \Gamma_1 X + 1 \\ 0, & \Gamma_1 X + 1 \le \varphi \le \infty \end{cases} \\ c_2(X,\varphi) = \begin{cases} 0, & 0 \le \varphi \le \Gamma_2 X \\ c_2^{(J)}, & \Gamma_2 X \le \varphi \le \Gamma_2 X + 1 \\ 0, & \Gamma_2 X + 1 \le \varphi \le \infty \end{cases} \\ \vdots \\ c_n(X,\varphi) = \begin{cases} 0, & 0 \le \varphi \le \Gamma_n X \\ c_n^{(J)}, & \Gamma_n X \le \varphi \le \Gamma_n X + 1 \\ 0, & \Gamma_n X + 1 \le \varphi \le \infty \end{cases} \end{cases} \tag{85}$$

This solution divides the plane into regions separated by straight lines (shock waves) (Figure 16), similarly to the case of a water slug containing three polymers presented previously. The number of regions (N_R) and the number of crossing points dividing regions of constant concentration (N_P) can be expressed as functions of the number of components (n):

$$N_R(n) = 2n + 1 + \sum_{r=1}^{n} (n - r) \tag{86}$$

$$N_P(n) = \sum_{r=0}^{n-1} [(n-1)-r] \tag{87}$$

The points that separate the regions of the auxiliary physical plane are determined by the intersection of two shocks. The coordinates of the intersection points of shock trajectories $\varphi = \Gamma_i X$ and $\varphi = \Gamma_j + 1$, where $i = 1, 2, \ldots, n-1$, $j = 2, 3, \ldots, n$, and $j > i$, are given by the following expressions:

$$X_{ij} = \frac{1}{\Gamma_j - \Gamma_i}; \quad \varphi_{ij} = \frac{\Gamma_j}{\Gamma_j - \Gamma_i} \tag{88}$$

It can be noted that:

- There are $n + 1$ regions where: $c_1 = c_2 = \ldots = c_n = 0$;
- There are n regions where only one component is present;
- There is only one region where all the n components are present, so that: $c_1 = c_2 = \ldots = c_n = 1$.

From the solution of the thermodynamic part of the problem, it is possible to determine, from the lifting equation, the saturation solution following a procedure analogous to the one presented in the previous section. For regions of constant concentration, we have:

$$\frac{\partial F}{\partial U}\frac{\partial U}{\partial \varphi} + \frac{\partial U}{\partial X} = -\frac{\partial F}{\partial c_1}\frac{\partial c_1}{\partial \varphi} = -\frac{\partial F}{\partial c_2}\frac{\partial c_2}{\partial \varphi} = \ldots = -\frac{\partial F}{\partial c_n}\frac{\partial c_n}{\partial \varphi} = 0 \tag{89}$$

The expression $\frac{d\varphi}{dX} = \frac{\partial F}{\partial U}$ defines the speed of the U characteristics. Since the concentration in each region is constant ($\frac{\partial c_i}{\partial \varphi} = 0$), each characteristic carries a constant value of U.

In order to map the solution in plane ($X \times T$), we need to invert the solution using the expression:

$$dT = \frac{d\varphi}{f\left(s(X,\varphi)\vec{c}(X,\varphi)\right)} + \frac{s}{f\left(s(X,\varphi)\vec{c}(X,\varphi)\right)}dX \tag{90}$$

For this case we can also generalize the expression for time in a region R. We consider the following nomenclature:

- R is a region of constant concentration in plane ($X \times \varphi$);
- $\Gamma^{(R)}$ is the adsorption constant of the upper limit of region R;
- $X^{(R)}$ is the position of the shock with slope $\Gamma^{(R)}$.

So, for the self-similar region ($R = n$);

$$\frac{X}{T} = \frac{\partial f}{\partial s} \tag{91}$$

For the region where $R = n - 1$ (first non-self-similar region):

$$T = \frac{\left(\Gamma^{(n)} + s^{(n)}\right)X^{(n)} + 1}{f^{(n)}} - \frac{\left(\Gamma^{(R+1)} + s^{(R)}\right)X^{(R+1)} + 1}{f^{(R)}} + \frac{X}{\frac{\partial f}{\partial s}} \tag{92}$$

For the other regions ($R < n - 1$):

$$\begin{aligned} T = {} & \frac{\left(\Gamma^{(n)} + s^{(n)}\right)X^{(n)} + 1}{f^{(n)}} + \sum_{k=1}^{R-1} \frac{\left(\Gamma^{(k)} + s^{(k)}\right)X^{(k)} - \left(\Gamma^{(k+1)} + s^{(k)}\right)}{f^{(k)}} \\ & - \frac{\left(\Gamma^{(R+1)} + s^{(R)}\right)X^{(R+1)} + 1}{f^{(R)}} + \frac{X}{\frac{\partial f}{\partial s}} \end{aligned} \tag{93}$$

Note that this general solution comprises $2n$ concentration shocks and one saturation shock (Buckley-Leverett shock type). It is important to point out that the chromatographic cycle also takes place (complete separation of components in porous media) and interactions between the rarefaction families appear. The procedure to develop a solution for any number of chemical components follows the steps presented in the previous section (three component system).

4 | CONCLUSIONS

In this paper the analytical solution for the problem of oil displacement by a chemical slug containing n components displaced by pure water is presented. By using a splitting technique based on the water conservation, a new independent variable was introduced and the system of $n + 1$ conservation laws is splitted into an $n \times n$ auxiliary system and a lifting equation. The auxiliary system depends only on the thermodynamics features of the problem, which in this case is the Henry's adsorption isotherm. The lifting equation is a function of the solution of the auxiliary system and of the transport properties (phases relative permeabilities and viscosities).

For Henry's adsorption isotherm, the solution of the auxiliary system is composed by $2n$ shock waves separated by constant states. Expressions for the number of regions and for the coordinates of the intersection points between the shock waves in the auxiliary plane are also presented. The solution in the auxiliary plane is mapped to space–time plane through simple expressions. A detailed construction of the solution is presented for the case of a slug containing 3 components.

The solution in the physical plane shows the complete development of the chromatographic cycle (separation of the components in porous media) and the saturation profiles along the porous media.

The procedure presented in this paper can be applied to several other physical systems that arise in enhanced oil recovery, like polymer and surfactant flooding, low salinity waterflooding with polymers, etc.

ACKNOWLEDGMENT

This study was financed in part by the Coordenação de Aperfeiçoamento de Pessoal de Nível Superior - Brasil (CAPES) - Finance Code 001.

ORCID

Felipe de O. Apolinário https://orcid.org/0000-0003-1606-2946

REFERENCES

1. Buckley SE, Leverett MC. Mechanism of fluid displacement in sands. *Trans AIME*. 1942;146(1):107-116.
2. Delamaide E, Moreau P, Tabary R. A new approach for offshore chemical oil recovery. In: Offshore Technology Conference, Houston, 2015.
3. Helfferich FG. Theory of multicomponent, multiphase displacement in porous media. *SPE J*. 1981;21(1):51-62.
4. Hirasaki GJ. Application of theory of multicomponent, multiphase displacement to three-component, two-phase surfactant flooding. *SPE J*. 1981;21(2):191-204.
5. Johansen T, Winther R. The Riemann problem for multicomponent polymer flooding. *SIAM J Math Anal*. 1989;19(3):908-929.
6. Bedrikovetsky PG. *Mathematical theory of oil and gas recovery: with applications to ex-USSR oil and gas fields*. Dordrecht: Kluwer Academic Publishers; 1993.
7. Pires AP, Bedrikovetsky PG, Shapiro AA. A splitting technique for analytical modelling of two-phase multicomponent flow in porous media. *J Petrol Sci Eng*. 2006;51:54-67.
8. Boa PMF, Pires AP. Salt effects on polymer adsorption in chemical flooding of oil reservoirs. In: 11th Brazilian Congress of Thermal Sciences and Engineering, Curitiba, 2006.
9. Silva RCA, Cardoso CB, Pires AP. The role of adsorption isotherms on chemical flooding oil recovery. In: SPE Annual Technical Conference and Exhibition, Anaheim, 2007.
10. Ribeiro PM, Pires AP. The displacement of oil by polymer slugs considering adsorption effects. In: SPE Annual Technical Conference and Exhibition, Denver, 2008.
11. Borazjani S, Bedrikovetsky PG, Farajzadeh R. Exact solution for non-self-similar wave-interaction problem during two-phase four-component flow in porous media. *Abs Appl Anal*. 2014;2014:1-13.
12. De Paula AS, Pires AP. Analytical solution for oil displacement by polymer slugs containing salt in porous media. *J Petrol Sci Eng*. 2015;135:323-335.
13. Borazjani S, Roberts AJ, Bedrikovetsky P. Splitting in systems of PDEs for two-phase multicomponent flow in porous media. *Appl Math Lett*. 2015;53:25-32.
14. Borazjani S, Bedrikovetsky PG, Farajzadeh R. Analytical solutions of oil displacement by a polymer slug with varying salinity. *J Petrol Sci Eng*. 2016;140:28-40.
15. Khorsandi S, Changhe Q, Johns RT. Displacement efficiency for low salinity polymer flooding including wettability alteration. *SPE J*. 2017;22(2):417-430.
16. Hamid SAA, Muggeridge AH. Analytical solution of polymer slug injection with viscous fingering. *Comput Geosci*. 2018;22(3):711-723.

How to cite this article: S. de Paula A, de O. Apolinário F, P. Pires A. Water slug injection containing *n* polymers in porous media. *AIChE J*. 2019;e16735. https://doi.org/10.1002/aic.16735

Chapter 2 – Injection of Water Slug Containing Two Polymers in Porous Media: Analytical Solution for Two-Phase Flow Accounting for Adsorption Effects

Journal of Petroleum Science and Engineering 188 (2020) 106927

Contents lists available at ScienceDirect

Journal of Petroleum Science and Engineering

journal homepage: http://www.elsevier.com/locate/petrol

Injection of water slug containing two polymers in porous media: Analytical solution for two-phase flow accounting for adsorption effects

Felipe de O Apolinário [a,*], Anália S. de Paula [b], Adolfo P. Pires [a]

[a] Universidade Estadual do Norte Fluminense Darcy Ribeiro, Brazil
[b] Petróleo Brasileiro S.A, Brazil

ARTICLE INFO

Keywords:
Enhanced oil recovery
Chemical enhanced oil recovery
Polymer flooding
Conservation laws
Hyperbolic systems of partial differential equations

ABSTRACT

Polymer flooding is the most applied chemical method of enhanced oil recovery (EOR). Usually this process consists of injecting a slug containing dissolved chemicals displaced by water. This technique is modeled by a system of conservation laws with constant initial condition and not constant boundary conditions. In this paper we extend the two solute one-dimensional chromatography problem solution (Rhee et al., 2001) for a two-phase environment. The exact solution for the injection of a slug containing two dissolved polymers driven by water in an oil reservoir is developed. It is considered that both polymers may adsorb in porous media following Langmuir's adsorption isotherm. The solution is built splitting the original system into a purely chromatographic problem (auxiliary system), and a lifting equation that considers the hydrodynamics properties of the system. Due to the chase water drive, interactions between waves arise along the space-time plane and change the path of the characteristics at the rear of the slug. The presented solution is composed by rarefaction and shock waves, and constant states. Moreover, a complete chromatography cycle develops in the porous media (complete separation of the chemical components).

1. Introduction

Injection of aqueous polymer solutions is the most applied chemical method of enhanced oil recovery (Sheng et al., 2015). Adding polymers to injection water increases the viscosity of the solution and reduces its mobility, avoiding viscous fingering and early water breakthrough (Kargozarfard et al., 2018). The polymers commonly used in enhanced oil recovery (EOR) do not modify the interfacial tension between aqueous and oleic phase, and therefore do not change the residual oil saturation. In fact, the remarkable effect of polymers solution injection in a reservoir is the increase of oil production, *i.e.*, a larger volume of oil is produced for a particular volume of polymeric solution injected when compared to the same volume of pure water (Sorbie, 1991). This effect results in a higher oil recovery at the end of the production life of reservoirs subjected to polymer injection.

The design of a polymer flooding process depends on the adsorption of the chemicals on the rock. The presence of divalent cations in the reservoir, either on the rock or in the connate water, can increase the adsorption of the polymer by the rock, which reduces the viscosity of the polymeric solution and the efficiency of the process (Sorbie, 1991; Taber et al., 1997). The injection of a water pre-flush slug containing low concentration of divalent cations can minimize the adsorption of the polymers in sandstone reservoirs (Maitin and Volz, 1981; Davison and Mentzer, 1982; Algharaib et al., 2014). For carbonate reservoirs, use of salinity resistant biopolymers or neutral pH water pre-flush with low concentration of Ca^{2+} and high concentration of SO_4^{2-} are the best options to avoid severe polymer adsorption (Ali and Barrufet, 1984; Lee et al., 2019).

Due to injectivity issues, to presence of divalent cations and to chemical components storage, polymer flooding is most used in onshore high permeable sandstone reservoirs saturated with low/medium viscosity oil (Taber et al., 1997; Torrealba and Hoteit, 2019). However, it has been reported successful implementation of this technique in different environments, including offshore reservoirs (Boardman et al., 1982). In Bohai Bay field, in China, the injection of polymers in an offshore reservoir containing heavy oil resulted in an increase of 3% in oil recovery, and a reduction of 5% in water cut (Zhou et al., 2008). In a deep-water field in Angola, despite of the heavy oil, polymer injection resulted in 7% incremental oil production and 10% water cut reduction (Morel et al., 2012).

Numerical simulation and analytical models are two of the most

---

* Corresponding author.
E-mail address: felipe_apolinario03@hotmail.com (F. de O Apolinário).

https://doi.org/10.1016/j.petrol.2020.106927
Received 20 August 2019; Received in revised form 2 January 2020; Accepted 6 January 2020

important tools to design polymer flooding projects. Numerical simulators can model complex scenarios and reduce the uncertainty of polymer flooding projects design (Alsofi & Blunt, 2010, 2014). On the other hand, analytical models can provide effective sensitive analysis on the performance of this technique under more restrictive assumptions (Bedrikovetsky, 1993).

The mathematical model that governs the flow of water containing dissolved chemicals is composed by the water volume conservation and mass conservation of each component. These equations result in a hyperbolic system of conservation laws. For a one-dimensional problem with constant initial and boundary conditions, the solution can be obtained by the method of characteristics and is composed by rarefaction and shock waves, and constant states (Bedrikovetsky, 1993).

For the case of water containing one polymer, the mathematical problem is composed by a 2×2 hyperbolic system of conservation laws. The solution is obtained by an extension of Buckley and Leverett (1942) theory, and its structure is formed by a saturation rarefaction wave followed by a concentration shock and the Buckley-Leverett shock (Patton et al., 1971). This structure can be generalized to include other enhanced oil recovery methods (Pope, 1980), such as surfactant or alkali injection, and to different adsorption isotherms (Langmuir, Henry or Freundlich adsorption isotherms) (Johansen and Winther, 1988).

The multicomponent polymer injection is modeled by a system of $(n+1) \times (n+1)$ conservation laws, where n is the number of polymers dissolved in water. The solution to the continuous injection problem was presented in Johansen and Winther (1989), and it was developed from the associated chromatography problem (one-phase multicomponent problem), followed by an extension to the two-phase problem. It is important to point out that this solution is not applied for varying boundary conditions (slug injection).

Despite the efficiency of the continuous injection of chemicals to increase oil production, due to economic criteria and injectivity issues, usually a finite volume of polymeric solution is injected in the reservoir (polymer slug) followed by pure water (water drive) (Torrealba and Hoteit, 2019). In this case, a discontinuity arises in the boundary condition at the beginning of the water drive. At this point, interaction between waves of different families occurs along the space-time plane. Therefore, in the case of slug injection of chemicals, the solution is not self-similar (Vicente et al., 2014).

A theory to solve chemicals slug injection into oil reservoirs problems is presented in Pires et al. (2006). A potential function related to the conservation of water volume replaces the independent variable time in the system of hyperbolic equations. Considering a slug containing n chemical components dissolved, the potential function splits the original $(n+1) \times (n+1)$ system into an auxiliary system of n equations and a lifting equation. The auxiliary system depends on the thermodynamic model and represents a pure chromatographic process (one-phase problem), whereas the lifting equation depends on the transport properties of the flow and on the solution of the auxiliary system. For a multicomponent polymer slug injection, it can be noted that after applying the splitting technique, the auxiliary system is similar to the one obtained in multicomponent chromatography (Rhee et al., 2001, Borazjani et al., 2016).

The splitting technique has been applied to solve several problems involving polymer injection in porous media. Boa and Pires (2006) considered the case of one polymer continuous injection where the polymer may adsorb according to Langmuir isotherm, and the amount adsorbed is affected by the water salt concentration. Silva et al. (2007) presented the solution for the continuous multicomponent polymer injection. Ribeiro and Pires (2008) considered different adsorption isotherms and fractional flow functions to solve the polymer slug injection problem.

Vicente et al. (2014) presented the solution to the problem of slug injection containing one polymer that adsorbs following Langmuir adsorption isotherm. The solution presented was built using the splitting technique and compared to the results obtained in numerical simulators.

Borazjani et al. (2014) developed the exact solution to the case of polymer slug injection considering salt effects, and the polymer adsorbs following Henry's isotherm. de Paula and Pires (2015) considered Langmuir's adsorption isotherm and salt effects in the adsorption curve to model polymer slug injection in porous media.

Borazjani et al. (2016) applied the splitting technique to solve the two-phase problem of polymer slug injection with varying salinity. It was considered that the polymer follows a linear adsorption isotherm and that the salt does not adsorb in porous media. The solution includes implicit formulae for saturation, polymer and salt concentrations and front trajectories of the components.

Khorsandi et al. (2016) presented the exact solution to the problem of low salinity polymer slug injection considering cation exchange effects that lead to wettability alteration. The results were compared to experimental data and numerical simulations.

De Paula et. al. (2019) presented the solution to the problem of slug injection containing n dissolved polymers that may adsorb following Henry's isotherm. The solution was composed by a water saturation rarefaction, $2n$ concentration shock waves and the Buckley-Leverett shock. The solution also included the effects of the interaction between saturation and concentration waves. Due to the separation of the chemicals in the porous media, water banks appeared in the water saturation solution.

It has been shown that it is also possible to build a solution to EOR problems considering advective transport, parabolic terms and relaxation non-equilibrium equations applying the splitting technique for the cases where the auxiliary system allows the development of an analytical solution (Borazjani et al., 2016).

In this paper we present the solution for the one-dimensional two-phase isothermal two-component polymer slug injection followed by water drive problem. It is considered that both polymers may be adsorbed by the porous media following Langmuir's isotherm. It was also considered that the slug and water drive salinity are the same as the connate water. The presented solution is a two-phase generalization of the one-dimensional two-component chromatography solution presented by Rhee et al. (2001). This solution is general and may be applied to any problem with two dissolved chemical components, for instance: one polymer and one surfactant, one polymer and one salt, and so on. The restriction is that the adsorption must follow Langmuir adsorption isotherm.

Next section presents the mathematical description of the physical model followed by the detailed procedure of solution using the splitting technique (Pires et al., 2006) and the chromatography theory (Rhee et al., 2001). Then, the solution in auxiliary space is mapped onto the space-time plane. The paper ends with some discussions and conclusions.

2. Mathematical model

We consider the injection of a water slug containing two dissolved polymers displaced by pure water. The following assumptions are adopted:

- Two-phase, one-dimensional isothermal flow;
- Incompressible system;
- Homogeneous porous media;
- Dispersion, gravity and capillarity are neglected;
- Polymers are dissolved only in the aqueous phase;
- Water density is not a function of polymer concentration;
- Newtonian flow.

According to these hypotheses, the physical model is governed by the volume balance of water and by the mass conservation of each dissolved polymer in the slug. The resulting system of equations is given by:

$$\begin{cases} \phi \dfrac{\partial s}{\partial t} + u_T \dfrac{\partial f(s, c_1, c_2)}{\partial x} = 0 \\ \phi \dfrac{\partial (c_1 s + a_1(c_1, c_2))}{\partial t} + u_T \dfrac{\partial (c_1 f(s, c_1, c_2))}{\partial x} = 0 \\ \phi \dfrac{\partial (c_2 s + a_2(c_1, c_2))}{\partial t} + u_T \dfrac{\partial (c_2 f(s, c_1, c_2))}{\partial x} = 0 \end{cases} \tag{1}$$

where s is the water saturation, c_1 and c_2 are the concentration of the components in the flowing phase, a_1 and a_2 the amount adsorbed by the rock, f is the water fractional flow, ϕ is the rock porosity and u_T is the total flow velocity. We introduce the following dimensionless variables in the system of equation (1):

$$x_D = \frac{x}{\frac{\Omega_s}{A}} \tag{2}$$

$$t_D = \frac{\int_0^t u_T(\tau) d\tau}{\phi \frac{\Omega_s}{A}} \tag{3}$$

where x_D is the dimensionless position related to the length of the slug, t_D represents the number of slug volumes injected, Ω_S is the injected slug volume and A is the cross-sectional area of the reservoir.

So, we can rewrite (1) in dimensionless form:

$$\begin{cases} \dfrac{\partial s}{\partial t_D} + \dfrac{\partial f(s, c_1, c_2)}{\partial x_D} = 0 \\ \dfrac{\partial (c_1 s + a_1(c_1, c_2))}{\partial t_D} + \dfrac{\partial (c_1 f(s, c_1, c_2))}{\partial x_D} = 0 \\ \dfrac{\partial (c_2 s + a_2(c_1, c_2))}{\partial t_D} + \dfrac{\partial (c_2 f(s, c_1, c_2))}{\partial x_D} = 0 \end{cases} \tag{4}$$

Water saturation is normalized using the relation:

$$s = \frac{s(x_D, t_D) - s^{(I)}}{s^{(J)} - s^{(I)}} \tag{5}$$

where $s^{(I)}$ is the reservoir initial water saturation and $s^{(J)}$ is the water saturation at the injection point.

In this problem, the adsorption of both polymers is governed by Langmuir's isotherm:

$$a_i(\overrightarrow{c}) = \frac{K_i c_i}{1 + \sum_{j=1}^{2} K_j c_j} \tag{6}$$

where $\overrightarrow{c} = (c_1, c_2)$.

When the slug injection begins ($t_D = 0$), there is no polymer in the reservoir ($c_1^{(I)} = c_2^{(I)} = 0$), and the water saturation is irreducible ($s = 0$). During the injection of the slug, the water fractional flow is 1 at the inlet point ($x_D = 0$), and the injection concentration is constant ($c_1^{(J)}$, $c_2^{(J)}$). After the injection of the slug ($x_D = 0, t_D = 1$), the water drive begins ($c_1 = c_2 = 0$). Thus, the initial and boundary conditions of the problem are given by:

$$t_D = 0, \begin{cases} s(x_D, 0) = 0, \\ c_1(x_D, 0) = c_1^{(I)}, & 0 < x_D < \dfrac{L}{\frac{\Omega_s}{A}} \\ c_2(x_D, 0) = c_2^{(I)}, \end{cases} \tag{7}$$

$$x_D = 0, \begin{cases} f(0, t_D) = f^{(J)} & t_D > 0 \\ c_1(0, t_D) = \begin{cases} c_1^{(J)}, & 0 < t_D < 1 \\ 0, & t_D > 1 \end{cases} \\ c_2(0, t_D) = \begin{cases} c_2^{(J)}, & 0 < t_D < 1 \\ 0, & t_D > 1 \end{cases} \end{cases} \tag{8}$$

2.1. Splitting between thermodynamics and hydrodynamics

At this point we introduce the following potential function associated to water conservation:

$$d\varphi = f(s, \overrightarrow{c}) dt_D - s dx_D \tag{9}$$

in the system of conservation laws in dimensionless form (Equation (4)), leading to:

$$\frac{\partial}{\partial \varphi} \left(\frac{s}{f(s, c_1, c_2)} \right) - \frac{\partial}{\partial x_D} \left(\frac{1}{f(s, c_1, c_2)} \right) = 0 \tag{10}$$

$$\begin{cases} \dfrac{\partial a_1(c_1, c_2)}{\partial \varphi} + \dfrac{\partial c_1}{\partial x_D} = 0 \\ \dfrac{\partial a_2(c_1, c_2)}{\partial \varphi} + \dfrac{\partial c_2}{\partial x_D} = 0 \end{cases} \tag{11}$$

This procedure splits the original 3×3 system of equations (Equation (4)) into a 2×2 system (Equation (11)), which is a function of thermodynamic properties only and is similar to the chromatography problem (Rhee et al., 2001), and a lifting equation (Equation (10)), which is a function of hydrodynamic properties of the system and of the solution of the auxiliary system (Pires et al., 2006).

The initial and boundary conditions (Equations (7) and (8)) in $x_D \times \varphi$ space become:

$$\varphi = 0, \begin{cases} s(x_D, 0) = 0, \\ c_1(x_D, 0) = c_1^{(I)}, & 0 < x_D < \dfrac{L}{\frac{\Omega_s}{A}} \\ c_2(x_D, 0) = c_2^{(I)}, \end{cases} \tag{12}$$

$$x_D = 0, \begin{cases} f(0, \varphi) = f^{(J)}(\varphi) = 1 & \varphi > 0 \\ c_1(0, \varphi) = \begin{cases} c_1^{(J)}, & 0 < \varphi < 1 \\ 0, & \varphi > 1 \end{cases} \\ c_2(0, \varphi) = \begin{cases} c_2^{(J)}, & 0 < \varphi < 1 \\ 0, & \varphi > 1 \end{cases} \end{cases} \tag{13}$$

Defining $\frac{1}{f(s, c_1, c_2)}$ as $U(s, c_1, c_2)$ and $-\frac{s}{f(s, c_1, c_2)}$ as $F(U, c_1, c_2)$, the lifting equation (Equation (11)) becomes:

$$\frac{\partial F(U, c_1, c_2)}{\partial \varphi} + \frac{\partial U(s, c_1, c_2)}{\partial x_D} = 0 \tag{14}$$

The initial and boundary conditions (Equations (12) and (13)) for the lifting equation (Equation (14)) are:

$$\phi = 0, \begin{cases} U \to +\infty \\ F \to -\infty \end{cases} \tag{15}$$

$$x_D = 0, \begin{cases} U = 1 \\ F = -1 \end{cases} \tag{16}$$

After both auxiliary system (Equation (10)) and lifting equation (Equation (14)) are solved in $x_D \times \varphi$ plane, the inverse mapping to $x_D \times t_D$ plane is obtained from the following expression:

$$dt_D = \frac{d\varphi}{f(s(x_D, \varphi), c_1(x_D, \varphi), c_2(x_D, \varphi))} + \frac{s}{f(s(x_D, \varphi), c_1(x_D, \varphi), c_2(x_D, \varphi))} dx_D \tag{17}$$

2.2. Solution of the auxiliary 2×2 problem

The methodology to build the solution of the auxiliary problem follows the steps presented in Rhee et al. (2001) for the problem of two-component chromatography:

- Apply the hodograph transformation to determine the concentration waves in the $c_1 \times c_2$ plane;
- Build the solution path in $c_1 \times c_2$ plane;
- Map the solution from $c_1 \times c_2$ plane onto $x_D \times \varphi$ plane.

The derivation of the characteristic and shock waves in the hodograph plane for the system of equation (11) is presented in Appendix A. The detailed theory for the two-component chromatography problem can be found in chapters 1 and 2 of Rhee et al. (2001).

In the hodograph plane, the slopes of the characteristic curves are given by:

$$\Gamma_+ : \alpha = \left(\frac{dc_1}{dc_2}\right)_+ = \xi_+ = \frac{1}{2} a_{21}^{-1} \left[(a_{11} - a_{22}) + \sqrt{(a_{11} - a_{22})^2 + 4a_{21}a_{12}} \right] \quad (18)$$

$$\Gamma_- : \beta = \left(\frac{dc_1}{dc_2}\right)_- = \xi_- = \frac{1}{2} a_{21}^{-1} \left[(a_{11} - a_{22}) - \sqrt{(a_{11} - a_{22})^2 + 4a_{21}a_{12}} \right] \quad (19)$$

The characteristic velocities of the rarefaction waves are:

$$\lambda_+ = \frac{d\varphi}{dx_D} = K_2 \gamma a b^2 \quad (20)$$

$$\lambda_- = \frac{d\varphi}{dx_D} = K_2 \gamma a^2 b \quad (21)$$

where the parameters a and b are functions of α and β, which are defined as:

$$a = a(\alpha) = \frac{\alpha + 1}{\alpha + \gamma} \quad (22)$$

$$b = b(\beta) = \frac{\beta + 1}{\beta + \gamma} \quad (23)$$

From Rankine-Hugoniot conditions, it is possible to determine the shock velocity:

$$V_+(a, b^-, b^+) = \frac{\varphi}{x_D} = K_2 \gamma a b^- b^+ \quad (24)$$

$$V_-(a^-, a^+, b) = \frac{\varphi}{x_D} = K_2 \gamma b a^- a^+ \quad (25)$$

where the superscripts + and – represent the value of a or b before and after the shock, respectively.

In equations (18-21), (24) and (25), the subscripts + and – denote the slow and fast wave family, respectively.

At this point we present a solution for an arbitrary initial and boundary condition. Fig. 1 shows the solution path in the concentration plane. The injection condition is represented by the point (J), and the initial condition is represented by the point (I). Points (A) and (P) are intermediary points along the solution path. We indicate a rarefaction wave as "–", and a shock wave as "→".

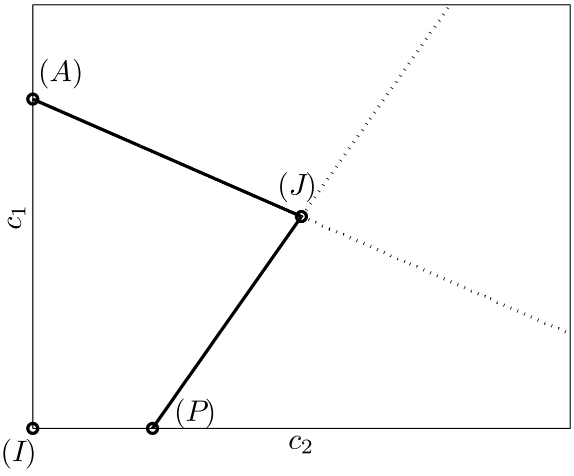

Fig. 1. Solution path in the concentration plane.

During the slug injection ($\varphi < 1$), the solution is self-similar and is composed by two shock waves: $(J) \rightarrow (A) \rightarrow (I)$. The first shock velocity is denoted as V_+ and is a b characteristic parameter jump. On the other hand, V_- is the second shock velocity and is an a parameter jump in auxiliary space (Fig. 2).

Across the shock $(J) \rightarrow (A)$ (b parameter jump), the concentration c_2 jumps to the initial condition, whereas the concentration c_1 increases to a value higher than the injection condition (point A). On the other hand, the component 1 concentration jumps to the initial condition through the shock $(A) \rightarrow (I)$.

For $\varphi > 1$, the injected fluid does not contain dissolved polymers, and the solution in the concentration plane is composed by two rarefaction waves: $(I) - (P)$ and $(P) - (J)$. The first rarefaction wave is a Γ_+ type family, whereas the second rarefaction is a Γ_- characteristic family in concentration plane.

The characteristic curves C_+, with slope λ_+ in $x_D \times \varphi$ plane, correspond to the segment $(I) - (P)$ in the hodograph plane; and the characteristic curves C_-, with slope λ_- in $x_D \times \varphi$ plane, correspond to the segment $(P) - (J)$ in the hodograph plane. The slope of the rarefaction waves, which is a function of polymers concentration, is given by (Fig. 2):

$$C_+ : \lambda_+ = K_2 [b(\beta)]^2 \quad (26)$$

$$C_- : \lambda_- = K_2 a(\alpha) b^{(J)} \quad (27)$$

where $b^{(J)}$ denotes the value of b at injection condition. Along the rarefaction family C_+, there is only component 2 in water (segment $(I) - (P)$ in Fig. 1, where $c_1 = c_1^{(I)} = 0$), and the concentration c_2 is inversely proportional to the slope of the rarefaction characteristic. Along the family C_-, both chemicals are dissolved in water, and their concentrations are inversely proportional to the characteristic slope (Fig. 2).

The water drive (used to displace the polymer slug) leads to interactions between the characteristic waves. Waves of different families (Γ_+ and Γ_-) are transmitted through each other and their slopes change. Waves of same families (Γ_+ and Γ_+ or Γ_- and Γ_-) adsorb each other, and a shock wave appears at the intersection point. The theory of interaction between rarefaction and shock waves is detailed in Rhee et al., 2001et al

Fig. 2 shows the characteristic diagram in $x_D \times \varphi$ plane. The shock waves $\overline{OB}$ and $\overline{OE}$ are straight lines whose slope is given by:

$$V_+(OB)\left(a = a^{(J)}, b^- = 1, b^+ = b^{(J)}\right) = K_2 \gamma a^{(J)} b^{(J)} \quad (28)$$

$$V_-(OE)\left(a^- = \frac{1}{\gamma}, a^+ = a^{(J)}, b = 1\right) = K_2 \gamma a^{(J)} \quad (29)$$

The coordinates of point B are:

$$x_B = \frac{1}{K_2 \gamma a^{(J)} b^{(J)} \left(1 - a^{(J)}\right)} \quad (30)$$

$$\varphi_B = \frac{1}{\left(1 - a^{(J)}\right)} \quad (31)$$

At point B the interaction between the shock V_+ and rarefaction C_- begins (Fig. 2). At this point the shock wave is transmitted through the rarefaction wave, and the rarefaction wave through the shock wave. Each rarefaction characteristic C_- carries a constant a value, whereas b jumps from $b^{(J)}$ to $b^{(I)}$ through the shock wave. Therefore, to calculate the shock path along the interaction, it is necessary to solve the Rankine-Hugoniot conditions considering the value of a carried by each rarefaction wave. So, the new shock path is given by:

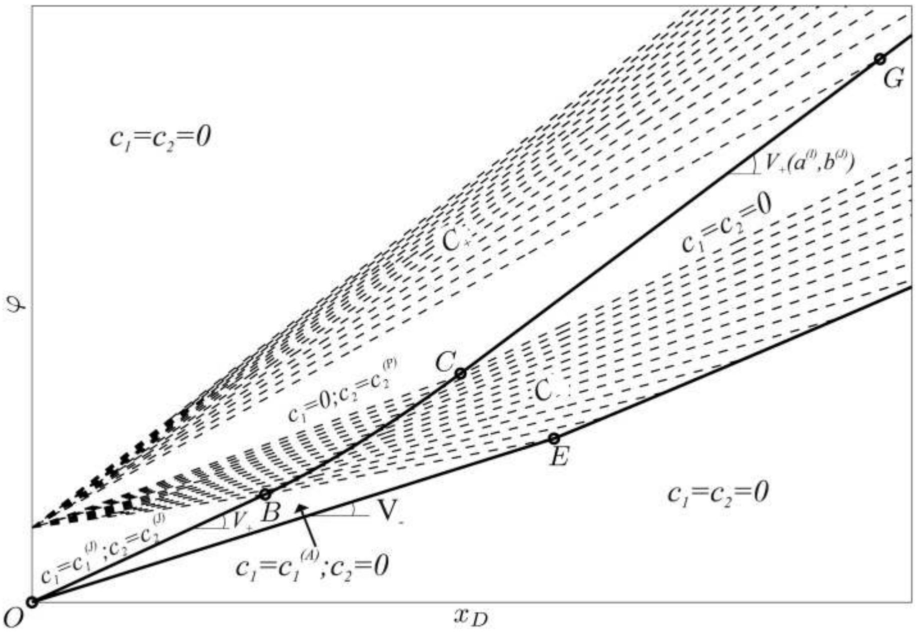

Fig. 2. Solution of the auxiliary system in plane $x_D \times \phi$.

$$x_D^{(BC)}(a) = x_B \frac{\left(1-a^{(J)}\right)^2}{(1-a)^2} \tag{32}$$

and $\varphi^{(BC)}$ can be calculated by:

$$\varphi^{(BC)}(a) = \left(\sqrt{K_2\gamma b^{(J)} x_D^{(BC)}} - \sqrt{\frac{1}{a^{(J)}}-1}\right)^2 + 1 \tag{33}$$

This shock path generated by its interaction with the rarefaction C_- is part of a parabola where the shock velocity decreases. At point C the interaction ends and the shock path of V_+ is a straight line with slope $K_2 b^{(J)}$. Ahead of the shock V_+ the component 2 no longer exists, *i.e.*, $c_2 = 0$. The coordinates of point C are (Fig. 2):

$$x_C = \frac{\gamma^2\left(1-a^{(J)}\right)}{K_2\gamma a^{(J)} b^{(J)} (\gamma-1)^2} \tag{34}$$

$$\varphi_C = \frac{\left(1-a^{(J)}\right)}{a^{(J)}(1-\gamma)^2} \tag{35}$$

and the shock path $\overline{CG}$ is:

$$x_D^{(CG)} = \frac{\varphi-\varphi_C}{K_2 b^{(J)}} \tag{36}$$

As the rarefaction C_- intercepts shock V_+, the slope of the characteristics changes due to the jump of b. Thus, the new slope of rarefaction C_- is given by:

$$\lambda_-^{(-)} = K_2\gamma a^2 \tag{37}$$

After the interaction with shock V_+, the rarefaction C_- intercepts shock V_-. As both waves belong to the same family, the shock adsorbs the rarefaction, but its slope changes. The first interaction between the shock V_- and the rarefaction C_- occurs at point E, whose coordinates are (Fig. 2):

$$x_E = \frac{\varphi_B - K_2\gamma\left(a^{(J)}\right)^2 x_B}{K_2 a^{(J)}\left(1-a^{(J)}\right)} \tag{38}$$

$$\varphi_E = K_2\gamma\left(a^{(J)}\right)^2 (x_E - x_B) \tag{39}$$

The shock path of V_- along the interaction with C_- is:

$$x_D^{(E\infty)} = x_E \frac{\left(\frac{1}{\gamma}-a^{(J)}\right)^2}{\left(\frac{1}{\gamma}-a\right)^2} \tag{40}$$

$$\varphi^{(E\infty)} = K_2 a x_D^{(E\infty)} \tag{41}$$

and when $x_D \to +\infty$ the shock slope tends to the last rarefaction characteristic slope.

After the interaction with rarefaction family C_-, shock V_+ catches up rarefaction C_+, and the shock adsorbs the rarefaction and its trajectory changes continuously (shock and rarefaction belong to the same family). The interaction begins at point G (Fig. 2):

$$x_G = \frac{\left(1-\varphi_D + K_2 b^{(J)} x_C\right)}{K_2 b^{(J)}\left(1-b^{(J)}\right)} \tag{42}$$

$$\varphi_G = K_2 b^{(J)} (x_G - x_C) + \varphi_C \tag{43}$$

After point G the shock path of V_+ is given by:

$$x_D^{(G\infty)} = x_G \frac{\left(1-b^{(J)}\right)^2}{(1-b)^2} \tag{44}$$

$$\varphi^{(G\infty)} = K_2 b^2 x_D^{(G\infty)} + 1 \tag{45}$$

Analogously to the case of the interaction between C_- and V_-, when $x_D \to +\infty$ the shock slope tends to the last rarefaction characteristic slope.

The solution of the auxiliary system is divided in 6 parts (c_I, c_{II}, c_{III}, c_{IV}, c_V, and c_{VI}), which are bounded by the end of the polymer slug injection ($\varphi = 1$), and by the first and the last points of the regions where waves interaction take place (points B, E, C, and G). Thus, the overall solution is:

$$c(x_D,\varphi) = \begin{cases} c_I, & \varphi < 1 \\ c_{II}, & 1 < \varphi < \varphi_B \\ c_{III}, & \varphi_B < \varphi < \varphi_E \\ c_{IV}, & \varphi_E < \varphi < \varphi_C \\ c_V, & \varphi_C < \varphi < \varphi_G \\ c_{VI}, & \varphi_G < \varphi \end{cases} \tag{46}$$

where, $c_I(x_D,\varphi)$ is the self-similar part of the solution, given by:

$$c_I(x_D,\varphi)=\begin{cases} c_1=c_1^{(J)},c_2=c_2^{(J)}, & x_D<\dfrac{\phi}{V_+(OB)} \\ c_1=c_1^{(A)},c_2=c_2^{(I)}, & \dfrac{\varphi}{V_+(OB)}<x_D<\dfrac{\varphi}{V_-(OE)} \\ c_1=c_1^{(I)},c_2=c_2^{(I)}, & \dfrac{\varphi}{V_-(OE)}<x_D \end{cases} \tag{47}$$

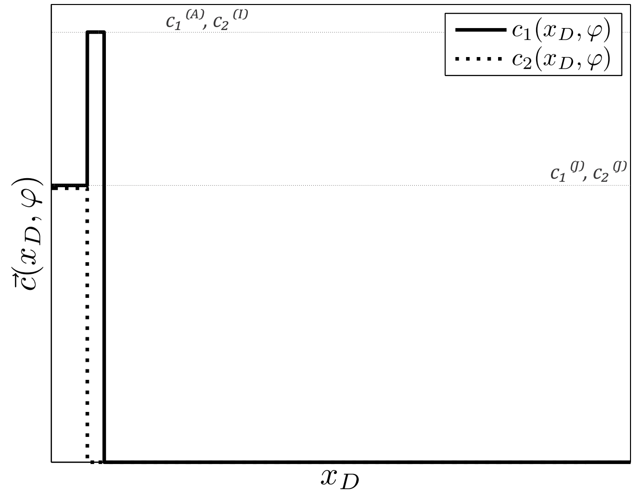

Fig. 3. Concentration profile for solution $c_I(x_D,\varphi)$.

The other parts of the solution are:

$$c_{II}(x_D,\varphi)=\begin{cases} c_1=0,c_2=0, & x_D<\dfrac{\varphi-1}{\lambda_+\left(a^{(I)},b^{(I)}\right)} \\ c_1=0,c_2=c_{2r+}(x_D,\varphi), & \dfrac{\varphi-1}{\lambda_+\left(a^{(I)},b^{(I)}\right)}<x_D<\dfrac{\varphi-1}{\lambda_+\left(a^{(I)},b^{(J)}\right)} \\ c_1=0,c_2=c_2^{(P)}, & \dfrac{\varphi-1}{\lambda_+\left(a^{(I)},b^{(J)}\right)}<x_D<\dfrac{\varphi-1}{\lambda_-\left(a^{(I)},b^{(J)}\right)} \\ c_1=c_{1r-}(x_D,\varphi),c_2=c_{2r-}(x_D,\varphi), & \dfrac{\varphi-1}{\lambda_-\left(a^{(I)},b^{(J)}\right)}<x_D<\dfrac{\varphi-1}{\lambda_-\left(a^{(J)},b^{(J)}\right)} \\ c_1=c_1^{(J)},c_2=c_2^{(J)}, & \dfrac{\varphi-1}{\lambda_-\left(a^{(J)},b^{(J)}\right)}<x_D<\dfrac{\varphi}{V_+(OB)} \\ c_1=c_1^{(A)},c_2=c_2^{(I)}, & \dfrac{\varphi}{V_+(OB)}<x_D<\dfrac{\varphi}{V_-(OE)} \\ c_1=c_1^{(I)},c_2=c_2^{(I)}, & \dfrac{\varphi}{V_-(OE)}<x_D \end{cases} \tag{48}$$

$$c_{III}(x_D,\varphi)=\begin{cases} c_1=0,\ c_2=0, & x_D<\dfrac{\varphi-1}{\lambda_+\left(a^{(I)},b^{(I)}\right)} \\ c_1=0,\ c_2=c_{2r+}(x_D,\varphi), & \dfrac{\varphi-1}{\lambda_+\left(a^{(I)},b^{(I)}\right)}<x_D<\dfrac{\varphi-1}{\lambda_+\left(a^{(I)},b^{(J)}\right)} \\ c_1=0,\ c_2=c_2^{(P)}, & \dfrac{\varphi-1}{\lambda_+\left(a^{(I)},b^{(J)}\right)}<x_D<\dfrac{\varphi-1}{\lambda_-\left(a^{(I)},b^{(J)}\right)} \\ c_1=c_{1r-}^{+}(x_D,\varphi),\ c_2=c_{2r-}^{+}(x_D,\varphi), & \dfrac{\varphi-1}{\lambda_-\left(a^{(I)},b^{(J)}\right)}<x_D<x_D^{(BC)}(a(x_D,\varphi)) \\ c_1=c_{1r-}^{-}(x_D,\varphi),\ c_2=c_2^{(I)}, & x_D^{(BC)}(a(x_D,\varphi))<x_D<\dfrac{\varphi-\varphi^{(BC)}(a(x_D,\varphi))}{\lambda_-\left(a^{(A)},b^{(I)}=b^-\right)} \\ c_1=c_1^{(A)},c_2=c_2^{(I)}, & \dfrac{\varphi-\varphi^{(BC)}(a(x_D,\varphi))}{\lambda_-\left(a^{(A)},b^{(I)}=b^-\right)}<x_D<\dfrac{\varphi}{V_-(OE)} \\ c_1=c_1^{(I)},c_2=c_2^{(I)}, & \dfrac{\varphi}{V_-(OE)}<x_D \end{cases} \tag{49}$$

$$c_{IV}(x_D,\varphi)=\begin{cases} c_1=0,\ c_2=0, & x_D<\dfrac{\varphi-1}{\lambda_+\left(a^{(I)},b^{(I)}\right)} \\ c_1=0,\ c_2=c_{2r+}(x_D,\varphi), & \dfrac{\varphi-1}{\lambda_+\left(a^{(I)},b^{(I)}\right)}<x_D<\dfrac{\varphi-1}{\lambda_+\left(a^{(I)},b^{(J)}\right)} \\ c_1=0,\ c_2=c_2^{(P)}, & \dfrac{\varphi-1}{\lambda_+\left(a^{(I)},b^{(J)}\right)}<x_D<\dfrac{\varphi-1}{\lambda_-\left(a^{(I)},b^{(J)}\right)} \\ c_1=c_{1r-}^{+}(x_D,\varphi),\ c_2=c_{2r-}^{+}(x_D,\varphi), & \dfrac{\varphi-1}{\lambda_-\left(a^{(I)},b^{(J)}\right)}<x_D<x_D^{(BC)}(a(x_D,\varphi)) \\ c_1=c_{1r-}^{-}(x_D,\varphi),\ c_2=c_2^{(I)}, & x_D^{(BC)}(a(x_D,\varphi))<x_D<x_D^{(E\infty)}(a^+(x_D,\varphi)) \\ c_1=c_1^{-(I)},c_2=c_2^{(I)}, & x_D^{(E\infty)}(a^+(x_D,\varphi))<x_D \end{cases} \tag{50}$$

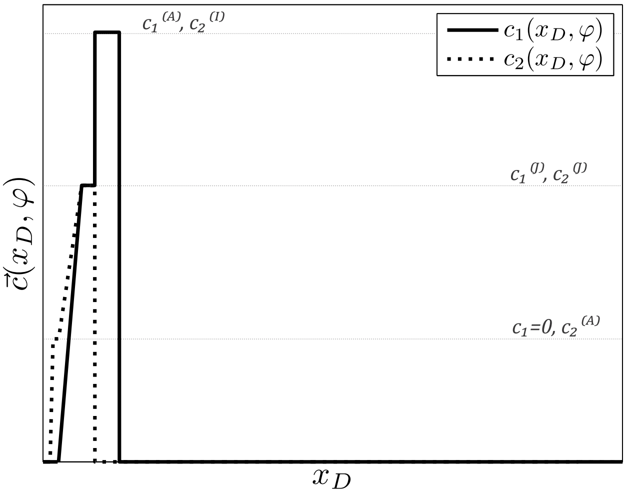

Fig. 4. Concentration profile for solution $c_{II}(x_D, \varphi)$.

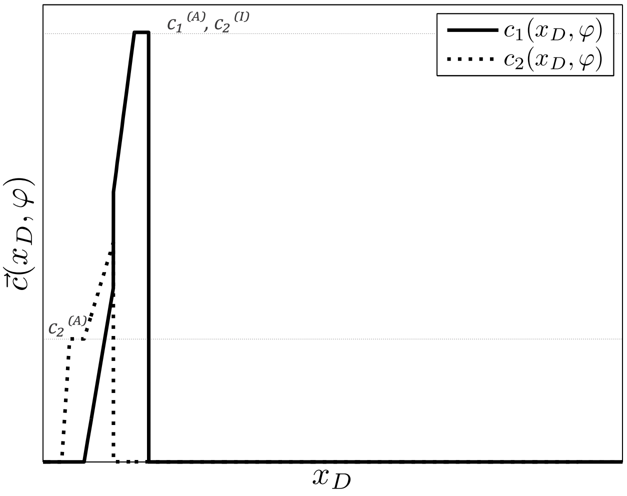

Fig. 5. Concentration profile for solution $c_{III}(x_D, \varphi)$.

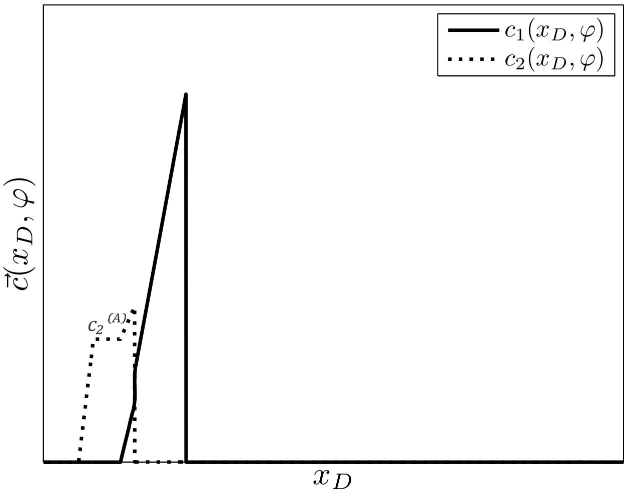

Fig. 6. Concentration profile for solution $c_{IV}(x_D, \varphi)$.

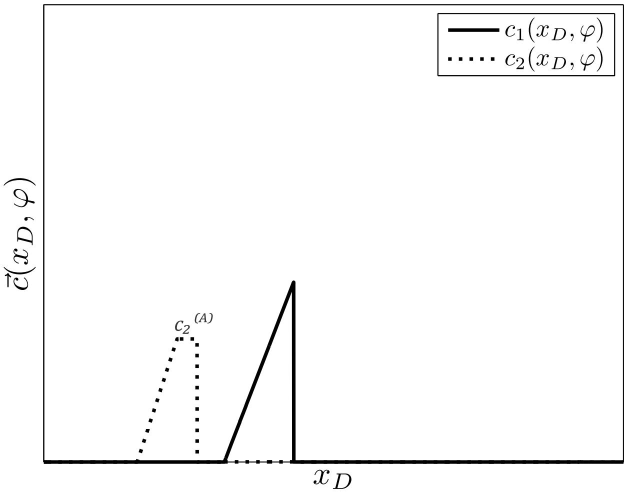

Fig. 7. Concentration profile for solution $c_V(x_D, \varphi)$.

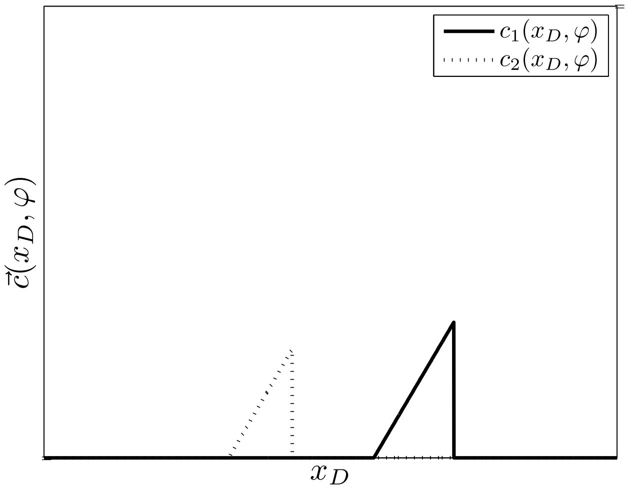

Fig. 8. Concentration profile for solution $c_{VI}(x_D, \varphi)$.

$$c_V(x_D,\varphi)=\begin{cases} c_1=0,\ c_2=0, & x_D<\dfrac{\varphi-1}{\lambda_+\left(a^{(I)},b^{(I)}\right)} \\ c_1=0,\ c_2=c_{2r+}(x_D,\varphi), & \dfrac{\varphi-1}{\lambda_+\left(a^{(I)},b^{(I)}\right)}<x_D<\dfrac{\varphi-1}{\lambda_+\left(a^{(I)},b^{(J)}\right)} \\ c_1=0,\ c_2=c_2^{(P)}, & \dfrac{\varphi-1}{\lambda_+\left(a^{(I)},b^{(J)}\right)}<x_D<x_D^{(CG)} \\ c_1=0, c_2=0, & x_D^{(CG)}<x_D<\dfrac{\varphi-\varphi_C}{\lambda_-\left(a^{(I)},b^{(I)}\right)} \\ c_1=c_{1r-}^{+}(x_D,\varphi), c_2=0, & \dfrac{\varphi-\varphi_C}{\lambda_-\left(a^{(I)},b^{(I)}\right)}<x_D<x_D^{(E\infty)}\left(a^+(x_D,\varphi)\right) \\ c_1=c_1^{(I)}, c_2=c_2^{(I)}, & x_D^{(E\infty)}\left(a^+(x_D,\varphi)\right)<x_D \end{cases} \tag{51}$$

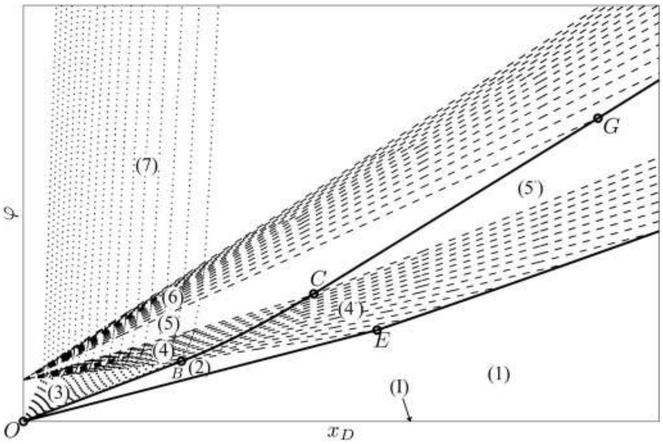

Fig. 9. Lifting equation solution in auxiliary plane.

$$c_{VI}(x_D,\varphi)=\begin{cases} c_1=0,\ c_2=0, & x_D<\dfrac{\varphi-1}{\lambda_+\left(a^{(I)},b^{(I)}\right)} \\ c_1=0,\ c_2=c^+_{2r+}(x_D,\varphi), & \dfrac{\varphi-1}{\lambda_+\left(a^{(I)},b^{(I)}\right)}<x_D<x_D^{(G\infty)} \\ c_1=0, c_2=0, & x_D^{(G\infty)}<x_D<\dfrac{\varphi-\varphi_C}{\lambda_-\left(a^{(I)},b^{(I)}\right)} \\ c_1=c^+_{1r-}(x_D,\varphi), c_2=0, & \dfrac{\varphi-\varphi_C}{\lambda_-\left(a^{(I)},b^{(I)}\right)}<x_D<x_D^{(E\infty)}\left(a^+(x_D,\varphi)\right) \\ c_1=c_1^{(I)}, c_2=c_2^{(I)}, & x_D^{(E\infty)}\left(a^+(x_D,\varphi)\right)<x_D \end{cases} \tag{52}$$

In equations (47)–(52), $c_j(x_D,\varphi)$ denotes the rarefaction wave where component j concentration changes, subscripts $r+$ and $r-$ denote the rarefaction waves C_+ and C_-, respectively, and the superscript in parenthesis denotes a constant state in the phase plane.

Figs. 3–8 show the concentration profiles for each part of the solution (Equation (46)) along the $x_D\times\varphi$ plane.

In Figs. 3–8 it is possible to see the development of the chromatographic cycle. Note that component 1 front travels ahead of component 2 due to its lower adsorption rate.

In Fig. 3 there is a region where the concentration of both components is the injection condition concentration ($c_1^{(J)}\ c_2^{(J)}$). This region is followed by a shock wave where the concentration of both components change. After the shock wave, the concentration of component 2 jumps to its initial condition, whereas the concentration of component 1 increases to a higher value than the injection condition (see Fig. 1).

In Fig. 4, the water drive has begun, and a rarefaction wave appears at the rear of the polymer slug. Note that at this part of the solution the chromatographic cycle begins. Figs. 5 and 6 stress, besides the separation of the components, the development of a sharp edge on the concentration profile of both components.

In Fig. 7, components 1 and 2 are completely separated and travel in porous media as two single component slugs separated by a pure water region. In Fig. 8, it is possible to see the spreading of the concentration at the rear part of each component slug. This effect is dependent on the adsorption isotherm.

When $\varphi\to+\infty$, the rarefaction waves are completely absorbed by the shock waves, thus components 1 and 2 concentration along the porous media is equal to their water drive concentration (Rhee et al., 2001).

2.3. Solution of the lifting equation

In this subsection we present the solution of the lifting equation, which depends on the solution of the auxiliary system (previous section) and the transport properties (relative permeability and viscosity of each phase), using the method of characteristics. Applying the chain rule in equation (10) we find:

$$\frac{\partial F}{\partial U}\frac{\partial U}{\partial\varphi}+\frac{\partial U}{\partial x_D}=-\frac{\partial F}{\partial c_1}\frac{\partial c_1}{\partial\varphi}-\frac{\partial F}{\partial c_2}\frac{\partial c_2}{\partial\varphi} \tag{53}$$

In constant concentration regions of the solution, we have $\frac{\partial c_1}{\partial\varphi}=\frac{\partial c_2}{\partial\varphi}=0$. Thus,

$$\frac{\partial F}{\partial U}\frac{\partial U}{\partial\varphi}+\frac{\partial U}{\partial x_D}=0 \tag{54}$$

In these regions each characteristic curve carries a constant value of U, and its velocity is given by:

$$\frac{d\varphi}{dx_D}=\frac{\partial F(U,c_1,c_2)}{\partial U} \tag{55}$$

In regions where c_1 and/or c_2 vary, U is no longer constant along the characteristic. In this case, U can be found through the following equation:

$$\frac{dU}{dx_D}=-\frac{\partial F}{\partial c_1}\frac{\partial c_1}{\partial\varphi}-\frac{\partial F}{\partial c_2}\frac{\partial c_2}{\partial\varphi} \tag{56}$$

The viscosity of the polymer solution is calculated by:

$$\mu_w(c_1,c_2)=\mu_w^0(1+\eta_1c_1+\eta_2c_2) \tag{57}$$

where μ_w^0 is the viscosity of pure water, and the coefficient η_i is an empiric parameter that represents the effect of the polymer concentration in the solution viscosity. In this work, we assume $\eta_1>\eta_2$.

Fig. 9 presents the solution of the lifting equation in the $x_D\times\phi$ plane,

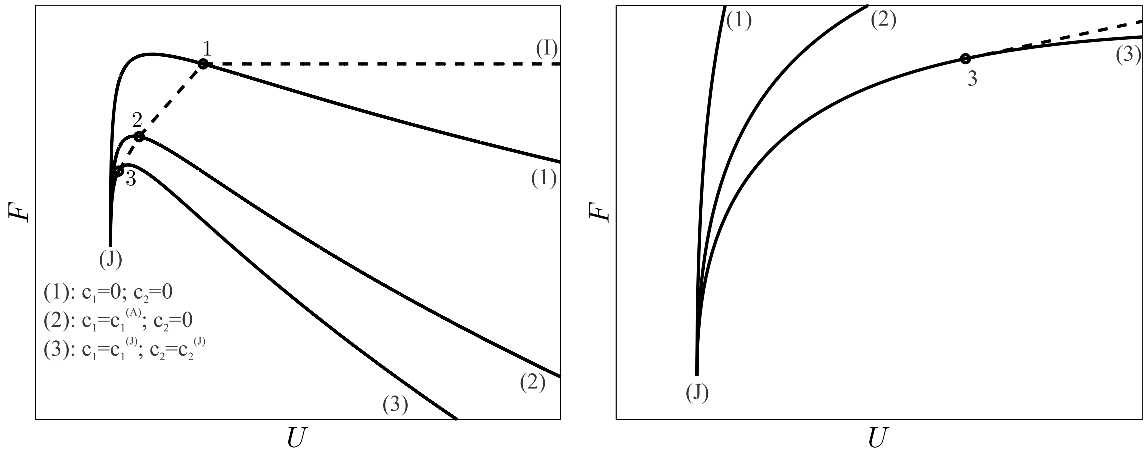

Fig. 10. Solution U_I in $F\times U$ plane.

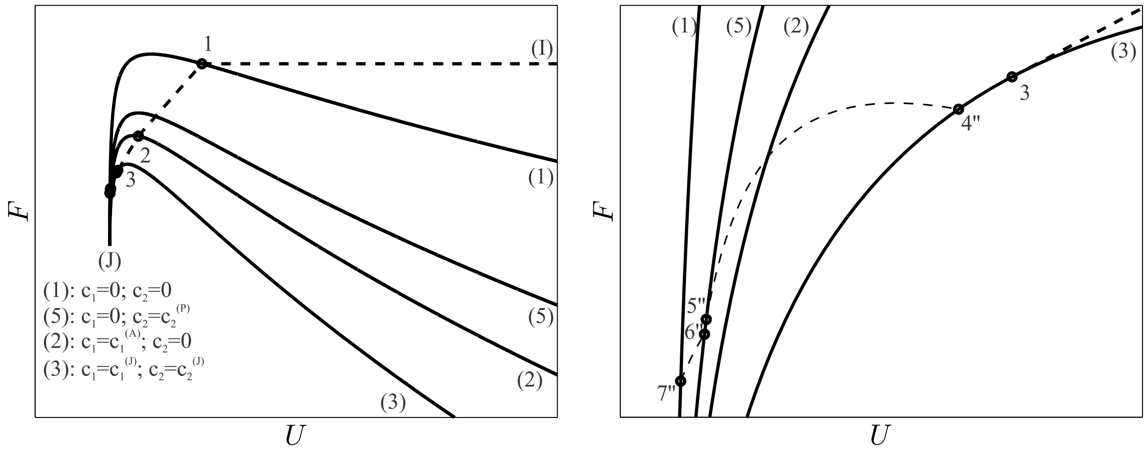

Fig. 11. Solution U_{II} in $F \times U$ plane.

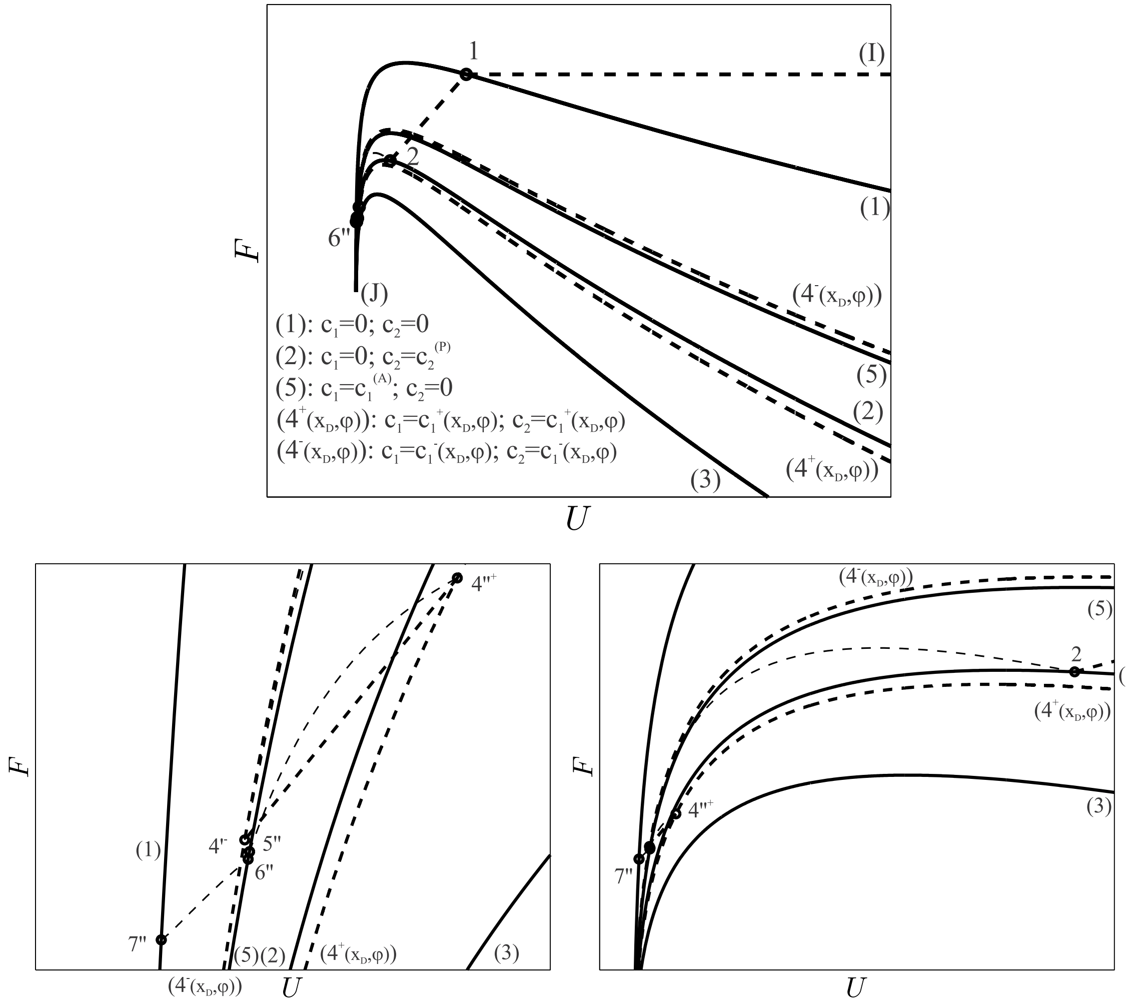

Fig. 12. Solution U_{III} in $F \times U$ plane.

which is divided in 9 regions:

- Region (I): constant state: $U = U^{(I)}$, $c_1 = c_2 = 0$ (x_D axis);
- Region (1): constant state: $U = U^{(1)}$, $c_1 = c_2 = 0$;
- Region (2): constant state: $U = U^{(2)}$, $c_1 = c_1^{(A)}$ and $c_2 = 0$ (Fig. 1);
- Region (3): U_3 rarefaction, $c_1 = c_1^{(J)}$ and $c_2 = c_2^{(J)}$;
- Region (4): interaction between U_4 rarefaction and C_-, concentrations vary from injection condition (J) to the intermediate state (P) (Fig. 1);

- Region (5): U_5 rarefaction, $c_1 = 0$ and $c_2 = c_2^{(P)}$;
- Region (6): interaction between U_6 rarefaction and C_+, $c_1 = 0$ and c_2 varies from $c_2^{(P)}$ to $c_2^{(I)} = 0$ (Fig. 1);
- Region (7): U_7 rarefaction, $c_1 = c_2 = 0$;
- Region (4^-): U_4^- rarefaction, c_1 varies from $c_1^{(A)}$ to $c_1^{(I)}$ and $c_2 = c_2^{(I)} = 0$;
- Region (5^-): constant state: $U = U^{(5-)}$, $c_1 = c_2 = 0$.

The solution of $U(x_D, \varphi)$ is presented in six parts. When $\varphi < 1$, the solution is self-similar. The remaining regions are bounded by $\varphi = 1$ (part II), and by the waves interaction (points B, E, C, and G):

$$U(x_D,\varphi) = \begin{cases} U_I, & \varphi < 1 \\ U_{II}, & 1 < \varphi < \varphi_B \\ U_{III}, & \varphi_B < \varphi < \varphi_E \\ U_{IV}, & \varphi_E < \varphi < \varphi_C \\ U_V, & \varphi_C < \varphi < \varphi_G \\ U_{VI}, & \varphi_G < \varphi \end{cases} \tag{58}$$

The self-similar part is given by:

$$U_I(x_D,\varphi) = \begin{cases} U^{(J)}, & x_D < \varphi \left(\dfrac{\partial F\left(U^{(3)}, c_1^{(J)}, c_2^{(J)}\right)}{\partial U} \right)^{-1} \\ U_3(x_D,\varphi), & \varphi \left(\dfrac{\partial F\left(U^{(3)}, c_1^{(J)}, c_2^{(J)}\right)}{\partial U} \right)^{-1} < x_D < \dfrac{\varphi}{V_+} \\ U^{(2)}, & \dfrac{\varphi}{V_+} < x_D < \dfrac{\varphi}{V_-} \\ U^{(1)}, & \dfrac{\varphi}{V_-} < x_D < +\infty \\ U^{(I)}, & x_D \to +\infty \end{cases} \tag{59}$$

The structural formula for this part is $(I) \to (1) \to (2) \to (3) - (J)$ (Fig. 10).

The solution $U_{II}(x_D, \varphi)$ is (Fig. 11):

$$U_{II}(x_D,\varphi) = \begin{cases} U^{(J)}, & x_D < (\varphi - 1) \left(\dfrac{\partial F\left(U^{(7)}, c_1 = 0, c_2 = 0\right)}{\partial U} \right)^{-1} \\ U_7(x_D,\varphi), & (\varphi - 1) \left(\dfrac{\partial F\left(U^{(7)}, c_1 = 0, c_2 = 0\right)}{\partial U} \right)^{-1} < x_D < \dfrac{\varphi - 1}{\lambda_+\left(a^{(I)}, b^{(I)}\right)} \\ U_6(x_D,\varphi), & \dfrac{\varphi - 1}{\lambda_+\left(a^{(I)}, b^{(I)}\right)} < x_D < \dfrac{\varphi - 1}{\lambda_+\left(a^{(I)}, b^{(J)}\right)} \\ U_5(x_D,\varphi), & \dfrac{\varphi - 1}{\lambda_+\left(a^{(I)}, b^{(J)}\right)} < x_D < \dfrac{\varphi - 1}{\lambda_-\left(a^{(I)}, b^{(J)}\right)} \\ U_4(x_D,\varphi), & \dfrac{\varphi - 1}{\lambda_-\left(a^{(I)}, b^{(J)}\right)} < x_D < \dfrac{\varphi - 1}{\lambda_-\left(a^{(J)}, b^{(J)}\right)} \\ U_3(x_D,\varphi), & \dfrac{\varphi - 1}{\lambda_-\left(a^{(J)}, b^{(J)}\right)} < x_D < \dfrac{\varphi}{V_+} \\ U^{(2)}, & \dfrac{\varphi}{V_+} < x_D < \dfrac{\varphi}{V_-} \\ U^{(1)}, & \dfrac{\varphi}{V_-} < x_D < +\infty \\ U^{(I)}, & x_D \to +\infty \end{cases} \tag{60}$$

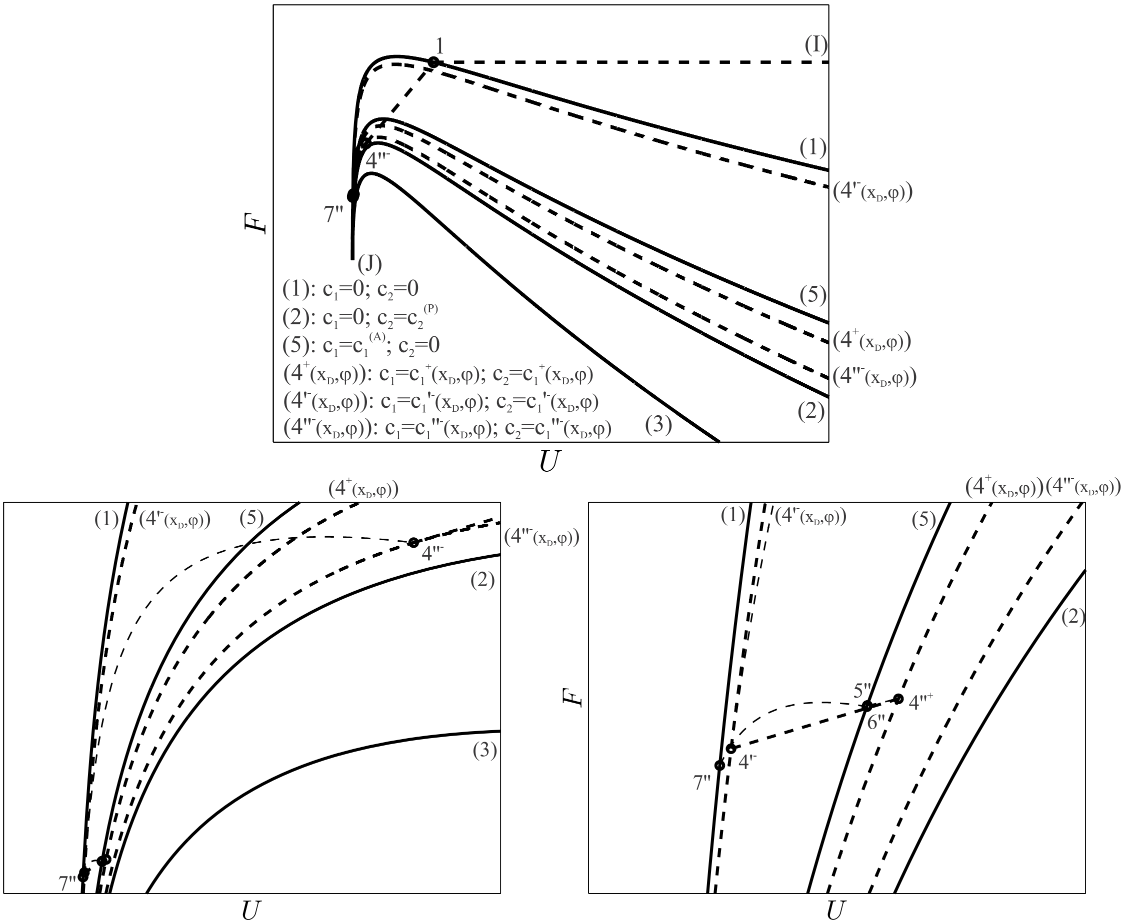

Fig. 13. Solution U_{IV} in $F \times U$ plane.

and its structural formula is $(I)\rightarrow(1)\rightarrow(2)\rightarrow 3'' - 4'' - 5'' - 6'' - 7'' - (J)$. The superscript '' denotes the first rarefaction wave in the region.

For $U_{III}(x_D, \varphi)$ we have

$$U_{III}(x_D,\varphi)=\begin{cases} U^{(J)}, & x_D<(\varphi-1)\left(\dfrac{\partial F\left(U^{(7)},c_1=0,c_2=0\right)}{\partial U}\right)^{-1} \\ U_7(x_D,\varphi), & (\varphi-1)\left(\dfrac{\partial F\left(U^{(7)},c_1=0,c_2=0\right)}{\partial U}\right)^{-1}<x_D<\dfrac{\varphi-1}{\lambda_+\left(a^{(I)},b^{(I)}\right)} \\ U_6(x_D,\varphi), & \dfrac{\varphi-1}{\lambda_+\left(a^{(I)},b^{(I)}\right)}<x_D<\dfrac{\varphi-1}{\lambda_+\left(a^{(I)},b^{(J)}\right)} \\ U_5(x_D,\varphi), & \dfrac{\varphi-1}{\lambda_+\left(a^{(I)},b^{(J)}\right)}<x_D<\dfrac{\varphi-1}{\lambda_-\left(a^{(I)},b^{(J)}\right)} \\ U_4^+(x_D,\varphi), & \dfrac{\varphi-1}{\lambda_-\left(a^{(I)},b^{(J)}\right)}<x_D<x_D^{(BC)} \\ U_4^-(x_D,\varphi), & x_D^{(BC)}<x_D<\dfrac{\varphi-\varphi_B}{\lambda_-\left(a^{(J)},b^{(I)}\right)} \\ U^{(2)}, & \dfrac{\varphi-\varphi_B}{\lambda_-\left(a^{(J)},b^{(I)}\right)}<x_D<\dfrac{\varphi}{V_-} \\ U^{(1)}, & \dfrac{\varphi}{V_-}<x_D<+\infty \\ U^{(I)}, & x_D\rightarrow+\infty \end{cases} \tag{61}$$

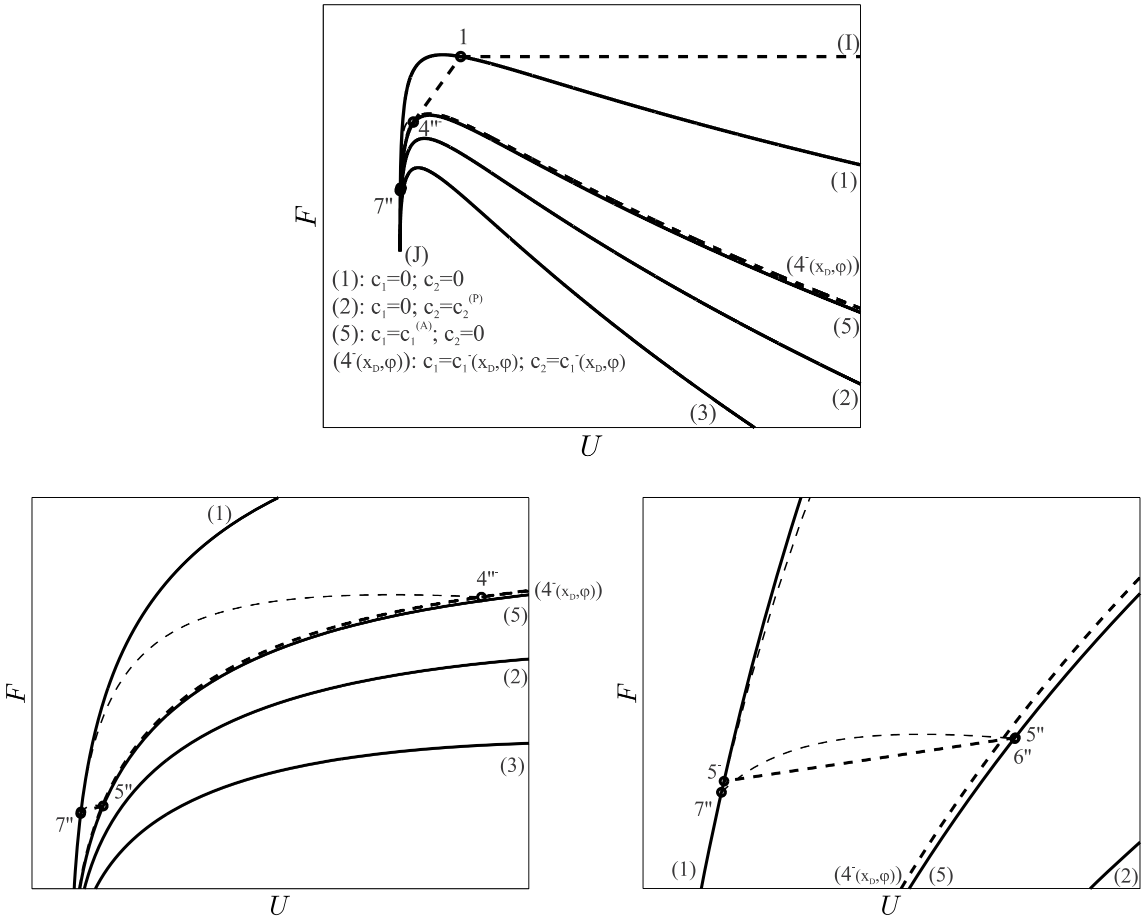

Fig. 14. Solution $U_V(x_D,\phi)$ in $F\times U$ plane.

The structural formula is $(I)\to(1)\to(2)-4''^{-}-4'^{-}\to4''^{+}-5''-6''-7''-(J)$ (Fig. 12). The superscript ' denotes the last rarefaction wave in the region. We also add superscripts " + " and " − " in the rarefaction notation (either Y' or Y'') to indicate that the rarefaction is a left or a right state of a shock wave, respectively. In Fig. 12, $Y^{\pm}(x_D,\varphi)$ denotes the concentration rarefaction waves in region Y connected through a shock. This structure appears in concentration profiles that cross the shock waves $\varphi^{(BC)}$, $\varphi^{(E\infty)}$ and $\varphi^{(G\infty)}$ (regions where concentration rarefactions waves interact with shock waves).

The solution $U_{IV}(x_D,\varphi)$ is given by

$$U_{IV}(x_D,\varphi)=\begin{cases} U^{(J)}, & x_D<(\varphi-1)\left(\dfrac{\partial F\left(U^{(7)},c_1=0,c_2=0\right)}{\partial U}\right)^{-1} \\ U_7(x_D,\varphi), & (\varphi-1)\left(\dfrac{\partial F\left(U^{(7)},c_1=0,c_2=0\right)}{\partial U}\right)^{-1}<x_D<\dfrac{\varphi-1}{\lambda_+\left(a^{(I)},b^{(I)}\right)} \\ U_6(x_D,\varphi), & \dfrac{\varphi-1}{\lambda_+\left(a^{(I)},b^{(I)}\right)}<x_D<\dfrac{\varphi-1}{\lambda_+\left(a^{(I)},b^{(J)}\right)} \\ U_5(x_D,\varphi), & \dfrac{\varphi-1}{\lambda_+\left(a^{(I)},b^{(J)}\right)}<x_D<\dfrac{\varphi-1}{\lambda_-\left(a^{(I)},b^{(J)}\right)} \\ U_4^{+}(x_D,\varphi), & \dfrac{\varphi-1}{\lambda_-\left(a^{(I)},b^{(J)}\right)}<x_D<x_D^{(BC)} \\ U_4^{-}(x_D,\varphi), & x_D^{(BC)}<x_D<x_D^{(E\infty)} \\ U^{(1)}, & x_D^{(E\infty)}<x_D<+\infty \\ U^{(I)}, & x_D\to+\infty \end{cases} \tag{62}$$

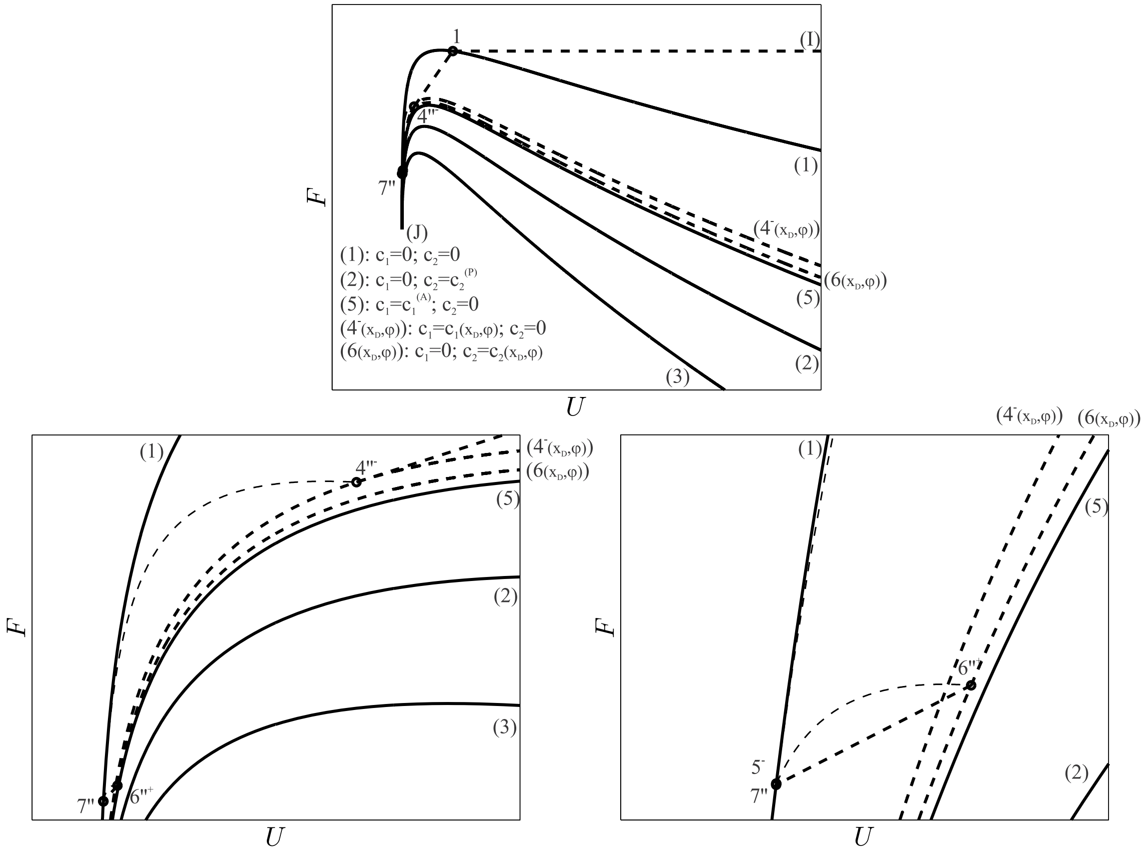

Fig. 15. Solution U_{VI} in $F \times U$ plane.

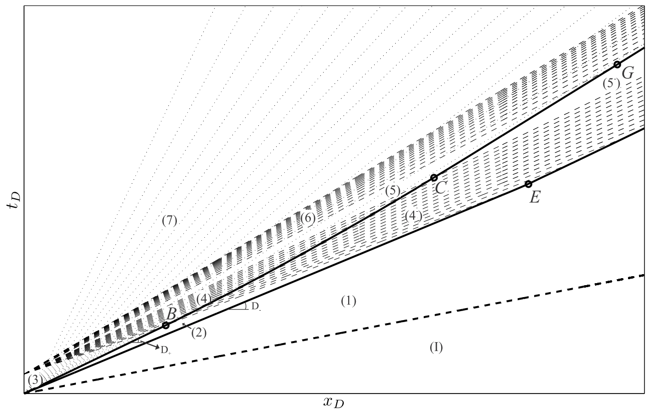

Fig. 16. Characteristic diagram in $x_D \times t_D$ plane.

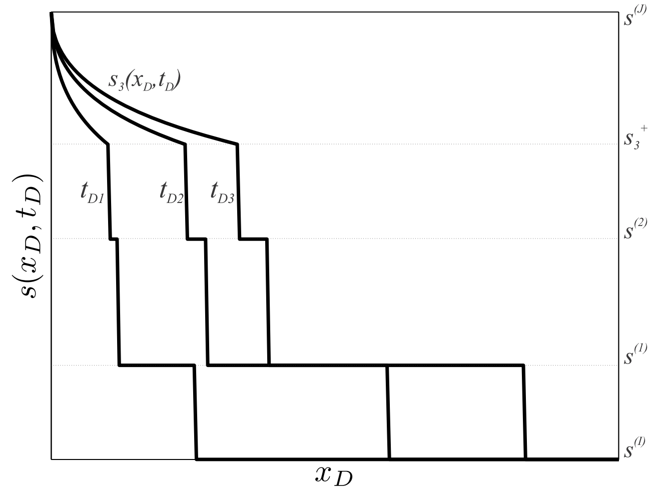

Fig. 17. Self-similar part of the solution.

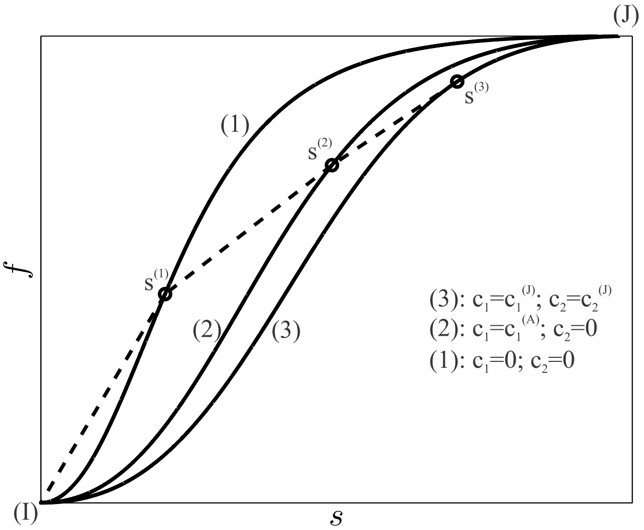

Fig. 18. Solution path for s_I in phase plane.

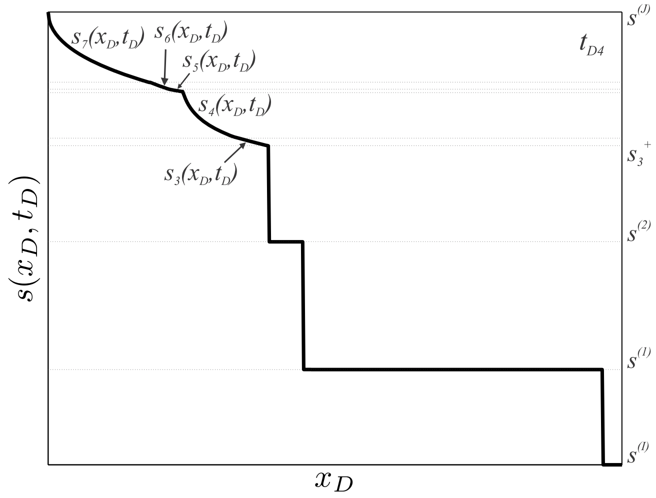

Fig. 19. Solution profile for $s_{II}(x_D,t_D)$ for t_{D4} $(1 < t_{D4} < t_B)$.

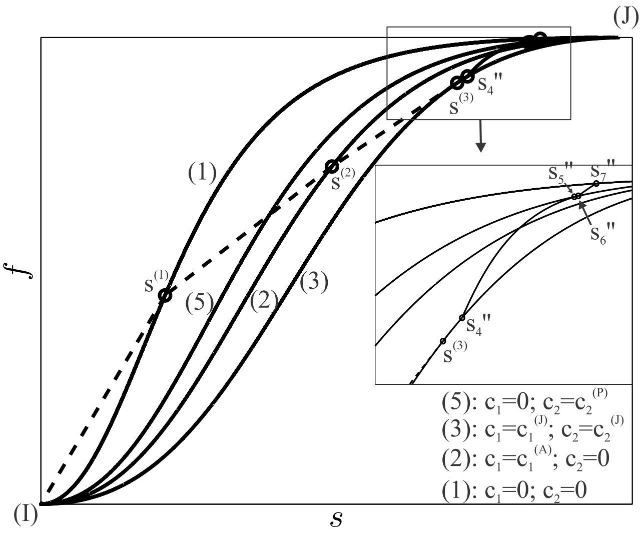

Fig. 20. Solution path for s_{II} in phase plane.

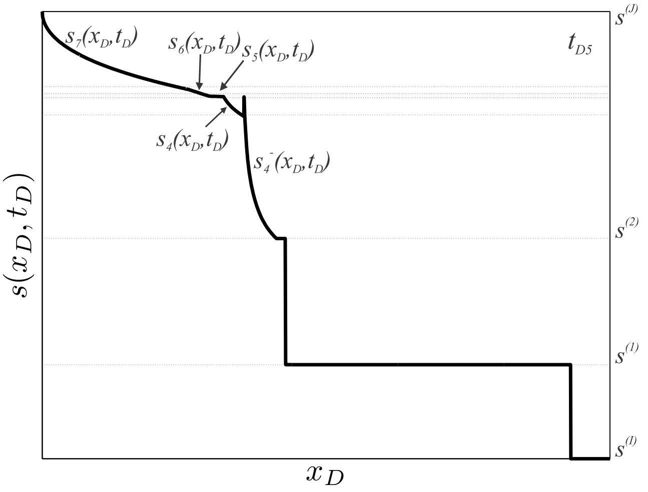

Fig. 21. Solution profile for $s_{III}(x_D,t_D)$ for t_{D5} $(t_B < t_{D5} < t_E)$.

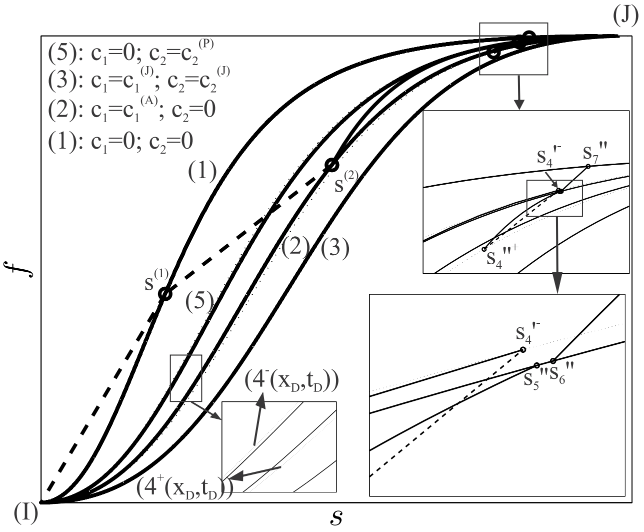

Fig. 22. Solution path for s_{III} in phase plane.

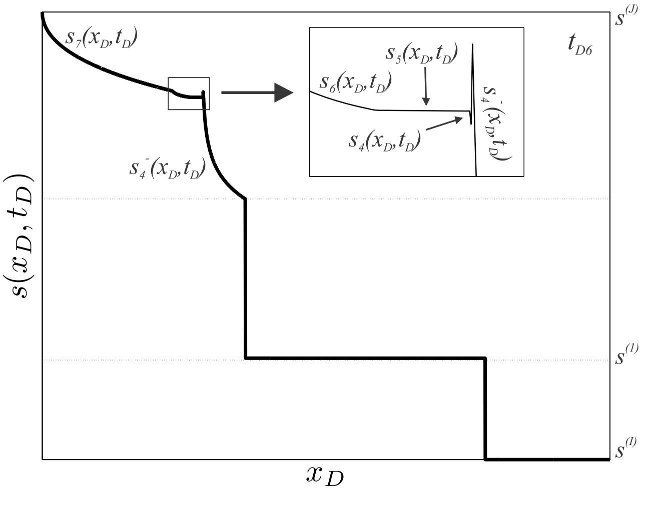

Fig. 23. Solution profile for $s_{IV}(x_D,t_D)$ for t_{D6} $(t_E < t_{D6} < t_C)$.

and its path in $F \times U$ plane is shown in Fig. 13. The structural formula for this part of the solution is $(I)\rightarrow(1)\rightarrow 4^{''-} - 4^{'-}\rightarrow 4^{''+} - 5^{''} - 6'' - 7^{''} - (J)$.

For the region of solution $U_V(x_D,\varphi)$, we have:

$$U_V(x_D,\varphi) = \begin{cases} U^{(J)}, & x_D < (\varphi-1)\left(\dfrac{\partial F\left(U^{(7)}, c_1 = 0, c_2 = 0\right)}{\partial U}\right)^{-1} \\ U_7(x_D,\varphi), & (\varphi-1)\left(\dfrac{\partial F\left(U^{(7)}, c_1 = 0, c_2 = 0\right)}{\partial U}\right)^{-1} < x_D < \dfrac{\varphi-1}{\lambda_+\left(a^{(I)}, b^{(I)}\right)} \\ U_6(x_D,\varphi), & \dfrac{\varphi-1}{\lambda_+\left(a^{(I)}, b^{(I)}\right)} < x_D < \dfrac{\varphi-1}{\lambda_+\left(a^{(I)}, b^{(J)}\right)} \\ U_5(x_D,\varphi), & \dfrac{\varphi-1}{\lambda_+\left(a^{(I)}, b^{(J)}\right)} < x_D < x_D^{(CG)} \\ U^{(5-)}, & x_D^{(CG)} < x_D < \dfrac{\varphi-\varphi_C}{\lambda_-^{(-)}\left(a^{(I)}, b^{(I)}\right)} \\ U_4^-(x_D,\varphi), & \dfrac{\varphi-\varphi_C}{\lambda_-^{(-)}\left(a^{(I)}, b^{(I)}\right)} < x_D < x_D^{(E\infty)} \\ U^{(1)}, & x_D^{(E\infty)} < x_D < +\infty \\ U^{(I)}, & x_D \rightarrow +\infty \end{cases} \tag{63}$$

Fig. 14 presents the solution path of U_V in $F \times U$ plane, whose structural formula is $(I)\rightarrow(1)\rightarrow 4^{''-} - (5^-)\rightarrow 5^{''+} - 6^{''} - 7'' - (J)$.

Finally, the solution $U_{VI}(x_D,\varphi)$ is given by

$$U_{VI}(x_D,\varphi) = \begin{cases} U^{(J)}, & x_D < (\varphi-1)\left(\dfrac{\partial F\left(U^{(7)}, c_1 = 0, c_2 = 0\right)}{\partial U}\right)^{-1} \\ U_7(x_D,\varphi), & (\varphi-1)\left(\dfrac{\partial F\left(U^{(7)}, c_1 = 0, c_2 = 0\right)}{\partial U}\right)^{-1} < x_D < \dfrac{\varphi-1}{\lambda_+\left(a^{(I)}, b^{(I)}\right)} \\ U_6(x_D,\varphi), & \dfrac{\varphi-1}{\lambda_+\left(a^{(I)}, b^{(I)}\right)} < x_D < x_D^{(G\infty)} \\ U^{(5-)}, & x_D^{(G\infty)} < x_D < \dfrac{\varphi-\varphi_C}{\lambda_-^{(-)}\left(a^{(I)}, b^{(I)}\right)} \\ U_4^-(x_D,\varphi), & \dfrac{\varphi-\varphi_C}{\lambda_-^{(-)}\left(a^{(I)}, b^{(I)}\right)} < x_D < x_D^{(E\infty)} \\ U^{(1)}, & x_D^{(E\infty)} < x_D < +\infty \\ U^{(I)}, & x_D \rightarrow +\infty \end{cases} \tag{64}$$

Fig. 15 shows the solution path of U_{VI} in $F \times U$ plane. Its structural formula is $(I)\rightarrow(1)\rightarrow 4^{''-} - (5^-)\rightarrow 6^{''+} - 7'' - (J)$.

From the definition of the variables U and F, the water fractional flow function $f(s(x_D,\varphi), c_1, c_2)$ and saturation $s(x_D,\varphi)$ can be easily determined through the following expressions:

$$f = \frac{1}{U(x_D,\varphi)} \tag{65}$$

$$s(x_D,\varphi) = -\frac{F\left(U(x_D,\varphi), c_1, c_2\right)}{U(x_D,\varphi)} \tag{66}$$

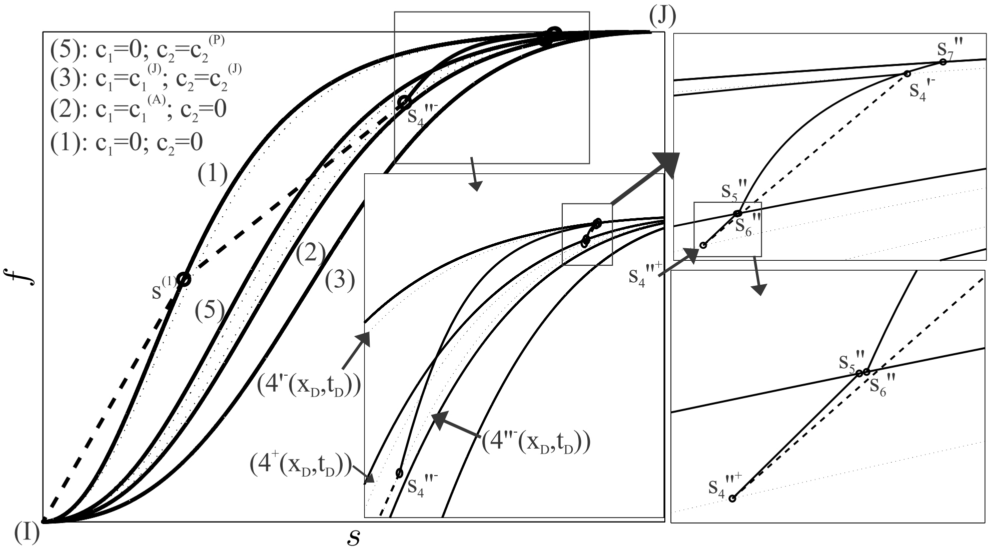

Fig. 24. Solution path for s_{IV} in phase plane.

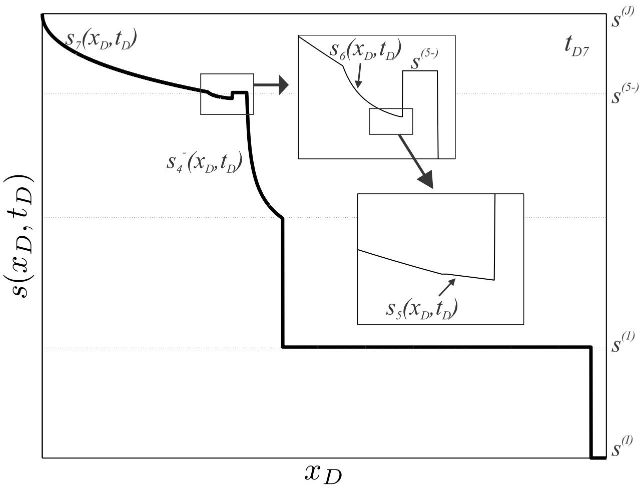

Fig. 25. Solution profile for $s_V(x_D, t_D)$ for t_{D7} ($t_C < t_{D7} < t_G$).

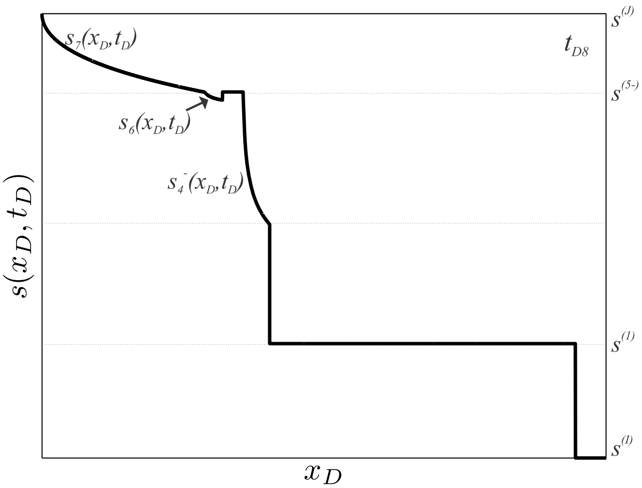

Fig. 27. Solution profile for $s_{VI}(x_D, t_D)$ for t_{D8} ($t_{D8} > t_G$).

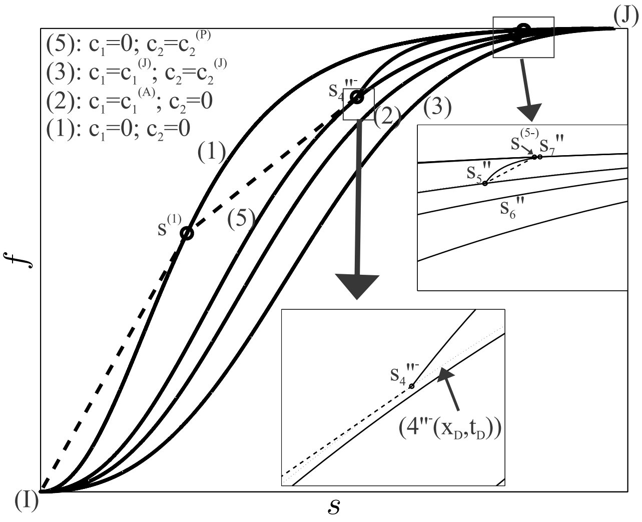

Fig. 26. Solution path for $s_V$in $f \times s$ plane.

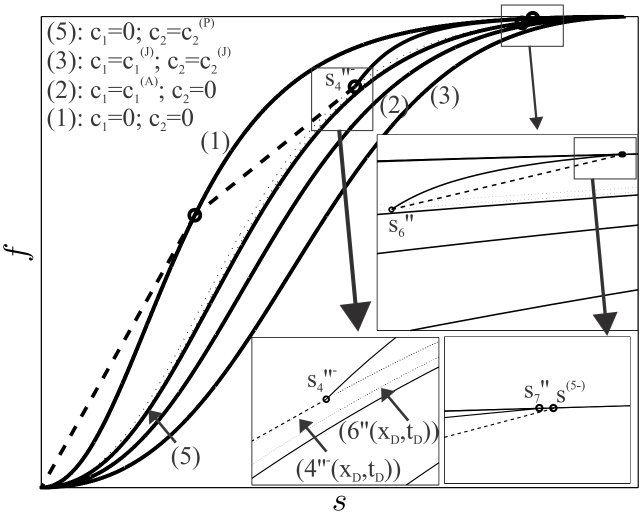

Fig. 28. Solution path for s_{VI} in phase plane.

2.4. Inverse mapping to time domain

At this point we have already calculated the solution of s, c_1 and c_2 in the $x_D \times \varphi$ plane. The next step is the inverse mapping of these solutions onto the space-time plane through the relation:

$$dt_D = \frac{d\varphi}{f(s(x_D,\varphi), c_1(x_D,\varphi), c_2(x_D,\varphi))} + \frac{s}{f(s(x_D,\varphi), c_1(x_D,\varphi), c_2(x_D,\varphi))} dx_D \tag{67}$$

Rarefaction waves and constant states are calculated directly from expression (75), whereas the shock trajectories are determined by (Pires et al., 2006):

$$D_i = \frac{f^{\pm}}{s^{\pm} + V_i}, \; i = +, - \tag{68}$$

where V_i is the respective shock velocity in the auxiliary plane (Equations (24) and (25)).

The complete mathematical derivation and the exact equations for the inverse mapping are presented in Appendix B. Fig. 16 presents the characteristic diagram of the solution in $x_D \times t_D$ plane.

The solution is also divided in six regions. For $t_D < 1$ the solution is self-similar. Beyond this point, the solution is bounded by the start and end of the waves interactions regions (points B, E, C, and G):

$$s(x_D, \phi) = \begin{cases} s_I, & t_D < 1 \\ s_{II}, & 1 < t_D < t_B \\ s_{III}, & t_B < t_D < t_E \\ s_{IV}, & t_E < t_D < t_C \\ s_V, & t_C < t_D < t_G \\ s_{VI}, & t_G < t_D \end{cases} \tag{69}$$

The self-similar part of the solution (s_I) is given by:

$$s_I(x_D, t_D) = \begin{cases} s^{(J)}, & x_D < \dfrac{f\left(s^{(J)}, c_1^{(J)}, c_2^{(J)}\right)}{s^{(J)}} t_D \\ s_3(x_D, t_D). & \dfrac{f\left(s^{(J)}, c_1^{(J)}, c_2^{(J)}\right)}{s^{(J)}} t_D < x_D < t_D D_+ \\ s^{(2)}, & t_D D_+ < x_D < t_D D_- \\ s^{(1)}, & t_D D_- < x_D < D_{BL} t_D \\ s^{(I)}, & D_{BL} t_D < x_D \end{cases} \tag{70}$$

Fig. 17 presents the self-similar part of the solution for three different times ($t_{D1} < t_{D2} < t_{D3} < 1$).

The path of the solution s_I in the $f \times s$ plane (phase plane) is shown in Fig. 18 (structural formula: $(J) - (3) \rightarrow (2) \rightarrow (1) \rightarrow (I)$). This part of the solution is equivalent to the solution of continuous water injection containing two dissolved polymers.

The solution s_{II} is

$$s_{II}(x_D, t_D) = \begin{cases} s^{(J)}, & x_D < \dfrac{f\left(s^{(J)}, c_1^{(I)}, c_2^{(I)}\right)}{s^{(J)}} (t_D - 1) \\ s_7(x_D, t_D), & \dfrac{f\left(s^{(J)}, c_1^{(I)}, c_2^{(I)}\right)}{s^{(J)}} (t_D - 1) < x_D < \dfrac{f\left(s_7^{''}, c_1^{(I)}, c_2^{(I)}\right)}{s_7^{''} + K_2 \gamma a^{(I)} \left[b^{(I)}\right]^2} (t_D - 1) \\ s_6(x_D, t_D), & \dfrac{f\left(s_7^{''}, c_1^{(I)}, c_2^{(I)}\right)}{s_7^{''} + K_2 \gamma a^{(I)} \left[b^{(I)}\right]^2} (t_D - 1) < x_D < \dfrac{f\left(s_6^{''}, c_1^{(I)}, c_2^{(P)}\right)}{s_6^{''} + K_2 \gamma a^{(I)} \left[b^{(J)}\right]^2} (t_D - 1) \\ s_5(x_D, t_D), & \dfrac{f\left(s_6^{''}, c_1^{(I)}, c_2^{(P)}\right)}{s_6^{''} + K_2 \gamma a^{(I)} \left[b^{(J)}\right]^2} (t_D - 1) < x_D < \dfrac{f\left(s_5^{''}, c_1^{(I)}, c_2^{(P)}\right)}{s_5^{''} + K_2 \gamma \left[a^{(I)}\right]^2 b^{(J)}} (t_D - 1) \\ s_4(x_D, t_D), & \dfrac{f\left(s_5^{''}, c_1^{(I)}, c_2^{(P)}\right)}{s_5^{''} + K_2 \gamma \left[a^{(I)}\right]^2 b^{(J)}} (t_D - 1) < x_D < \dfrac{f\left(s^{(3)}, c_1^{(J)}, c_2^{(J)}\right)}{s^{(3)} + K_2 \gamma \left[a^{(J)}\right]^2 b^{(J)}} (t_D - 1) \\ s_3(x_D, t_D), & \dfrac{f\left(s^{(3)}, c_1^{(J)}, c_2^{(J)}\right)}{s^{(3)} + K_2 \gamma \left[a^{(J)}\right]^2 b^{(J)}} (t_D - 1) < x_D < t_D D_+ \\ s^{(2)}, & t_D D_+ < x_D < t_D D_- \\ s^{(1)}, & t_D D_- < x_D < D_{BL} t_D \\ s^{(I)}, & D_{BL} t_D < x_D \end{cases} \tag{71}$$

The profile of the solution s_{II} is presented in Fig. 19 and its path in the phase plane is shown in Fig. 20. The structural formula is $(J) - 7^{''} - 6^{''} - 5^{''} - 4^{''} - (3) \rightarrow (2) \rightarrow (1) \rightarrow (I)$. The same notation previously used for the $F \times U$ solution is followed for $f \times s$ plane.

At the beginning of water drive, for $1 < t_D < t_B$ (Fig. 19), two concentration rarefaction waves appear at the rear of the slug. These rarefactions interact with the saturation rarefaction waves from region 3 (Fig. 16). Note that the separation of the components begins (chromatographic cycle), where component 1 travels ahead of component 2 in porous media.

The solution S_{III} is given by:

$$s_{III}(x_D,t_D)=\begin{cases} s^{(J)}, & x_D<\dfrac{f\left(s^{(J)},c_1^{(I)},c_2^{(I)}\right)}{s^{(J)}}(t_D-1)\\ s_7(x_D,t_D), & \dfrac{f\left(s^{(J)},c_1^{(I)},c_2^{(I)}\right)}{s^{(J)}}(t_D-1)<x_D<\dfrac{f\left(s_7^{''},c_1^{(I)},c_2^{(I)}\right)}{s_7^{''}+K_2\gamma a^{(I)}\left[b^{(I)}\right]^2}(t_D-1)\\ s_6(x_D,t_D), & \dfrac{f\left(s_7^{''},c_1^{(I)},c_2^{(I)}\right)}{s_7^{''}+K_2\gamma a^{(I)}\left[b^{(I)}\right]^2}(t_D-1)<x_D<\dfrac{f\left(s_6^{''},c_1^{(I)},c_2^{(P)}\right)}{s_6^{''}+K_2\gamma a^{(I)}\left[b^{(J)}\right]^2}(t_D-1)\\ s_5(x_D,t_D), & \dfrac{f\left(s_6^{''},c_1^{(I)},c_2^{(P)}\right)}{s_6^{''}+K_2\gamma a^{(I)}\left[b^{(J)}\right]^2}(t_D-1)<x_D<\dfrac{f\left(s_5^{''},c_1^{(I)},c_2^{(P)}\right)}{s_5^{''}+K_2\gamma\left[a^{(I)}\right]^2b^{(J)}}(t_D-1)\\ s_4(x_D,t_D), & \dfrac{f\left(s_5^{''},c_1^{(I)},c_2^{(P)}\right)}{s_5^{''}+K_2\gamma\left[a^{(I)}\right]^2b^{(J)}}(t_D-1)<x_D<\left(\dfrac{dx_D}{dt_D}\right)_{BC}(t_D-t_B)+x_B\\ s_4^{-}(x_D,t_D), & \left(\dfrac{dx_D}{dt_D}\right)_{BC}(t_D-t_B)+x_B<x_D<\dfrac{f\left(s_4^{''-},c_{1r-}^{-},c_2^{(I)}\right)}{s_4^{''-}+K_2\gamma\left[a_{r-}^{-}\right]^2b^{(I)}}(t_D-1)\\ s^{(2)}, & \dfrac{f\left(s_4^{''-},c_{1r-}^{-},c_2^{(I)}\right)}{s_4^{''-}+K_2\gamma\left[a_{r-}^{-}\right]^2b^{(I)}}(t_D-1)<x_D<t_DD_-\\ s^{(1)}, & t_DD_-<x_D<D_{BL}t_D\\ s^{(I)}, & D_{BL}t_D<x_D \end{cases}\tag{72}$$

where a_{r-}^{-} is the value of a on a rarefaction wave C_- after its interaction with shock D_+. Fig. 21 shows the profile of the solution s_{III}, and in Fig. 22 we present its path in the phase plane. The structural formula for this region is: $(J)-7''-6''-5''-4''^{+}\rightarrow 4'^{-}-(2)\rightarrow(1)\rightarrow(I)$.

In this part of the solution, a lower viscosity water region between two regions of higher viscosity appears (Fig. 21). This effect is caused by the separation of the dissolved polymers. In the low viscosity region, a peak in water saturation can be observed in the solution profile (see beginning of $s_4^{-}(x_D,t_D)$ in Fig. 21).

For the solution s_{IV}we have

Fig. 23 presents the saturation profile for the solution s_{IV} and Fig. 24 shows its path in $f\times s$ plane. For this case the structural expression is $(J)-7''-6''-5''-4''^{+}\rightarrow 4'^{-}-4''^{-}\rightarrow(1)\rightarrow(I)$.

At this point the polymers are almost separated, and there is only a small region where both components coexist ($s_4(x_D,t_D)$ in Fig. 23). The peak of water saturation increases and the constant state (2) no longer appears in the solution.

The solution s_V is

$$s_{IV}(x_D,t_D)=\begin{cases} s^{(J)}, & x_D<\dfrac{f\left(s^{(J)},c_1^{(I)},c_2^{(I)}\right)}{s^{(J)}}(t_D-1)\\ s_7(x_D,t_D), & \dfrac{f\left(s^{(J)},c_1^{(I)},c_2^{(I)}\right)}{s^{(J)}}(t_D-1)<x_D<\dfrac{f\left(s_7^{''},c_1^{(I)},c_2^{(I)}\right)}{s_7^{''}+K_2\gamma a^{(I)}\left[b^{(I)}\right]^2}(t_D-1)\\ s_6(x_D,t_D), & \dfrac{f\left(s_7^{''},c_1^{(I)},c_2^{(I)}\right)}{s_7^{''}+K_2\gamma a^{(I)}\left[b^{(I)}\right]^2}(t_D-1)<x_D<\dfrac{f\left(s_6^{''},c_1^{(I)},c_2^{(P)}\right)}{s_6^{''}+K_2\gamma a^{(I)}\left[b^{(J)}\right]^2}(t_D-1)\\ s_5(x_D,t_D), & \dfrac{f\left(s_6^{''},c_1^{(I)},c_2^{(P)}\right)}{s_6^{''}+K_2\gamma a^{(I)}\left[b^{(J)}\right]^2}(t_D-1)<x_D<\dfrac{f\left(s_5^{''},c_1^{(I)},c_2^{(P)}\right)}{s_5^{''}+K_2\gamma\left[a^{(I)}\right]^2b^{(J)}}(t_D-1)\\ s_4(x_D,t_D), & \dfrac{f\left(s_5^{''},c_1^{(I)},c_2^{(P)}\right)}{s_5^{''}+K_2\gamma\left[a^{(I)}\right]^2b^{(J)}}(t_D-1)<x_D<\left(\dfrac{dx_D}{dt_D}\right)_{BC}(t_D-t_B)+x_B\\ s_4^{-}(x_D,t_D), & \left(\dfrac{dx_D}{dt_D}\right)_{BC}(t_D-t_B)+x_B<x_D<\dfrac{f\left(s_4^{''-},c_{1r-}^{-},c_2^{(I)}\right)}{s_4^{''-}+K_2\gamma a_{r-}^{-}}(t_D-t_E)+x_E\\ s^{(1)}, & \dfrac{f\left(s_4^{''-},c_{1r-}^{-},c_2^{(I)}\right)}{s_4^{''-}+K_2\gamma a_{r-}^{-}}(t_D-t_E)+x_E<x_D<D_{BL}t_D\\ s^{(I)}, & D_{BL}t_D<x_D \end{cases}\tag{73}$$

$$s_V(x_D,t_D)=\begin{cases} s^{(J)}, & x_D<\dfrac{f\left(s^{(J)},c_1^{(I)},c_2^{(I)}\right)}{s^{(J)}}(t_D-1) \\ s_7(x_D,t_D), & \dfrac{f\left(s^{(J)},c_1^{(I)},c_2^{(I)}\right)}{s^{(J)}}(t_D-1)<x_D<\dfrac{f\left(s_7^{''},c_1^{(I)},c_2^{(I)}\right)}{s_7^{''}+K_2\gamma a^{(I)}\left[b^{(I)}\right]^2}(t_D-1) \\ s_6(x_D,t_D), & \dfrac{f\left(s_7^{''},c_1^{(I)},c_2^{(I)}\right)}{s_7^{''}+K_2\gamma a^{(I)}\left[b^{(I)}\right]^2}(t_D-1)<x_D<\dfrac{f\left(s_6^{''},c_1^{(I)},c_2^{(P)}\right)}{s_6^{''}+K_2\gamma a^{(I)}\left[b^{(J)}\right]^2}(t_D-1) \\ s_5(x_D,t_D), & \dfrac{f\left(s_6^{''},c_1^{(I)},c_2^{(P)}\right)}{s_6^{''}+K_2\gamma a^{(I)}\left[b^{(J)}\right]^2}(t_D-1)<x_D<\dfrac{f\left(s_5^{''},c_1^{(I)},c_2^{(P)}\right)}{s_5^{''}+K_2b^{(J)}}(t_D-t_C)+x_C \\ s^{(5-)}, & \dfrac{f\left(s_5^{''},c_1^{(I)},c_2^{(P)}\right)}{s_5^{''}+K_2b^{(J)}}(t_D-t_C)+x_C<x_D<\dfrac{f\left(s^{(5-)},c_1^{(I)},c_2^{(I)}\right)}{s^{(5-)}+K_2\gamma\left[a^{(I)}\right]^2b^{(I)}}(t_D-t_C)+x_C \\ s_4^-(x_D,t_D), & \dfrac{f\left(s^{(5-)},c_1^{(I)},c_2^{(I)}\right)}{s^{(5-)}+K_2\gamma\left[a^{(I)}\right]^2b^{(I)}}(t_D-t_C)+x_C<x_D<\dfrac{f\left(s_4^{''-},c_{1r-}^-,c_2^{(I)}\right)}{s_4^{''-}+K_2\gamma a_{r-}^-}(t_D-t_E)+x_E \\ s^{(1)}, & \dfrac{f\left(s_4^{''-},c_{1r-}^-,c_2^{(I)}\right)}{s_4^{''-}+K_2\gamma a_{r-}^-}(t_D-t_E)+x_E<x_D<D_{BL}t_D \\ s^{(I)}, & D_{BL}t_D<x_D \end{cases} \tag{74}$$

Fig. 25 shows the profile for s_V for t_{D7}, where $t_C<t_{D7}<t_G$. The path of s_V in the phase plane is presented in Fig. 26. Its structural representation is $(J)-7^{''}-6^{''}-5^{''+}\to(5^-)-4^{''-}\to(1)\to(I)$.

Note that the components are completely separated in porous media (full chromatographic cycle) (Fig. 25). The chemical components are traveling in two different slugs separated by a pure water bank (constant state $s^{(5-)}$).

Finally, s_{VI} is given by:

$$s_{VI}(x_D,t_D)=\begin{cases} s^{(J)}, & x_D<\dfrac{f\left(s^{(J)},c_1^{(I)},c_2^{(I)}\right)}{s^{(J)}}(t_D-1) \\ s_7(x_D,t_D), & \dfrac{f\left(s^{(J)},c_1^{(I)},c_2^{(I)}\right)}{s^{(J)}}(t_D-1)<x_D<\dfrac{f\left(s_7^{''},c_1^{(I)},c_2^{(I)}\right)}{s_7^{''}+K_2\gamma a^{(I)}\left[b^{(I)}\right]^2}(t_D-1) \\ s_6(x_D,t_D), & \dfrac{f\left(s_7^{''},c_1^{(I)},c_2^{(I)}\right)}{s_7^{''}+K_2\gamma a^{(I)}\left[b^{(I)}\right]^2}(t_D-1)<x_D<\dfrac{f\left(s_6^{''+},c_1^{(I)},c_{2r+}^+\right)}{s_6^{''+}+K_2b_{r+}^+}(t_D-t_G)+x_G \\ s^{(5-)}, & \dfrac{f\left(s_6^{''+},c_1^{(I)},c_{2r+}^+\right)}{s_6^{''+}K_2b_{r+}^+}(t_D-t_G)+x_G<x_D<\dfrac{f\left(s^{(5-)},c_1^{(I)},c_2^{(I)}\right)}{s^{(5-)}+K_2\gamma\left[a^{(I)}\right]^2b^{(I)}}(t_D-t_C)+x_C \\ s_4^-(x_D,t_D), & \dfrac{f\left(s^{(5-)},c_1^{(I)},c_2^{(I)}\right)}{s^{(5-)}+K_2\gamma\left[a^{(I)}\right]^2b^{(I)}}(t_D-t_C)+x_C<x_D<\dfrac{f\left(s_4^{''-},c_{1r-}^-,c_2^{(I)}\right)}{s_4^{''-}+K_2\gamma a_{r-}^-}(t_D-t_E)+x_E \\ s^{(1)}, & \dfrac{f\left(s_4^{''-},c_{1r-}^-,c_2^{(I)}\right)}{s_4^{''-}+K_2\gamma a_{r-}^-}(t_D-t_E)+x_E<x_D<D_{BL}t_D \\ s^{(I)}, & D_{BL}t_D<x_D \end{cases} \tag{75}$$

where b_{r+}^+ is the value of b on a rarefaction wave C_+ before its interaction with the shock D_+. The saturation profile of the solution s_{VI} is shown in Fig. 27.

In Fig. 28 we present the solution path of $s_{VI}(x_D,t_D)$in $f\times s$ plane. The structural representation of the solution in this region is $(J)-7''-6''^+\to(5^-)-4''^-\to(1)\to(I)$.

In this part of the solution, the slugs containing the chemical components travel with different velocities in the porous media, and the high water saturation region (water bank) becomes larger. Moreover, the constant state (5) no longer exists, which implies in no constant concentration regions in porous media.

For $t_D\to+\infty$, both concentration rarefaction waves are completely adsorbed by the respective shock waves of the same family. Thus, the chemical components concentrations are $c_1=c_2=0$ and the water saturation is $s=s^{(J)}$ (boundary condition for $t_D>1$) (Rhee et al., 2001).

3. Conclusions

In this paper we derive the analytical solution to the one-dimensional two-phase water slug injection containing two dissolved polymers problem. The solution was built using the splitting technique, which consists in applying a potential function that splits the original system of equations into an auxiliary system and a lifting equation. The solution of the problem was obtained in the auxiliary plane and subsequently mapped to the space-time plane. Effects of interactions between waves of different families and between waves of same family were considered in the construction of the solution.

The solution is divided in six regions bounded by the crossing points of the waves in the space-time plane. Analytical expressions and profiles for water saturation and polymer concentrations were presented for each region.

It was shown the development of a full chromatographic cycle, and how the separation of the chemicals influences the saturation profile. It is highlighted that in regions where a lower viscosity aqueous solution appears between two regions of higher viscosity aqueous solution, water banks without polymers appear. We also showed that the water bank region increases with time due to the different velocities of the polymer slugs.

The presented solution can be used to validate reservoir simulators and to evaluate the most important parameters to polymer flooding projects design. It is also possible to forecast fluids production, and water and polymer breakthrough.

The solution methodology shown in this paper can be applied to solve similar slug injection problems, such as surfactant-polymer systems or low-salinity polymer systems. The only restriction is that the adsorption of the chemicals must follow Langmuir adsorption isotherm.

CRediT authorship contribution statement

Felipe de O Apolinário: Methodology, Software, Formal analysis, Investigation, Writing - original draft, Writing - review & editing. **Anália S. de Paula:** Methodology, Formal analysis, Investigation. **Adolfo P. Pires:** Methodology, Formal analysis, Investigation, Writing - review & editing, Supervision.

Acknowledgements

This study was financed in part by the Coordenação de Aperfeiçoamento de Pessoal de Nível Superior - Brasil (CAPES) - Finance Code 001.

Appendix A

In this appendix we present the detailed derivation of the solution of the auxiliary problem in the hodograph space, following the procedure presented in chapters 1 and 2 of Rhee et al. (2001). For the sake of clarity, we adopted the same notation as the one of Rhee et al. (2001).

Applying the chain rule in the auxiliary system (Equation (11)), we find:

$$\begin{cases} a_{11}\dfrac{\partial c_1}{\partial \varphi} + a_{12}\dfrac{\partial c_2}{\partial \varphi} + \dfrac{\partial c_1}{\partial x_D} = 0 \\ a_{21}\dfrac{\partial c_1}{\partial \varphi} + a_{22}\dfrac{\partial c_2}{\partial \varphi} + \dfrac{\partial c_2}{\partial x_D} = 0 \end{cases} \tag{A.1}$$

where,

$$a_{ij} = \frac{\partial a_i}{\partial c_j}\ ,\ i = 1,2; j = 1,2 \tag{A.2}$$

It is possible to write x_D and φ as a function of c_1 and c_2 applying the hodograph transformation. This procedure can only be applied if the Jacobian matrix does not vanish nor approaches infinite for any concentration pair:

$$J = \begin{vmatrix} \dfrac{\partial c_1}{\partial \varphi} & \dfrac{\partial c_1}{\partial x_D} \\ \dfrac{\partial c_2}{\partial \varphi} & \dfrac{\partial c_2}{\partial x_D} \end{vmatrix} = \frac{\partial c_1}{\partial \varphi}\frac{\partial c_2}{\partial x_D} - \frac{\partial c_1}{\partial x_D}\frac{\partial c_2}{\partial \varphi} \neq 0,\ J \in \mathbb{R} \tag{A.3}$$

If equation (A.3) is satisfied, we can write $x_D = x_D(c_1, c_2)$and $\varphi = \varphi(c_1, c_2)$, and apply the chain rule to find the relation between the partial derivatives of c_1 and c_2, and the hodograph variables:

$$\frac{\partial x_D}{\partial c_1} = -\frac{\frac{\partial c_2}{\partial \varphi}}{J} \tag{A.4}$$

$$\frac{\partial x_D}{\partial c_2} = \frac{\frac{\partial c_1}{\partial \varphi}}{J} \tag{A.5}$$

$$\frac{\partial \varphi}{\partial c_1} = \frac{\frac{\partial c_2}{\partial x_D}}{J} \tag{A.6}$$

$$\frac{\partial \varphi}{\partial c_2} = -\frac{\frac{\partial c_1}{\partial x_D}}{J} \tag{A.7}$$

Replacing equations A.4-A.7 in equation (A.1), we find the system of equations in the hodograph space:

$$\begin{cases} -\dfrac{\partial\varphi}{\partial c_2} + a_{11}\dfrac{\partial x_D}{\partial c_2} - a_{12}\dfrac{\partial x_D}{\partial c_1} = 0 \\ \dfrac{\partial\varphi}{\partial c_1} + a_{21}\dfrac{\partial x_D}{\partial c_2} - a_{22}\dfrac{\partial x_D}{\partial c_1} = 0 \end{cases} \tag{A.8}$$

The characteristic velocity of system of equation (A.8) are the roots of:

$$a_{21}\xi^2 - (a_{11} - a_{22})\xi - a_{12} = 0 \tag{A.9}$$

where $\xi = \frac{dc_1}{dc_2}$(see section 1.3 of Rhee et al. (2001) for details).

Solving equation (A.9) for ξ, we find

$$\xi = \left\{ \begin{matrix} \alpha \\ \beta \end{matrix} \right\} = \frac{1}{2}a_{21}^{-1}\left[(a_{11} - a_{22}) \pm \sqrt{(a_{11} - a_{22})^2 + 4a_{21}a_{12}}\right] \tag{A.10}$$

The characteristic curves Γ_+ and $\Gamma_-$are denoted as:

$$\Gamma_- : \alpha = \left(\frac{dc_1}{dc_2}\right)_- = \xi_- = \frac{1}{2}a_{21}^{-1}\left[(a_{11} - a_{22}) - \sqrt{(a_{11} - a_{22})^2 + 4a_{21}a_{12}}\right] \tag{A.11}$$

$$\Gamma_+ : \beta = \left(\frac{dc_1}{dc_2}\right)_+ = \xi_+ = \frac{1}{2}a_{21}^{-1}\left[(a_{11} - a_{22}) + \sqrt{(a_{11} - a_{22})^2 + 4a_{21}a_{12}}\right] \tag{A.12}$$

In the phase plane (plane $c_1 \times c_2$), the characteristic parameter α varies along Γ_+ and it is always negative, whereas β varies along Γ_- and it is positive.

From Langmuir's adsorption isotherm, we calculate the partial derivatives of the adsorption isotherm with respect to the dissolved polymer concentrations:

$$a_{11} = \frac{K_1(1 + K_2c_2)}{(1 + K_1c_1 + K_2c_2)^2} \tag{A.13}$$

$$a_{12} = \frac{-K_1K_2c_1}{(1 + K_1c_1 + K_2c_2)^2} \tag{A.14}$$

$$a_{21} = \frac{-K_1K_2c_2}{(1 + K_1c_1 + K_2c_2)^2} \tag{A.15}$$

$$a_{22} = \frac{K_2(1 + K_1c_1)}{(1 + K_1c_1 + K_2c_2)^2} \tag{A.16}$$

Substituting equations A.13-A.16 in equation (A.9) it is possible to obtain:

$$c_2\left(\frac{dc_1}{dc_2}\right)^2 - (M - c_2 + c_1)\frac{dc_1}{dc_2} - c_1 = 0 \tag{A.17}$$

where,

$$M = \frac{K_1 - K_2}{K_1K_2} \tag{A.18}$$

Differentiating equation (A.17) with respect to $c_2$leads to:

$$\frac{d^2c_1}{dc_2^2}\left[c_2\frac{dc_1}{dc_2} - (M - c_2 + c_1)\right] = 0 \tag{A.19}$$

Solving the ordinary differential equation (A.19) we find:

$$c_1 = \xi c_2 - \frac{M\xi}{\xi + 1} \tag{A.20}$$

$$(M + c_1 - c_2)^2 + 4c_1c_2 = 0 \tag{A.21}$$

Equation (A.20) represents the characteristic curves (straight lines) in the phase plane. The equations for the two characteristic waves are found applying the parameters α and β in equation (A.20):

$$\Gamma_+ : \ c_1 = \beta c_2 - \frac{M\beta}{\beta + 1} \tag{A.22}$$

$$\Gamma_- : \ c_1 = \alpha c_2 - \frac{M\alpha}{\alpha + 1} \tag{A.23}$$

As the parameter α is negative and β is positive, the family Γ_+ is composed by straight lines with positive slopes, and the family Γ_- by straight lines with negative slopes.

For any pair (α,β), the constant concentration state can be determined by the following relations (derived from equations A.22 and A.23):

$$c_1 = -\frac{M\alpha\beta}{(\alpha+1)(\beta+1)} \tag{A.24}$$

$$c_2 = \frac{M}{(\alpha+1)(\beta+1)} \tag{A.25}$$

We now establish a relation between the phase plane and the $x_D \times \varphi$ plane. Consider the linear combination of the auxiliary system equations (Equation (A.1)):

$$\lambda_1\frac{\partial c_1}{\partial x_D} + (\lambda_1 a_{11} + \lambda_2 a_{21})\frac{\partial c_1}{\partial \varphi} + \lambda_2\frac{\partial c_2}{\partial x_D} + (\lambda_1 a_{12} + \lambda_2 a_{22})\frac{\partial c_2}{\partial \varphi} = 0 \tag{A.26}$$

where $\lambda_1$and $\lambda_2$are the eigenvalues of equation (A.1). If ωrepresents a characteristic parameter (either αor β), the derivatives $\frac{\partial c_1}{\partial \omega}$and $\frac{\partial c_2}{\partial \omega}$will be in the same direction if the following system of equations (Rhee et al., 2001):

$$\lambda_1\frac{\partial \varphi}{\partial \omega} - (\lambda_1 a_{11} + \lambda_2 a_{21})\frac{\partial x_D}{\partial \omega} = 0 \tag{A.27}$$

$$\lambda_2\frac{\partial \varphi}{\partial \omega} - (\lambda_1 a_{12} + \lambda_2 a_{22})\frac{\partial x_D}{\partial \omega} = 0 \tag{A.28}$$

$$\lambda_1\frac{\partial c_1}{\partial \omega} + \lambda_2\frac{\partial c_2}{\partial \omega} = 0 \tag{A.29}$$

$$(\lambda_1 a_{11} + \lambda_2 a_{21})\frac{\partial c_1}{\partial \omega} + (\lambda_1 a_{12} + \lambda_2 a_{22})\frac{\partial c_2}{\partial \omega} = 0 \tag{A.30}$$

is satisfied.

From equations A.27 and A.29, one can find that:

$$\frac{\partial \varphi}{\partial \omega} - (a_{11} - \xi a_{21})\frac{\partial x_D}{\partial \omega} = 0 \tag{A.31}$$

Moreover, we consider that the independent variables x_D and φ can be written as a function of the parameter ω. The eigenvalues of the auxiliary system are given by

$$\lambda = \frac{\partial \varphi}{\partial x_D} = \frac{\frac{\partial \varphi}{\partial \omega}}{\frac{\partial x_D}{\partial \omega}} \tag{A.32}$$

Thus,

$$\frac{\partial \varphi}{\partial \omega} - \lambda\frac{\partial x_D}{\partial \omega} = 0 \tag{A.33}$$

Defining βas the characteristic parameter for the family C_+(Γ_+ family on the hodograph plane), and $\alpha$for the family C_-(family Γ_-on the hodograph plane), we have

$$\frac{\partial \varphi}{\partial \beta} - \lambda_+\frac{\partial x_D}{\partial \beta} = 0 \tag{A.34}$$

$$\frac{\partial \varphi}{\partial \alpha} - \lambda_-\frac{\partial x_D}{\partial \alpha} = 0 \tag{A.35}$$

Comparing equations A.34 and A.35 with equation (A.31), we can establish the relation between the hodograph plane and the $x_D \times \varphi$ plane:

$$\lambda_+ = \frac{d\varphi}{dx_D} = a_{11} - \beta a_{21} \tag{A.36}$$

$$\lambda_- = \frac{d\varphi}{dx_D} = a_{11} - \alpha a_{21} \tag{A.37}$$

Replacing equation A13.-A.16 in equations A.36 and A.37, we find

$$\lambda_+ = K_2\gamma\left(\frac{\alpha+1}{\alpha+\gamma}\right)\left(\frac{\beta+1}{\beta+\gamma}\right)^2 \tag{A.38}$$

$$\lambda_- = K_2\gamma\left(\frac{\alpha+1}{\alpha+\gamma}\right)^2\left(\frac{\beta+1}{\beta+\gamma}\right) \tag{A.39}$$

where $\gamma = \frac{K_2}{K_1}$. For convenience, we denote

$$a = a(\alpha) = \frac{\alpha+1}{\alpha+\gamma} \tag{A.40}$$

$$b = b(\beta) = \frac{\beta + 1}{\beta + \gamma} \tag{A.41}$$

The functions $a(\alpha)$ and $b(\beta)$ represent a pair of characteristic parameters and their values lie between $0 \le a(\alpha) \le \frac{1}{\gamma} \le b(\beta) \le 1$. The plane $a(\alpha) \times b(\beta)$ is spanned by orthogonal straight lines, where the a waves are vertical and b waves are horizontal. The characteristic velocities are now recast as:

$$\lambda_+ = K_2\gamma a b^2 \tag{A.42}$$

$$\lambda_- = K_2\gamma a^2 b \tag{A.43}$$

After deriving the expressions for the characteristic waves of the auxiliary problem, the shock velocities are found from the Rankine-Hugoniot conditions:

$$V_+(a, b^-, b^+) = \frac{\varphi}{x_D} = K_2\gamma a b^- b^+ \tag{A.44}$$

$$V_-(a^-, a^+, b) = \frac{\varphi}{x_D} = K_2\gamma b a^- a^+ \tag{A.45}$$

where the superscripts $+$ and $-$ represent the value of a or b before and after the shock wave, respectively.

Now we analyze how λ_+ and λ_- change along the phase plane. We denote D_- the derivative of λ_+ with respect to the concentration along the family Γ_- and D_+ the derivative of λ_- with respect to the concentration along the family Γ_+. We will consider $K_2 > K_1$, and therefore, $\gamma > 1$. Thus, we have:

$$\frac{D_-\lambda_+}{Dc_2} = \frac{\frac{\partial\lambda_+}{\partial\beta}}{\frac{\partial c_2}{\partial\beta}} = -2K_2^2\gamma\frac{(\alpha+1)^2(\beta+1)^3}{(\alpha+\gamma)(\beta+\gamma)^3} = -2K_2^2\gamma\frac{(1-\gamma)}{(a-1)}a^2b^3 < 0 \tag{A.46}$$

$$\frac{D_+\lambda_-}{Dc_2} = \frac{\frac{\partial\lambda_+}{\partial\alpha}}{\frac{\partial c_2}{\partial\alpha}} = -2K_2^2\gamma\frac{(\alpha+1)^3(\beta+1)^2}{(\alpha+\gamma)^3(\beta+\gamma)} = -2K_2^2\gamma\frac{(1-\gamma)}{(b-1)}a^3b^2 < 0 \tag{A.47}$$

Since both derivatives (Equations A.46 and A.47) are negative, we conclude that λ decreases along Γ_+ and Γ_- as c_2 increases.

Appendix B

In this appendix the inverse mapping of the waves from the $x_D \times \varphi$ plane to the $x_D \times t_D$ plane is presented. We also derive the exact coordinates of the crossing points of these waves related to the beginning and the ending points of the interactions between the waves.

The relation between the shock waves in the $x_D \times \varphi$ plane and $x_D \times t_D$ plane is given by (Pires et al., 2006):

$$D_i = \frac{f^\pm}{s^\pm + V_i}, \; i = +, - \tag{B.1}$$

where D_i is the shock velocity in the $x_D \times t_D$ plane and V_i is the shock velocity in the $x_D \times \phi$ plane.

From equations (75) and (A.38), the velocity of the rarefaction family C_+ in $x_D \times t_D$ plane is:

$$\frac{dx_D}{dt_D} = \frac{f}{K_2\gamma a b^2 + s} \tag{B.2}$$

and the velocity of the rarefaction family C_- (Equations 75 and A.39):

$$\frac{dx_D}{dt_D} = \frac{f}{K_2\gamma a^2 b + s} \tag{B.3}$$

From equation (B.1), the shock path $\overline{OB}$ is given by:

$$x_D = t_D\frac{f^+}{K_2\gamma a^{(J)} b^{(J)} + s^+} \tag{B.4}$$

Following the same procedure, the shock path $\overline{OE}$ is:

$$x_D = t_D\frac{f^+}{K_2\gamma a^{(J)} + s^+} \tag{B.5}$$

From equations (A.43) and (A.44), we find the shock velocity BC in $x_D \times \phi$ plane:

$$\left(\frac{d\varphi}{dx_D}\right)_{BC} = K_2\gamma b^{(J)} - \frac{\sqrt{\frac{1}{a^{(J)}} - 1}}{K_2\gamma b^{(J)}\sqrt{K_2\gamma b^{(J)} x_D^{(BC)}}} \tag{B.6}$$

Then, through equation (B.1), the velocity of shock BC in $x_D \times t_D$ plane is:

$$\left(\frac{dx_D}{dt_D}\right)_{BC} = \frac{f^+}{s^+ + \left(\frac{d\varphi}{dx_D}\right)_{BC}} \tag{B.7}$$

Therefore, we can write the shock path BCas:

$$x_D = \left(\frac{dx_D}{dt_D}\right)_{BC}(t_D - t_B) + x_B \tag{B.8}$$

where $(x_B, t_B)$is the point where the shock $\overline{OB}$intercepts the first rarefaction characteristic of C_-, given by:

$$t_B = \frac{K_2\gamma a^{(J)}b^{(J)} + s^+}{K_2\gamma a^{(J)}b^{(J)}(1 - a^{(J)})} \tag{B.9}$$

$$x_B = \frac{f^+}{K_2\gamma a^{(J)}b^{(J)} + s^+}t_B \tag{B.10}$$

The rarefaction $C_-$is transmitted through the shock BC, its new slope is:

$$\frac{dx_D}{dt_D} = \frac{f}{K_2\gamma a^2 b^{(I)} + s} \tag{B.11}$$

The shock BCfinishes at point C, which is the point where the last characteristic of the rarefaction C_-intercepts the shock BC. The coordinates of point $C$are:

$$t_C = \frac{\frac{f^+}{K_2\gamma[a^{(I)}]^2 b^{(J)} + s^+} - \frac{f^+}{K_2 b^{(J)} + s^+}t_B + x_B}{\frac{f^+}{K_2\gamma[a^{(I)}]^2 b^{(J)} + s^+} - \frac{f^+}{K_2 b^{(J)} + s^+}} \tag{B.12}$$

$$x_C = \frac{f^+}{K_2\gamma[a^{(I)}]^2 b^{(J)} + s^+}(t_C - 1) \tag{B.13}$$

After the interaction with the rarefaction C_-, the shock path continues from point Cas a straight line up to point G, which is the point where the interaction between shock $V_+$with the rarefaction C_+begins. The shock path $\overline{CG}$is:

$$x_D = \frac{f^+}{K_2 b^{(J)} + s^+}(t_D - t_C) + x_C \tag{B.14}$$

and point Gcoordinates are:

$$t_G = \frac{\frac{f^+}{K_2 b^{(J)} + s^+}t_C - \frac{f^+}{K_2\gamma a^{(I)}\left[b^{(J)}\right]^2 + s^+} - x_C}{\frac{f^+}{K_2 b^{(J)} + s^+} - \frac{f^+}{K_2\gamma a^{(I)}\left[b^{(J)}\right]^2 + s^+}} \tag{B.15}$$

$$x_G = \frac{f^+}{K_2\gamma a^{(I)}\left[b^{(J)}\right]^2 + s^+}[t_G - 1] \tag{B.16}$$

After point G, the rarefaction $C_-$is absorbed and the path of shock $G\infty$is:

$$x_D = \frac{f^+}{K_2 b + s^+}(t_D - t_G) + x_G \tag{B.17}$$

The last interaction occurs between the transmitted rarefaction $C_-$and the shock $\overline{OE}$. The rarefaction is absorbed by the shock wave, and the new shock path is defined as:

$$x_D = \frac{f^+}{K_2\gamma a + s^+}(t_D - t_E) + x_E \tag{B.18}$$

where the point $(x_E, t_E)$is given by:

$$t_E = \frac{\frac{f^+}{K_2\gamma[a^{(J)}]^2 b^{(I)} + s^+}t_B - x_B}{\frac{f^+}{K_2\gamma[a^{(J)}]^2 b^{(I)} + s^+} - \frac{f^+}{K_2\gamma a^{(J)} + s^+}} \tag{B.19}$$

$$x_E = \frac{f^+}{K_2\gamma a^{(J)} + s^+}t_E \tag{B.20}$$

References

Algharaib, M., Alajmi, A., Gharbi, R., 2014. Improving polymer flood performance in high salinity reservoirs. J. Pet. Sci. Eng. 115, 17–23. https://doi.org/10.1016/j.petrol.2014.02.003.

Ali, L., Barrufet, M.A., 1984. Profile modification due to polymer adsorption in reservoir rocks. Energy Fuels 8 (6), 1217–1222. https://doi.org/10.1021/ef00048a008.

Alsofi, A.M., Blunt, M.J., 2010. Streamline-based simulation of non-Newtonian polymer flooding. SPE J. 15 (4), 901–911. https://doi.org/10.2118/123971-PA.

Alsofi, A.M., Blunt, M.J., 2014. Polymer flooding design and optimization under economic uncertainty. J. Pet. Sci. Eng. 124, 46–59. https://doi.org/10.1016/j.petrol.2014.10.014.

Bedrikovetsky, P.G., 1993. Mathematical Theory of Oil and Gas Recovery. Kluwer Academic Publishers, London.

Boa, P.M.F., Pires, A.P., 2006. Salt effects on polymer adsorption in chemical flooding of oil reservoirs. In: 11th Brazilian Congress of Thermal Sciences and Engineering, Curitiba, Brazil.

Boardman, R.S., Moore, L.J., Julian, M.H., Bilbrey, D.G., Moore, J.S., 1982. Design and implementation of four enhanced oil recovery in Bay fields of South Louisiana. In: SPE Enhanced Oil Recovery Symposium. Tulsa, Oklahoma, USA.

Borazjani, S., Bedrikovetsky, P.G., Farajzadeh, R., 2014. Exact Solution for Non-self-similar Wave-Interaction Problem during Two-phase Four-Component Flow in Porous Media. Abstract and Applied Analysis. https://doi.org/10.1155/2014/731567, 2014.

Borazjani, S., Bedrikovetsky, P.G., Farajzadeh, R., 2016a. Analytical solutions of oil displacement by a polymer slug with varying salinity. J. Pet. Sci. Eng. 140, 28–40. https://doi.org/10.1016/j.petrol.2016.01.001.

Borazjani, S., Roberts, A.J., Bedrikovetsky, P.G., 2016b. Splitting in systems of PDEs for two-phase multicomponent flow in porous media. Appl. Math. Lett. 53, 25–32. https://doi.org/10.1016/j.aml.2015.09.014.

Buckley, S.E., Leverett, M.C., 1942. Mechanism of fluid displacement in sands. Transactions of the AIME 146 (1), 107–116. https://doi.org/10.2118/942107-G.

Davison, P., Mentzer, E., 1982. Polymer flooding in north Sea reservoirs. SPE J. 22 (3), 353–362. https://doi.org/10.2118/9300-PA.

de Paula, A.S., Pires, A.P., 2015. Analytical solution for oil displacement by polymer slugs containing salt in porous media. J. Pet. Sci. Eng. 135, 323–335. https://doi.org/10.1016/j.petrol.2015.09.001.

de Paula, A.S., Apolinário, F.O., Pires, A.P., 2019. Water slug injection containing *n* polymers in porous media. AIChE J. 65 (11) https://doi.org/10.1002/aic.16735.

Johansen, T., Winther, R., 1988. The solution of the riemann problem for a hyperbolic system of conservation laws modeling polymer flooding. SIAM J. Math. Anal. 19 (3), 541–566. https://doi.org/10.1137/0519039.

Johansen, T., Winther, R., 1989. The riemann problem for multicomponent polymer flooding. SIAM J. Math. Anal. 20 (4), 908–929. https://doi.org/10.1137/0520061.

Kargozarfard, Z., Ruai, M., Ayatollahi, S., 2018. Viscous fingering and its effect on areal Sweep efficiency during waterflooding: an experimental study. Pet. Sci. 16 (7), 105–116. https://doi.org/10.1007/s12182-018-0258-6.

Khorsandi, S., Changhe, Q., Johns, R.T., 2016. Displacement efficiency for low salinity polymer flooding including wettability alteration. In: SPE Improved Oil Recovery Conference, Tulsa, USA.

Lee, Y., Lee, W., Jang, Y., Sung, W., 2019. Oil recovery by low-salinity polymer flooding in carbonate oil reservoirs. J. Pet. Sci. Eng. 181, 1–9. https://doi.org/10.1016/j.petrol.2019.106211.

Maitin, B.K., Volz, H., 1981. Performance of deutsche texaco Ag's oerrel and hankensbuettel polymer floods. In: SPE/DOE Enhanced Oil Recovery Symposium, Tulsa, USA. https://doi.org/10.2118/9794-MS.

Morel, D., Vert, M., Jouenne, S., Gauchet, R., Bouger, Y., 2012. First polymer injection in deep offshore field Angola: recent advances in the dalia/carmelia field case. SPE Oil and Gas Facilities 1 (2), 43–52. https://doi.org/10.2118/135735-PA.

Patton, J.T., Coats, K.H., Colegrove, G.T., 1971. Prediction of polymer flood performance. SPE J. 11 (1), 72–84. https://doi.org/10.2118/2546-PA.

Pires, A.P., Bedrikovetsky, P.G., Shapiro, A.A., 2006. A splitting technique for analytical modeling of two-phase multicomponent flow in porous media. J. Pet. Sci. Eng. 51 (1–2), 54–67. https://doi.org/10.1016/j.petrol.2005.11.009.

Pope, G.A., 1980. The application of fractional flow theory to enhanced oil recovery. SPE J. 20 (3), 191–205. https://doi.org/10.2118/7660-PA.

Rhee, H.-K., Aris, R., Amundson, N.R., 2001. First-Order Partial Differential Equations: Theory and Application of Hyperbolic Systems of Quasilinear Equations, vol. 2. Prentience-Hall, New Jersey, USA. Englewood Cliffs.

Ribeiro, P.M., Pires, A.P., 2008. The displacement of oil by polymer slugs considering adsorption effects. In: SPE Annual Technical Conference and Exhibition, Denver, USA.

Sheng, J.J., Leonhardt, B., Azri, N., 2015. Status of polymer-flooding technology. J. Can. Pet. Technol. 54 (2), 116–126. https://doi.org/10.2118/174541-PA.

Silva, R.C.A., Cardoso, C.B., Pires, A.P., 2007. The role of adsorption isotherms on chemical flooding oil recovery. In: SPE Annual Technical Conference and Exhibition, Anaheim, USA.

Sorbie, K.S., 1991. Polymer-Improved Oil Recovery. Springer Science and Business Media, New York, USA.

Taber, J.J., Martin, F.D., Seright, R.S., 1997. EOR Screening criteria revisited – Part 1: introduction to Screening criteria and enhanced oil recovery field projects. SPE Reserv. Eng. 12 (3), 189–198. https://doi.org/10.2118/35385-PA.

Torrealba, V.A., Hoteit, H., 2019. Improved polymer flooding injectivity and displacement by considering compositionally-tuned slugs. J. Pet. Sci. Eng. 178, 14–26. https://doi.org/10.1016/j.petrol.2019.03.019.

Vicente, B.J., Viatcheslav, I.P., Pires, A.P., 2014. Semi-analytical solution for a hyperbolic system modeling 1D polymer slug flow in porous media. J. Pet. Sci. Eng. 115, 102–109. https://doi.org/10.1016/j.petrol.2014.02.005.

Zhou, W., Zhang, J., Feng, G., Jiang, W., Sun, F., Zhou, S., Liu, Y., 2008. Key technologies of polymer flooding in offshore oilfield of Bohai Bay. In: SPE Asia Pacific Oil and Gas Conference and Exhibition. Perth, Australia.

Chapter 3 – Oil Displacement by Multicomponent Slug Injection: An Analytical Solution for Langmuir Adsorption Isotherm

Journal of Petroleum Science and Engineering 197 (2021) 107939

Contents lists available at ScienceDirect

Journal of Petroleum Science and Engineering

journal homepage: http://www.elsevier.com/locate/petrol

Oil displacement by multicomponent slug injection: An analytical solution for Langmuir adsorption isotherm

Felipe de O. Apolinário *, Adolfo P. Pires **

Universidade Estadual do Norte Fluminense Darcy Ribeiro, Brazil

ARTICLE INFO

Keywords:
Enhanced oil recovery
Polymer flooding
Conservation laws
Hyperbolic systems of partial differential equations

ABSTRACT

Injection of water containing dissolved chemical components is one of the most important enhanced oil recovery (EOR) techniques. This problem can be modeled by an $(n+1)\times(n+1)$ system of hyperbolic partial differential equations representing the conservation of water and chemical components. In this paper we present the solution to the problem of oil displacement by a water slug containing n dissolved chemicals driven by pure water. It is considered that the chemicals can be adsorbed by the rock following Langmuir adsorption isotherm. The solution for any number of dissolved chemicals was obtained from a generalization of the case where three polymers are dissolved in the slug. To build the solution we first introduced a potential function replacing time as an independent variable. This procedure splits the original system of equations into a one-phase purely chromatographic problem and a scalar hyperbolic equation. The one-phase problem was solved using multicomponent chromatography theory, and its solution was used to solve the scalar equation. Both solution procedures are based on the method of characteristics. Finally, the solution of the scalar equation was mapped onto the space-time plane. The concentration solution shows the development of a complete chromatographic cycle in the porous media, and due to the separation of the chemicals, water banks appear in the water saturation solution. These results are new and present important insights for two-phase multicomponent flows in porous media.

1. Introduction

Waterflooding is the most used oil recovery technique. However, it may not achieve high ultimate recovery factors (Ogbeiwi, 2018). The performance of a waterflooding project is highly dependent on the displacement efficiency, which is a function of the relative permeabilities and viscosities of the fluids saturating the porous media (Zhao et al., 2016).

To increase the displacement efficiency, chemical components can be dissolved in the injection water aiming to reduce its mobility and increase the oil-water mobility ratio. The adding of chemicals to injection water is defined as a chemical method of Enhanced Oil Recovery (EOR) (Lake, 1989). Surfactants reduce interfacial tension between oil and water phases, and modify the displacement efficiency by changing wettability and relative permeabilities (Fayers and Perrine, 1958; Adams and Schievelbein, 1987; Pal et al., 2018).

Polymers can also be dissolved in injection water. The polymeric solution is more viscous than pure water, thus, its mobility is lower and the displacement efficiency is improved (Needham and Doe, 1987; Mishra et al., 2014). The most important feature of this technique is the increase of oil production when compared to waterflooding (Ustick, 1967). It also reduces viscous fingering and increases the efficiency of a posterior waterflooding due to the reduced permeability after polymer flooding (Sheng et al., 2015; Kargozarfard et al., 2018). The mobilization of residual oil in polymer flooding processes is relevant only for highly concentrated solutions (Asghari and Nakutnyy, 2008; Koh et al., 2018; Seright et al., 2018). Due to its efficiency, polymer flooding is the most applied chemical method of EOR (Sorbie, 1991).

Adsorption of the polymer by the pore rock surface plays an important role in screening and designing a polymer flooding project. Polymer flooding is mostly applied in sandstone reservoirs (Sorbie, 1991; Taber et al., 1997; Sheng et al., 2015).

Connate water salinity is also an important parameter in a polymer flooding project design. The mixture of formation water containing divalent cations with polyacrylamides solution (PA), which is the most used polymer in EOR, reduces its viscosity (Amro et al., 2002). So, it is necessary to use a higher polymer concentration in order to achieve the same viscosity, or to inject a water pre-flush containing divalent cations

---

* Corresponding author.
** Corresponding author.
E-mail addresses: felipe_apolinario03@hotmail.com (F.O. Apolinário), adolfo.puime@gmail.com (A.P. Pires).

https://doi.org/10.1016/j.petrol.2020.107939
Received 20 March 2020; Received in revised form 26 August 2020; Accepted 11 September 2020

in low concentration (Maitin and Volz, 1981; Davison and Mentzer, 1982; Algharaib et al., 2014). Biopolymers (*e.g.* xantham gum) are salinity resistant and can be injected in both carbonate and siliciclastic reservoirs (Ali and Barrufet, 1994). However, for high temperature reservoirs, xantham gum solutions gradually lose its viscosity (Sofia and Aliouche, 2016).

Mathematical models are important tools to analyze fluid flow through porous media for EOR techniques. A set of partial differential equations (PDE's) based on the balance laws of water and each chemical component governs the one-dimensional incompressible two-phase oil displacement. From the solution of these systems of PDE's it is possible to build saturation and concentration profiles, analyze the positions of the water and chemical components fronts, and forecast the production profile (Buckley and Leverett, 1942; Welge, 1952; Patton et al., 1971). The solutions of these systems of equations can be obtained by the method of characteristics (MOC) and are composed by sets of rarefaction and shock waves, and constant states (Wachmann, 1964; Claridge and Bondor, 1974; Bedrikovetsky, 1993).

Relevant effects of the physical model, such as adsorption or mass transfer between phases must be included in the system of conservation laws (Pope, 1980; Johns and Orr Jr, 1996). The adsorption phenomena can be modeled by an adsorption isotherm, which is a relation between the concentration of the chemical in the flowing phase and in the stationary phase (rock). The adsorption of some chemicals used in EOR processes is described by the Langmuir adsorption isotherm (Langmuir, 1918; Danq et al., 2011; Ali and Mahmud, 2015). The adsorption of the chemical components delays its concentration front with respect to the water saturation front (Patton et al., 1971; Entov and Polishchuk, 1975; Farajzadeh et al., 2016).

Non-isothermal displacement is also modeled by a system of conservation laws. For these problems, the energy conservation equation must be included in the system of PDE's to evaluate the energy transfer and the temperature influence on the displacement (Braginskaya and Entov, 1980).

The case of continuous injection of water containing one dissolved polymer in an oil reservoir is composed by a 2×2 system of conservation laws with constant initial and boundary conditions. For an "S" shape fractional flow curve and considering a convex adsorption isotherm, the solution is composed by a saturation rarefaction, followed by a concentration shock wave and by a Buckley-Leverett shock type (Patton et al., 1971). For a concave adsorption isotherm, the structure of the solution is composed by a saturation rarefaction followed by a concentration rarefaction wave and by a Buckley-Leverett shock type (Johansen and Winther, 1988).

Entov and Zazovskii (1982) presented the solution of oil displacement by a solution containing two chemical components: one active component that will change the displacement efficiency and a passive additive that increases/decreases the adsorption of the active component. The problem is composed by a 3×3 system of conservation laws.

Multicomponent chemical injection in oil reservoirs is modeled by an $(n+1) \times (n+1)$ system of conservation laws, where n is the number of chemicals dissolved. Helfferich (1981) developed a theory to solve two-phase multicomponent problems neglecting adsorption effects. This theory was later applied to solve the problem of two-phase three-component surfactant displacement in oil reservoirs (Hirasaki, 1981).

When the adsorption is considered for two-phase multicomponent flow problems, the components split along the reservoir due to their different adsorption rates, and the lower adsorption ones travel ahead of the chemicals with higher adsorption rates (chromatographic cycle) (Rhee et al., 2001; Lüftenegger and Clemens, 2017). The solution for constant concentration injection problems can be built by a generalization of the chromatography theory, and consists in solving the associated multicomponent chromatographic problem, followed by the extension of the solution for a two-phase environment (Johansen and Winther, 1989; Dahl et al., 1992). This procedure was applied to solve the problem of two-phase multicomponent polymer injection, considering that the adsorption of the i^{th} component is only a function of the concentration of component i (Johansen and Winther, 1989). Later, a Riemann solver was developed for the same physical model (Johansen et al., 1989). Next, the solution was extended for a general adsorption isotherm (Dahl et al., 1992).

The efficiency of polymer flooding is a function of the amount of polymer injected. Continuous injection and high concentration slug injection displaced by water yield to similar results if the amount of injected polymer is the same (Sheng et al., 2015). However, for polymer slug injection, the cost is smaller. Therefore, polymers are commonly injected in high concentration slugs displaced by water rather than continuous injection.

The boundary condition of the slug injection problem is discontinuous, and the solution is no longer self-similar. In such cases, the methodology presented in Dahl et al. (1992) cannot be applied. Considering a slug containing one polymer dissolved, the hodograph transformation can be used to recast the 2×2 system of conservation laws in terms of Riemann invariants (Bedrikovetsky, 1982; Logan, 1994; Dafermos, 2000; Rhee et al., 2001). A similar problem considering viscous fingering can be solved by a graphical method analogous to the one presented in Bedrikovetsky (1982) (Hamid and Muggeridge, 2018).

Pires et al. (2006) presented a methodology to solve complex problems of chemical slugs injection in porous media. A potential function related to water conservation replaces time as an independent variable. For the case of slugs containing n chemicals dissolved, the introduction of the potential function splits the original system of $(n+1) \times (n+1)$ conservation laws into an auxiliary system of n equations and a scalar equation. The auxiliary system contains only thermodynamic properties (one-phase chromatography process), whereas the scalar equation is a function of the transport properties of the flow and of the solution of the auxiliary system. For multicomponent polymer slug injection, the auxiliary system is analogous to the multicomponent chromatography problem (Rhee et al., 1970; Borazjani et al., 2016b).

This technique was applied to solve different EOR problems. The solution for the case of one polymer continuous injection considering that the polymer may adsorb according to the Langmuir adsorption isotherm and the effects of salinity in polymer adsorption was presented in Boa and Pires (2006). Silva et al. (2007) developed the solution for the case of oil displacement by continuous multicomponent polymer injection using this technique. Injection of a slug containing one polymer that may be adsorbed by the rock was solved for different adsorption isotherms (convex, linear and Langmuir type) and for a concave fractional flow curve (Ribeiro and Pires, 2008).

The solution for the case of slug injection containing one polymer that may be adsorbed by the porous media following Langmuir adsorption isotherm and an "S" shape fractional flow curve is presented in Vicente et al. (2014). The results were compared to a numerical simulator with close agreement. Borazjani et al. (2014) included the effect of salinity in the polymer adsorption isotherm, and it was considered that the polymer followed a linear adsorption isotherm. de Paula and Pires (2015) extended the Borazjani et al. (2014) solution to the case of polymer adsorption modeled by Langmuir isotherm.

Borazjani et al. (2016a) applied this technique to solve the problem of oil displacement by the injection of a polymer slug with varying salinity. It was assumed that the salt was not adsorbed by the rock but changed the polymer adsorption, which followed a linear adsorption isotherm. Khorsandi et al. (2016) presented the solution for the case of a slug containing one polymer dissolved in low salinity water injection. The low salinity effects were included in the polymer adsorption isotherm and rock wettability. The results were compared with experimental data and numerical simulators.

de Paula et al. (2019) developed a general solution for the multicomponent polymer slug injection in oil reservoirs for a linear adsorption isotherm. It was considered that the adsorption of the i^{th} polymer was a function of its own concentration in flowing phase. The solution showed that the components splitting in porous media (chromatography cycle) led to the appearance of water banks with different viscosities.

Apolinário et al. (2020) used the two-component chromatography theory presented in Rhee et al. (2001) to model the injection of a slug containing two dissolved polymers in an oil reservoir. It was assumed that both polymers adsorbed in porous media following Langmuir adsorption isotherm. Beyond the development of the full chromatographic cycle, the solution showed that for long times the chemicals concentrations are constant along the porous media.

The splitting technique can also be applied to solve problems considering advective transport, parabolic terms and relaxation non-equilibrium equations in cases where the auxiliary system allows the construction of an analytical solution (Borazjani et al., 2015).

In this paper the solution for the injection of a slug containing n chemicals dissolved and displaced by water in an oil reservoir is presented. It is considered that the chemicals can be adsorbed by the porous media following Langmuir adsorption isotherm. The solution is a generalization of the model presented in Vicente et al. (2014) and Apolinário et al. (2020) for any number of components dissolved in the water slug, which has not been published.

Several problems of chemicals injection in porous media can be modeled by the solution presented in this paper, such as multicomponent polymer slug injection, alkali-polymer injection, low salinity waterflooding, etc. The main constraint is that the chemical adsorption by the rock must follow Langmuir adsorption isotherm.

The solution also presents important features regarding the flow of chemicals in a reservoir: the impact of the chemical separation in the water saturation profiles, the generalized water saturation behavior in a multicomponent injection for long times, and the impact of each adsorption constant in the saturation and concentration profiles.

In the following sections we present the general formulation, followed by the solution of the problem of slug injection containing three dissolved polymers in an oil reservoir. The solution is built applying the technique presented in Pires et al. (2006) and the multicomponent chromatography theory of Rhee et al. (1970). Then, we present the solution for the case of n dissolved chemicals in the slug.

2. Mathematical model

In this section we present the mathematical formulation for the problem of one-dimensional two-phase oil displacement by a water slug containing n dissolved chemicals driven by water. Further assumptions are:

- Homogeneous porous media;
- Incompressible system;
- Dispersion, gravity and capillarity are neglected;
- The chemical components are dissolved only in the water phase;
- Water density is not a function of the chemicals concentrations.

These assumptions are better suited for horizontal flow of two low compressibility immiscible liquid phases, or, from a mathematical point of view, advection dominated flow (water and oil). As phases velocities in reservoirs are very small, dispersive effects are usually neglected. Moreover, as the injected polymer concentrations are small, the infinite dilution condition can be applied.

Under these hypotheses, the flow of fluids through porous media is governed by a hyperbolic system of partial differential equations (PDE), composed by the conservation of water and of each chemical component. This system of PDE's is written as:

$$\begin{cases} \phi\dfrac{\partial s}{\partial t}+u_T\partial f(s,\dfrac{\vec{c})}{\partial x}=0 \\ \phi\partial(c_is+a_i\dfrac{(\vec{c}))}{\partial t}+u_T\partial(c_if(s,\dfrac{\vec{c}))}{\partial x}=0, i=1,2,\ldots,n \end{cases} \tag{1}$$

where $\vec{c}=[c_1,c_2,\ldots,c_n]$ is the concentration of each component in the flowing phase, a_i is the adsorbed chemical amount on the rock surface, f is the water fractional flow, ϕ is the rock porosity, and u_T is the total flux velocity.

We define the following dimensionless variables:

$$x_D=\frac{x}{\frac{\Omega_s}{A}} \tag{2}$$

$$t_D=\frac{\int_0^t u_T(\tau)d\tau}{\phi\frac{\Omega_s}{A}} \tag{3}$$

in which x_D is the dimensionless position related to the length of the slug, t_D represents the number of slug volumes injected, Ω_S is the volume of the injected slug and A is the cross-sectional area of the reservoir. Introducing equations (3) and (4) in the system of equation (1), we have:

$$\begin{cases} \dfrac{\partial s}{\partial t_D}+\dfrac{\partial f(s,c_1,c_2)}{\partial x_D}=0 \\ \dfrac{\partial(c_is+a_i(\vec{c}))}{\partial t_D}+\dfrac{\partial(c_if(s,\vec{c}))}{\partial x_D}=0,\ i=1,2,\ldots,n \end{cases} \tag{4}$$

We consider that the adsorption of the chemicals on the rock surface is governed by the multicomponent Langmuir adsorption isotherm (Langmuir, 1918):

$$a_i(\vec{c})=\frac{K_ic_i}{1+\sum_{j=1}^n K_jc_j} \tag{5}$$

where K_i is the Langmuir adsorption constant of i.

At the beginning of the slug injection ($t_D=0$), there is no polymer in the reservoir ($\vec{c}=\vec{c}^{(I)}=0$), and the water saturation is irreducible ($s=s^{(I)}$). During the slug injection, the water fractional flow is 1 at the inlet ($x_D=0$), and the injected chemicals concentration will be denoted as $\vec{c}^{(J)}$. The water drive begins at $t_D=1$, and no more chemicals are injected. Thus, the initial and boundary conditions of the problem are:

$$t_D=0,\ \begin{cases} s(x_D,0)=s^{(I)}, \\ \vec{c}(x_D,0)=\vec{c}^{(I)}=0, \end{cases} \quad 0< x_D<\frac{L}{\frac{\Omega_s}{A}} \tag{6}$$

$$x_D=0,\ \begin{cases} f(0,t_D)=f^{(J)}=1 & t_D>0 \\ \vec{c}(0,t_D)=\begin{cases} \vec{c}^{(J)}, & 0<t_D<1 \\ 0, & t_D>1 \end{cases} \end{cases} \tag{7}$$

2.1. Splitting between thermodynamics and hydrodynamics

We now define the following potential function associated to the water volume conservation:

$$d\varphi=f(s,\vec{c})dt_D-sdx_D \tag{8}$$

Introducing equation (8) in the system of equation (4), we obtain:

$$\frac{\partial}{\partial\varphi}\left(\frac{s}{f(s,\vec{c})}\right)-\frac{\partial}{\partial x_D}\left(\frac{1}{f(s,\vec{c})}\right)=0 \tag{9}$$

$$\partial a_i\frac{(\vec{c})}{\partial\varphi}+\frac{\partial c_i}{\partial x_D}=0,\ i=1,2,\ldots,n \tag{10}$$

This procedure splits the original system (Equation (4)) into an $n\times n$ auxiliary system of equations (Equation (10)), which is a function of the concentration of chemicals, and a scalar equation (Equation (9)) that includes the hydrodynamic properties of the flow and the solution of the auxiliary system (Pires et al., 2006). Note that the potential function replaces time as one independent variable of the problem, and the problem is defined in the auxiliary plane $x_D\times\varphi$. The auxiliary system is analogous to the system of PDE's that models multicomponent chromatography problems (Rhee et al., 1970).

The initial and boundary conditions (Equations (6) and (7)) in the auxiliary plane are given by:

$$\varphi = -s^{(I)}x_D, \begin{cases} s\left(x_D, -s^{(I)}x_D\right) = s^{(I)}, \\ \vec{c}\left(x_D, -s^{(I)}x_D\right) = \vec{c}^{(I)} = 0, 0 < x_D < \frac{L}{\frac{\Omega_s}{A}} \end{cases} \tag{11}$$

$$x_D = 0, \begin{cases} f(0,\varphi) = f^{(J)} = 1 & \varphi > 0 \\ \vec{c}(0,\varphi) = \begin{cases} \vec{c}^{(J)}, & 0 < \varphi < 1 \\ 0, & \varphi > 1 \end{cases} \end{cases} \tag{12}$$

Defining $\frac{1}{f(s,\vec{c})}$ as $U(s,\vec{c})$ and $-\frac{s}{f(s,\vec{c})}$ as $F(U,\vec{c})$, equation (9) becomes:

$$\partial F(U,\frac{\vec{c})}{\partial\varphi} + \partial U(s,\frac{\vec{c})}{\partial x_D} = 0 \tag{13}$$

The initial and boundary conditions for the variables F and U are:

$$\varphi = -s^{(I)}x_D, \begin{cases} U \rightarrow +\infty \\ F \rightarrow -\infty \end{cases} \tag{14}$$

$$x_D = 0, \begin{cases} U = 1 \\ F = -s^{(J)} \end{cases} \tag{15}$$

where $s^{(J)} = 1 - s_{or}$, and s_{or} is the residual oil saturation.

The solution for this new problem is built following the steps:

- Solution of the auxiliary system (Equation (10)) using the chromatography theory (Rhee et al., 1970);
- Solution of equation (9) by the method of characteristics (MOC);
- Inverse mapping of the solution from the auxiliary plane to the $x_D \times t_D$ plane using the following expression:

$$dt_D = \frac{d\varphi}{f\left(s(x_D,\varphi), \vec{c}(x_D,\varphi)\right)} + \frac{s}{f\left(s(x_D,\varphi), \vec{c}(x_D,\varphi)\right)} dx_D \tag{16}$$

Note that in equation (16) $s(x_D,\varphi)$ is the solution of equation (9) and $\vec{c}(x_D,\varphi)$ is the solution of the auxiliary system. Therefore, the path of the solution in the $x_D \times t_D$ plane is a function of the solutions of the auxiliary system and equation (9), and of the path of the waves in the auxiliary plane. For a bounded system, there is a one-to-one correspondence between the solution in the auxiliary plane and in $x_D \times t_D$ plane (Wagner, 1982; Pires et al., 2006).

2.2. Slug injection containing three dissolved polymers

For the sake of simplicity, we present the solution of the two-phase oil displacement by a slug containing three dissolved polymers followed by water drive.

The water saturation is redefined as:

$$s(x_D, t_D) = \frac{s(x_D, t_D) - s^{(I)}}{s^{(J)} - s^{(I)}} \tag{17}$$

Equation (17) normalizes water saturation and leads to a new set of dimensionless variables, given by:

$$x_D = \frac{x}{\frac{\Omega_s}{A}} \tag{18}$$

$$t_D = \frac{\int_0^t u_T(\tau)d\tau}{\phi\left(s^{(J)} - s^{(I)}\right)\frac{\Omega_s}{A}} \tag{19}$$

Applying the new dimensionless variables (Equations (18) and (19)), the system of equation (1) becomes:

$$\begin{cases} \frac{\partial s}{\partial t_D} + \frac{\partial f(s,c_1,c_2)}{\partial x_D} = 0 \\ \frac{\partial(c_i s + a_i(\vec{c}))}{\partial t_D} + \frac{\partial(c_i f(s,\vec{c}))}{\partial x_D} = 0, \ i = 1,2,3 \end{cases} \tag{20}$$

with initial and boundary conditions given by:

$$t_D = 0, \begin{cases} s(x_D, 0) = 0, \\ \vec{c}(x_D, 0) = \vec{c}^{(I)} = 0, \end{cases} 0 < x_D < \frac{L}{\frac{\Omega_s}{A}} \tag{21}$$

$$x_D = 0, \begin{cases} f(0,t_D) = f^{(J)} = 1 & t_D > 0 \\ \vec{c}(0,t_D) = \begin{cases} \vec{c}^{(J)}, & 0 < t_D < 1 \\ 0, & t_D > 1 \end{cases} \end{cases} \tag{22}$$

where $\vec{c} = [c_1, c_2, c_3]$.

Applying equation (8) in system (20), we split the original problem into a 3 × 3 auxiliary system and a scalar equation:

$$\frac{\partial}{\partial\varphi}\left(\frac{s}{f(s,\vec{c})}\right) - \frac{\partial}{\partial x_D}\left(\frac{1}{f(s,\vec{c})}\right) = 0 \tag{23}$$

$$\partial a_i\frac{(\vec{c})}{\partial\varphi} + \frac{\partial c_i}{\partial x_D} = 0, \ i = 1,2,3 \tag{24}$$

with the following initial and boundary conditions:

$$\varphi = 0, \begin{cases} s(x_D, 0) = 0, \\ \vec{c}(x_D, 0) = \vec{c}^{(I)} = 0, 0 < x_D < \frac{L}{\frac{\Omega_s}{A}} \end{cases} \tag{25}$$

$$x_D = 0, \begin{cases} f(0,\varphi) = f^{(J)} = 1 & \varphi > 0 \\ \vec{c}(0,\varphi) = \begin{cases} \vec{c}^{(J)}, & 0 < \varphi < 1 \\ 0, & \varphi > 1 \end{cases} \end{cases} \tag{26}$$

2.2.1. Solution of the auxiliary system

The first step is the solution of the auxiliary system (Equation (24)), which is given by:

$$\begin{cases} \partial a_1\frac{(\vec{c})}{\partial\varphi} + \frac{\partial c_1}{\partial x_D} = 0 \\ \partial a_2\frac{(\vec{c})}{\partial\varphi} + \frac{\partial c_2}{\partial x_D} = 0 \\ \partial a_3\frac{(\vec{c})}{\partial\varphi} + \frac{\partial c_3}{\partial x_D} = 0 \end{cases} \tag{27}$$

with the following initial and boundary conditions:

$$\varphi = 0, \ \vec{c}(x_D, 0) = \vec{c}^{(I)} = 0, \ 0 < x_D < \frac{L}{\frac{\Omega_s}{A}} \tag{28}$$

$$x_D = 0, \ \vec{c}(0,\varphi) = \begin{cases} \vec{c}^{(J)}, \ 0 < \varphi < 1 \\ 0, \quad \varphi > 1 \end{cases} \tag{29}$$

In this paper we applied the methodology of multicomponent chromatography developed by Rhee et al. (1970) to solve the auxiliary system (Equation (27)). The detailed solution procedure is presented in supplementary material.

The chemical components are sorted in ascending order of adsorption constant, *i.e.*:

$$K_1 < K_2 < K_3 \tag{30}$$

The concentration states are written as a function of a parameter ω which decouples the auxiliary system (see supplementary material for details). The characteristic slope $\sigma_{(k)}$ of the k^{th} wave family was calculated as a function of the parameter ω using the expression (Rhee et al., 1970):

$$\sigma_{(k)} = \frac{d\varphi}{dx_D} = \omega_k^{(k)} \prod_{i=1}^{3} \frac{\omega_i^{(k)}}{K_i} \tag{31}$$

The k^{th} shock path is defined by the relation:

$$V_{(k)} = \left(\frac{d\varphi}{dx_D}\right)_s^{(k)} = \omega_k^+ \prod_{i=1}^{k-1} \frac{\omega_i^{(J)}}{K_i} \tag{32}$$

Equation (32) is derived from Rankine-Hugoniot conditions (Rhee et al., 1970). Note that equations 31 and 32 can be applied for any number of components.

After computing all ω waves, we can calculate the concentration waves from the relation (Rhee et al., 1970):

$$K_i c_i = \left(\frac{K_i}{\omega_i} - 1\right) \prod\nolimits_{j=1, j\neq i}^{3} \frac{\frac{K_i}{\omega_j} - 1}{\frac{K_i}{K_j} - 1} \tag{33}$$

Due to the discontinuity in the boundary condition (Equation (29)), two types of wave interactions appear in the solution of the auxiliary system: interactions between rarefaction and shock waves from different families and between rarefaction and shock waves from the same family.

Along the interaction between a rarefaction and a shock wave of different families, the waves are transmitted through each other and their paths change (Rhee et al., 1970). The k^{th} family rarefaction slope after the interaction with a ω_j shock wave is given by:

$$\sigma_{(k)}^{-} = \left(\frac{d\varphi}{dx_D}\right)^{(k)-} = \omega_k^{(k)} \frac{\omega_j^{-}}{K_j} \prod_{i=1, i\neq j}^{k-1} \frac{\omega_i^{(k)}}{K_i} \tag{34}$$

where the superscript – denotes the value of ω_j and $\sigma_{(k)}$ after the shock. A rarefaction wave can cross more than one shock wave. In such cases, we denote the new rarefaction slope as $\sigma_{(k)}^{--}$. Note that for a multicomponent system there will be up to $k-1$ rarefaction-shock interactions for the k^{th} family.

The k^{th} family shock path along the interaction with a ω_j rarefaction is:

$$V_{(k)} = \left(\frac{d\varphi}{dx_D}\right)_s^{(k)} = \omega_k^{+} \frac{\omega_j}{K_j} \prod_{i=1, i\neq j}^{k-1} \frac{\omega_i^{(J)}}{K_i} \tag{35}$$

where ω_j varies continuously along the interaction. Therefore, the shock path is no longer a straight line.

When waves of the same family interact, the rarefaction is adsorbed by the shock wave, *i.e.* it is not transmitted, and the new shock path can be obtained from the relation:

$$V_{(k)} = \left(\frac{d\varphi}{dx_D}\right)_s^{(k)} = \omega_k^{+} \frac{\omega_k^{-}}{K_k} \prod_{i=1}^{k-1} \frac{\omega_i^{(J)}}{K_i} \tag{36}$$

where the superscripts + and – denote the value of ω at the right and at the left state of the shock wave, and ω_k^{+} changes continuously along the interaction. We denote the shock path along an interaction region as $x_{s,r}(\varphi)$, where the subscript s denotes the shock family, and the subscript r denotes the rarefaction family. The shock path $x_{s,r}(\varphi)$ can be calculated integrating equation (36) along the interaction region.

The characteristic diagram of the auxiliary problem solution presenting all wave interactions can be seen in figure (1).

The solution of the auxiliary problem in $x_D \times \varphi$ plane is divided in 16 regions, each one contains either a concentration rarefaction wave or a constant state (Fig. 1). Table 1 summarizes the concentration states in each region of the solution of the auxiliary system.

Concentration profiles of the auxiliary system solution ($c(x_D, \varphi)$) can be calculated for different φ (Fig. 2). We present the solution $c(x_D, \varphi)$ divided in 11 regions, bounded by the end of the slug injection ($\varphi < 1$)

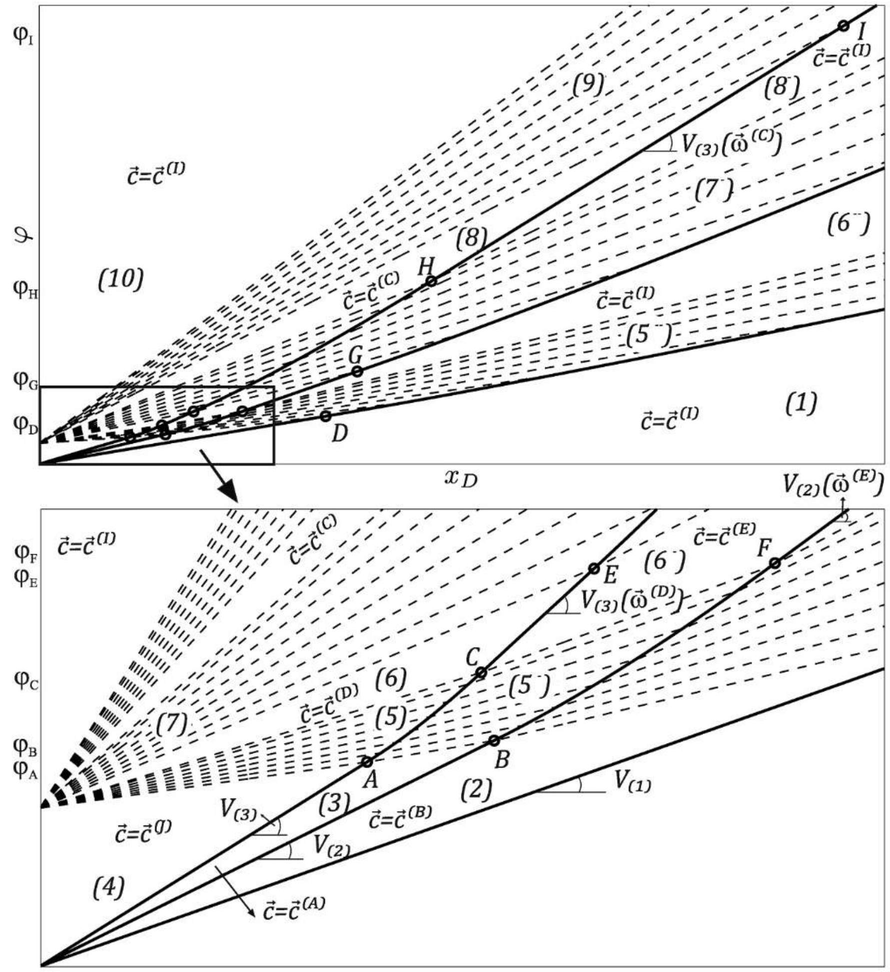

Fig. 1. Characteristic diagram of the solution of the auxiliary problem.

and by the crossing points of the waves (points *A* to *I* in Fig. 1):

$$c(x_D,\varphi)=\begin{cases} c_I, & \varphi<1\\ c_{II}, & 1<\varphi<\varphi_{(A)}\\ c_{III}, & \varphi_{(A)}<\varphi<\varphi_{(B)}\\ c_{IV}, & \varphi_{(B)}<\varphi<\varphi_{(C)}\\ c_V, & \varphi_{(C)}<\varphi<\varphi_{(D)}\\ c_{VI}, & \varphi_{(D)}<\varphi<\varphi_{(E)}\\ c_{VII}, & \varphi_{(E)}<\varphi<\varphi_{(F)}\\ c_{VIII}, & \varphi_{(F)}<\varphi<\varphi_{(G)}\\ c_{IX}, & \varphi_{(G)}<\varphi<\varphi_{(H)}\\ c_X, & \varphi_{(H)}<\varphi<\varphi_{(I)}\\ c_{XI}, & \varphi_{(I)}<\varphi \end{cases} \tag{37}$$

In equation (37) $\varphi_{(Y)}$ represents the coordinate φ of the point Y in figure (3), where $Y = A, B, C, \ldots, I$. The complete description and exact expressions for each part of the solution of the auxiliary system (Equation (37)) is presented in the supplementary material. The concentration waves travel with different velocities in the porous media, which leads to the development of a complete chromatographic cycle. Note that from the beginning of the solution c_X, all three chemical components become completely separated in the reservoir. When $\varphi \to +\infty$, the concentrations of the three components approach their concentration in the water drive.

2.2.2. Solution of the scalar problem (lifting equation)

The second step of the solution procedure is to solve the scalar equation (23). At this point it is considered the transport properties of the displacement (relative permeabilities and viscosity of each phase). The scalar problem solution is built from the solution of the auxiliary system (Equation (37) and Figs. 1–2), and it extends the associated one-phase problem solution (auxiliary system solution) to a two-phase environment.

The following new variables

$$U(s,\vec{c})=\frac{1}{f(s,\vec{c})} \tag{38}$$

$$F(U,\vec{c})=-\frac{s}{f(s,\vec{c})} \tag{39}$$

are applied in equation (23) to get

$$\frac{\partial F(U,\vec{c})}{\partial\varphi}+\frac{\partial U(s,\vec{c})}{\partial x_D}=0 \tag{40}$$

Table 1
Auxiliary system solution.

Region	$\vec{c}$
(1)	Constant state ($\vec{c}^{(I)}$)
(2)	Constant state ($\vec{c}^{(B)}$)
(3)	Constant state ($\vec{c}^{(A)}$)
(4)	Constant state ($\vec{c}^{(J)}$)
(5)	Rarefaction wave ($\vec{c}^{(D)} - \vec{c}^{(J)}$)
(5^-)	Rarefaction wave ($\vec{c}^{(E)} - \vec{c}^{(A)}$)
(5^{--})	Rarefaction wave ($\vec{c}^{(I)} - \vec{c}^{(B)}$)
(6)	Constant state ($\vec{c}^{(D)}$)
(6^-)	Constant state ($\vec{c}^{(E)}$)
(6^{--})	Constant state ($\vec{c}^{(I)}$)
(7)	Rarefaction wave ($\vec{c}^{(C)} - \vec{c}^{(D)}$)
(7^-)	Rarefaction wave ($\vec{c}^{(I)} - \vec{c}^{(E)}$)
(8)	Constant state ($\vec{c}^{(C)}$)
(8^-)	Constant state ($\vec{c}^{(I)}$)
(9)	Rarefaction wave ($\vec{c}^{(I)} - \vec{c}^{(C)}$)
(10)	Constant state ($\vec{c}^{(I)}$)

The initial and boundary conditions (Equations (25) and (26)) for equation (40) are:

$$\varphi=0,\begin{cases} U\to+\infty\\ F\to-\infty \end{cases} \tag{41}$$

$$x_D=0,\begin{cases} U=1\\ F=-1 \end{cases} \tag{42}$$

Equation (40) will be solved for U. Further details regarding the construction of the solution of the lifting equation are presented in the supplementary material.

We define the viscosity of the polymeric solution as:

$$\mu_w(\vec{c})=\mu_w^0\left(1+\sum_{i=1}^{3}\eta_i c_i\right) \tag{43}$$

where μ_w^0 is the pure water viscosity, and the coefficients η_i are experimental parameters that represent the effect of the polymer concentration in aqueous viscosity. We assume that the higher adsorption rate, the higher η_i, *i.e.*:

$$\eta_1<\eta_2<\eta_3 \tag{44}$$

The characteristic diagram for the solution of the lifting equation is presented in Fig. 3. The different waves families and their interactions divide the solution plane in 17 regions. Compared to the concentration solution, there is only one new region (region I^+) and two new rarefaction U-waves appear in regions where the concentrations are constant. One of them is a centered rarefaction wave in region 4 and the other one appears in region I^+ (also a centered wave). The region 4 centered rarefaction wave leads to 3 new interactions between waves at the rear of the slug. Thus, a new type of interaction appears: interaction between rarefaction waves of different families (Rhee et al., 2001).

The U-wave path in regions 5, 7 and 9 (regions where interactions between U-waves and concentration waves take place) is affected by the concentration waves. However, the concentration waves paths are not affected by the U-wave because the trajectories of the concentration waves are not a function of U.

The U-rarefaction slope along its interaction with a concentration wave is given by:

$$\sigma_U(U,\vec{c}(x_D,\varphi))=\frac{\partial F(U,\vec{c}(x_D,\varphi))}{\partial U} \tag{45}$$

There is an infinity slope semi-shock at the end of region (I^+), which is equivalent to the Buckley-Leverett shock (Buckley and Leverett, 1942) for one dimensional two-phase incompressible flow. Table 2 summarizes the solution of the lifting equation.

We present the lifting equation solution for the same φ used to describe the auxiliary system solution. Thus, we have:

$$U(x_D,\varphi)=\begin{cases} U_I, & \varphi<1\\ U_{II}, & 1<\varphi<\varphi_{(A)}\\ U_{III}, & \varphi_{(A)}<\varphi<\varphi_{(B)}\\ U_{IV}, & \varphi_{(B)}<\varphi<\varphi_{(C)}\\ U_V, & \varphi_{(C)}<\varphi<\varphi_{(D)}\\ U_{VI}, & \varphi_{(D)}<\varphi<\varphi_{(E)}\\ U_{VII}, & \varphi_{(E)}<\varphi<\varphi_{(F)}\\ U_{VIII}, & \varphi_{(F)}<\varphi<\varphi_{(G)}\\ U_{IX}, & \varphi_{(G)}<\varphi<\varphi_{(H)}\\ U_X, & \varphi_{(H)}<\varphi<\varphi_{(I)}\\ U_{XI}, & \varphi_{(I)}<\varphi \end{cases} \tag{46}$$

where each solution U_i is built for a value of φ_i presented in Fig. 3. The exact expressions and complete description of equation (46) can be found in the supplementary material.

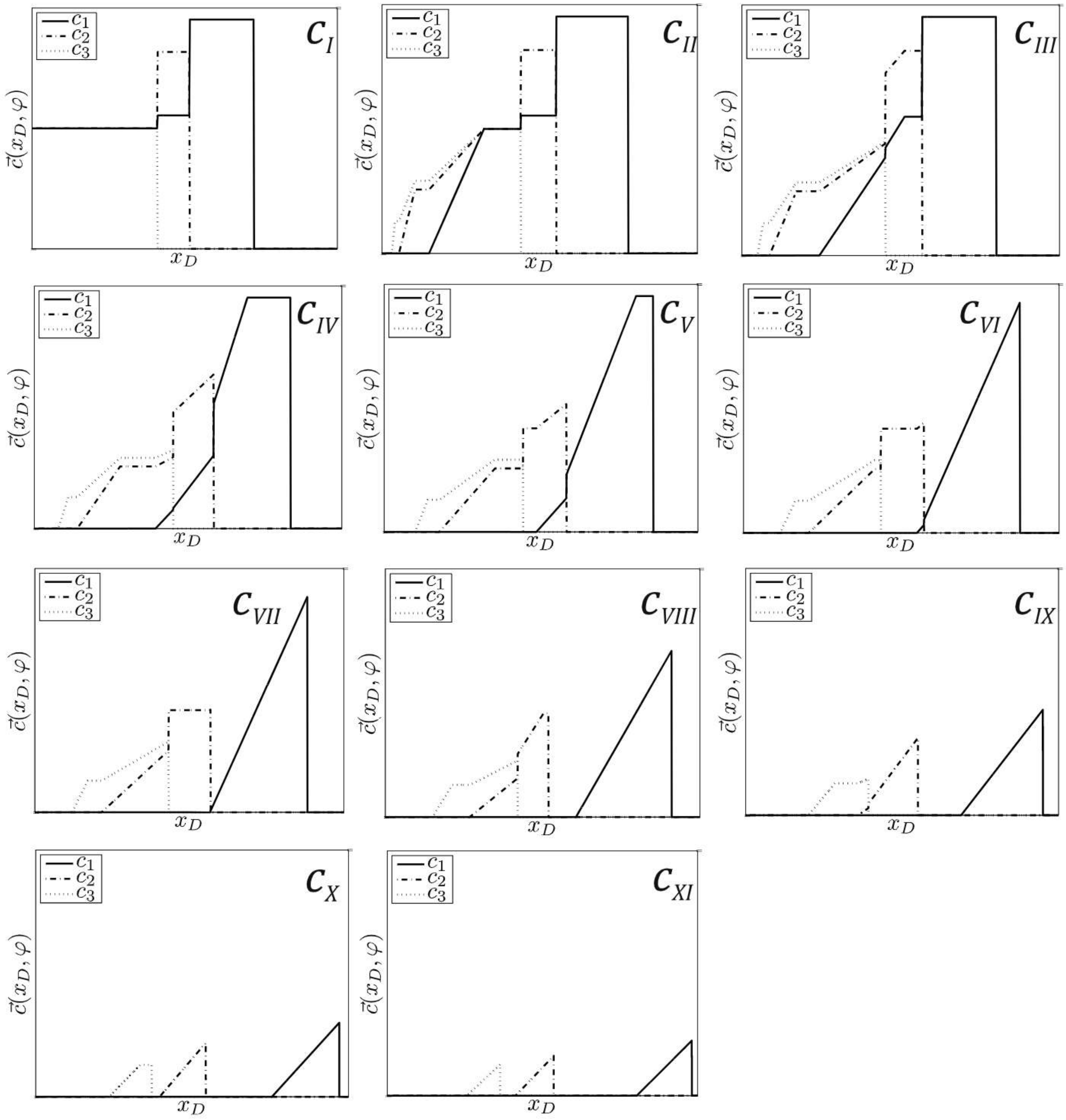

Fig. 2. Concentration profiles for the auxiliary system solution.

2.2.3. *Inverse mapping to $\mathbf{x_D} \times \mathbf{t_D}$ plane*

Once the lifting equation is solved, the inverse mapping of the solution onto the $x_D \times t_D$ plane is developed. From the relation given by:

$$dt_D = \frac{d\varphi}{f(s(x_D,\varphi), c_1(x_D,\varphi), c_2(x_D,\varphi), c_3(x_D,\varphi))} + \frac{s}{f(s(x_D,\varphi), c_1(x_D,\varphi), c_2(x_D,\varphi), c_3(x_D,\varphi))} dx_D \tag{47}$$

it is possible to map equation (37) (solution of the auxiliary system) and equation (46) onto the $x_D \times t_D$ plane.

The path of the k^{th} rarefaction wave in space-time plane is obtained integrating the expression:

$$\lambda_{(k)} = \left(\frac{dt_D}{dx_D}\right)_{(k)} = \frac{1}{f(s(x_D,\varphi), c_1(x_D,\varphi), c_2(x_D,\varphi), c_3(x_D,\varphi))}\sigma_{(k)} + \frac{s}{f(s(x_D,\varphi), c_1(x_D,\varphi), c_2(x_D,\varphi), c_3(x_D,\varphi))} \tag{48}$$

where $\sigma_{(k)}$ is the rarefaction slope in the auxiliary plane.

The shock paths are given by (Pires et al., 2006):

$$D_{(k)} = \left(\frac{dt_D}{dx_D}\right)_{(k)} = \frac{f^{\pm}}{s^{\pm} + V_{(k)}} \tag{49}$$

where the superscripts " + " and "–"indicate the value of the variable before and after the shock wave. The concentration waves follow the same notation used for the auxiliary plane solution ($k = 1, 2, 3$). The velocities of the saturation rarefaction waves will be denoted as $\lambda_{(s)}$ or

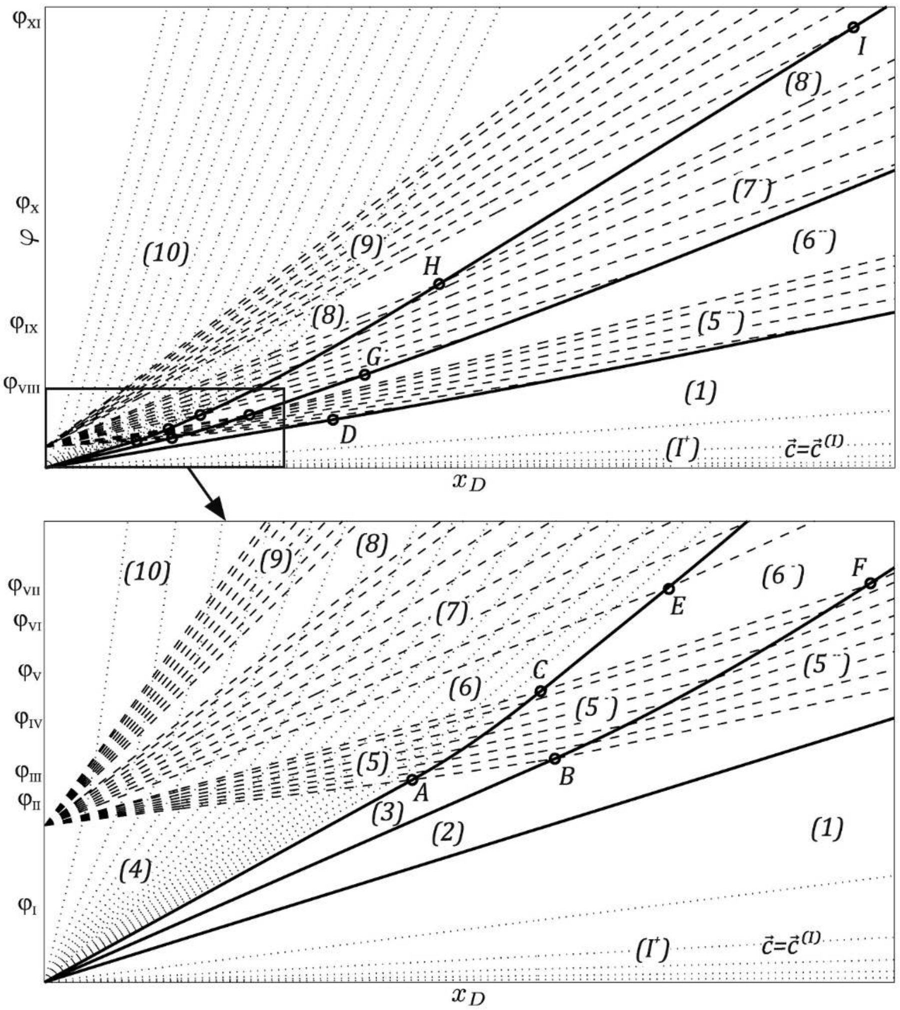

Fig. 3. Characteristic diagram for the lifting equation.

Table 2
Lifting equation solution.

Region	$\boldsymbol{U}$	$\overrightarrow{c}$
(I^{+})	Rarefaction wave $(U^{(1)} - U^{(I+)})$	Constant state $(\overrightarrow{c}^{(I)})$
(1)	Constant state $(U^{(1)})$	Constant state $(\overrightarrow{c}^{(I)})$
(2)	Constant state $(U^{(2)})$	Constant state $(\overrightarrow{c}^{(B)})$
(3)	Constant state $(U^{(3)})$	Constant state $(\overrightarrow{c}^{(A)})$
(4)	Rarefaction wave $(U^{(J)} - U^{(4)})$	Constant state $(\overrightarrow{c}^{(J)})$
(5)	Rarefaction wave $(U^{(J)} - U^{(5)})$	Rarefaction wave $(\overrightarrow{c}^{(D)} - \overrightarrow{c}^{(J)})$
(5^{-})	Rarefaction wave $(U^{(6-)} - U^{(3)})$	Rarefaction wave $(\overrightarrow{c}^{(E)} - \overrightarrow{c}^{(A)})$
(5^{--})	Rarefaction wave $(U^{(6--)} - U^{(5--)})$	Rarefaction wave $(\overrightarrow{c}^{(I)} - \overrightarrow{c}^{(B)})$
(6)	Rarefaction wave $(U^{(J)} - U^{(6)})$	Constant state $(\overrightarrow{c}^{(D)})$
(6^{-})	Constant state $(U^{(6-)})$	Constant state $(\overrightarrow{c}^{(E)})$
(6^{--})	Constant state $(U^{(6--)})$	Constant state $(\overrightarrow{c}^{(I)})$
(7)	Rarefaction wave $(U^{(J)} - U^{(7)})$	Rarefaction wave $(\overrightarrow{c}^{(C)} - \overrightarrow{c}^{(D)})$
(7^{-})	Rarefaction wave $(U^{(8-)} - U^{(6-)})$	Rarefaction wave $(\overrightarrow{c}^{(I)} - \overrightarrow{c}^{(E)})$
(8)	Rarefaction wave $(U^{(J)} - U^{(8)})$	Constant state $(\overrightarrow{c}^{(C)})$
(8^{-})	Constant state $(U^{(8-)})$	Constant state $(\overrightarrow{c}^{(I)})$
(9)	Rarefaction wave $(U^{(J)} - U^{(9)})$	Rarefaction wave $(\overrightarrow{c}^{(I)} - \overrightarrow{c}^{(C)})$
(10)	Rarefaction wave $(U^{(J)} - U^{(10)})$	Constant state $(\overrightarrow{c}^{(I)})$

$\lambda_{(I)}$, and the Buckley-Leverett type shock will be denoted as $D_{(I)}$.

The characteristic diagram for the solution in the $x_D \times t_D$ plane is presented in Fig. 4. The space-time plane is divided in 17 regions, similarly to the solution of the lifting equation (Table 3). Note that the rarefaction paths depend on saturation and concentration (Equation (48)). Thus, in the interaction regions (5), (7) and (9), the concentration rarefactions are not straight lines. Furthermore, the Buckley-Leverett shock wave does not lay on the x_D axis and there is an initial condition (I) region.

Analogously to the solution of the lifting equation, the saturation profile in the $x_D \times t_D$ plane is calculated for 11 different times t_D's. Thus, $s(x_D, t_D)$ is given by:

$$s(x_D, t_D) = \begin{cases} s_I, & t_D < 1 \\ s_{II}, & 1 < t_D < t_{(A)} \\ s_{III}, & t_{(A)} < t_D < t_{(B)} \\ s_{IV}, & t_{(B)} < t_D < t_{(C)} \\ s_V, & t_{(C)} < t_D < t_{(IV)} \\ s_{VI}, & t_{(IV)} < t_D < t_{(E)} \\ s_{VII}, & t_{(E)} < t_D < t_{(F)} \\ s_{VIII}, & t_{(F)} < t_D < t_{(G)} \\ s_{IX}, & t_{(G)} < t_D < t_{(H)} \\ s_X, & t_{(H)} < t_D < t_{(I)} \\ s_{XI}, & t_{(I)} < t_D \end{cases} \tag{50}$$

In equation (50) the notation $t_{(Y)}$ represents the coordinate t_D of point Y in Fig. 4, where $Y = A, B, C, \ldots, I$. The exact expressions for each part of equation (50), water saturation profiles, and solution path in $f \times s$ plane

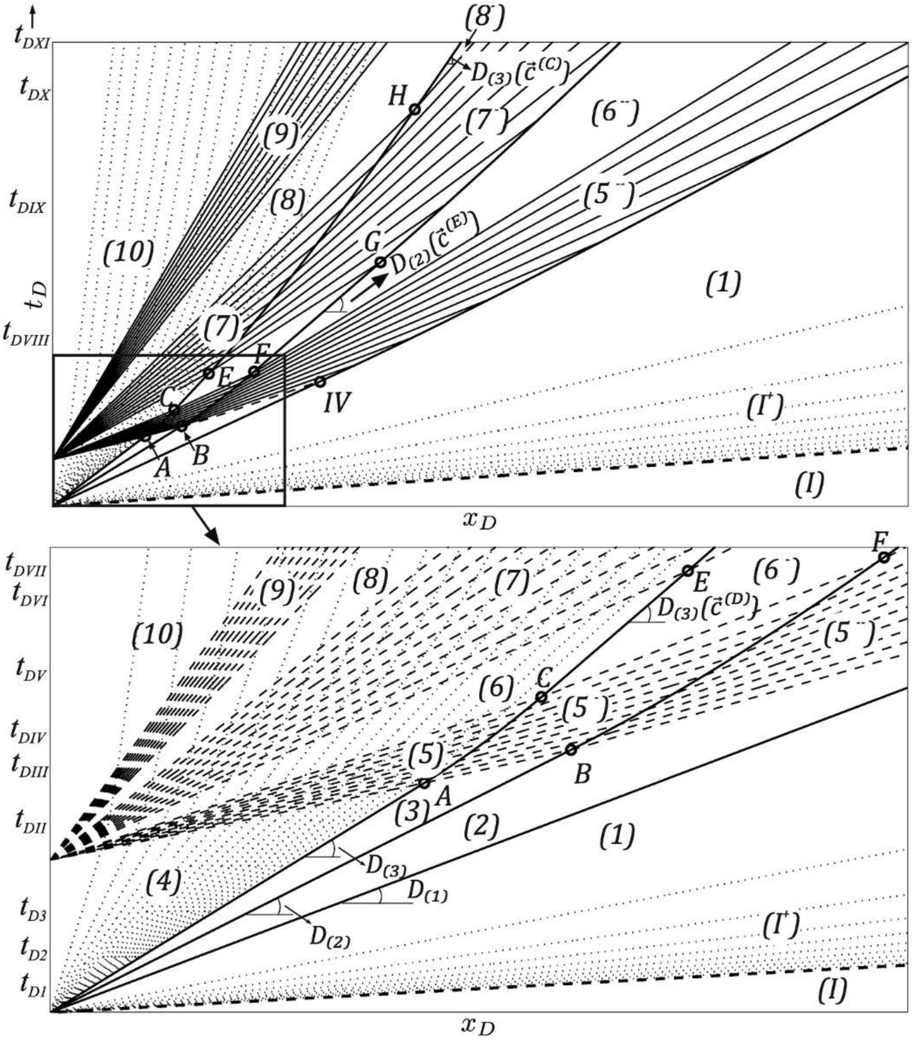

Fig. 4. Characteristic diagram of the solution in the $x_D \times t_D$ plane.

are presented in a supplementary material. From now on we present some important aspects of the solution of equation (50).

During polymer slug injection ($t_D < 1$), the solution is self-similar and is equal to the solution of the continuous polymer injection problem (Dahl et al., 1992) for Langmuir adsorption isotherm. Thus, $s_I(x_D, t_D)$ is given by:

$$s_I(x_D,t_D)=\begin{cases} s^{(J)}, & x_D<\dfrac{t_D}{\lambda_{(s)}\left(s^{(J)},\overrightarrow{c}^{(J)}\right)}\\ s_4(x_D,t_D), & \dfrac{t_D}{\lambda_{(s)}\left(s^{(J)},\overrightarrow{c}^{(J)}\right)}<x_D<\dfrac{t_D}{D_{(3)}}\\ s^{(3)}, & \dfrac{t_D}{D_{(3)}}<x_D<\dfrac{t_D}{D_{(2)}}\\ s^{(2)}, & \dfrac{t_D}{D_{(2)}}<x_D<\dfrac{t_D}{D_{(1)}}\\ s^{(1)}, & \dfrac{t_D}{D_{(1)}}<x_D<\dfrac{t_D}{\lambda_{(s)}\left(s^{(1)},\overrightarrow{c}^{(I)}\right)}\\ s_{I^+}(x_D,t_D), & \dfrac{t_D}{\lambda_{(s)}\left(s^{(1)},\overrightarrow{c}^{(I)}\right)}<x_D<\dfrac{t_D}{\lambda_{(s)}\left(s^{(I^+)},\overrightarrow{c}^{(I)}\right)}\\ s^{(I)}, & x_D>\dfrac{t_D}{\lambda_{(s)}\left(s^{(I^+)},\overrightarrow{c}^{(I)}\right)} \end{cases} \tag{51}$$

The saturation profile for three different t_D, where $t_{D1} < t_{D2} < t_{D3} < 1$, is presented in Fig. 5. The solution path of s_I in $f \times s$ plane is shown in Fig. 6, and the structural formula is: $(J) - (4) \rightarrow (3) \rightarrow (2) \rightarrow (1) - I^{+''} \rightarrow (I)$.

As time evolves, the polymers separate in porous media and water banks appear in the water saturation profiles. Note that when $t_{(H)} < t_D < t_{(I)}$, s_X part of the solution, two components are already splited from the other, thus, two water banks with constant water saturation appear (Fig. 7). In figure (8) the $f \times s$ plane of solution s_X is presented.

For $t_D = t_I$, the rarefaction wave $\lambda_{(3)}$ meets the shock wave $D_{(3)}$ (solution $s_{XI}(x_D,t_D)$). At this part of the solution, the region (8) no longer exists and the constant concentration state is $\overrightarrow{c} = \overrightarrow{c}^{(I)} = 0$.

When $t_D \rightarrow +\infty$, the rarefaction waves are completely absorbed by the shock waves of the same family (Rhee et al., 2001). Therefore, the chemicals concentration and water saturation along all the reservoir are $\overrightarrow{c} = 0$ and $s = s^{(J)}$, respectively.

3. Generalized solution for *n* components

The generalized solution for the problem of slug injection containing *n* dissolved components (Equations (4), (6) and (7)) is built following the same steps presented in the previous section.

The problem in the auxiliary plane is given by:

$$\frac{\partial}{\partial \varphi}\left(\frac{s}{f(s,\overrightarrow{c})}\right)-\frac{\partial}{\partial x_D}\left(\frac{1}{f(s,\overrightarrow{c})}\right)=0 \tag{52}$$

Table 3
Solution in $x_D \times t_D$ plane.

Region	s	$\vec{c}$
(I)	Constant state ($s^{(I)}$)	Constant state ($\vec{c}^{(I)}$)
(I^+)	Rarefaction wave ($s^{(1)} - s^{(I+)}$)	Constant state ($\vec{c}^{(I)}$)
(1)	Constant state ($s^{(1)}$)	Constant state ($\vec{c}^{(I)}$)
(2)	Constant state ($s^{(2)}$)	Constant state ($\vec{c}^{(B)}$)
(3)	Constant state ($s^{(3)}$)	Constant state ($\vec{c}^{(A)}$)
(4)	Rarefaction wave ($s^{(J)} - s^{(4)}$)	Constant state ($\vec{c}^{(J)}$)
(5)	Rarefaction wave ($s^{(J)} - s^{(5)}$)	Rarefaction wave ($\vec{c}^{(D)} - \vec{c}^{(J)}$)
(5^-)	Rarefaction wave ($s^{(6-)} - s^{(3)}$)	Rarefaction wave ($\vec{c}^{(E)} - \vec{c}^{(A)}$)
(5^{--})	Rarefaction wave ($s^{(6--)} - s^{(5--)}$)	Rarefaction wave ($\vec{c}^{(I)} - \vec{c}^{(B)}$)
(6)	Rarefaction wave ($s^{(J)} - s^{(6)}$)	Constant state ($\vec{c}^{(D)}$)
(6^-)	Constant state ($s^{(6-)}$)	Constant state ($\vec{c}^{(E)}$)
(6^{--})	Constant state ($s^{(6--)}$)	Constant state ($\vec{c}^{(I)}$)
(7)	Rarefaction wave ($s^{(J)} - s^{(7)}$)	Rarefaction wave ($\vec{c}^{(C)} - \vec{c}^{(D)}$)
(7^-)	Rarefaction wave ($s^{(8-)} - s^{(6-)}$)	Rarefaction wave ($\vec{c}^{(I)} - \vec{c}^{(E)}$)
(8)	Rarefaction wave ($s^{(J)} - s^{(8)}$)	Constant state ($\vec{c}^{(C)}$)
(8^-)	Constant state ($s^{(8-)}$)	Constant state ($\vec{c}^{(I)}$)
(9)	Rarefaction wave ($s^{(J)} - s^{(9)}$)	Rarefaction wave ($\vec{c}^{(I)} - \vec{c}^{(C)}$)
(10)	Rarefaction wave ($s^{(J)} - s^{(10)}$)	Constant state ($\vec{c}^{(I)}$)

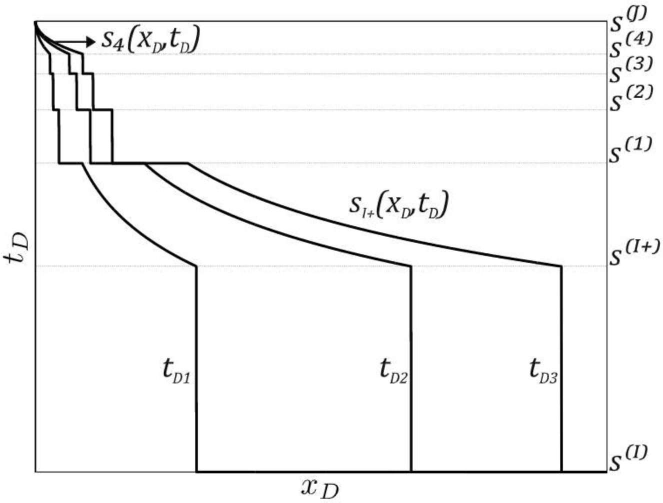

Fig. 5. Saturation profiles of the solution.$s_I(x_D, t_D)$

$$\partial a_i \frac{(\vec{c})}{\partial \varphi} + \frac{\partial c_i}{\partial x_D} = 0,\ i = 1, 2, \ldots, n \tag{53}$$

with the following initial and boundary conditions:

$$\varphi = 0,\ \begin{cases} s(x_D, 0) = s^{(I)}, \\ \vec{c}(x_D, 0) = \vec{c}^{(I)} = 0, 0 <\ x_D < \frac{L}{\frac{\Omega_s}{A}} \end{cases} \tag{54}$$

$$x_D = 0, \begin{cases} f(0, \varphi) = f^{(J)} = 1 & \varphi > 0 \\ \vec{c}(0, \varphi) = \begin{cases} \vec{c}^{(J)}, & 0 < \varphi < 1 \\ 0, & \varphi > 1 \end{cases} \end{cases} \tag{55}$$

where $\vec{c} = [c_1, c_2, \ldots, c_n]$. The general Langmuir adsorption isotherm is given by equation (5) and the adsorption constants also follow:

$$K_1 < K_2 < \ldots < K_n \tag{56}$$

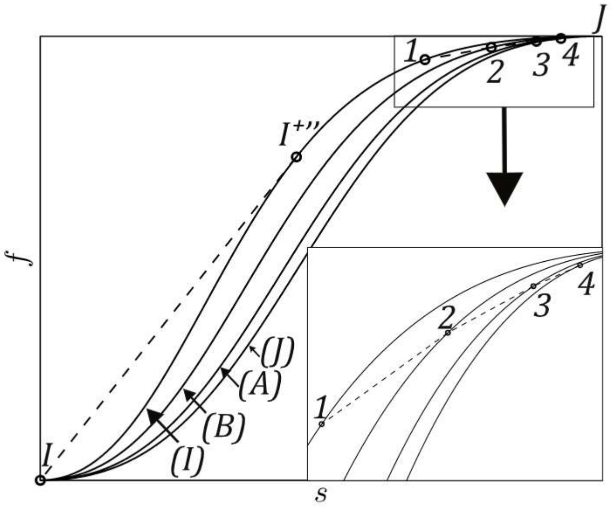

Fig. 6. Solution path of s_I in $f \times s$ plane.

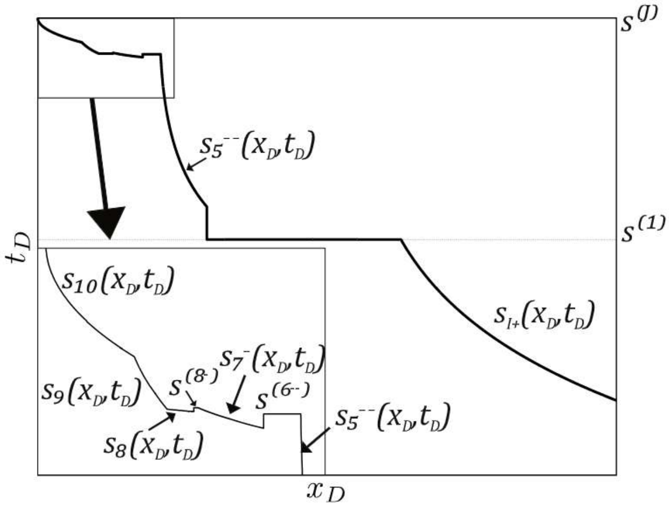

Fig. 7. Saturation profile of the solution.$s_X(x_D, t_D)$

The i^{th} Riemann invariant J_i is calculated from (Rhee et al., 1970):

$$J_i = \frac{K_i a_i(\vec{c})}{K_i - \omega},\ i = 1, 2, \ldots, n \tag{57}$$

and the parameter ω is calculated by (Rhee et al., 1970):

$$\sum_{i=1}^{n} \frac{K_i a_i(\vec{c})}{K_i - \omega} = 1 \tag{58}$$

The constant concentration states are obtained from the following expression:

$$K_i c_i = \left(\frac{K_i}{\omega_i} - 1\right) \prod_{j=1, j \neq i}^{n} \frac{\frac{K_i}{\omega_j} - 1}{\frac{K_i}{K_j} - 1} \tag{59}$$

The path of the waves in the multicomponent solution can also be determined as a function of ω. The rarefaction slopes are given by:

$$\sigma_{(k)} = \frac{d\varphi}{dx_D} = \omega_k^{(k)} \prod_{i=1}^{n} \frac{\omega_i^{(k)}}{K_i} \tag{60}$$

and the shock waves by

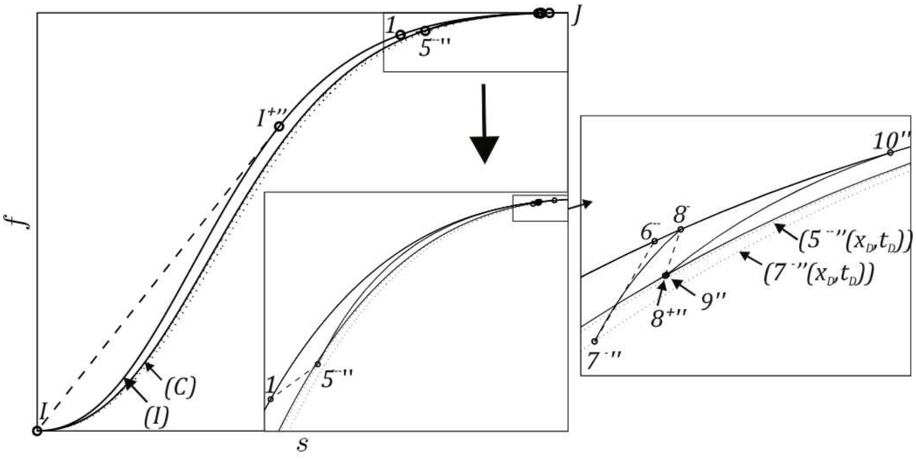

Fig. 8. Solution path of s_X in $f \times s$ plane.

$$V_{(k)} = \left(\frac{d\varphi}{dx_D}\right)_s^{(k)} = \omega_k^+ \prod_{i=1}^{k-1} \frac{\omega_i^{(J)}}{K_i} \tag{61}$$

The interaction between waves are calculated from equations 34–36 (Rhee et al., 1970).

In figure (9) we present the characteristic diagram of the auxiliary system solution for 1, 2 and 3 chemical components dissolved in the slug. For 1 component, the plane is divided into 4 regions (Fig. 9a); for 2 components, the plane is divided into 9 regions (Fig. 9b); for 3 chemicals, there are 16 regions (Figs. 9c and 1), and so on. Thus, for the general case of n dissolved chemical components, the solution divides the $x_D \times \varphi$ plane in $(n+1)^2$ regions. Moreover, note that the fastest rarefaction wave ($k = 1$) interacts with $(n-1)$ shock waves before it is absorbed by the $k = 1$ shock; the $k = 2$ rarefaction wave interacts with $(n-2)$ shock waves and then it is absorbed by the $k = 2$ shock. Thus, the k^{th} rarefaction wave interacts with $(n-k)$ shock waves before it is absorbed by the k^{th} shock wave.

The concentration solution for $\varphi < 1$ is given by:

$$c(x_D,\varphi) = \begin{cases} c_1 = c_1^{(J)}, c_2 = c_2^{(J)}, \ldots, c_n = c_n^{(J)}, & x_D < \dfrac{\varphi}{V_{(n)}} \\ c_1 = c_1^{(A)}, c_2 = c_2^{(A)}, \ldots, c_n = c_n^{(I)}, & \dfrac{\varphi}{V_{(n)}} < x_D < \dfrac{\varphi}{V_{(n-1)}} \\ \vdots & \vdots \\ c_1 = c_1^{(I)}, c_2 = c_2^{(I)}, \ldots, c_n = c_n^{(I)}, & \dfrac{\varphi}{V_{(1)}} < x_D \end{cases} \tag{62}$$

For high values of φ (denoted by φ_∞), all dissolved chemicals will be separated in porous media, and the solution of the auxiliary system is:

$$c(x_D,\varphi) = \begin{cases} c_1 = 0, c_2 = 0, \ldots, c_n = 0, & x_D < \dfrac{\varphi - 1}{\sigma_{(n)}\left(\overrightarrow{\omega}^{(I)}\right)} \\ c_1 = 0, c_2 = 0, \ldots, c_n = c_n^+(x_D,\varphi), & \dfrac{\varphi - 1}{\sigma_{(n)}\left(\overrightarrow{\omega}^{(I)}\right)} < x_D < x_{(n,n)}(\varphi) \\ c_1 = 0, c_2 = 0, \ldots, c_n = c_n^{(I)}, & x_{(n,n)}(\varphi) < x_D < \dfrac{\varphi - \varphi_\infty}{\sigma_{(n-1)}^-\left(\overrightarrow{\omega}^{(I)}\right)} + x_\infty \\ c_1 = 0, \ldots, c_{n-1} = c_{n-1}^-(x_D,\varphi), c_n = c_n^{(I)}, & \dfrac{\varphi - \varphi_\infty}{\sigma_{(\infty)}^-\left(\overrightarrow{\omega}^{(I)}\right)} + x_\infty < x_D < x_{(n-1,n-1)}(\varphi) \\ \vdots & \vdots \\ c_1 = c_1^{(I)}, c_2 = c_2^{(I)}, \ldots, c_n = c_n^{(I)}, & x_{(1,1)}(\varphi) < x_D \end{cases} \tag{63}$$

For intermediate φ, the calculation of the general solution follows the same procedure for three components presented in the previous section. However, due to the high dependence of the solution on the viscosity parameters and adsorption constants, it is not straightforward to write a generalized description of all intermediate regions ($1 < \varphi < \varphi_\infty$).

Applying equations (38) and (39) in the lifting equation (Equation (52)), we have:

$$\frac{\partial F(U,\overrightarrow{c})}{\partial\varphi} + \frac{\partial U(s,\overrightarrow{c})}{\partial x_D} = 0 \tag{64}$$

with the following initial and boundary conditions:

$$\varphi = 0, \begin{cases} U \rightarrow +\infty \\ F \rightarrow -\infty \end{cases} \tag{65}$$

$$x_D = 0, \begin{cases} U = 1 \\ F = -1 \end{cases} \tag{66}$$

Equation (66) can be rewritten as:

$$\frac{\partial F}{\partial U}\frac{\partial U}{\partial\varphi} + \frac{\partial U}{\partial x_D} = -\frac{\partial F}{\partial c_1}\frac{\partial c_1}{\partial\varphi} - \frac{\partial F}{\partial c_2}\frac{\partial c_2}{\partial\varphi} - \ldots - \frac{\partial F}{\partial c_n}\frac{\partial c_n}{\partial\varphi} \tag{67}$$

In regions where the concentrations are constant,

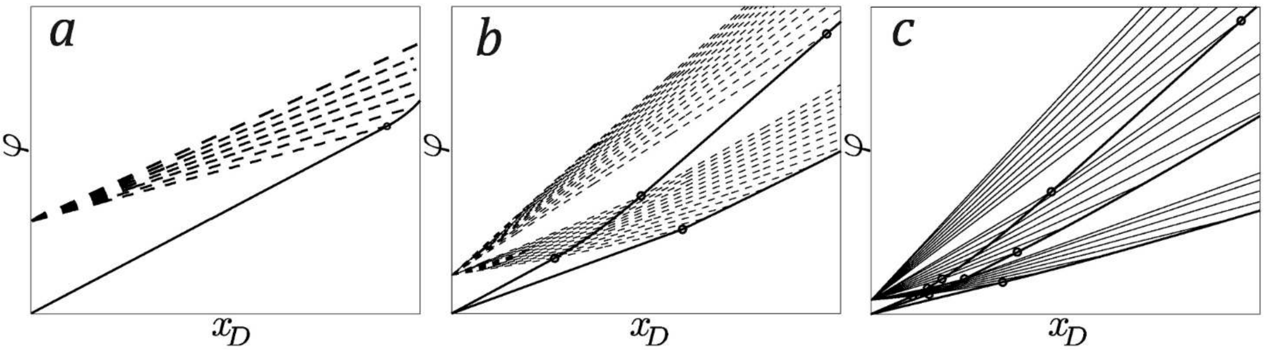

Fig. 9. Auxiliary system solution characteristic diagram for: a) 1 component; b) 2 components; c) 3 components.

$$\frac{\partial c_1}{\partial \varphi} = \frac{\partial c_2}{\partial \varphi} = \ldots = \frac{\partial c_n}{\partial \varphi} = 0 \tag{68}$$

and the lifting equation becomes:

$$\frac{\partial F}{\partial U}\frac{\partial U}{\partial \varphi} + \frac{\partial U}{\partial x_D} = 0 \tag{69}$$

The characteristics velocities are given by:

$$\frac{d\varphi}{dx_D} = \sigma_U = \frac{\partial F(U, \overrightarrow{c})}{\partial U} \tag{70}$$

In regions where the concentration is not constant, along each characteristic U is calculated by:

$$\frac{dU}{dx_D} = -\frac{\partial F}{\partial c_1}\frac{\partial c_1}{\partial \varphi} - \frac{\partial F}{\partial c_2}\frac{\partial c_2}{\partial \varphi} - \ldots - \frac{\partial F}{\partial c_n}\frac{\partial c_n}{\partial \varphi} \tag{71}$$

For the generalized problem, the viscosity of the polymeric solution is defined by:

$$\mu_w(\overrightarrow{c}) = \mu_w^0\left(1 + \sum_{i=1}^{n}\eta_i c_i\right) \tag{72}$$

where:

$$\eta_1 < \eta_2 < \ldots < \eta_n \tag{73}$$

If a U-rarefaction wave at initial concentration state exists, the characteristic diagram of the lifting equation solution for the generalized problem is divided into $[(n+1)^2+1]$ regions. In this case, the solution $U(x_D, t_D)$ for $\varphi < 1$ is:

$$U(x_D,\varphi) = \begin{cases} U^{(J)}, & x_D < \dfrac{\varphi}{\sigma_U\left(U^{(J)},\ \overrightarrow{c}^{(J)}\right)} \\ U_{n+1}(x_D,\varphi), & \dfrac{\varphi}{\sigma_U\left(U^{(J)},\ \overrightarrow{c}^{(J)}\right) < x_D < \dfrac{\varphi}{V_{(n)}}} \\ U^{(n)}, & \dfrac{\varphi}{V_{(n)}} < x_D < \dfrac{\varphi}{V_{(n-1)}} \\ U^{(n-1)}, & \dfrac{\varphi}{V_{(n-1)}} < x_D < \dfrac{\varphi}{V_{(n-2)}} \\ \vdots & \vdots \\ U_{I^+}(x_D,\varphi), & \dfrac{\varphi}{\sigma_U\left(U^{(1)},\ \overrightarrow{c}^{(I)}\right)} < x_D < \dfrac{\varphi}{\sigma_U\left(U^{(I^+)},\ \overrightarrow{c}^{(I)}\right)} \\ U^{(I)}, & x_D \rightarrow +\infty \end{cases} \tag{74}$$

When all chemical components are completely separated in porous media ($\varphi > \varphi_\infty$), the solution of the lifting equation is composed by sequences of a rarefaction wave connecting the curve $F(U, \overrightarrow{c}^{(I)})$ (points $(3n+1)''$, $(3n-1)'$, and $(3n-2)'$ at curve (I) in Fig. 10) to an intermediate concentration point on the curve $F(U, \overrightarrow{c}(x_D,\varphi))$ (point $(3n)''$ at curve 1 and point $(3n-1)''$ at curve 2 in Fig. 10), and a shock wave from the intermediate concentration point on the curve $F(U, \overrightarrow{c}(x_D,\varphi))$ (point $(3n)''$ at curve 1 and point $(3n-1)''$ at curve 2 in Fig. 10), to the curve $F(U, \overrightarrow{c}^{(I)})$ (points $(3n-1)'$ and $(3n-2)'$ at curve (I) in Fig. 10). After the sequence of concentration waves, a U-rarefaction wave in the region (I^+) completes the solution.

The inverse mapping from the auxiliary plane $x_D \times \varphi$ to the plane $x_D \times t_D$ is given by:

$$dt_D = \frac{d\varphi}{f(s(x_D,\varphi),}\ \overrightarrow{c}(x_D,\varphi)) + \frac{s}{f(s(x_D,\varphi),}\ \overrightarrow{c}(x_D,\varphi))\, dx_D \tag{75}$$

The rarefaction waves in the $x_D \times t_D$ plane are found from the expression:

$$\left(\frac{dt_D}{dx_D}\right)_{(k)} = \frac{1}{f(s(x_D,\varphi),}\ \overrightarrow{c}(x_D,\varphi))\left(\frac{d\varphi}{dx_D}\right)_{(k)} + \frac{s}{f(s(x_D,\varphi),}\ \overrightarrow{c}(x_D,\varphi)) \tag{76}$$

and the shock waves by:

$$D_{(k)} = \left(\frac{dt_D}{dx_D}\right)_{(k)} = \frac{f^{\pm}}{s^{\pm} + V_{(k)}} \tag{77}$$

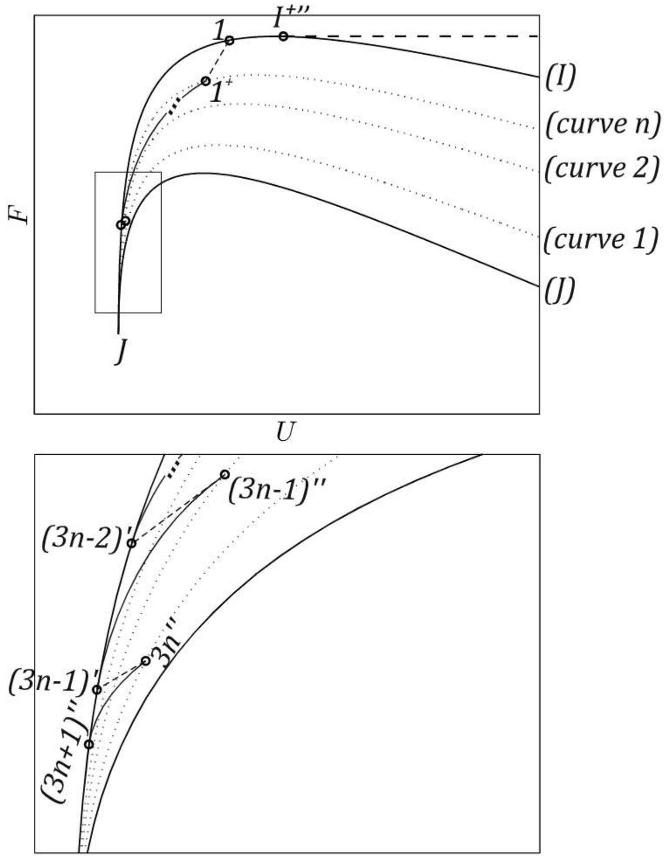

Fig. 10. Schematic solution path in $F \times U$ plane for $t_D > t_\infty$.

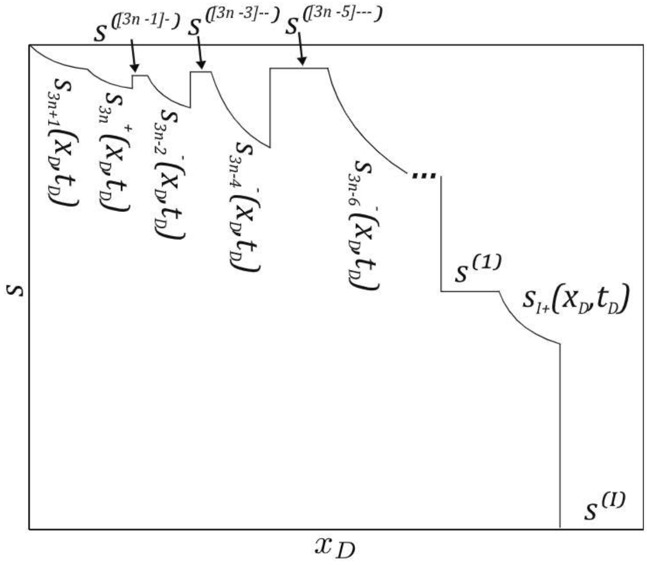

Fig. 11. Schematic saturation profile for $t_D > t_\infty$.

For $t_D < 1$, the solution of the generalized problem is given by:

$$s(x_D,t_D)=\begin{cases} s^{(J)}, & x_D < \dfrac{t_D}{\lambda_{(s)}\left(s^{(J)},\overrightarrow{c}^{(J)}\right)} \\ s_n(x_D,t_D), & \dfrac{t_D}{\lambda_{(s)}\left(s^{(J)},\overrightarrow{c}^{(J)}\right)} < x_D < \dfrac{t_D}{D_{(n)}} \\ s^{(n-1)}, & \dfrac{t_D}{D_{(n-1)}} < x_D < \dfrac{t_D}{D_{(n-2)}} \\ s^{(n-2)}, & \dfrac{t_D}{D_{(n-2)}} < x_D < \dfrac{t_D}{D_{(n-3)}} \\ \vdots & \vdots \\ s^{(1)}, & \dfrac{t_D}{D_{(1)}} < x_D < \dfrac{t_D}{\lambda_{(s)}\left(s^{(1)},\overrightarrow{c}^{(I)}\right)} \\ s_{I^+}(x_D,t_D), & \dfrac{t_D}{\lambda_{(s)}\left(s^{(1)},\overrightarrow{c}^{(I)}\right)} < x_D < \dfrac{t_D}{\lambda_{(s)}\left(s^{(I^+)},\overrightarrow{c}^{(I)}\right)} \\ s^{(I)}, & x_D > \dfrac{t_D}{\lambda_{(s)}\left(s^{(I^+)},\overrightarrow{c}^{(I)}\right)} \end{cases} \tag{78}$$

For long t_D, when all chemicals are completely separated in the reservoir (denoted as $t_D = t_\infty$), the saturation solution is (Fig. 11):

$$s(x_D,t_D)=\begin{cases} s^{(J)}, & x_D < \dfrac{t_D}{\lambda_{(s)}\left(s^{(J)},\overrightarrow{c}=0\right)} \\ s_{3n+1}(x_D,t_D), & \dfrac{t_D}{\lambda_{(s)}\left(s^{(J)},\overrightarrow{c}=0\right)} < x_D < \dfrac{t_D-1}{\lambda_{(n)}\left(s_{3n+1}(x_D,\phi),\overrightarrow{c}=0\right)} \\ s_{3n}^{+}(x_D,t_D), & \dfrac{t_D-1}{\lambda_{(n)}\left(s_{10}(x_D,\phi),\overrightarrow{c}=0\right)} < x_D < x_{n,n}\left(t_D\right) \\ s^{([3n-1]-)}, & x_{n,n}\left(t_D\right) < x_D < \dfrac{t_D-t_{\infty-1}}{\lambda_{(n-1)}^{-}\left(s_{3n-1}(x_D,\phi),\overrightarrow{c}=0\right)} + x_{\infty-1} \\ s_{3n-2}^{-}(x_D,t_D), & \dfrac{t_D-t_{\infty-1}}{\lambda_{(n-1)}^{-}\left(s_{3n-1}(x_D,\phi),\overrightarrow{c}=0\right)} + x_{\infty-1} < x_D < x_{n-1,n-1}(t_D) \\ s^{([3n-3]--)}, & x_{n-1,n-1}(t_D) < x_D < \dfrac{t_D-t_{\infty-2}}{\lambda_{(n-2)}^{--}\left(s^{([3n-3]--)},\overrightarrow{c}=0\right)} - x_{\infty-2} \\ \vdots & \vdots \\ s^{(1)}, & x_{1,1}(t_D) < x_D < \dfrac{t_D}{\lambda_{(s)}\left(s^{(1)},\overrightarrow{c}^{(I)}\right)} \\ s_{I^+}(x_D,t_D), & \dfrac{t_D}{\lambda_{(s)}\left(s^{(1)},\overrightarrow{c}^{(I)}\right)} < x_D < \dfrac{t_D}{\lambda_{(s)}\left(s^{(I^+)},\overrightarrow{c}^{(I)}\right)} \\ s^{(I)}, & x_D > \dfrac{t_D}{\lambda_{(s)}\left(s^{(I^+)},\overrightarrow{c}^{(I)}\right)} \end{cases} \tag{79}$$

Note that when $t_D > t_\infty$, the saturation solution will be a sequence of n rarefaction waves (each one carrying one component) separated by a jump to the curve $f(s,\overrightarrow{c}^{(I)})$ (slope given by equation (77)), and a constant state (pure water bank). Then, there may be a rarefaction wave s_{I^+}, and the Buckley-Leverett shock. Observe that for n components, there will be $(n-1)$ water banks in the solution after all chemical components are separated in the reservoir.

4. Summary and conclusions

In this paper we present the solution for the multicomponent chemical slug injection driven by water in oil reservoirs. The mathematical model is composed by a system of $(n+1)$ hyperbolic equations representing the conservation of water and each chemical component. It was considered that the chemical components can be adsorbed by the rock following Langmuir isotherm.

The system of hyperbolic equations was splitted into an associated one-phase multicomponent problem (auxiliary system), and a scalar hyperbolic equation. This solution extends the multicomponent chromatography theory for a two-phase environment.

The detailed solution was derived for the case of three polymers. First, the problem was splitted and solved in an auxiliary plane; then the solution was mapped on the $x_D \times t_D$ plane. Exact solutions were developed for concentration and saturation, whose profiles clearly show the complete separation of the components in the reservoir (chromatographic cycle) and the development of water banks.

A generalized solution for n components showed that the space-time plane is divided in $(n+1)^2$ regions. After all chemicals are separated in the reservoir, $(n-1)$ pure water regions appear.

The results of this paper can be used to solve other chemical enhanced oil recovery problems, such as alkali-polymer injection, low salinity waterflooding, etc. This solution presents new insights for saturation and concentration behavior in two-phase flows in oil reservoirs: the impact of the chemical separation in the water saturation profiles, the generalized water saturation behavior in a multicomponent injection for long times, and the impact of each adsorption constant in the saturation and concentration profiles. It can also be applied to validate numerical simulators.

CRediT authorship contribution statement

Felipe de O. Apolinário: Methodology, Software, Formal analysis, Investigation, Writing - original draft, Writing - review & editing. **Adolfo P. Pires:** Methodology, Formal analysis, Investigation, Writing - review & editing, Supervision.

Declaration of competing interest

The authors declare that they have no known competing financial interests or personal relationships that could have appeared to influence the work reported in this paper.

Acknowledgements

This study was financed in part by the Coordenação de Aperfeiçoamento de Pessoal de Nivel Superior - Brasil (CAPES) - Finance Code 001.

Appendix A. Supplementary data

Supplementary data to this article can be found online at https://doi.org/10.1016/j.petrol.2020.107939.

References

Adams, W.T., Schievelbein, V.H., 1987. Surfactant flooding carbonate reservoirs. SPE Reservoir Eng. 2 (4), 619–626. https://doi.org/10.2118/12686-PA.

Ali, L., Barrufet, M.A., 1994. Profile modification due to polymer adsorption in reservoir rocks. Energy Fuel. 8 (6), 1217–1222. https://doi.org/10.1021/ef00048a008.

Ali, M., Mahmud, B., 2015. The effects of concentration and salinity on polymer adsorption isotherm at sandstone rock surface. IOP Conf. Ser. Mater. Sci. Eng. 78 (1) https://doi.org/10.1088/1757-899X/78/1/012038.

Algharaib, M., Alajmi, A., Gharbi, R., 2014. Improving polymer flood performance in high salinity reservoirs. J. Petrol. Sci. Eng. 115, 17–23. https://doi.org/10.1016/j.petrol.2014.02.003.

Amro, M.M., El-Sayed, A.-A.H., Al-Homahdi, E.S., Al-Saddique, M.A., Al-Awad, M.N., 2002. Investigation of polymer adsorption on rock surface of highly saline reservoirs. Chem. Eng. Technol. 25 (10), 1005–1013. https://doi.org/10.1002/1521-4125(20021008)25:10<1005::aid-ceat1005>3.0.co;2-p.

Apolinário, F.O., de Paula, A.S., Pires, A.P., 2020. Injection of water slug containing two polymers in porous media: analytical solution for two-phase flow accounting for adsorption effects. J. Petrol. Sci. Eng. 188 https://doi.org/10.1016/j.petrol.2020.106927.

Asghari, K., Nakutnyy, P., 2008. Experimental results of polymer flooding of heavy oil reservoirs. In: Canadian International Petroleum Conference, Calgary, Canada. https://doi.org/10.2118/2008-189.

Bedrikovetsky, P.G., 1982. Displacement of oil by a slug of an active additive forced by water through a stratum. Fluid Dynam. 17 (3), 409–417. https://doi.org/10.1007/BF01091279.

Bedrikovetsky, P.G., 1993. Mathematical Theory of Oil and Gas Recovery. Kluwer Academic Publishers, London.

Braginskaya, G.S., Entov, V.M., 1980. Non-isothermal displacement of oil by a solution of an active additive. Fluid Dynam. 15 (6), 873–880. https://doi.org/10.1007/BF01096638.

Boa, P.M.F., Pires, A.P., 2006. Salt effects on polymer adsorption in chemical flooding of oil reservoirs. In: 11th Brazilian Congress of Thermal Sciences and Engineering, Curitiba, Brazil.

Borazjani, S., Bedrikovetsky, P.G., Farajzadeh, R., 2014. Exact Solution for Non-self-similar Wave-Interaction Problem during Two-phase Four-Component Flow in Porous Media. Abstract and Applied Analysis, 2014. https://doi.org/10.1155/2014/731567.

Borazjani, S., Bedrikovetsky, P.G., Farajzadeh, R., 2016a. Analytical solutions of oil displacement by a polymer slug with varying salinity. J. Petrol. Sci. Eng. 140, 28–40. https://doi.org/10.1016/j.petrol.2016.01.001.

Borazjani, S., Roberts, A.J., Bedrikovetsky, 2016b. Splitting in systems of PDEs for two-phase multicomponent flow in porous media. Appl. Math. Lett. 53, 25–32. https://doi.org/10.1016/j.aml.2015.09.014.

Buckley, S.E., Leverett, M.C., 1942. Mechanism of fluid displacement in sands. Transactions of the AIME 146, 107–116. https://doi.org/10.2118/942107-G, 01.

Claridge, E.L., Bondor, P.L., 1974. A graphical method for calculating linear displacement with mass transfer and continuously changing mobilities. SPE J. 14 (6), 609–618. https://doi.org/10.2118/4673-PA.

Dafermos, C.M., 2000. Hyperbolic Conservation Laws in Continuum Physics. Springer Verlag, Berlin.

Dahl, O., Johansen, T., Tveito, A., Winther, R., 1992. Multicomponent chromatography in a two-phase environment. SIAM J. Appl. Math. 52 (1), 65–104. https://doi.org/10.1137/0152005.

Danq, C.T., Chen, Z.J., Nguyen, N.T.B., Bae, W., Phung, T.H., 2011. Development of isotherm polymer/surfactant adsorption models in chemical flooding. In: SPE Asia Pacific Oil and Gas Conference and Exhibition, Jakarta, Indonesia. https://doi.org/10.2118/147872-MS.

Davison, P., Mentzer, E., 1982. Polymer flooding in north sea reservoirs. SPE J. 22, 353–362. https://doi.org/10.2118/9300-PA, 03.

Entov, V.M., Polishchuk, A.M., 1975. Role of sorption process with the motion of polymer solutions in a porous medium. Fluid Dynam. 10 (3), 422–428. https://doi.org/10.1007/BF01015266.

Entov, V.M., Zazovskii, A.F., 1982. Displacement of oil by a solution of an active and a passive additive. Fluid Dynam. 17 (6), 876–884. https://doi.org/10.1007/BF01090381.

Farajzadeh, R., Bedrikovetsky, P.G., Lotfollahi, M., Lake, L.W., 2016. Simultaneous sorption and mechanical entrapment during polymer flow through porous media. Water Resour. Res. 52 (3), 2279–2298. https://doi.org/10.1002/2015WR017885.

Fayers, F.J., Perrine, R.L., 1958. Mathematical description of detergent flooding in oil reservoirs. In: Fall Meeting of the Society of Petroleum Engineers of AIME, Houston, USA. https://doi.org/10.2118/1132-G.

Hamid, S.A., Muggeridge, A.H., 2018. Analytical solution of polymer slug injection with viscous fingering. Comput. Geosci. 22 (3), 711–723. https://doi.org/10.1007/s10596-018-9721-0.

Helfferich, F.G., 1981. Theory of multicomponent, multiphase displacement in porous media. SPE J. 21, 51–62. https://doi.org/10.2118/8372-PA, 01.

Hirasaki, G.J., 1981. Application of the theory of multicomponent, multiphase displacement to three-component, two-phase surfactant flooding. SPE J. 21 (2), 191–204. https://doi.org/10.2118/8373-PA.

Johansen, T., Winther, R., 1988. The solution of the Riemann problem for a hyperbolic system of conservation laws modeling polymer flooding. SIAM J. Math. Anal. 19 (3), 541–566. https://doi.org/10.1137/0519039.

Johansen, T., Tveito, A., Winther, R., 1989. A Riemann solver for a two-phase multicomponent process. SIAM J. Sci. Stat. Comput. 10 (5), 846–879. https://doi.org/10.1137/0910050.

Johansen, T., Winther, R., 1989. The Riemann problem for multicomponent polymer flooding. SIAM J. Math. Anal. 20 (4), 908–929. https://doi.org/10.1137/0520061.

Johns, R., Orr Jr., F.M., 1996. Miscible gas displacement of multicomponent oils. SPE J. 1 (1), 846–879. https://doi.org/10.2118/30798-PA.

Kargozarfard, Z., Ruai, M., Ayatollahi, S., 2018. Viscous fingering and its effect on areal sweep efficiency during waterflooding: an experimental study. Petrol. Sci. 16 (7), 105–116. https://doi.org/10.1007/s12182-018-0258-6.

Khorsandi, S., Changhe, Q., Johns, R.T., 2016. Displacement efficiency for low salinity polymer flooding including wettability alteration. SPE J. 22, 417–430. https://doi.org/10.2118/179695-PA, 02.

Koh, H., Lee, V.B., Pope, G.A., 2018. Experimental investigation of the effect of polymers on residual oil saturation. SPE J. 23, 1–17. https://doi.org/10.2118/179683-PA, 01.

Lake, L.W., 1989. Enhanced Oil Recovery. Prentice-Hall Inc, Englewood Cliffs.

Langmuir, I., 1918. The adsorption of gases on plane surfaces of glass, mica and platinum. J. Am. Chem. Soc. 40 (9), 1361–1403. https://doi.org/10.1021/ja02242a004.

Logan, J.D., 1994. An Introduction to Nonlinear Partial Differential Equations. John Wiley & Sons Inc, New York.

Lüftenegger, M., Clemens, T., 2017. Chromatography effects in alkali surfactant polymer flooding. In: *SPE Europec in 79th EAGE Conference and Exhibition*, Paris, France. https://doi.org/10.2118/185793-MS.

Maitin, B.K., Volz, H., 1981. Performance of deutsche texaco Ag's oerrel and hankensbuettel polymer floods. In: SPE/DOE Enhanced Oil Recovery Symposium, Tulsa, USA. https://doi.org/10.2118/9794-MS.

Mishra, S., Bera, A., Mandal, A., 2014. Effect of polymer adsorption on permeability reduction in enhanced oil recovery. J. Petrol. Eng. https://doi.org/10.1155/2014/395857.

Needham, R.B., Doe, P.H., 1982. Polymer flooding review. J. Petrol. Technol. 39 (12), 1503–1507. https://doi.org/10.2118/17140-PA.

Ogbeiwi, P., 2018. An approach to waterflood optimization: case study of the reservoir X. J. Petrol. Explor. Prod. Technol. 8 (1), 271–289. https://doi.org/10.1007/s13202-017-0368-5.

Pal, S., Mushtaq, M., Banat, F., Al Sumaiti, A.M., 2018. Review of surfactant-assisted chemical enhanced oil recovery for carbonate reservoirs: challenges and future perspectives. Petrol. Sci. 15 (1), 77–102. https://doi.org/10.1007/s12182-017-0198-6.

Patton, J.T., Coats, K.H., Colegrove, G.T., 1971. Prediction of polymer flood performance. SPE J. 11 (1), 72–84. https://doi.org/10.2118/2546-PA.

de Paula, A.S., Pires, A.P., 2015. Analytical solution for oil displacement by polymer slugs containing salt in porous media. J. Petrol. Sci. Eng. 135, 323–335. https://doi.org/10.1016/j.petrol.2015.09.001.

de Paula, A.S., Apolinário, F.O., Pires, A.P., 2019. Water slug injection containing *n* polymers in porous media. AIChE J. 65 (11) https://doi.org/10.1002/aic.16735.

Pires, A.P., Bedrikovetsky, P.G., Shapiro, A.A., 2006. A splitting technique for analytical modeling of two-phase multicomponent flow in porous media. J. Petrol. Sci. Eng. 51 (1–2), 54–67. https://doi.org/10.1016/j.petrol.2005.11.009.

Pope, G.A., 1980. The application of fractional flow theory to enhanced oil recovery. SPE J. 20 (3), 191–205. https://doi.org/10.2118/7660-PA.

Rhee, H.-K., Aris, R., Amundson, N.R., 1970. On the theory of multicomponent chromatography. Phil. Trans. Roy. Soc. A 267 (1182), 419–455. https://doi.org/10.1098/rsta.1970.0050.

Rhee, H.-K., Aris, R., Amundson, N.R., 2001. First-Order Partial Differential Equations: Theory and Application of Hyperbolic Systems of Quasilinear Equations, vol. 2. Prentience-Hall Inc, Englewood Cliffs.

Ribeiro, P.M., Pires, A.P., 2008. The displacement of oil by polymer slugs considering adsorption effects. In: SPE Annual Technical Conference and Exhibition, Denver, USA.

Seright, R.S., Wang, D., Lerner, N., Nguyen, A., Sabid, J., Tochor, R., 2018. Beneficial relative permeabilities for polymer flooding. In: SPE Improved Oil Recovery Conference, Tulsa, USA. https://doi.org/10.2118/190321-MS.

Sheng, J.J., Leonhardt, B., Azri, N., 2015. Status of polymer-flooding technology. J. Can. Petrol. Technol. 54 (2), 116–126. https://doi.org/10.2118/174541-PA.

Silva, R.C.A., Cardoso, C.B., Pires, A.P., 2007. The role of adsorption isotherms on chemical flooding oil recovery. In: SPE Annual Technical Conference and Exhibition. Anaheim, USA.

Sofia, G.-B., Aliouche, D., 2016. A rheological study of xantham polymer for enhanced oil recovery. J. Macromol. Sci. Part B 55 (8), 793–809. https://doi.org/10.1080/00222348.2016.1207544.

Sorbie, K.S., 1991. Polymer-Improved Oil Recovery. Springer Science and Business Media, New York.

Taber, J.J., Martin, F.D., Seright, R.S., 1997. EOR screening criteria revisited – Part 1: introduction to screening criteria and enhanced oil recovery field projects. SPE Reservoir Eng. 12 (3), 189–198. https://doi.org/10.2118/35385-PA.

Ustick, R.E., 1967. Comparison of polymer flooding and waterflooding at huntington beach, California. J. Petrol. Technol. 19 (9), 1103–1111. https://doi.org/10.2118/1734-PA.

Vicente, B.J., Viatcheslav, I.P., Pires, A.P., 2014. Semi-analytical solution for a hyperbolic system modeling 1D polymer slug flow in porous media. J. Petrol. Sci. Eng. 115, 102–109.

Wachmann, C., 1964. A mathematical theory for the displacement of oil and water by alcohol. SPE J. 4 (3), 250–266. https://doi.org/10.2118/879-PA.

Wagner, D.H., 1982. Equivalence of the euler and Lagrangian equations of gas dynamics for weak solutions. J. Differ. Equ. 68 (1), 118–136. https://doi.org/10.1016/0022-0396(87)90188-4.

Welge, H.J., 1952. A simplified method for computing oil recovery by gas or water drive. J. Petrol. Technol. 4 (4), 91–98. https://doi.org/10.2118/124-G.

Zhao, L., Wu, L.L.Z., Zhang, C., 2016. Analytical model of waterflood sweep efficiency in vertical heterogeneous reservoirs under constant pressure. Math. Probl Eng. https://doi.org/10.1155/2016/6273492, 2016.

Chapter 4 – Mathematical Modeling of Low Salinity Waterflooding in Sandstone Reservoirs: Enhanced Oil Recovery by Multicomponent Cation Exchange

Mathematical Modeling of Low Salinity Waterflooding in Sandstone Reservoirs: Enhanced Oil Recovery by Multicomponent Cation Exchange

Felipe de O. Apolinário (Corresponding Author)

e-mail: felipe_apolinario03@hotmail.com

Universidade Estadual do Norte Fluminense Darcy Ribeiro

Adolfo P. Pires

e-mail: adolfo.puime@gmail.com

Universidade Estadual do Norte Fluminense Darcy Ribeiro

Abstract

Low salinity waterflooding is the injection of water with smaller salt concentration than the connate water. The control of the pH of injection water, and the amount of dissolved monovalent and divalent cations in the water affect the cation exchange in the reservoir and the mobilization of residual oil. This process is modeled by an $(n+2)\times(n+2)$ system of hyperbolic partial differential equations representing the conservation law of each dissolved cation, pH, and water. In this work we present the solution for the problem of low salinity slug injection driven by seawater considering three dissolved cations and pH effects. It was considered that the cations and H^+ adsorbed on the rock follow a Langmuir adsorption isotherm type. The adsorption parameters of the cations depend on the water pH. The introduction of a potential function replacing time as an independent variable splits the original problem into three decoupled problems: a pH equation, a one-phase chromatographic system, and a scalar equation. First, the pH problem is solved, and its solution is used to calculate the one-phase chromatographic problem, and both results are applied in the scalar equation solution. Next, the solution is mapped onto space-time plane. The solution shows that due to the high adsorption rate, the pH effects take place close to the injection point and disappear. Moreover, the high contrast between the adsorption rates creates regions where salinity changes, but these regions disappear. Cations separation in the porous media, similar to a chromatographic cycle, lead to the generation of several small oil and water banks along the reservoir. The oil banks contain residual oil which was mobilized by the cation exchange.

Keywords: Low Salinity Flooding; Multicomponent Cation Exchange; Enhanced Oil Recovery; Conservation Laws; Hyperbolic Systems of Partial Differential Equations.

1. Introduction

Low Salinity waterflooding is a low-cost Enhanced Oil Recovery (EOR) method used to optimize reservoir's production by injecting water with controlled ionic composition and salinity smaller than the connate water (Sheng, 2014). The injection of low salinity water can increase the displacement efficiency up to 38% when compared to injection of seawater (Jerauld *et al.*, 2008).

Several physical phenomena take place in the reservoir when the low salinity water interacts with the reservoir fluid and pore surface. In siliciclastic reservoirs the main phenomena are clay swelling and cation exchange (Morrow and Buckley, 2011). Clay swelling changes relative permeability and increases the displacement efficiency (Tang & Morrow, 1999).

Cation exchange in low salinity waterflooding is the replacement of a divalent by a monovalent cation on the clay mineral surface (which has negative charge) according to the following chemical reaction:

$$((Clay\ Mineral)^{-} - X^{2+})^{+} + Y^{+} \leftrightarrow (Clay\ Mineral)^{-} - Y^{+} + X^{2+} \qquad (1)$$

This phenomenon is directly related to the mobilization of residual oil in low salinity waterflooding processes (Romero *et al.*, 2013). The replacement of divalent by monovalent cations can also change wettability (Morrow & Buckley, 2011), expand double layer (Ligthelm *et al.*, 2009; Lima *et al.*, 2020), increase pH and decrease interfacial tension (McGuire *et al.*, 2005). These effects change the relative permeability curves and increase the recovery factor of the reservoir (Lager *et al.*, 2006). Data collected from 411 coreflooding experiments have shown that better recovery factors are obtained in reservoirs that were originally oil-wet and changed wettability to mixed-wet after the low salinity waterflooding (Aladasani, 2014).

In sandstone reservoirs the clay content, the adsorbed cations on the mineral surface and the dissolved cations in the connate water directly affect the cationic exchange capacity (CEC). CEC is greater where the clay content and the concentration of divalent cations are higher (Austad *et al.*, 2010). The presence of calcium on the clay mineral surface enhances its reactivity. A similar behavior is observed for magnesium, but its reactivity is smaller (Aghaeifar *et al.*, 2015).

Injection water composition also plays an important role on low salinity flooding in sandstone reservoirs. Low concentration of divalent cations in injected water led to greater recovery factors (Austad *et al.,* 2010; Nasralla & Nasr-el-din, 2011; Nasralla & Nasr-el-din, 2014; Xie *et al.*, 2014; Al-Saedi et *al.*, 2018). The pH of the injected water also affects the method. The cation H^+ is a high reactivity monovalent cation (Austad *et al.*, 2010), and changes the adsorption-desorption isotherm of divalent cations on the rock surface. Higher pH enhances the cationic exchange on the rock surface (Aksulu *et al.*, 2012; Xie *et al.*, 2014; Brady *et al.*, 2015).

The cation exchange equilibrium is governed by a modified Langmuir's Adsorption Isotherm (Langmuir, 1918; Akai *et al.*, 2020; Lima *et al.*, 2020). Moreover, the two-phase flow of oil and water containing dissolved cations in a porous media can be modeled by a system of hyperbolic partial differential equations that represents the conservation law of water and of each dissolved ion. It is possible to build water saturation, cation concentration profiles and recovery factor curves from the solution of this system of equations (Jerauld *et al.*, 2008; Borazjani *et al.*, 2016; Khorsandi *et al.*, 2016). These solutions are found by the method of characteristics (Wachmann, 1964; Claridge & Bondor, 1974; Bedrikovestky, 1993). The adsorption of the chemical components on the rock surface results in a delay of the cation-front when compared to the water-front (Patton *et al.*, 1971; Entov & Polischuk, 1975; Pope, 1980; Farajzadeh *et al.*, 2016).

During low salinity waterflooding in sandstone reservoirs, the most active chemical species are the cations Ca^{2+}, Mg^{2+} and Na^{+}, and the anion Cl^{-} (Brady *et al.*, 2015; Dang *et al.*, 2016; Pouryousefy *et al.*, 2016). Balance laws generate a 4×4 system of hyperbolic partial differential equations. For the case of constant concentration injection and neglecting adsorption effects, the solution of the system of equations is self-similar and can be found applying the theory presented in Helfferich (1981). This theory was also used to solve the problem of two-phase flow containing three surfactants dissolved in water (Hirasaki, 1981).

If the adsorption effects are considered, the concentration front of each ion travels with a different velocity due to their different adsorption rates, and analogously to a chromatographic cycle, these components separate in the porous media (Rhee *et al.*, 1970; Luftenegger & Clemens, 2017). In such cases, the solution can be developed generalizing the chromatography theory for two-phase flow (Johansen & Winther, 1989; Dahl *et al.*, 1991).

Low salinity waterflooding usually takes place after a secondary recovery water injection period, or eventually a slug of low salinity water is injected and displaced by seawater (Lager *et al.*, 2008; Seccombe *et al.*, 2010; Mahani *et al.*, 2011). This mathematical problem is modeled by a varying boundary condition. Therefore, the solution is no longer self-similar, and the procedure presented in Dahl *et al.* (1991) can't be applied. The solution of the problem of water slug containing one dissolved chemical component injection displaced by pure water can be developed through the hodograph transformation and written in terms of Riemann Invariants (Bedrikovetsky, 1982; Logan, 1994; Dafermos, 2000; Rhee *et al.*, 2001).

For multicomponent slug injection displaced by water ($(n+1) \times (n+1)$ system of equations), it is necessary to use a different approach. A potential function replacing time as a new independent variable decouples the original system of equations into a system of $n \times n$ partial differential equations, where n is the number of chemical species dissolved; and a partial differential equation that depends on the solution of the $n \times n$ system and on the hydrodynamic properties of the flow in the reservoir. The $n \times n$ system is called auxiliary system and can be solved using the theory of one-phase chromatography (Rhee *et al.*, 1970; Borazjani *et al.*, 2016; Apolinário & Pires, 2021). The hyperbolic equation that depends on the flow properties is called lifting equation (Pires *et al.*, 2006).

The theory developed in Pires *et al.* (2006) is called splitting technique, and it was used to solve several mathematical problems related to enhanced oil recovery (Cardoso *et al.*, 2007; Ribeiro & Pires, 2008; Dutra *et al.*, 2009; Vicente *et al.*, 2014; de Paula & Pires, 2015; Borazjani *et al.*, 2016; Garcia, 2019; de Paula *et al.*, 2019; Apolinário *et al.*, 2020; Apolinário & Pires, 2021), and several other EOR associated mathematical problems.

In this work we present the analytical solution to the problem of the injection of a low salinity slug containing calcium, magnesium, and sodium in a sandstone oil reservoir. The low salinity slug is displaced by seawater and pH effects are considered. Cations' adsorption follows a modified Langmuir's adsorption isotherm, and the anions are not adsorbed by the rock.

2. Mathematical Model

In this section we present the formulation of the one-dimensional two-phase flow problem of low salinity slug injection containing three dissolved cations driven by seawater considering pH effects in a sandstone reservoir. The chemical species in the system are the cations H^+, Ca^{2+}, Mg^{2+} and Na^+, and the anions OH^- and Cl^-. Note that the ions H^+ and OH^- are products of water dissociation. The adsorption sites (clay minerals) are negatively charged, thus only the cationic species adsorb on the pore surface. Further assumptions are:

- Homogeneous porous media;
- Incompressible system;
- Gravitational, dispersive, and capillary effects are negligible;
- Electrical charges in equilibrium.

From the conservation law of water and of each ion, we find:

$$\begin{cases} \frac{\partial s}{\partial t_D} + \frac{\partial f(s,\vec{C})}{\partial x_D} = 0 \\ \frac{\partial\left(c_i s + a_i(\vec{C})\right)}{\partial t_D} + \frac{\partial c_i f(s,\vec{C})}{\partial x_D} = 0, \; i = 1,2,3 \\ \frac{\partial(c_{Cl} s)}{\partial t_D} + \frac{\partial c_{Cl} f(s,\vec{C})}{\partial x_D} = 0 \\ \frac{\partial(c_H s + a_H(c_H))}{\partial t_D} + \frac{\partial c_H f(s,\vec{C})}{\partial x_D} + R_i = 0 \\ \frac{\partial(c_{OH} s)}{\partial t_D} + \frac{\partial c_{OH} f(s,\vec{C})}{\partial x_D} + R_i = 0 \end{cases} \tag{2}$$

where x_D and t_D are dimensionless variables defined as

$$x_D = \frac{x}{\frac{\Omega_S}{A}} \tag{3}$$

$$t_D = \frac{\int_0^t u_T(\tau)d\tau}{\frac{\Omega_S}{A}} \tag{4}$$

in which x is the space coordinate, Ω_s is the low salinity slug volume, t is the time coordinate, and A is the cross-sectional area of the reservoir. In equation (2) s is the water saturation, f is water fractional flow, $\vec{C}$ is the concentration vector $[c_1, c_2, c_3, c_H]$, c_1, c_2 and c_3 are the concentrations of calcium, magnesium and sodium, c_{Cl} is chloride concentration, c_H and c_{OH} are the concentrations of the ions H^+ and OH^-, R_i is the source term related to water ionization, and a_i is the adsorbed concentration of the cation species i, given by a modified Langmuir's adsorption isotherm type (Lima *et al.*, 2020):

$$a_i(\vec{C}) = \frac{\alpha_i(c_H)c_i}{1+\sum_{j=1}^{3}\beta_j(c_H)c_j} \tag{5}$$

in which α_i and β_i are adsorption parameters that depend on the pH following the relations:

$$\alpha_i(c_H) = g_i\left(c_H - \frac{K_w}{c_H}\right)^{k_1} \tag{6}$$

$$\beta_i(c_H) = h_i\left(c_H - \frac{K_w}{c_H}\right)^{k_2} \tag{7}$$

where g_i, k_1, h_i and k_2 are experimental constants, and K_w is the water ionization constant:

$$K_w = c_H c_{OH} \tag{8}$$

In equation (2) a_H is the adsorbed concentration of hydrogen, given by (Lima *et al.*, 2020):

$$a_H(c_H) = \frac{\alpha_H c_H^{n_H}}{1+\beta_H c_H^{m_H}} \tag{9}$$

where α_H, β_H, n_H and m_H are constants related to the hydrogen adsorption rate.

The adsorption parameters are ordered according to the chemical reactivity of the cations on clay surfaces (Austad *et al.*, 2010):

$$H^+ >>> Ca^{2+} > Mg^{2+} > K^+ > Na^+ > Li^+ \quad (10)$$

Thus, in equation (5) we have

$$\alpha_H >>> \alpha_1 > \alpha_2 > \alpha_3 \quad (11)$$

and

$$\beta_H >>> \beta_1 > \beta_2 > \beta_3 \quad (12)$$

In our model we assume that the cations Ca^{2+}, Mg^{2+} and Na^+ are associated with anions Cl^-:

$$c_1 + c_2 + c_3 = 5c_{Cl} \quad (13)$$

and the chloride concentration equation does not have to be solved.

Subtracting the last conservation law (OH^-) from the H^+ balance in system (2), we obtain:

$$\frac{\partial\big((c_H - c_{OH})s + a_H(c_H)\big)}{\partial t_D} + \frac{\partial(c_H - c_{OH})f(s,\vec{C})}{\partial x_D} = 0 \quad (14)$$

From the water ionization constant (Equation 8), we can write OH^- concentration as a function of H^+ concentration:

$$c_{OH} = \frac{K_w}{c_H} \quad (8)$$

Applying equation (15) in equation (14), we find

$$\frac{\partial\left((c_H - \frac{K_w}{c_H})s + a_H(c_H)\right)}{\partial t_D} + \frac{\partial(c_H - \frac{K_w}{c_H})f(s,\vec{C})}{\partial x_D} = 0 \quad (14)$$

Denoting the variable ξ as:

$$\xi(c_H) = c_H - \frac{K_w}{c_H} \tag{15}$$

equation (14) becomes:

$$\frac{\partial\left(\xi s + a_H(c_H)\right)}{\partial t_D} + \frac{\partial \xi f(s,\vec{c})}{\partial x_D} = 0 \tag{16}$$

From the definition of c_{OH} we can write c_H as a function of ξ:

$$c_H = \frac{\xi + \sqrt{\xi^2 + 4K_w}}{2} \tag{17}$$

therefore, it is straightforward to rewrite equations (2), (5)-(7) and (9) as a function of ξ.

Using equations (13) and (16) in the system of equations (2) we obtain the following system of partial differential equations:

$$\begin{cases} \frac{\partial s}{\partial t_D} + \frac{\partial f(s,\vec{c},\xi)}{\partial x_D} = 0 \\ \frac{\partial\left(c_i s + a_i(\vec{c},\xi)\right)}{\partial t_D} + \frac{\partial c_i f(s,\vec{c},\xi)}{\partial x_D} = 0, \ i = 1,2,3 \\ \frac{\partial\left(\xi s + a_H(\xi)\right)}{\partial t_D} + \frac{\partial \xi f(s,\vec{c},\xi)}{\partial x_D} = 0 \end{cases} \tag{18}$$

where $\vec{c} = [c_1, c_2, c_3]$ is the vector containing the cations concentrations.

At the beginning of the low salinity waterflooding ($t_D = 0$), the reservoir is saturated with high salinity water and oil ($s^{(I)}$, $\vec{c}^{(I)}$). At the inlet point ($x_D = 0$) low salinity water ($f^{(J)} = 1$, $\vec{c}^{(J1)}$) with controlled pH ($c_H^{(J1)}$ which leads to $\xi^{(J1)}$ using equation 15) is injected until time t_{HS}. After t_{HS} seawater is injected into the reservoir ($\vec{c}^{(J2)}$,$\xi^{(J2)}$). Therefore, the initial and boundary conditions are:

$$t_D = 0, \begin{cases} s(x_D, t_D = 0) = s^{(I)} \\ \vec{c}(x_D, t_D = 0) = \vec{c}^{(I)} \\ \xi(x_D, t_D = 0) = \xi^{(I)} \end{cases} \tag{19}$$

$$x_D = 0, \begin{cases} f(x_D = 0, t_D) = f^{(J)} = 1 \\ \vec{c}(x_D = 0, t_D) = \begin{cases} \vec{c}^{(J1)}, t_D < t_{HS} \\ \vec{c}^{(J2)}, t_D > t_{HS} \end{cases} \\ \xi(x_D = 0, t_D) = \begin{cases} \xi^{(J1)}, t_D < t_{HS} \\ \xi^{(J2)}, t_D > t_{HS} \end{cases} \end{cases} \quad (20)$$

where $\vec{c}^{(J1)} < \vec{c}^{(J2)} < \vec{c}^{(I)}$. Moreover, we consider that the reservoir is acidic $(pH < 7)$, the low salinity slug is alkaline, and the seawater drive pH will be slightly greater than the low salinity slug pH. Thus, we will have $c_H^{(I)} > 10^{-7}\left[\frac{mol}{L}\right] > c_H^{(J1)} > c_H^{(J2)}$, resulting in $\xi^{(I)} > 0 > \xi^{(J1)} > \xi^{(J2)}$.

2.1. Splitting between thermodynamics and hydrodynamics

Introducing the following potential function (Pires *et al.*, 2006)

$$d\varphi = f(s, \vec{c}, \xi)dt_D - sdx_D \quad (21)$$

in system of equations (18) we find:

$$\frac{\partial}{\partial\varphi}\left(\frac{s}{f(s,\vec{c},\xi)}\right) - \frac{\partial}{\partial x_D}\left(\frac{1}{f(s,\vec{c},\xi)}\right) = 0 \quad (22)$$

$$\frac{\partial a_i(\vec{c},\xi)}{\partial\varphi} + \frac{\partial c_i}{\partial x_D} = 0, i = 1,2,3 \quad (23)$$

$$\frac{\partial a_H(\xi)}{\partial\varphi} + \frac{\partial\xi}{\partial x_D} = 0 \quad (24)$$

Equation (24) is decoupled and is a function of pH only. Equation (23) is a 3×3 auxiliary system that depends on the cations concentrations and the solution of the pH problem (Equation 24). Equation (22) is a function of the hydrodynamics properties of the flow and depends on the solution of the auxiliary system and the solution of the pH problem (Pires *et al.*, 2006). The potential function (Equation 21) replaces time as an independent variable, and the problem is placed on the auxiliary plane $x_D \times \varphi$

(Apolinário & Pires, 2021). Equation (24) is analogous to a one-component chromatography problem, whereas equation (23) is similar to a three-component chromatography problem (Rhee *et al.*, 2001).

The initial and boundary conditions of the problem (22)-(24) can be obtained mapping the conditions given by equations (19)-(20) using equation (21), which leads to:

$$\varphi = -s^{(I)}x_D, \begin{cases} s\left(x_D, -s^{(I)}x_D\right) = s^{(I)}, \\ \vec{c}\left(x_D, -s^{(I)}x_D\right) = \vec{c}^{(I)}, \quad 0 < x_D < \frac{L}{\frac{\Omega_S}{A}} \\ \xi\left(x_D, -s^{(I)}x_D\right) = \xi^{(I)} \end{cases} \tag{25}$$

$$x_D = 0, \begin{cases} f(0,\varphi) = f^{(J)} = 1, \ \varphi > 0 \\ \vec{c}(0,\varphi) = \begin{cases} \vec{c}^{(J1)} \ , 0 < \varphi < \varphi_{HS} \\ \vec{c}^{(J2)}, \ \ \varphi > \varphi_{HS} \end{cases} \\ \xi(0,\varphi) = \begin{cases} \xi^{(J1)} \ , 0 < \varphi < \varphi_{HS} \\ \xi^{(J2)}, \ \ \varphi > \varphi_{HS} \end{cases} \end{cases} \tag{26}$$

Note that in equation (25) the initial condition no longer lays on the x_D axis, but on a straight line with slope given by $-s^{(I)}$.

The algorithm to build the solution to the problem given by equations (22)-(26) is:

- Solution of the pH problem (Equation (24) by the method of characteristics;
- Compute the adsorption parameters $\alpha_i(\xi), \beta_i(\xi),\ i = 1,2,3$ using equations (6) and (7) throughout the auxiliary plane using the pH solution;
- Solution of the auxiliary system (Equation 23) using the one-phase chromatography theory (Rhee *et al.*, 1970);
- Use the solution of the auxiliary system and pH problem to solve the lifting equation problem by the method of characteristics.

After the development of the solution in the auxiliary plane $x_D \times \varphi$, it can be mapped on the $x_D \times t_D$ plane using the expression:

$$dt_D = \frac{d\varphi}{f(s(x_D,\varphi),\vec{c}(x_D,\varphi),\xi(x_D,\varphi))} + \frac{s}{f(s(x_D,\varphi),\vec{c}(x_D,\varphi),\xi(x_D,\varphi))} dx_D \tag{27}$$

where $s(x_D,\varphi)$, $\vec{c}(x_D,\varphi)$ and $\xi(x_D,\varphi)$ are the solutions of water saturation, cations concentrations and pH in the auxiliary plane, respectively.

3. Solution of the pH problem

The pH problem is composed by:

$$\frac{\partial a_H(\xi)}{\partial \varphi} + \frac{\partial \xi}{\partial x_D} = 0 \tag{28}$$

and the following initial and boundary conditions:

$$\varphi = -s^{(I)} x_D, \xi\left(x_D, -s^{(I)} x_D\right) = \xi^{(I)} \tag{29}$$

$$x_D = 0, \xi(0,\varphi) = \begin{cases} \xi^{(J1)} \ , 0 < \varphi < \varphi_{HS} \\ \xi^{(J2)}, \ \ \varphi > \varphi_{HS} \end{cases} \tag{30}$$

The hydrogen adsorption constants (Equation 9) are presented in table (1).

Table 1: Hydrogen adsorption constants (Lima *et al*., 2020)

α_H	14
β_H	1
n_H	0.2
m_H	0.6

Applying the chain rule in equation (28) we obtain:

$$\frac{da_H}{d\xi}\frac{\partial \xi}{\partial \varphi} + \frac{\partial \xi}{\partial x_D} = 0 \tag{31}$$

Therefore, the characteristics slope σ_{pH} is given by:

$$\sigma_{pH} = \frac{d\varphi}{dx_D} = \frac{da_H}{d\xi} \tag{32}$$

From equation (9) and the definition of $c_H(\xi)$ given by equation (17), we can rewrite hydrogen adsorption isotherm as a function of ξ:

$$a_H(\xi) = \frac{\alpha_H\left(\frac{\xi+\sqrt{\xi^2+4K_w}}{2}\right)^{n_H}}{1+\beta_H\left(\frac{\xi+\sqrt{\xi^2+4K_w}}{2}\right)^{m_H}} \tag{33}$$

Thus, the exact expression for the characteristic slope is:

$$\begin{aligned} \sigma_{pH} = \frac{da_H}{d\xi} = {} & \frac{\frac{\alpha_H}{2^{n_H}} n_H \left(\xi+\sqrt{\xi^2+4K_w}\right)^{n_H-1}\left(1+\frac{\xi}{\sqrt{\xi^2+4K_w}}\right)}{1+\beta_H\left(\frac{\xi+\sqrt{\xi^2+4K_w}}{2}\right)^{m_H}} - \\ & \frac{\frac{\alpha_H\beta_H m_H}{2^{n_H+m_H}}\left(\xi+\sqrt{\xi^2+4K_w}\right)^{n_H+m_H-1}\left(1+\frac{\xi}{\sqrt{\xi^2+4K_w}}\right)}{\left[1+\beta_H\left(\frac{\xi+\sqrt{\xi^2+4K_w}}{2}\right)^{m_H}\right]^2} \end{aligned} \tag{34}$$

The shock waves are calculated using the Rankine-Hugoniot condition:

$$V_{pH} = \frac{[a_H]}{[\xi]} = \frac{a_H(\xi^{(+)})-a_H(\xi^{(-)})}{\xi^{(+)}-\xi^{(-)}} \tag{35}$$

where the superscripts $+$ and $-$ represent a condition before and after the shock wave, respectively.

The characteristic diagram of the solution of the pH problem (Equations 28-30) is presented in figure (1) and it is divided in two parts: the injection of the low salinity slug (Figure 1a), and the seawater drive after the low salinity slug (Figure 1b).

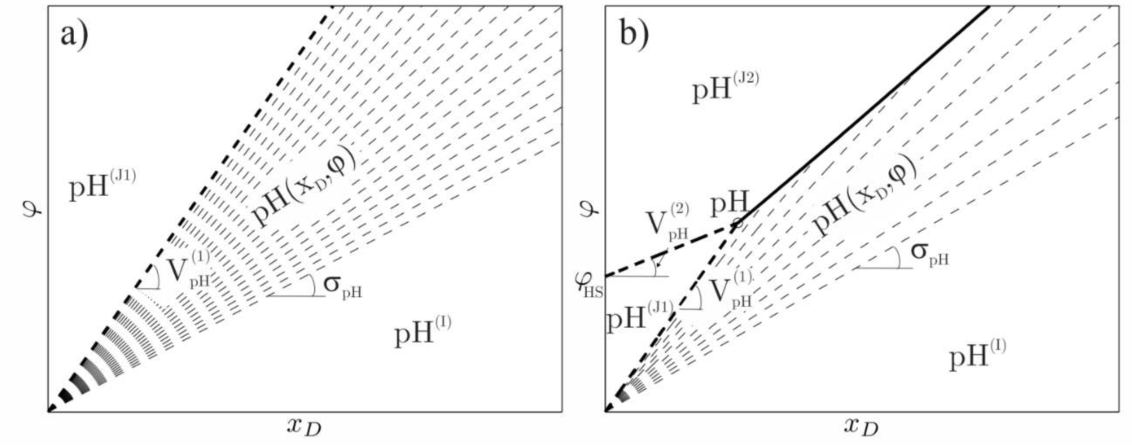

Figure 1: Characteristic diagram of the pH solution: a) during low salinity slug injection; b) during the injection of seawater

In figure (1), the thick dashed lines represent shock paths, the thin dashed lines are the rarefaction wave, and the thick continuous line is a shock path with varying velocity. The shock slope $V_{pH}^{(1)}$ is given by:

$$V_{pH}^{(1)} = \frac{a_H(\xi^{(J1)}) - a_H(\xi^{(-)})}{\xi^{(J1)} - \xi^{(-)}} \tag{36}$$

The shock wave $V_{pH}^{(1)}$ is a semi-shock where $\xi(x_D, \varphi) = \xi^{(-)}$ along its path (Rhee & Amundson, 1970). The rarefactions slopes are calculated using equation (34) with ξ varying from $\xi^{(-)}$ to $\xi^{(I)}$.

After the injection of the low salinity slug ($\varphi > \varphi_{HS}$, Figure 1b), the boundary condition changes and a shock wave with slope $V_{pH}^{(2)}$ arises at $\varphi = \varphi_{HS}$. The shock slope $V_{pH}^{(2)}$ is calculated applying the Rankine Hugoniot condition (Equation 35):

$$V_{pH}^{(2)} = \frac{a_H(\xi^{(J2)}) - a_H(\xi^{(J1)})}{\xi^{(J2)} - \xi^{(J1)}} \tag{37}$$

At point (x_{pH}, φ_{pH}) in figure (1b), the shock waves with slopes $V_{pH}^{(1)}$ and $V_{pH}^{(2)}$ interact generating a new shock wave with slope

$$V_{pH}^{(-)} = \frac{a_H(\xi^{(J2)}) - a_H(\xi^{(-)})}{\xi^{(J2)} - \xi^{(-)}} \tag{38}$$

This shock interacts with the rarefaction wave changing the shock path ($x_{pH}^{-}(\varphi)$). The derivative of the new shock path can be calculated by the relation:

$$V_{pH}^{(-)}(\xi) = \frac{da_H}{d\xi}(\xi) = \frac{a_H(\xi^{(J2)}) - a_H(\xi)}{\xi^{(J2)} - \xi}, \quad \xi^{(J2)} < \xi < \xi^{(I)} \tag{39}$$

The solution of the pH problem (Equations 28-30) is divided in three parts:

$$\xi(x_D, \varphi) = \begin{cases} \xi_I, \ x_D < \varphi_{HS} \\ \xi_{II}, \ , \varphi_{HS} < x_D < \varphi_{PH} \\ \xi_{III}, x_D > \varphi_{PH} \end{cases} \tag{40}$$

For $\varphi < \varphi_{HS}$ (solution ξ_I):

$$\xi_I(x_D, \varphi) = \begin{cases} \xi^{(J1)}, x_D < \frac{\varphi}{V_{pH}^{(1)}} \\ \xi(x_D, t_D), \frac{\varphi}{V_{pH}^{(1)}} < x_D < \frac{\varphi}{\sigma_{pH}(\xi^{(I)})} \\ \xi^{(I)}, \frac{\varphi}{\sigma_{pH}(\xi^{(I)})} < x_D \end{cases} \tag{41}$$

If $\varphi_{HS} < \varphi < \varphi_{pH}$ (solution ξ_{II}) the solution is:

$$\xi_{II}(x_D, \varphi) = \begin{cases} \xi^{(J2)}, x_D < \frac{\varphi - \varphi_{HS}}{V_{pH}^{(2)}} \\ \xi^{(J1)}, \frac{\varphi - \varphi_{HS}}{V_{pH}^{(2)}} < x_D < \frac{\varphi}{V_{pH}^{(1)}} \\ \xi(x_D, t_D), \frac{\varphi}{V_{pH}^{(1)}} < x_D < \frac{\varphi}{\sigma_{pH}(\xi^{(I)})} \\ \xi^{(I)}, \frac{\varphi}{\sigma_{pH}(\xi^{(I)})} < x_D \end{cases} \tag{42}$$

Finally, when solution ξ_{III} is:

$$\xi_{III}(x_D, \varphi) = \begin{cases} \xi^{(J2)}, x_D < x_{pH}^{-}(\varphi) \\ \xi(x_D, t_D), x_{pH}^{-}(\varphi) < x_D < \frac{\varphi}{\sigma_{pH}(\xi^{(I)})} \\ \xi^{(I)}, \frac{\varphi}{\sigma_{pH}(\xi^{(I)})} < x_D \end{cases} \tag{43}$$

The characteristics velocities for $\xi^{(J2)} < \xi < \xi^{(I)}$, and the solution path for $\varphi < \varphi_{HS}$ and for $\varphi > \varphi_{HS}$ are presented in figure 2.

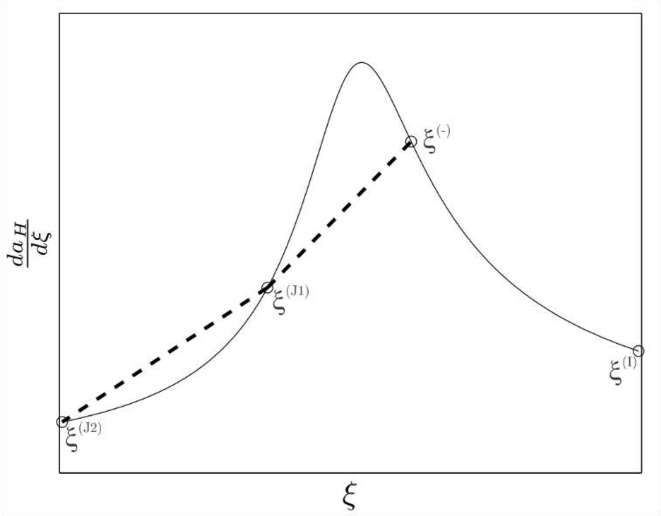

Figure 2: Characteristics velocities for $\xi^{(J2)} < \xi < \xi^{(I)}$ and solution path for pH problem

4. Solution of the auxiliary system

The auxiliary system, given by:

$$\frac{\partial a_i(\vec{c},\xi)}{\partial\varphi} + \frac{\partial c_i}{\partial x_D} = 0, i = 1,2,3 \quad (44)$$

with the following initial and boundary conditions:

$$\varphi = -s^{(I)}x_D,\ \vec{c}\left(x_D, -s^{(I)}x_D\right) = \vec{c}^{(I)},\ \ 0 < x_D < \frac{L}{\frac{\Omega_S}{A}} \quad (45)$$

$$x_D = 0, \vec{c}(0,\varphi) = \begin{cases} \vec{c}^{(J1)}\ , 0 < \varphi < \varphi_{HS} \\ \vec{c}^{(J2)},\ \ \varphi > \varphi_{HS} \end{cases} \quad (46)$$

is solved after the pH problem.

The first step is the calculation of the adsorption parameters $\alpha_i(\xi)$ and $\beta_i(\xi)$ on the $x_D \times \varphi$ plane according to the solution of the pH problem through the relations:

$$\alpha_i(c_H) = g_i \xi^{k_1} \tag{47}$$

$$\beta_i(c_H) = h_i \xi^{k_2} \tag{48}$$

Constants g_i, h_i, k_1 and k_2 were obtained interpolating the data presented in Lima *et al*. (2010) and Lima *et al*. (2020) (Table 2).

Table 2: Constants for parameters α_i and β_i

g_1	0.012
g_2	0.06
g_3	0.12
h_1	0.0325
h_2	0.039
h_3	0.065
k_1	−0.568
k_2	−0.549

The problem defined by equations (44)-(46) is analogous to the system of partial differential equations that models one-phase multicomponent chromatography processes. The solution procedure for multicomponent Langmuir adsorption isotherm is presented in Rhee *et al*. (2001). In this work we followed these steps to extend the multicomponent chromatography theory to pH-dependent adsorption coefficients.

The Riemann invariants J_i are calculated by:

$$J_i(\vec{c}, \xi) = \frac{\beta_i(\xi)\alpha_i(\vec{c}, \xi)}{\alpha_i(\xi) - \omega}, \; i = 1,2,3 \tag{49}$$

where ω is a characteristic parameter of the problem. It is also known that (Rhee *et al.*, 2001):

$$\sum_{i=1}^{3} J_i = 1 \tag{50}$$

Thus,

$$\sum_{i=1}^{3} \frac{\beta_i(\xi) a_i(\vec{c},\xi)}{\alpha_i(\xi)-\omega} = 1 \tag{51}$$

Equation (51) is an n-order polynomial in ω, and n is the number of the dissolved cations in the water ($n = 3$ in this example). This polynomial has n distinct positive roots for any concentration and pH state. For a fixed pH condition and a concentration state $\vec{c} = [c_1, c_2, c_3]$ there is only one vector $\vec{\omega} = [\omega_1, \omega_2, \omega_3]$, where its components are the roots of equation (51) (Rhee *et al.*, 2001; Apolinário & Pires, 2021). Thus, equation (51) maps the concentration state on the ω-space. In a constant pH region, all concentrations change along a $\vec{c}$-wave but only one ω changes. In a region where the pH changes, the coefficients α_i and β_i also change, and therefore all components of $\vec{\omega}$ change.

The initial and boundary conditions (Equations 45-46) are constant pH regions ($pH^{(I)}$, and $pH^{(J1)}$ and $pH^{(J2)}$ respectively), therefore it can be mapped on the ω-space solving equation (51) for each condition, which will result in states $\vec{\omega}^{(I)}$, $\vec{\omega}^{(J1)}$ and $\vec{\omega}^{(J2)}$.

The characteristic slopes of the kth rarefaction family $\sigma_{(k)}$ can also be written as a function of ω (Rhee *et al.*, 2001; Apolinário & Pires, 2021):

$$\sigma_{(k)}(\omega_k, \xi) = \omega_k(\xi) \prod_{j=1}^{3} \frac{\omega_j(\xi)}{\alpha_j(\xi)} \tag{52}$$

For a constant pH, if $\omega_k^{(k+1)} < \omega_k^{(k)}$, we have $\sigma_{(k)}\left(\omega_k^{(k+1)}\right) > \sigma_{(k)}\left(\omega_k^{(k)}\right)$, which leads to a rarefaction wave whose slope is defined by equation (52). In this case, ω_k changes from $\omega_k^{(k+1)}$ to $\omega_k^{(k)}$, and all other $\omega_{j\neq k}$ remain constant. For the case of a constant pH and $\omega_k^{(k+1)} > \omega_k^{(k)}$, a shock wave from $\omega_k^{(k+1)}$ to $\omega_k^{(k)}$ appears, and all other $\omega_{j\neq k}$ remain constant. In this case, the shock slope $V_{(k)}$ is defined by:

$$V_{(k)}(\omega_k, \xi) = \omega_k^{+}(\xi) \prod_{j=1}^{3} \frac{\omega_j^{-}(\xi)}{\alpha_j(\xi)} = \omega_k^{-}(\xi) \prod_{j=1}^{3} \frac{\omega_j^{+}(\xi)}{\alpha_j(\xi)} \tag{53}$$

Note that the characteristic and shock speeds depend on the pH of the media. Therefore, when a k^{th} family wave crosses a pH wave, the new pH will change the concentration (and $\vec{\omega}$), and the characteristic or the shock slope of the k^{th} family.

In regions where pH varies, the compatibility condition (Rhee *et al.*, 2001) for non-isothermal chromatography is valid, and therefore for any pH wave (either shock or rarefaction wave), here is a concentration wave with same velocity. So, for a pH rarefaction wave interacting with concentration characteristics, we must solve the 3 × 3 system of equations:

$$\sigma_{(1)}(\omega_1, \xi) = \sigma_{pH}(\xi) = \omega_1(\xi) \prod_{j=1}^{3} \frac{\omega_j(\xi)}{\alpha_j(\xi)} \tag{54}$$

$$\sigma_{(2)}(\omega_1, \xi) = \sigma_{pH}(\xi) = \omega_2(\xi) \prod_{j=1}^{3} \frac{\omega_j(\xi)}{\alpha_j(\xi)} \tag{55}$$

$$\sigma_{(3)}(\omega_1, \xi) = \sigma_{pH}(\xi) = \omega_3(\xi) \prod_{j=1}^{3} \frac{\omega_j(\xi)}{\alpha_j(\xi)} \tag{56}$$

where ω_1, ω_2 and ω_3 are the unknowns. In the case of a pH shock wave, we must solve the following system for ω_1, ω_2 and ω_3:

$$V_{(1)}(\omega_1, \xi) = V_{pH} = \omega_1(\xi^+) \prod_{j=1}^{3} \frac{\omega_j(\xi^-)}{\alpha_j(\xi^-)} = \omega_1(\xi^-) \prod_{j=1}^{3} \frac{\omega_j(\xi^+)}{\alpha_j(\xi^+)} \tag{57}$$

$$V_{(2)}(\omega_2, \xi) = V_{pH} = \omega_2(\xi^+) \prod_{j=1}^{3} \frac{\omega_j(\xi^-)}{\alpha_j(\xi^-)} = \omega_2(\xi^-) \prod_{j=1}^{3} \frac{\omega_j(\xi^+)}{\alpha_j(\xi^+)} \tag{58}$$

$$V_{(3)}(\omega_3, \xi) = V_{pH} = \omega_3(\xi^+) \prod_{j=1}^{3} \frac{\omega_j(\xi^-)}{\alpha_j(\xi^-)} = \omega_3(\xi^-) \prod_{j=1}^{3} \frac{\omega_j(\xi^+)}{\alpha_j(\xi^+)} \tag{59}$$

The initial condition $\vec{\omega}^{(I)}$ is calculated using $\xi^{(I)}$. For $\varphi < \varphi_{HS}$, the boundary condition $\vec{\omega}^{(J1)}$ is determined using $\xi^{(J1)}$. The boundary condition waves interact with the self-similar part of the pH solution, resulting in a new state $\vec{\omega}^{(J1-)}$. The conditions $\vec{\omega}^{(I)}$ and $\vec{\omega}^{(J1-)}$ are used to compute the ω-waves using chromatography theory (Rhee *et al.*, 1970). Table 3 summarizes the $\vec{\omega}$ solution for $\varphi < \varphi_{HS}$.

Table 3: Concentration solution for $\varphi < \varphi_{HS}$

Boundary condition	$\omega_1^{(J1)}$	$\omega_2^{(J1)}$	$\omega_3^{(J1)}$
pH interaction	$\omega_1^{(J1-)}$	$\omega_2^{(J1-)}$	$\omega_3^{(J1-)}$
ω_3-wave	$\omega_1^{(J1-)}$	$\omega_2^{(J1-)}$	$\omega_3^{(I)}$
ω_2-wave	$\omega_1^{(J1-)}$	$\omega_2^{(I)}$	$\omega_3^{(I)}$
ω_1-wave (initial condition)	$\omega_1^{(I)}$	$\omega_2^{(I)}$	$\omega_3^{(I)}$

Seawater injection starts at $\varphi = \varphi_{HS}$ and the boundary condition changes to $(J2)$. The pH solution for $\varphi > \varphi^{HS}$ is composed by two shocks and a rarefaction wave (Section 3). The pH solution rear shock wave interacts with the boundary condition $(J2)$ ω-waves. We will denote the ω-state before the pH-shock as $\vec{\omega}^{(J2)}$ and the ω-state after the shock as $\vec{\omega}^{(J2-)}$. The condition $\vec{\omega}^{(J2-)}$ and state $\vec{\omega}^{(J1)}$ are used to compute the concentration waves at the rear of the low salinity slug. Table 4 presents the ω-waves solution for $\varphi > \varphi_{HS}$.

Table 4: Concentration solution for $\varphi > \varphi_{HS}$

Boundary condition $(J2)$	$\omega_1^{(J2)}$	$\omega_2^{(J2)}$	$\omega_3^{(J2)}$
pH shock wave (rear)	$\omega_1^{(J2-)}$	$\omega_2^{(J2-)}$	$\omega_3^{(J2-)}$
ω_3-wave (rear)	$\omega_1^{(J2-)}$	$\omega_2^{(J2-)}$	$\omega_3^{(J1)}$
ω_2-wave (rear)	$\omega_1^{(J2-)}$	$\omega_2^{(J1)}$	$\omega_3^{(J1)}$
ω_1-wave (boundary condition $(J1)$)	$\omega_1^{(J1)}$	$\omega_2^{(J1)}$	$\omega_3^{(J1)}$
pH-waves (front)	$\omega_1^{(J1-)}$	$\omega_2^{(J1-)}$	$\omega_3^{(J1-)}$
ω_3-wave (front)	$\omega_1^{(J1-)}$	$\omega_2^{(J1-)}$	$\omega_3^{(I)}$
ω_2-wave (front)	$\omega_1^{(J1-)}$	$\omega_2^{(I)}$	$\omega_3^{(I)}$
ω_1-wave (initial condition)	$\omega_1^{(I)}$	$\omega_2^{(I)}$	$\omega_3^{(I)}$

When φ increases, the ω-waves from the rear of the slug interact with the pH waves from the front of the low salinity slug. The new wave paths along and after the interaction can be computed using equations (54)-(59). The transmitted waves from the rear of the slug will interact with the waves from the front of the low salinity slug, leading to several types of interactions: transmission of a rarefaction wave through a shock wave of a different family, transmission of two rarefaction waves of different families, cancelation of a rarefaction wave by a shock wave of the same family (Rhee *et al.*, 2001).

The slope of the wave generated by the transmission of a rarefaction wave through a shock wave is given by:

$$\sigma_{(k)}^{-}(\omega_k) = \omega_k(x_D, \varphi)\frac{\omega_s^{+}}{\alpha_s}\prod_{\substack{j=1 \\ j\neq s}}^{3}\frac{\omega_j(\xi)}{\alpha_j(\xi)} \tag{60}$$

where $\sigma_{(k)}^{-}$ is the slope of the transmitted rarefaction wave of the k^{th} family, ω_s^{+} is the value of ω after the shock of the s^{th} family. Moreover, the shock path of the s^{th} family will be continuously changed by its interaction with the k^{th} rarefaction. The shock path can be calculated integrating the following expression:

$$\left(\frac{d\varphi}{dx_D}\right)_{(s)} = \omega_s^{+}\frac{\omega_k(x_D,\varphi)}{\alpha_k}\prod_{\substack{j=1 \\ j\neq k}}^{3}\frac{\omega_j^{-}}{\alpha_j} = \omega_s^{-}\frac{\omega_k(x_D,\varphi)}{\alpha_k}\prod_{\substack{j=1 \\ j\neq k}}^{3}\frac{\omega_j^{+}}{\alpha_j} \tag{61}$$

where $\omega_k(x_D, \varphi)$ is the value of ω along the k^{th} rarefaction wave, and ω_s^{-} is the value of ω_s before the shock.

The characteristic path resulting from the interaction of two rarefaction waves of different families $k1$ and $k2$ is computed by the ordinary differential equation:

$$\left(\frac{d\varphi}{dx_D}\right)_{(k1)} = \omega_{k1}(x_D, \varphi)\frac{\omega_{k2}(x_D,\varphi)}{\alpha_{k2}}\prod_{\substack{j=1 \\ j\neq k2}}^{3}\frac{\omega_j}{\alpha_j} \tag{62}$$

A rarefaction wave is cancelled when it reaches a shock wave of the same family, and the shock path changes continuously while it crosses the k^{th} rarefaction. The new shock path can be found from the following equation:

$$\left(\frac{d\varphi}{dx_D}\right)_{(k)} = \omega_k^- \frac{\omega_k(x_D,\varphi)}{\alpha_k} \prod_{\substack{j=1 \\ j\neq k}}^{3} \frac{\omega_j^+}{\alpha_j} \tag{63}$$

A detailed description of the theory of the interaction between waves in multicomponent chromatography can be found in chapter 4 of Rhee *et al.* (2001).

After the determination of the ω solution in the $x_D \times \varphi$ plane, the concentration solution is calculated through the relation:

$$c_i = \frac{1}{\beta_i(\xi)} \frac{(\omega_i - \alpha_i(\xi))}{\omega_i} \prod_{\substack{j=1 \\ j\neq i}}^{n} \frac{\alpha_j(\xi)[\omega_j - \alpha_j(\xi)]}{\omega_j[\alpha_j(\xi) - \alpha_i(\xi)]} \tag{64}$$

Equation (64) generalizes the inverse mapping equation presented in Rhee *et al.* (1970) for the case of pH-dependent coefficients of the Langmuir adsorption isotherm.

The characteristic diagram of the solution of the auxiliary system is presented in figure (3). Note that due to the difference between the adsorption rates of H^+ and the other cations (Equations 10-12), the slope of the pH waves is much greater than the slope of the concentration waves (Zoom in the upper left corner of the figure). Moreover, due to the low adsorption rate of the cation Na^+, the slope of $\omega_{(1)}$ waves is close to zero. Consequently, the interaction between waves of the family $k = 1$ will take place when x_D tends to infinite. The solution of this problem presents slopes approaching zero and infinite leading to very small regions in the characteristic diagram. To observe these regions and clearly illustrate the solution, several zooms are displayed in figure (3).

In figure (3), the thick lines represent shock waves, and the thin lines denote rarefaction waves. At the shock slopes $V_{(k)}^{HS}$ and rarefaction characteristics slopes $\sigma_{(k)}^{HS}$, the superscript "HS" indicate the rear of the low salinity slug, and the superscript "–" denotes that the wave path was changed due to an interaction with another wave. The number of "-" is equal to the number of interactions. The letters "A" to "N" refer to points (x_X, φ_X) used as reference for the construction of concentration profiles, and the numbers in parenthesis represent regions of constant state $\vec{\omega}$, which are described in detail in table

(5). The dashed lines represent the pH waves, the continuous lines denote the family $k = 3$, the dotted lines the family $k = 2$, and the dashed-dotted lines the family $k = 1$.

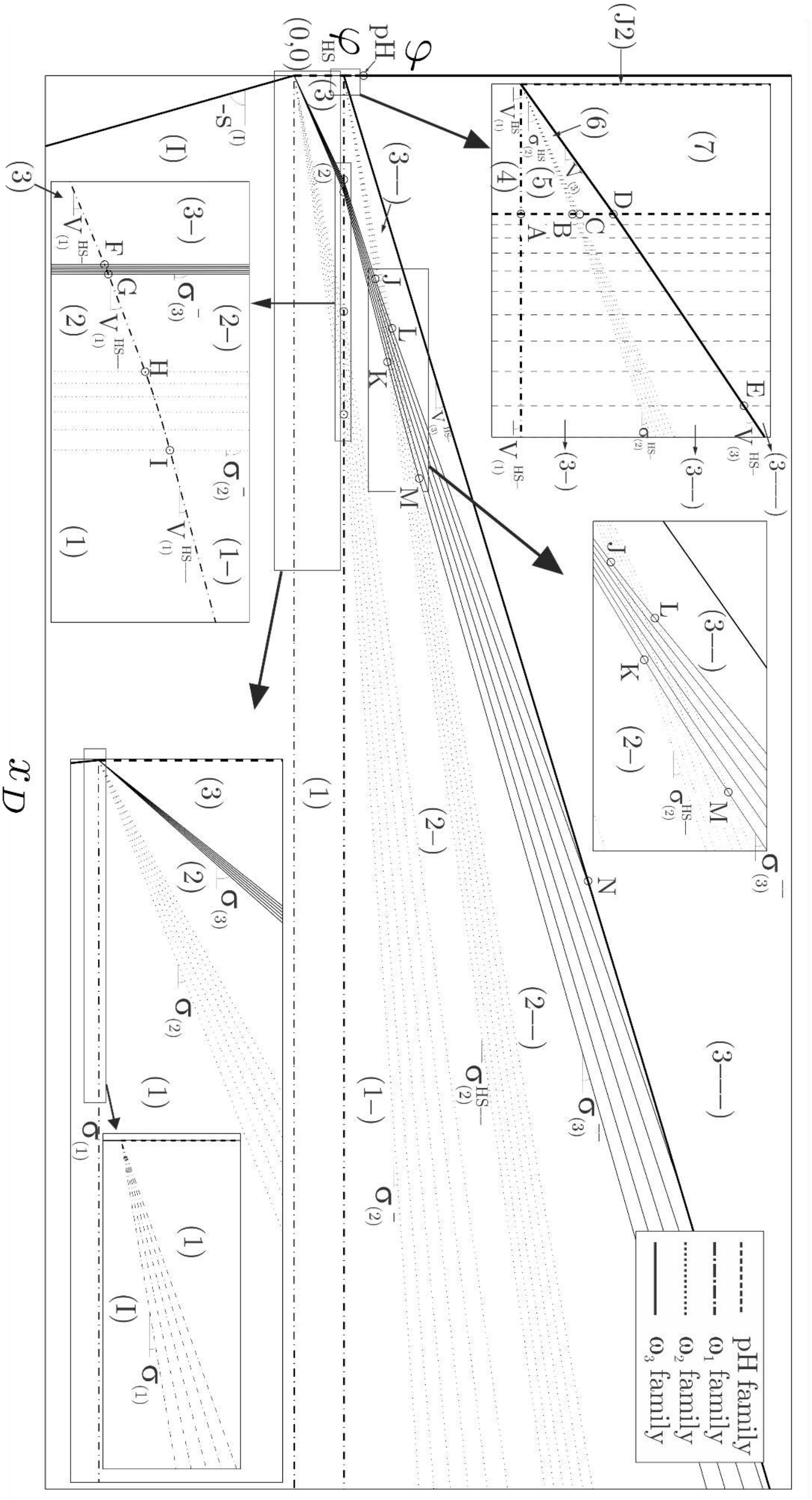

Figure 3: Characteristic diagram of the auxiliary system solution

Table 5: Solution of the auxiliary system

Region	$\vec{\omega}$ state	$\vec{c}$ state
(I)	$\left[\omega_1^{(I)}, \omega_2^{(I)}, \omega_3^{(I)}\right]$	$\left[c_1^{(I)}, c_2^{(I)}, c_3^{(I)}\right]$
(1)	$\left[\omega_1^{(J1-)}, \omega_2^{(I)}, \omega_3^{(I)}\right]$	$\left[c_1^{(1)}, c_2^{(1)}, c_3^{(1)}\right]$
(2)	$\left[\omega_1^{(J1-)}, \omega_2^{(J1-)}, \omega_3^{(I)}\right]$	$\left[c_1^{(2)}, c_2^{(2)}, c_3^{(2)}\right]$
(3)	$\left[\omega_1^{(J1-)}, \omega_2^{(J1-)}, \omega_3^{(J1-)}\right]$	$\left[c_1^{(3)}, c_2^{(3)}, c_3^{(3)}\right]$
(4)	$\left[\omega_1^{(J1)}, \omega_2^{(J1)}, \omega_3^{(J1)}\right]$	$\left[c_1^{(J1)}, c_2^{(J1)}, c_3^{(J1)}\right]$
(5)	$\left[\omega_1^{(J2-)}, \omega_2^{(J1)}, \omega_3^{(J1)}\right]$	$\left[c_1^{(5)}, c_2^{(5)}, c_3^{(5)}\right]$
(6)	$\left[\omega_1^{(J2-)}, \omega_2^{(J2-)}, \omega_3^{(J1)}\right]$	$\left[c_1^{(6)}, c_2^{(6)}, c_3^{(6)}\right]$
(7)	$\left[\omega_1^{(J2-)}, \omega_2^{(J2-)}, \omega_3^{(J2-)}\right]$	$\left[c_1^{(7)}, c_2^{(7)}, c_3^{(7)}\right]$
(J2)	$\left[\omega_1^{(J2)}, \omega_2^{(J2)}, \omega_3^{(J2)}\right]$	$\left[c_1^{(J2)}, c_2^{(J2)}, c_3^{(J2)}\right]$
(1-)	$\left[\omega_1^{(J2--)}, \omega_2^{(I)}, \omega_3^{(I)}\right]$	$\left[c_1^{(1-)}, c_2^{(1-)}, c_3^{(1-)}\right]$
(2-)	$\left[\omega_1^{(J2--)}, \omega_2^{(J1-)}, \omega_3^{(I)}\right]$	$\left[c_1^{(2-)}, c_2^{(2-)}, c_3^{(2-)}\right]$
(2--)	$\left[\omega_1^{(J2--)}, \omega_2^{(J2--)}, \omega_3^{(I)}\right]$	$\left[c_1^{(2--)}, c_2^{(2--)}, c_3^{(2--)}\right]$
(3-)	$\left[\omega_1^{(J2--)}, \omega_2^{(J1-)}, \omega_3^{(J1-)}\right]$	$\left[c_1^{(3-)}, c_2^{(3-)}, c_3^{(3-)}\right]$
(3--)	$\left[\omega_1^{(J2--)}, \omega_2^{(J2--)}, \omega_3^{(J1-)}\right]$	$\left[c_1^{(3--)}, c_2^{(3--)}, c_3^{(3--)}\right]$
(3---)	$\left[\omega_1^{(J2--)}, \omega_2^{(J2--)}, \omega_3^{(J2-)}\right]$	$\left[c_1^{(3---)}, c_2^{(3---)}, c_3^{(3---)}\right]$

Note that only one ω_k changes along each ω-wave, but all concentrations change when this wave is mapped on $\vec{c}$-space. In pH waves (transition from region (J2) to region (7), and transition from region (4) to region (3)), both $\vec{\omega}$ and $\vec{c}$ change.

The solution of the auxiliary system can be divided into 17 regions (Figure 3) separated by the points (x_A, φ_A)-(x_N, φ_N) and the point $\left(x_{pH}, \varphi_{pH}\right)$ that comes from the pH solution (Equation 64).

$$\vec{c}(x_D, \varphi) = \begin{cases} \overrightarrow{c_I}, & \varphi < \varphi_{HS} \\ \overrightarrow{c_{II}}, & \varphi_{HS} < \varphi < \varphi_A \\ \overrightarrow{c_{III}}, & \varphi_A < \varphi < \varphi_B \\ \overrightarrow{c_{IV}}, & \varphi_B < \varphi < \varphi_C \\ \overrightarrow{c_V}, & \varphi_C < \varphi < \varphi_D \\ \overrightarrow{c_{VI}}, & \varphi_D < \varphi < \varphi_E \\ \overrightarrow{c_{VII}}, & \varphi_E < \varphi < \varphi_F \\ \overrightarrow{c_{VIII}}, & \varphi_F < \varphi < \varphi_G \\ \overrightarrow{c_{IX}}, & \varphi_G < \varphi < \varphi_H \\ \overrightarrow{c_X}, & \varphi_H < \varphi < \varphi_I \\ \overrightarrow{c_{XI}}, & \varphi_I < \varphi < \varphi_{pH} \\ \overrightarrow{c_{XII}}, & \varphi_{pH} < \varphi < \varphi_J \\ \overrightarrow{c_{XIII}}, & \varphi_J < \varphi < \varphi_K \\ \overrightarrow{c_{XIV}}, & \varphi_K < \varphi < \varphi_L \\ \overrightarrow{c_{XV}}, & \varphi_L < \varphi < \varphi_M \\ \overrightarrow{c_{XVI}}, & \varphi_M < \varphi < \varphi_N \\ \overrightarrow{c_{XVII}}, & \varphi_N < \varphi \end{cases} \tag{65}$$

The solution parts $\overrightarrow{c_I}$ (self-similar), $\overrightarrow{c_{II}}$ (beginning of seawater drive), $\overrightarrow{c_{IV}}$ (interaction between pH waves and rarefaction waves from the rear of the low salinity slug) and $\overrightarrow{c_{XIII}}$ (interaction between concentration rarefaction waves) are detailed in this section. The remaining part of the complete solution can be found in the supplementary material.

The self-similar part of the solution takes place when $\varphi < \varphi_{HS}$ ($\overrightarrow{c_I}$ in equation 65). The concentration profile is detailed in equation (66):

$$\overrightarrow{c_I} = \begin{cases} \vec{c}^{(J1)}, & x_D < \frac{\varphi}{V_{pH}^{(1)}} \\ \vec{c}^{(4)-(3)}(x_D,\varphi), & \frac{\varphi}{V_{pH}^{(1)}} < x_D < \frac{\varphi}{\sigma_{pH}(\xi^{(I)})} \\ \vec{c}^{(3)}, & \frac{\varphi}{\sigma_{pH}(\xi^{(I)})} < x_D < \frac{\varphi}{\sigma_{(3)}(\vec{\omega}^{(3)},\xi^{(I)})} \\ \vec{c}^{(3)-(2)}(x_D,\varphi), & \frac{\varphi}{\sigma_{(3)}(\vec{\omega}^{(3)},\xi^{(I)})} < x_D < \frac{\varphi}{\sigma_{(3)}(\vec{\omega}^{(2)},\xi^{(I)})} \\ \vec{c}^{(2)}, & \frac{\varphi}{\sigma_{(3)}(\vec{\omega}^{(2)},\xi^{(I)})} < x_D < \frac{\varphi}{\sigma_{(2)}(\vec{\omega}^{(2)},\xi^{(I)})} \\ \vec{c}^{(2)-(1)}(x_D,\varphi), & \frac{\varphi}{\sigma_{(2)}(\vec{\omega}^{(2)},\xi^{(I)})} < x_D < \frac{\varphi}{\sigma_{(2)}(\vec{\omega}^{(1)},\xi^{(I)})} \\ \vec{c}^{(1)}, & \frac{\varphi}{\sigma_{(2)}(\vec{\omega}^{(1)},\xi^{(I)})} < x_D < \frac{\varphi}{\sigma_{(1)}(\vec{\omega}^{(1)},\xi^{(I)})} \\ \vec{c}^{(1)-(I)}(x_D,\varphi), & \frac{\varphi}{\sigma_{(1)}(\vec{\omega}^{(1)},\xi^{(I)})} < x_D < \frac{\varphi}{\sigma_{(1)}(\vec{\omega}^{(I)},\xi^{(I)})} \\ \vec{c}^{(I)}, & \frac{\varphi}{\sigma_{(1)}(\vec{\omega}^{(I)},\xi^{(I)})} < x_D < \frac{\varphi}{-s^{(I)}} \end{cases} \qquad (66)$$

In equation (66) we denote $\vec{c}^{(X)}$ as a constant concentration state in region X (see table 5 for $\vec{\omega}$ and $\vec{c}$), and $\vec{c}^{(X)-(Y)}(x_D,\varphi)$ as the rarefaction wave from a region (X) to a region (Y), where $\vec{\omega}$ is known and the concentration is calculated using equation (64). A concentration profile of $\overrightarrow{c_I}$ is presented in figure (4) emphasizing the effect of pH waves on the solution.

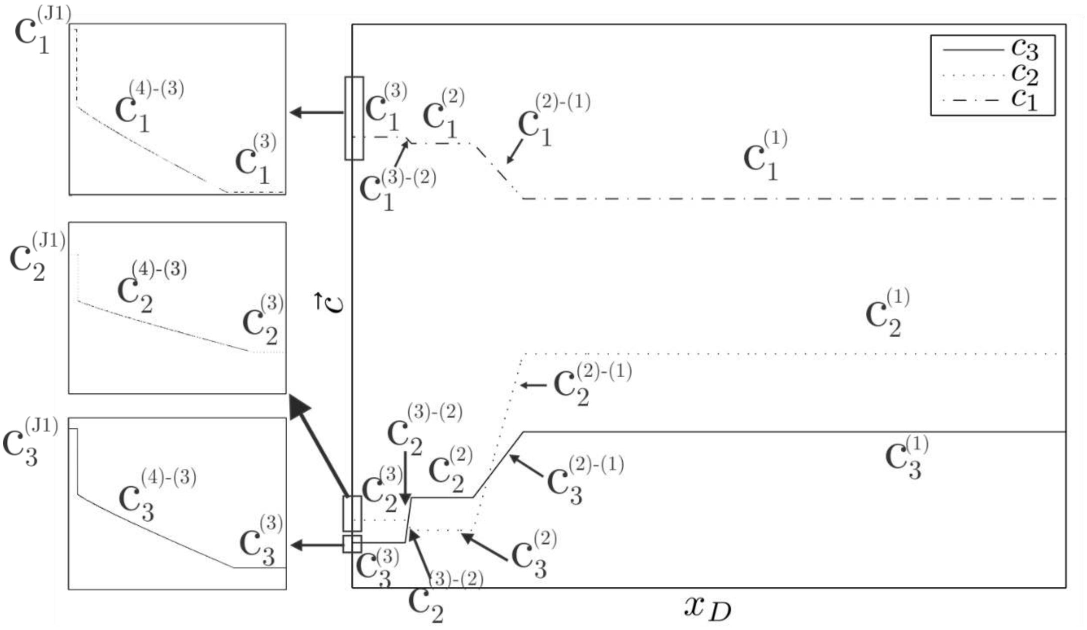

Figure 4: Solution of the auxiliary system ($\overrightarrow{c_I}$)

Along $\varphi_{HS} < \varphi < \varphi_A$, after the beginning of seawater drive, a new set of waves appear. The solution of the auxiliary system for this region is defined as $\overrightarrow{c_{II}}$ (Equation (65), and it is given by:

$$\overrightarrow{c_{II}} = \begin{cases} \vec{c}^{(J2)}, & x_D < \frac{\varphi-\varphi_{HS}}{V_{pH}^{(2)}} \\ \vec{c}^{(7)}, & \frac{\varphi-\varphi_{HS}}{V_{pH}^{(2)}} < x_D < \frac{\varphi-\varphi_{HS}}{V_{(3)}} \\ \vec{c}^{(6)}, & \frac{\varphi-\varphi_{HS}}{V_{(3)}} < x_D < \frac{\varphi-\varphi_{HS}}{\sigma_{(2)}\left(\vec{\omega}^{(6)},\xi^{(J1)}\right)} \\ \vec{c}^{(6)-(5)}(x_D,\varphi), & \frac{\varphi-\varphi_{HS}}{\sigma_{(2)}\left(\vec{\omega}^{(6)},\xi^{(J1)}\right)} < x_D < \frac{\varphi-\varphi_{HS}}{\sigma_{(2)}\left(\vec{\omega}^{(5)},\xi^{(J1)}\right)} \\ \vec{c}^{(5)}, & \frac{\varphi-\varphi_{HS}}{\sigma_{(2)}\left(\vec{\omega}^{(5)},\xi^{(J1)}\right)} < x_D < \frac{\varphi-\varphi_{HS}}{V_{(1)}} \\ \vec{c}^{(J1)}, & \frac{\varphi-\varphi_{HS}}{V_{(1)}} < x_D < \frac{\varphi}{V_{pH}^{(1)}} \\ \vec{c}^{(4)-(3)}(x_D,\varphi), & \frac{\varphi}{V_{pH}^{(1)}} < x_D < \frac{\varphi}{\sigma_{pH}(\xi^{(I)})} \\ \vec{c}^{(3)}, & \frac{\varphi}{\sigma_{pH}(\xi^{(I)})} < x_D < \frac{\varphi}{\sigma_{(3)}(\vec{\omega}^{(3)},\xi^{(I)})} \\ \vec{c}^{(3)-(2)}(x_D,\varphi), & \frac{\varphi}{\sigma_{(3)}(\vec{\omega}^{(3)},\xi^{(I)})} < x_D < \frac{\varphi}{\sigma_{(3)}(\vec{\omega}^{(2)},\xi^{(I)})} \\ \vec{c}^{(2)}, & \frac{\varphi}{\sigma_{(3)}(\vec{\omega}^{(2)},\xi^{(I)})} < x_D < \frac{\varphi}{\sigma_{(2)}(\vec{\omega}^{(2)},\xi^{(I)})} \\ \vec{c}^{(2)-(1)}(x_D,\varphi), & \frac{\varphi}{\sigma_{(2)}(\vec{\omega}^{(2)},\xi^{(I)})} < x_D < \frac{\varphi}{\sigma_{(2)}(\vec{\omega}^{(1)},\xi^{(I)})} \\ \vec{c}^{(1)}, & \frac{\varphi}{\sigma_{(2)}(\vec{\omega}^{(1)},\xi^{(I)})} < x_D < \frac{\varphi}{\sigma_{(1)}(\vec{\omega}^{(1)},\xi^{(I)})} \\ \vec{c}^{(1)-(I)}(x_D,\varphi), & \frac{\varphi}{\sigma_{(1)}(\vec{\omega}^{(1)},\xi^{(I)})} < x_D < \frac{\varphi}{\sigma_{(1)}(\vec{\omega}^{(I)},\xi^{(I)})} \\ \vec{c}^{(I)}, & \frac{\varphi}{\sigma_{(1)}(\vec{\omega}^{(I)},\xi^{(I)})} < x_D < \frac{\varphi}{-s^{(I)}} \end{cases} \tag{67}$$

Figure (5) presents the concentration profile of the solution $\overrightarrow{c_{II}}$.

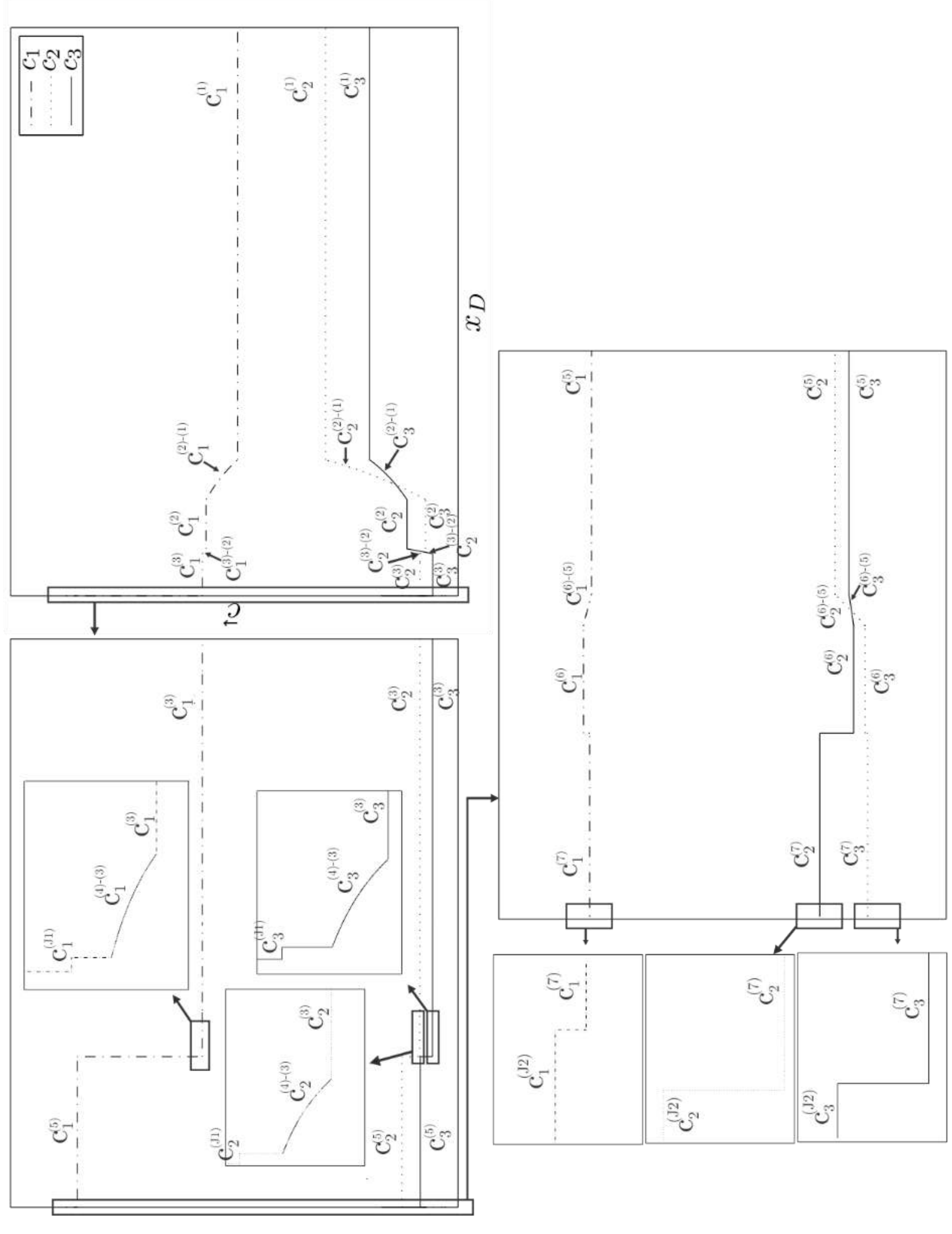

Figure 5: Solution of the auxiliary system for $\varphi_{HS} < \varphi < \varphi_A$ ($\overrightarrow{c_{II}}$)

For $\varphi_B < \varphi < \varphi_C$ (solution $\overrightarrow{c_{IV}}$), the rarefaction wave $\vec{c}^{(6)-(5)}$ interacts with the pH waves. In this region part of that rarefaction is located at the left of the pH shock (constant pH) and the other part at the right, a pH-concentration rarefaction wave. The characteristic path of the rarefaction $\vec{c}^{(6)-(5)}$ changes along the interaction. The shock path of the family

X after its first interaction is denoted as $x_{(X)}^{-}(\varphi)$, and the rarefaction wave $(X)-(Y)$ after its first interaction as $x_{(X)-(Y)}^{-(\pm)}(\varphi)$, in which $x_{(X)-(Y)}^{-(+)}(\varphi)$ is the first characteristic curve and $x_{(X)-(Y)}^{-(-)}(\varphi)$ is the last characteristic curve of the rarefaction wave. From now on the number of "$-$" in the wave superscript indicates its number of interactions. Equation (68) details $\overrightarrow{c_{IV}}$ and the concentration profile is shown in figure (6).

$$\overrightarrow{c_{IV}} = \begin{cases} \vec{c}^{(J2)}, & x_D < \frac{\varphi-\varphi_{HS}}{V_{pH}^{(2)}} \\ \vec{c}^{(7)}, & \frac{\varphi-\varphi_{HS}}{V_{pH}^{(2)}} < x_D < \frac{\varphi-\varphi_{HS}}{V_{(3)}} \\ \vec{c}^{(6)}, & \frac{\varphi-\varphi_{HS}}{V_{(3)}} < x_D < \frac{\varphi-\varphi_{HS}}{\sigma_{(2)}\left(\overrightarrow{\omega}^{(6)},\xi^{(J1)}\right)} \\ \vec{c}^{(6)-(5)}(x_D,\varphi), & \frac{\varphi-\varphi_{HS}}{\sigma_{(2)}\left(\overrightarrow{\omega}^{(6)},\xi^{(J1)}\right)} < x_D < \frac{\varphi}{V_{(pH)}^{(1)}} \\ \vec{c}^{(6)-(5)-}(x_D,\varphi), & \frac{\varphi}{V_{(pH)}^{(1)}} < x_D < x_{(6)-(5)}^{-(-)}(\varphi) \\ \vec{c}^{(5)-(3-)}(x_D,\varphi), & x_{(6)-(5)}^{-(-)}(\varphi) < x_D < \frac{\varphi}{\sigma_{pH}(\xi^{(I)})} \\ \vec{c}^{(3-)}, & \frac{\varphi}{\sigma_{pH}(\xi^{(I)})} < x_D < x_{(1)}^{-}(\varphi) \\ \vec{c}^{(3)}, & x_{(1)}^{-}(\varphi) < x_D < \frac{\varphi}{\sigma_{(3)}(\overrightarrow{\omega}^{(3)},\xi^{(I)})} \\ \vec{c}^{(3)-(2)}(x_D,\varphi), & \frac{\varphi}{\sigma_{(3)}(\overrightarrow{\omega}^{(3)},\xi^{(I)})} < x_D < \frac{\varphi}{\sigma_{(3)}(\overrightarrow{\omega}^{(2)},\xi^{(I)})} \\ \vec{c}^{(2)}, & \frac{\varphi}{\sigma_{(3)}(\overrightarrow{\omega}^{(2)},\xi^{(I)})} < x_D < \frac{\varphi}{\sigma_{(2)}(\overrightarrow{\omega}^{(2)},\xi^{(I)})} \\ \vec{c}^{(2)-(1)}(x_D,\varphi), & \frac{\varphi}{\sigma_{(2)}(\overrightarrow{\omega}^{(2)},\xi^{(I)})} < x_D < \frac{\varphi}{\sigma_{(2)}(\overrightarrow{\omega}^{(1)},\xi^{(I)})} \\ \vec{c}^{(1)}, & \frac{\varphi}{\sigma_{(2)}(\overrightarrow{\omega}^{(1)},\xi^{(I)})} < x_D < \frac{\varphi}{\sigma_{(1)}(\overrightarrow{\omega}^{(1)},\xi^{(I)})} \\ \vec{c}^{(1)-(I)}(x_D,\varphi), & \frac{\varphi}{\sigma_{(1)}(\overrightarrow{\omega}^{(1)},\xi^{(I)})} < x_D < \frac{\varphi}{\sigma_{(1)}(\overrightarrow{\omega}^{(I)},\xi^{(I)})} \\ \vec{c}^{(I)}, & \frac{\varphi}{\sigma_{(1)}(\overrightarrow{\omega}^{(I)},\xi^{(I)})} < x_D < \frac{\varphi}{-s^{(I)}} \end{cases} \tag{68}$$

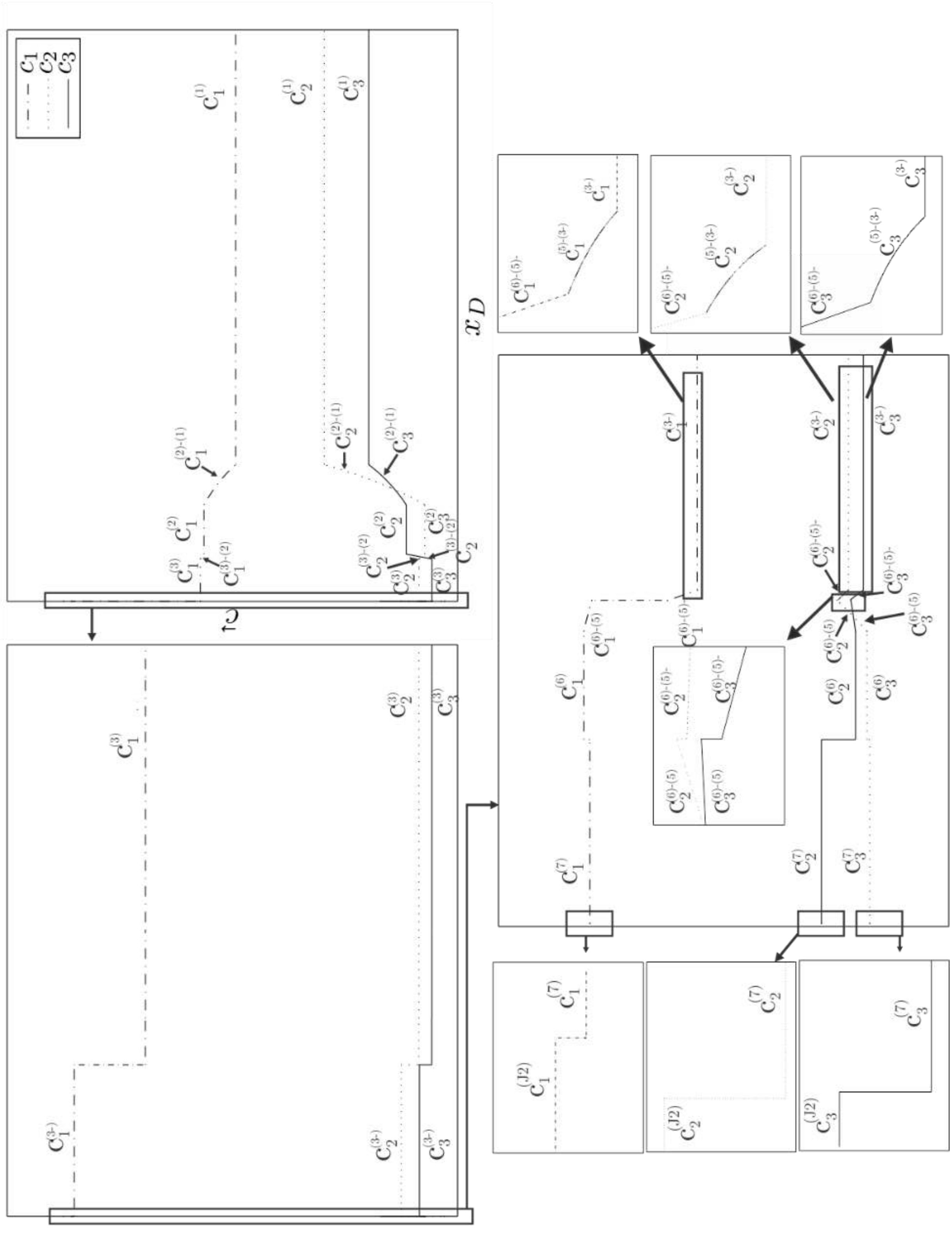

Figure 6: Concentration profile for the solution $\overrightarrow{c_{IV}}$

In the solution $\overrightarrow{c_{XIII}}$ the interaction between rarefaction waves of the families $k = 2$ and $k = 3$ begins. This interaction region is bounded by the curves $(J - L) =$

$x^{--(+)}_{(3)-(2)}(\varphi)$, $(K-M) = x^{--(-)}_{(3)-(2)}(\varphi)$, $(J-K) = x^{--(-)}_{(6)-(5)}(\varphi)$ and $(L-M) = x^{--(+)}_{(6)-(5)}(\varphi)$. In this part of the solution the region (3-) disappears. In equation (69) we detail $\overrightarrow{c_{XIII}}$, and its concentration profile is shown in figure (7).

$$\overrightarrow{c_{XIII}} = \begin{cases} \vec{c}^{(J2)}, & x_D < x^{-}_{pH}(\varphi) \\ \vec{c}^{(7)-(3---)}(x_D,\varphi), & x^{-}_{pH}(\varphi) < x_D < \frac{\varphi}{\sigma_{pH}(\xi^{(I)})} \\ \vec{c}^{(3---)}, & \frac{\varphi}{\sigma_{pH}(\xi^{(I)})} < x_D < x^{-}_{(3)} \\ \vec{c}^{(3--)}, & x^{-}_{(3)} < x_D < x^{-(+)}_{(6)-(5)}(\varphi) \\ \vec{c}^{(6)-(5)-}(x_D,\varphi), & x^{-(+)}_{(6)-(5)}(\varphi) < x_D < x^{--(+)}_{(3)-(2)}(\varphi) \\ \vec{c}^{(3)-(2)--}(x_D,\varphi), & x^{--(+)}_{(3)-(2)}(\varphi) < x_D < x^{-(-)}_{(6)-(5)}(\varphi) \\ \vec{c}^{(3)-(2)-}(x_D,\varphi), & x^{-(-)}_{(6)-(5)}(\varphi) < x_D < x^{--(-)}_{(3)-(2)}(\varphi) \\ \vec{c}^{(2-)}, & x^{--(-)}_{(3)-(2)}(\varphi) < x_D < x^{-(+)}_{(2)-(1)}(\varphi) \\ \vec{c}^{(2)-(1)-}, & x^{-(+)}_{(2)-(1)}(\varphi) < x_D < x^{-(-)}_{(2)-(1)}(\varphi) \\ \vec{c}^{(1-)}, & x^{-(-)}_{(2)-(1)}(\varphi) < x_D < x^{---}_{(1)}(\varphi) \\ \vec{c}^{(1)}, & x^{---}_{(1)}(\varphi) < x_D < \frac{\varphi}{\sigma_{(1)}(\overrightarrow{\omega}^{(1)},\xi^{(I)})} \\ \vec{c}^{(1)-(I)}(x_D,\varphi), & \frac{\varphi}{\sigma_{(1)}(\overrightarrow{\omega}^{(1)},\xi^{(I)})} < x_D < \frac{\varphi}{\sigma_{(1)}(\overrightarrow{\omega}^{(I)},\xi^{(I)})} \\ \vec{c}^{(I)}, & \frac{\varphi}{\sigma_{(1)}(\overrightarrow{\omega}^{(I)},\xi^{(I)})} < x_D < \frac{\varphi}{-s^{(I)}} \end{cases} \tag{69}$$

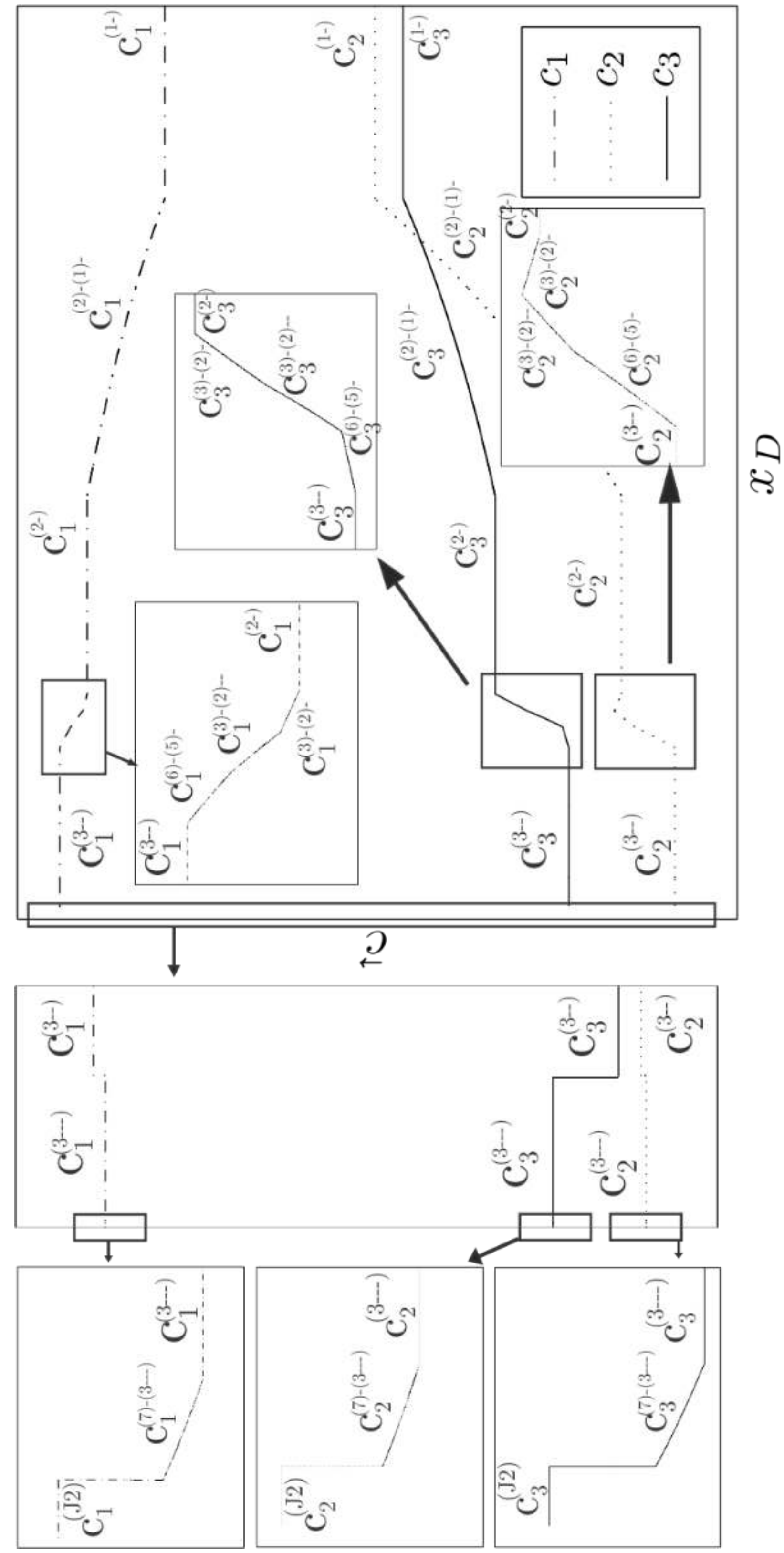

Figure 7: Concentration profile of the solution $\overrightarrow{c_{XIII}}$

5. Solution of the lifting equation

The lifting equation (Equation 22) is solved after the auxiliary system, considering the hydrodynamic and transport properties of the flow (relative permeability curves and viscosities of the flowing phases). The solution of the lifting equation extends the solution of the auxiliary system (analogous to a one-phase chromatography problem) to a two-phase environment.

First, we introduce the following variables in equation (22):

$$U(s,\vec{c},\xi) = \frac{1}{f(s,\vec{c},\xi)} \tag{70}$$

$$F(U,s,\vec{c},\xi) = \frac{-s}{f(s,\vec{c},\xi)} = -sU(s,\vec{c},\xi) \tag{71}$$

to obtain the hyperbolic equation:

$$\frac{\partial F(U,s,\vec{c},\xi)}{\partial \varphi} + \frac{\partial U(s,\vec{c},\xi)}{\partial x_D} = 0 \tag{72}$$

to find U.

The initial and boundary conditions for the lifting equation problem (Equations 25-26) are:

$$\varphi = -s^{(I)}x_D, \begin{cases} U \to +\infty \\ F \to -\infty \end{cases} \tag{73}$$

$$x_D = 0, \begin{cases} U = 1 \\ F = -s^{(I)} \end{cases} \tag{74}$$

The water fractional flow is defined as:

$$f(s,\vec{c},\xi) = \frac{\frac{k_{rw}(s,\vec{c},\xi)}{\mu_w(\vec{c})}}{\frac{k_{rw}(s,\vec{c},\xi)}{\mu_w(\vec{c},\xi)} + \frac{k_{ro}(s,\vec{c},\xi)}{\mu_o}} \tag{75}$$

in which the oil viscosity μ_o is considered constant for this problem. The water viscosity μ_w was calculated using a correlation for brine fluids in reservoir conditions (McCain Jr., 1991):

$$\mu_B(T) = AT^{-B} \tag{76}$$

$$A = 109.574 - 8.40564\, S_{al} + 0.313314\, S_{al}^2 + 8.72213.10^{-3}\, S_{al}^3 \tag{77}$$

$$B = 1.12166 - 2.63951.10^{-2}\, S_{al} + 6.79461.10^{-3} S_{al}^2 + 5.47119.10^{-5} S_{al}^3 - 1.55586.10^{-6} S_{al}^4 \tag{78}$$

$$\mu_w(T, P) = \mu_B(T)(0.9994 + 4.0295.10^{-5} p + 3.1062.10^{-9} p^2) \tag{79}$$

where T is the temperature (°F), S_{al} is the salinity (total dissolved solids), and p is the pressure ($psia$).

Corey's model (Corey, 1954) was used to calculate the relative permeabilities, and the residual oil saturation (s_{or}), Corey's exponents (n_w and n_o) and the permeability end points (k_{rw}^* and k_{ro}^*) are functions of the salinity and water pH. Thus, the permeability curves are given by:

$$k_{rw}(s, \vec{c}, \xi) = k_{rw}^*(\vec{c}, \xi) \left(\frac{s - s^{(I)}}{1 - s_{or}(\vec{c}, \xi) - s^{(I)}} \right)^{n_w(\vec{c}, \xi)} \tag{80}$$

$$k_{ro}(s, \vec{c}, \xi) = k_{ro}^*(\vec{c}, \xi) \left(\frac{1 - s_{or}(\vec{c}, \xi) - s}{1 - s_{or}(\vec{c}, \xi) - s^{(I)}} \right)^{n_o(\vec{c}, \xi)} \tag{81}$$

Expressions for the parameters s_{or}, n_w, n_o, k_{rw}^* and k_{ro}^* were obtained adjusting experimental data from 47 coreflooding experiments (Table 6) and are given by:

$$s_{or}(\vec{c}, \xi) = 10^{-6} S_{al} + 0.225 - 0.0978.pH \tag{82}$$

$$n_w(\vec{c}, \xi) = -10^{-5} S_{al} + 2.8554 + 0.05214.pH \tag{83}$$

$$n_o(\vec{c},\xi) = 10^{-5}S_{al} + 2.4258 - 0.4873.pH \tag{84}$$

$$k_{rw}^{*}(\vec{c},\xi) = 2.10^{-6}S_{al} + 0.3311 - 0.00517.pH \tag{85}$$

$$k_{ro}^{*}(\vec{c},\xi) = -2.10^{-6}S_{al} + 05913 + 0.0181.pH \tag{86}$$

	Salinity range	pH range
Aladasani *et al.* (2014)	249-38522 ppm	6.5-7.2
Al-Shalabi *et al.* (2016)	600-60000 ppm	6.3-7.5
Etemadi *et al.* (2016)	1000-45000 ppm	7-7.6
Holter (2012)	0-45000 ppm	7.2-75
Lima *et al.* (2020)	6500-32000 ppm	4-7
Omekeh & Evje (2013)	450-45000 ppm	7
Rivet *et al.* (2010)	200-32000 ppm	6.2-7.1
Shojaei *et al.* (2015)	3500-714000 ppm	7-7.2
Tang & Morrow (1999)	151.5-35960 ppm	6.3-7.3

From equation (72), we find:

$$\frac{\partial F(U,\vec{c},\xi)}{\partial U}\frac{\partial U(s,\vec{c},\xi)}{\partial \varphi} + \frac{\partial U(s,\vec{c},\xi)}{\partial x_D} = -\frac{\partial F(U,\vec{c},\xi)}{\partial \vec{c}}\frac{\partial \vec{c}}{\partial \varphi} - \frac{\partial F(U,\vec{c},\xi)}{\partial \xi}\frac{\partial \xi}{\partial \varphi} \tag{87}$$

and the characteristic velocity of U-characteristics is given by:

$$\sigma_U = \frac{d\varphi}{dx_D} = \frac{\partial F(U,\vec{c},\xi)}{\partial U} \tag{88}$$

In regions where both concentration and pH are constant, equation (87) becomes:

$$\frac{\partial F(U,\vec{c},\xi)}{\partial U}\frac{\partial U(s,\vec{c},\xi)}{\partial \varphi} + \frac{\partial U(s,\vec{c},\xi)}{\partial x_D} = 0 \tag{89}$$

and U is constant along the characteristic curves. However, in regions where the pH and/or concentration change, we have:

$$\frac{dU}{dx_D} = -\frac{\partial F(U,\vec{c},\xi)}{\partial \vec{c}}\frac{\partial \vec{c}}{\partial \varphi} - \frac{\partial F(U,\vec{c},\xi)}{\partial \xi}\frac{\partial \xi}{\partial \varphi} \tag{90}$$

The shock condition for the lifting equation (Equation 72) is:

$$V_U = \frac{d\varphi}{dx_D} = \frac{[F]}{[U]} \tag{91}$$

Note that the lifting equation solution depends on concentration and pH, however, the auxiliary system solution does not depend on U, and therefore it is not affected by the lifting equation solution. Thus, wave interactions between U-waves and $\vec{c}$-waves changes the paths of the U-waves. The characteristic diagram of the solution of the lifting equation can be seen in figure (8). The thick dotted lines are the waves where only U changes (U waves).

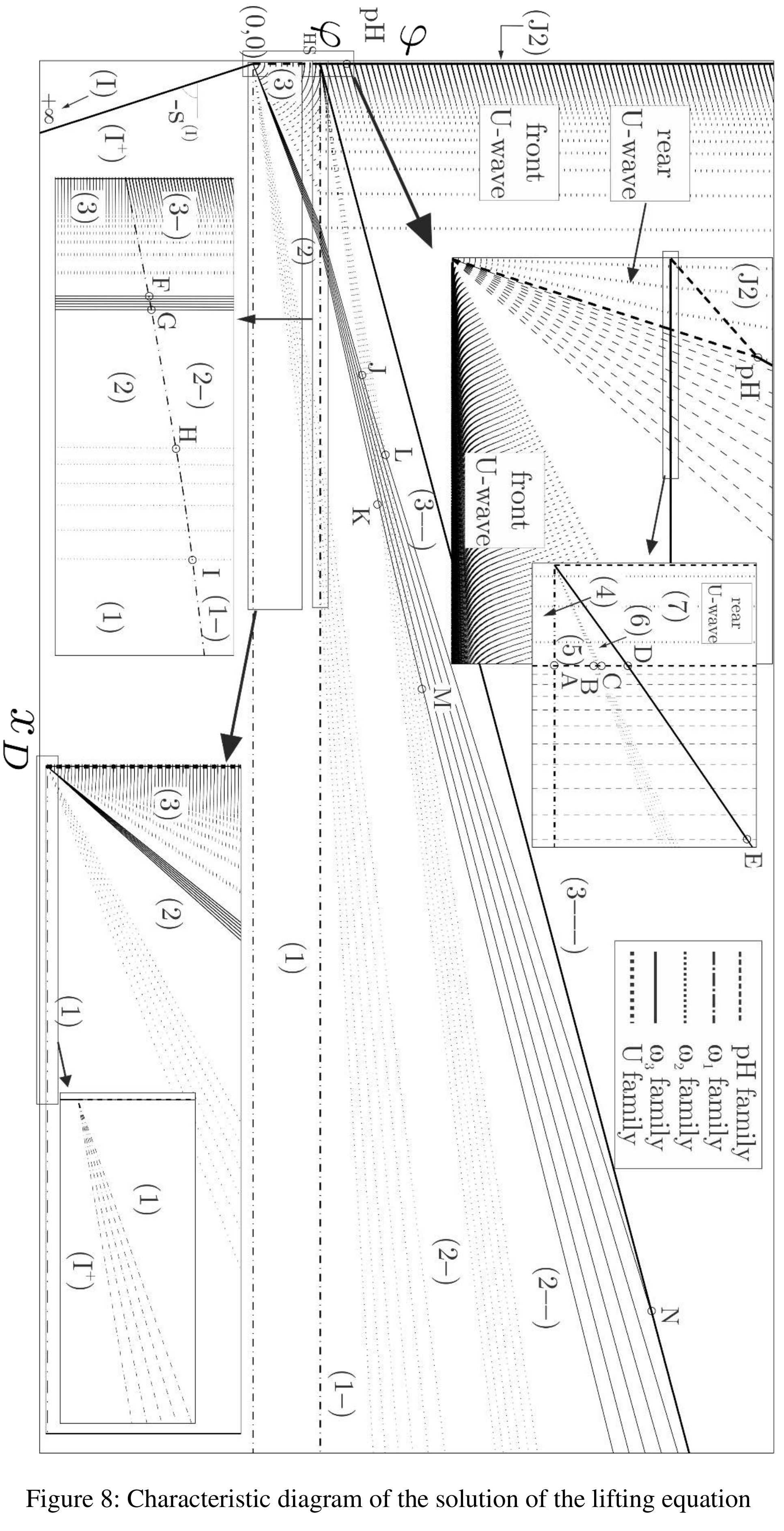

Figure 8: Characteristic diagram of the solution of the lifting equation

The solution of the lifting equation is divided into the same 17 regions of the auxiliary solution:

$$U(x_D,\varphi)=\begin{cases}U_I, & \varphi<\varphi_{HS}\\ U_{II}, & \varphi_{HS}<\varphi<\varphi_A\\ U_{III}, & \varphi_A<\varphi<\varphi_B\\ U_{IV}, & \varphi_B<\varphi<\varphi_C\\ U_V, & \varphi_C<\varphi<\varphi_D\\ U_{VI}, & \varphi_D<\varphi<\varphi_E\\ U_{VII}, & \varphi_E<\varphi<\varphi_F\\ U_{VIII}, & \varphi_F<\varphi<\varphi_G\\ U_{IX}, & \varphi_G<\varphi<\varphi_H\\ U_X, & \varphi_H<\varphi<\varphi_I\\ U_{XI}, & \varphi_I<\varphi<\varphi_{pH}\\ U_{XII}, & \varphi_{pH}<\varphi<\varphi_J\\ U_{XIII}, & \varphi_J<\varphi<\varphi_K\\ U_{XIV}, & \varphi_K<\varphi<\varphi_L\\ U_{XV}, & \varphi_L<\varphi<\varphi_M\\ U_{XVI}, & \varphi_M<\varphi<\varphi_N\\ U_{XVII}, & \varphi_N<\varphi\end{cases} \tag{92}$$

For the lifting equation solution, we denote $U_X(x_D,\varphi)$ the U-rarefaction in region X. Along these waves only U changes, both concentration and pH are constant. For the U-waves where concentration and/or pH change, the notation created for the auxiliary system solution is followed: $U^{(X)-(Y)}$ is a rarefaction wave from the region X to the region Y, and $U^{(X)}$ is a constant state in region X.

Similar to the auxiliary system solution, we present regions U_I, U_{II}, U_{IV} and U_{XIII} of the lifting equation solution (Equation 91), the other parts are shown in the supplementary material.

Each flow function $F\left(U,\vec{c}^{(X)},\xi^{(X)}\right)$ presented in figures (9)-(12) is built using the constant concentration and pH of the region (X) of the characteristic diagram (Figure 8).

The continuous lines connecting two points of different curves $F\left(U,\vec{c}^{(X)},\xi^{(X)}\right)$ represent a rarefaction wave where U, concentration and/or pH change. The continuous lines connecting two points on the same $F\left(U,\vec{c}^{(X)},\xi^{(X)}\right)$ curve represent a rarefaction wave where only U changes. The dashed lines denote shock waves, and X is the constant state $U^{(X)}$. When $U \to +\infty$, $U = U^{(I)}$, thus the shock wave from $U^{(I+)}$ to $U^{(I)}$ is shown as a dashed line that starting at I^+.

$$U_I = \begin{cases} U_4(x_D, \varphi), & x_D < \frac{\varphi}{V_{pH}^{(1)}} \\ U^{(4)-(3)}(x_D, \varphi), & \frac{\varphi}{V_{pH}^{(1)}} < x_D < \frac{\varphi}{\sigma_{pH}^{(1)}(\xi^{(I)})} \\ U_3(x_D, \varphi), & \frac{\varphi}{\sigma_{pH}^{(1)}(\xi^{(I)})} < x_D < \frac{\varphi}{\sigma_{(3)}(\vec{\omega}^{(3)},\xi^{(I)})} \\ U^{(3)-(2)}(x_D, \varphi), & \frac{\varphi}{\sigma_{(3)}(\vec{\omega}^{(3)},\xi^{(I)})} < x_D < \frac{\varphi}{\sigma_{(3)}(\vec{\omega}^{(2)},\xi^{(I)})} \\ U^{(2)}, & \frac{\varphi}{\sigma_{(3)}(\vec{\omega}^{(2)},\xi^{(I)})} < x_D < \frac{\varphi}{\sigma_{(2)}(\vec{\omega}^{(2)},\xi^{(I)})} \\ U^{(2)-(1)}(x_D, \varphi), & \frac{\varphi}{\sigma_{(2)}(\vec{\omega}^{(2)},\xi^{(I)})} < x_D < \frac{\varphi}{\sigma_{(2)}(\vec{\omega}^{(1)},\xi^{(I)})} \\ U^{(1)}, & \frac{\varphi}{\sigma_{(2)}(\vec{\omega}^{(1)},\xi^{(I)})} < x_D < \frac{\varphi}{\sigma_{(1)}(\vec{\omega}^{(1)},\xi^{(I)})} \\ U^{(1)-(I+)}(x_D, \varphi), & \frac{\varphi}{\sigma_{(1)}(\vec{\omega}^{(1)},\xi^{(I)})} < x_D < \frac{\varphi}{\sigma_{(1)}(\vec{\omega}^{(I)},\xi^{(I)})} \\ U^{(I+)}, & \frac{\varphi}{\sigma_{(1)}(\vec{\omega}^{(I)},\xi^{(I)})} < x_D < +\infty \\ U^{(I)}, & x_D \to +\infty \end{cases} \tag{93}$$

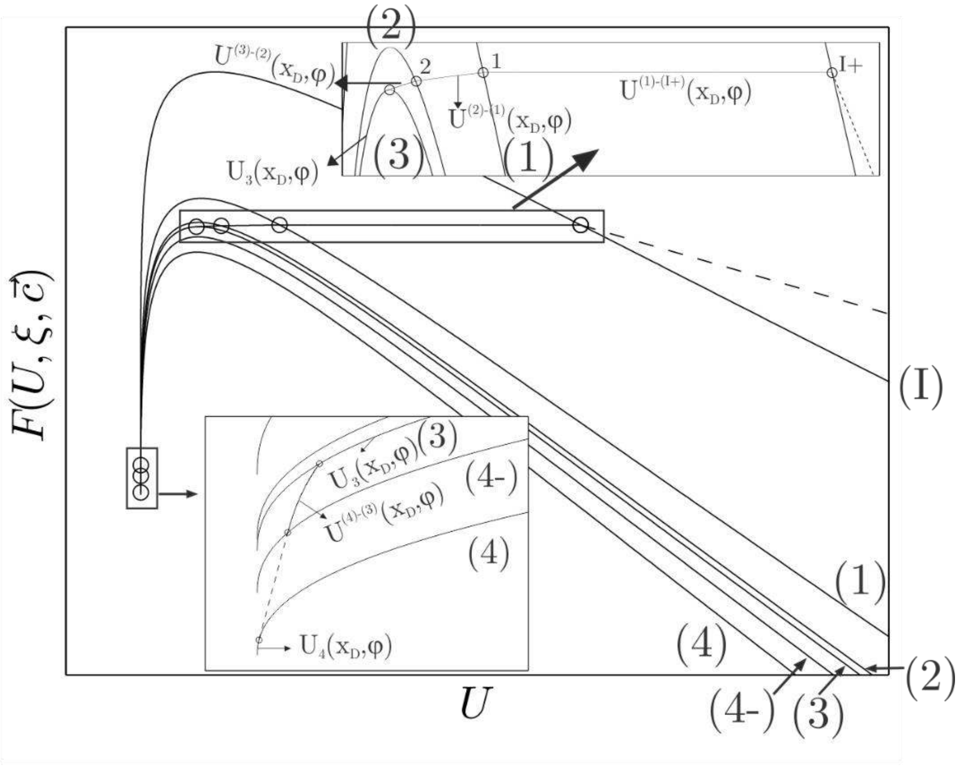

Figure 9: Solution path of U_I in the $F \times U$ plane

$$U_{II} = \begin{cases} U_{J2}(x_D, \varphi), & x_D < \frac{\varphi - \varphi_{HS}}{V_{pH}^{(2)}} \\ U_7(x_D, \varphi), & \frac{\varphi - \varphi_{HS}}{V_{pH}^{(2)}} < x_D < \frac{\varphi - \varphi_{HS}}{V_{(3)}} \\ U_6(x_D, \varphi), & \frac{\varphi - \varphi_{HS}}{V_{(3)}} < x_D < \frac{\varphi - \varphi_{HS}}{\sigma_{(2)}\left(\vec{\omega}^{(6)}, \xi^{(J1)}\right)} \\ U^{(6)-(5)}(x_D, \varphi), & \frac{\varphi - \varphi_{HS}}{\sigma_{(2)}\left(\vec{\omega}^{(6)}, \xi^{(J1)}\right)} < x_D < \frac{\varphi - \varphi_{HS}}{\sigma_{(2)}\left(\vec{\omega}^{(5)}, \xi^{(J1)}\right)} \\ U_5(x_D, \varphi), & \frac{\varphi - \varphi_{HS}}{\sigma_{(2)}\left(\vec{\omega}^{(5)}, \xi^{(J1)}\right)} < x_D < \frac{\varphi - \varphi_{HS}}{V_{(1)}} \\ U_4(x_D, \varphi), & \frac{\varphi - \varphi_{HS}}{V_{(1)}} < x_D < \frac{\varphi}{V_{pH}^{(1)}} \\ U^{(4)-(3)}(x_D, \varphi), & \frac{\varphi}{V_{pH}^{(1)}} < x_D < \frac{\varphi}{\sigma_{pH}^{(1)}\left(\xi^{(I)}\right)} \\ U_3(x_D, \varphi), & \frac{\varphi}{\sigma_{pH}^{(1)}\left(\xi^{(I)}\right)} < x_D < \frac{\varphi}{\sigma_{(3)}(\vec{\omega}^{(3)}, \xi^{(I)})} \\ U^{(3)-(2)}(x_D, \varphi), & \frac{\varphi}{\sigma_{(3)}(\vec{\omega}^{(3)}, \xi^{(I)})} < x_D < \frac{\varphi}{\sigma_{(3)}(\vec{\omega}^{(2)}, \xi^{(I)})} \\ U^{(2)}, & \frac{\varphi}{\sigma_{(3)}(\vec{\omega}^{(2)}, \xi^{(I)})} < x_D < \frac{\varphi}{\sigma_{(2)}(\vec{\omega}^{(2)}, \xi^{(I)})} \\ U^{(2)-(1)}(x_D, \varphi), & \frac{\varphi}{\sigma_{(2)}(\vec{\omega}^{(2)}, \xi^{(I)})} < x_D < \frac{\varphi}{\sigma_{(2)}(\vec{\omega}^{(1)}, \xi^{(I)})} \\ U^{(1)}, & \frac{\varphi}{\sigma_{(2)}(\vec{\omega}^{(1)}, \xi^{(I)})} < x_D < \frac{\varphi}{\sigma_{(1)}(\vec{\omega}^{(1)}, \xi^{(I)})} \\ U^{(1)-(I+)}(x_D, \varphi), & \frac{\varphi}{\sigma_{(1)}(\vec{\omega}^{(1)}, \xi^{(I)})} < x_D < \frac{\varphi}{\sigma_{(1)}(\vec{\omega}^{(I)}, \xi^{(I)})} \\ U^{(I+)}, & \frac{\varphi}{\sigma_{(1)}(\vec{\omega}^{(I)}, \xi^{(I)})} < x_D < +\infty \\ U^{(I)}, & x_D \to +\infty \end{cases} \tag{94}$$

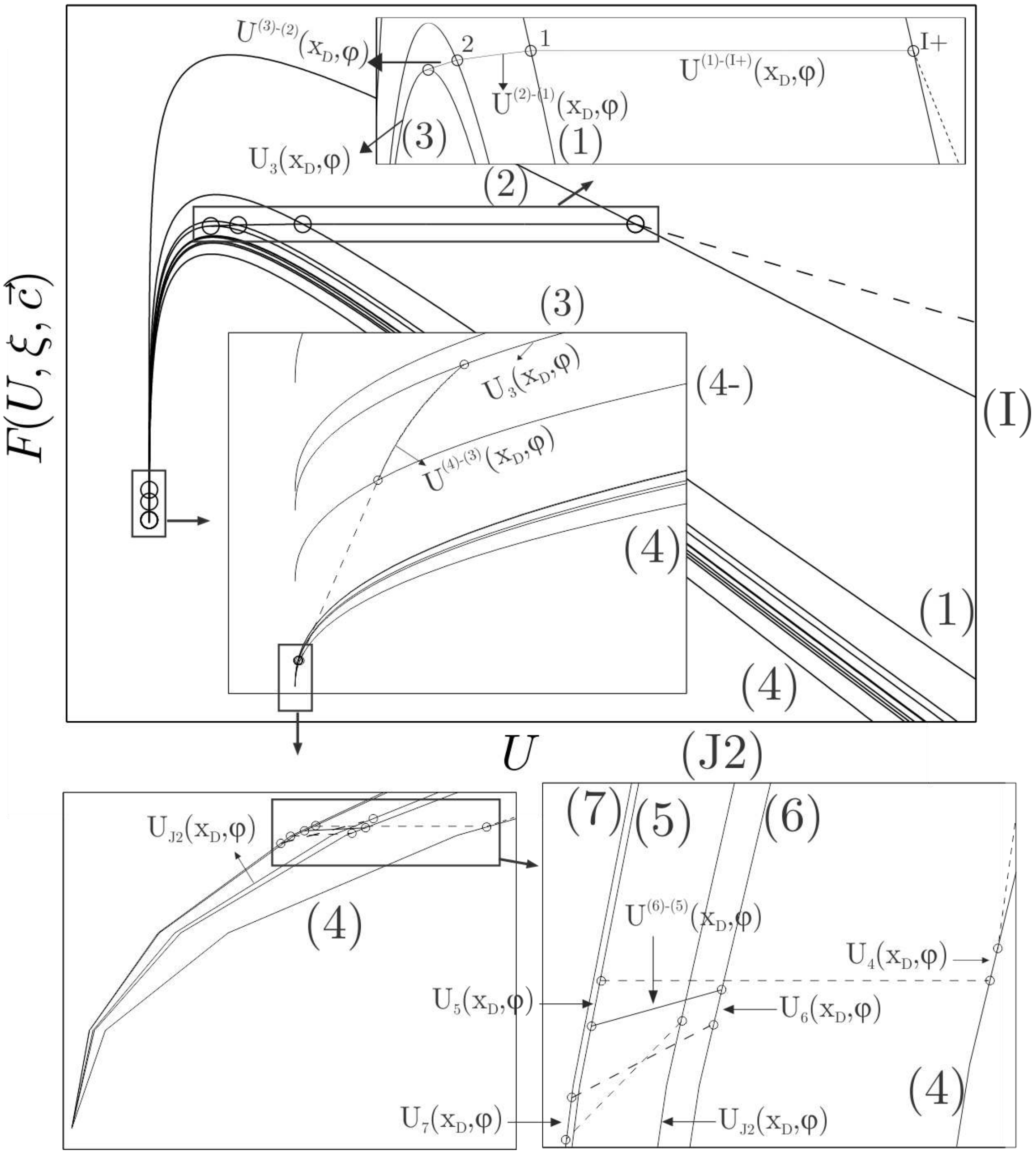

Figure 10: Solution path of U_{II} in the $F \times U$ plane

For $\varphi_B < \varphi < \varphi_C$ (solution U_{IV}) we have:

$$U_{IV}=\begin{cases}U_{J2}(x_D,\varphi), & x_D<\frac{\varphi-\varphi_{HS}}{V_{pH}^{(2)}}\\ U_7(x_D,\varphi), & \frac{\varphi-\varphi_{HS}}{V_{pH}^{(2)}}<x_D<\frac{\varphi-\varphi_{HS}}{V_{(3)}}\\ U_6(x_D,\varphi), & \frac{\varphi-\varphi_{HS}}{V_{(3)}}<x_D<\frac{\varphi-\varphi_{HS}}{\sigma_{(2)}\left(\vec{\omega}^{(6)},\xi^{(J1)}\right)}\\ U^{(6)-(5)}(x_D,\varphi), & \frac{\varphi-\varphi_{HS}}{\sigma_{(2)}\left(\vec{\omega}^{(6)},\xi^{(J1)}\right)}<x_D<\frac{\varphi}{V_{(pH)}^{(1)}}\\ U^{(6)-(5)-}(x_D,\varphi), & \frac{\varphi}{V_{(pH)}^{(1)}}<x_D<x_{(6)-(5)}^{-}(\varphi)\\ U^{(5)-(3-)}(x_D,\varphi), & x_{(6)-(5)}^{-}(\varphi)<x_D<\frac{\varphi}{\sigma_{pH}(\xi^{(I)})}\\ U_{3-}(x_D,\varphi), & \frac{\varphi}{\sigma_{pH}(\xi^{(I)})}<x_D<x_{(1)}^{-}(\varphi)\\ U_3(x_D,\varphi), & x_{(1)}^{-}(\varphi)<x_D<\frac{\varphi}{\sigma_{(3)}(\vec{\omega}^{(3)},\xi^{(I)})}\\ U^{(3)-(2)}(x_D,\varphi), & \frac{\varphi}{\sigma_{(3)}(\vec{\omega}^{(3)},\xi^{(I)})}<x_D<\frac{\varphi}{\sigma_{(3)}(\vec{\omega}^{(2)},\xi^{(I)})}\\ U^{(2)}, & \frac{\varphi}{\sigma_{(3)}(\vec{\omega}^{(2)},\xi^{(I)})}<x_D<\frac{\varphi}{\sigma_{(2)}(\vec{\omega}^{(2)},\xi^{(I)})}\\ U^{(2)-(1)}(x_D,\varphi), & \frac{\varphi}{\sigma_{(2)}(\vec{\omega}^{(2)},\xi^{(I)})}<x_D<\frac{\varphi}{\sigma_{(2)}(\vec{\omega}^{(1)},\xi^{(I)})}\\ U^{(1)}, & \frac{\varphi}{\sigma_{(2)}(\vec{\omega}^{(1)},\xi^{(I)})}<x_D<\frac{\varphi}{\sigma_{(1)}(\vec{\omega}^{(1)},\xi^{(I)})}\\ U^{(1)-(I+)}(x_D,\varphi), & \frac{\varphi}{\sigma_{(1)}(\vec{\omega}^{(1)},\xi^{(I)})}<x_D<\frac{\varphi}{\sigma_{(1)}(\vec{\omega}^{(I)},\xi^{(I)})}\\ U^{(I+)}, & \frac{\varphi}{\sigma_{(1)}(\vec{\omega}^{(I)},\xi^{(I)})}<x_D<+\infty\\ U^{(I)}, & x_D\to+\infty\end{cases}\tag{95}$$

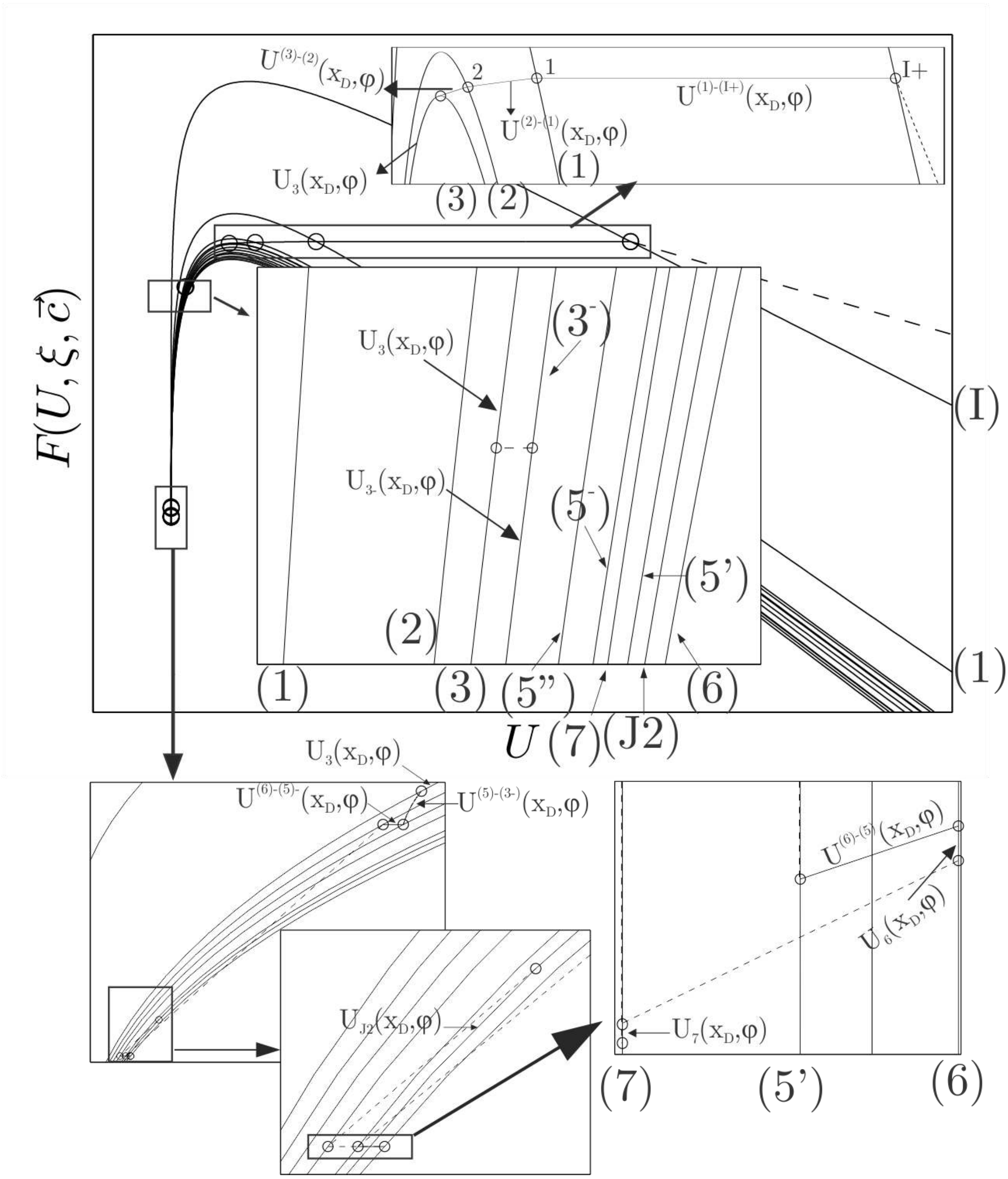

Figure 11: Solution path of U_{IV} in the $F \times U$ plane

$$U_{XIII} = \begin{cases} U_{J2}(x_D,\varphi), & x_D < x_{pH}^{-}(\varphi) \\ U^{(7)-(3---)}(x_D,\varphi), & x_{pH}^{-}(\varphi) < x_D < \frac{\varphi}{\sigma_{pH}(\xi^{(I)})} \\ U_{3---}(x_D,\varphi), & \frac{\varphi}{\sigma_{pH}(\xi^{(I)})} < x_D < x_{(3)}^{-} \\ U_{3--}(x_D,\varphi), & x_{(3)}^{-} < x_D < x_{(6)-(5)}^{-(+)}(\varphi) \\ U^{(6)-(5)-}(x_D,\varphi), & x_{(6)-(5)}^{-(+)}(\varphi) < x_D < x_{(3)-(2)}^{--(+)}(\varphi) \\ U^{(3)-(2)--}(x_D,\varphi), & x_{(3)-(2)}^{--(+)}(\varphi) < x_D < x_{(6)-(5)}^{-(-)}(\varphi) \\ U^{(3)-(2)-}(x_D,\varphi), & x_{(6)-(5)}^{-(-)}(\varphi) < x_D < x_{(3)-(2)}^{--(-)}(\varphi) \\ U^{(2-)}, & x_{(3)-(2)}^{--(-)}(\varphi) < x_D < x_{(2)-(1)}^{-(+)}(\varphi) \\ U^{(2)-(1)-}, & x_{(2)-(1)}^{-(+)}(\varphi) < x_D < x_{(2)-(1)}^{-(-)}(\varphi) \\ U^{(1-)}, & x_{(2)-(1)}^{-(-)}(\varphi) < x_D < x_{(1)}^{---}(\varphi) \\ U^{(1)}, & x_{(1)}^{---}(\varphi) < x_D < \frac{\varphi}{\sigma_{(1)}(\vec{\omega}^{(1)},\xi^{(I)})} \\ U^{(1)-(I+)}(x_D,\varphi), & \frac{\varphi}{\sigma_{(1)}(\vec{\omega}^{(1)},\xi^{(I)})} < x_D < \frac{\varphi}{\sigma_{(1)}(\vec{\omega}^{(I)},\xi^{(I)})} \\ U^{(I+)}, & \frac{\varphi}{\sigma_{(1)}(\vec{\omega}^{(I)},\xi^{(I)})} < x_D < +\infty \\ U^{(I)} & x_D \to +\infty \end{cases} \tag{96}$$

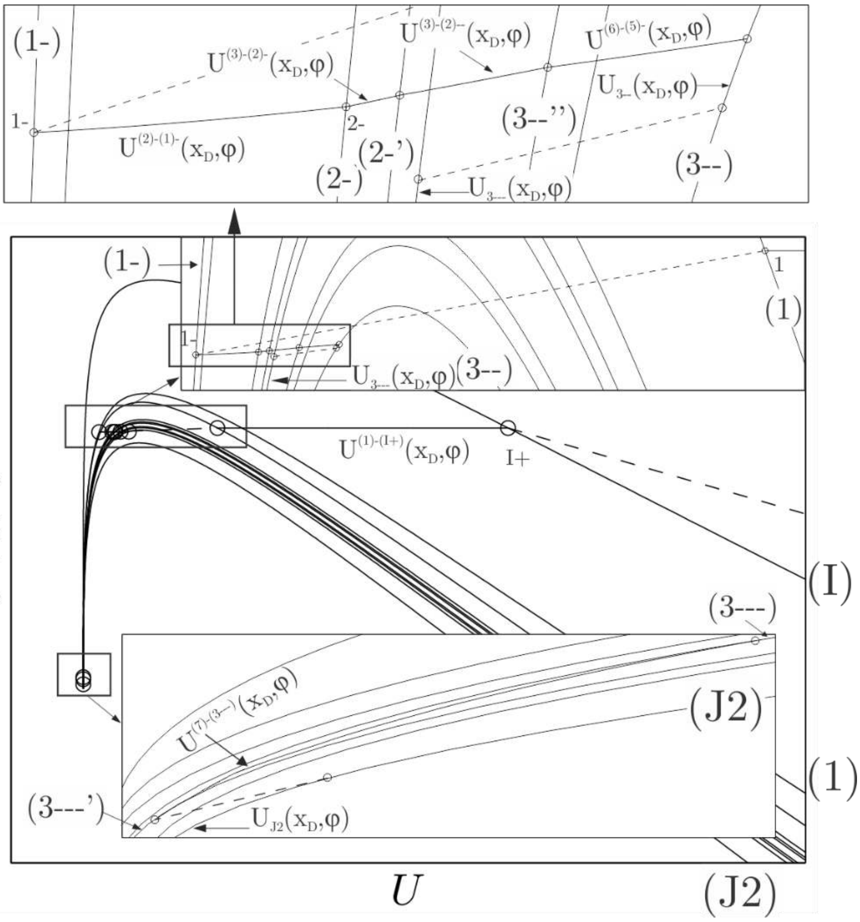

Figure 12: Solution path of U_{XIII} in $F \times U$ plane

6. Inverse mapping to $x_D \times t_D$ plane

In this section the solution in the auxiliary plane is mapped onto the $x_D \times t_D$ plane. First the saturation and fractional flow solutions are calculated from the expressions (70) and (71) and the waves are mapped using the potential function:

$$dt_D = \frac{d\varphi}{f(s(x_D,\varphi),\vec{c}(x_D,\varphi),\xi(x_D,\varphi))} + \frac{s}{f(s(x_D,\varphi),\vec{c}(x_D,\varphi),\xi(x_D,\varphi))} dx_D \tag{97}$$

The path of each rarefaction wave can be determined on the $x_D \times t_D$ plane by:

$$\lambda_{(X)} = \left(\frac{dt_D}{dx_D}\right)_{(X)} = U(x_D,\varphi)\sigma_{(X)} - F(U,\vec{c},\xi) \tag{98}$$

and the shock paths are mapped through the relation (Pires *et al.*, 2006):

$$D_{(X)} = \left(\frac{dt_D}{dx_D}\right)_{(k)} = \frac{1}{U^{\pm}(x_D,\varphi)V_{(k)} - F(U^{\pm},\vec{c}^{\pm},\xi^{\pm})} \tag{99}$$

In equations (98)-(99) X corresponds to the wave family (U, pH, $k = 1,2,3$). The U-waves on the auxiliary plane will be named as s-waves on $x_D \times t_D$ plane.

Note that all wave families interact with each other in $x_D \times t_D$ plane, including s-waves with concentration and pH waves. Thus, the waves from the rear of the low salinity slug are not straight lines.

The Buckley-Leverett shock velocity (water saturation shock at initial concentration and pH) is given by:

$$D_{(s)} = \frac{[f]}{[s]} = \frac{f^{-} - f^{(I)}}{s^{-} - s^{(I)}} = \frac{f^{-}}{s^{-} - s^{(I)}} \tag{100}$$

The characteristic diagram in $x_D \times t_D$ plane is presented in figure 13. We denote as $x_{XY}^{S}(t_D)$ and $x_{XY}^{R}(t_D)$ the shock wave and the rarefaction wave between points (x_X, t_X)-(x_Y, t_Y), respectively. The paths $x_{XY}^{R}(t_D)$ and $x_{XY}^{S}(t_D)$ are calculated integrating equations (98) and (99) in the region between points (x_X, t_X)-(x_Y, t_Y).

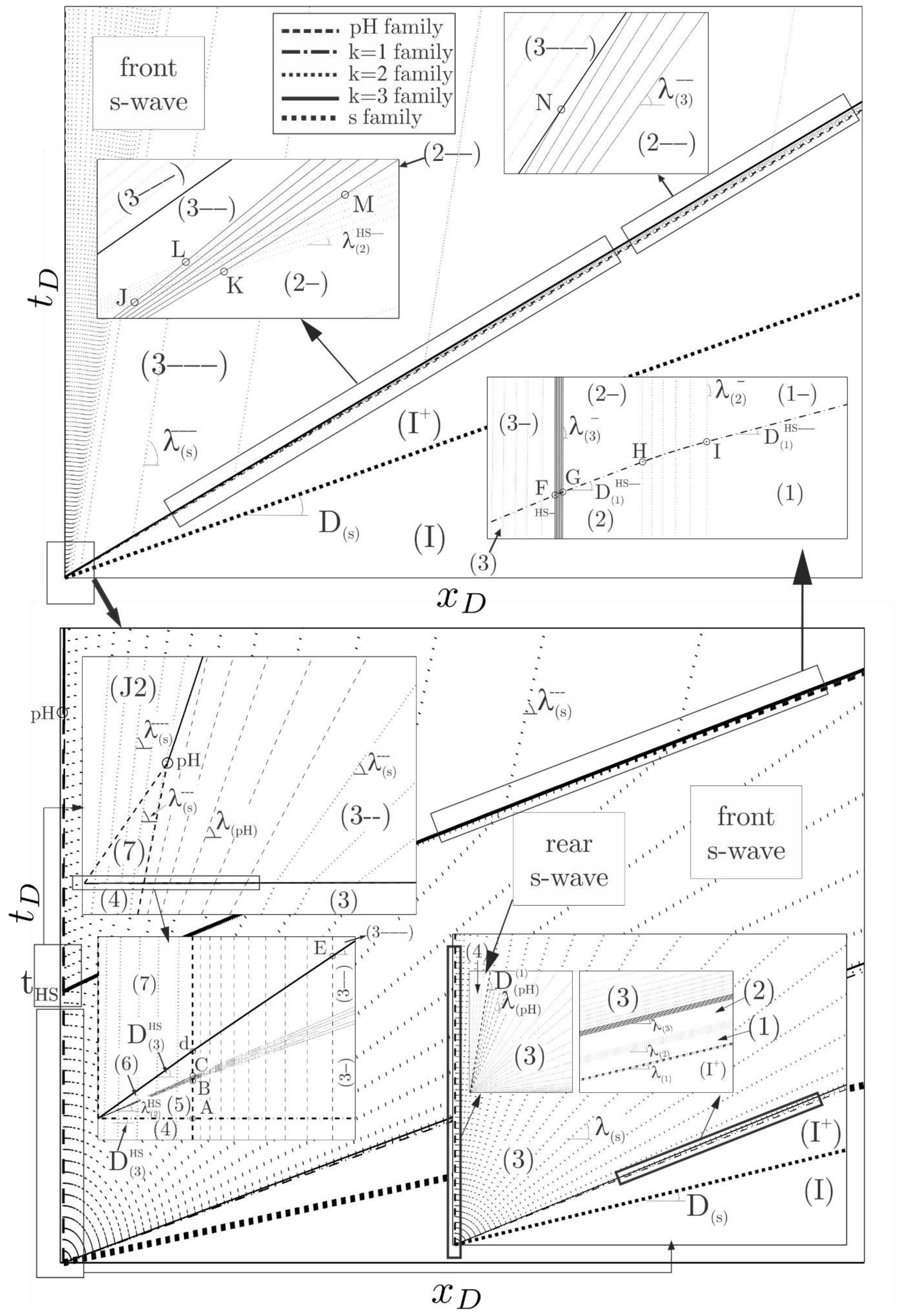

Figure 13: Characteristic diagram of the solution in $x_D \times t_D$ plane

The solution in $x_D \times t_D$ plane is also divided in 17 regions:

$$s(x_D, t_D) = \begin{cases} s_I, & t_D < t_{HS} \\ s_{II}, & t_{HS} < t_D < t_A \\ s_{III}, & t_A < t_D < t_B \\ s_{IV}, & t_B < t_D < t_C \\ s_V, & t_C < t_D < t_d \\ s_{VI}, & t_d < t_D < t_E \\ s_{VII}, & t_E < t_D < t_F \\ s_{VIII}, & t_F < t_D < t_G \\ s_{IX}, & t_G < t_D < t_H \\ s_X, & t_H < t_D < t_I \\ s_{XI}, & t_I < t_D < t_{pH} \\ s_{XII}, & t_{pH} < t_D < t_J \\ s_{XIII}, & t_J < t_D < t_K \\ s_{XIV}, & t_K < t_D < t_L \\ s_{XV}, & t_L < t_D < t_M \\ s_{XVI}, & t_M < t_D < t_N \\ s_{XVII}, & t_N < t_D \end{cases} \tag{101}$$

The solutions s_I,, s_{II},, s_{IV}, and s_{XIII} are described in equations (102)-(105). Water saturation profile and salinity profile are presented in figures (14)-(21). The complete solution is detailed in the supplementary material.

The self-similar part of the solution takes place when $t_D < t_{HS}$, solution s_I (Equation 102).

$$s_I = \begin{cases} s_4(x_D, t_D), & x_D < D^{(1)}_{(pH)} t_D \\ s^{(4)-(3)}(x_D, t_D), & D^{(1)}_{(pH)} t_D < x_D < \lambda_{(pH)}\left(\xi^{(I)}\right) t_D \\ s_3(x_D, t_D), & \lambda_{(pH)}\left(\xi^{(I)}\right) t_D < x_D < \lambda_{(3)}\left(\vec{c}^{(3)}, \xi^{(I)}\right) t_D \\ s^{(3)-(2)}(x_D, t_D), & \lambda_{(3)}\left(\vec{c}^{(3)}, \xi^{(I)}\right) t_D < x_D < \lambda_{(3)}\left(\vec{c}^{(2)}, \xi^{(I)}\right) t_D \\ s^{(2)}, & \lambda_{(3)}\left(\vec{c}^{(2)}, \xi^{(I)}\right) t_D < x_D < \lambda_{(2)}\left(\vec{c}^{(2)}, \xi^{(I)}\right) t_D \\ s^{(2)-(1)}(x_D, t_D), & \lambda_{(2)}\left(\vec{c}^{(2)}, \xi^{(I)}\right) t_D < x_D < \lambda_{(2)}\left(\vec{c}^{(1)}, \xi^{(I)}\right) t_D \\ s^{(1)}, & \lambda_{(2)}\left(\vec{c}^{(1)}, \xi^{(I)}\right) t_D < x_D < \lambda_{(1)}\left(\vec{c}^{(1)}, \xi^{(I)}\right) t_D \\ s^{(1)-(I+)}(x_D, t_D), & \lambda_{(1)}\left(\vec{c}^{(1)}, \xi^{(I)}\right) t_D < x_D < \lambda_{(1)}\left(\vec{c}^{(I)}, \xi^{(I)}\right) t_D \\ s^{(I+)}, & \lambda_{(1)}\left(\vec{c}^{(I)}, \xi^{(I)}\right) t_D < x_D < D_{(s)} t_D \\ s^{(I)}, & x_D > D_{(s)} t_D \end{cases} \tag{102}$$

In figures (14)-(15) it is shown the saturation and salinity profiles. It is possible to note that the pH change plays an important role in water saturation solution (saturation jump between s_4 and $s^{(4)-(3)}$). The solution path of s_I is depicted in figure (16).

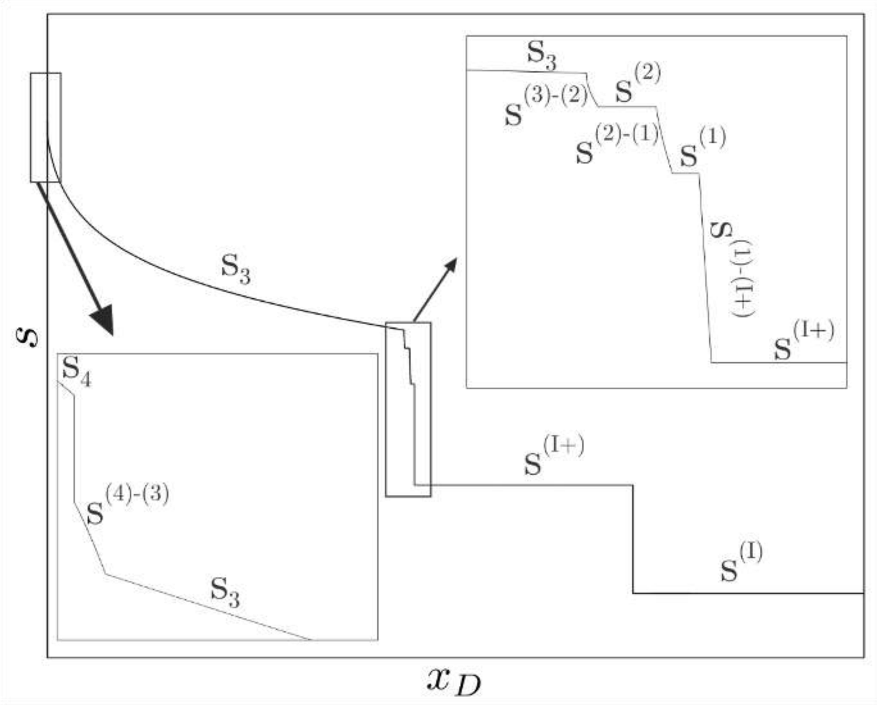

Figure 14: Water saturation profile for s_I

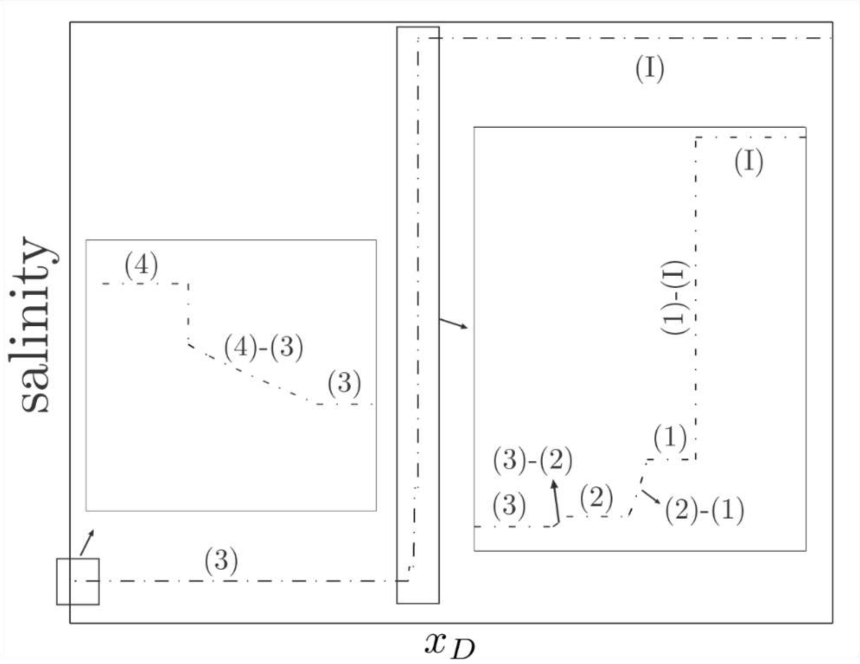

Figure 15: Salinity profile for $t_D < t_{HS}$

Solution s_{II} (Equation 103) starts at the injection of the seawater drive, while $t_{HS} < t_D < t_A$. The water saturation profile is shown in figure (16) and the salinity profile in figure (17). The pH and salinity waves centered in t_{HS} change the saturation behavior (Figure 16). Note that the decreasing salinity followed by its increase in regions (7), (6) and (6)-(5) (Figure 17) result in the creation of a small oil bank in saturation solution (saturation s_6 in Figure 16).

$$s_{II} = \begin{cases} s_{J2}(x_D, t_D), & x_D < x^S_{HS\,pH}(t_D) \\ s_7(x_D, t_D), & x^S_{HS\,pH}(t_D) < x_D < x^S_{HS\,d}(t_D) \\ s_6(x_D, t_D), & x^S_{HS\,d}(t_D) < x_D < x^R_{HS\,C}(t_D) \\ s^{(6)-(5)}(x_D, t_D), & x^R_{HS\,C}(t_D) < x_D < x^R_{HS\,B}(t_D) \\ s_5(x_D, t_D), & x^R_{HS\,B}(t_D) < x_D < x^S_{HS\,A}(t_D) \\ s_4(x_D, t_D), & x^S_{HS\,A}(t_D) < x_D < D^{(1)}_{(pH)} t_D \\ s^{(4)-(3)}(x_D, t_D), & D^{(1)}_{(pH)} t_D < x_D < \lambda_{(pH)}\left(\xi^{(I)}\right) t_D \\ s_3(x_D, t_D), & \lambda_{(pH)}\left(\xi^{(I)}\right) t_D < x_D < \lambda_{(3)}\left(\vec{c}^{(3)}, \xi^{(I)}\right) t_D \\ s^{(3)-(2)}(x_D, t_D), & \lambda_{(3)}\left(\vec{c}^{(3)}, \xi^{(I)}\right) t_D < x_D < \lambda_{(3)}\left(\vec{c}^{(2)}, \xi^{(I)}\right) t_D \\ s^{(2)}, & \lambda_{(3)}\left(\vec{c}^{(2)}, \xi^{(I)}\right) t_D < x_D < \lambda_{(2)}\left(\vec{c}^{(2)}, \xi^{(I)}\right) t_D \\ s^{(2)-(1)}(x_D, t_D), & \lambda_{(2)}\left(\vec{c}^{(2)}, \xi^{(I)}\right) t_D < x_D < \lambda_{(2)}\left(\vec{c}^{(1)}, \xi^{(I)}\right) t_D \\ s^{(1)}, & \lambda_{(2)}\left(\vec{c}^{(1)}, \xi^{(I)}\right) t_D < x_D < \lambda_{(1)}\left(\vec{c}^{(1)}, \xi^{(I)}\right) t_D \\ s^{(1)-(I+)}(x_D, t_D), & \lambda_{(1)}\left(\vec{c}^{(1)}, \xi^{(I)}\right) t_D < x_D < \lambda_{(1)}\left(\vec{c}^{(I)}, \xi^{(I)}\right) t_D \\ s^{(I+)}, & \lambda_{(1)}\left(\vec{c}^{(I)}, \xi^{(I)}\right) t_D < x_D < D_{(s)} t_D \\ s^{(I)}, & x_D > D_{(s)} t_D \end{cases} \tag{103}$$

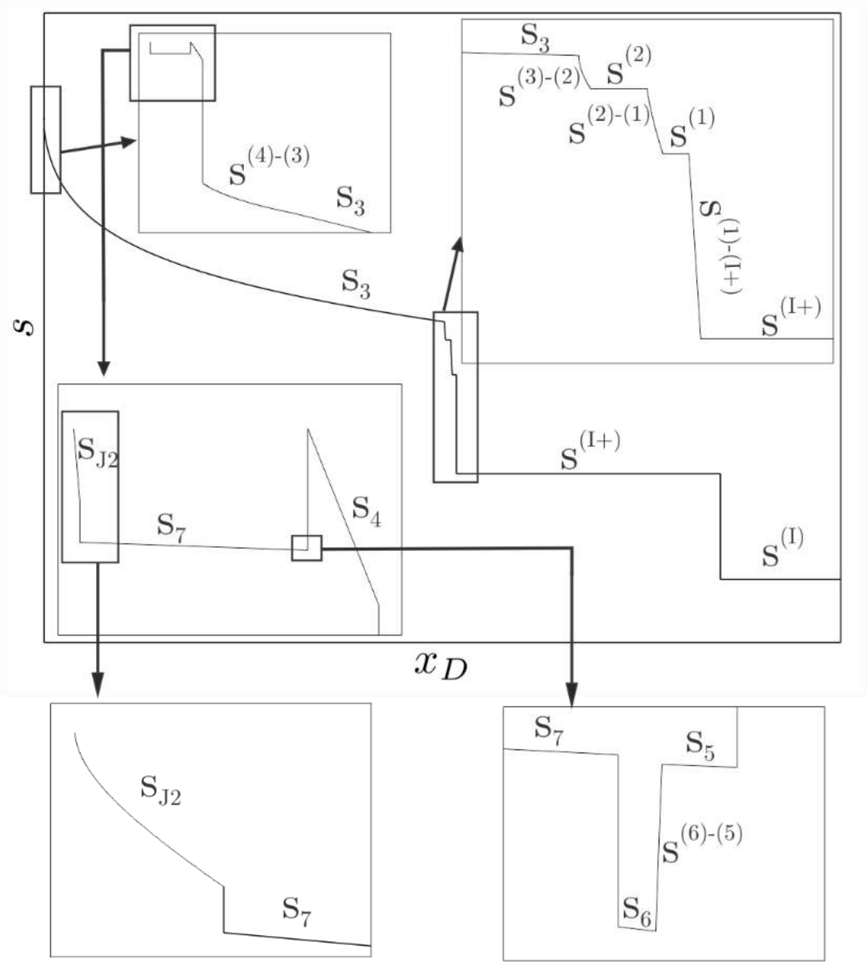

Figure 16: Water saturation profile for s_{II}

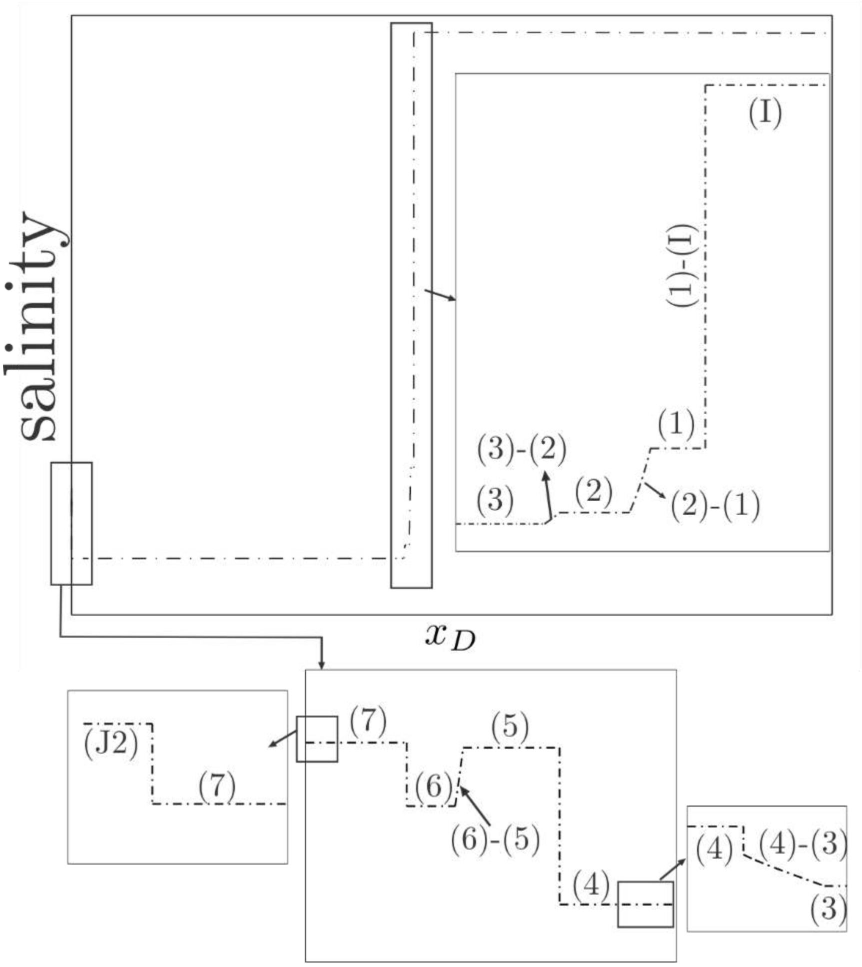

Figure 17: Salinity profile for $t_{HS} < t_D < t_A$

Solution s_{IV} ($t_B < t_D < t_C$) is characterized by the interaction between the rarefaction wave of family $k = 2$ and the pH waves from the front of the slug. The pH shock to a more acidic media changes the adsorption parameters of the cations, and the salinity that increased along x_D for family $k = 2$ starts to decrease (Figure 19). This behavior impacts water saturation solution: it increases along x_D before the pH shock (saturation wave $s^{(6)-(5)}$ in figure 18) and decreases after the pH shock (saturation wave $s^{(6)-(5)-}$ in figure 21).

$$s_{IV} = \begin{cases} s_{J2}(x_D, t_D), & x_D < x^S_{HS\,pH}(t_D) \\ s_7(x_D, t_D), & x^S_{HS\,pH}(t_D) < x_D < x^S_{HS\,d}(t_D) \\ s_6(x_D, t_D), & x^S_{HS\,d}(t_D) < x_D < x^R_{HS\,C}(t_D) \\ s^{(6)-(5)}(x_D, t_D), & x^R_{HS\,C}(t_D) < x_D < x^S_{B\,C}(t_D) \\ s^{(6)-(5)-}(x_D, t_D), & x^S_{B\,C}(t_D) < x_D < x^R_{B\,J}(t_D) \\ s^{(5)-(3-)}(x_D, t_D), & x^R_{B\,J}(t_D) < x_D < x^R_{0\,E}(t_D) \\ s_{3-}(x_D, t_D), & x^R_{0\,E}(t_D) < x_D < x^S_{A\,F}(t_D) \\ s_3(x_D, t_D), & x^S_{A\,F}(t_D) < x_D < \lambda_{(3)}\left(\vec{c}^{(3)}, \xi^{(I)}\right)t_D \\ s^{(3)-(2)}(x_D, t_D), & \lambda_{(3)}\left(\vec{c}^{(3)}, \xi^{(I)}\right)t_D < x_D < \lambda_{(3)}\left(\vec{c}^{(2)}, \xi^{(I)}\right)t_D \\ s^{(2)}, & \lambda_{(3)}\left(\vec{c}^{(2)}, \xi^{(I)}\right)t_D < x_D < \lambda_{(2)}\left(\vec{c}^{(2)}, \xi^{(I)}\right)t_D \\ s^{(2)-(1)}(x_D, t_D), & \lambda_{(2)}\left(\vec{c}^{(2)}, \xi^{(I)}\right)t_D < x_D < \lambda_{(2)}\left(\vec{c}^{(1)}, \xi^{(I)}\right)t_D \\ s^{(1)}, & \lambda_{(2)}\left(\vec{c}^{(1)}, \xi^{(I)}\right)t_D < x_D < \lambda_{(1)}\left(\vec{c}^{(1)}, \xi^{(I)}\right)t_D \\ s^{(1)-(I+)}(x_D, t_D), & \lambda_{(1)}\left(\vec{c}^{(1)}, \xi^{(I)}\right)t_D < x_D < \lambda_{(1)}\left(\vec{c}^{(I)}, \xi^{(I)}\right)t_D \\ s^{(I+)}, & \lambda_{(1)}\left(\vec{c}^{(I)}, \xi^{(I)}\right)t_D < x_D < D_{(s)}t_D \\ s^{(I)}, & x_D > D_{(s)}t_D \end{cases} \tag{104}$$

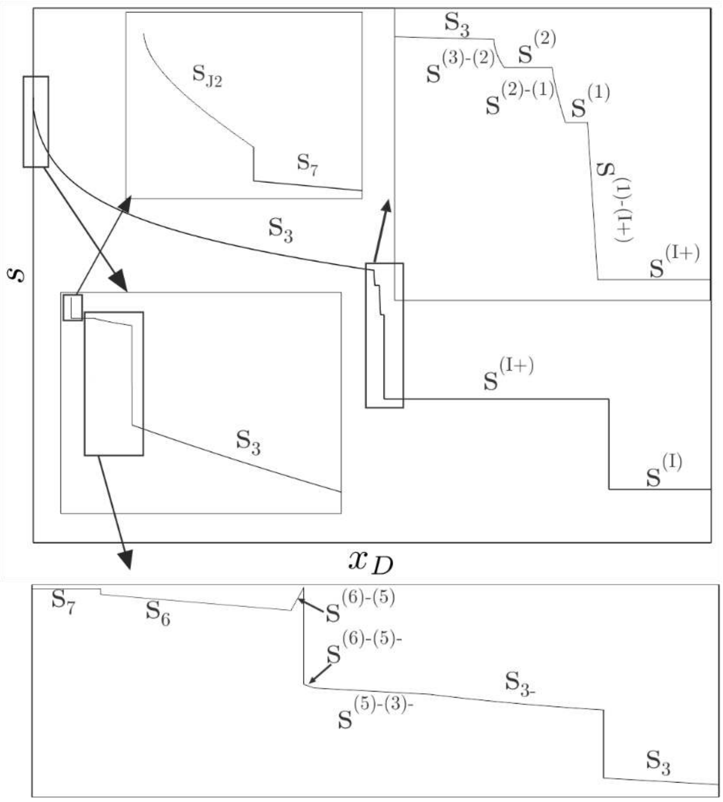

Figure 18: Water saturation profile for s_{IV}

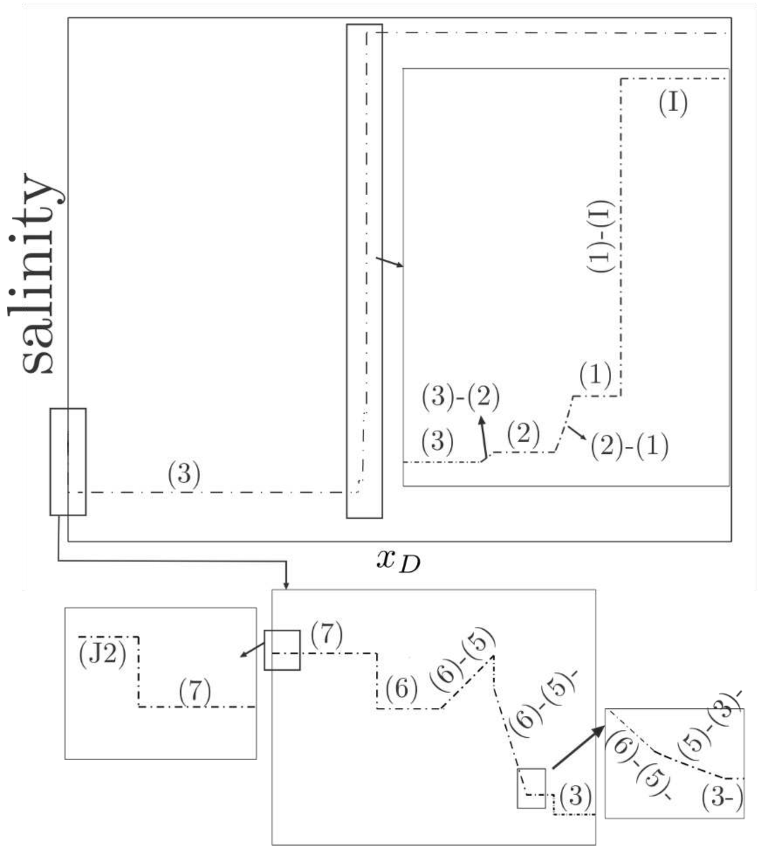

Figure 19: Salinity profile for $t_B < t_D < t_C$

In solution s_{XIII} (Equation 105) the rarefaction wave $k = 2$ from the rear and $k = 3$ from the front of the low salinity slug interact, which leads to the disappearance of region (3-) (Figure 21) and rarefaction s_{3-} (Figure 20), and the appearance of the region where these two waves interact: region (3)-(2)-- in salinity solution and rarefaction $s^{(3)-(2)--}$ in saturation solution. In the region where the two waves interact there is a slight salinity increase, and a slight increase of water saturation.

$$s_{XIII} = \begin{cases} s_{J2}(x_D, t_D), & x_D < x^S_{pH\,\infty}(t_D) \\ s^{(7)-(3---)}(x_D, t_D), & x^S_{pH\,\infty}(t_D) < x_D < x^R_{E\,\infty}(t_D) \\ s_{3---}(x_D, t_D), & x^R_{E\,\infty}(t_D) < x_D < x^S_{E\,N}(t_D) \\ s_{3--}(x_D, t_D), & x^S_{E\,N}(t_D) < x_D < x^R_{C\,L}(t_D) \\ s^{(6)-(5)-}(x_D, t_D), & x^R_{C\,L}(t_D) < x_D < x^R_{J\,L}(t_D) \\ s^{(3)-(2)--}(x_D, t_D), & x^R_{J\,L}(t_D) < x_D < x^R_{J\,K}(t_D) \\ s^{(3)-(2)-}(x_D, t_D), & x^R_{J\,K}(t_D) < x_D < x^R_{G\,K}(t_D) \\ s^{(2-)}, & x^R_{G\,K}(t_D) < x_D < x^R_{H\,\infty}(t_D) \\ s^{(2)-(1)-}(x_D, t_D), & x^R_{H\,\infty}(t_D) < x_D < x^R_{I\,\infty}(t_D) \\ s^{(1-)}, & x^R_{I\,\infty}(t_D) < x_D < x^S_{I\,\infty}(t_D) \\ s^{(1)}, & x^S_{I\,\infty}(t_D) < x_D < \lambda_{(1)}\left(\vec{c}^{(1)}, \xi^{(I)}\right)t_D \\ s^{(1)-(I+)}(x_D, t_D), & \lambda_{(1)}\left(\vec{c}^{(1)}, \xi^{(I)}\right)t_D < x_D < \lambda_{(1)}\left(\vec{c}^{(I)}, \xi^{(I)}\right)t_D \\ s^{(I+)}, & \lambda_{(1)}\left(\vec{c}^{(I)}, \xi^{(I)}\right)t_D < x_D < D_{(s)}t_D \\ s^{(I)}, & x_D > D_{(s)}t_D \end{cases} \tag{105}$$

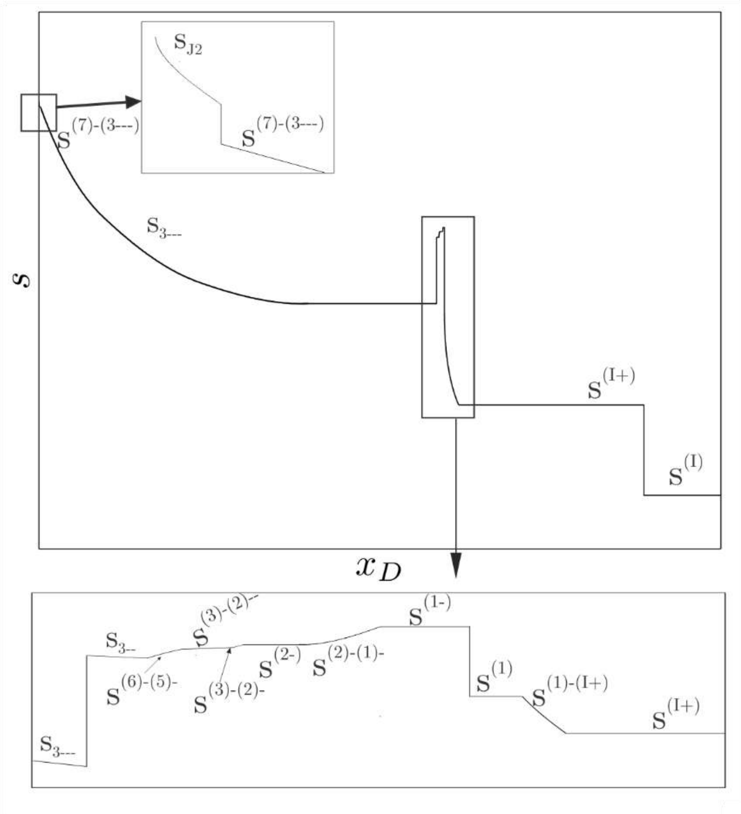

Figure 20: Water saturation profile for s_{XIII}

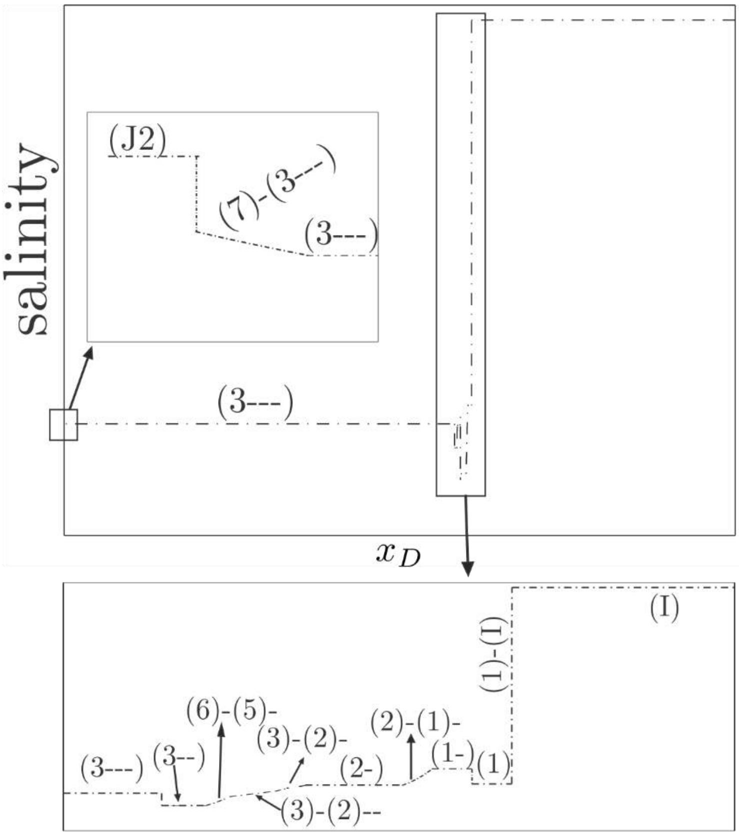

Figure 21: Salinity profile for $t_J < t_D < t_K$

Note that due to the low adsorption rate of sodium, the waves of the family $k = 1$ from the rear and from the front of the slug will never interact with each other. Moreover, the rarefaction waves of the family $k = 2$ don´t interact either, given that the last characteristic from the rear wave and the first characteristic from the front wave have the same slope. Another useful insight is that the waves of different families are completely separated from each other for $t_D > t_M$.

7. Summary and conclusions

We presented the complete analytical solution for the injection of a low salinity slug driven by seawater in oil reservoirs. It was considered three dissolved cations in the injection water and pH effects, which resulted in a system of $(n + 2) \times (n + 2)$ partial differential equations, where n is the number of dissolved cations.

The solution of this problem was built applying the splitting technique, which decoupled the original system of partial differential equations into a pH equation, an auxiliary system, and a lifting equation. Each problem was solved by the method of characteristics, and the solution extended the multicomponent chromatography theory for a two-phase flow in porous media considering non-constant adsorption coefficients and a different adsorption isotherm for the ion H^+.

The high difference between the adsorption rate of H^+ and the other cations leads to the appearance of small constant state regions in the space-time plane, which quickly disappear over time.

The pH of the initial water in porous media has an important effect on cations adsorption and water saturation solution, however, due to the high adsorption rates of H^+ the pH effects take place close to injection point for most of the time. The pH effects will be important only for a large number of pore volumes injected, which agrees with experimental data (Austad *et al.*, 2010; Aksulu *et al.*, 2012).

Different wave interaction types occur in the solution of this problem, which lead to several patterns in water saturation profiles. Moreover, the different salinity states resulting from interactions result in the appearance of oil and water banks along the porous media. This feature generates a large water bank when the k-waves from the rear of the low salinity slug begin to interact with the waves from the front. The low salinity effect (mobilization of residual oil) leads to the generation of an oil bank behind the large water bank. This behavior of water saturation profile can give useful insights to better understand and analyze recovery factor curves in reservoirs produced under low salinity waterflooding.

The solution procedure applied in this problem can be used in several other enhanced oil recovery techniques, including non-isothermal chemical flooding, low-salinity-polymer flooding, and others.

References

Aghaeifar, Z., Strand, S., Puntervold, T., Austad, T. & Aarnes, S. (2015). Adsorption/Desorption of Ca^{2+} and Mg^{2+} to/from Kaolinite Clay in Relation to the Low Salinity EOR Effect. In *18th European Symposium on Improved Oil Recovery*, Dresden, Germany. DOI: 10.3997/2214-4609.201412132

Akai, T., Blunt, M. & Bijeljic, B. (2020). Pore-Scale Numerical Simulation of Low Salinity Water Flooding Using the Lattice Boltzmann Method. *Journal of Colloid and Interface Science*, 566, pp. 444-453. DOI: 10.1016/j.jcis.2020.01.065

Aksulu, H., Hamso, D., Strand, S., Puntervold, T. & Austad, T. (2012). Evaluation of Low-Salinity Enhanced Oil Recovery Effects in Sandstone: Effects of the temperature and pH Gradient. *Energy & Fuels*, 26(06), pp. 3497-3503. DOI: 10.1021/ef300162n

Al-Saedi, H.N., Flori, R.E. & Mortadha, A. (2018). Investigation of Smart Water Flooding in Sandstone Reservoirs: Experimental and Simulation Study Part 2. In *Abu Dhabi International Petroleum Exhibition and Conference*, Abu Dhabi, UAE. DOI: 10.2118/193238-MS

Al-Shalabi, E.W., Sepehrnoori, K. & Pope, G. (2016). A Mechanistic Modeling of Oil Recovery Caused by Low-Salinity-Water Injection in Oil Reservoirs. *SPE Journal*, 21(03), pp. 730-743. DOI: 10.2118/172770-PA

Aladasani, A., Bai, B. Wu, Y. & Salehi, S. (2014). Studying Low-Salinity Waterflooding Recovery Effects in Sandstone Reservoirs. *Journal of Petroleum Science and Engineering*, 120, pp. 39-51. DOI: 10.1016/j.petrol.2014.03.008

Apolinário, F.O., de Paula, A.S. & Pires, A.P. (2020). Injection of Water Slug Containing Two Polymers in Porous media: Analytical Solution for Two-Phase Flow accounting for

Adsorption Effects. *Journal of Petroleum Science and Engineering*, 188. DOI: 10.1016/j.petrol.2020.106927

Apolinário, F.O. & Pires, A.P. (2021). Oil Displacement by Multicomponent Slug Injection: An Analytical Solution for Langmuir Adsorption Isotherm. *Journal of Petroleum Science and Engineering*, 188. DOI: 10.1016/j.petrol.2020.107939

Austad, T., Doust, A., Puntervold, T. (2010). Chemical Mechanism of Low Salinity Water Flooding in Sandstone Reservoirs. In *SPE Improved Oil Recovery Symposium*, Tulsa, USA. DOI: 10.2118/129767-MS

Bedrikovetsky, P.G. (1982). Displacement of Oil by a Slug of an Active Additive Forced by Water Through a Stratum. *Fluid Dynamics*, 17(03), pp. 409-417.

Bedrikovetsky, P.G (1993). Mathematical Theory of Oil and Gas Recovery: with Applications to ex-USSR Oil and Gas Fields. Kluwer Academic, London.

Borazjani, S., Bedrikovetsky, P.G. & Farajzadeh, R. (2016). Analytical Solutions of Oil Displacement by a Polymer Slug with Varying Salinity. *Journal of Petroleum Science and Engineering*, 140, pp. 28-40. DOI: 10.1016/j.petrol.2016.01.001

Borazjani, S., Roberts, A. & Bedrikovetsky, P.G. (2016). Splitting in Systems of PDEs for Two-Phase Multicomponent Flow in Porous Media. *Applied Mathematic Letters*, 53, pp. 25-32. DOI: 10.1016/j.aml.2015.09.014

Brady, P., Morrow, N.R., Fogden, A., Deniz, V. & Loahardjio, N. (2015). Electrostatics and the Low Salinity Effect in Sandstone Reservoirs. *Energy & Fuels*, 29(02), pp. 666-677. DOI: 10.1021/ef502474a

Cardoso, C.B., Silva, R.C.A. & Pires, A.P. (2007). The Role of Adsorption Isotherms on Chemical-Flooding Oil Recovery. In *SPE Annual Technical Conference and Exhibition*, Anaheim, USA. DOI: 10.2118/109642-MS

Claridge, E.L. & Bondor, P.L. (1974). A Graphical Method for Calculating Linear Displacement with Mass Transfer and Continuously Changing Mobilities. *SPE Journal*, 14(06), pp. 609-618. DOI: 10.2118/4673-PA

Corey, A.T. (1954). The Interrelation Between Gas and Oil Relative Permeabilities. *Producers Monthly*, 19(11), pp 38-41

Dafermos, C. (2000). Hyperbolic Conservation Laws on Continuum Physics, 3rd edition, Springer-Verlag Berlin Heidelberg, vol. 325.

Dahl, O., Johansen, T., Tveito, A. & Winther, R. (1991). Multicomponent Chromatography in a Two-Phase Environment. *SIAM Journal on Applied Mathematics*, 52(01), pp. 65-104. DOI: 10.1137/0152005

Dang, C., Nghiem, L., Nguyen, N., Chen, Z. & Nguyen, Q. (2016). Mechanistic Modeling of Low Salinity Waterflooding. *Journal of Petroleum Science and Engineering*, 146, pp. 191-209. DOI: 10.1016/j.petrol.2016.04.024

Dutra, T.A., Pires, A.P. & Bedrikovetsky, P.G. (2009). A New Splitting Scheme and Existence of Elliptic Region for Gasflood Modeling. *SPE Journal*, 14(01), pp. 101-111. DOI: 10.2118/107886-PA

Entov, V.M. & Polischuk (1975). Role of Sorption Processes with the Motion of Polymer Solutios in a Porous Medium. *Fluid Dynamics*, 10, pp. 422-428

Etemadi, A., Khodapanah, E. & Nejad, S.A.T.-(2016). Modelling Low-Salinity Waterflooding: Effect of Divalent Cations and Capillary Pressure. *Journal of Petroleum Science and Engineering*, 149, pp. 1-8. DOI: 10.1016/j.petrol.2016.10.012.

Farajzadeh, R., Bedrikovetsky, P.G., Lotfollahi, M. & Lake, L.W. (2016). Simultaneous Sorption and Mechanical Entrapment During Polymer Flow Through Porous Media. *Water Resources Research*, 52(03), pp. 2279-2298. DOI: 10.1002/2015WR017885

Garcia, D.T.G.F. (2019). Mathematical Modeling of Low-Salinity Wateflooding. Master Thesis at Universidade Estadual do Norte Fluminense, Macaé, Brazil

Helfferich, F.G. (1981). Theory of Multicomponent, Multiphase Displacement in Porous Media. *SPE Journal*, 21(01), pp. 51-62. DOI: 10.2118/8372-PA

Hirasaki, G.J. (1981). Application of the Theory of Multicomponent, Multiphase Displacement to Three-Component, Two-Phase Surfactant Flooding. *SPE Journal*, 21(02), pp. 51-62. DOI: 10.2118/8373-PA

Holter, K.E. (2016). Simulation of Low Salinity Waterflooding in a Synthetic Reservoir Model and Frϕy Field Reservoir Model. PhD dissertation, Norwegian University of Science and Technology, Trondheim, Norway

Jerauld, G., Lin, C. & Seccombe, J. (2008). Modeling Low-Salinity Waterflooding. *SPE Reservoir Evaluation & Engineering*, 11(06), pp 1000-1012. DOI: 10.2118/102239-PA

Khorsandi, S., Qiao, C. & Johns, R. (2016). Displacement efficiency for Low Salinity Polymer Flooding Including Wettability Alteration. In *SPE Improved Oil Recovery Conference*, Tulsa, USA. DOI: 10.2118/179695-PA

Johansen, T. & Winther, R. (1989). The Riemann Problem for Multicomponent Polymer Flooding. *SIAM Journal on Mathematical Analysis*, 20(04), pp. 908-929. DOI: 10.1137/0520061

Lager, A., Webb, K.J., Black, C.J. & Sorbie, K.S. (2006). Low Salinity Oil Recovery – an Experimental Investigation. *Petrophysics*, 49(01), pp 28-35.

Lager, A., Webb, K.J., Collins, I.R. & Richmond, D.M. (2008). LoSal Enhanced Oil Recovery: Evidence of Enhanced Oil Recovery at the Reservoir Scale. In *SPE Symposium on Improved Oil Recovery*, Tulsa, USA. DOI: 10.2118/113976-MS

Langmuir, I. (1918). The Adsorption of Gases on Plane Surface of Glass, Mica and Platinum. *Journal of American Chemical Society*, 40, pp. 1361-1403. DOI: 10.1021/ja02242a004

Ligthelm, D., Gronsveld, J., Hofman, J., Brussee, N., Marcelis, F. & van der Linde, H. (2009). Novel Waterflooding Strategy by Manipulation of Injection Brine Composition. In *EUROPEC/EAGE Conference and Exhibition*, Netherlands. DOI: 10.2118/119835-MS

Lima, S.A., Murad, M.A., Moyne, C. & Stemmelen, D. (2010). A Three-Scale Model of pH-Dependent Flows and Ion Transport with Equilibrium Adsorption in Kaolinite Clays: I. Homogenization Analysis. *Transport in Porous Media*, 85(01), pp. 23-44. DOI: 10.1007/s11242-010-9545-4

Lima, S.A., Murad, M.A., Vicente, B.J. & Pires, A.P. (2020). A New Mutiscale Computational Model for Low Salinity Waterflooding in Clay Bearing Sandstones. *Transport in Porous Media*, 135, pp. 361-408. DOI: 10.1007/s11242-020-01480-3

Logan, J. (1994). An Introduction to Nonlinear Partial Differential Equations, 2nd edition, John Wiley & Sons.

Luftenegger, M. & Clemens, T. (2017). Chromatography Effects in Alkali Surfactant Polymer Flooding. In *79th EAGE Conference and Exhibition*, Paris, France. DOI: 10.2118/185793-MS

Mahani, H., Sorop, T., Ligthelm, D., Brooks, A., Vledder, P. Mozagem, F. & Ali, Y. (2011). Analysis of Field Responses to Low-Salinity Waterflooding in Secundary and Tertiary Mode in Syria. In SPE EUROPEC/EAGE Annual Conference and Exhibition, Vienna, Austria. DOI: 10.2118/142960-MS

McCain Jr., W.D. (1991). Reservoir Fluid Property Correlations – State of the Art. *SPE Reservoir Engineering*, 6(02), pp. 266-272. DOI: 10.2118/18571-PA

McGuire, P.L., Chatham, J.R., Paskvan, F.K., Sommer, D.M. & Carini, F.H. (2005). Low Salinity Oil Recovery: An Exciting New EOR Opportunity for Alaska's North Slope. In *SPE Western Regional Meeting*, Irvine, USA. DOI: 10.2118/93903-MS

Morrow, N.R. & Buckley, J.S. (2011). Improved Oil Recovery by Low-Salinity Waterflooding. *Journal of Petroleum Technology*, 63(05), pp. 106-112. DOI: 10.2118/129421-JPT

Nasralla, R.A. & Nasr-el-din, H.A. (2011). Impact of Electric Surface Charges and Cation Exchange on Oil Recovery by Low Salinity Water. In *SPE Asia Pacific Oil and Gas Conference and Exhibition*, Jakarta, Indonesia. DOI: 10.2118/147937-MS

Nasralla, R.A. & Nasr-el-din, H.A. (2014). Impact of Cation Type and Concentration in Injected Brine on Oil Recovery in Sandstone Reservoirs. *Journal of Petroleum Science and Engineering*, 122. DOI: 10.1016/j.petrol.2014.07.038

Omekeh, A.V. & Evje, S. (2013). Modeling of Low Salinity Effects in Sandstone Oil Rocks. *International Journal of Numerical Analysis and Modeling*, 2(02), pp. 95-128

de Paula, A.S., Apolinário, F.O. & Pires, A.P. (2019). Water Slug Injection Containing n Polymers in Porous Media. *AIChE Journal*, 65(11). DOI: 10.1002/aic.16735

de Paula, A.S. & Pires, A.P. (2015). Analytical Solution for Oil Displacement by Polymer Slugs Containing Salt in Porous Media. *Journal of Petroleum Science and Engineering*, 197. DOI: 10.1016/j.petrol.2015.09.001

Patton, J.T., Coats, K.H. & Colegrove, G.T. (1971). Prediction of Polymer Flood Performance. *SPE Journal*, 11(01), pp. 72-84. DOI: 10.2118/2546-PA

Pires, A.P., Bedrikovetsky, P.G. & Shapiro, A.A. (2006). A Splitting Technique for Analytical Modelling of Two-Phase Multicomponent Flow in Porous Media. *Journal of Petroleum Science and Engineering*, 51, pp. 54-67. DOI: 10.1016/j.petrol.2005.11.009

Pope, G.A. (1980). The Application of Fractional Flow Theory to Enhanced Oil Recovery. *SPE Journal*, 20(03), pp. 191-205. DOI: 10.2118/7660-PA

Pouryousefy, E., Xie, Q. & Saeedi, A. (2016). Effect of Multi-component Ions Exchange on Low Salinity EOR: Coupled Geochemical Simulation Study. *Petroleum*, 2(03), pp. 191-209. DOI: 10.1016/j.petlm.2016.05.004

Rhee, H.K. & Amundson, N.R. (1970). An Analysis of an Adiabatic Adsorption Column: Part 1. Theoretical Development. *The Chemical Engineering Journal*, 1(03), pp. 241-254. DOI: 10.1016/0300-9467(70)80007-7

Rhee, H.K., Aris, R. & Amundson, N.R. (1970). On the Theory of Multicomponent Chromatography. *Philosophical Transactions of The Royal Society A: Mathematical,* *Physical and Engineering Sciences*, 267(1182), pp. 419-455. DOI: 10.1098/rsta.1970.0050

Rhee, H.K., Aris, R. & Amundson, N.R. (2001). First-Order Partial Differential Equations, vol. 2, 2nd edition, Dover Publications.

Ribeiro, P.M. & Pires, A.P. (2008). The Displacement of Oil by Polymer Slugs Considering Adsorption Effects. In *SPE Annual Technical Conference and Exhibition*, Denver, USA. DOI: 10.2118/115272-MS

Rivet, S.M., Lake. L.W. & Pope, G.A. (2010). A Coreflood Investigation of Low Salinity Enhanced Oil Recovery. In *SPE Annual Technical Conference and Exhibition*, Florence, Italy. DOI: 10.2118/134297-MS

Romero, M.I., Gamage, P., Jiang, H. & Thyne, G. (2013). Study of Low-Salinity Waterflooding for Single and Two-Phase Experiments in Berea Sandstone Cores. *Journal of Petroleum Science and Engineering*, 110, pp 149-154. DOI: 10.1016/j.petrol.2013.08.050

Seccombe, J., Lager, A., Jerauld, G., Jhaveri, B., Buikema, T., Bassler, S., Denis, J. Webb, K., Cockin, A., Fueg, E. & Paskvan, F. (2010). Demonstration of Low-Salinity EOR at Interwell Scale, Endicott Field, Alaska. In *SPE Improved Oil Recovery Symposium*, Tulsa, USA. DOI: 10.2118/129692-MS

Sheng, J.J. (2014). Critical Review of Low-Salinity Waterflooding. *Journal of Petroleum Science and Engineering*, 120, pp. 216-224. DOI: 10.1016/j.petrol.2014.05.026

Shojaei, M.-J., Ghazanfari, M. & Masihi, M. (2015). Relative Permeability and Capillary Pressure Curves for Low Salinity Water Flooding in Sandstone Rocks. *Journal of Natural Gas Science and Engineering*, 25, pp. 30-38. DOI: 10.1016/j.jngse.2015.04.023

Tang, G.-Q. & Morrow, N.R. (1999). Influence of Brine Composition and Fines Migration on Crude Oil/Brine/Rock Interactions and Oil Recovery. *Journal of Petroleum Science and Engineering*, 24(2-4), pp. 99-111. DOI: 10.1016/S0920-4105(99)00034-0

Vicente, B.J., Priimenko, V.I. & Pires, A.P. (2014). Semi-Analytical Solution for a Hyperbolic System Modeling 1D Polymer Slug Flow in Porous Media. *Journal of Petroleum Science and Engineering*, 15, pp. 102-109. DOI: 10.1016/j.petrol.2014.02.005

Wachmann, C. (1964). A Mathematical Theory for the Displacement of Oil and Water by Alcohol. *SPE Journal*, 4(03), pp. 250-266. DOI: 10.2118/879-PA

Xie, Q., Liu, Y., Wu, J. & Liu, Q. (2014). Ions Tuning Water Flooding Experiments and Interpretations by Thermodynamics of Wettability. *Journal of Petroleum Science and Engineering*, 124. DOI: 10.1016/j.petrol.2014.07.015

Appendix A – Supplementary Material of the Paper “Oil Displacement by Multicomponent Slug Injection: An Analytical Solution for Langmuir Adsorption Isotherm

In this supplementary material we present the detailed solution of the concentration and saturation in the auxiliary plane and saturation in physical plane.

The auxiliary problem for the injection of 3 polymers is given by:

$$\begin{cases} \dfrac{\partial a_1(\vec{c})}{\partial \varphi} + \dfrac{\partial c_1}{\partial x_D} = 0 \\ \dfrac{\partial a_2(\vec{c})}{\partial \varphi} + \dfrac{\partial c_2}{\partial x_D} = 0 \\ \dfrac{\partial a_3(\vec{c})}{\partial \varphi} + \dfrac{\partial c_3}{\partial x_D} = 0 \end{cases} \tag{1}$$

with the following initial and boundary conditions:

$$\varphi = 0, \quad \vec{c}\,(x_D, 0) = \vec{c}^{(I)} = 0, \; 0 < \; x_D < \frac{L}{\frac{\Omega_S}{A}} \tag{2}$$

$$x_D = 0, \; \vec{c}(0, \varphi) = \begin{cases} \vec{c}^{(J)}, & 0 < t_D < 1 \\ 0, & t_D > 1 \end{cases} \tag{3}$$

The i^{th} Riemann invariant J_i can be calculated from the relation (Rhee *et al.*, 1970):

$$J_i = \frac{K_i a_i(\vec{c})}{K_i - \omega}, \; i = 1,2,3 \tag{4}$$

where ω is a parameter of the problem. Moreover, we know that (Rhee *et al.*, 1970):

$$\sum_{i=1}^{3} J_i = 1 \tag{5}$$

Thus,

$$\sum_{i=1}^{3} \frac{K_i a_i(\vec{c})}{K_i - \omega} = 1 \tag{6}$$

The parameter ω can be calculated for any given concentration state solving equation (6), which has three distinct and positive roots (Rhee *et al.*, 2001). Thus, for each concentration state $\vec{c} = [c_1, c_2, c_3]$, there is an equivalent $\vec{\omega} = [\omega_1, \omega_2, \omega_3]$ state, where the components of the $\vec{\omega}$ vector are the roots of the polynomial (Equation 6) for the respective concentration state (Rhee *et al.*, 1970). Along a $\vec{c}$ wave, one or more concentrations can change. However, when this wave is mapped on the ω-space, only one coordinate of $\vec{\omega}$ varies and the other remain constant.

We calculate the initial and boundary $\vec{\omega}$ from equation (6) for any initial and boundary conditions (Equations 2 and 3), which will be denoted as $\vec{\omega}^{(I)}$ and $\vec{\omega}^{(J)}$, respectively. In each wave only one ω_i $(i = 1,2,3)$ changes. So, to connect the injection condition (J) to the initial condition (I), we must have three ω waves for $\varphi < 1$. For $\varphi > 1$, interaction between waves appear, thus there are at least six ω waves to connect the boundary condition to the initial condition of the problem (Rhee *et al.*, 2001).

After computing all ω waves, we can calculate the respective concentration waves from the relation (Rhee *et al.*, 1970):

$$K_i c_i = \left(\frac{K_i}{\omega_i} - 1\right) \prod_{j=1, j\neq i}^{3} \frac{\frac{K_i}{\omega_j} - 1}{\frac{K_i}{K_j} - 1} \tag{7}$$

We can also determine the characteristic slope $\sigma_{(k)}$ of the k^{th} family as a function of ω using the expression (Rhee *et al.*, 1970):

$$\sigma_{(k)} = \frac{d\varphi}{dx_D} = \omega_k^{(k)} \prod_{i=1}^{3} \frac{\omega_i^{(k)}}{K_i} \tag{8}$$

Note that for $\omega_k^{(k+1)} < \omega_k^{(k)}$, we have $\sigma_{(k+1)} > \sigma_{(k)}$, and therefore there is a ω_k rarefaction wave defined by equation (8), where all terms in the product remain constant, and ω_k varies continuously from $\omega_k^{(k)}$ to $\omega_k^{(k+1)}$. If $\omega_k^{(k+1)} > \omega_k^{(k)}$, there is a ω_k jump from $\omega_k^{(k)}$ to $\omega_k^{(k+1)}$ where all $\omega_{i\neq k}$ remaining constant. The k^{th} shock path is defined by the relation:

$$V_{(k)} = \left(\frac{d\varphi}{dx_D}\right)_s^{(k)} = \omega_k^{+} \prod_{i=1}^{k-1} \frac{\omega_i^{(J)}}{K_i} \tag{9}$$

Equation (9) is derived from Rankine-Hugoniot conditions (Rhee *et al.*, 1970). Note that equations (8)-(9) can be applied for any number of components.

When $\varphi = 0$, there is no polymer in the reservoir (Equation 2), therefore $\omega_i^{(J)} < \omega_i^{(I)}$ for all $\vec{\omega}$ vector components, and the solution path in ω-space for $\varphi < 1$ is composed by three shock waves (Table 1).

Table 1: ω-waves for $\varphi < 1$

Injection state	$\omega_1^{(J)}$	$\omega_2^{(J)}$	$\omega_3^{(J)}$
Intermediate state A	$\omega_1^{(J)}$	$\omega_2^{(J)}$	$\omega_3^{(I)}$
Intermediate state B	$\omega_1^{(J)}$	$\omega_2^{(I)}$	$\omega_3^{(I)}$
Initial state	$\omega_1^{(I)}$	$\omega_2^{(I)}$	$\omega_3^{(I)}$

The solution path in ω-space for $\varphi < 1$ is given by $(J) \rightarrow (A) \rightarrow (B) \rightarrow (I)$, where "→" denotes a shock wave (Figure 1). From equation (7) we can calculate the constant concentration states associated to the ω-waves described in table (1). In figure (1) the shock waves are presented as continuous lines between two states.

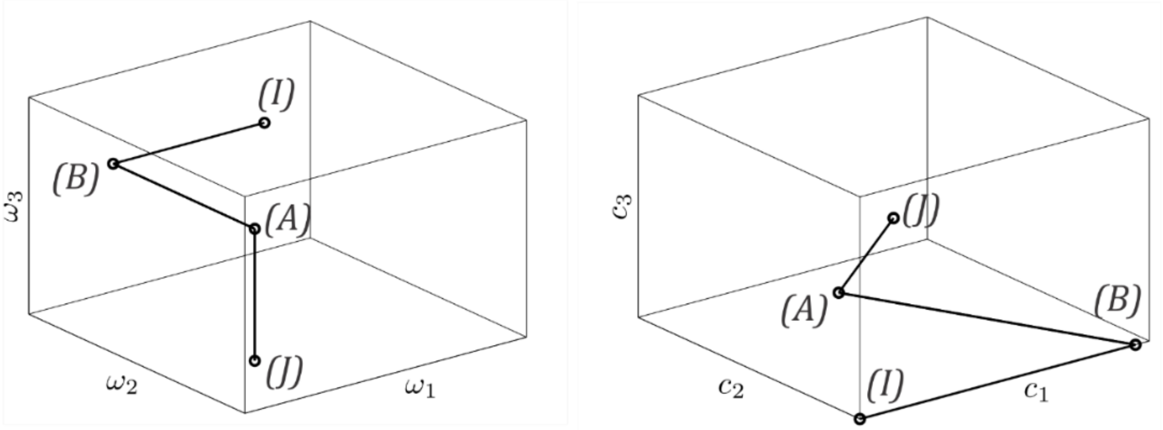

Figure 1: Solution path for $\varphi < 1$ in ω-space and in concentration space

The water drive composition is similar to the connate water, so, for $\varphi > 1$ the ω injection state is equal to the initial state, and $\omega_i^{(I)} < \omega_i^{(J)}$. Thus, after the beginning of the water drive, rarefaction waves appear at the rear of the slug. The structure of the ω-waves for $\varphi > 1$ at the beginning of water drive are presented in table (2).

Table 2: ω-waves for $\varphi > 1$

Injection state	$\omega_1^{(I)}$	$\omega_2^{(I)}$	$\omega_3^{(I)}$
Intermediate state C	$\omega_1^{(I)}$	$\omega_2^{(I)}$	$\omega_3^{(J)}$
Intermediate state D	$\omega_1^{(I)}$	$\omega_2^{(J)}$	$\omega_3^{(J)}$
Intermediate state J	$\omega_1^{(J)}$	$\omega_2^{(J)}$	$\omega_3^{(J)}$
Intermediate state A	$\omega_1^{(J)}$	$\omega_2^{(J)}$	$\omega_3^{(I)}$
Intermediate state B	$\omega_1^{(J)}$	$\omega_2^{(I)}$	$\omega_3^{(I)}$
Initial state	$\omega_1^{(I)}$	$\omega_2^{(I)}$	$\omega_3^{(I)}$

The solution path in ω-space for $\varphi > 1$ is presented in figure (2), and its structural formula is given by $(I) - (C) - (D) - (J) \rightarrow (A) \rightarrow (B) \rightarrow (I)$, where "$-$" denotes a rarefaction wave. Analogously to the self-similar part of the solution, we can calculate the constant states of the solution when $\varphi > 1$ applying equation (34). In figure (2), the shock waves are presented as continuous lines between two points, and the rarefaction waves by dashed lines.

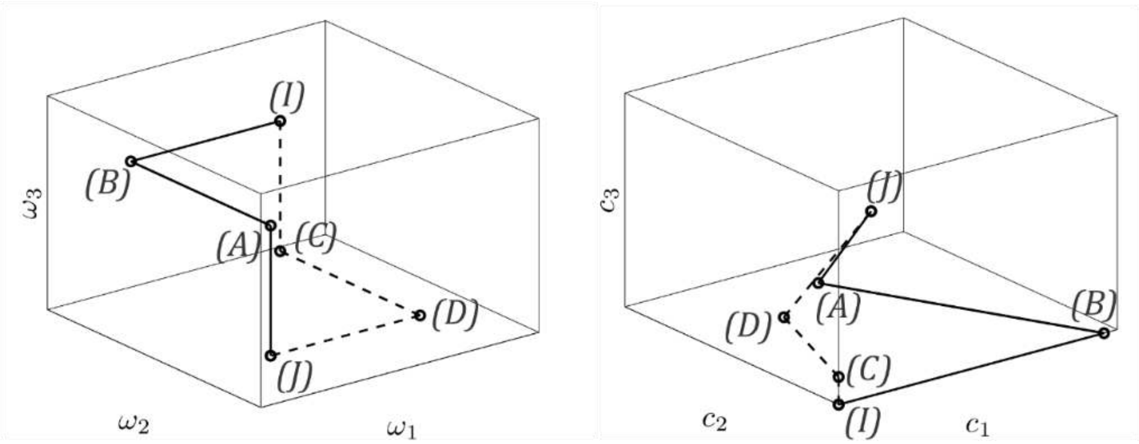

Figure 2: Solution path for $\varphi > 1$ in ω-space and in concentration space

Note that in figures (1) and (2), the ω-waves are straight lines parallel to one of the three axes, showing that only one ω_i changes.

As the slug propagates along the $x_D \times \varphi$ plane, interaction between waves may appear. Thus, the paths of the waves will be changed and the structure of ω waves solution also change. The theory of waves interactions is discussed in chapter 4 of Rhee *et al.* (2001).

The solution of the auxiliary problem presents two types of wave interactions: interactions between rarefaction and shock waves from different families and between rarefaction and shock waves from the same family.

Along the interaction between a rarefaction and a shock wave of different families, the waves are transmitted through each other and their paths change. The k^{th} family rarefaction slope after the interaction with a ω_j shock wave is given by:

$$\sigma_{(k)}^{-} = \left(\frac{d\varphi}{dx_D}\right)^{(k)-} = \omega_k^{(k)} \frac{\omega_j^{-}}{K_j} \prod_{i=1, i\neq j}^{k-1} \frac{\omega_i^{(k)}}{K_i} \tag{10}$$

where the superscript – denotes the value of ω_j and $\sigma_{(k)}$ after the shock. A rarefaction wave can cross more than one shock wave. In such cases, we denote the new rarefaction slope as $\sigma_{(k)}^{--}$. Note that for a multicomponent system there will be up to $k-1$ rarefaction-shock interactions for the k^{th} family.

The k^{th} family shock path along the interaction with a ω_j rarefaction is:

$$V_{(k)} = \left(\frac{d\varphi}{dx_D}\right)_S^{(k)} = \omega_k^{+} \frac{\omega_j}{K_j} \prod_{i=1, i\neq j}^{k-1} \frac{\omega_i^{(J)}}{K_i} \tag{11}$$

where ω_j varies continuously along the interaction. Therefore, the shock path is no longer a straight line.

When waves of the same family interact, the rarefaction is adsorbed by the shock wave, *i.e.* it is not transmitted, and the new shock path can be obtained from the relation:

$$V_{(k)} = \left(\frac{d\varphi}{dx_D}\right)_s^{(k)} = \omega_k^+ \frac{\omega_k^-}{K_k} \prod_{i=1}^{k-1} \frac{\omega_i^{(J)}}{K_i} \tag{12}$$

where the superscripts $+$ and $-$ denote the value of ω at the right and at the left state of the shock wave respectively, and ω_k^+ changes continuously along the interaction. We denote the shock path along an interaction region as $x_{s,r}(\varphi)$, where the subscript s denotes the shock family, and the subscript r denotes the rarefaction family. The shock path $x_{s,r}(\varphi)$ can be calculated integrating equation (12) along the interaction region.

We now present the complete description of the solution of the auxiliary system, which is composed by 11 parts separated by the end of the chemical injection ($\varphi = 1$) and by the crossing points between the waves:

$$c(x_D, \varphi) = \begin{cases} c_I, & \varphi < 1 \\ c_{II}, & 1 < \varphi < \varphi_A \\ c_{III}, & \varphi_A < \varphi < \varphi_B \\ c_{IV}, & \varphi_B < \varphi < \varphi_C \\ c_V, & \varphi_C < \varphi < \varphi_D \\ c_{VI}, & \varphi_D < \varphi < \varphi_E \\ c_{VII}, & \varphi_E < \varphi < \varphi_F \\ c_{VIII}, & \varphi_F < \varphi < \varphi_G \\ c_{IX}, & \varphi_G < \varphi < \varphi_H \\ c_X, & \varphi_H < \varphi < \varphi_I \\ c_{XI}, & \varphi_I < \varphi \end{cases} \tag{13}$$

The self-similar part of the solution $c_I(x_D, \varphi)$ is composed by four constant states:

$$c_I(x_D, \varphi) = \begin{cases} c_1 = c_1^{(J)}, c_2 = c_2^{(J)}, c_3 = c_3^{(J)}, & x_D < \frac{\varphi}{V_{(3)}} \\ c_1 = c_1^{(A)}, c_2 = c_2^{(A)}, c_3 = c_3^{(I)}, & \frac{\varphi}{V_{(3)}} < x_D < \frac{\varphi}{V_{(2)}} \\ c_1 = c_1^{(B)}, c_2 = c_2^{(I)}, c_3 = c_3^{(I)}, & \frac{\varphi}{V_{(2)}} < x_D < \frac{\varphi}{V_{(1)}} \\ c_1 = c_1^{(I)}, c_2 = c_2^{(I)}, c_3 = c_3^{(I)}, & \frac{\varphi}{V_{(1)}} < x_D \end{cases} \tag{14}$$

For $1 < \varphi < \varphi_A$ there is no wave interaction. Thus, $c_{II}(x_D, \varphi)$ is composed by three rarefaction waves and three shock waves, and is given by:

$$c_{II}(x_D,\varphi)=\begin{cases} c_1=0, c_2=0, c_3=0, & x_D<\frac{\varphi-1}{\sigma_{(3)}\left(\vec{\omega}^{(I)}\right)} \\ c_1=0, c_2=0, c_3=c_3(x_D,\varphi), & \frac{\varphi-1}{\sigma_{(3)}\left(\vec{\omega}^{(I)}\right)}<x_D<\frac{\varphi-1}{\sigma_{(3)}\left(\vec{\omega}^{(C)}\right)} \\ c_1=0, c_2=0, c_3=c_3^{(C)}, & \frac{\varphi-1}{\sigma_{(3)}\left(\vec{\omega}^{(C)}\right)}<x_D<\frac{\varphi-1}{\sigma_{(2)}\left(\vec{\omega}^{(C)}\right)} \\ c_1=0, c_2=c_2(x_D,\varphi), c_3=c_3(x_D,\varphi), & \frac{\varphi-1}{\sigma_{(2)}\left(\vec{\omega}^{(C)}\right)}<x_D<\frac{\varphi-1}{\sigma_{(2)}\left(\vec{\omega}^{(D)}\right)} \\ c_1=0, c_2=c_2^{(D)}, c_3=c_3^{(D)}, & \frac{\varphi-1}{\sigma_{(2)}\left(\vec{\omega}^{(D)}\right)}<x_D<\frac{\varphi-1}{\sigma_{(1)}\left(\vec{\omega}^{(D)}\right)} \\ c_1=c_1(x_D,\varphi), c_2=c_2(x_D,\varphi), c_3=c_3(x_D,\varphi), & \frac{\varphi-1}{\sigma_{(1)}\left(\vec{\omega}^{(D)}\right)}<x_D<\frac{\varphi-1}{\sigma_{(1)}\left(\vec{\omega}^{(J)}\right)} \\ c_1=c_1^{(J)}, c_2=c_2^{(J)}, c_3=c_3^{(J)}, & \frac{\varphi-1}{\sigma_{(1)}\left(\vec{\omega}^{(J)}\right)}<x_D<\frac{\varphi}{V_{(3)}} \\ c_1=c_1^{(A)}, c_2=c_2^{(A)}, c_3=c_3^{(I)}, & \frac{\varphi}{V_{(3)}}<x_D<\frac{\varphi}{V_{(2)}} \\ c_1=c_1^{(B)}, c_2=c_2^{(I)}, c_3=c_3^{(I)}, & \frac{\varphi}{V_{(2)}}<x_D<\frac{\varphi}{V_{(1)}} \\ c_1=c_1^{(I)}, c_2=c_2^{(I)}, c_3=c_3^{(I)}, & \frac{\varphi}{V_{(1)}}<x_D \end{cases}$$

(15)

At $\varphi=\varphi_A$ the rarefaction wave with slope $\sigma_{(1)}\left(\vec{\omega}^{(J)}\right)$ crosses the shock wave with slope $V_{(3)}$ and the first wave interaction appears. So, from now on, the constant state $\vec{c}^{(J)}$ is no longer present in the solution. Thus, the solution part $c_{III}(x_D,\varphi)$ is:

$c_{III}(x_D, \varphi) =$

$$\begin{cases} c_1 = 0, c_2 = 0, c_3 = 0, & x_D < \frac{\varphi-1}{\sigma_{(3)}(\vec{\omega}^{(I)})} \\ c_1 = 0, c_2 = 0, c_3 = c_3(x_D, \varphi), & \frac{\varphi-1}{\sigma_{(3)}(\vec{\omega}^{(I)})} < x_D < \frac{\varphi-1}{\sigma_{(3)}(\vec{\omega}^{(C)})} \\ c_1 = 0, c_2 = 0, c_3 = c_3^{(C)}, & \frac{\varphi-1}{\sigma_{(3)}(\vec{\omega}^{(C)})} < x_D < \frac{\varphi-1}{\sigma_{(2)}(\vec{\omega}^{(C)})} \\ c_1 = 0, c_2 = c_2(x_D, \varphi), c_3 = c_3(x_D, \varphi), & \frac{\varphi-1}{\sigma_{(2)}(\vec{\omega}^{(C)})} < x_D < \frac{\varphi-1}{\sigma_{(2)}(\vec{\omega}^{(D)})} \\ c_1 = 0, c_2 = c_2^{(D)}, c_3 = c_3^{(D)}, & \frac{\varphi-1}{\sigma_{(2)}(\vec{\omega}^{(D)})} < x_D < \frac{\varphi-1}{\sigma_{(1)}(\vec{\omega}^{(D)})} \\ c_1 = c_1^{+}(x_D, \varphi), c_2 = c_2^{+}(x_D, \varphi), c_3 = c_3^{+}(x_D, \varphi), & \frac{\varphi-1}{\sigma_{(1)}(\vec{\omega}^{(D)})} < x_D < x_{(3,1)}(\varphi) \\ c_1 = c_1^{-}(x_D, \varphi), c_2 = c_2^{-}(x_D, \varphi), c_3 = c_3^{(I)}, & x_{(3,1)}(\varphi) < x_D < \frac{\varphi-\varphi_A}{\sigma_{(1)}^{-}(\vec{\omega}^{(A)})} + x_A \\ c_1 = c_1^{(A)}, c_2 = c_2^{(A)}, c_3 = c_3^{(I)}, & \frac{\varphi-\varphi_A}{\sigma_{(1)}^{-}(\vec{\omega}^{(A)})} + x_A < x_D < \frac{\varphi}{V_{(2)}} \\ c_1 = c_1^{(B)}, c_2 = c_2^{(I)}, c_3 = c_3^{(I)}, & \frac{\varphi}{V_{(2)}} < x_D < \frac{\varphi}{V_{(1)}} \\ c_1 = c_1^{(I)}, c_2 = c_2^{(I)}, c_3 = c_3^{(I)}, & \frac{\varphi}{V_{(1)}} < x_D \end{cases} \tag{16}$$

For $c_{IV}(x_D, \varphi)$, the rarefaction wave $\sigma_{(1)}^{-}$ crosses the shock wave $V_{(2)}$ and the constant state *(A)* no longer exists. Thus, we have:

$c_{IV}(x_D, \varphi) =$

$$\begin{cases} c_1 = 0, c_2 = 0, c_3 = 0, & x_D < \frac{\varphi-1}{\sigma_{(3)}(\vec{\omega}^{(I)})} \\ c_1 = 0, c_2 = 0, c_3 = c_3(x_D, \varphi), & \frac{\varphi-1}{\sigma_{(3)}(\vec{\omega}^{(I)})} < x_D < \frac{\varphi-1}{\sigma_{(3)}(\vec{\omega}^{(C)})} \\ c_1 = 0, c_2 = 0, c_3 = c_3^{(C)}, & \frac{\varphi-1}{\sigma_{(3)}(\vec{\omega}^{(C)})} < x_D < \frac{\varphi-1}{\sigma_{(2)}(\vec{\omega}^{(C)})} \\ c_1 = 0, c_2 = c_2(x_D, \varphi), c_3 = c_3(x_D, \varphi), & \frac{\varphi-1}{\sigma_{(2)}(\vec{\omega}^{(C)})} < x_D < \frac{\varphi-1}{\sigma_{(2)}(\vec{\omega}^{(D)})} \\ c_1 = 0, c_2 = c_2^{(D)}, c_3 = c_3^{(D)}, & \frac{\varphi-1}{\sigma_{(2)}(\vec{\omega}^{(D)})} < x_D < \frac{\varphi-1}{\sigma_{(1)}(\vec{\omega}^{(D)})} \\ c_1 = c_1^{+}(x_D, \varphi), c_2 = c_2^{+}(x_D, \varphi), c_3 = c_3^{+}(x_D, \varphi), & \frac{\varphi-1}{\sigma_{(1)}(\vec{\omega}^{(D)})} < x_D < x_{(3,1)}(\varphi) \\ c_1 = c_1^{-}(x_D, \varphi), c_2 = c_2^{-}(x_D, \varphi), c_3 = c_3^{(I)}, & x_{(3,1)}(\varphi) < x_D < x_{(2,1)}(\varphi) \\ c_1 = c_1^{--}(x_D, \varphi), c_2 = c_2^{(I)}, c_3 = c_3^{(I)}, & x_{(2,1)}(\varphi) < x_D < \frac{\varphi-\varphi_B}{\sigma_{(1)}^{--}(\vec{\omega}^{(B)})} + x_B \\ c_1 = c_1^{(B)}, c_2 = c_2^{(I)}, c_3 = c_3^{(I)}, & \frac{\varphi-\varphi_B}{\sigma_{(1)}^{--}(\vec{\omega}^{(B)})} + x_B < x_D < \frac{\varphi}{V_{(1)}} \\ c_1 = c_1^{(I)}, c_2 = c_2^{(I)}, c_3 = c_3^{(I)}, & \frac{\varphi}{V_{(1)}} < x_D \end{cases} \tag{17}$$

At $\varphi = \varphi_C$ the interaction between the rarefaction wave $\sigma_{(1)}$ and the shock wave $V_{(3)}$ ends, and from now on the components c_1 and c_3 no longer coexist in any region. Thus, c_V is given by:

$$c_V(x_D, \varphi) =$$

$$\begin{cases}
c_1 = 0, c_2 = 0, c_3 = 0, & x_D < \frac{\varphi - 1}{\sigma_{(3)}\left(\vec{\omega}^{(I)}\right)} \\
c_1 = 0, c_2 = 0, c_3 = c_3(x_D, \varphi), & \frac{\varphi - 1}{\sigma_{(3)}\left(\vec{\omega}^{(I)}\right)} < x_D < \frac{\varphi - 1}{\sigma_{(3)}\left(\vec{\omega}^{(C)}\right)} \\
c_1 = 0, c_2 = 0, c_3 = c_3^{(C)}, & \frac{\varphi - 1}{\sigma_{(3)}\left(\vec{\omega}^{(C)}\right)} < x_D < \frac{\varphi - 1}{\sigma_{(2)}\left(\vec{\omega}^{(C)}\right)} \\
c_1 = 0, c_2 = c_2(x_D, \varphi), c_3 = c_3(x_D, \varphi), & \frac{\varphi - 1}{\sigma_{(2)}\left(\vec{\omega}^{(C)}\right)} < x_D < \frac{\varphi - 1}{\sigma_{(2)}\left(\vec{\omega}^{(D)}\right)} \\
c_1 = 0, c_2 = c_2^{+(D)}, c_3 = c_3^{+(D)}, & \frac{\varphi - 1}{\sigma_{(2)}\left(\vec{\omega}^{(D)}\right)} < x_D < \frac{\varphi - \varphi_C}{V_{(3)}\left(\vec{\omega}^{(D)}\right)} + x_C \\
c_1 = 0, c_2 = c_2^{(E)}, c_3 = c_3^{(I)}, & \frac{\varphi - \varphi_C}{V_{(3)}\left(\vec{\omega}^{(D)}\right)} + x_C < x_D < \frac{\varphi - \varphi_C}{\sigma_{(1)}^{-}\left(\vec{\omega}^{(E)}\right)} + x_C \\
c_1 = c_1^{-}(x_D, \varphi), c_2 = c_2^{-}(x_D, \varphi), c_3 = c_3^{(I)}, & \frac{\varphi - \varphi_C}{\sigma_{(1)}^{-}\left(\vec{\omega}^{(E)}\right)} + x_C < x_D < x_{(2,1)}(\varphi) \\
c_1 = c_1^{--}(x_D, \varphi), c_2 = c_2^{(I)}, c_3 = c_3^{(I)}, & x_{(2,1)}(\varphi) < x_D < \frac{\varphi - \varphi_B}{\sigma_{(1)}^{--}\left(\vec{\omega}^{(B)}\right)} + x_B \\
c_1 = c_1^{(B)}, c_2 = c_2^{(I)}, c_3 = c_3^{(I)}, & \frac{\varphi - \varphi_B}{\sigma_{(1)}^{--}\left(\vec{\omega}^{(B)}\right)} + x_B < x_D < \frac{\varphi}{V_{(1)}} \\
c_1 = c_1^{(I)}, c_2 = c_2^{(I)}, c_3 = c_3^{(I)}, & \frac{\varphi}{V_{(1)}} < x_D
\end{cases} \tag{18}$$

When $\varphi = \varphi_D$, the rarefaction $\sigma_{(1)}$ meets the shock wave $V_{(1)}$, which is the first interaction between waves of the same family, and the constant state $\vec{c}^{(B)}$ no longer exists. Thus, the solution $c_{VI}(x_D, \varphi)$ is:

$c_{VI}(x_D, \varphi) =$

$$\begin{cases} c_1 = 0, c_2 = 0, c_3 = 0, & x_D < \frac{\varphi - 1}{\sigma_{(3)}\left(\vec{\omega}^{(I)}\right)} \\ c_1 = 0, c_2 = 0, c_3 = c_3(x_D, \varphi), & \frac{\varphi - 1}{\sigma_{(3)}\left(\vec{\omega}^{(I)}\right)} < x_D < \frac{\varphi - 1}{\sigma_{(3)}\left(\vec{\omega}^{(C)}\right)} \\ c_1 = 0, c_2 = 0, c_3 = c_3^{(C)}, & \frac{\varphi - 1}{\sigma_{(3)}\left(\vec{\omega}^{(C)}\right)} < x_D < \frac{\varphi - 1}{\sigma_{(2)}\left(\vec{\omega}^{(C)}\right)} \\ c_1 = 0, c_2 = c_2(x_D, \varphi), c_3 = c_3(x_D, \varphi), & \frac{\varphi - 1}{\sigma_{(2)}\left(\vec{\omega}^{(C)}\right)} < x_D < \frac{\varphi - 1}{\sigma_{(2)}\left(\vec{\omega}^{(D)}\right)} \\ c_1 = 0, c_2 = c_2^{+(D)}, c_3 = c_3^{+(D)}, & \frac{\varphi - 1}{\sigma_{(2)}\left(\vec{\omega}^{(D)}\right)} < x_D < \frac{\varphi - \varphi_C}{V_{(3)}\left(\vec{\omega}^{(D)}\right)} + x_C \\ c_1 = 0, c_2 = c_2^{(E)}, c_3 = c_3^{(I)}, & \frac{\varphi - \varphi_C}{V_{(3)}\left(\vec{\omega}^{(D)}\right)} + x_C < x_D < \frac{\varphi - \varphi_C}{\sigma_{(1)}^{-}\left(\vec{\omega}^{(E)}\right)} + x_C \\ c_1 = c_1^{-}(x_D, \varphi), c_2 = c_2^{-}(x_D, \varphi), c_3 = c_3^{(I)}, & \frac{\varphi - \varphi_C}{\sigma_{(1)}^{-}\left(\vec{\omega}^{(E)}\right)} + x_C < x_D < x_{(2,1)}(\varphi) \\ c_1 = c_1^{--}(x_D, \varphi), c_2 = c_2^{(I)}, c_3 = c_3^{(I)}, & x_{(2,1)}(\varphi) < x_D < x_{(1,1)}(\varphi) \\ c_1 = c_1^{(I)}, c_2 = c_2^{(I)}, c_3 = c_3^{(I)}, & x_{(1,1)}(\varphi) < x_D \end{cases} \tag{19}$$

At $\varphi = \varphi_E$, the rarefaction $\sigma_{(2)}$ crosses the shock wave $V_{(3)}$, the constant state $\vec{c}^{(D)}$ disappears and a new rarefaction wave appears ($\sigma_{(2)}^{-}$). Thus, the solution $c_{VII}(x_D, \varphi)$ is given by:

$c_{VII}(x_D, \varphi) =$

$$\begin{cases} c_1 = 0, c_2 = 0, c_3 = 0, & x_D < \frac{\varphi - 1}{\sigma_{(3)}\left(\vec{\omega}^{(I)}\right)} \\ c_1 = 0, c_2 = 0, c_3 = c_3(x_D, \varphi), & \frac{\varphi - 1}{\sigma_{(3)}\left(\vec{\omega}^{(I)}\right)} < x_D < \frac{\varphi - 1}{\sigma_{(3)}\left(\vec{\omega}^{(C)}\right)} \\ c_1 = 0, c_2 = 0, c_3 = c_3^{(C)}, & \frac{\varphi - 1}{\sigma_{(3)}\left(\vec{\omega}^{(C)}\right)} < x_D < \frac{\varphi - 1}{\sigma_{(2)}\left(\vec{\omega}^{(C)}\right)} \\ c_1 = 0, c_2 = c_2^{+}(x_D, \varphi), c_3 = c_3^{+}(x_D, \varphi), & \frac{\varphi - 1}{\sigma_{(2)}\left(\vec{\omega}^{(C)}\right)} < x_D < x_{(3,2)}(\varphi) \\ c_1 = 0, c_2 = c_2^{-}(x_D, \varphi), c_3 = c_3^{(I)}, & x_{(3,2)}(\varphi) < x_D < \frac{\varphi - \varphi_E}{\sigma_{(2)}^{-}\left(\vec{\omega}^{(E)}\right)} + x_E \\ c_1 = 0, c_2 = c_2^{(E)}, c_3 = c_3^{(I)}, & \frac{\varphi - \varphi_E}{\sigma_{(2)}^{-}\left(\vec{\omega}^{(E)}\right)} + x_E < x_D < \frac{\varphi - \varphi_C}{\sigma_{(1)}^{-}\left(\vec{\omega}^{(E)}\right)} + x_C \\ c_1 = c_1^{-}(x_D, \varphi), c_2 = c_2^{-}(x_D, \varphi), c_3 = c_3^{(I)}, & \frac{\varphi - \varphi_C}{\sigma_{(1)}^{-}\left(\vec{\omega}^{(E)}\right)} + x_C < x_D < x_{(2,1)}(\varphi) \\ c_1 = c_1^{--}(x_D, \varphi), c_2 = c_2^{(I)}, c_3 = c_3^{(I)}, & x_{(2,1)}(\varphi) < x_D < x_{(1,1)}(\varphi) \\ c_1 = c_1^{(I)}, c_2 = c_2^{(I)}, c_3 = c_3^{(I)}, & x_{(1,1)}(\varphi) < x_D \end{cases} \tag{20}$$

After $\varphi = \varphi_F$, component 1 is completely separated from the other chemicals and a region without any chemicals appears. So, the solution $c_{VIII}(x_D, \varphi)$ is:

$c_{VIII}(x_D, \varphi) =$

$$\begin{cases} c_1 = 0, c_2 = 0, c_3 = 0, & x_D < \frac{\varphi - 1}{\sigma_{(3)}(\vec{\omega}^{(I)})} \\ c_1 = 0, c_2 = 0, c_3 = c_3(x_D, \varphi), & \frac{\varphi - 1}{\sigma_{(3)}(\vec{\omega}^{(I)})} < x_D < \frac{\varphi - 1}{\sigma_{(3)}(\vec{\omega}^{(C)})} \\ c_1 = 0, c_2 = 0, c_3 = c_3^{(C)}, & \frac{\varphi - 1}{\sigma_{(3)}(\vec{\omega}^{(C)})} < x_D < \frac{\varphi - 1}{\sigma_{(2)}(\vec{\omega}^{(C)})} \\ c_1 = 0, c_2 = c_2^{+}(x_D, \varphi), c_3 = c_3^{+}(x_D, \varphi), & \frac{\varphi - 1}{\sigma_{(2)}(\vec{\omega}^{(C)})} < x_D < x_{(3,2)}(\varphi) \\ c_1 = 0, c_2 = c_2^{-}(x_D, \varphi), c_3 = c_3^{(I)}, & x_{(3,2)}(\varphi) < x_D < \frac{\varphi - \varphi_E}{\sigma_{(2)}^{-}(\vec{\omega}^{(E)})} + x_E \\ c_1 = 0, c_2 = c_2^{+(E)}, c_3 = c_3^{(I)}, & \frac{\varphi - \varphi_E}{\sigma_{(2)}^{-}(\vec{\omega}^{(E)})} + x_E < x_D < \frac{\varphi - \varphi_F}{V_{(F)}(\vec{\omega}^{(E)})} + x_F \\ c_1 = 0, c_2 = c_2^{(I)}, c_3 = c_3^{(I)}, & \frac{\varphi - \varphi_F}{V_{(F)}(\vec{\omega}^{(E)})} + x_F < x_D < \frac{\varphi - \varphi_F}{\sigma_{(1)}^{--}(\vec{\omega}^{(I)})} + x_F \\ c_1 = c_1^{--}(x_D, \varphi), c_2 = c_2^{(I)}, c_3 = c_3^{(I)}, & \frac{\varphi - \varphi_F}{\sigma_{(1)}^{--}(\vec{\omega}^{(I)})} + x_F < x_D < x_{(1,1)}(\varphi) \\ c_1 = c_1^{(I)}, c_2 = c_2^{(I)}, c_3 = c_3^{(I)}, & x_{(1,1)}(\varphi) < x_D \end{cases} \qquad (21)$$

For $\varphi = \varphi_G$ the rarefaction $\sigma_{(2)}^{-}$ meets the shock $V_{(2)}$ and it is absorbed. Therefore, the constant state $\vec{c}^{(E)}$ is no longer present in the solution. So, $c_{IX}(x_D, \varphi)$ is:

$$c_{IX}(x_D, \varphi) = \begin{cases} c_1 = 0, c_2 = 0, c_3 = 0, & x_D < \frac{\varphi - 1}{\sigma_{(3)}(\vec{\omega}^{(I)})} \\ c_1 = 0, c_2 = 0, c_3 = c_3(x_D, \varphi), & \frac{\varphi - 1}{\sigma_{(3)}(\vec{\omega}^{(I)})} < x_D < \frac{\varphi - 1}{\sigma_{(3)}(\vec{\omega}^{(C)})} \\ c_1 = 0, c_2 = 0, c_3 = c_3^{(C)}, & \frac{\varphi - 1}{\sigma_{(3)}(\vec{\omega}^{(C)})} < x_D < \frac{\varphi - 1}{\sigma_{(2)}(\vec{\omega}^{(C)})} \\ c_1 = 0, c_2 = c_2^{+}(x_D, \varphi), c_3 = c_3^{+}(x_D, \varphi), & \frac{\varphi - 1}{\sigma_{(2)}(\vec{\omega}^{(C)})} < x_D < x_{(3,2)}(\varphi) \\ c_1 = 0, c_2 = c_2^{-}(x_D, \varphi), c_3 = c_3^{(I)}, & x_{(3,2)}(\varphi) < x_D < x_{(2,2)}(\varphi) \\ c_1 = 0, c_2 = c_2^{(I)}, c_3 = c_3^{(I)}, & x_{(2,2)}(\varphi) < x_D < \frac{\varphi - \varphi_F}{\sigma_{(1)}^{--}(\vec{\omega}^{(I)})} + x_F \\ c_1 = c_1^{--}(x_D, \varphi), c_2 = c_2^{(I)}, c_3 = c_3^{(I)}, & \frac{\varphi - \varphi_F}{\sigma_{(1)}^{--}(\vec{\omega}^{(I)})} + x_F < x_D < x_{(1,1)}(\varphi) \\ c_1 = c_1^{(I)}, c_2 = c_2^{(I)}, c_3 = c_3^{(I)}, & x_{(1,1)}(\varphi) < x_D \end{cases}$$

(22)

After $\varphi = \varphi_H$, all the components are completely separated (chromatographic cycle) by two regions where all concentrations are zero. Therefore, $c_X(x_D, \varphi)$ is:

$$c_X(x_D,\varphi) = \begin{cases} c_1 = 0, c_2 = 0, c_3 = 0, & x_D < \frac{\varphi-1}{\sigma_{(3)}\left(\vec{\omega}^{(I)}\right)} \\ c_1 = 0, c_2 = 0, c_3 = c_3(x_D,\varphi), & \frac{\varphi-1}{\sigma_{(3)}\left(\vec{\omega}^{(I)}\right)} < x_D < \frac{\varphi-1}{\sigma_{(3)}\left(\vec{\omega}^{(C)}\right)} \\ c_1 = 0, c_2 = 0, c_3 = c_3^{+(C)}, & \frac{\varphi-1}{\sigma_{(3)}\left(\vec{\omega}^{(C)}\right)} < x_D < \frac{\varphi-\varphi_H}{V_{(3)}\left(\vec{\omega}^{(C)}\right)} + x_H \\ c_1 = 0, c_2 = 0, c_3 = c_3^{(I)}, & \frac{\varphi-\varphi_H}{V_{(3)}\left(\vec{\omega}^{(C)}\right)} + x_H < x_D < \frac{\varphi-\varphi_H}{\sigma_{(2)}^{-}\left(\vec{\omega}^{(I)}\right)} + x_H \\ c_1 = 0, c_2 = c_2^{-}(x_D,\varphi), c_3 = c_3^{(I)}, & \frac{\varphi-\varphi_H}{\sigma_{(2)}^{-}\left(\vec{\omega}^{(I)}\right)} + x_H < x_D < x_{(2,2)}(\varphi) \\ c_1 = 0, c_2 = c_2^{(I)}, c_3 = c_3^{(I)}, & x_{(2,2)}(\varphi) < x_D < \frac{\varphi-\varphi_F}{\sigma_{(1)}^{--}\left(\vec{\omega}^{(I)}\right)} + x_F \\ c_1 = c_1^{--}(x_D,\varphi), c_2 = c_2^{(I)}, c_3 = c_3^{(I)}, & \frac{\varphi-\varphi_F}{\sigma_{(1)}^{--}\left(\vec{\omega}^{(I)}\right)} + x_F < x_D < x_{(1,1)}(\varphi) \\ c_1 = c_1^{(I)}, c_2 = c_2^{(I)}, c_3 = c_3^{(I)}, & x_{(1,1)}(\varphi) < x_D \end{cases}$$

(23)

For $\varphi > \varphi_I$, the rarefaction wave $\sigma_{(3)}$ is absorbed by the shock of same family $V_{(3)}$. As a consequence, the constant state $\vec{c}^{(C)}$ disappears. We can write $c_{XI}(x_D,\varphi)$ as:

$$c_{XI}(x_D,\varphi) = \begin{cases} c_1 = 0, c_2 = 0, c_3 = 0, & x_D < \frac{\varphi-1}{\sigma_{(3)}\left(\vec{\omega}^{(I)}\right)} \\ c_1 = 0, c_2 = 0, c_3 = c_3^{+}(x_D,\varphi), & \frac{\varphi-1}{\sigma_{(3)}\left(\vec{\omega}^{(I)}\right)} < x_D < x_{(3,3)}(\varphi) \\ c_1 = 0, c_2 = 0, c_3 = c_3^{(I)}, & x_{(3,3)}(\varphi) < x_D < \frac{\varphi-\varphi_H}{\sigma_{(2)}^{-}\left(\vec{\omega}^{(I)}\right)} + x_H \\ c_1 = 0, c_2 = c_2^{-}(x_D,\varphi), c_3 = c_3^{(I)}, & \frac{\varphi-\varphi_H}{\sigma_{(2)}^{-}\left(\vec{\omega}^{(I)}\right)} + x_H < x_D < x_{(2,2)}(\varphi) \\ c_1 = 0, c_2 = c_2^{(I)}, c_3 = c_3^{(I)}, & x_{(2,2)}(\varphi) < x_D < \frac{\varphi-\varphi_F}{\sigma_{(1)}^{--}\left(\vec{\omega}^{(I)}\right)} + x_F \\ c_1 = c_1^{--}(x_D,\varphi), c_2 = c_2^{(I)}, c_3 = c_3^{(I)}, & \frac{\varphi-\varphi_F}{\sigma_{(1)}^{--}\left(\vec{\omega}^{(I)}\right)} + x_F < x_D < x_{(1,1)}(\varphi) \\ c_1 = c_1^{(I)}, c_2 = c_2^{(I)}, c_3 = c_3^{(I)}, & x_{(1,1)}(\varphi) < x_D \end{cases} \quad (24)$$

From this point we present the solution of the lifting equation, given by:

$$\frac{\partial\, F(U,\vec{c})}{\partial\varphi} + \frac{\partial U(s,\vec{c})}{\partial x_D} = 0 \quad (25)$$

Applying the chain rule, we have:

$$\frac{\partial F}{\partial U}\frac{\partial U}{\partial\varphi} + \frac{\partial U}{\partial x_D} = -\frac{\partial F}{\partial c_1}\frac{\partial c_1}{\partial\varphi} - \frac{\partial F}{\partial c_2}\frac{\partial c_2}{\partial\varphi} - \frac{\partial F}{\partial c_3}\frac{\partial c_3}{\partial\varphi} \quad (26)$$

In regions where the concentrations are constant we find

$$\frac{\partial c_1}{\partial \varphi} = 0 \tag{27}$$

$$\frac{\partial c_2}{\partial \varphi} = 0 \tag{28}$$

$$\frac{\partial c_3}{\partial \varphi} = 0 \tag{29}$$

In such regions, the lifting equation is a homogeneous hyperbolic PDE given by:

$$\frac{\partial F}{\partial U}\frac{\partial U}{\partial \varphi} + \frac{\partial U}{\partial x_D} = 0 \tag{30}$$

where each characteristic carries a constant value of U, and its velocity is defined by:

$$\frac{d\varphi}{dx_D} = \sigma_U = \frac{\partial F(U,\vec{c})}{\partial U} \tag{31}$$

In rarefaction regions, where concentration changes continuously, along each characteristic (Equation 26) we have:

$$\frac{dU}{dx_D} = -\frac{\partial F}{\partial c_1}\frac{\partial c_1}{\partial \varphi} - \frac{\partial F}{\partial c_2}\frac{\partial c_2}{\partial \varphi} - \frac{\partial F}{\partial c_3}\frac{\partial c_3}{\partial \varphi} \tag{32}$$

The solution of the lifting equation is divided in 11 parts:

$$U(x_D,\varphi) = \begin{cases} U_I, & \varphi < 1 \\ U_{II}, & 1 < \varphi < \varphi_A \\ U_{III}, & \varphi_A < \varphi < \varphi_B \\ U_{IV}, & \varphi_B < \varphi < \varphi_C \\ U_V, & \varphi_C < \varphi < \varphi_D \\ U_{VI}, & \varphi_D < \varphi < \varphi_E \\ U_{VII}, & \varphi_E < \varphi < \varphi_F \\ U_{VIII}, & \varphi_F < \varphi < \varphi_G \\ U_{IX}, & \varphi_G < \varphi < \varphi_H \\ U_X, & \varphi_H < \varphi < \varphi_I \\ U_{XI}, & \varphi_I < \varphi \end{cases} \tag{33}$$

The solution $U_I(x_D,\varphi)$ is presented for φ_I, where $\varphi_I < 1$:

$$U_I(x_D,\varphi) = \begin{cases} U^{(J)}, & x_D < \frac{\varphi}{\sigma_U(U^{(J)},\vec{c}^{(J)})} \\ U_4(x_D,\varphi), & \frac{\varphi}{\sigma_U(U^{(J)},\vec{c}^{(J)})} < x_D < \frac{\varphi}{V_{(3)}} \\ U^{(3)}, & \frac{\varphi}{V_{(3)}} < x_D < \frac{\varphi}{V_{(2)}} \\ U^{(2)}, & \frac{\varphi}{V_{(2)}} < x_D < \frac{\varphi}{V_{(1)}} \\ U^{(1)}, & \frac{\varphi}{V_{(1)}} < x_D < \frac{\varphi}{\sigma_U(U^{(1)},\vec{c}^{(I)})} \\ U_{I^+}(x_D,\varphi), & \frac{\varphi}{\sigma_U(U^{(1)},\vec{c}^{(I)})} < x_D < \frac{\varphi}{\sigma_U(U^{(I^+)},\vec{c}^{(I)})} \\ U^{(I)}, & x_D \to +\infty \end{cases} \tag{34}$$

The structural formula of $U_I(x_D,\varphi)$ is $(I) \to I^{+''} - (1) \to (2) \to (3) \to (4) - (J)$, where "→" denotes a shock wave, and "$-$" a rarefaction wave (Figure 3). Note that the subscript "i" in the solution of U represents a U-rarefaction wave in a region i of figure (3), the superscript "(i)" represents a constant state of U in a region i of figure (3), and the superscript "$''$" in the structural formula denotes the first point of a rarefaction wave in the region.

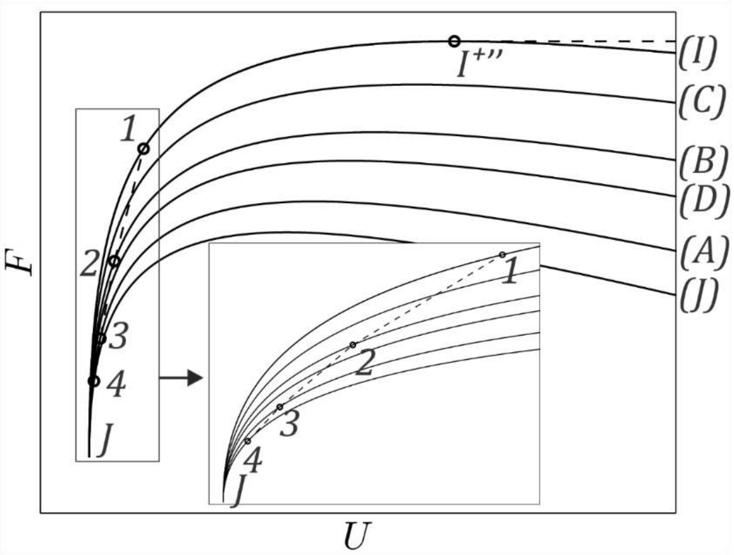

Figure 3: Solution U_I in $F \times U$ plane

For $U_{II}(x_D,\varphi)$ we have:

$$U_{II}(x_D,\varphi)=\begin{cases} U^{(J)}, & x_D<\frac{\varphi-1}{\sigma_U(U^{(J)},\vec{c}=0)} \\ U_{10}(x_D,\varphi), & \frac{\varphi-1}{\sigma_U(U^{(J)},\vec{c}=0)}<x_D<\frac{\varphi-1}{\sigma_{(3)}\left(\overrightarrow{\omega}^{(I)}\right)} \\ U_9(x_D,\varphi), & \frac{\varphi-1}{\sigma_{(3)}\left(\overrightarrow{\omega}^{(I)}\right)}<x_D<\frac{\varphi-1}{\sigma_{(3)}\left(\overrightarrow{\omega}^{(C)}\right)} \\ U_8(x_D,\varphi), & \frac{\varphi-1}{\sigma_{(3)}\left(\overrightarrow{\omega}^{(C)}\right)}<x_D<\frac{\varphi-1}{\sigma_{(2)}\left(\overrightarrow{\omega}^{(C)}\right)} \\ U_7(x_D,\varphi), & \frac{\varphi-1}{\sigma_{(2)}\left(\overrightarrow{\omega}^{(C)}\right)}<x_D<\frac{\varphi-1}{\sigma_{(2)}\left(\overrightarrow{\omega}^{(D)}\right)} \\ U_6(x_D,\varphi), & \frac{\varphi-1}{\sigma_{(2)}\left(\overrightarrow{\omega}^{(D)}\right)}<x_D<\frac{\varphi-1}{\sigma_{(1)}\left(\overrightarrow{\omega}^{(D)}\right)} \\ U_5(x_D,\varphi), & \frac{\varphi-1}{\sigma_{(1)}\left(\overrightarrow{\omega}^{(D)}\right)}<x_D<\frac{\varphi-1}{\sigma_{(1)}\left(\overrightarrow{\omega}^{(J)}\right)} \\ U_4(x_D,\varphi), & \frac{\varphi-1}{\sigma_U(U_4(x_D,\varphi),\vec{c}^{(J)})}<x_D<\frac{\varphi}{V_{(3)}} \\ U^{(3)}, & \frac{\varphi}{V_{(3)}}<x_D<\frac{\varphi}{V_{(2)}} \\ U^{(2)}, & \frac{\varphi}{V_{(2)}}<x_D<\frac{\varphi}{V_{(1)}} \\ U^{(1)}, & \frac{\varphi}{V_{(1)}}<x_D<\frac{\varphi}{\sigma_U(U^{(1)},\vec{c}^{(I)})} \\ U_{I^+}(x_D,\varphi), & \frac{\varphi}{\sigma_U(U^{(1)},\vec{c}^{(I)})}<x_D<\frac{\varphi}{\sigma_U(U^{(I^+)},\vec{c}^{(I)})} \\ U^{(I)}, & x_D\to+\infty \end{cases} \tag{35}$$

The structural formula for $U_{II}(x_D,\varphi)$ is $(I)\to I^{+\prime\prime}-(1)\to(2)\to(3)\to(4)-5''-6''-7''-8''-9''-10''-(J)$ (Figure 4).

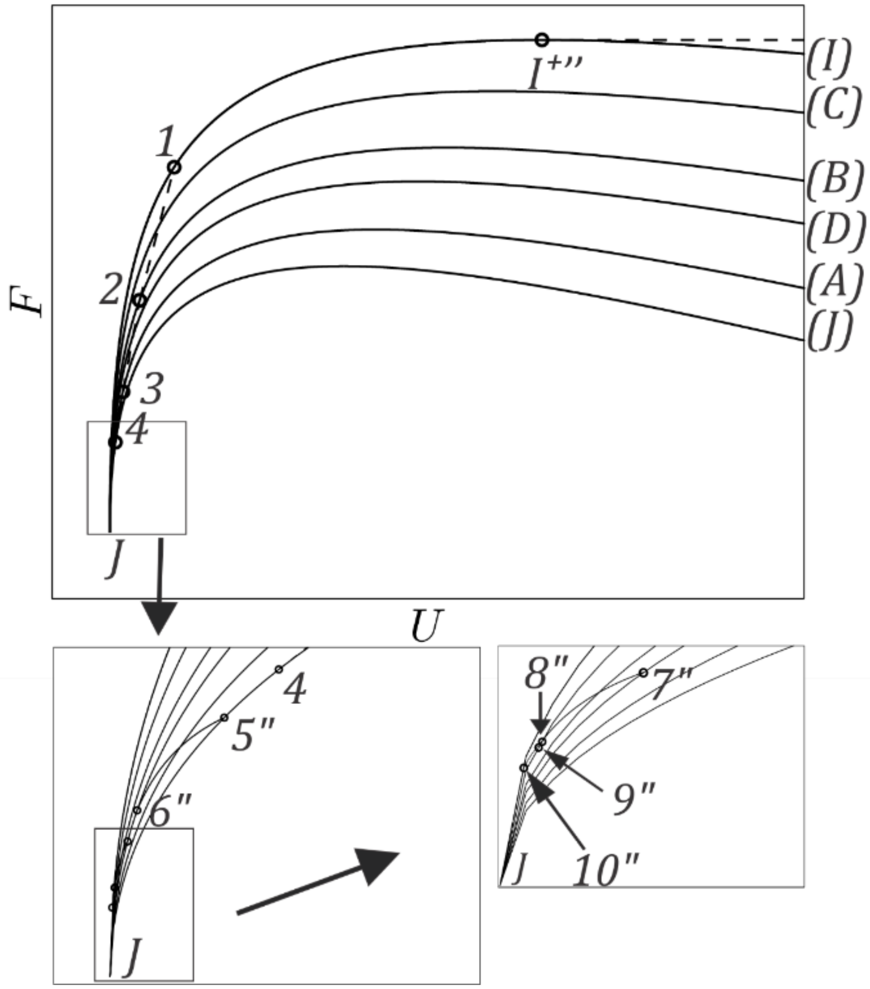

Figure 4: Solution U_{II} in $F \times U$ plane

State (4) disappears in solution U_{III}. We must also calculate new curves $F(U_5^+, \vec{c}_5{}^+)$ and $F(U_5^-, \vec{c}_5{}^-)$ to compute the solution. $U_{III}(x_D, \varphi)$:

$$U_{III}(x_D,\varphi)=\begin{cases} U^{(J)}, & x_D<\frac{\varphi-1}{\sigma_U(U^{(J)},\vec{c}=0)} \\ U_{10}(x_D,\varphi), & \frac{\varphi-1}{\sigma_U(U^{(J)},\vec{c}=0)}<x_D<\frac{\varphi-1}{\sigma_{(3)}(\vec{\omega}^{(I)})} \\ U_9(x_D,\varphi), & \frac{\varphi-1}{\sigma_{(3)}(\vec{\omega}^{(I)})}<x_D<\frac{\varphi-1}{\sigma_{(3)}(\vec{\omega}^{(C)})} \\ U_8(x_D,\varphi), & \frac{\varphi-1}{\sigma_{(3)}(\vec{\omega}^{(C)})}<x_D<\frac{\varphi-1}{\sigma_{(2)}(\vec{\omega}^{(C)})} \\ U_7(x_D,\varphi), & \frac{\varphi-1}{\sigma_{(2)}(\vec{\omega}^{(C)})}<x_D<\frac{\varphi-1}{\sigma_{(2)}(\vec{\omega}^{(D)})} \\ U_6(x_D,\varphi), & \frac{\varphi-1}{\sigma_{(2)}(\vec{\omega}^{(D)})}<x_D<\frac{\varphi-1}{\sigma_{(1)}(\vec{\omega}^{(D)})} \\ U_5^{+}(x_D,\varphi), & \frac{\varphi-1}{\sigma_{(1)}(\vec{\omega}^{(D)})}<x_D<x_{3,1}(\varphi) \\ U_5^{-}(x_D,\varphi), & x_{3,1}(\varphi)<x_D<\frac{\varphi-\varphi_A}{\sigma_{(1)}^{-}(\vec{\omega}^{(A)})}+x_A \\ U^{(3)}, & \frac{\varphi-\varphi_A}{\sigma_{(1)}^{-}(\vec{\omega}^{(A)})}+x_A<x_D<\frac{\varphi}{V_{(2)}} \\ U^{(2)}, & \frac{\varphi}{V_{(2)}}<x_D<\frac{\varphi}{V_{(1)}} \\ U^{(1)}, & \frac{\varphi}{V_{(1)}}<x_D<\frac{\varphi}{\sigma_U(U^{(1)},\vec{c}^{(I)})} \\ U_{I^+}(x_D,\varphi), & \frac{\varphi}{\sigma_U(U^{(1)},\vec{c}^{(I)})}<x_D<\frac{\varphi}{\sigma_U(U^{(I^+)},\vec{c}^{(I)})} \\ U^{(I)}, & x_D\to+\infty \end{cases} \tag{36}$$

The structural formula for U_{III} is: $(I)\to I^{+''}-(1)\to(2)\to(3)-5^{-''}\to 5^{+'}-5''-6''-7''-8''-9''-10''-(J)$. The superscript "$'$" in the structural formula denotes the last point of a rarefaction wave in the region. The segments $U_5^{+}(x_D,\varphi)$ and $U_5^{-}(x_D,\varphi)$ indicate the U states at the right and left of the shock path x_{AC}, which is the region where shock $V_{(3)}$ interacts with rarefaction $\sigma_{(1)}$. The $U_{III}(x_D,\varphi)$ solution in $F\times U$ plane is presented in figure 5.

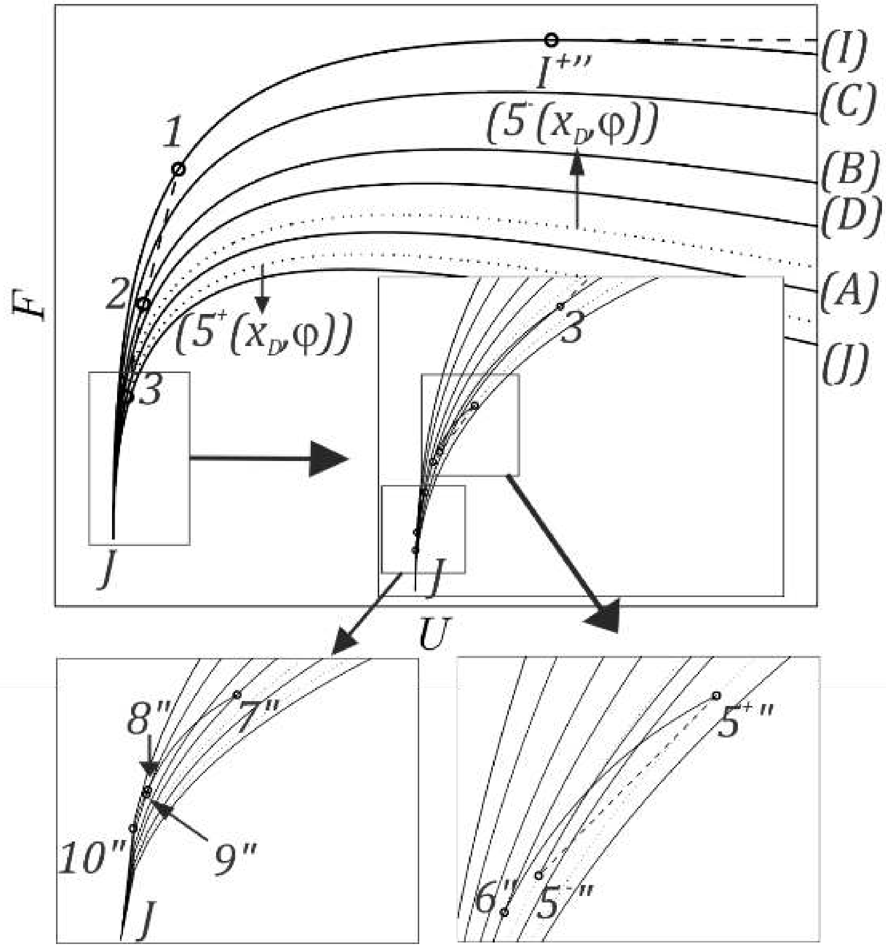

Figure 5: Solution U_{III} in $F \times U$ plane

$U_{IV}(x_D, \varphi)$ is defined by:

$$U_{IV}(x_D,\varphi)=\begin{cases} U^{(J)}, & x_D<\frac{\varphi-1}{\sigma_U(U^{(J)},\vec{c}=0)} \\ U_{10}(x_D,\varphi), & \frac{\varphi-1}{\sigma_U(U^{(J)},\vec{c}=0)}<x_D<\frac{\varphi-1}{\sigma_{(3)}\left(\vec{\omega}^{(I)}\right)} \\ U_9(x_D,\varphi), & \frac{\varphi-1}{\sigma_{(3)}\left(\vec{\omega}^{(I)}\right)}<x_D<\frac{\varphi-1}{\sigma_{(3)}\left(\vec{\omega}^{(C)}\right)} \\ U_8(x_D,\varphi), & \frac{\varphi-1}{\sigma_{(3)}\left(\vec{\omega}^{(C)}\right)}<x_D<\frac{\varphi-1}{\sigma_{(2)}\left(\vec{\omega}^{(C)}\right)} \\ U_7(x_D,\varphi), & \frac{\varphi-1}{\sigma_{(2)}\left(\vec{\omega}^{(C)}\right)}<x_D<\frac{\varphi-1}{\sigma_{(2)}\left(\vec{\omega}^{(D)}\right)} \\ U_6(x_D,\varphi), & \frac{\varphi-1}{\sigma_{(2)}\left(\vec{\omega}^{(D)}\right)}<x_D<\frac{\varphi-1}{\sigma_{(1)}\left(\vec{\omega}^{(D)}\right)} \\ U_5^{+}(x_D,\varphi), & \frac{\varphi-1}{\sigma_{(1)}\left(\vec{\omega}^{(D)}\right)}<x_D<x_{3,1}(\varphi) \\ U_5^{-}(x_D,\varphi), & x_{3,1}(\varphi)<x_D<x_{2,1}(\varphi) \\ U_5^{--}(x_D,\varphi), & x_{2,1}(\varphi)<x_D<\frac{\varphi-\varphi_B}{\sigma_{(1)}^{--}\left(\vec{\omega}^{(B)}\right)}+x_B \\ U^{(2)}, & \frac{\varphi-\varphi_B}{\sigma_{(1)}^{--}\left(\vec{\omega}^{(B)}\right)}+x_B<x_D<\frac{\varphi}{V_{(1)}} \\ U^{(1)}, & \frac{\varphi}{V_{(1)}}<x_D<\frac{\varphi}{\sigma_U(U^{(1)},\vec{c}^{(I)})} \\ U_{I^+}(x_D,\varphi), & \frac{\varphi}{\sigma_U(U^{(1)},\vec{c}^{(I)})}<x_D<\frac{\varphi}{\sigma_U(U^{(I^+)},\vec{c}^{(I)})} \\ U^{(I)}, & x_D\to+\infty \end{cases} \tag{37}$$

The solution path for U_{IV} in $F \times U$ plane is presented in figure 6. For the sake of simplicity, from now on the constant state curves of $F(U,\vec{c})$ that are not part of the solution will not be shown in the figures. The structural formula for U_{IV} is: $(I) \to I^{+''} - (1) \to (2) - 5^{--''} \to 5^{-''} - 5^{-'} \to 5'' - 6'' - 7'' - 8'' - 9'' - 10'' - (J)$.

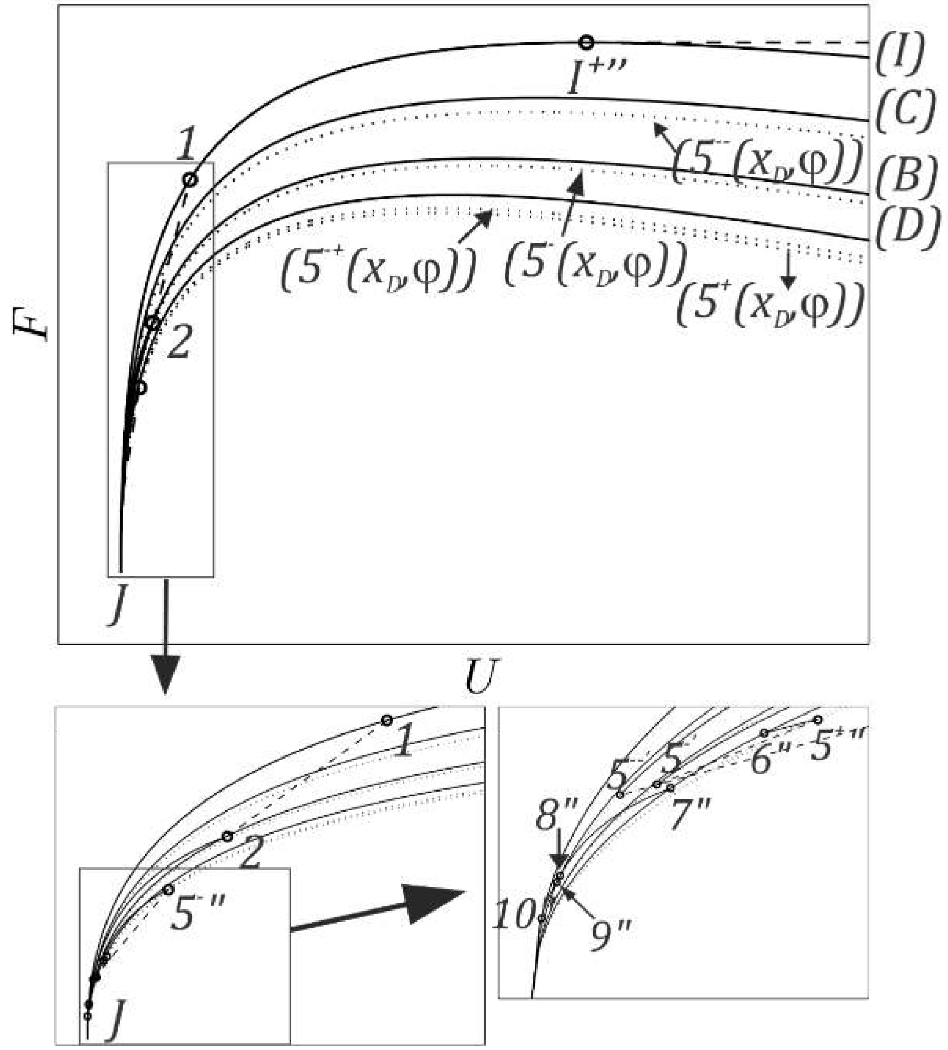

Figure 6: Solution U_{IV} in $F \times U$ plane

The rarefaction region (5) no longer exists in the solution path U_V. This solution is given by:

$$U_V(x_D,\varphi)=\begin{cases} U^{(J)}, & x_D<\frac{\varphi-1}{\sigma_U(U^{(J)},\vec{c}=0)} \\ U_{10}(x_D,\varphi), & \frac{\varphi-1}{\sigma_U(U^{(J)},\vec{c}=0)}<x_D<\frac{\varphi-1}{\sigma_{(3)}\left(\vec{\omega}^{(I)}\right)} \\ U_9(x_D,\varphi), & \frac{\varphi-1}{\sigma_{(3)}\left(\vec{\omega}^{(I)}\right)}<x_D<\frac{\varphi-1}{\sigma_{(3)}\left(\vec{\omega}^{(C)}\right)} \\ U_8(x_D,\varphi), & \frac{\varphi-1}{\sigma_{(3)}\left(\vec{\omega}^{(C)}\right)}<x_D<\frac{\varphi-1}{\sigma_{(2)}\left(\vec{\omega}^{(C)}\right)} \\ U_7(x_D,\varphi), & \frac{\varphi-1}{\sigma_{(2)}\left(\vec{\omega}^{(C)}\right)}<x_D<\frac{\varphi-1}{\sigma_{(2)}\left(\vec{\omega}^{(D)}\right)} \\ U_6(x_D,\varphi), & \frac{\varphi-1}{\sigma_{(2)}\left(\vec{\omega}^{(D)}\right)}<x_D<x_{3,1}(\varphi) \\ U^{(6-)}, & x_{3,1}(\varphi)<x_D<\frac{\varphi-\varphi_C}{\sigma_{(1)}^{-}\left(\vec{\omega}^{(E)}\right)}+x_C \\ U_5^{-}(x_D,\varphi), & \frac{\varphi-\varphi_C}{\sigma_{(1)}^{-}\left(\vec{\omega}^{(E)}\right)}+x_C<x_D<x_{2,1}(\varphi) \\ U_5^{--}(x_D,\varphi), & x_{2,1}(\varphi)<x_D<\frac{\varphi-\varphi_B}{\sigma_{(1)}^{--}\left(\vec{\omega}^{(B)}\right)}+x_B \\ U^{(2)}, & \frac{\varphi-\varphi_B}{\sigma_{(1)}^{--}\left(\vec{\omega}^{(B)}\right)}+x_B<x_D<\frac{\varphi}{V_{(1)}} \\ U^{(1)}, & \frac{\varphi}{V_{(1)}}<x_D<\frac{\varphi}{\sigma_U(U^{(1)},\vec{c}^{(I)})} \\ U_{I^+}(x_D,\varphi), & \frac{\varphi}{\sigma_U(U^{(1)},\vec{c}^{(I)})}<x_D<\frac{\varphi}{\sigma_U(U^{(I^+)},\vec{c}^{(I)})} \\ U^{(I)}, & x_D\to+\infty \end{cases} \tag{38}$$

In figure 7, we present the solution path for U_V in $F\times U$ plane. The structural formula is composed by $(I)\to I^{+''}-(1)\to(2)-5^{--''}\to 5^{-''}-5^{-'}\to 6''-7''-8''-9''-10''-(J)$.

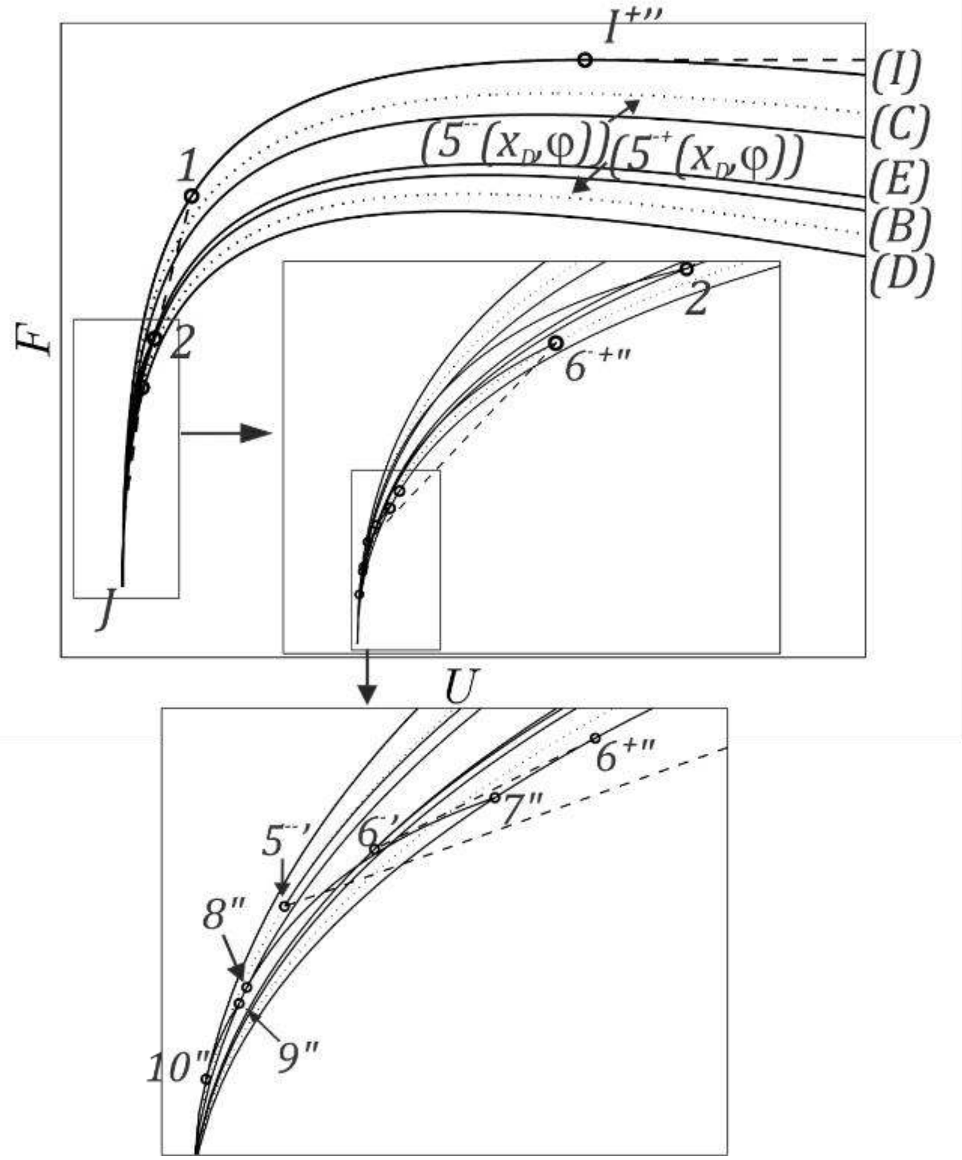

Figure 7: Solution U_V in $F \times U$ plane

Solution $U_{VI}(x_D, \varphi)$ is given by:

$$U_{VI}(x_D,\varphi)=\begin{cases} U^{(J)}, & x_D<\frac{\varphi-1}{\sigma_U(U^{(J)},\vec{c}=0)} \\ U_{10}(x_D,\varphi), & \frac{\varphi-1}{\sigma_U(U^{(J)},\vec{c}=0)}<x_D<\frac{\varphi-1}{\sigma_{(3)}\left(\vec{\omega}^{(I)}\right)} \\ U_9(x_D,\varphi), & \frac{\varphi-1}{\sigma_{(3)}\left(\vec{\omega}^{(I)}\right)}<x_D<\frac{\varphi-1}{\sigma_{(3)}\left(\vec{\omega}^{(C)}\right)} \\ U_8(x_D,\varphi), & \frac{\varphi-1}{\sigma_{(3)}\left(\vec{\omega}^{(C)}\right)}<x_D<\frac{\varphi-1}{\sigma_{(2)}\left(\vec{\omega}^{(C)}\right)} \\ U_7(x_D,\varphi), & \frac{\varphi-1}{\sigma_{(2)}\left(\vec{\omega}^{(C)}\right)}<x_D<\frac{\varphi-1}{\sigma_{(2)}\left(\vec{\omega}^{(D)}\right)} \\ U_6(x_D,\varphi), & \frac{\varphi-1}{\sigma_{(2)}\left(\vec{\omega}^{(D)}\right)}<x_D<x_{3,1}(\varphi) \\ U^{(6-)}, & x_{3,1}(\varphi)<x_D<\frac{\varphi-\varphi_C}{\sigma_{(1)}^{-}\left(\vec{\omega}^{(E)}\right)}+x_C \\ U_5^{-}(x_D,\varphi), & \frac{\varphi-\varphi_C}{\sigma_{(1)}^{-}\left(\vec{\omega}^{(E)}\right)}+x_C<x_D<x_{2,1}(\varphi) \\ U_5^{--}(x_D,\varphi), & x_{2,1}(\varphi)<x_D<x_{1,1}(\varphi) \\ U^{(1)}, & x_{1,1}(\varphi)<x_D<\frac{\varphi}{\sigma_U(U^{(1)},\vec{c}^{(I)})} \\ U_{I^+}(x_D,\varphi), & \frac{\varphi}{\sigma_U(U^{(1)},\vec{c}^{(I)})}<x_D<\frac{\varphi}{\sigma_U(U^{(I^+)},\vec{c}^{(I)})} \\ U^{(I)}, & x_D\to+\infty \end{cases} \tag{39}$$

In figure 8 we present the solution path for U_{VI} in $F\times U$ plane. The structural formula of the solution is: $(I)\to I^{+\prime\prime}-(1)\to 5^{--\prime\prime}-5^{--\prime}\to 5^{-\prime\prime}-5^{-\prime}\to 6^{\prime\prime}-7^{\prime\prime}-8^{\prime\prime}-9^{\prime\prime}-10^{\prime\prime}-(J)$.

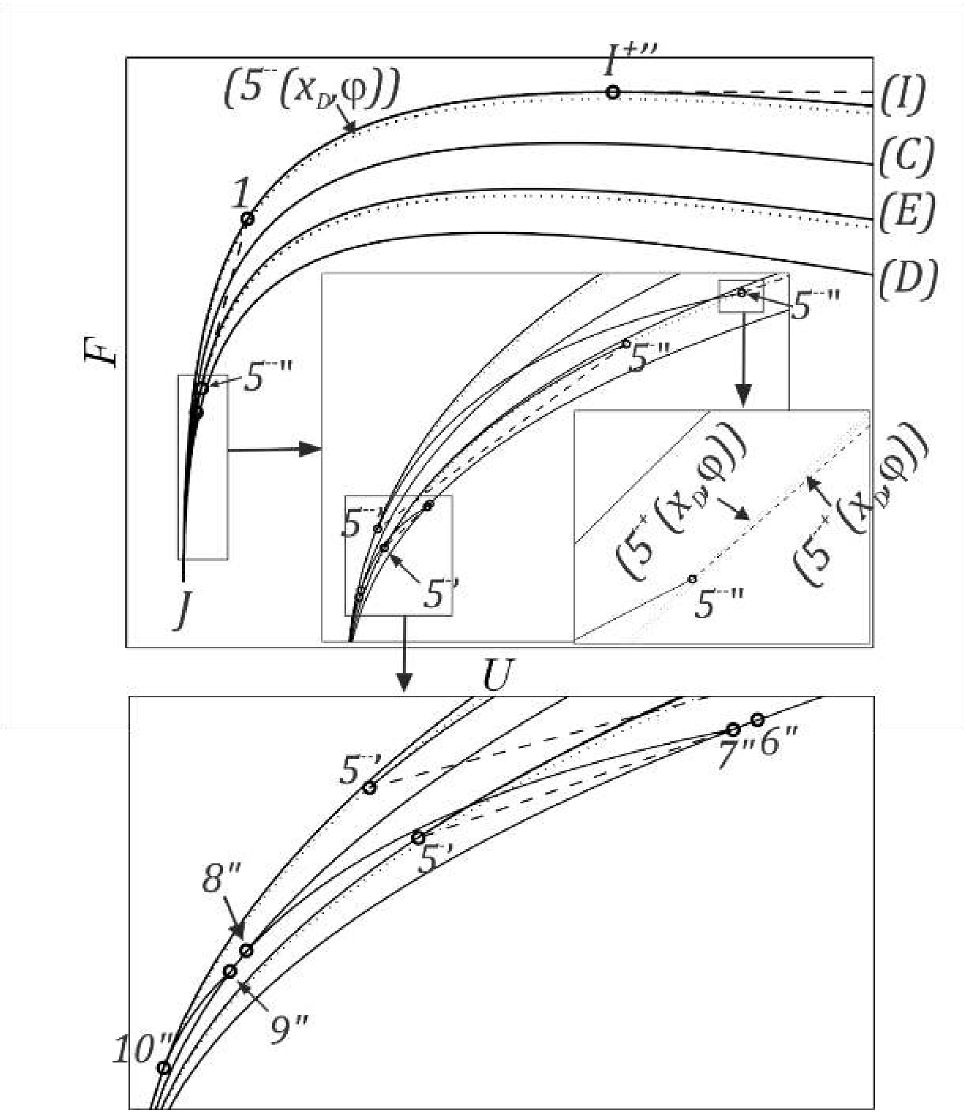

Figure 8: Solution U_{VI} in $F \times U$ plane

For $U_{VII}(x_D, \varphi)$ we have:

$$U_{VII}(x_D,\varphi)=\begin{cases} U^{(J)}, & x_D<\frac{\varphi-1}{\sigma_U(U^{(J)},\vec{c}=0)} \\ U_{10}(x_D,\varphi), & \frac{\varphi-1}{\sigma_U(U^{(J)},\vec{c}=0)}<x_D<\frac{\varphi-1}{\sigma_{(3)}\left(\vec{\omega}^{(I)}\right)} \\ U_9(x_D,\varphi), & \frac{\varphi-1}{\sigma_{(3)}\left(\vec{\omega}^{(I)}\right)}<x_D<\frac{\varphi-1}{\sigma_{(3)}\left(\vec{\omega}^{(C)}\right)} \\ U_8(x_D,\varphi), & \frac{\varphi-1}{\sigma_{(3)}\left(\vec{\omega}^{(C)}\right)}<x_D<\frac{\varphi-1}{\sigma_{(2)}\left(\vec{\omega}^{(C)}\right)} \\ U_7^+(x_D,\varphi), & \frac{\varphi-1}{\sigma_{(2)}\left(\vec{\omega}^{(C)}\right)}<x_D<x_{3,2}(\varphi) \\ U_7^-(x_D,\varphi), & x_{3,2}(\varphi)<x_D<\frac{\varphi-\varphi_E}{\sigma_{(2)}^-(\vec{\omega}(x_D,\varphi))} \\ U^{(6-)}, & \frac{\varphi-\varphi_E}{\sigma_{(2)}^-(\vec{\omega}(x_D,\varphi))}<x_D<\frac{\varphi-\varphi_C}{\sigma_{(1)}^-\left(\vec{\omega}^{(E)}\right)}+x_C \\ U_5^-(x_D,\varphi), & \frac{\varphi-\varphi_C}{\sigma_{(1)}^-\left(\vec{\omega}^{(E)}\right)}+x_C<x_D<x_{2,1}(\varphi) \\ U_5^{--}(x_D,\varphi), & x_{2,1}(\varphi)<x_D<x_{1,1}(\varphi) \\ U^{(1)}, & x_{1,1}(\varphi)<x_D<\frac{\varphi}{\sigma_U(U^{(1)},\vec{c}^{(I)})} \\ U_{I^+}(x_D,\varphi), & \frac{\varphi}{\sigma_U(U^{(1)},\vec{c}^{(I)})}<x_D<\frac{\varphi}{\sigma_U(U^{(I^+)},\vec{c}^{(I)})} \\ U^{(I)}, & x_D\to+\infty \end{cases} \tag{40}$$

The solution path for U_{VII} in $F\times U$ plane is presented in figure 9. The structural formula of the solution is: $(I)\to I^{+\prime\prime}-(1)\to 5^{--\prime\prime}-5^{--\prime}\to 5^{-\prime\prime}-(6^-)-7^{-\prime}\to 7^{\prime\prime}-8^{\prime\prime}-9^{\prime\prime}-10^{\prime\prime}-(J)$.

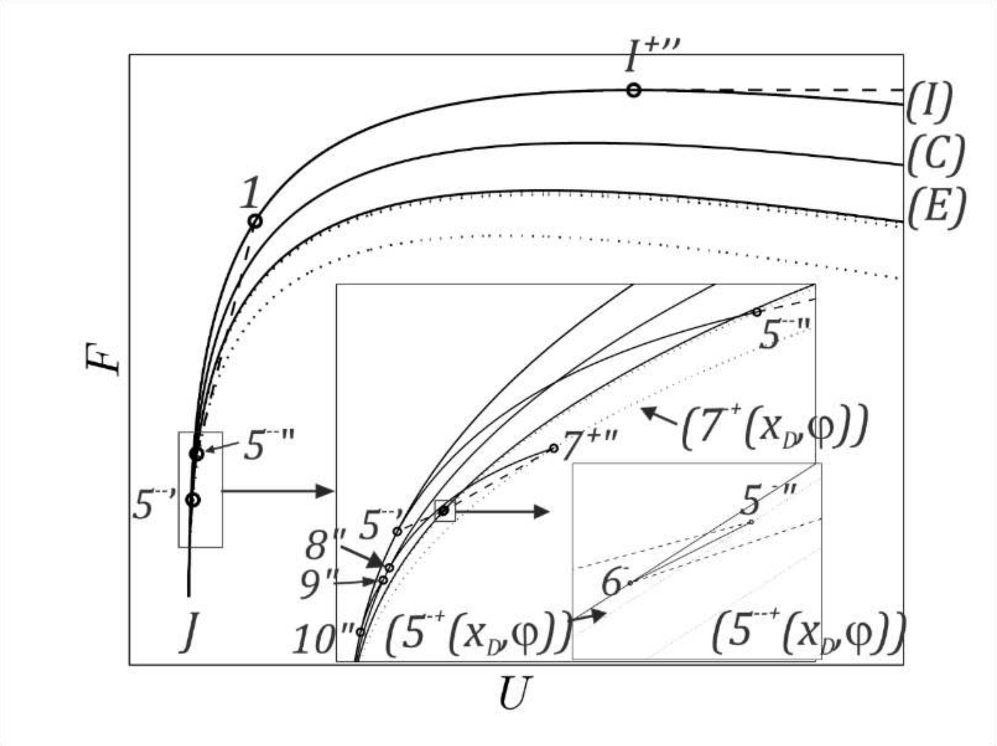

Figure 9: Solution U_{VII} in $F \times U$ plane

Solution $U_{VIII}(x_D,\varphi)$ is given by:

$$U_{VIII}(x_D,\varphi) = \begin{cases} U^{(J)}, & x_D < \frac{\varphi-1}{\sigma_U(U^{(J)},\vec{c}=0)} \\ U_{10}(x_D,\varphi), & \frac{\varphi-1}{\sigma_U(U^{(J)},\vec{c}=0)} < x_D < \frac{\varphi-1}{\sigma_{(3)}(\overrightarrow{\omega}^{(I)})} \\ U_9(x_D,\varphi), & \frac{\varphi-1}{\sigma_{(3)}(\overrightarrow{\omega}^{(I)})} < x_D < \frac{\varphi-1}{\sigma_{(3)}(\overrightarrow{\omega}^{(C)})} \\ U_8(x_D,\varphi), & \frac{\varphi-1}{\sigma_{(3)}(\overrightarrow{\omega}^{(C)})} < x_D < \frac{\varphi-1}{\sigma_{(2)}(\overrightarrow{\omega}^{(C)})} \\ U_7^+(x_D,\varphi), & \frac{\varphi-1}{\sigma_{(2)}(\overrightarrow{\omega}^{(C)})} < x_D < x_{3,2}(\varphi) \\ U_7^-(x_D,\varphi), & x_{3,2}(\varphi) < x_D < \frac{\varphi-\varphi_E}{\sigma_{(2)}^-(\overrightarrow{\omega}(x_D,\varphi))} \\ U^{(6-)}, & \frac{\varphi-\varphi_E}{\sigma_{(2)}^-(\overrightarrow{\omega}(x_D,\varphi))} < x_D < x_{2,1}(\varphi) \\ U^{(6--)} & x_{2,1}(\varphi) < x_D < \frac{\varphi-\varphi_F}{\sigma_{(1)}^{--}(\overrightarrow{\omega}^{(I)})} \\ U_5^{--}(x_D,\varphi), & \frac{\varphi-\varphi_F}{\sigma_{(1)}^{--}(\overrightarrow{\omega}^{(I)})} < x_D < x_{1,1}(\varphi) \\ U^{(1)}, & x_{1,1}(\varphi) < x_D < \frac{\varphi}{\sigma_U(U^{(1)},\vec{c}^{(I)})} \\ U_{I^+}(x_D,\varphi), & \frac{\varphi}{\sigma_U(U^{(1)},\vec{c}^{(I)})} < x_D < \frac{\varphi}{\sigma_U(U^{(I^+)},\vec{c}^{(I)})} \\ U^{(I)}, & x_D \to +\infty \end{cases} \tag{41}$$

For this solution profile, the smallest adsorption chemical separates from the other two components (region 6^{--}) at the jump from $U^{(6-)}$ to $U^{(6--)}$ (Figure 10). The structural formula for this part of the solution is: $(I) \rightarrow I^{+''} - (1) \rightarrow 5^{--''} - (6^{--}) \rightarrow (6^{-}) - 7^{-'} \rightarrow 7'' - 8'' - 9'' - 10'' - (J)$.

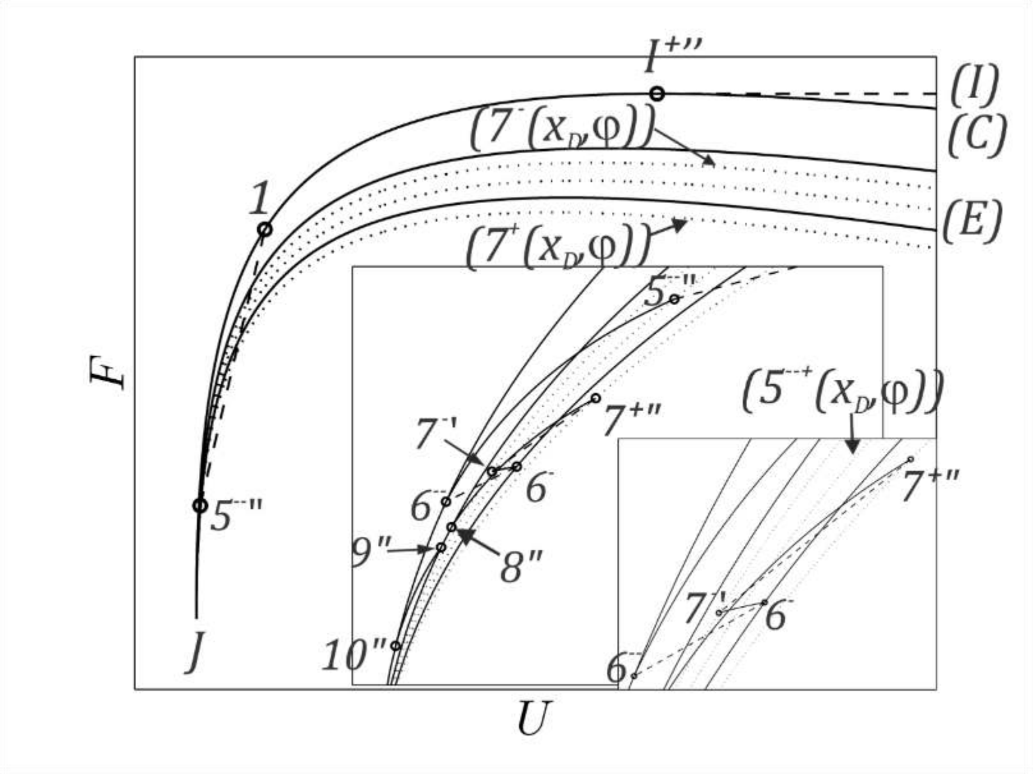

Figure 10: Solution U_{VIII} in the $F \times U$ plane

The solution $U_{IX}(x_D, \varphi)$ is:

$$U_{IX}(x_D,\varphi)=\begin{cases} U^{(J)}, & x_D<\frac{\varphi-1}{\sigma_U(U^{(J)},\vec{c}=0)} \\ U_{10}(x_D,\varphi), & \frac{\varphi-1}{\sigma_U(U^{(J)},\vec{c}=0)}<x_D<\frac{\varphi-1}{\sigma_{(3)}\left(\vec{\omega}^{(I)}\right)} \\ U_9(x_D,\varphi), & \frac{\varphi-1}{\sigma_{(3)}\left(\vec{\omega}^{(I)}\right)}<x_D<\frac{\varphi-1}{\sigma_{(3)}\left(\vec{\omega}^{(C)}\right)} \\ U_8(x_D,\varphi), & \frac{\varphi-1}{\sigma_{(3)}\left(\vec{\omega}^{(C)}\right)}<x_D<\frac{\varphi-1}{\sigma_{(2)}\left(\vec{\omega}^{(C)}\right)} \\ U_7^+(x_D,\varphi), & \frac{\varphi-1}{\sigma_{(2)}\left(\vec{\omega}^{(C)}\right)}<x_D<x_{3,2}(\varphi) \\ U_7^-(x_D,\varphi), & x_{3,2}(\varphi)<x_D<x_{2,2}(\varphi) \\ U^{(6--)} & x_{2,2}(\varphi)<x_D<\frac{\varphi-\varphi_F}{\sigma_{(1)}^{--}\left(\vec{\omega}^{(I)}\right)} \\ U_5^{--}(x_D,\varphi), & \frac{\varphi-\varphi_F}{\sigma_{(1)}^{--}\left(\vec{\omega}^{(I)}\right)}<x_D<x_{1,1}(\varphi) \\ U^{(1)}, & x_{1,1}(\varphi)<x_D<\frac{\varphi}{\sigma_U(U^{(1)},\vec{c}^{(I)})} \\ U_{I^+}(x_D,\varphi), & \frac{\varphi}{\sigma_U(U^{(1)},\vec{c}^{(I)})}<x_D<\frac{\varphi}{\sigma_U(U^{(I^+)},\vec{c}^{(I)})} \\ U^{(I)}, & x_D\to+\infty \end{cases} \tag{42}$$

The structural formula for U_{IX} is: $(I)\to I^{+\prime\prime}-(1)\to 5^{--\prime\prime}-(6^{--})\to 7^{-\prime\prime}-7^{-\prime}\to 7^{\prime\prime}-8^{\prime\prime}-9^{\prime\prime}-10^{\prime\prime}-(J)$. The solution path for U_{IX} in $F\times U$ plane is presented in figure 11.

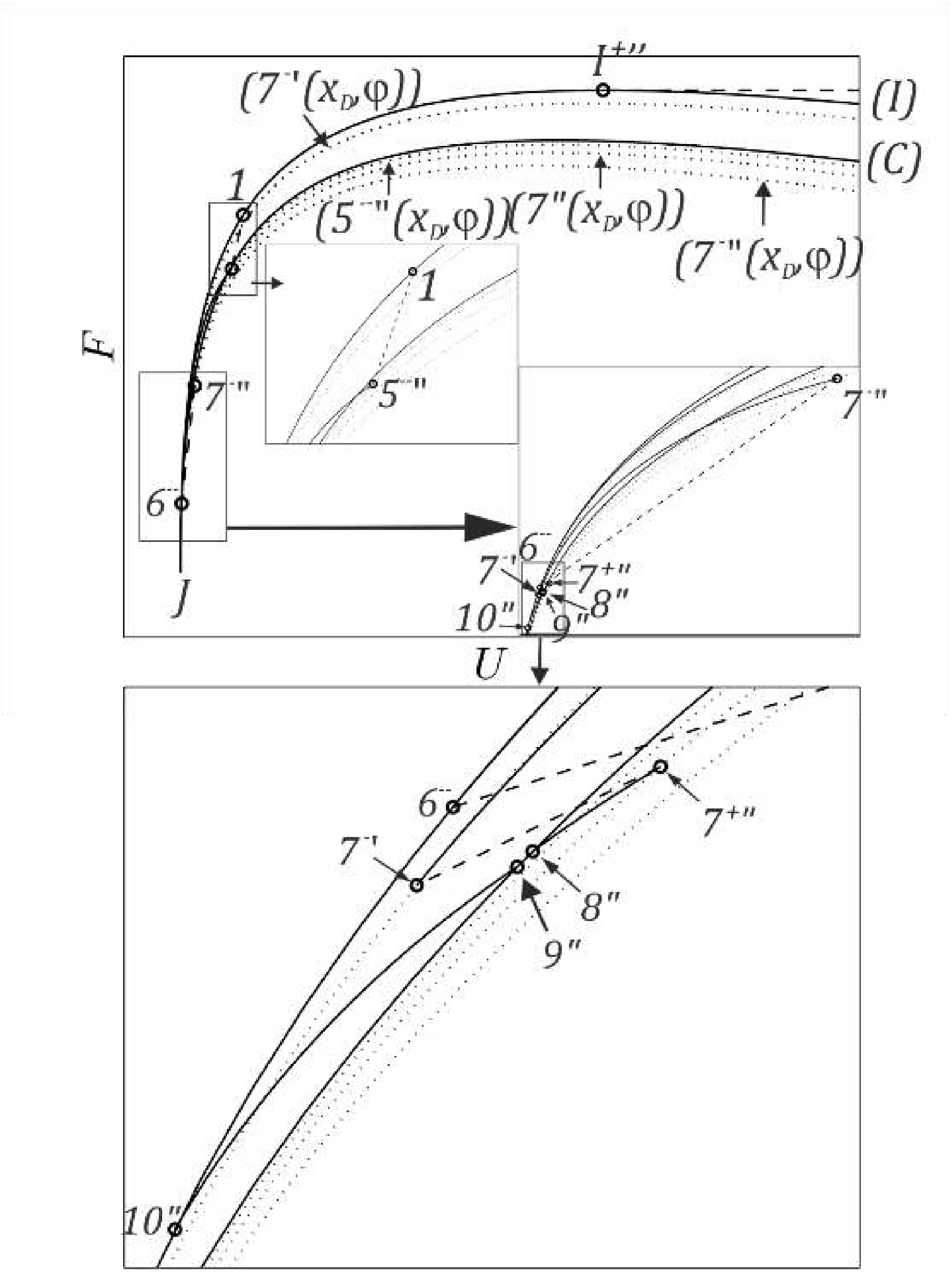

Figure 11: Solution U_{IX} in $F \times U$ plane

The three components are completely separated in solution $U_X(x_D, \varphi)$. Thus, there is no longer a region (7) in the solution profile and $U_X(x_D, \varphi)$ is given by:

$$U_X(x_D,\varphi)=\begin{cases} U^{(J)}, & x_D < \frac{\varphi-1}{\sigma_U(U^{(J)},\vec{c}=0)} \\ U_{10}(x_D,\varphi), & \frac{\varphi-1}{\sigma_U(U^{(J)},\vec{c}=0)} < x_D < \frac{\varphi-1}{\sigma_{(3)}\left(\overrightarrow{\omega}^{(I)}\right)} \\ U_9(x_D,\varphi), & \frac{\varphi-1}{\sigma_{(3)}\left(\overrightarrow{\omega}^{(I)}\right)} < x_D < \frac{\varphi-1}{\sigma_{(3)}\left(\overrightarrow{\omega}^{(C)}\right)} \\ U_8^{+}(x_D,\varphi), & \frac{\varphi-1}{\sigma_{(3)}\left(\overrightarrow{\omega}^{(C)}\right)} < x_D < \frac{\varphi-\varphi_H}{V_{(3)}\left(\overrightarrow{\omega}^{(C)}\right)} + x_H \\ U^{(8-)}, & \frac{\varphi-\varphi_H}{V_{(3)}\left(\overrightarrow{\omega}^{(C)}\right)} + x_H < x_D < \frac{\varphi-\varphi_H}{\sigma_{(2)}\left(\overrightarrow{\omega}^{(I)}\right)} + x_H \\ U_7^{-}(x_D,\varphi), & \frac{\varphi-\varphi_H}{\sigma_{(2)}\left(\overrightarrow{\omega}^{(I)}\right)} + x_H < x_D < x_{2,2}(\varphi) \\ U^{(6--)} & x_{2,2}(\varphi) < x_D < \frac{\varphi-\varphi_F}{\sigma_{(1)}^{--}\left(\overrightarrow{\omega}^{(I)}\right)} \\ U_5^{--}(x_D,\varphi), & \frac{\varphi-\varphi_F}{\sigma_{(1)}^{--}\left(\overrightarrow{\omega}^{(I)}\right)} < x_D < x_{1,1}(\varphi) \\ U^{(1)}, & x_{1,1}(\varphi) < x_D < \frac{\varphi}{\sigma_U(U^{(1)},\vec{c}^{(I)})} \\ U_{I^+}(x_D,\varphi), & \frac{\varphi}{\sigma_U(U^{(1)},\vec{c}^{(I)})} < x_D < \frac{\varphi}{\sigma_U(U^{(I^+)},\vec{c}^{(I)})} \\ U^{(I)}, & x_D \to +\infty \end{cases} \tag{43}$$

The structural formula for U_X is: $(I) \to I^{+\prime\prime} - (1) \to 5^{--}" - (6^{--}) \to 7^{-\prime\prime} - (8^{-}) \to 8'' - 9'' - 10'' - (J)$. The solution in $F \times U$ plane is presented in figure 12.

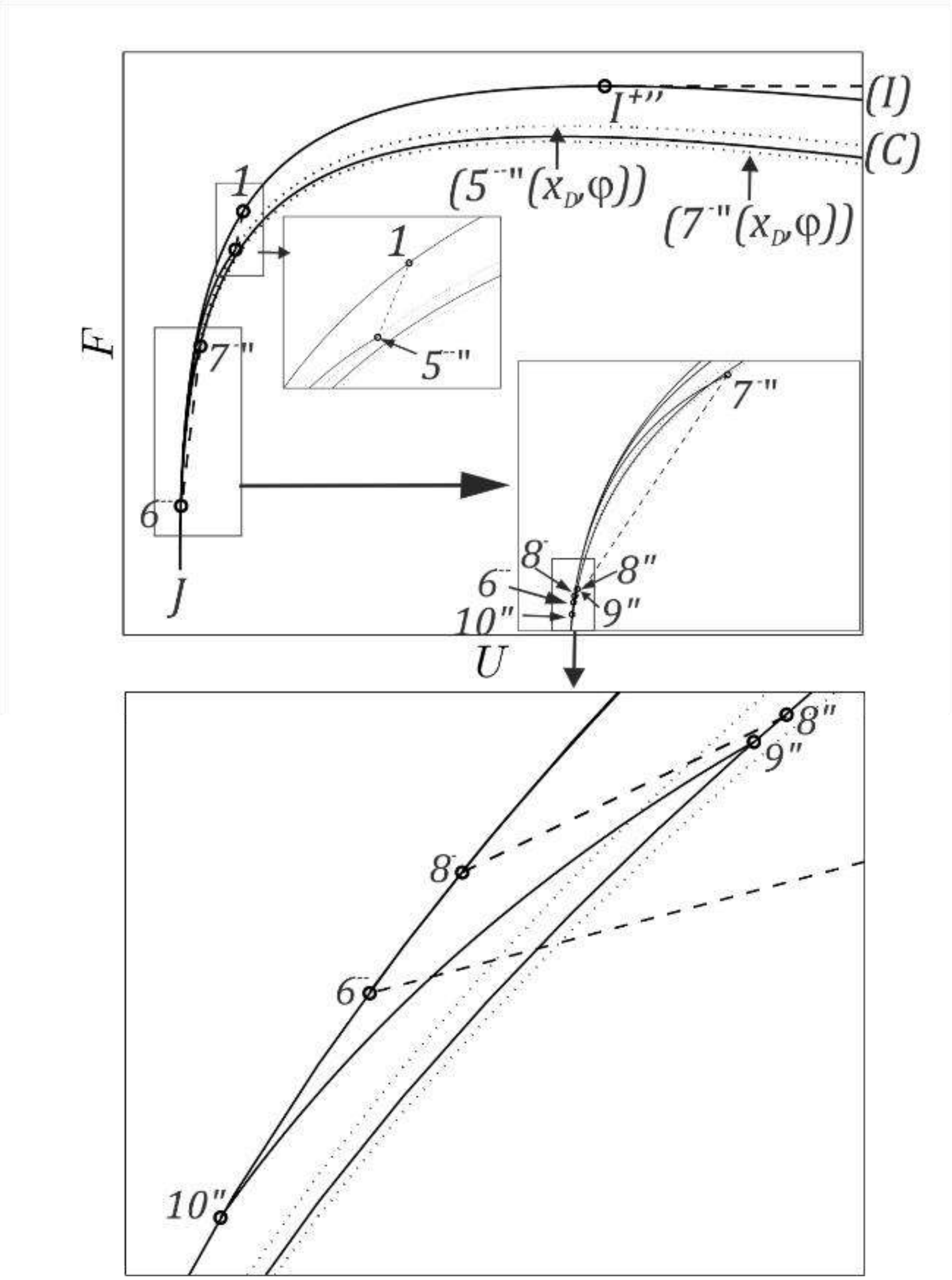

Figure 12: Solution U_X in $F \times U$ plane

Finally, for $U_{XI}(x_D, \varphi)$ we have:

$$U_{XI}(x_D,\varphi)=\begin{cases} U^{(J)}, & x_D<\frac{\varphi-1}{\sigma_U(U^{(J)},\vec{c}=0)} \\ U_{10}(x_D,\varphi), & \frac{\varphi-1}{\sigma_U(U^{(J)},\vec{c}=0)}<x_D<\frac{\varphi-1}{\sigma_{(3)}\left(\vec{\omega}^{(I)}\right)} \\ U_9^{+}(x_D,\varphi), & \frac{\varphi-1}{\sigma_{(3)}\left(\vec{\omega}^{(I)}\right)}<x_D<x_{3,3}(\varphi) \\ U^{(8-)}, & x_{3,3}(\varphi)<x_D<\frac{\varphi-\varphi_H}{\sigma_{(2)}\left(\vec{\omega}^{(I)}\right)}+x_H \\ U_7^{-}(x_D,\varphi), & \frac{\varphi-\varphi_H}{\sigma_{(2)}\left(\vec{\omega}^{(I)}\right)}+x_H<x_D<x_{2,2}(\varphi) \\ U^{(6--)} & x_{2,2}(\varphi)<x_D<\frac{\varphi-\varphi_F}{\sigma_{(1)}^{--}\left(\vec{\omega}^{(I)}\right)} \\ U_5^{--}(x_D,\varphi), & \frac{\varphi-\varphi_F}{\sigma_{(1)}^{--}\left(\vec{\omega}^{(I)}\right)}<x_D<x_{1,1}(\varphi) \\ U^{(1)}, & x_{1,1}(\varphi)<x_D<\frac{\varphi}{\sigma_U(U^{(1)},\vec{c}^{(I)})} \\ U_{I^+}(x_D,\varphi), & \frac{\varphi}{\sigma_U(U^{(1)},\vec{c}^{(I)})}<x_D<\frac{\varphi}{\sigma_U(U^{(I^+)},\vec{c}^{(I)})} \\ U^{(I)}, & x_D\to+\infty \end{cases} \tag{44}$$

The structural formula is given by: $(I)\to I^{+\prime\prime}-(1)\to 5^{--\prime\prime}-(6^{--})\to 7^{-\prime\prime}-(8^{-})\to 9^{\prime\prime}-10^{\prime\prime}-(J)$. Figure 13 presents the solution path of U_{XI} in $F\times U$ plane.

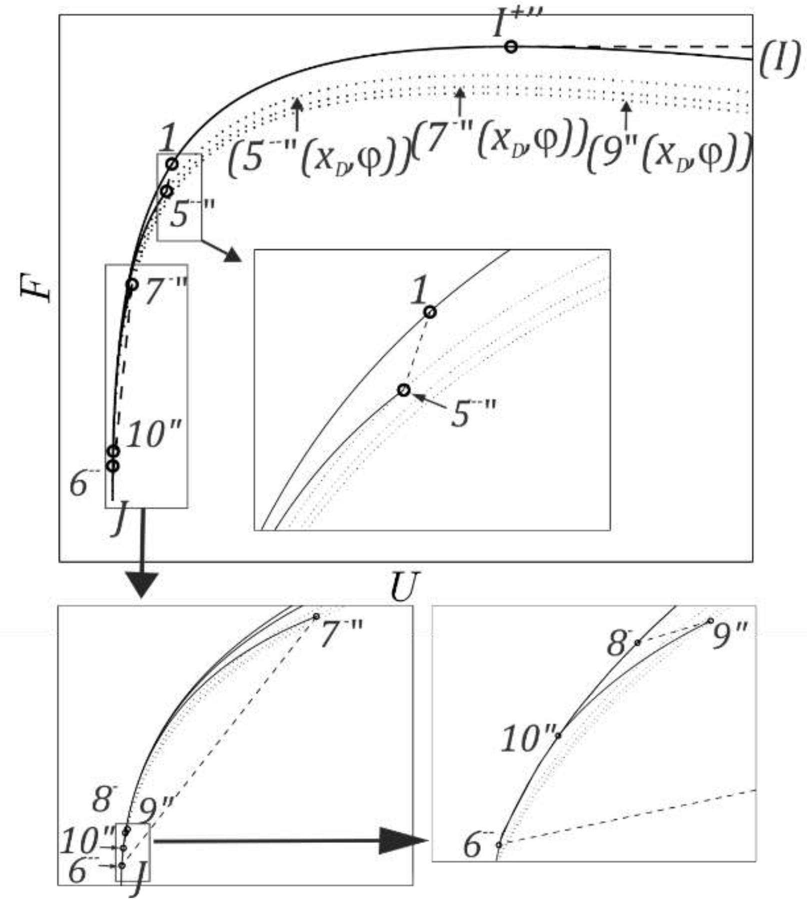

Figure 13: Solution U_{XI} in $F \times U$ plane

We now present the exact expressions for each part of water saturation solution obtained from the inverse mapping of the lifting equation solution. We also show water saturation profiles, the solution path in the $f \times s$ plane and some comments regarding each part of the solution.

The saturation solution is divided in 11 parts and is given by:

$$s(x_D, t_D) = \begin{cases} s_I, & t_D < 1 \\ s_{II}, & 1 < t_D < t_{(A)} \\ s_{III}, & t_{(A)} < t_D < t_{(B)} \\ s_{IV}, & t_{(B)} < t_D < t_{(C)} \\ s_V, & t_{(C)} < t_D < t_{(IV)} \\ s_{VI}, & t_{(IV)} < t_D < t_{(E)} \\ s_{VII}, & t_{(E)} < t_D < t_{(F)} \\ s_{VIII}, & t_{(F)} < t_D < t_{(G)} \\ s_{IX}, & t_{(G)} < t_D < t_{(H)} \\ s_X, & t_{(H)} < t_D < t_{(I)} \\ s_{XI}, & t_{(I)} < t_D \end{cases} \tag{45}$$

During polymer slug injection ($t_D < 1$), the solution is self-similar and is equal to the solution of the continuous polymer injection problem (Dahl *et al.*, 1992) for Langmuir adsorption isotherm. Thus, $s_I(x_D, t_D)$ is given by:

$$s_I(x_D, t_D) = \begin{cases} s^{(J)}, & x_D < \frac{t_D}{\lambda_{(s)}(s^{(J)}, \vec{c}^{(J)})} \\ s_4(x_D, t_D), & \frac{t_D}{\lambda_{(s)}(s^{(J)}, \vec{c}^{(J)})} < x_D < \frac{t_D}{D_{(3)}} \\ s^{(3)}, & \frac{t_D}{D_{(3)}} < x_D < \frac{t_D}{D_{(2)}} \\ s^{(2)}, & \frac{t_D}{D_{(2)}} < x_D < \frac{t_D}{D_{(1)}} \\ s^{(1)}, & \frac{t_D}{D_{(1)}} < x_D < \frac{t_D}{\lambda_{(s)}(s^{(1)}, \vec{c}^{(I)})} \\ s_{I^+}(x_D, t_D), & \frac{t_D}{\lambda_{(s)}(s^{(1)}, \vec{c}^{(I)})} < x_D < \frac{t_D}{\lambda_{(s)}(s^{(I^+)}, \vec{c}^{(I)})} \\ s^{(I)}, & x_D > \frac{t_D}{\lambda_{(s)}(s^{(I^+)}, \vec{c}^{(I)})} \end{cases} \tag{46}$$

The saturation profile for three different t_D, where $t_{D1} < t_{D2} < t_{D3} < 1$, is presented in figure (14). The solution path of s_I in $f \times s$ plane is shown in figure (15), and the structural formula is: $(J) - (4) \rightarrow (3) \rightarrow (2) \rightarrow (1) - I^{+''} \rightarrow (I)$.

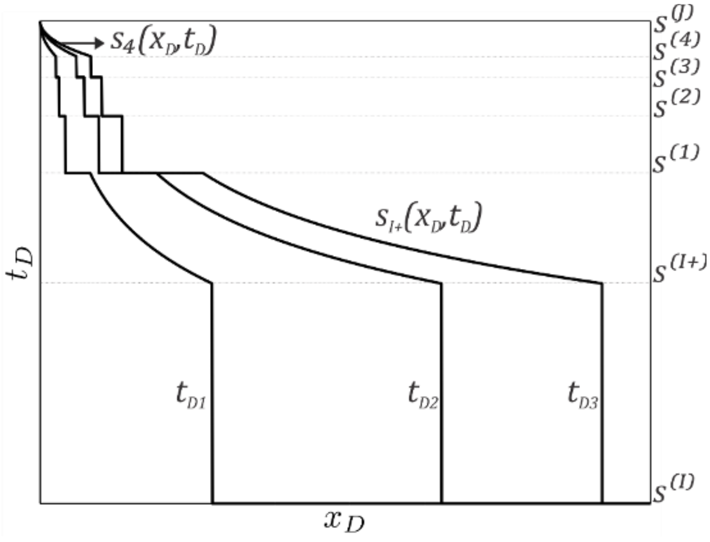

Figure 14: Saturation profiles of the solution $s_I(x_D, t_D)$

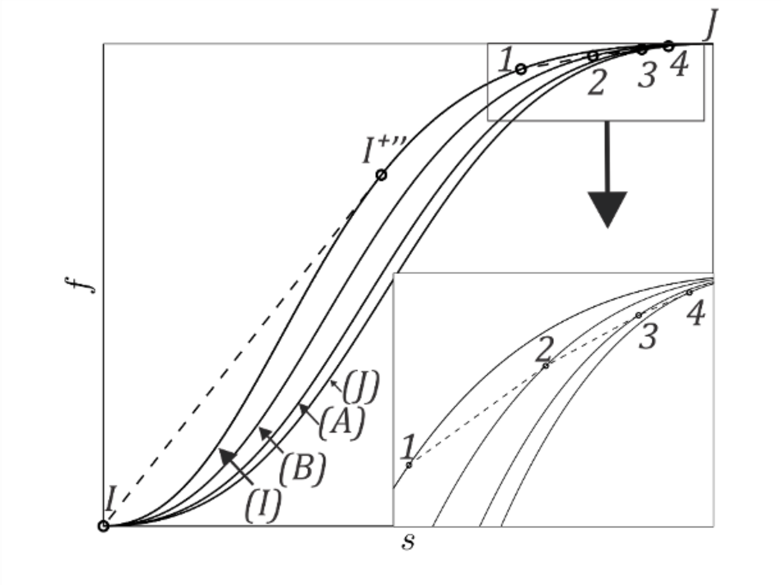

Figure 15: Solution path of s_I in $f \times s$ plane

For $t_D > 1$, the water drive begins and interactions between waves appear. Solution $s_{II}(x_D, t_D)$ is given by:

$$
s_{II}(x_D,t_D)=\begin{cases}
s^{(J)}, & x_D<\frac{t_D}{\lambda_{(s)}(s^{(J)},\vec{c}=0)}\\
s_{10}(x_D,t_D), & \frac{t_D}{\lambda_{(s)}(s^{(J)},\vec{c}=0)}<x_D<\frac{t_D-1}{\lambda_{(3)}(s_{10}(x_D,\varphi),\vec{c}=0)}\\
s_9(x_D,t_D), & \frac{t_D-1}{\lambda_{(3)}(s_{10}(x_D,\varphi),\vec{c}=0)}<x_D<\frac{t_D-1}{\lambda_{(3)}(s_9(x_D,\varphi),\vec{c}^{(C)})}\\
s_8(x_D,t_D), & \frac{t_D-1}{\lambda_{(3)}(s_9(x_D,\varphi),\vec{c}^{(C)})}<x_D<\frac{t_D-1}{\lambda_{(2)}(s_8(x_D,\varphi),\vec{c}^{(C)})}\\
s_7(x_D,t_D), & \frac{t_D-1}{\lambda_{(2)}(s_8(x_D,\varphi),\vec{c}^{(C)})}<x_D<\frac{t_D-1}{\lambda_{(2)}(s_7(x_D,\varphi),\vec{c}^{(D)})}\\
s_6(x_D,t_D), & \frac{t_D-1}{\lambda_{(2)}(s_7(x_D,\varphi),\vec{c}^{(D)})}<x_D<\frac{t_D-1}{\lambda_{(1)}(s_6(x_D,\varphi),\vec{c}^{(D)})}\\
s_5(x_D,t_D), & \frac{t_D-1}{\lambda_{(1)}(s_6(x_D,\varphi),\vec{c}^{(D)})}<x_D<\frac{t_D-1}{\lambda_{(1)}(s_5(x_D,\varphi),\vec{c}^{(J)})}\\
s_4(x_D,t_D), & \frac{t_D-1}{\lambda_{(1)}(s_5(x_D,\varphi),\vec{c}^{(J)})}<x_D<\frac{t_D}{D_{(3)}}\\
s^{(3)}, & \frac{t_D}{D_{(3)}}<x_D<\frac{t_D}{D_{(2)}}\\
s^{(2)}, & \frac{t_D}{D_{(2)}}<x_D<\frac{t_D}{D_{(1)}}\\
s^{(1)}, & \frac{t_D}{D_{(1)}}<x_D<\frac{t_D}{\lambda_{(s)}(s^{(1)},\vec{c}^{(I)})}\\
s_{I^+}(x_D,t_D), & \frac{t_D}{\lambda_{(s)}(s^{(1)},\vec{c}^{(I)})}<x_D<\frac{t_D}{\lambda_{(s)}(s^{(I^+)},\vec{c}^{(I)})}\\
s^{(I)}, & x_D>\frac{t_D}{\lambda_{(s)}(s^{(I^+)},\vec{c}^{(I)})}
\end{cases}
\tag{47}
$$

We present the saturation profile of $s_{II}(x_D,t_D)$ in figure (16). The solution path for $s_{II}(x_D,t_D)$ in $f\times s$ plane is shown in figure (17), and its structural formula is: $(J)-10''-9''-8''-7''-5''-(4)\rightarrow(3)\rightarrow(2)\rightarrow(1)-I^{+''}\rightarrow(I)$.

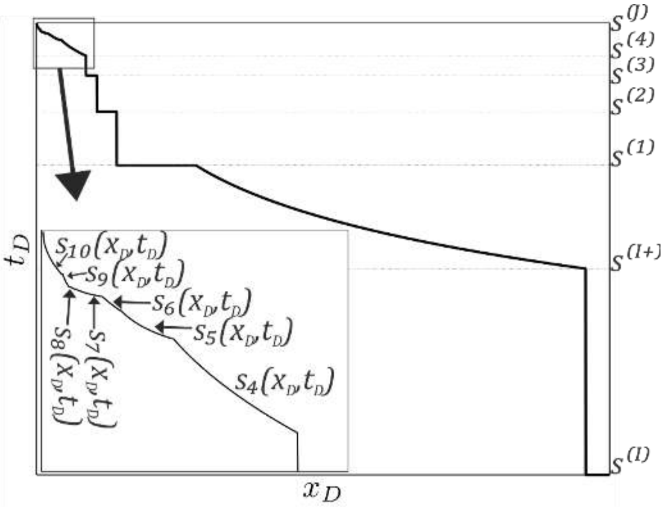

Figure 16: Saturation profile of the solution $s_{II}(x_D,t_D)$

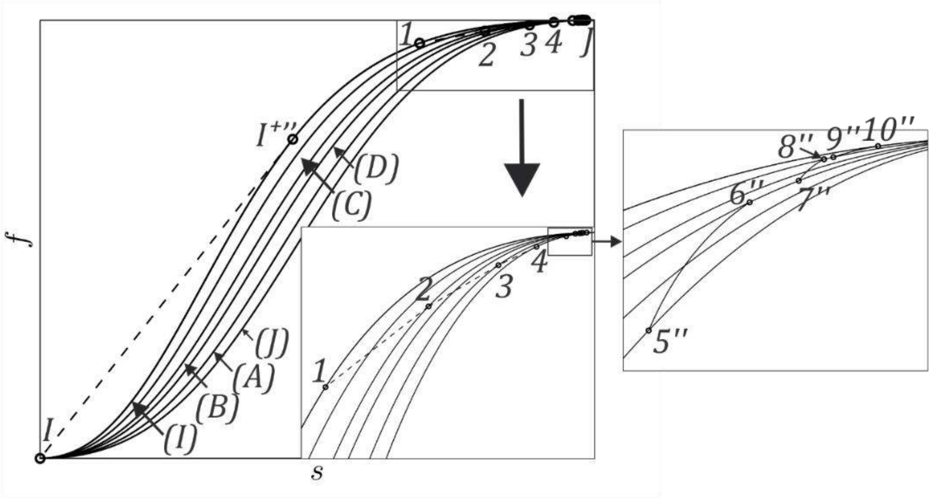

Figure 17: Solution path of s_{II} in $f \times s$ plane

In $s_{III}(x_D, t_D)$ the rarefaction $\lambda_{(1)}$ interacts with the shock wave $D_{(3)}$, which is the first interaction between two concentration waves in the solution, and region (4) disappears. Thus, we have:

$$s_{III}(x_D, t_D) = \begin{cases} s^{(J)}, & x_D < \frac{t_D}{\lambda_{(s)}(s^{(J)}, \vec{c}=0)} \\ s_{10}(x_D, t_D), & \frac{t_D}{\lambda_{(s)}(s^{(J)}, \vec{c}=0)} < x_D < \frac{t_D - 1}{\lambda_{(3)}(s_{10}(x_D, \varphi), \vec{c}=0)} \\ s_9(x_D, t_D), & \frac{t_D - 1}{\lambda_{(3)}(s_{10}(x_D, \varphi), \vec{c}=0)} < x_D < \frac{t_D - 1}{\lambda_{(3)}(s_9(x_D, \varphi), \vec{c}^{(C)})} \\ s_8(x_D, t_D), & \frac{t_D - 1}{\lambda_{(3)}(s_9(x_D, \varphi), \vec{c}^{(C)})} < x_D < \frac{t_D - 1}{\lambda_{(2)}(s_8(x_D, \varphi), \vec{c}^{(C)})} \\ s_7(x_D, t_D), & \frac{t_D - 1}{\lambda_{(2)}(s_8(x_D, \varphi), \vec{c}^{(C)})} < x_D < \frac{t_D - 1}{\lambda_{(2)}(s_7(x_D, \varphi), \vec{c}^{(D)})} \\ s_6(x_D, t_D), & \frac{t_D - 1}{\lambda_{(2)}(s_7(x_D, \varphi), \vec{c}^{(D)})} < x_D < \frac{t_D - 1}{\lambda_{(1)}(s_6(x_D, \varphi), \vec{c}^{(D)})} \\ s_5^+(x_D, t_D), & \frac{t_D - 1}{\lambda_{(1)}(s_6(x_D, \varphi), \vec{c}^{(D)})} < x_D < x_{3,1}(t_D) \\ s_5^-(x_D, t_D), & x_{3,1}(t_D) < x_D < \frac{t_D - t_A}{\lambda_{(1)}^-(s^{(3)}, \vec{c}^{(A)})} - x_A \\ s^{(3)}, & \frac{t_D - t_A}{\lambda_{(1)}^-(s^{(3)}, \vec{c}^{(A)})} - x_A < x_D < \frac{t_D}{D_{(2)}} \\ s^{(2)}, & \frac{t_D}{D_{(2)}} < x_D < \frac{t_D}{D_{(1)}} \\ s^{(1)}, & \frac{t_D}{D_{(1)}} < x_D < \frac{t_D}{\lambda_{(s)}(s^{(1)}, \vec{c}^{(I)})} \\ s_{I^+}(x_D, t_D), & \frac{t_D}{\lambda_{(s)}(s^{(1)}, \vec{c}^{(I)})} < x_D < \frac{t_D}{\lambda_{(s)}(s^{(I^+)}, \vec{c}^{(I)})} \\ s^{(I)}, & x_D > \frac{t_D}{\lambda_{(s)}(s^{(I^+)}, \vec{c}^{(I)})} \end{cases} \tag{48}$$

The saturation profile of $s_{III}(x_D, t_D)$ is presented in figure (18), and the solution path in the $f \times s$ plane is shown in figure (19). The structural formula of $s_{III}(x_D, t_D)$ is: $(J) - 10'' - 9'' - 8'' - 7'' - 6'' - 5^{+''} \rightarrow 5^{-'} - 5^{-''} - (3) \rightarrow (2) \rightarrow (1) - I^{+''} \rightarrow (I)$. Observe that a water bank created by two surrounding higher viscosity waves appears in the solution in region (5^{-}). This phenomena will also take place in other parts of the solution where there is a lower viscosity fluid surrounded by two higher viscosity fluids.

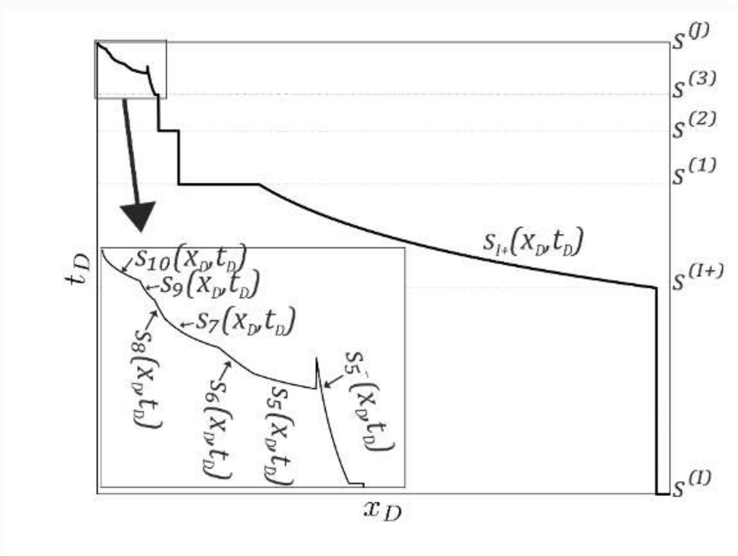

Figure 18: Saturation profile of the solution $s_{III}(x_D, t_D)$

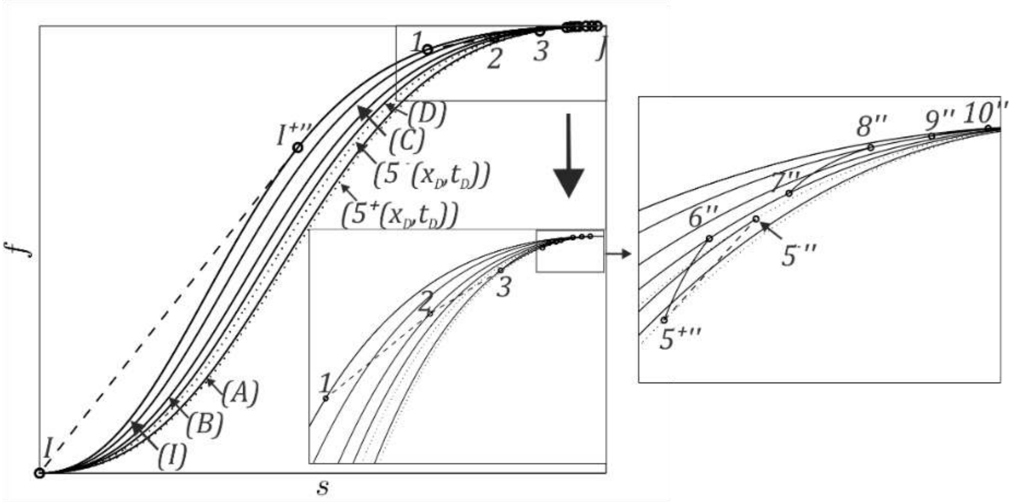

Figure 19: Solution path of s_{III} in $f \times s$ plane

The rarefaction $\lambda_{(1)}^{-}$ crosses the shock $D_{(2)}$ and the region (3) disappears in solution $s_{IV}(x_D, t_D)$. Therefore,

$$s_{IV}(x_D,t_D) = \begin{cases} s^{(J)}, & x_D < \frac{t_D}{\lambda_{(s)}(s^{(J)},\vec{c}=0)} \\ s_{10}(x_D,t_D), & \frac{t_D}{\lambda_{(s)}(s^{(J)},\vec{c}=0)} < x_D < \frac{t_D-1}{\lambda_{(3)}(s_{10}(x_D,\varphi),\vec{c}=0)} \\ s_9(x_D,t_D), & \frac{t_D-1}{\lambda_{(3)}(s_{10}(x_D,\varphi),\vec{c}=0)} < x_D < \frac{t_D-1}{\lambda_{(3)}(s_9(x_D,\varphi),\vec{c}^{(C)})} \\ s_8(x_D,t_D), & \frac{t_D-1}{\lambda_{(3)}(s_9(x_D,\varphi),\vec{c}^{(C)})} < x_D < \frac{t_D-1}{\lambda_{(2)}(s_8(x_D,\varphi),\vec{c}^{(C)})} \\ s_7(x_D,t_D), & \frac{t_D-1}{\lambda_{(2)}(s_8(x_D,\varphi),\vec{c}^{(C)})} < x_D < \frac{t_D-1}{\lambda_{(2)}(s_7(x_D,\varphi),\vec{c}^{(D)})} \\ s_6(x_D,t_D), & \frac{t_D-1}{\lambda_{(2)}(s_7(x_D,\varphi),\vec{c}^{(D)})} < x_D < \frac{t_D-1}{\lambda_{(1)}(s_6(x_D,\varphi),\vec{c}^{(D)})} \\ s_5^{+}(x_D,t_D), & \frac{t_D-1}{\lambda_{(1)}(s_6(x_D,\varphi),\vec{c}^{(D)})} < x_D < x_{3,1}(t_D) \\ s_5^{-}(x_D,t_D), & x_{3,1}(t_D) < x_D < x_{2,1}(t_D) \\ s_5^{--}(x_D,t_D), & x_{2,1}(t_D) < x_D < \frac{t_D-t_B}{\lambda_{(1)}^{--}(s^{(3)},\vec{c}^{(A)})} - x_B \\ s^{(2)}, & \frac{t_D-t_B}{\lambda_{(1)}^{--}(s^{(3)},\vec{c}^{(A)})} - x_B < x_D < \frac{t_D}{D_{(1)}} \\ s^{(1)}, & \frac{t_D}{D_{(1)}} < x_D < \frac{t_D}{\lambda_{(s)}(s^{(1)},\vec{c}^{(I)})} \\ s_{I^+}(x_D,t_D), & \frac{t_D}{\lambda_{(s)}(s^{(1)},\vec{c}^{(I)})} < x_D < \frac{t_D}{\lambda_{(s)}(s^{(I^+)},\vec{c}^{(I)})} \\ s^{(I)}, & x_D > \frac{t_D}{\lambda_{(s)}(s^{(I^+)},\vec{c}^{(I)})} \end{cases} \tag{49}$$

In figure (20) we present the saturation profile of solution $s_{IV}(x_D, t_D)$, and in figure (21) the solution path of $s_{IV}(x_D, t_D)$ in $f \times s$ plane is shown, which structural formula is given by: $(J) - 10'' - 9'' - 8'' - 7'' - 6'' - 5^{+''} \rightarrow 5^{-'} - 5^{-''} \rightarrow 5^{--'} - (2) \rightarrow (1) - I^{+''} \rightarrow (I)$.

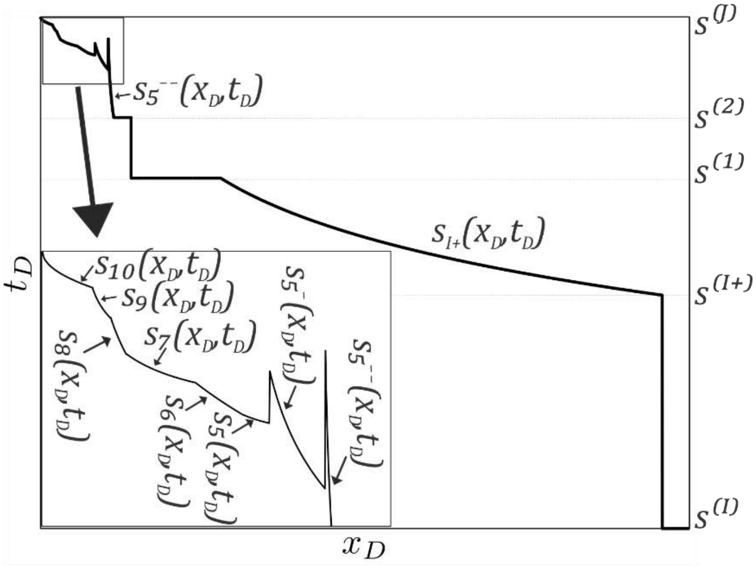

Figure 20: Saturation profile of solution $s_{IV}(x_D, t_D)$

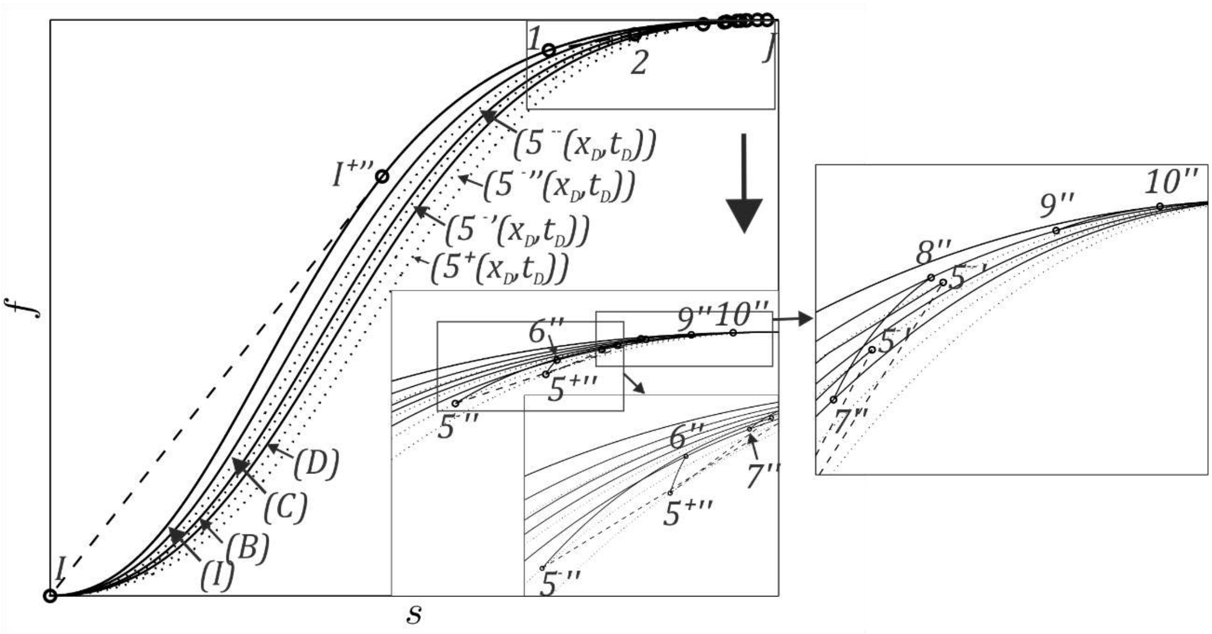

Figure 21: Solution path of s_{IV} in $f \times s$ plane

In $s_V(x_D, t_D)$ the constant state $\vec{c} = \vec{c}^{(D)}$ (region 6^-) appears in the solution and the region (5) no longer exists. Thus,

$$s_V(x_D,t_D)=\begin{cases} s^{(J)}, & x_D<\frac{t_D}{\lambda_{(s)}(s^{(J)},\vec{c}=0)} \\ s_{10}(x_D,t_D), & \frac{t_D}{\lambda_{(s)}(s^{(J)},\vec{c}=0)}<x_D<\frac{t_D-1}{\lambda_{(3)}(s_{10}(x_D,\varphi),\vec{c}=0)} \\ s_9(x_D,t_D), & \frac{t_D-1}{\lambda_{(3)}(s_{10}(x_D,\varphi),\vec{c}=0)}<x_D<\frac{t_D-1}{\lambda_{(3)}(s_9(x_D,\varphi),\vec{c}^{(C)})} \\ s_8(x_D,t_D), & \frac{t_D-1}{\lambda_{(3)}(s_9(x_D,\varphi),\vec{c}^{(C)})}<x_D<\frac{t_D-1}{\lambda_{(2)}(s_8(x_D,\varphi),\vec{c}^{(C)})} \\ s_7(x_D,t_D), & \frac{t_D-1}{\lambda_{(2)}(s_8(x_D,\varphi),\vec{c}^{(C)})}<x_D<\frac{t_D-1}{\lambda_{(2)}(s_7(x_D,\varphi),\vec{c}^{(D)})} \\ s_6(x_D,t_D), & \frac{t_D-1}{\lambda_{(2)}(s_7(x_D,\varphi),\vec{c}^{(D)})}<x_D<x_{3,1}(t_D) \\ s^{(6-)}, & x_{3,1}(t_D)<x_D<\frac{t_D-t_C}{\lambda^{-}_{(1)}\left(s^{(6-)},\vec{c}^{(D)}\right)}-x_C \\ s_5^{-}(x_D,t_D), & \frac{t_D-t_C}{\lambda^{-}_{(1)}\left(s^{(6-)},\vec{c}^{(D)}\right)}-x_C<x_D<x_{2,1}(t_D) \\ s_5^{--}(x_D,t_D), & x_{2,1}(t_D)<x_D<\frac{t_D-t_B}{\lambda^{--}_{(1)}\left(s^{(3)},\vec{c}^{(A)}\right)}-x_B \\ s^{(2)}, & \frac{t_D-t_B}{\lambda^{--}_{(1)}\left(s^{(3)},\vec{c}^{(A)}\right)}-x_B<x_D<\frac{t_D}{D_{(1)}} \\ s^{(1)}, & \frac{t_D}{D_{(1)}}<x_D<\frac{t_D}{\lambda_{(s)}(s^{(1)},\vec{c}^{(I)})} \\ s_{I^+}(x_D,t_D), & \frac{t_D}{\lambda_{(s)}(s^{(1)},\vec{c}^{(I)})}<x_D<\frac{t_D}{\lambda_{(s)}(s^{(I^+)},\vec{c}^{(I)})} \\ s^{(I)}, & x_D>\frac{t_D}{\lambda_{(s)}(s^{(I^+)},\vec{c}^{(I)})} \end{cases} \qquad (50)$$

The saturation profile of $s_V(x_D,t_D)$ is shown in figure (22) and the solution path in $f \times s$ plane is presented in figure (23). The structural formula of $s_V(x_D,t_D)$ is: $(J)-10''-9''-8''-7''-6''\rightarrow(6^-)-5^{-''}\rightarrow5^{--'}-(2)\rightarrow(1)-I^{+''}\rightarrow(I)$.

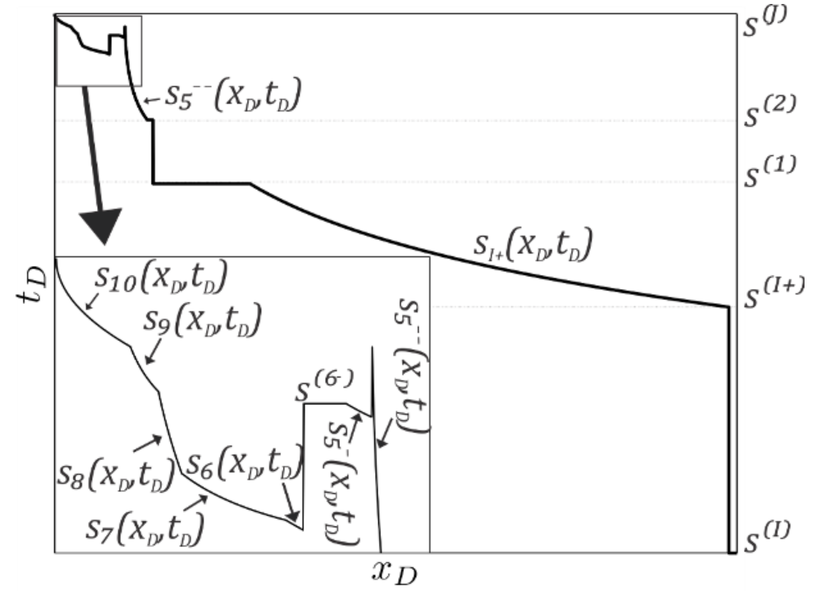

Figure 22: Saturation profile of the solution $s_V(x_D, t_D)$

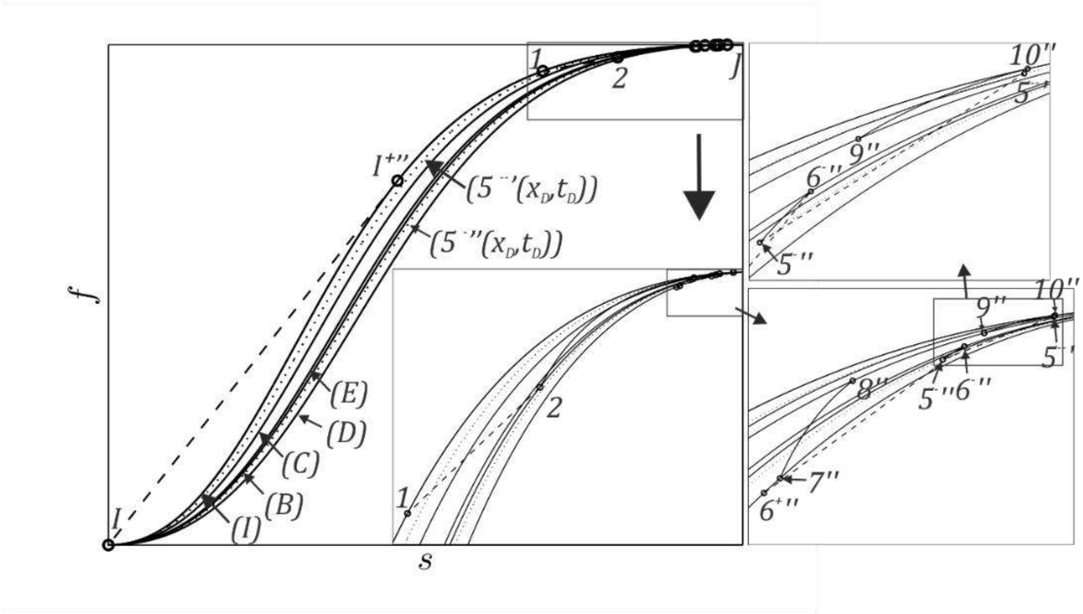

Figure 23: Solution path of s_V in $f \times s$ plane

In solution $s_{VI}(x_D, t_D)$ the rarefaction $\lambda_{(1)}$ is absorbed by shock $D_{(1)}$. Thus, the solution is:

$$s_{VI}(x_D,t_D)=\begin{cases} s^{(J)}, & x_D<\frac{t_D}{\lambda_{(s)}(s^{(J)},\vec{c}=0)} \\ s_{10}(x_D,t_D), & \frac{t_D}{\lambda_{(s)}(s^{(J)},\vec{c}=0)}<x_D<\frac{t_D-1}{\lambda_{(3)}(s_{10}(x_D,\varphi),\vec{c}=0)} \\ s_9(x_D,t_D), & \frac{t_D-1}{\lambda_{(3)}(s_{10}(x_D,\varphi),\vec{c}=0)}<x_D<\frac{t_D-1}{\lambda_{(3)}(s_9(x_D,\varphi),\vec{c}^{(C)})} \\ s_8(x_D,t_D), & \frac{t_D-1}{\lambda_{(3)}(s_9(x_D,\varphi),\vec{c}^{(C)})}<x_D<\frac{t_D-1}{\lambda_{(2)}(s_8(x_D,\varphi),\vec{c}^{(C)})} \\ s_7(x_D,t_D), & \frac{t_D-1}{\lambda_{(2)}(s_8(x_D,\varphi),\vec{c}^{(C)})}<x_D<\frac{t_D-1}{\lambda_{(2)}(s_7(x_D,\varphi),\vec{c}^{(D)})} \\ s_6(x_D,t_D), & \frac{t_D-1}{\lambda_{(2)}(s_7(x_D,\varphi),\vec{c}^{(D)})}<x_D<x_{3,1}(t_D) \\ s^{(6-)}, & x_{3,1}(t_D)<x_D<\frac{t_D-t_C}{\lambda_{(1)}^{-}(s^{(6-)},\vec{c}^{(D)})}-x_C \\ s_5^{-}(x_D,t_D), & \frac{t_D-t_C}{\lambda_{(1)}^{-}(s^{(6-)},\vec{c}^{(D)})}-x_C<x_D<x_{2,1}(t_D) \\ s_5^{--}(x_D,t_D), & x_{2,1}(t_D)<x_D<x_{1,1}(t_D) \\ s^{(1)}, & x_{1,1}(t_D)<x_D<\frac{t_D}{\lambda_{(s)}(s^{(1)},\vec{c}^{(I)})} \\ s_{I^+}(x_D,t_D), & \frac{t_D}{\lambda_{(s)}(s^{(1)},\vec{c}^{(I)})}<x_D<\frac{t_D}{\lambda_{(s)}(s^{(I^+)},\vec{c}^{(I)})} \\ s^{(I)}, & x_D>\frac{t_D}{\lambda_{(s)}(s^{(I^+)},\vec{c}^{(I)})} \end{cases} \tag{51}$$

Next, we present the saturation profile (Figure 24) and the solution path in $f\times s$ plane (Figure 25) of the solution $s_{VI}(x_D,\varphi)$, which has the structural formula: $(J)-10''-9''-8''-7''-6''\to(6^-)-5^{-''}\to5^{--'}-5^{--''}\to(1)-I^{+''}\to(I)$.

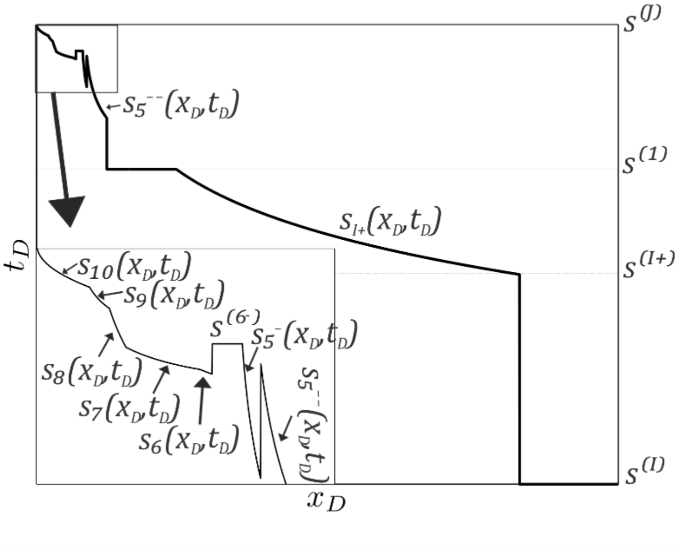

Figure 24: Saturation profile of the solution $s_{VI}(x_D,t_D)$

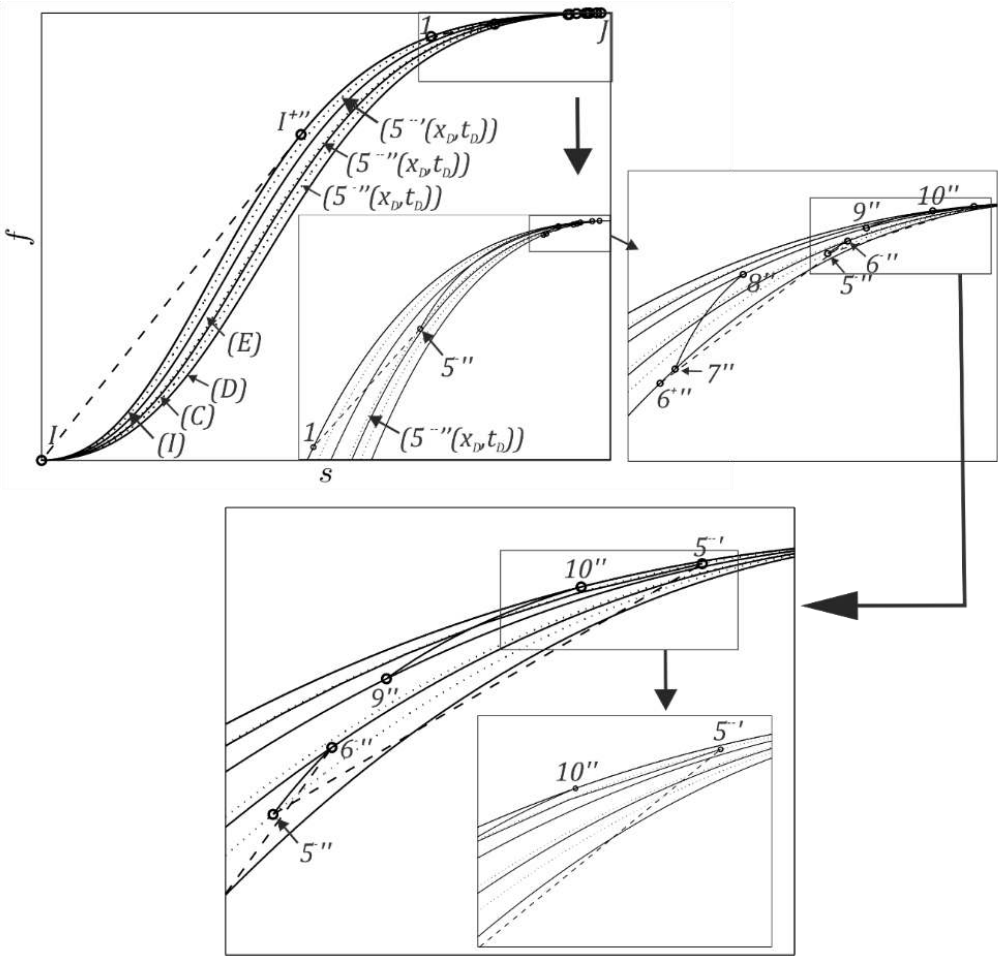

Figure 25: Solution path of s_{VI} in $f \times s$ plane

In the next part of the solution ($s_{VII}(x_D, t_D)$), the rarefaction $\lambda_{(2)}$ crosses the shock wave $D_{(3)}$ at point E, and region (6) disappears. Therefore,

$$s_{VII}(x_D,t_D)=\begin{cases} s^{(J)}, & x_D<\frac{t_D}{\lambda_{(s)}(s^{(J)},\vec{c}=0)}\\ s_{10}(x_D,t_D), & \frac{t_D}{\lambda_{(s)}(s^{(J)},\vec{c}=0)}<x_D<\frac{t_D-1}{\lambda_{(3)}(s_{10}(x_D,\varphi),\vec{c}=0)}\\ s_9(x_D,t_D), & \frac{t_D-1}{\lambda_{(3)}(s_{10}(x_D,\varphi),\vec{c}=0)}<x_D<\frac{t_D-1}{\lambda_{(3)}(s_9(x_D,\varphi),\vec{c}^{(C)})}\\ s_8(x_D,t_D), & \frac{t_D-1}{\lambda_{(3)}(s_9(x_D,\varphi),\vec{c}^{(C)})}<x_D<\frac{t_D-1}{\lambda_{(2)}(s_8(x_D,\varphi),\vec{c}^{(C)})}\\ s_7^{+}(x_D,t_D), & \frac{t_D-1}{\lambda_{(2)}(s_8(x_D,\varphi),\vec{c}^{(C)})}<x_D<x_{3,2}(t_D)\\ s_7^{-}(x_D,t_D), & x_{3,2}(t_D)<x_D<\frac{t_D-t_E}{\lambda_{(2)}^{-}(s^{(6-)},\vec{c}^{(D)})}-x_E\\ s^{(6-)}, & \frac{t_D-t_E}{\lambda_{(2)}^{-}(s^{(6-)},\vec{c}^{(D)})}-x_E<x_D<\frac{t_D-t_C}{\lambda_{(1)}^{-}(s^{(6-)},\vec{c}^{(D)})}-x_C\\ s_5^{-}(x_D,t_D), & \frac{t_D-t_C}{\lambda_{(1)}^{-}(s^{(6-)},\vec{c}^{(D)})}-x_C<x_D<x_{2,1}(t_D)\\ s_5^{--}(x_D,t_D), & x_{2,1}(t_D)<x_D<x_{1,1}(t_D)\\ s^{(1)}, & x_{1,1}(t_D)<x_D<\frac{t_D}{\lambda_{(s)}(s^{(1)},\vec{c}^{(I)})}\\ s_{I^+}(x_D,t_D), & \frac{t_D}{\lambda_{(s)}(s^{(1)},\vec{c}^{(I)})}<x_D<\frac{t_D}{\lambda_{(s)}(s^{(I^+)},\vec{c}^{(I)})}\\ s^{(I)}, & x_D>\frac{t_D}{\lambda_{(s)}(s^{(I^+)},\vec{c}^{(I)})} \end{cases} \tag{52}$$

The saturation profile of solution $s_{VII}(x_D,t_D)$ is shown in figure (26), and the solution path in $f \times s$ plane is presented in figure (27). The structural formula is given by: $(J) - 10'' - 9'' - 8'' - 7'' \to 7^{-\prime} - (6^{-}) - 5^{-\prime\prime} \to -5^{--\prime} - 5^{--\prime\prime} \to (1) - I^{+\prime\prime} \to (I)$.

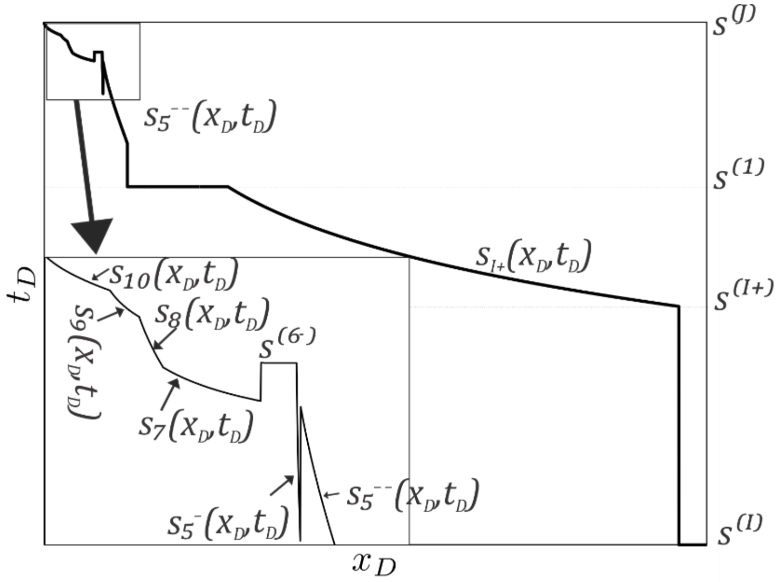

Figure 26: Saturation profile of the solution $s_{VII}(x_D,t_D)$

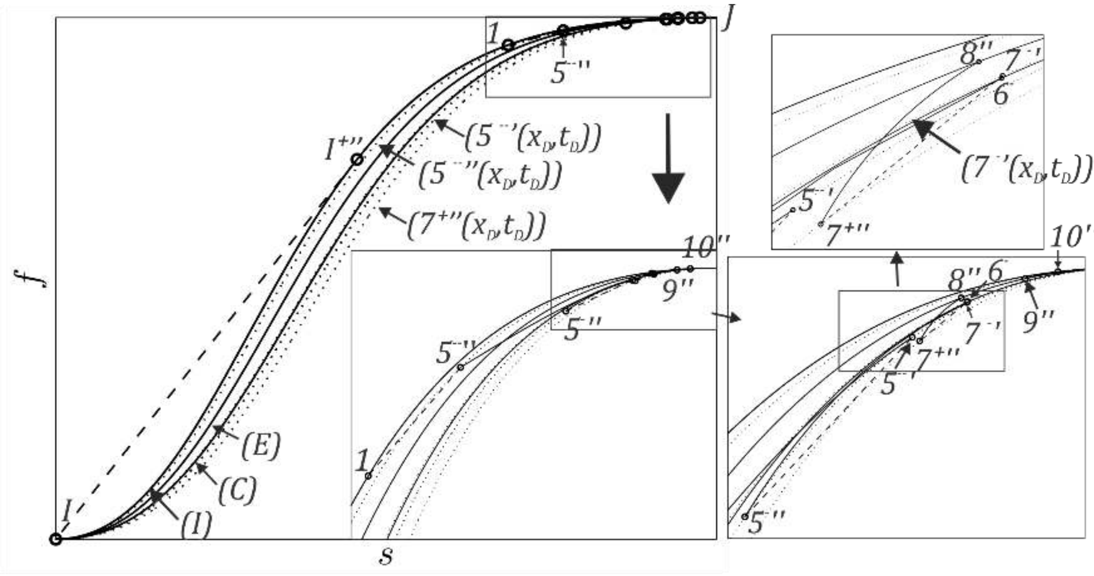

Figure 27: Solution path of s_{VII} in $f \times s$ plane

In $s_{VIII}(x_D, t_D)$, the interaction between rarefaction $\lambda_{(1)}$ and the shock wave $D_{(2)}$ ends, and a pure water bank appears in the solution (region 6^{--}). Thus,

$$s_{VIII}(x_D,t_D)=\begin{cases} s^{(J)}, & x_D<\frac{t_D}{\lambda_{(s)}(s^{(J)},\vec{c}=0)} \\ s_{10}(x_D,t_D), & \frac{t_D}{\lambda_{(s)}(s^{(J)},\vec{c}=0)}<x_D<\frac{t_D-1}{\lambda_{(3)}(s_{10}(x_D,\varphi),\vec{c}=0)} \\ s_9(x_D,t_D), & \frac{t_D-1}{\lambda_{(3)}(s_{10}(x_D,\varphi),\vec{c}=0)}<x_D<\frac{t_D-1}{\lambda_{(3)}(s_9(x_D,\varphi),\vec{c}^{(C)})} \\ s_8(x_D,t_D), & \frac{t_D-1}{\lambda_{(3)}(s_9(x_D,\varphi),\vec{c}^{(C)})}<x_D<\frac{t_D-1}{\lambda_{(2)}(s_8(x_D,\varphi),\vec{c}^{(C)})} \\ s_7^{+}(x_D,t_D), & \frac{t_D-1}{\lambda_{(2)}(s_8(x_D,\varphi),\vec{c}^{(C)})}<x_D<x_{3,2}(t_D) \\ s_7^{-}(x_D,t_D), & x_{3,2}(t_D)<x_D<\frac{t_D-t_E}{\lambda_{(2)}^{-}\left(s^{(6-)},\vec{c}^{(D)}\right)}-x_E \\ s^{(6-)}, & \frac{t_D-t_E}{\lambda_{(2)}^{-}\left(s^{(6-)},\vec{c}^{(D)}\right)}-x_E<x_D<\frac{t_D-t_F}{D_{(2)}\left(s^{(6-)},\vec{c}^{(D)}\right)}-x_F \\ s^{(6--)}, & \frac{t_D-t_F}{D_{(2)}\left(s^{(6-)},\vec{c}^{(D)}\right)}-x_F<x_D<\frac{t_D-t_F}{\lambda_{(1)}^{--}\left(s^{(6--)},\vec{c}=0\right)}-x_F \\ s_5^{--}(x_D,t_D), & \frac{t_D-t_F}{\lambda_{(1)}^{--}\left(s^{(6--)},\vec{c}=0\right)}-x_F<x_D<x_{1,1}(t_D) \\ s^{(1)}, & x_{1,1}(t_D)<x_D<\frac{t_D}{\lambda_{(s)}(s^{(1)},\vec{c}^{(I)})} \\ s_{I^+}(x_D,t_D), & \frac{t_D}{\lambda_{(s)}(s^{(1)},\vec{c}^{(I)})}<x_D<\frac{t_D}{\lambda_{(s)}(s^{(I^+)},\vec{c}^{(I)})} \\ s^{(I)}, & x_D>\frac{t_D}{\lambda_{(s)}(s^{(I^+)},\vec{c}^{(I)})} \end{cases} \tag{53}$$

We present the saturation profile of equation (53) in figure (28), and the solution path in $f \times s$ plane in figure (29). The structural formula is given by: $(J) - 10'' - 9'' - 8'' - 7'' \to 7^{-\prime} - (6^{-}) \to (6^{--}) - 5^{--\prime\prime} \to (1) - I^{+\prime\prime} \to (I)$.

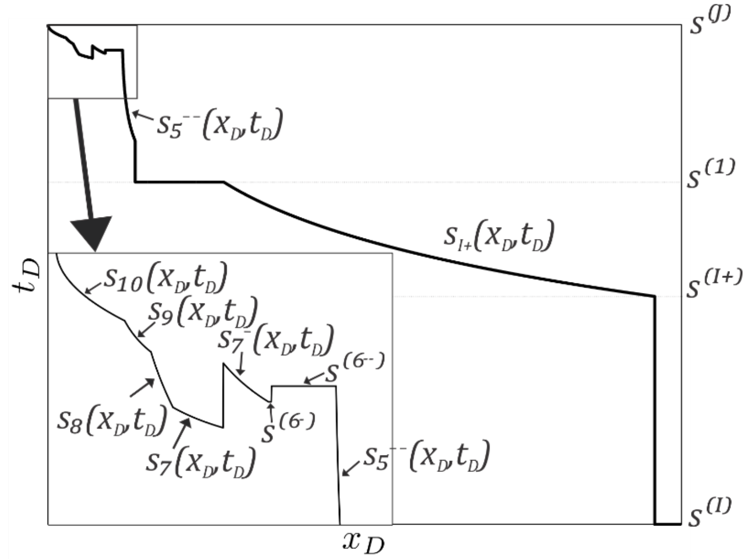

Figure 28: Saturation profile of the solution $s_{VIII}(x_D, t_D)$

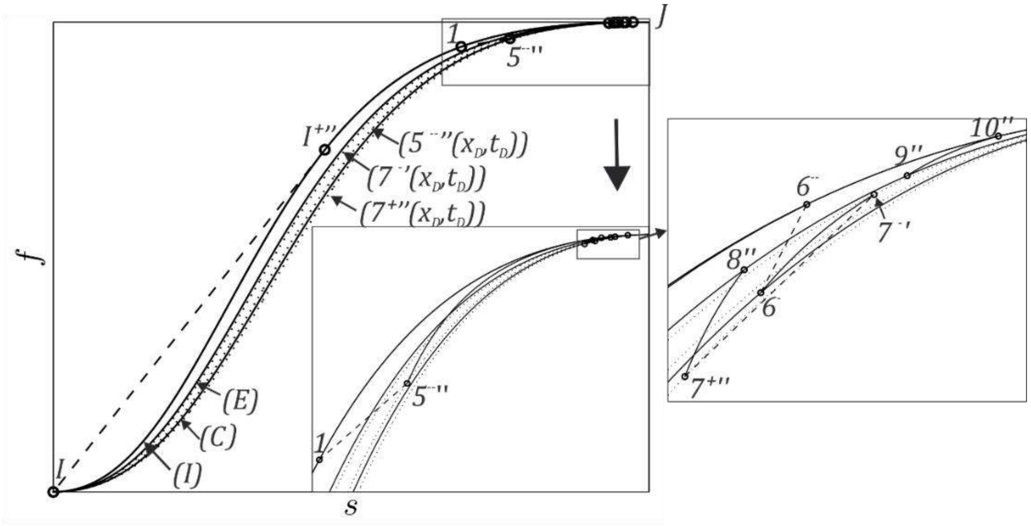

Figure 29: Solution path of s_{VIII} in the $f \times s$ plane

For $t_D > t_G$ (solution $s_{IX}(x_D, t_D)$), the rarefaction $\lambda_{(2)}$ is absorbed by the shock $D_{(2)}$. Therefore, the solution for this region is given by:

$$s_{IX}(x_D,t_D)=\begin{cases} s^{(J)}, & x_D<\frac{t_D}{\lambda_{(s)}(s^{(J)},\vec{c}=0)} \\ s_{10}(x_D,t_D), & \frac{t_D}{\lambda_{(s)}(s^{(J)},\vec{c}=0)}<x_D<\frac{t_D-1}{\lambda_{(3)}(s_{10}(x_D,\varphi),\vec{c}=0)} \\ s_9(x_D,t_D), & \frac{t_D-1}{\lambda_{(3)}(s_{10}(x_D,\varphi),\vec{c}=0)}<x_D<\frac{t_D-1}{\lambda_{(3)}(s_9(x_D,\varphi),\vec{c}^{(C)})} \\ s_8(x_D,t_D), & \frac{t_D-1}{\lambda_{(3)}(s_9(x_D,\varphi),\vec{c}^{(C)})}<x_D<\frac{t_D-1}{\lambda_{(2)}(s_8(x_D,\varphi),\vec{c}^{(C)})} \\ s_7^{+}(x_D,t_D), & \frac{t_D-1}{\lambda_{(2)}(s_8(x_D,\varphi),\vec{c}^{(C)})}<x_D<x_{3,2}(t_D) \\ s_7^{-}(x_D,t_D), & x_{3,2}(t_D)<x_D<x_{2,2}(t_D) \\ s^{(6--)}, & x_{2,2}(t_D)<x_D<\frac{t_D-t_F}{\lambda_{(1)}^{--}(s^{(6--)},\vec{c}=0)}-x_F \\ s_5^{--}(x_D,t_D), & \frac{t_D-t_F}{\lambda_{(1)}^{--}(s^{(6--)},\vec{c}=0)}-x_F<x_D<x_{1,1}(t_D) \\ s^{(1)}, & x_{1,1}(t_D)<x_D<\frac{t_D}{\lambda_{(s)}(s^{(1)},\vec{c}^{(I)})} \\ s_{I^+}(x_D,t_D), & \frac{t_D}{\lambda_{(s)}(s^{(1)},\vec{c}^{(I)})}<x_D<\frac{t_D}{\lambda_{(s)}(s^{(I^+)},\vec{c}^{(I)})} \\ s^{(I)}, & x_D>\frac{t_D}{\lambda_{(s)}(s^{(I^+)},\vec{c}^{(I)})} \end{cases} \tag{54}$$

In figure (30) the saturation profile of solution $s_{IX}(x_D,t_D)$ is presented. In figure (31) we show the solution path in $f\times s$ plane, which has structural formula $(J)-10''-9''-8''-7''\rightarrow 7^{-\prime}-7^{-\prime\prime}\rightarrow(6^{--})-5^{--\prime\prime}\rightarrow(1)-I^{+\prime\prime}\rightarrow(I)$.

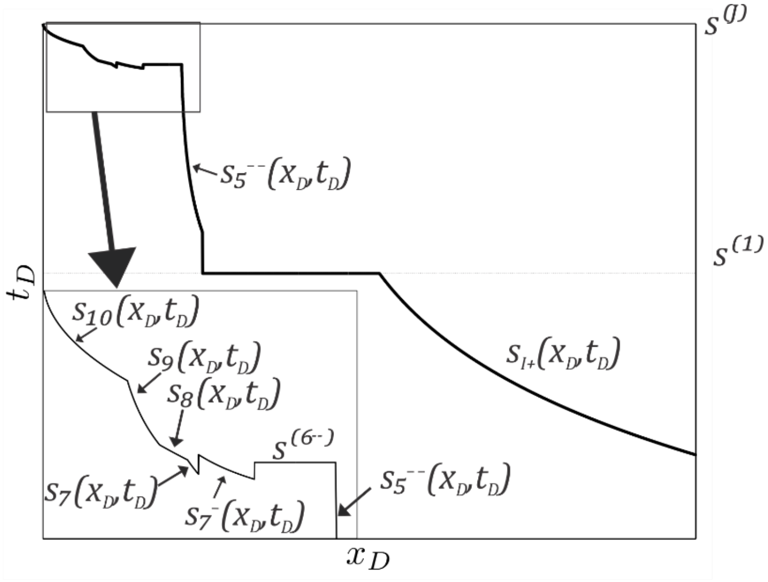

Figure 30: Saturation profile of the solution $s_{IX}(x_D,t_D)$

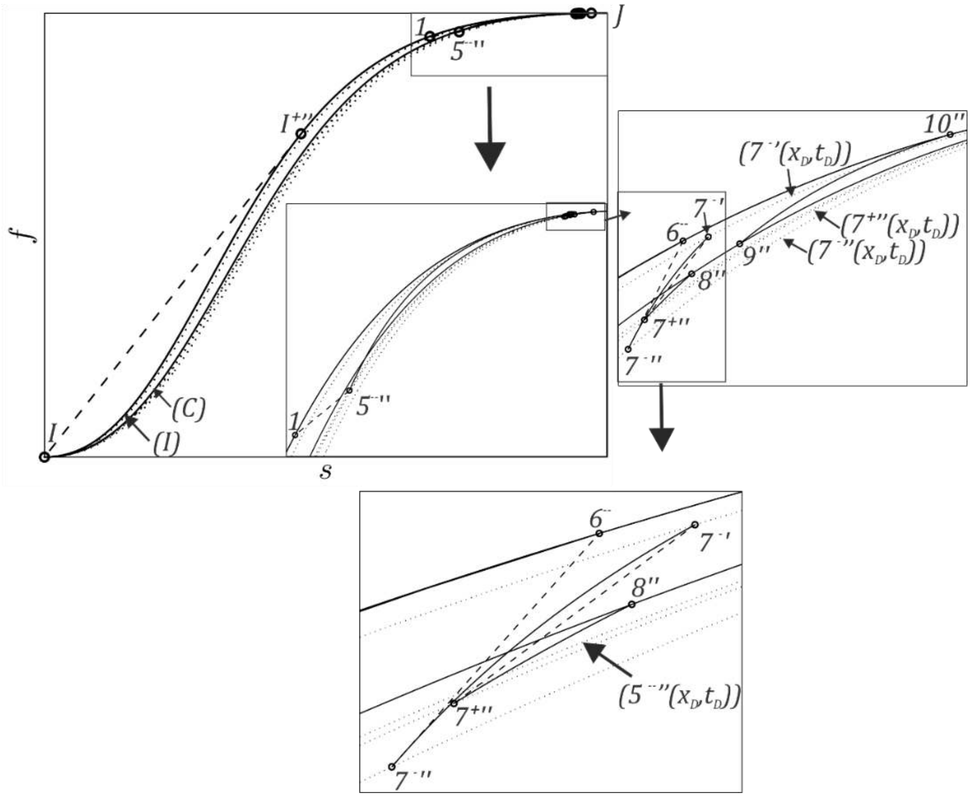

Figure 31: Solution path of s_{IX} in $f \times s$ plane

For $t_D > t_H$ (solution $s_X(x_D, t_D)$), the interaction between rarefaction $\lambda_{(2)}$ and the shock $D_{(3)}$ ends, and region 7 is no longer present in the solution. Moreover, at this point the separation of the chemical components is completed. Note that due to the separation of the chemicals, a new pure water bank region appears (region 8^-). Thus, $s_X(x_D, t_D)$ is given by:

$$s_X(x_D,t_D)=\begin{cases} s^{(J)}, & x_D<\frac{t_D}{\lambda_{(s)}(s^{(J)},\vec{c}=0)} \\ s_{10}(x_D,t_D), & \frac{t_D}{\lambda_{(s)}(s^{(J)},\vec{c}=0)}<x_D<\frac{t_D-1}{\lambda_{(3)}(s_{10}(x_D,\varphi),\vec{c}=0)} \\ s_9(x_D,t_D), & \frac{t_D-1}{\lambda_{(3)}(s_{10}(x_D,\varphi),\vec{c}=0)}<x_D<\frac{t_D-1}{\lambda_{(3)}(s_9(x_D,\varphi),\vec{c}^{(C)})} \\ s_8^+(x_D,t_D), & \frac{t_D-1}{\lambda_{(3)}(s_9(x_D,\varphi),\vec{c}^{(C)})}<x_D<\frac{t_D-t_H}{D_{(3)}(s_8(x_D,\varphi),\vec{c}^{(C)})}+x_H \\ s^{(8-)}, & \frac{t_D-t_H}{D_{(3)}(s_8(x_D,\varphi),\vec{c}^{(C)})}+x_H<x_D<\frac{t_D-t_H}{\lambda_{(2)}^-(s_8(x_D,\varphi),\vec{c}=0)}+x_H \\ s_7^-(x_D,t_D), & \frac{t_D-t_H}{\lambda_{(2)}^-(s_8(x_D,\varphi),\vec{c}=0)}+x_H<x_D<x_{2,2}(t_D) \\ s^{(6--)}, & x_{2,2}(t_D)<x_D<\frac{t_D-t_F}{\lambda_{(1)}^{--}(s^{(6--)},\vec{c}=0)}-x_F \\ s_5^{--}(x_D,t_D), & \frac{t_D-t_F}{\lambda_{(1)}^{--}(s^{(6--)},\vec{c}=0)}-x_F<x_D<x_{1,1}(t_D) \\ s^{(1)}, & x_{1,1}(t_D)<x_D<\frac{t_D}{\lambda_{(s)}(s^{(1)},\vec{c}^{(I)})} \\ s_{I^+}(x_D,t_D), & \frac{t_D}{\lambda_{(s)}(s^{(1)},\vec{c}^{(I)})}<x_D<\frac{t_D}{\lambda_{(s)}(s^{(I^+)},\vec{c}^{(I)})} \\ s^{(I)}, & x_D>\frac{t_D}{\lambda_{(s)}(s^{(I^+)},\vec{c}^{(I)})} \end{cases} \tag{55}$$

Next, we present the saturation profile of $s_X(x_D,t_D)$ (Figure 32) and the solution path in $f\times s$ plane (Figure 33). The structural formula of the solution is: $(J)-10''-9''-8''\rightarrow(8^-)-7^{-''}\rightarrow(6^{--})-5^{--''}\rightarrow(1)-I^{+''}\rightarrow(I)$.

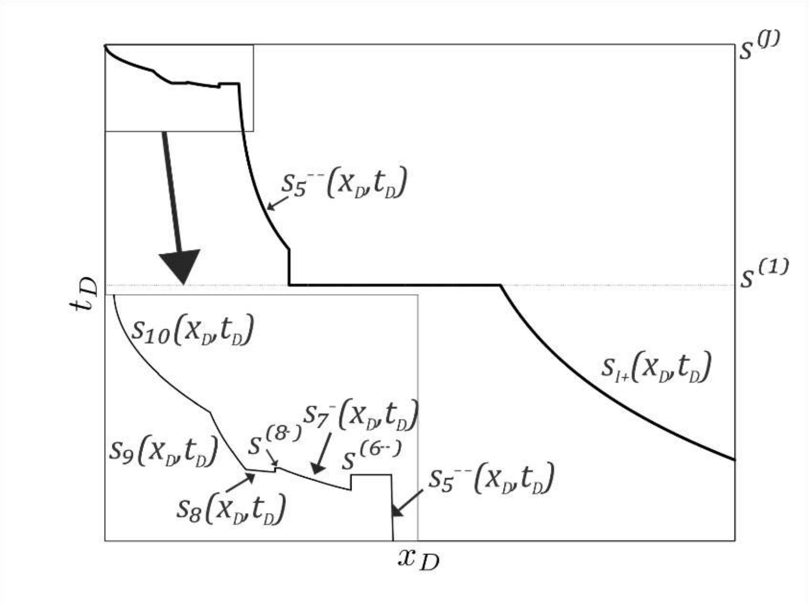

Figure 32: Saturation profile of the solution $s_X(x_D,t_D)$

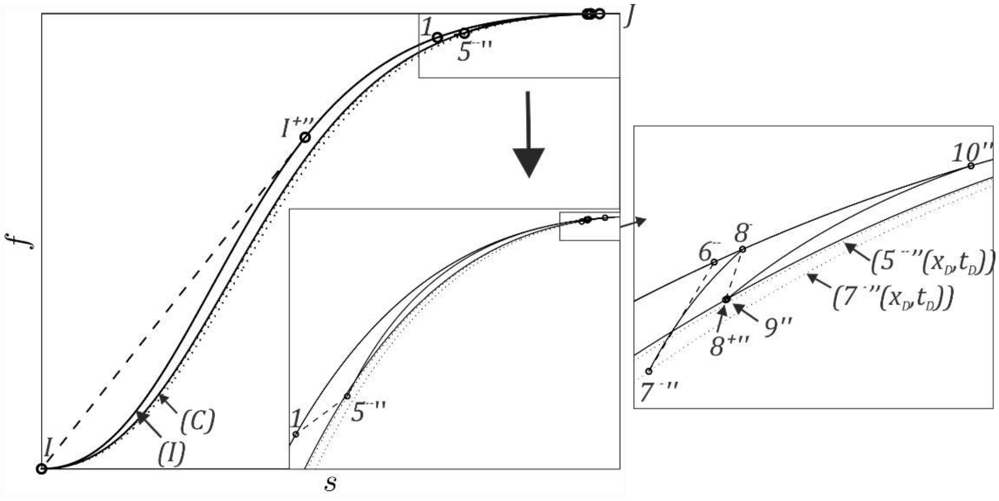

Figure 33: Solution path of s_X in $f \times s$ plane

For $t_D = t_I$, the rarefaction wave $\lambda_{(3)}$ meets the shock wave $D_{(3)}$ (solution $s_{XI}(x_D, t_D)$). At this part of the solution, the region (8) no longer exists and the constant concentration state is $\vec{c} = \vec{c}^{(I)} = 0$; $s_{XI}(x_D, t_D)$ is given by:

$$
s_{XI}(x_D,t_D) = \begin{cases}
s^{(J)}, & x_D < \frac{t_D}{\lambda_{(s)}(s^{(J)},\vec{c}=0)} \\
s_{10}(x_D,t_D), & \frac{t_D}{\lambda_{(s)}(s^{(J)},\vec{c}=0)} < x_D < \frac{t_D-1}{\lambda_{(3)}(s_{10}(x_D,\varphi),\vec{c}=0)} \\
s_9^+(x_D,t_D), & \frac{t_D-1}{\lambda_{(3)}(s_{10}(x_D,\varphi),\vec{c}=0)} < x_D < x_{3,3}(t_D) \\
s^{(8-)}, & x_{3,3}(t_D) < x_D < \frac{t_D-t_H}{\lambda_{(2)}^{-}(s_8(x_D,\varphi),\vec{c}=0)} + x_H \\
s_7^-(x_D,t_D), & \frac{t_D-t_H}{\lambda_{(2)}^{-}(s_8(x_D,\varphi),\vec{c}=0)} + x_H < x_D < x_{2,2}(t_D) \\
s^{(6--)}, & x_{2,2}(t_D) < x_D < \frac{t_D-t_F}{\lambda_{(1)}^{--}(s^{(6--)},\vec{c}=0)} - x_F \\
s_5^{--}(x_D,t_D), & \frac{t_D-t_F}{\lambda_{(1)}^{--}(s^{(6--)},\vec{c}=0)} - x_F < x_D < x_{1,1}(t_D) \\
s^{(1)}, & x_{1,1}(t_D) < x_D < \frac{t_D}{\lambda_{(s)}(s^{(1)},\vec{c}^{(I)})} \\
s_{I^+}(x_D,t_D), & \frac{t_D}{\lambda_{(s)}(s^{(1)},\vec{c}^{(I)})} < x_D < \frac{t_D}{\lambda_{(s)}(s^{(I^+)},\vec{c}^{(I)})} \\
s^{(I)}, & x_D > \frac{t_D}{\lambda_{(s)}(s^{(I^+)},\vec{c}^{(I)})}
\end{cases} \tag{56}
$$

When $t_D \rightarrow +\infty$, the rarefaction waves are completely absorbed by the shock waves of the same family (Rhee *et al.*, 2001). Therefore, the chemicals concentration and water saturation along all the reservoir are $\vec{c} = 0$ and $s = s^{(J)}$, respectively.

Appendix B – Supplementary material of the paper “Mathematical Modeling of Low Salinity Waterflooding in Sandstone Reservoirs: Enhanced Oil Recovery by Multicomponent Cation Exchange”

This supplementary material presents the complete solution description of the auxiliary system (section A), lifting equation (section B) and $x_D \times t_D$ plane solution (section C) for the paper "Mathematical Modeling of Low Salinity Waterflooding in Sandstone Reservoirs: Enhanced Oil Recovery by Multicomponent Cation Exchange".

A. Auxiliary system solution

The solution of the auxiliary system can be divided into 17 regions (see figure 3 in the original paper) separated by the points (x_A, φ_A)-(x_N, φ_N) and the point $\left(x_{pH}, \varphi_{pH}\right)$ that comes from the pH solution (Equation B.1).

$$\vec{c}(x_D, \varphi) = \begin{cases} \overrightarrow{c_I}, & \varphi < \varphi_{HS} \\ \overrightarrow{c_{II}}, & \varphi_{HS} < \varphi < \varphi_A \\ \overrightarrow{c_{III}}, & \varphi_A < \varphi < \varphi_B \\ \overrightarrow{c_{IV}}, & \varphi_B < \varphi < \varphi_C \\ \overrightarrow{c_V}, & \varphi_C < \varphi < \varphi_D \\ \overrightarrow{c_{VI}}, & \varphi_D < \varphi < \varphi_E \\ \overrightarrow{c_{VII}}, & \varphi_E < \varphi < \varphi_F \\ \overrightarrow{c_{VIII}}, & \varphi_F < \varphi < \varphi_G \\ \overrightarrow{c_{IX}}, & \varphi_G < \varphi < \varphi_H \\ \overrightarrow{c_X}, & \varphi_H < \varphi < \varphi_I \\ \overrightarrow{c_{XI}}, & \varphi_I < \varphi < \varphi_{pH} \\ \overrightarrow{c_{XII}}, & \varphi_{pH} < \varphi < \varphi_J \\ \overrightarrow{c_{XIII}}, & \varphi_J < \varphi < \varphi_K \\ \overrightarrow{c_{XIV}}, & \varphi_K < \varphi < \varphi_L \\ \overrightarrow{c_{XV}}, & \varphi_L < \varphi < \varphi_M \\ \overrightarrow{c_{XVI}}, & \varphi_M < \varphi < \varphi_N \\ \overrightarrow{c_{XVII}}, & \varphi_N < \varphi \end{cases} \qquad \text{(B.1)}$$

The self-similar part of the solution takes place when $\varphi < \varphi_{HS}$ ($\overrightarrow{c_I}$ in equation B.1). The concentration profile is detailed in equation (B.2):

$$\overrightarrow{c_I} = \begin{cases} \vec{c}^{(J1)}, & x_D < \frac{\varphi}{V_{pH}^{(1)}} \\ \vec{c}^{(4)-(3)}(x_D,\varphi), & \frac{\varphi}{V_{pH}^{(1)}} < x_D < \frac{\varphi}{\sigma_{pH}(\xi^{(I)})} \\ \vec{c}^{(3)}, & \frac{\varphi}{\sigma_{pH}(\xi^{(I)})} < x_D < \frac{\varphi}{\sigma_{(3)}(\vec{\omega}^{(3)},\xi^{(I)})} \\ \vec{c}^{(3)-(2)}(x_D,\varphi), & \frac{\varphi}{\sigma_{(3)}(\vec{\omega}^{(3)},\xi^{(I)})} < x_D < \frac{\varphi}{\sigma_{(3)}(\vec{\omega}^{(2)},\xi^{(I)})} \\ \vec{c}^{(2)}, & \frac{\varphi}{\sigma_{(3)}(\vec{\omega}^{(2)},\xi^{(I)})} < x_D < \frac{\varphi}{\sigma_{(2)}(\vec{\omega}^{(2)},\xi^{(I)})} \\ \vec{c}^{(2)-(1)}(x_D,\varphi), & \frac{\varphi}{\sigma_{(2)}(\vec{\omega}^{(2)},\xi^{(I)})} < x_D < \frac{\varphi}{\sigma_{(2)}(\vec{\omega}^{(1)},\xi^{(I)})} \\ \vec{c}^{(1)}, & \frac{\varphi}{\sigma_{(2)}(\vec{\omega}^{(1)},\xi^{(I)})} < x_D < \frac{\varphi}{\sigma_{(1)}(\vec{\omega}^{(1)},\xi^{(I)})} \\ \vec{c}^{(1)-(I)}(x_D,\varphi), & \frac{\varphi}{\sigma_{(1)}(\vec{\omega}^{(1)},\xi^{(I)})} < x_D < \frac{\varphi}{\sigma_{(1)}(\vec{\omega}^{(I)},\xi^{(I)})} \\ \vec{c}^{(I)}, & \frac{\varphi}{\sigma_{(1)}(\vec{\omega}^{(I)},\xi^{(I)})} < x_D < \frac{\varphi}{-s^{(I)}} \end{cases} \tag{B.2}$$

A concentration profile of $\overrightarrow{c_I}$ is presented in figure (B.1) emphasizing the effect of pH waves on the solution.

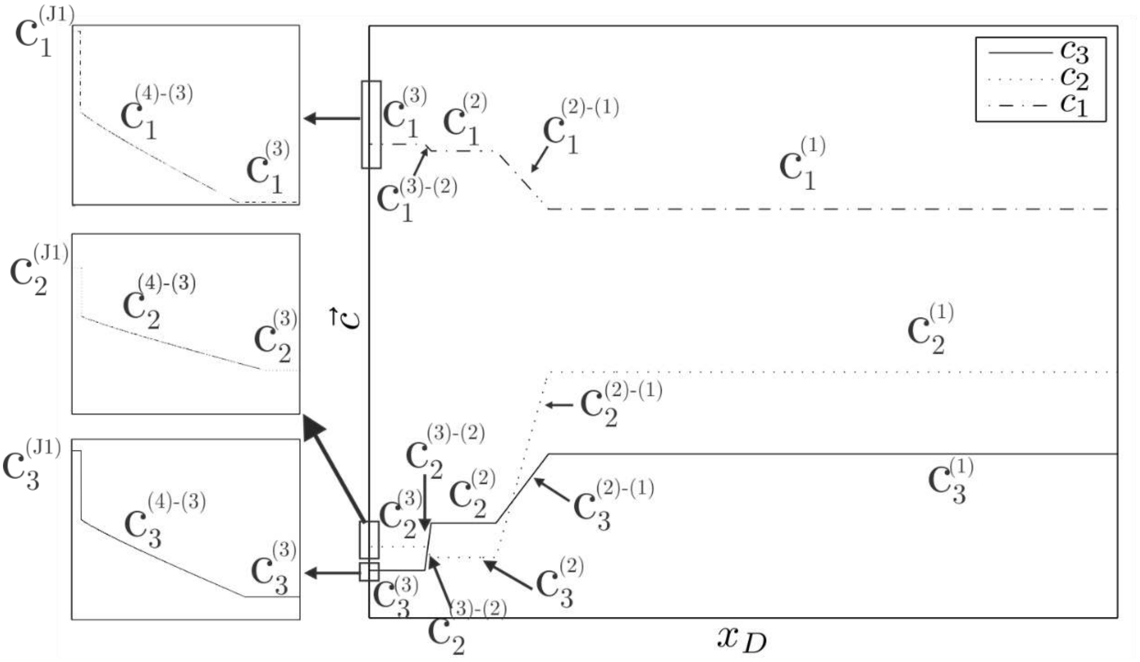

Figure B.1: Solution of the auxiliary system ($\overrightarrow{c_I}$)

The solution of the auxiliary system for this region is defined as $\overrightarrow{c_{II}}$ (Equation (B.3), and it is given by:

$$\overrightarrow{c_{II}} = \begin{cases} \vec{c}^{(J2)}, & x_D < \frac{\varphi-\varphi_{HS}}{V_{pH}^{(2)}} \\ \vec{c}^{(7)}, & \frac{\varphi-\varphi_{HS}}{V_{pH}^{(2)}} < x_D < \frac{\varphi-\varphi_{HS}}{V_{(3)}} \\ \vec{c}^{(6)}, & \frac{\varphi-\varphi_{HS}}{V_{(3)}} < x_D < \frac{\varphi-\varphi_{HS}}{\sigma_{(2)}\left(\overrightarrow{\omega}^{(6)},\xi^{(J1)}\right)} \\ \vec{c}^{(6)-(5)}(x_D,\varphi), & \frac{\varphi-\varphi_{HS}}{\sigma_{(2)}\left(\overrightarrow{\omega}^{(6)},\xi^{(J1)}\right)} < x_D < \frac{\varphi-\varphi_{HS}}{\sigma_{(2)}\left(\overrightarrow{\omega}^{(5)},\xi^{(J1)}\right)} \\ \vec{c}^{(5)}, & \frac{\varphi-\varphi_{HS}}{\sigma_{(2)}\left(\overrightarrow{\omega}^{(5)},\xi^{(J1)}\right)} < x_D < \frac{\varphi-\varphi_{HS}}{V_{(1)}} \\ \vec{c}^{(J1)}, & \frac{\varphi-\varphi_{HS}}{V_{(1)}} < x_D < \frac{\varphi}{V_{pH}^{(1)}} \\ \vec{c}^{(4)-(3)}(x_D,\varphi), & \frac{\varphi}{V_{pH}^{(1)}} < x_D < \frac{\varphi}{\sigma_{pH}(\xi^{(I)})} \\ \vec{c}^{(3)}, & \frac{\varphi}{\sigma_{pH}(\xi^{(I)})} < x_D < \frac{\varphi}{\sigma_{(3)}(\overrightarrow{\omega}^{(3)},\xi^{(I)})} \\ \vec{c}^{(3)-(2)}(x_D,\varphi), & \frac{\varphi}{\sigma_{(3)}(\overrightarrow{\omega}^{(3)},\xi^{(I)})} < x_D < \frac{\varphi}{\sigma_{(3)}(\overrightarrow{\omega}^{(2)},\xi^{(I)})} \\ \vec{c}^{(2)}, & \frac{\varphi}{\sigma_{(3)}(\overrightarrow{\omega}^{(2)},\xi^{(I)})} < x_D < \frac{\varphi}{\sigma_{(2)}(\overrightarrow{\omega}^{(2)},\xi^{(I)})} \\ \vec{c}^{(2)-(1)}(x_D,\varphi), & \frac{\varphi}{\sigma_{(2)}(\overrightarrow{\omega}^{(2)},\xi^{(I)})} < x_D < \frac{\varphi}{\sigma_{(2)}(\overrightarrow{\omega}^{(1)},\xi^{(I)})} \\ \vec{c}^{(1)}, & \frac{\varphi}{\sigma_{(2)}(\overrightarrow{\omega}^{(1)},\xi^{(I)})} < x_D < \frac{\varphi}{\sigma_{(1)}(\overrightarrow{\omega}^{(1)},\xi^{(I)})} \\ \vec{c}^{(1)-(I)}(x_D,\varphi), & \frac{\varphi}{\sigma_{(1)}(\overrightarrow{\omega}^{(1)},\xi^{(I)})} < x_D < \frac{\varphi}{\sigma_{(1)}(\overrightarrow{\omega}^{(I)},\xi^{(I)})} \\ \vec{c}^{(I)}, & \frac{\varphi}{\sigma_{(1)}(\overrightarrow{\omega}^{(I)},\xi^{(I)})} < x_D < \frac{\varphi}{-s^{(I)}} \end{cases} \tag{B.3}$$

Figure (B.2) presents the concentration profile of the solution $\overrightarrow{c_{II}}$.

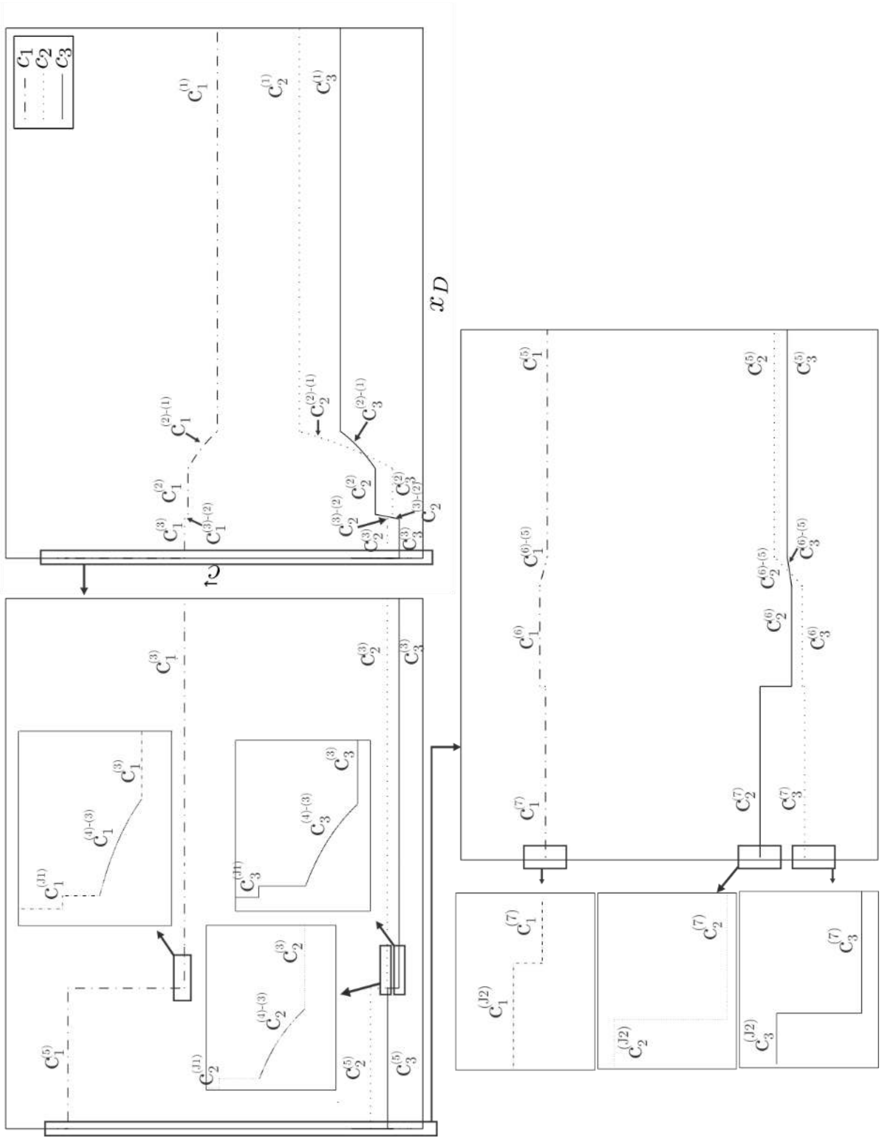

Figure B.2: Solution of the auxiliary system for $\varphi_{HS} < \varphi < \varphi_A$ ($\overrightarrow{c_{II}}$)

Region (4) disappears in $\overrightarrow{c_{III}}$, and a new rarefaction wave ($\vec{c}^{(5)-(3-)}$) and the constant state $\vec{c}^{(3-)}$ appear. The family $k = 1$ is separated from the pH wave.

Equation (B.4) presents the exact expression for the region $\overrightarrow{c_{III}}$ and the concentration profile of each component is shown in figure (B.3).

$$\overrightarrow{c_{III}} = \begin{cases} \vec{c}^{(J2)}, & x_D < \frac{\varphi-\varphi_{HS}}{V_{pH}^{(2)}} \\ \vec{c}^{(7)}, & \frac{\varphi-\varphi_{HS}}{V_{pH}^{(2)}} < x_D < \frac{\varphi-\varphi_{HS}}{V_{(3)}} \\ \vec{c}^{(6)}, & \frac{\varphi-\varphi_{HS}}{V_{(3)}} < x_D < \frac{\varphi-\varphi_{HS}}{\sigma_{(2)}\left(\overrightarrow{\omega}^{(6)},\xi^{(J1)}\right)} \\ \vec{c}^{(6)-(5)}(x_D,\varphi), & \frac{\varphi-\varphi_{HS}}{\sigma_{(2)}\left(\overrightarrow{\omega}^{(6)},\xi^{(J1)}\right)} < x_D < \frac{\varphi-\varphi_{HS}}{\sigma_{(2)}\left(\overrightarrow{\omega}^{(5)},\xi^{(J1)}\right)} \\ \vec{c}^{(5)}, & \frac{\varphi-\varphi_{HS}}{\sigma_{(2)}\left(\overrightarrow{\omega}^{(5)},\xi^{(J1)}\right)} < x_D < \frac{\varphi}{V_{(pH)}^{(1)}} \\ \vec{c}^{(5)-(3-)}(x_D,\varphi), & \frac{\varphi}{V_{pH}^{(1)}} < x_D < \frac{\varphi}{\sigma_{pH}(\xi^{(I)})} \\ \vec{c}^{(3-)}, & \frac{\varphi}{\sigma_{pH}(\xi^{(I)})} < x_D < x_{(1)}^{-}(\varphi) \\ \vec{c}^{(3)}, & x_{(1)}^{-}(\varphi) < x_D < \frac{\varphi}{\sigma_{(3)}(\overrightarrow{\omega}^{(3)},\xi^{(I)})} \\ \vec{c}^{(3)-(2)}(x_D,\varphi), & \frac{\varphi}{\sigma_{(3)}(\overrightarrow{\omega}^{(3)},\xi^{(I)})} < x_D < \frac{\varphi}{\sigma_{(3)}(\overrightarrow{\omega}^{(2)},\xi^{(I)})} \\ \vec{c}^{(2)}, & \frac{\varphi}{\sigma_{(3)}(\overrightarrow{\omega}^{(2)},\xi^{(I)})} < x_D < \frac{\varphi}{\sigma_{(2)}(\overrightarrow{\omega}^{(2)},\xi^{(I)})} \\ \vec{c}^{(2)-(1)}(x_D,\varphi), & \frac{\varphi}{\sigma_{(2)}(\overrightarrow{\omega}^{(2)},\xi^{(I)})} < x_D < \frac{\varphi}{\sigma_{(2)}(\overrightarrow{\omega}^{(1)},\xi^{(I)})} \\ \vec{c}^{(1)}, & \frac{\varphi}{\sigma_{(2)}(\overrightarrow{\omega}^{(1)},\xi^{(I)})} < x_D < \frac{\varphi}{\sigma_{(1)}(\overrightarrow{\omega}^{(1)},\xi^{(I)})} \\ \vec{c}^{(1)-(I)}(x_D,\varphi), & \frac{\varphi}{\sigma_{(1)}(\overrightarrow{\omega}^{(1)},\xi^{(I)})} < x_D < \frac{\varphi}{\sigma_{(1)}(\overrightarrow{\omega}^{(I)},\xi^{(I)})} \\ \vec{c}^{(I)}, & \frac{\varphi}{\sigma_{(1)}(\overrightarrow{\omega}^{(I)},\xi^{(I)})} < x_D < \frac{\varphi}{-s^{(I)}} \end{cases} \tag{B.4}$$

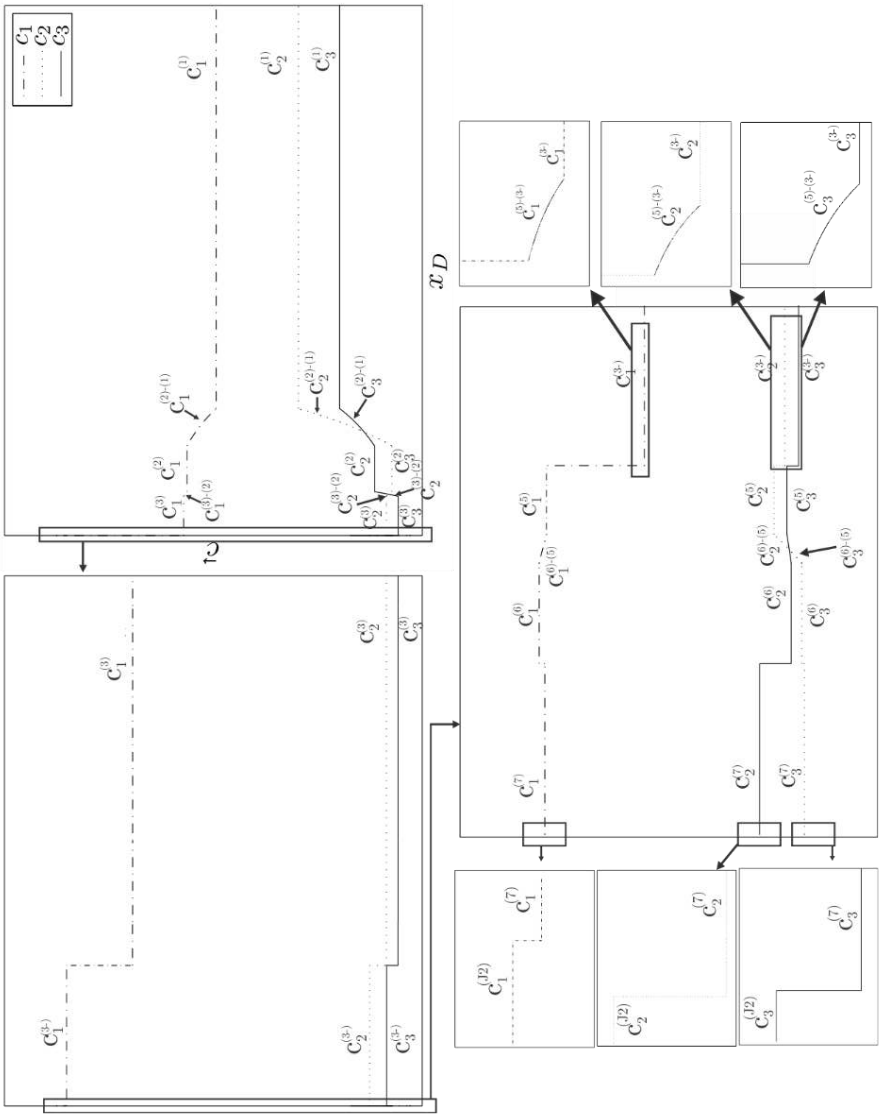

Figure B.3: Solution $\overrightarrow{c_{III}}$ of the auxiliary system

For $\varphi_B < \varphi < \varphi_C$ ($\overrightarrow{c_{IV}}$), the rarefaction wave $\vec{c}^{(6)-(5)}$ interacts with the pH waves. In this region part of that rarefaction is located at the left of the pH shock (constant pH) and the other part at the right, a pH-concentration rarefaction wave. The characteristic path of the rarefaction $\vec{c}^{(6)-(5)}$ changes along the interaction, and the new paths are denoted as $x^{-}_{(6)-(5)}(\varphi)$. Equation (B.5) details $\overrightarrow{c_{IV}}$ and the concentration profile is shown in figure (B.4).

$$\overrightarrow{c_{IV}} = \begin{cases} \vec{c}^{(J2)}, & x_D < \frac{\varphi - \varphi_{HS}}{V_{pH}^{(2)}} \\ \vec{c}^{(7)}, & \frac{\varphi - \varphi_{HS}}{V_{pH}^{(2)}} < x_D < \frac{\varphi - \varphi_{HS}}{V_{(3)}} \\ \vec{c}^{(6)}, & \frac{\varphi - \varphi_{HS}}{V_{(3)}} < x_D < \frac{\varphi - \varphi_{HS}}{\sigma_{(2)}\left(\vec{\omega}^{(6)}, \xi^{(J1)}\right)} \\ \vec{c}^{(6)-(5)}(x_D, \varphi), & \frac{\varphi - \varphi_{HS}}{\sigma_{(2)}\left(\vec{\omega}^{(6)}, \xi^{(J1)}\right)} < x_D < \frac{\varphi}{V_{(pH)}^{(1)}} \\ \vec{c}^{(6)-(5)-}(x_D, \varphi), & \frac{\varphi}{V_{(pH)}^{(1)}} < x_D < x_{(6)-(5)}^{-}(\varphi) \\ \vec{c}^{(5)-(3-)}(x_D, \varphi), & x_{(6)-(5)}^{-}(\varphi) < x_D < \frac{\varphi}{\sigma_{pH}(\xi^{(I)})} \\ \vec{c}^{(3-)}, & \frac{\varphi}{\sigma_{pH}(\xi^{(I)})} < x_D < x_{(1)}^{-}(\varphi) \\ \vec{c}^{(3)}, & x_{(1)}^{-}(\varphi) < x_D < \frac{\varphi}{\sigma_{(3)}(\vec{\omega}^{(3)}, \xi^{(I)})} \\ \vec{c}^{(3)-(2)}(x_D, \varphi), & \frac{\varphi}{\sigma_{(3)}(\vec{\omega}^{(3)}, \xi^{(I)})} < x_D < \frac{\varphi}{\sigma_{(3)}(\vec{\omega}^{(2)}, \xi^{(I)})} \\ \vec{c}^{(2)}, & \frac{\varphi}{\sigma_{(3)}(\vec{\omega}^{(2)}, \xi^{(I)})} < x_D < \frac{\varphi}{\sigma_{(2)}(\vec{\omega}^{(2)}, \xi^{(I)})} \\ \vec{c}^{(2)-(1)}(x_D, \varphi), & \frac{\varphi}{\sigma_{(2)}(\vec{\omega}^{(2)}, \xi^{(I)})} < x_D < \frac{\varphi}{\sigma_{(2)}(\vec{\omega}^{(1)}, \xi^{(I)})} \\ \vec{c}^{(1)}, & \frac{\varphi}{\sigma_{(2)}(\vec{\omega}^{(1)}, \xi^{(I)})} < x_D < \frac{\varphi}{\sigma_{(1)}(\vec{\omega}^{(1)}, \xi^{(I)})} \\ \vec{c}^{(1)-(I)}(x_D, \varphi), & \frac{\varphi}{\sigma_{(1)}(\vec{\omega}^{(1)}, \xi^{(I)})} < x_D < \frac{\varphi}{\sigma_{(1)}(\vec{\omega}^{(I)}, \xi^{(I)})} \\ \vec{c}^{(I)}, & \frac{\varphi}{\sigma_{(1)}(\vec{\omega}^{(I)}, \xi^{(I)})} < x_D < \frac{\varphi}{-s^{(I)}} \end{cases} \tag{B.5}$$

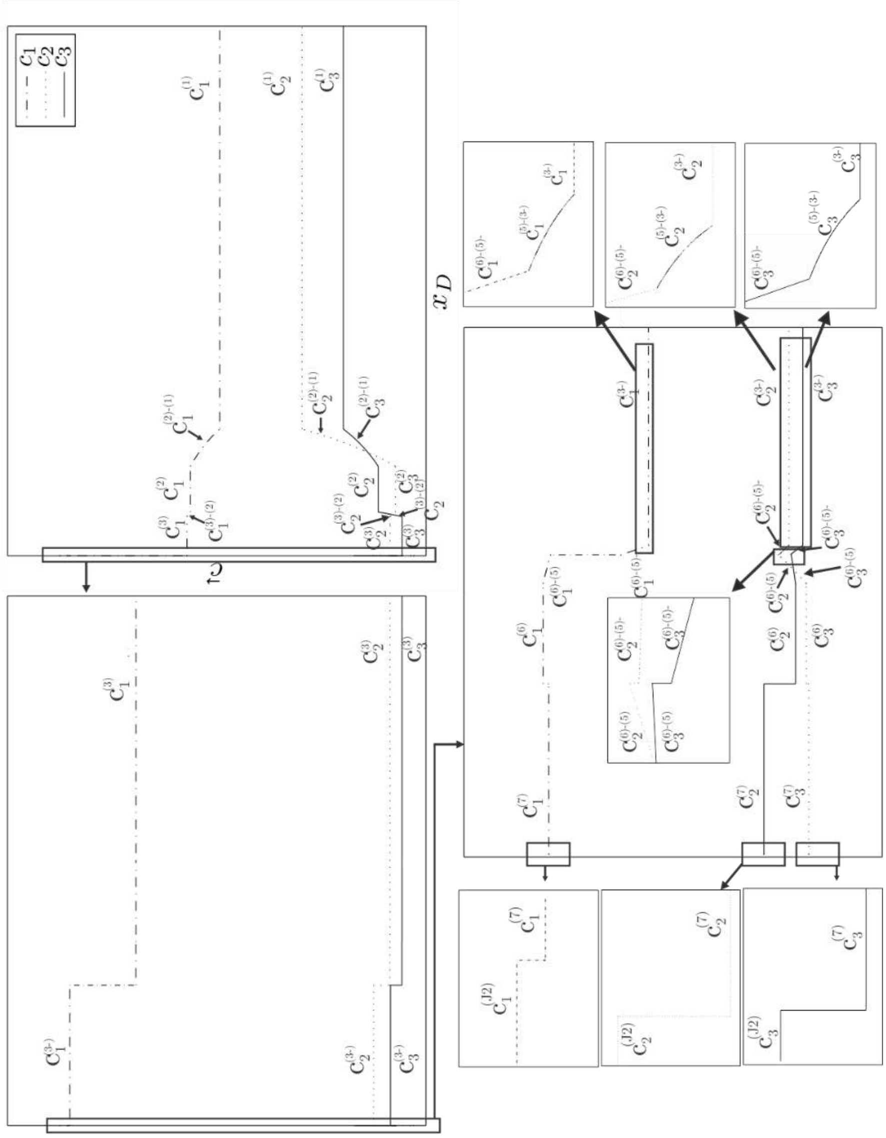

Figure B.4: Concentration profile for the solution $\overrightarrow{c_{IV}}$

If $\varphi_C < \varphi < \varphi_D$, there is an interaction between the pH rarefaction wave and the $k = 2$ family rarefaction wave, and a new rarefaction region appears ($\vec{c}^{(6)-(3--)}$), solution part $\overrightarrow{c_V}$ (Equation B.6 and figure B.5).

In equation (B.6) we call $x_{(6)-(5)}^{-(+)}$ the path of the first characteristic curve of the wave $(6) - (5)$ after it crosses the pH shock of the front of the low salinity slug. The last rarefaction characteristic path will be denoted as $x_{(6)-(5)}^{-(-)}$.

$$\overrightarrow{c_V} = \begin{cases} \vec{c}^{(J2)}, & x_D < \frac{\varphi - \varphi_{HS}}{V_{pH}^{(2)}} \\ \vec{c}^{(7)}, & \frac{\varphi - \varphi_{HS}}{V_{pH}^{(2)}} < x_D < \frac{\varphi - \varphi_{HS}}{V_{(3)}} \\ \vec{c}^{(6)}, & \frac{\varphi - \varphi_{HS}}{V_{(3)}} < x_D < \frac{\varphi}{V_{(pH)}^{(1)}} \\ \vec{c}^{(6)-(3--)}(x_D, \varphi), & \frac{\varphi}{V_{(pH)}^{(1)}} < x_D < x_{(6)-(5)}^{-(+)}(\varphi) \\ \vec{c}^{(6)-(5)-}(x_D, \varphi), & x_{(6)-(5)}^{-(+)}(\varphi) < x_D < x_{(6)-(5)}^{-(-)}(\varphi) \\ \vec{c}^{(5)-(3-)}(x_D, \varphi), & x_{(6)-(5)}^{-(-)}(\varphi) < x_D < \frac{\varphi}{\sigma_{pH}(\xi^{(I)})} \\ \vec{c}^{(3-)}, & \frac{\varphi}{\sigma_{pH}(\xi^{(I)})} < x_D < x_{(1)}^{-}(\varphi) \\ \vec{c}^{(3)}, & x_{(1)}^{-}(\varphi) < x_D < \frac{\varphi}{\sigma_{(3)}(\overrightarrow{\omega}^{(3)}, \xi^{(I)})} \\ \vec{c}^{(3)-(2)}(x_D, \varphi), & \frac{\varphi}{\sigma_{(3)}(\overrightarrow{\omega}^{(3)}, \xi^{(I)})} < x_D < \frac{\varphi}{\sigma_{(3)}(\overrightarrow{\omega}^{(2)}, \xi^{(I)})} \\ \vec{c}^{(2)}, & \frac{\varphi}{\sigma_{(3)}(\overrightarrow{\omega}^{(2)}, \xi^{(I)})} < x_D < \frac{\varphi}{\sigma_{(2)}(\overrightarrow{\omega}^{(2)}, \xi^{(I)})} \\ \vec{c}^{(2)-(1)}(x_D, \varphi), & \frac{\varphi}{\sigma_{(2)}(\overrightarrow{\omega}^{(2)}, \xi^{(I)})} < x_D < \frac{\varphi}{\sigma_{(2)}(\overrightarrow{\omega}^{(1)}, \xi^{(I)})} \\ \vec{c}^{(1)}, & \frac{\varphi}{\sigma_{(2)}(\overrightarrow{\omega}^{(1)}, \xi^{(I)})} < x_D < \frac{\varphi}{\sigma_{(1)}(\overrightarrow{\omega}^{(1)}, \xi^{(I)})} \\ \vec{c}^{(1)-(I)}(x_D, \varphi), & \frac{\varphi}{\sigma_{(1)}(\overrightarrow{\omega}^{(1)}, \xi^{(I)})} < x_D < \frac{\varphi}{\sigma_{(1)}(\overrightarrow{\omega}^{(I)}, \xi^{(I)})} \\ \vec{c}^{(I)}, & \frac{\varphi}{\sigma_{(1)}(\overrightarrow{\omega}^{(I)}, \xi^{(I)})} < x_D < \frac{\varphi}{-s^{(I)}} \end{cases} \tag{B.6}$$

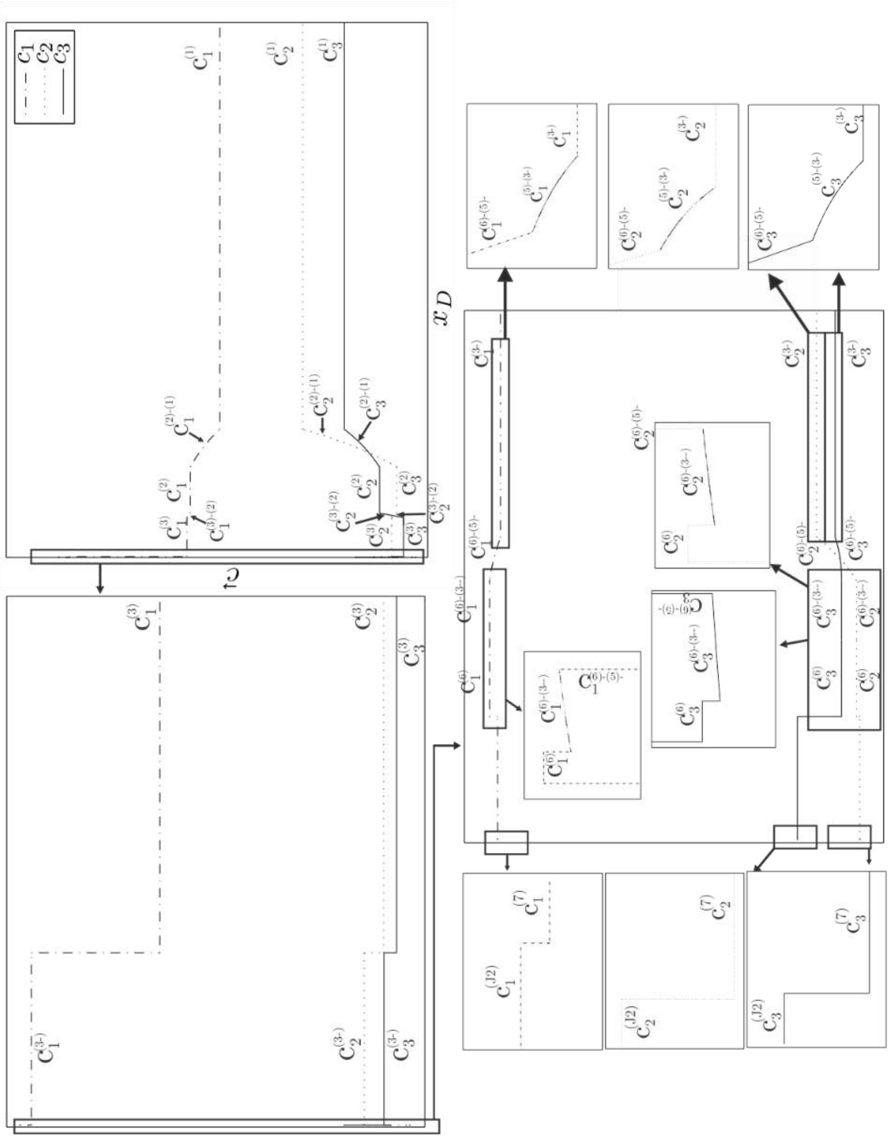

Figure B.5: Concentration profile for $\overrightarrow{c_V}$

The solution $\overrightarrow{c_{VI}}$ occurs when $\varphi_D < \varphi < \varphi_E$, where the shock wave of the family $k = 3$ from the rear of the low salinity slug reaches the pH waves of the front and interacts with them. As a result, the shock path is modified, and it is no longer a straight line. The region $\vec{c}^{(6)}$ disappears of the solution. The new shock path will be denoted as $x_{(3)}^{-}$. In equation (B.7) we present the mathematical description of this part of the solution of the auxiliary system. In figure (B.6) the concentration profile for the solution part $\overrightarrow{c_{VI}}$ is presented.

$$\overrightarrow{c_{VI}} = \begin{cases} \vec{c}^{(J2)}, & x_D < \frac{\varphi - \varphi_{HS}}{V_{pH}^{(2)}} \\ \vec{c}^{(7)}, & \frac{\varphi - \varphi_{HS}}{V_{pH}^{(2)}} < x_D < \frac{\varphi}{V_{(pH)}^{(1)}} \\ \vec{c}^{(7)-(3---)}(x_D, \varphi), & \frac{\varphi}{V_{(pH)}^{(1)}} < x_D < x_{(3)}^{-} \\ \vec{c}^{(6)-(3--)}(x_D, \varphi), & x_{(3)}^{-} < x_D < x_{(6)-(5)}^{-(+)}(\varphi) \\ \vec{c}^{(6)-(5)-}(x_D, \varphi), & x_{(6)-(5)}^{-(+)}(\varphi) < x_D < x_{(6)-(5)}^{-(-)}(\varphi) \\ \vec{c}^{(5)-(3-)}(x_D, \varphi), & x_{(6)-(5)}^{-(-)}(\varphi) < x_D < \frac{\varphi}{\sigma_{pH}(\xi^{(I)})} \\ \vec{c}^{(3-)}, & \frac{\varphi}{\sigma_{pH}(\xi^{(I)})} < x_D < x_{(1)}^{-}(\varphi) \\ \vec{c}^{(3)}, & x_{(1)}^{-}(\varphi) < x_D < \frac{\varphi}{\sigma_{(3)}(\vec{\omega}^{(3)}, \xi^{(I)})} \\ \vec{c}^{(3)-(2)}(x_D, \varphi), & \frac{\varphi}{\sigma_{(3)}(\vec{\omega}^{(3)}, \xi^{(I)})} < x_D < \frac{\varphi}{\sigma_{(3)}(\vec{\omega}^{(2)}, \xi^{(I)})} \\ \vec{c}^{(2)}, & \frac{\varphi}{\sigma_{(3)}(\vec{\omega}^{(2)}, \xi^{(I)})} < x_D < \frac{\varphi}{\sigma_{(2)}(\vec{\omega}^{(2)}, \xi^{(I)})} \\ \vec{c}^{(2)-(1)}(x_D, \varphi), & \frac{\varphi}{\sigma_{(2)}(\vec{\omega}^{(2)}, \xi^{(I)})} < x_D < \frac{\varphi}{\sigma_{(2)}(\vec{\omega}^{(1)}, \xi^{(I)})} \\ \vec{c}^{(1)}, & \frac{\varphi}{\sigma_{(2)}(\vec{\omega}^{(1)}, \xi^{(I)})} < x_D < \frac{\varphi}{\sigma_{(1)}(\vec{\omega}^{(1)}, \xi^{(I)})} \\ \vec{c}^{(1)-(I)}(x_D, \varphi), & \frac{\varphi}{\sigma_{(1)}(\vec{\omega}^{(1)}, \xi^{(I)})} < x_D < \frac{\varphi}{\sigma_{(1)}(\vec{\omega}^{(I)}, \xi^{(I)})} \\ \vec{c}^{(I)}, & \frac{\varphi}{\sigma_{(1)}(\vec{\omega}^{(I)}, \xi^{(I)})} < x_D < \frac{\varphi}{-s^{(I)}} \end{cases} \qquad \text{(B.7)}$$

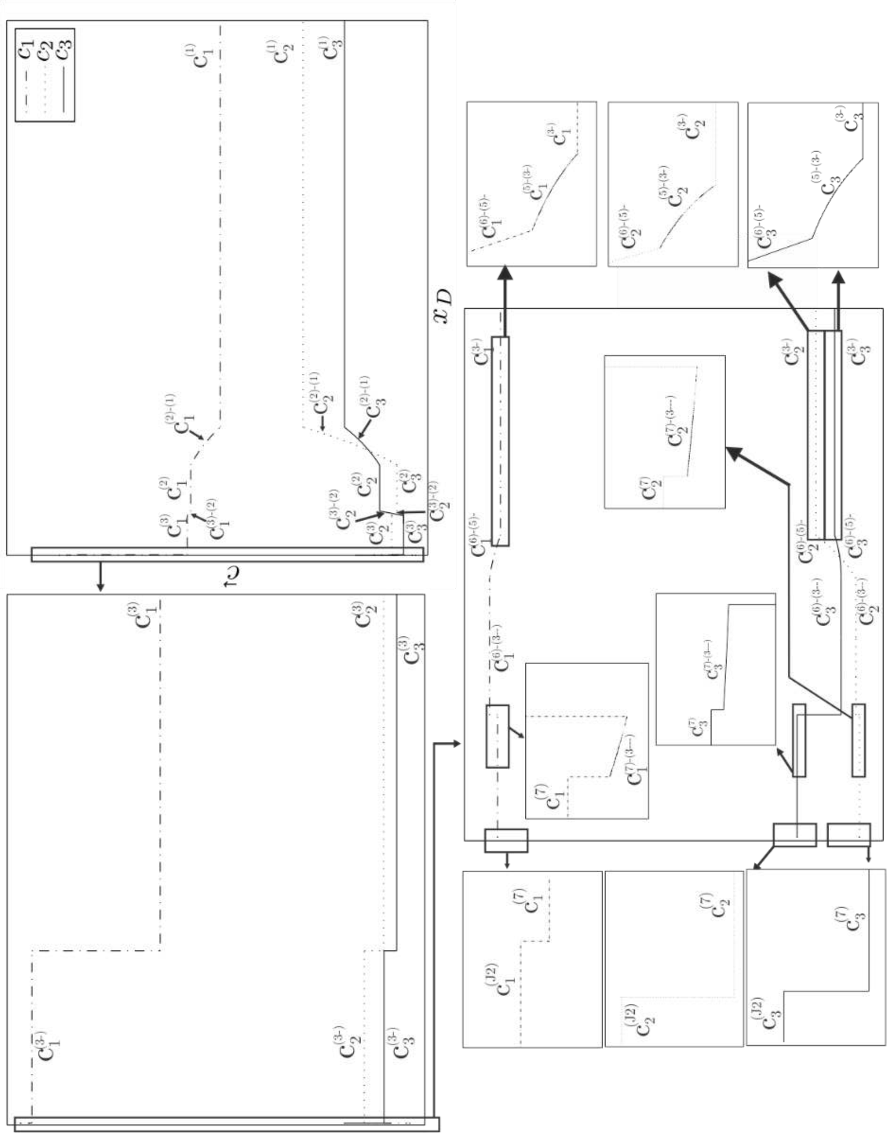

Figure B.6: Solution $\overrightarrow{c_{VI}}$ of the auxiliary system

For $\varphi_E < \varphi < \varphi_F$ (solution $\overrightarrow{c_{VII}}$), the k-waves are separated from the pH waves, and the region (6) and the rarefaction waves $\vec{c}^{(6)-(3--)}$ and $\vec{c}^{(5)-(3-)}$ no longer appear in the solution. In equation (B.8) we present the mathematical details of this part of the solution and the concentration profile can be seen in figure (B.7).

$$\overrightarrow{c_{VII}} = \begin{cases} \vec{c}^{(J2)}, & x_D < \frac{\varphi-\varphi_{HS}}{V_{pH}^{(2)}} \\ \vec{c}^{(7)}, & \frac{\varphi-\varphi_{HS}}{V_{pH}^{(2)}} < x_D < \frac{\varphi}{V_{(pH)}^{(1)}} \\ \vec{c}^{(7)-(3---)}(x_D,\varphi), & \frac{\varphi}{V_{(pH)}^{(1)}} < x_D < \frac{\varphi}{\sigma_{pH}(\xi^{(I)})} \\ \vec{c}^{(3---)}, & \frac{\varphi}{\sigma_{pH}(\xi^{(I)})} < x_D < x_{(3)}^{-} \\ \vec{c}^{(3--)}, & x_{(3)}^{-} < x_D < x_{(6)-(5)}^{-(+)}(\varphi) \\ \vec{c}^{(6)-(5)-}(x_D,\varphi), & x_{(6)-(5)}^{-(+)}(\varphi) < x_D < x_{(6)-(5)}^{-(-)}(\varphi) \\ \vec{c}^{(3-)}, & x_{(6)-(5)}^{-(-)}(\varphi) < x_D < x_{(1)}^{-}(\varphi) \\ \vec{c}^{(3)}, & x_{(1)}^{-}(\varphi) < x_D < \frac{\varphi}{\sigma_{(3)}(\vec{\omega}^{(3)},\xi^{(I)})} \\ \vec{c}^{(3)-(2)}(x_D,\varphi), & \frac{\varphi}{\sigma_{(3)}(\vec{\omega}^{(3)},\xi^{(I)})} < x_D < \frac{\varphi}{\sigma_{(3)}(\vec{\omega}^{(2)},\xi^{(I)})} \\ \vec{c}^{(2)}, & \frac{\varphi}{\sigma_{(3)}(\vec{\omega}^{(2)},\xi^{(I)})} < x_D < \frac{\varphi}{\sigma_{(2)}(\vec{\omega}^{(2)},\xi^{(I)})} \\ \vec{c}^{(2)-(1)}(x_D,\varphi), & \frac{\varphi}{\sigma_{(2)}(\vec{\omega}^{(2)},\xi^{(I)})} < x_D < \frac{\varphi}{\sigma_{(2)}(\vec{\omega}^{(1)},\xi^{(I)})} \\ \vec{c}^{(1)}, & \frac{\varphi}{\sigma_{(2)}(\vec{\omega}^{(1)},\xi^{(I)})} < x_D < \frac{\varphi}{\sigma_{(1)}(\vec{\omega}^{(1)},\xi^{(I)})} \\ \vec{c}^{(1)-(I)}(x_D,\varphi), & \frac{\varphi}{\sigma_{(1)}(\vec{\omega}^{(1)},\xi^{(I)})} < x_D < \frac{\varphi}{\sigma_{(1)}(\vec{\omega}^{(I)},\xi^{(I)})} \\ \vec{c}^{(I)}, & \frac{\varphi}{\sigma_{(1)}(\vec{\omega}^{(I)},\xi^{(I)})} < x_D < \frac{\varphi}{-s^{(I)}} \end{cases} \tag{B.8}$$

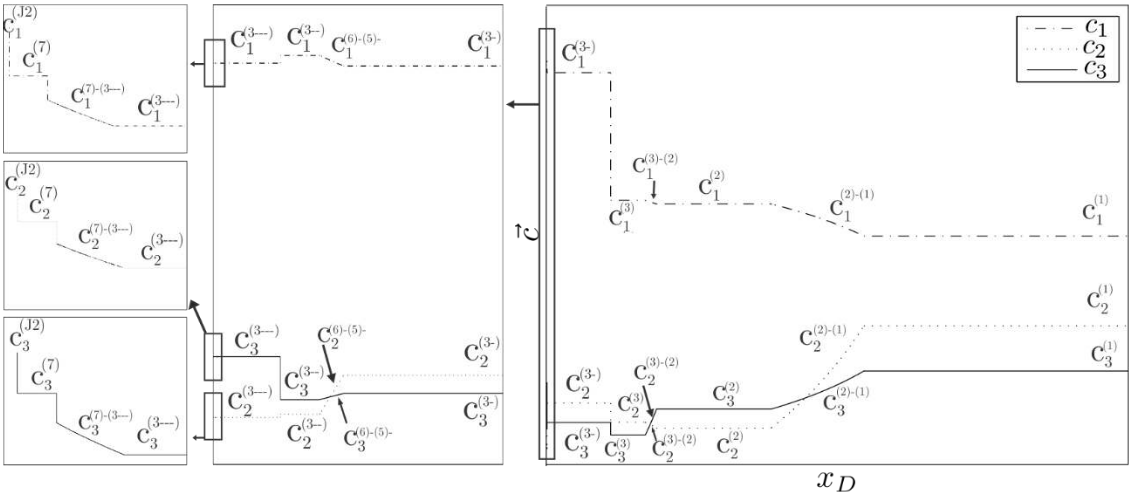

Figure B.7: Solution $\overrightarrow{c_{VII}}$ of the auxiliary system

In solution $\overrightarrow{c_{VIII}}$ ($\varphi_F < \varphi < \varphi_G$), the shock wave of the family $k = 1$ interacts with the rarefaction wave of the family $k = 3$, and region (3) disappears. The mathematical description of $\overrightarrow{c_{VIII}}$ is shown in equation (B.9). The concentration profile is presented in figure (B.8).

$$\overrightarrow{c_{VIII}} = \begin{cases} \vec{c}^{(J2)}, & x_D < \frac{\varphi-\varphi_{HS}}{V_{pH}^{(2)}} \\ \vec{c}^{(7)}, & \frac{\varphi-\varphi_{HS}}{V_{pH}^{(2)}} < x_D < \frac{\varphi}{V_{(pH)}^{(1)}} \\ \vec{c}^{(7)-(3---)}(x_D,\varphi), & \frac{\varphi}{V_{(pH)}^{(1)}} < x_D < \frac{\varphi}{\sigma_{pH}(\xi^{(I)})} \\ \vec{c}^{(3---)}, & \frac{\varphi}{\sigma_{pH}(\xi^{(I)})} < x_D < x_{(3)}^{-} \\ \vec{c}^{(3--)}, & x_{(3)}^{-} < x_D < x_{(6)-(5)}^{-(+)}(\varphi) \\ \vec{c}^{(6)-(5)-}(x_D,\varphi), & x_{(6)-(5)}^{-(+)}(\varphi) < x_D < x_{(6)-(5)}^{-(-)}(\varphi) \\ \vec{c}^{(3-)}, & x_{(6)-(5)}^{-(-)}(\varphi) < x_D < x_{(3)-(2)}^{-(+)}(\varphi) \\ \vec{c}^{(3)-(2)-}(x_D,\varphi), & x_{(3)-(2)}^{-(+)}(\varphi) < x_D < x_{(1)}^{--}(\varphi) \\ \vec{c}^{(3)-(2)}(x_D,\varphi), & x_{(1)}^{--}(\varphi) < x_D < \frac{\varphi}{\sigma_{(3)}(\vec{\omega}^{(2)},\xi^{(I)})} \\ \vec{c}^{(2)}, & \frac{\varphi}{\sigma_{(3)}(\vec{\omega}^{(2)},\xi^{(I)})} < x_D < \frac{\varphi}{\sigma_{(2)}(\vec{\omega}^{(2)},\xi^{(I)})} \\ \vec{c}^{(2)-(1)}(x_D,\varphi), & \frac{\varphi}{\sigma_{(2)}(\vec{\omega}^{(2)},\xi^{(I)})} < x_D < \frac{\varphi}{\sigma_{(2)}(\vec{\omega}^{(1)},\xi^{(I)})} \\ \vec{c}^{(1)}, & \frac{\varphi}{\sigma_{(2)}(\vec{\omega}^{(1)},\xi^{(I)})} < x_D < \frac{\varphi}{\sigma_{(1)}(\vec{\omega}^{(1)},\xi^{(I)})} \\ \vec{c}^{(1)-(I)}(x_D,\varphi), & \frac{\varphi}{\sigma_{(1)}(\vec{\omega}^{(1)},\xi^{(I)})} < x_D < \frac{\varphi}{\sigma_{(1)}(\vec{\omega}^{(I)},\xi^{(I)})} \\ \vec{c}^{(I)}, & \frac{\varphi}{\sigma_{(1)}(\vec{\omega}^{(I)},\xi^{(I)})} < x_D < \frac{\varphi}{-s^{(I)}} \end{cases} \tag{B.9}$$

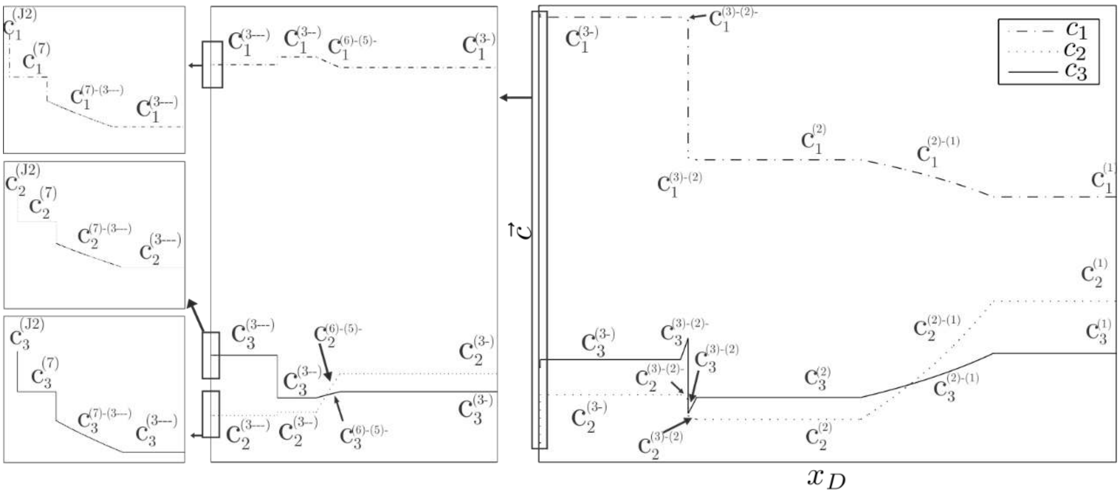

Figure B.8: Solution $\overrightarrow{c_{VIII}}$ of the auxiliary system

For $\varphi_G < \varphi < \varphi_H$, which corresponds to solution $\overrightarrow{c_{IX}}$, the wave family $k = 1$ is completely separated from the wave $k = 3$, and region (2-) appears. The exact solution $\overrightarrow{c_{IX}}$ is presented in equation (B.10) and its concentration profile is shown in figure (B.9).

$$\overrightarrow{c_{IX}} = \begin{cases} \vec{c}^{(J2)}, & x_D < \frac{\varphi-\varphi_{HS}}{V_{pH}^{(2)}} \\ \vec{c}^{(7)}, & \frac{\varphi-\varphi_{HS}}{V_{pH}^{(2)}} < x_D < \frac{\varphi}{V_{(pH)}^{(1)}} \\ \vec{c}^{(7)-(3---)}(x_D,\varphi), & \frac{\varphi}{V_{(pH)}^{(1)}} < x_D < \frac{\varphi}{\sigma_{pH}(\xi^{(I)})} \\ \vec{c}^{(3---)}, & \frac{\varphi}{\sigma_{pH}(\xi^{(I)})} < x_D < x_{(3)}^{-} \\ \vec{c}^{(3--)}, & x_{(3)}^{-} < x_D < x_{(6)-(5)}^{-(+)}(\varphi) \\ \vec{c}^{(6)-(5)-}(x_D,\varphi), & x_{(6)-(5)}^{-(+)}(\varphi) < x_D < x_{(6)-(5)}^{-(-)}(\varphi) \\ \vec{c}^{(3-)}, & x_{(6)-(5)}^{-(-)}(\varphi) < x_D < x_{(3)-(2)}^{-(+)}(\varphi) \\ \vec{c}^{(3)-(2)-}(x_D,\varphi), & x_{(3)-(2)}^{-(+)}(\varphi) < x_D < x_{(3)-(2)}^{-(-)}(\varphi) \\ \vec{c}^{(2-)}, & x_{(3)-(2)}^{-(-)}(\varphi) < x_D < x_{(1)}^{--}(\varphi) \\ \vec{c}^{(2)}, & x_{(1)}^{--}(\varphi) < x_D < \frac{\varphi}{\sigma_{(2)}(\overrightarrow{\omega}^{(2)},\xi^{(I)})} \\ \vec{c}^{(2)-(1)}(x_D,\varphi), & \frac{\varphi}{\sigma_{(2)}(\overrightarrow{\omega}^{(2)},\xi^{(I)})} < x_D < \frac{\varphi}{\sigma_{(2)}(\overrightarrow{\omega}^{(1)},\xi^{(I)})} \\ \vec{c}^{(1)}, & \frac{\varphi}{\sigma_{(2)}(\overrightarrow{\omega}^{(1)},\xi^{(I)})} < x_D < \frac{\varphi}{\sigma_{(1)}(\overrightarrow{\omega}^{(1)},\xi^{(I)})} \\ \vec{c}^{(1)-(I)}(x_D,\varphi), & \frac{\varphi}{\sigma_{(1)}(\overrightarrow{\omega}^{(1)},\xi^{(I)})} < x_D < \frac{\varphi}{\sigma_{(1)}(\overrightarrow{\omega}^{(I)},\xi^{(I)})} \\ \vec{c}^{(I)}, & \frac{\varphi}{\sigma_{(1)}(\overrightarrow{\omega}^{(I)},\xi^{(I)})} < x_D < \frac{\varphi}{-s^{(I)}} \end{cases} \tag{B.10}$$

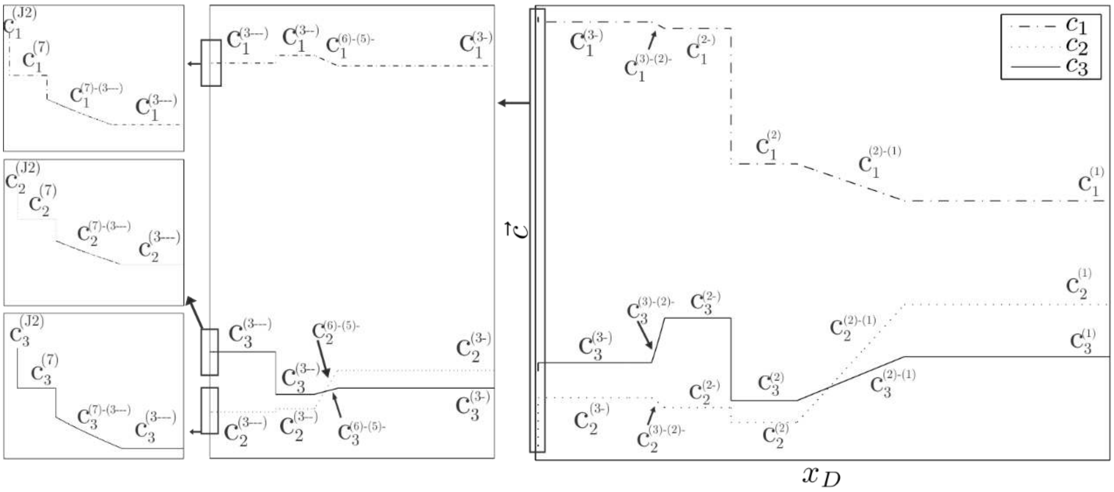

Figure B.9: Concentration profile of solution $\overrightarrow{c_{IX}}$

Solution $\overrightarrow{c_X}$ occurs when $\varphi_H < \varphi < \varphi_I$, where the rarefaction wave $\vec{c}^{(2)-(1)-}$ appears, which is a result of an interaction between the waves $k = 2$ from the front of the low salinity slug and $k = 1$ from the rear of the low salinity slug. In this part of the solution region (2) disappears. Equation (B.11) details $\overrightarrow{c_X}$, and figure (B.10) shows the concentration profile when $\varphi_H < \varphi < \varphi_I$.

$$\overrightarrow{c_X} = \begin{cases} \vec{c}^{(J2)}, & x_D < \frac{\varphi - \varphi_{HS}}{V_{pH}^{(2)}} \\ \vec{c}^{(7)}, & \frac{\varphi - \varphi_{HS}}{V_{pH}^{(2)}} < x_D < \frac{\varphi}{V_{(pH)}^{(1)}} \\ \vec{c}^{(7)-(3---)}(x_D, \varphi), & \frac{\varphi}{V_{(pH)}^{(1)}} < x_D < \frac{\varphi}{\sigma_{pH}(\xi^{(I)})} \\ \vec{c}^{(3---)}, & \frac{\varphi}{\sigma_{pH}(\xi^{(I)})} < x_D < x_{(3)}^{-} \\ \vec{c}^{(3--)}, & x_{(3)}^{-} < x_D < x_{(6)-(5)}^{-(+)}(\varphi) \\ \vec{c}^{(6)-(5)-}(x_D, \varphi), & x_{(6)-(5)}^{-(+)}(\varphi) < x_D < x_{(6)-(5)}^{-(-)}(\varphi) \\ \vec{c}^{(3-)}, & x_{(6)-(5)}^{-(-)}(\varphi) < x_D < x_{(3)-(2)}^{-(+)}(\varphi) \\ \vec{c}^{(3)-(2)-}(x_D, \varphi), & x_{(3)-(2)}^{-(+)}(\varphi) < x_D < x_{(3)-(2)}^{-(-)}(\varphi) \\ \vec{c}^{(2-)}, & x_{(3)-(2)}^{-(-)}(\varphi) < x_D < x_{(2)-(1)}^{-(+)}(\varphi) \\ \vec{c}^{(2)-(1)-}, & x_{(2)-(1)}^{-(+)}(\varphi) < x_D < x_{(1)}^{---}(\varphi) \\ \vec{c}^{(2)-(1)}(x_D, \varphi), & x_{(1)}^{---}(\varphi) < x_D < \frac{\varphi}{\sigma_{(2)}(\vec{\omega}^{(1)}, \xi^{(I)})} \\ \vec{c}^{(1)}, & \frac{\varphi}{\sigma_{(2)}(\vec{\omega}^{(1)}, \xi^{(I)})} < x_D < \frac{\varphi}{\sigma_{(1)}(\vec{\omega}^{(1)}, \xi^{(I)})} \\ \vec{c}^{(1)-(I)}(x_D, \varphi), & \frac{\varphi}{\sigma_{(1)}(\vec{\omega}^{(1)}, \xi^{(I)})} < x_D < \frac{\varphi}{\sigma_{(1)}(\vec{\omega}^{(I)}, \xi^{(I)})} \\ \vec{c}^{(I)}, & \frac{\varphi}{\sigma_{(1)}(\vec{\omega}^{(I)}, \xi^{(I)})} < x_D < \frac{\varphi}{-s^{(I)}} \end{cases} \tag{B.11}$$

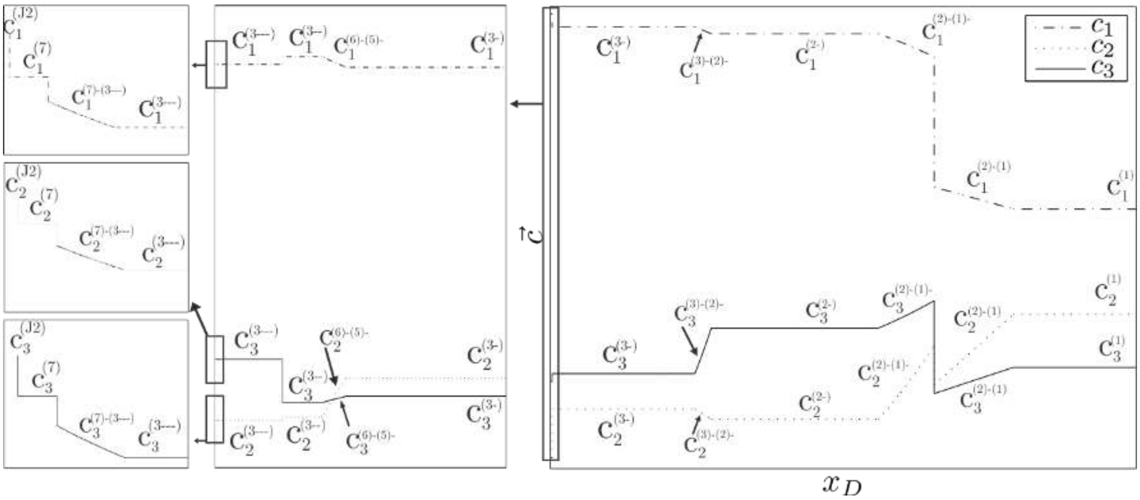

Figure B.10: Solution $\overrightarrow{c_X}$

The concentration solution when $\varphi_I < \varphi < \varphi_{pH}$ is defined as $\overrightarrow{c_{XI}}$. The wave family $k = 1$ is completely separated from the wave family $k = 2$. Thus, constant state region

(1-) appears. Equation (B.12) describes $\overrightarrow{c_{XI}}$, and figure (B.11) presents the concentration profile.

$$\overrightarrow{c_{XI}} = \begin{cases} \vec{c}^{(J2)}, & x_D < \frac{\varphi - \varphi_{HS}}{V_{pH}^{(2)}} \\ \vec{c}^{(7)}, & \frac{\varphi - \varphi_{HS}}{V_{pH}^{(2)}} < x_D < \frac{\varphi}{V_{(pH)}^{(1)}} \\ \vec{c}^{(7)-(3---)}(x_D, \varphi), & \frac{\varphi}{V_{(pH)}^{(1)}} < x_D < \frac{\varphi}{\sigma_{pH}(\xi^{(I)})} \\ \vec{c}^{(3---)}, & \frac{\varphi}{\sigma_{pH}(\xi^{(I)})} < x_D < x_{(3)}^{-} \\ \vec{c}^{(3--)}, & x_{(3)}^{-} < x_D < x_{(6)-(5)}^{-(+)}(\varphi) \\ \vec{c}^{(6)-(5)-}(x_D, \varphi), & x_{(6)-(5)}^{-(+)}(\varphi) < x_D < x_{(6)-(5)}^{-(-)}(\varphi) \\ \vec{c}^{(3-)}, & x_{(6)-(5)}^{-(-)}(\varphi) < x_D < x_{(3)-(2)}^{-(+)}(\varphi) \\ \vec{c}^{(3)-(2)-}(x_D, \varphi), & x_{(3)-(2)}^{-(+)}(\varphi) < x_D < x_{(3)-(2)}^{-(-)}(\varphi) \\ \vec{c}^{(2-)}, & x_{(3)-(2)}^{-(-)}(\varphi) < x_D < x_{(2)-(1)}^{-(+)}(\varphi) \\ \vec{c}^{(2)-(1)-}, & x_{(2)-(1)}^{-(+)}(\varphi) < x_D < x_{(2)-(1)}^{-(-)}(\varphi) \\ \vec{c}^{(1-)}, & x_{(2)-(1)}^{-(-)}(\varphi) < x_D < x_{(1)}^{---}(\varphi) \\ \vec{c}^{(1)}, & x_{(1)}^{---}(\varphi) < x_D < \frac{\varphi}{\sigma_{(1)}(\vec{\omega}^{(1)}, \xi^{(I)})} \\ \vec{c}^{(1)-(I)}(x_D, \varphi), & \frac{\varphi}{\sigma_{(1)}(\vec{\omega}^{(1)}, \xi^{(I)})} < x_D < \frac{\varphi}{\sigma_{(1)}(\vec{\omega}^{(I)}, \xi^{(I)})} \\ \vec{c}^{(I)}, & \frac{\varphi}{\sigma_{(1)}(\vec{\omega}^{(I)}, \xi^{(I)})} < x_D < \frac{\varphi}{-s^{(I)}} \end{cases} \tag{B.12}$$

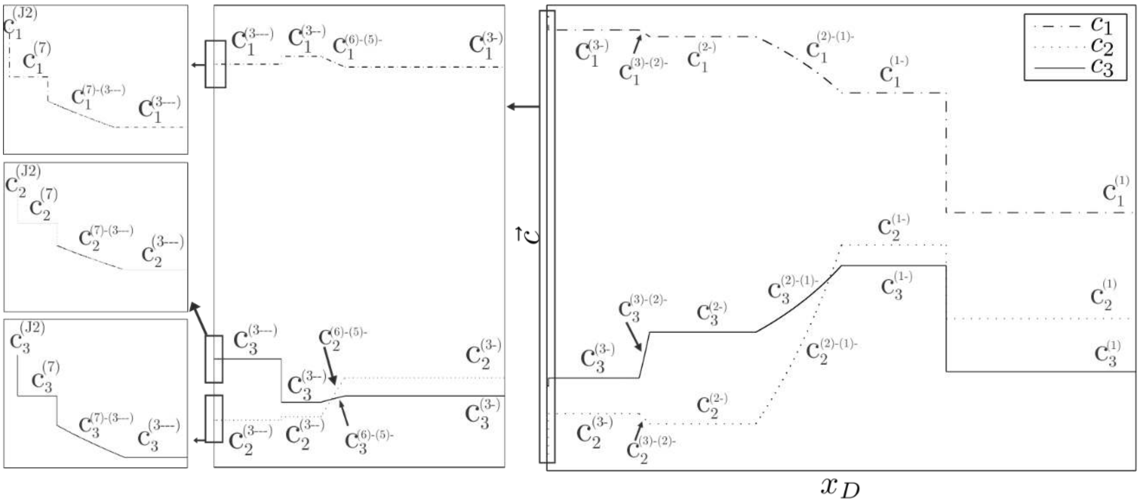

Figure B.11: Concentration profile of the solution part $\overrightarrow{c_{XI}}$

Solution $\overrightarrow{c_{XII}}$ takes place when $\varphi_{pH} < \varphi < \varphi_J$. Here the pH wave from the rear of the low salinity slug reaches the pH wave from the front, which leads to a wave interaction of the same family (Rhee *et al.*, 2001). The result is a shock wave that continuously absorb the pH rarefaction wave, and region (7) is no longer present in the solution of the auxiliary system. In equation (B.13) we present this part of the solution and the concentration profile is shown in figure (B.12).

$$\overrightarrow{c_{XII}} = \begin{cases} \vec{c}^{(J2)}, & x_D < x_{pH}^{-}(\varphi) \\ \vec{c}^{(7)-(3---)}(x_D,\varphi), & x_{pH}^{-}(\varphi) < x_D < \frac{\varphi}{\sigma_{pH}(\xi^{(I)})} \\ \vec{c}^{(3---)}, & \frac{\varphi}{\sigma_{pH}(\xi^{(I)})} < x_D < x_{(3)}^{-} \\ \vec{c}^{(3--)}, & x_{(3)}^{-} < x_D < x_{(6)-(5)}^{-(+)}(\varphi) \\ \vec{c}^{(6)-(5)-}(x_D,\varphi), & x_{(6)-(5)}^{-(+)}(\varphi) < x_D < x_{(6)-(5)}^{-(-)}(\varphi) \\ \vec{c}^{(3-)}, & x_{(6)-(5)}^{-(-)}(\varphi) < x_D < x_{(3)-(2)}^{-(+)}(\varphi) \\ \vec{c}^{(3)-(2)-}(x_D,\varphi), & x_{(3)-(2)}^{-(+)}(\varphi) < x_D < x_{(3)-(2)}^{-(-)}(\varphi) \\ \vec{c}^{(2-)}, & x_{(3)-(2)}^{-(-)}(\varphi) < x_D < x_{(2)-(1)}^{-(+)}(\varphi) \\ \vec{c}^{(2)-(1)-}, & x_{(2)-(1)}^{-(+)}(\varphi) < x_D < x_{(2)-(1)}^{-(-)}(\varphi) \\ \vec{c}^{(1-)}, & x_{(2)-(1)}^{-(-)}(\varphi) < x_D < x_{(1)}^{---}(\varphi) \\ \vec{c}^{(1)}, & x_{(1)}^{---}(\varphi) < x_D < \frac{\varphi}{\sigma_{(1)}(\vec{\omega}^{(1)},\xi^{(I)})} \\ \vec{c}^{(1)-(I)}(x_D,\varphi), & \frac{\varphi}{\sigma_{(1)}(\vec{\omega}^{(1)},\xi^{(I)})} < x_D < \frac{\varphi}{\sigma_{(1)}(\vec{\omega}^{(I)},\xi^{(I)})} \\ \vec{c}^{(I)}, & \frac{\varphi}{\sigma_{(1)}(\vec{\omega}^{(I)},\xi^{(I)})} < x_D < \frac{\varphi}{-s^{(I)}} \end{cases} \tag{B.13}$$

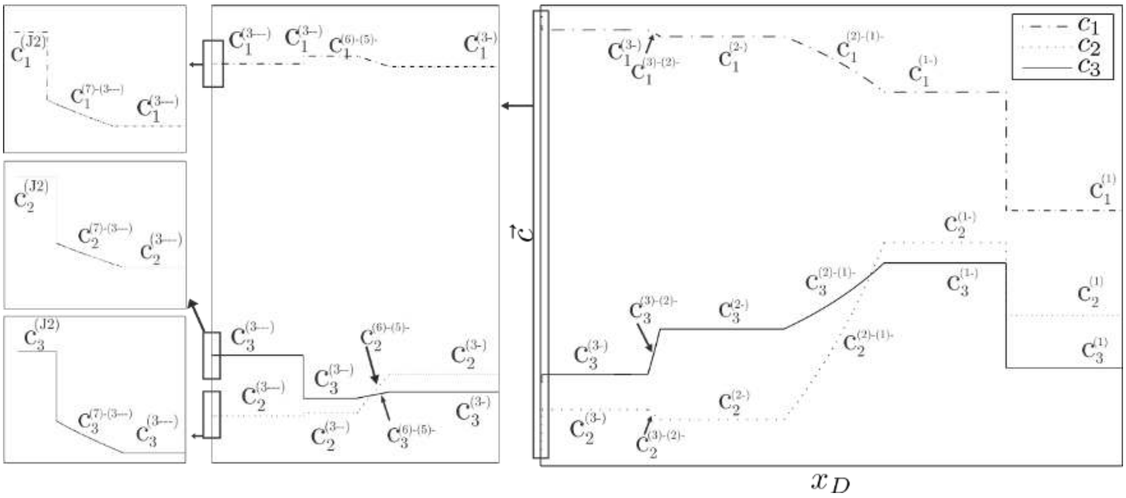

Figure B.12: Solution part $\overrightarrow{c_{XII}}$ of the auxiliary system

In the solution $\overrightarrow{c_{XIII}}$ the interaction between rarefaction waves of the families $k = 2$ and $k = 3$ begins. This interaction region is bounded by the curves $(J - L) = x_{(3)-(2)}^{--(+)}(\varphi)$, $(K - M) = x_{(3)-(2)}^{--(-)}(\varphi)$, $(J - K) = x_{(6)-(5)}^{--(-)}(\varphi)$ and $(L - M) =$

$x_{(6)-(5)}^{--(+)}(\varphi)$. In this part of the solution the region (3-) disappears. In equation (B.14) we detail $\overrightarrow{c_{XIII}}$, and its concentration profile is shown in figure (B.13).

$$\overrightarrow{c_{XIII}}=\begin{cases}\vec{c}^{(J2)}, & x_D < x_{pH}^{-}(\varphi)\\ \vec{c}^{(7)-(3---)}(x_D,\varphi), & x_{pH}^{-}(\varphi) < x_D < \frac{\varphi}{\sigma_{pH}(\xi^{(I)})}\\ \vec{c}^{(3---)}, & \frac{\varphi}{\sigma_{pH}(\xi^{(I)})} < x_D < x_{(3)}^{-}\\ \vec{c}^{(3--)}, & x_{(3)}^{-} < x_D < x_{(6)-(5)}^{-(+)}(\varphi)\\ \vec{c}^{(6)-(5)-}(x_D,\varphi), & x_{(6)-(5)}^{-(+)}(\varphi) < x_D < x_{(3)-(2)}^{--(+)}(\varphi)\\ \vec{c}^{(3)-(2)--}(x_D,\varphi), & x_{(3)-(2)}^{--(+)}(\varphi) < x_D < x_{(6)-(5)}^{-(-)}(\varphi)\\ \vec{c}^{(3)-(2)-}(x_D,\varphi), & x_{(6)-(5)}^{-(-)}(\varphi) < x_D < x_{(3)-(2)}^{--(-)}(\varphi)\\ \vec{c}^{(2-)}, & x_{(3)-(2)}^{--(-)}(\varphi) < x_D < x_{(2)-(1)}^{-(+)}(\varphi)\\ \vec{c}^{(2)-(1)-}, & x_{(2)-(1)}^{-(+)}(\varphi) < x_D < x_{(2)-(1)}^{-(-)}(\varphi)\\ \vec{c}^{(1-)}, & x_{(2)-(1)}^{-(-)}(\varphi) < x_D < x_{(1)}^{---}(\varphi)\\ \vec{c}^{(1)}, & x_{(1)}^{---}(\varphi) < x_D < \frac{\varphi}{\sigma_{(1)}(\vec{\omega}^{(1)},\xi^{(I)})}\\ \vec{c}^{(1)-(I)}(x_D,\varphi), & \frac{\varphi}{\sigma_{(1)}(\vec{\omega}^{(1)},\xi^{(I)})} < x_D < \frac{\varphi}{\sigma_{(1)}(\vec{\omega}^{(I)},\xi^{(I)})}\\ \vec{c}^{(I)}, & \frac{\varphi}{\sigma_{(1)}(\vec{\omega}^{(I)},\xi^{(I)})} < x_D < \frac{\varphi}{-s^{(I)}}\end{cases} \tag{B.14}$$

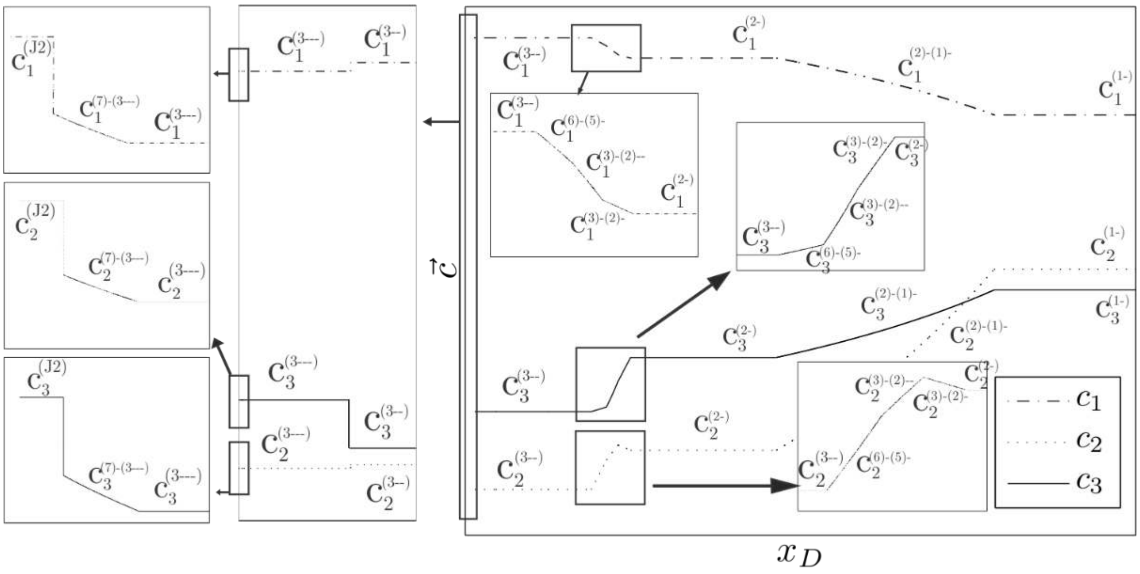

Figure B.13: Concentration profile of the solution $\overrightarrow{c_{XIII}}$

In the next part of the solution of the auxiliary system (solution $\overrightarrow{c_{XIV}}$), part of the rarefaction wave $k=2$ from the rear of the low salinity slug is separated from the rarefaction wave $k=3$ from the front. Thus, we have:

$$\overrightarrow{c_{XIV}} = \begin{cases} \vec{c}^{(J2)}, & x_D < x_{pH}^{-}(\varphi) \\ \vec{c}^{(7)-(3---)}(x_D,\varphi), & x_{pH}^{-}(\varphi) < x_D < \frac{\varphi}{\sigma_{pH}(\xi^{(I)})} \\ \vec{c}^{(3---)}, & \frac{\varphi}{\sigma_{pH}(\xi^{(I)})} < x_D < x_{(3)}^{-} \\ \vec{c}^{(3--)}, & x_{(3)}^{-} < x_D < x_{(6)-(5)}^{-(+)}(\varphi) \\ \vec{c}^{(6)-(5)-}(x_D,\varphi), & x_{(6)-(5)}^{-(+)}(\varphi) < x_D < x_{(3)-(2)}^{--(+)}(\varphi) \\ \vec{c}^{(3)-(2)--}(x_D,\varphi), & x_{(3)-(2)}^{--(+)}(\varphi) < x_D < x_{(3)-(2)}^{--(-)}(\varphi) \\ \vec{c}^{(6)-(5)--}(x_D,\varphi), & x_{(3)-(2)}^{--(-)}(\varphi) < x_D < x_{(6)-(5)}^{--(-)}(\varphi) \\ \vec{c}^{(2-)}, & x_{(6)-(5)}^{--(-)}(\varphi) < x_D < x_{(2)-(1)}^{-(+)}(\varphi) \\ \vec{c}^{(2)-(1)-}, & x_{(2)-(1)}^{-(+)}(\varphi) < x_D < x_{(2)-(1)}^{-(-)}(\varphi) \\ \vec{c}^{(1-)}, & x_{(2)-(1)}^{-(-)}(\varphi) < x_D < x_{(1)}^{---}(\varphi) \\ \vec{c}^{(1)}, & x_{(1)}^{---}(\varphi) < x_D < \frac{\varphi}{\sigma_{(1)}(\overrightarrow{\omega}^{(1)},\xi^{(I)})} \\ \vec{c}^{(1)-(I)}(x_D,\varphi), & \frac{\varphi}{\sigma_{(1)}(\overrightarrow{\omega}^{(1)},\xi^{(I)})} < x_D < \frac{\varphi}{\sigma_{(1)}(\overrightarrow{\omega}^{(I)},\xi^{(I)})} \\ \vec{c}^{(I)}, & \frac{\varphi}{\sigma_{(1)}(\overrightarrow{\omega}^{(I)},\xi^{(I)})} < x_D < \frac{\varphi}{-s^{(I)}} \end{cases} \tag{B.15}$$

The concentration profile for the solution $\overrightarrow{c_{XIV}}$ is shown in figure (B.14). Note that the difference from the solution $\overrightarrow{c_{XIII}}$ lies on the region where the rarefaction waves interact.

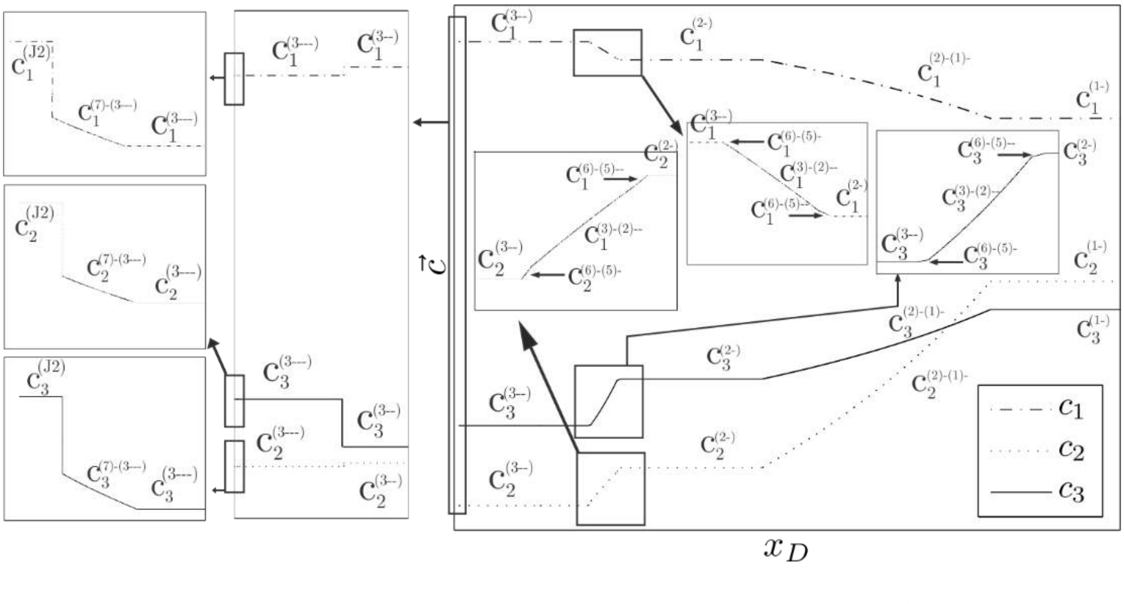

Figure B.14: Concentration profile of the solution $\overrightarrow{c_{XIV}}$

The solution $\overrightarrow{c_{XV}}$, which occurs when $\varphi_L < \varphi < \varphi_M$, is the last part of the solution of the auxiliary system where there is interaction between rarefaction waves. In this solution, part of the rarefaction wave $k = 3$ from the front of the low salinity slug is separated from the rarefaction wave $k = 2$ from the rear of the slug. Equation (B.16) presents the mathematical details for this part of the solution, and its concentration profile is shown in figure (B.15).

$$\overrightarrow{c_{XV}} = \begin{cases} \vec{c}^{(J2)}, & x_D < x_{pH}^{-}(\varphi) \\ \vec{c}^{(7)-(3---)}(x_D, \varphi), & x_{pH}^{-}(\varphi) < x_D < \frac{\varphi}{\sigma_{pH}(\xi^{(I)})} \\ \vec{c}^{(3---)}, & \frac{\varphi}{\sigma_{pH}(\xi^{(I)})} < x_D < x_{(3)}^{-} \\ \vec{c}^{(3--)}, & x_{(3)}^{-} < x_D < x_{(3)-(2)}^{--(+)}(\varphi) \\ \vec{c}^{(3)-(2)---}(x_D, \varphi), & x_{(3)-(2)}^{--(+)}(\varphi) < x_D < x_{(6)-(5)}^{--(+)}(\varphi) \\ \vec{c}^{(3)-(2)--}(x_D, \varphi), & x_{(6)-(5)}^{--(+)}(\varphi) < x_D < x_{(3)-(2)}^{--(-)}(\varphi) \\ \vec{c}^{(6)-(5)--}(x_D, \varphi), & x_{(3)-(2)}^{--(-)}(\varphi) < x_D < x_{(6)-(5)}^{--(-)}(\varphi) \\ \vec{c}^{(2-)}, & x_{(6)-(5)}^{--(-)}(\varphi) < x_D < x_{(2)-(1)}^{-(+)}(\varphi) \\ \vec{c}^{(2)-(1)-}, & x_{(2)-(1)}^{-(+)}(\varphi) < x_D < x_{(2)-(1)}^{-(-)}(\varphi) \\ \vec{c}^{(1-)}, & x_{(2)-(1)}^{-(-)}(\varphi) < x_D < x_{(1)}^{---}(\varphi) \\ \vec{c}^{(1)}, & x_{(1)}^{---}(\varphi) < x_D < \frac{\varphi}{\sigma_{(1)}(\vec{\omega}^{(1)}, \xi^{(I)})} \\ \vec{c}^{(1)-(I)}(x_D, \varphi), & \frac{\varphi}{\sigma_{(1)}(\vec{\omega}^{(1)}, \xi^{(I)})} < x_D < \frac{\varphi}{\sigma_{(1)}(\vec{\omega}^{(I)}, \xi^{(I)})} \\ \vec{c}^{(I)}, & \frac{\varphi}{\sigma_{(1)}(\vec{\omega}^{(I)}, \xi^{(I)})} < x_D < \frac{\varphi}{-s^{(I)}} \end{cases} \tag{B.16}$$

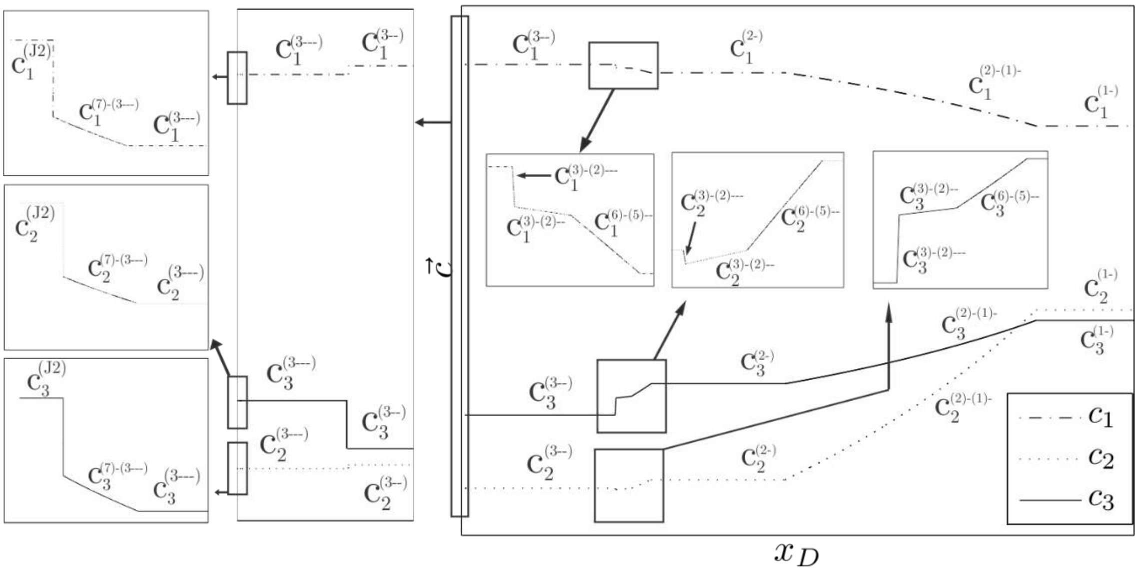

Figure B.15: Concentration profile of the solution $\overrightarrow{c_{XV}}$

For $\varphi_M < \varphi < \varphi_N$, $\vec{c} = \overrightarrow{c_{XVI}}$. In this part, the wave families $k = 2$ and $k = 3$ are fully separated, and the new region (2--) appears. In equation (B.17) it is possible to find the mathematical details regarding this part of the solution, and in figure (B.16) we present its concentration profile. As the concentration waves after $\vec{c}^{(2)-(1)-}$ appear for large x_D they are not shown in figure (B.16).

$$\overrightarrow{c_{XVI}} = \begin{cases} \vec{c}^{(J2)}, & x_D < x^{-}_{pH}(\varphi) \\ \vec{c}^{(7)-(3---)}(x_D,\varphi), & x^{-}_{pH}(\varphi) < x_D < \frac{\varphi}{\sigma_{pH}(\xi^{(I)})} \\ \vec{c}^{(3---)}, & \frac{\varphi}{\sigma_{pH}(\xi^{(I)})} < x_D < x^{-}_{(3)} \\ \vec{c}^{(3--)}, & x^{-}_{(3)} < x_D < x^{--(+)}_{(3)-(2)}(\varphi) \\ \vec{c}^{(3)-(2)---}(x_D,\varphi), & x^{--(+)}_{(3)-(2)}(\varphi) < x_D < x^{--(-)}_{(3)-(2)}(\varphi) \\ \vec{c}^{(2--)}, & x^{--(-)}_{(3)-(2)}(\varphi) < x_D < x^{--(+)}_{(6)-(5)}(\varphi) \\ \vec{c}^{(6)-(5)--}(x_D,\varphi), & x^{--(+)}_{(6)-(5)}(\varphi) < x_D < x^{--(-)}_{(6)-(5)}(\varphi) \\ \vec{c}^{(2-)}, & x^{--(-)}_{(6)-(5)}(\varphi) < x_D < x^{-(+)}_{(2)-(1)}(\varphi) \\ \vec{c}^{(2)-(1)-}, & x^{-(+)}_{(2)-(1)}(\varphi) < x_D < x^{-(-)}_{(2)-(1)}(\varphi) \\ \vec{c}^{(1-)}, & x^{-(-)}_{(2)-(1)}(\varphi) < x_D < x^{---}_{(1)}(\varphi) \\ \vec{c}^{(1)}, & x^{---}_{(1)}(\varphi) < x_D < \frac{\varphi}{\sigma_{(1)}(\vec{\omega}^{(1)},\xi^{(I)})} \\ \vec{c}^{(1)-(I)}(x_D,\varphi), & \frac{\varphi}{\sigma_{(1)}(\vec{\omega}^{(1)},\xi^{(I)})} < x_D < \frac{\varphi}{\sigma_{(1)}(\vec{\omega}^{(I)},\xi^{(I)})} \\ \vec{c}^{(I)}, & \frac{\varphi}{\sigma_{(1)}(\vec{\omega}^{(I)},\xi^{(I)})} < x_D < \frac{\varphi}{-s^{(I)}} \end{cases} \quad \text{(B.17)}$$

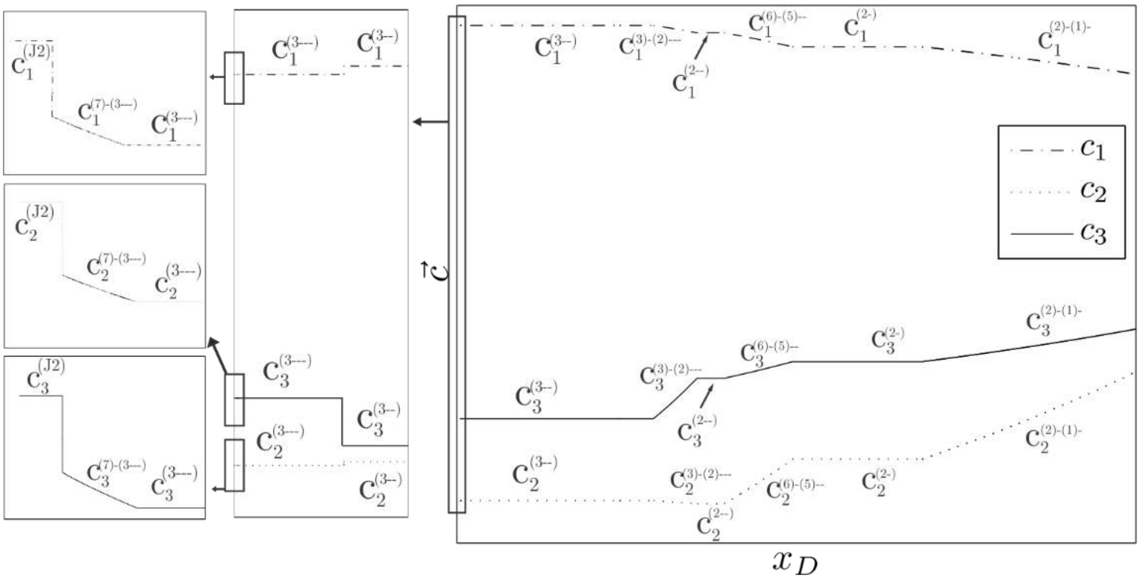

Figure B.16: Concentration profile of the solution $\overrightarrow{c_{XVI}}$

In solution $\overrightarrow{c_{XVII}}$ (for $\varphi > \varphi_N$), the waves from the family $k = 3$ of the rear of the slug catch up the waves of the same family of the front of the slug, an interaction between waves of the same family. The shock path of this interaction is denoted as $x_{(3)}^{--}$. Furthermore, the region (3--) disappears. In equation (B.18) we present the mathematical expression for $\overrightarrow{c_{XVII}}$ and in figure (B.17) we present its concentration profile.

$$\overrightarrow{c_{XVII}} = \begin{cases} \vec{c}^{(J2)}, & x_D < x_{pH}^{-}(\varphi) \\ \vec{c}^{(7)-(3---)}(x_D,\varphi), & x_{pH}^{-}(\varphi) < x_D < \frac{\varphi}{\sigma_{pH}(\xi^{(I)})} \\ \vec{c}^{(3---)}, & \frac{\varphi}{\sigma_{pH}(\xi^{(I)})} < x_D < x_{(3)}^{--} \\ \vec{c}^{(3)-(2)---}(x_D,\varphi), & x_{(3)}^{--} < x_D < x_{(3)-(2)}^{--(-)}(\varphi) \\ \vec{c}^{(2--)}, & x_{(3)-(2)}^{--(-)}(\varphi) < x_D < x_{(6)-(5)}^{--(+)}(\varphi) \\ \vec{c}^{(6)-(5)--}(x_D,\varphi), & x_{(6)-(5)}^{--(+)}(\varphi) < x_D < x_{(6)-(5)}^{--(-)}(\varphi) \\ \vec{c}^{(2-)}, & x_{(6)-(5)}^{--(-)}(\varphi) < x_D < x_{(2)-(1)}^{-(+)}(\varphi) \\ \vec{c}^{(2)-(1)-}, & x_{(2)-(1)}^{-(+)}(\varphi) < x_D < x_{(2)-(1)}^{-(-)}(\varphi) \\ \vec{c}^{(1-)}, & x_{(2)-(1)}^{-(-)}(\varphi) < x_D < x_{(1)}^{---}(\varphi) \\ \vec{c}^{(1)}, & x_{(1)}^{---}(\varphi) < x_D < \frac{\varphi}{\sigma_{(1)}(\overrightarrow{\omega}^{(1)},\xi^{(I)})} \\ \vec{c}^{(1)-(I)}(x_D,\varphi), & \frac{\varphi}{\sigma_{(1)}(\overrightarrow{\omega}^{(1)},\xi^{(I)})} < x_D < \frac{\varphi}{\sigma_{(1)}(\overrightarrow{\omega}^{(I)},\xi^{(I)})} \\ \vec{c}^{(I)}, & \frac{\varphi}{\sigma_{(1)}(\overrightarrow{\omega}^{(I)},\xi^{(I)})} < x_D < \frac{\varphi}{-s^{(I)}} \end{cases} \tag{B.18}$$

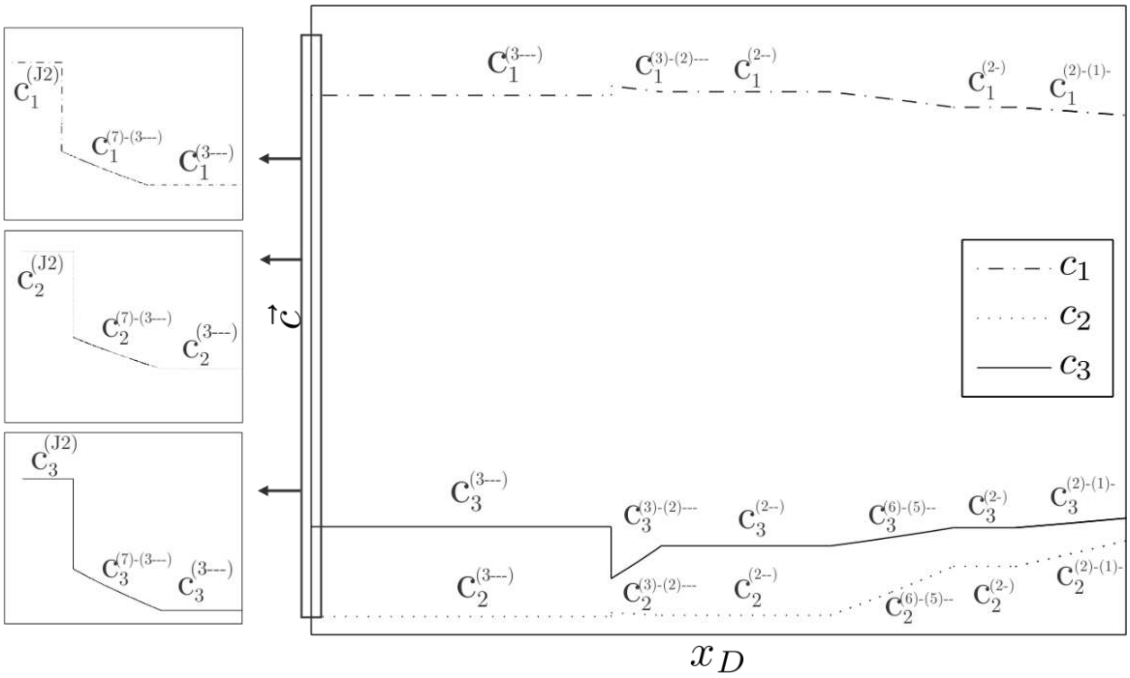

Figure B.17: Concentration profile of the solution $\overrightarrow{c_{XVII}}$

B. Lifting equation solution

The solution of the lifting equation is divided into the same 17 regions of the auxiliary solution:

$$U(x_D,\varphi)=\begin{cases} U_I, & \varphi<\varphi_{HS} \\ U_{II}, & \varphi_{HS}<\varphi<\varphi_A \\ U_{III}, & \varphi_A<\varphi<\varphi_B \\ U_{IV}, & \varphi_B<\varphi<\varphi_C \\ U_V, & \varphi_C<\varphi<\varphi_D \\ U_{VI}, & \varphi_D<\varphi<\varphi_E \\ U_{VII}, & \varphi_E<\varphi<\varphi_F \\ U_{VIII}, & \varphi_F<\varphi<\varphi_G \\ U_{IX}, & \varphi_G<\varphi<\varphi_H \\ U_X, & \varphi_H<\varphi<\varphi_I \\ U_{XI}, & \varphi_I<\varphi<\varphi_{pH} \\ U_{XII}, & \varphi_{pH}<\varphi<\varphi_J \\ U_{XIII}, & \varphi_J<\varphi<\varphi_K \\ U_{XIV}, & \varphi_K<\varphi<\varphi_L \\ U_{XV}, & \varphi_L<\varphi<\varphi_M \\ U_{XVI}, & \varphi_M<\varphi<\varphi_N \\ U_{XVII}, & \varphi_N<\varphi \end{cases} \tag{B.1}$$

Each solution part of equation (B.1) is presented in equations (B.2)-(B.18) and each solution path in $F\times U$ plane is shown in figures (B.1)-(B.17).

$$U_I = \begin{cases} U_4(x_D,\varphi), & x_D < \frac{\varphi}{V_{pH}^{(1)}} \\ U^{(4)-(3)}(x_D,\varphi), & \frac{\varphi}{V_{pH}^{(1)}} < x_D < \frac{\varphi}{\sigma_{pH}^{(1)}(\xi^{(I)})} \\ U_3(x_D,\varphi), & \frac{\varphi}{\sigma_{pH}^{(1)}(\xi^{(I)})} < x_D < \frac{\varphi}{\sigma_{(3)}(\overrightarrow{\omega}^{(3)},\xi^{(I)})} \\ U^{(3)-(2)}(x_D,\varphi), & \frac{\varphi}{\sigma_{(3)}(\overrightarrow{\omega}^{(3)},\xi^{(I)})} < x_D < \frac{\varphi}{\sigma_{(3)}(\overrightarrow{\omega}^{(2)},\xi^{(I)})} \\ U^{(2)}, & \frac{\varphi}{\sigma_{(3)}(\overrightarrow{\omega}^{(2)},\xi^{(I)})} < x_D < \frac{\varphi}{\sigma_{(2)}(\overrightarrow{\omega}^{(2)},\xi^{(I)})} \\ U^{(2)-(1)}(x_D,\varphi), & \frac{\varphi}{\sigma_{(2)}(\overrightarrow{\omega}^{(2)},\xi^{(I)})} < x_D < \frac{\varphi}{\sigma_{(2)}(\overrightarrow{\omega}^{(1)},\xi^{(I)})} \\ U^{(1)}, & \frac{\varphi}{\sigma_{(2)}(\overrightarrow{\omega}^{(1)},\xi^{(I)})} < x_D < \frac{\varphi}{\sigma_{(1)}(\overrightarrow{\omega}^{(1)},\xi^{(I)})} \\ U^{(1)-(I+)}(x_D,\varphi), & \frac{\varphi}{\sigma_{(1)}(\overrightarrow{\omega}^{(1)},\xi^{(I)})} < x_D < \frac{\varphi}{\sigma_{(1)}(\overrightarrow{\omega}^{(I)},\xi^{(I)})} \\ U^{(I+)}, & \frac{\varphi}{\sigma_{(1)}(\overrightarrow{\omega}^{(I)},\xi^{(I)})} < x_D < +\infty \\ U^{(I)}, & x_D \to +\infty \end{cases} \tag{B.2}$$

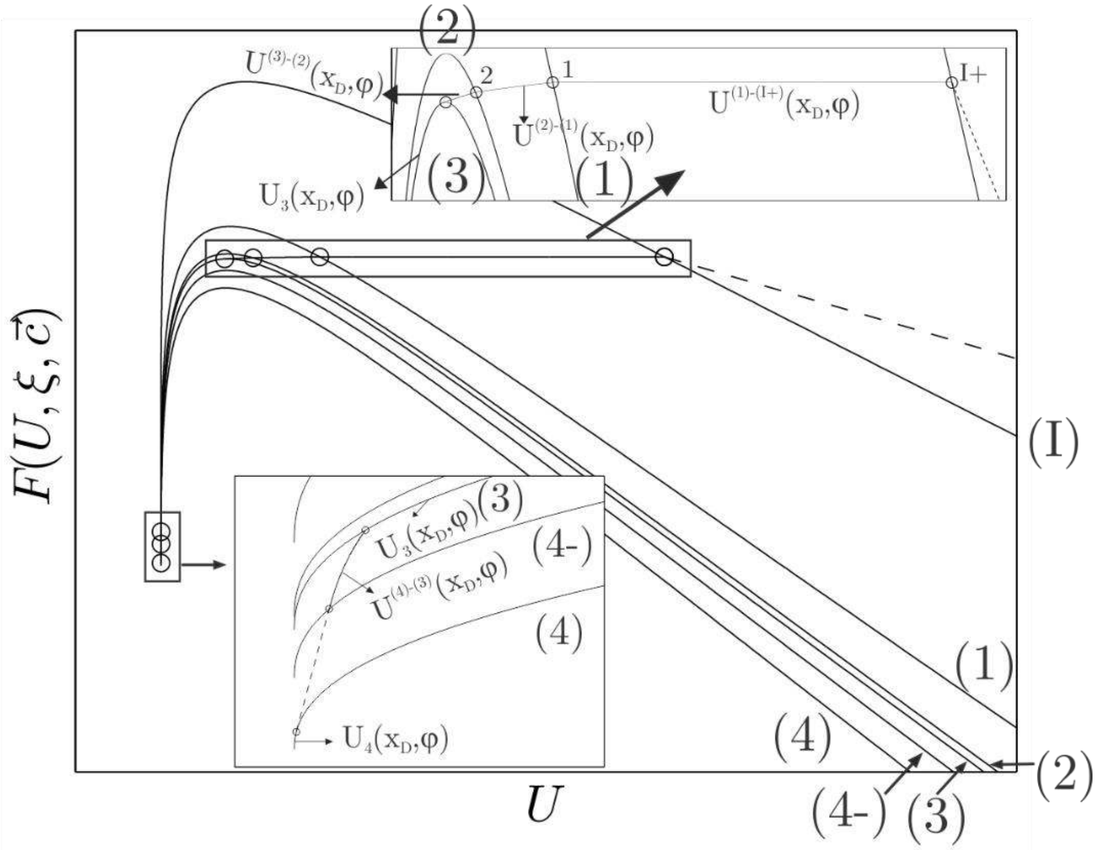

Figure B.1: Solution path of U_I in the $F \times U$ plane

$$U_{II} = \begin{cases} U_{J2}(x_D,\varphi), & x_D < \frac{\varphi-\varphi_{HS}}{V_{pH}^{(2)}} \\ U_7(x_D,\varphi), & \frac{\varphi-\varphi_{HS}}{V_{pH}^{(2)}} < x_D < \frac{\varphi-\varphi_{HS}}{V_{(3)}} \\ U_6(x_D,\varphi), & \frac{\varphi-\varphi_{HS}}{V_{(3)}} < x_D < \frac{\varphi-\varphi_{HS}}{\sigma_{(2)}\left(\vec{\omega}^{(6)},\xi^{(J1)}\right)} \\ U^{(6)-(5)}(x_D,\varphi), & \frac{\varphi-\varphi_{HS}}{\sigma_{(2)}\left(\vec{\omega}^{(6)},\xi^{(J1)}\right)} < x_D < \frac{\varphi-\varphi_{HS}}{\sigma_{(2)}\left(\vec{\omega}^{(5)},\xi^{(J1)}\right)} \\ U_5(x_D,\varphi), & \frac{\varphi-\varphi_{HS}}{\sigma_{(2)}\left(\vec{\omega}^{(5)},\xi^{(J1)}\right)} < x_D < \frac{\varphi-\varphi_{HS}}{V_{(1)}} \\ U_4(x_D,\varphi), & \frac{\varphi-\varphi_{HS}}{V_{(1)}} < x_D < \frac{\varphi}{V_{pH}^{(1)}} \\ U^{(4)-(3)}(x_D,\varphi), & \frac{\varphi}{V_{pH}^{(1)}} < x_D < \frac{\varphi}{\sigma_{pH}^{(1)}\left(\xi^{(I)}\right)} \\ U_3(x_D,\varphi), & \frac{\varphi}{\sigma_{pH}^{(1)}\left(\xi^{(I)}\right)} < x_D < \frac{\varphi}{\sigma_{(3)}(\vec{\omega}^{(3)},\xi^{(I)})} \\ U^{(3)-(2)}(x_D,\varphi), & \frac{\varphi}{\sigma_{(3)}(\vec{\omega}^{(3)},\xi^{(I)})} < x_D < \frac{\varphi}{\sigma_{(3)}(\vec{\omega}^{(2)},\xi^{(I)})} \\ U^{(2)}, & \frac{\varphi}{\sigma_{(3)}(\vec{\omega}^{(2)},\xi^{(I)})} < x_D < \frac{\varphi}{\sigma_{(2)}(\vec{\omega}^{(2)},\xi^{(I)})} \\ U^{(2)-(1)}(x_D,\varphi), & \frac{\varphi}{\sigma_{(2)}(\vec{\omega}^{(2)},\xi^{(I)})} < x_D < \frac{\varphi}{\sigma_{(2)}(\vec{\omega}^{(1)},\xi^{(I)})} \\ U^{(1)}, & \frac{\varphi}{\sigma_{(2)}(\vec{\omega}^{(1)},\xi^{(I)})} < x_D < \frac{\varphi}{\sigma_{(1)}(\vec{\omega}^{(1)},\xi^{(I)})} \\ U^{(1)-(I+)}(x_D,\varphi), & \frac{\varphi}{\sigma_{(1)}(\vec{\omega}^{(1)},\xi^{(I)})} < x_D < \frac{\varphi}{\sigma_{(1)}(\vec{\omega}^{(I)},\xi^{(I)})} \\ U^{(I+)}, & \frac{\varphi}{\sigma_{(1)}(\vec{\omega}^{(I)},\xi^{(I)})} < x_D < +\infty \\ U^{(I)}, & x_D \to +\infty \end{cases} \tag{B.3}$$

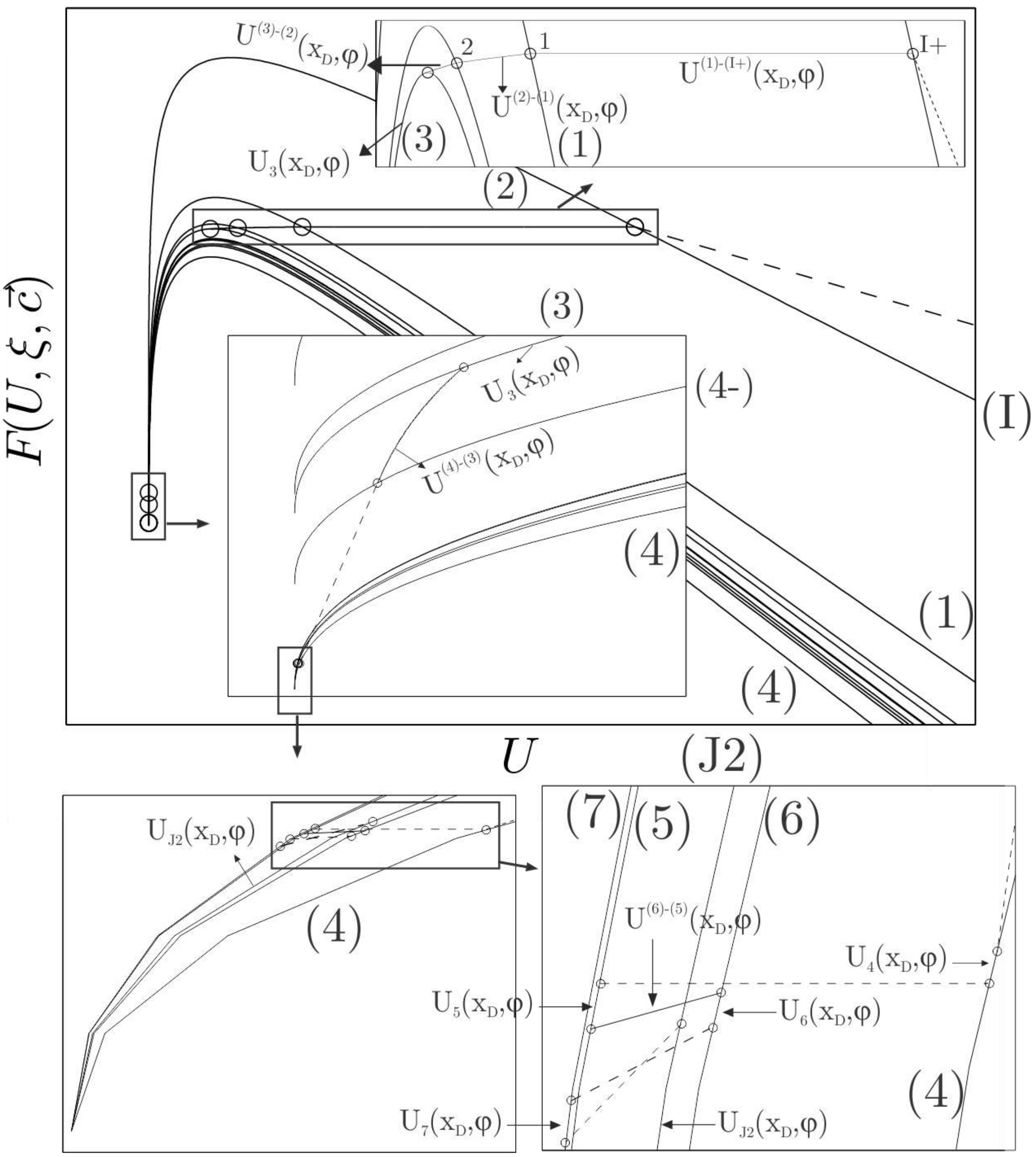

Figure B2: Solution path of U_{II} in the $F \times U$ plane

$$U_{III} = \begin{cases} U_{J2}(x_D, \varphi), & x_D < \frac{\varphi - \varphi_{HS}}{V_{pH}^{(2)}} \\ U_7(x_D, \varphi), & \frac{\varphi - \varphi_{HS}}{V_{pH}^{(2)}} < x_D < \frac{\varphi - \varphi_{HS}}{V_{(3)}} \\ U_6(x_D, \varphi), & \frac{\varphi - \varphi_{HS}}{V_{(3)}} < x_D < \frac{\varphi - \varphi_{HS}}{\sigma_{(2)}\left(\vec{\omega}^{(6)}, \xi^{(J1)}\right)} \\ U^{(6)-(5)}(x_D, \varphi), & \frac{\varphi - \varphi_{HS}}{\sigma_{(2)}\left(\vec{\omega}^{(6)}, \xi^{(J1)}\right)} < x_D < \frac{\varphi - \varphi_{HS}}{\sigma_{(2)}\left(\vec{\omega}^{(5)}, \xi^{(J1)}\right)} \\ U_5(x_D, \varphi), & \frac{\varphi - \varphi_{HS}}{\sigma_{(2)}\left(\vec{\omega}^{(5)}, \xi^{(J1)}\right)} < x_D < \frac{\varphi}{V_{(pH)}^{(1)}} \\ U^{(5)-(3-)}(x_D, \varphi), & \frac{\varphi}{V_{pH}^{(1)}} < x_D < \frac{\varphi}{\sigma_{pH}(\xi^{(I)})} \\ U^{(3-)}, & \frac{\varphi}{\sigma_{pH}(\xi^{(I)})} < x_D < x_{(1)}^{-}(\varphi) \\ U^{(3)}, & x_{(1)}^{-}(\varphi) < x_D < \frac{\varphi}{\sigma_{(3)}(\vec{\omega}^{(3)}, \xi^{(I)})} \\ U^{(3)-(2)}(x_D, \varphi), & \frac{\varphi}{\sigma_{(3)}(\vec{\omega}^{(3)}, \xi^{(I)})} < x_D < \frac{\varphi}{\sigma_{(3)}(\vec{\omega}^{(2)}, \xi^{(I)})} \\ U^{(2)}, & \frac{\varphi}{\sigma_{(3)}(\vec{\omega}^{(2)}, \xi^{(I)})} < x_D < \frac{\varphi}{\sigma_{(2)}(\vec{\omega}^{(2)}, \xi^{(I)})} \\ U^{(2)-(1)}(x_D, \varphi), & \frac{\varphi}{\sigma_{(2)}(\vec{\omega}^{(2)}, \xi^{(I)})} < x_D < \frac{\varphi}{\sigma_{(2)}(\vec{\omega}^{(1)}, \xi^{(I)})} \\ U^{(1)}, & \frac{\varphi}{\sigma_{(2)}(\vec{\omega}^{(1)}, \xi^{(I)})} < x_D < \frac{\varphi}{\sigma_{(1)}(\vec{\omega}^{(1)}, \xi^{(I)})} \\ U^{(1)-(I+)}(x_D, \varphi), & \frac{\varphi}{\sigma_{(1)}(\vec{\omega}^{(1)}, \xi^{(I)})} < x_D < \frac{\varphi}{\sigma_{(1)}(\vec{\omega}^{(I)}, \xi^{(I)})} \\ U^{(I+)}, & \frac{\varphi}{\sigma_{(1)}(\vec{\omega}^{(I)}, \xi^{(I)})} < x_D < +\infty \\ U^{(I)}, & x_D \to +\infty \end{cases} \tag{B.4}$$

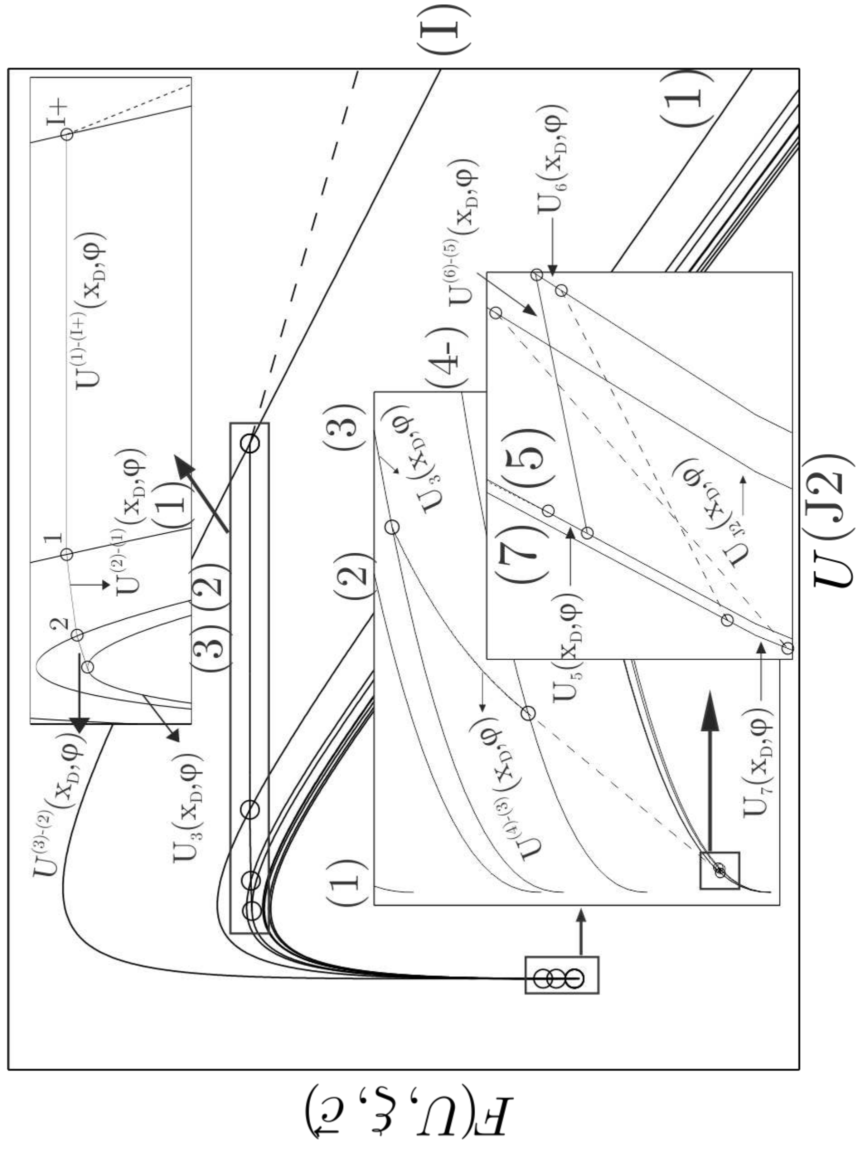

Figure B3: Solution path of U_{III} in the $F \times U$ plane

$$U_{IV} = \begin{cases} U_{J2}(x_D,\varphi), & x_D < \frac{\varphi-\varphi_{HS}}{V_{pH}^{(2)}} \\ U_7(x_D,\varphi), & \frac{\varphi-\varphi_{HS}}{V_{pH}^{(2)}} < x_D < \frac{\varphi-\varphi_{HS}}{V_{(3)}} \\ U_6(x_D,\varphi), & \frac{\varphi-\varphi_{HS}}{V_{(3)}} < x_D < \frac{\varphi-\varphi_{HS}}{\sigma_{(2)}\left(\vec{\omega}^{(6)},\xi^{(J1)}\right)} \\ U^{(6)-(5)}(x_D,\varphi), & \frac{\varphi-\varphi_{HS}}{\sigma_{(2)}\left(\vec{\omega}^{(6)},\xi^{(J1)}\right)} < x_D < \frac{\varphi}{V_{(pH)}^{(1)}} \\ U^{(6)-(5)-}(x_D,\varphi), & \frac{\varphi}{V_{(pH)}^{(1)}} < x_D < x_{(6)-(5)}^{-}(\varphi) \\ U^{(5)-(3-)}(x_D,\varphi), & x_{(6)-(5)}^{-}(\varphi) < x_D < \frac{\varphi}{\sigma_{pH}(\xi^{(I)})} \\ U_{3-}(x_D,\varphi), & \frac{\varphi}{\sigma_{pH}(\xi^{(I)})} < x_D < x_{(1)}^{-}(\varphi) \\ U_3(x_D,\varphi), & x_{(1)}^{-}(\varphi) < x_D < \frac{\varphi}{\sigma_{(3)}(\vec{\omega}^{(3)},\xi^{(I)})} \\ U^{(3)-(2)}(x_D,\varphi), & \frac{\varphi}{\sigma_{(3)}(\vec{\omega}^{(3)},\xi^{(I)})} < x_D < \frac{\varphi}{\sigma_{(3)}(\vec{\omega}^{(2)},\xi^{(I)})} \\ U^{(2)}, & \frac{\varphi}{\sigma_{(3)}(\vec{\omega}^{(2)},\xi^{(I)})} < x_D < \frac{\varphi}{\sigma_{(2)}(\vec{\omega}^{(2)},\xi^{(I)})} \\ U^{(2)-(1)}(x_D,\varphi), & \frac{\varphi}{\sigma_{(2)}(\vec{\omega}^{(2)},\xi^{(I)})} < x_D < \frac{\varphi}{\sigma_{(2)}(\vec{\omega}^{(1)},\xi^{(I)})} \\ U^{(1)}, & \frac{\varphi}{\sigma_{(2)}(\vec{\omega}^{(1)},\xi^{(I)})} < x_D < \frac{\varphi}{\sigma_{(1)}(\vec{\omega}^{(1)},\xi^{(I)})} \\ U^{(1)-(I+)}(x_D,\varphi), & \frac{\varphi}{\sigma_{(1)}(\vec{\omega}^{(1)},\xi^{(I)})} < x_D < \frac{\varphi}{\sigma_{(1)}(\vec{\omega}^{(I)},\xi^{(I)})} \\ U^{(I+)}, & \frac{\varphi}{\sigma_{(1)}(\vec{\omega}^{(I)},\xi^{(I)})} < x_D < +\infty \\ U^{(I)}, & x_D \to +\infty \end{cases} \tag{B.5}$$

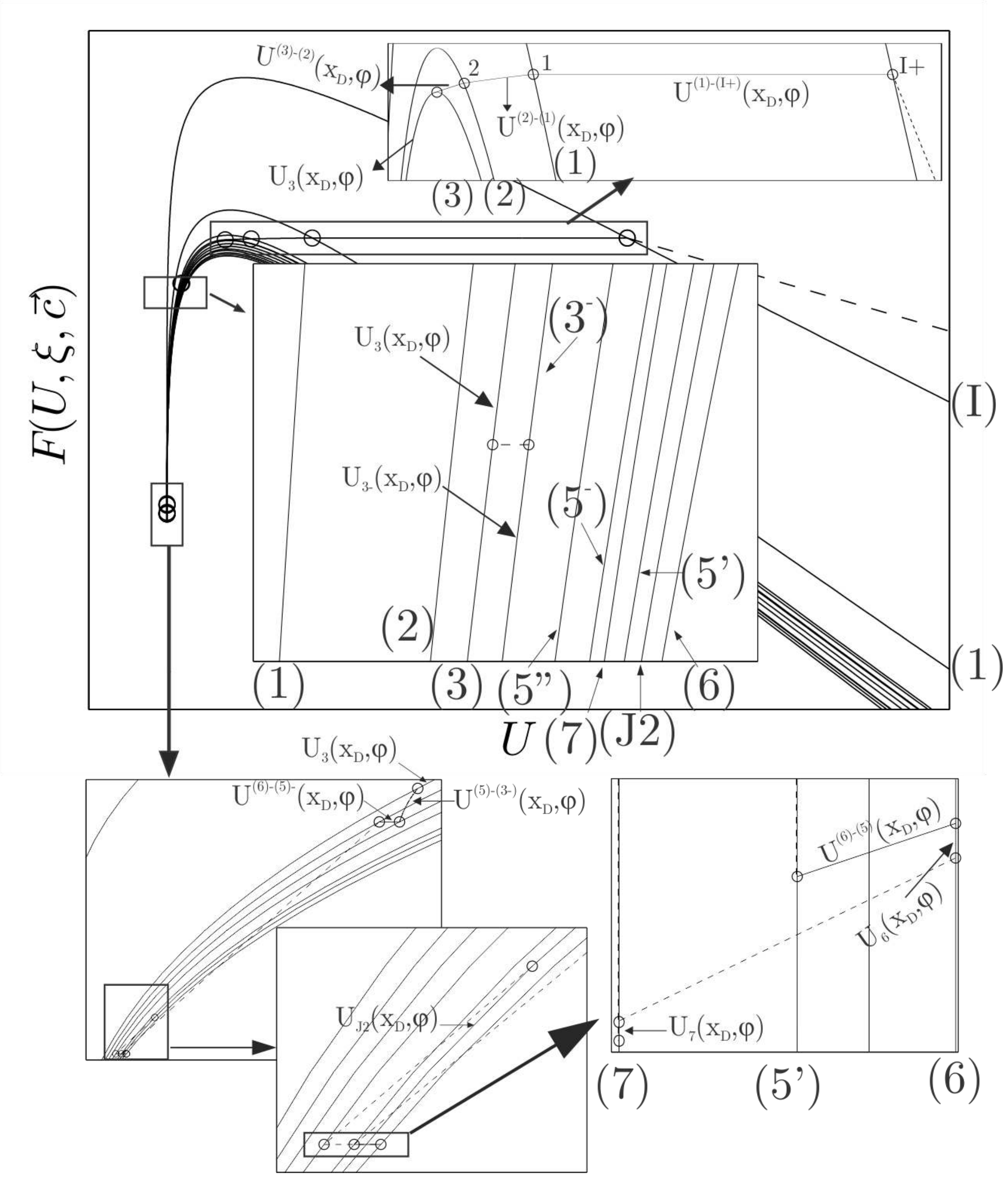

Figure B.4: Solution path of U_{IV} in the $F \times U$ plane

$$U_V = \begin{cases} U_{J2}(x_D, \varphi), & x_D < \frac{\varphi - \varphi_{HS}}{V_{pH}^{(2)}} \\ U_7(x_D, \varphi), & \frac{\varphi - \varphi_{HS}}{V_{pH}^{(2)}} < x_D < \frac{\varphi - \varphi_{HS}}{V_{(3)}} \\ U_6(x_D, \varphi), & \frac{\varphi - \varphi_{HS}}{V_{(3)}} < x_D < \frac{\varphi}{V_{(pH)}^{(1)}} \\ U^{(6)-(3--)}(x_D, \varphi), & \frac{\varphi}{V_{(pH)}^{(1)}} < x_D < x_{(6)-(5)}^{-(+)}(\varphi) \\ U^{(6)-(5)-}(x_D, \varphi), & x_{(6)-(5)}^{-(+)}(\varphi) < x_D < x_{(6)-(5)}^{-(-)}(\varphi) \\ U^{(5)-(3-)}(x_D, \varphi), & x_{(6)-(5)}^{-(-)}(\varphi) < x_D < \frac{\varphi}{\sigma_{pH}(\xi^{(I)})} \\ U_{3-}(x_D, \varphi), & \frac{\varphi}{\sigma_{pH}(\xi^{(I)})} < x_D < x_{(1)}^{-}(\varphi) \\ U_3(x_D, \varphi), & x_{(1)}^{-}(\varphi) < x_D < \frac{\varphi}{\sigma_{(3)}(\vec{\omega}^{(3)}, \xi^{(I)})} \\ U^{(3)-(2)}(x_D, \varphi), & \frac{\varphi}{\sigma_{(3)}(\vec{\omega}^{(3)}, \xi^{(I)})} < x_D < \frac{\varphi}{\sigma_{(3)}(\vec{\omega}^{(2)}, \xi^{(I)})} \\ U^{(2)}, & \frac{\varphi}{\sigma_{(3)}(\vec{\omega}^{(2)}, \xi^{(I)})} < x_D < \frac{\varphi}{\sigma_{(2)}(\vec{\omega}^{(2)}, \xi^{(I)})} \\ U^{(2)-(1)}(x_D, \varphi), & \frac{\varphi}{\sigma_{(2)}(\vec{\omega}^{(2)}, \xi^{(I)})} < x_D < \frac{\varphi}{\sigma_{(2)}(\vec{\omega}^{(1)}, \xi^{(I)})} \\ U^{(1)}, & \frac{\varphi}{\sigma_{(2)}(\vec{\omega}^{(1)}, \xi^{(I)})} < x_D < \frac{\varphi}{\sigma_{(1)}(\vec{\omega}^{(1)}, \xi^{(I)})} \\ U^{(1)-(I+)}(x_D, \varphi), & \frac{\varphi}{\sigma_{(1)}(\vec{\omega}^{(1)}, \xi^{(I)})} < x_D < \frac{\varphi}{\sigma_{(1)}(\vec{\omega}^{(I)}, \xi^{(I)})} \\ U^{(I+)}, & \frac{\varphi}{\sigma_{(1)}(\vec{\omega}^{(I)}, \xi^{(I)})} < x_D < +\infty \\ U^{(I)}, & x_D \to +\infty \end{cases} \tag{B.6}$$

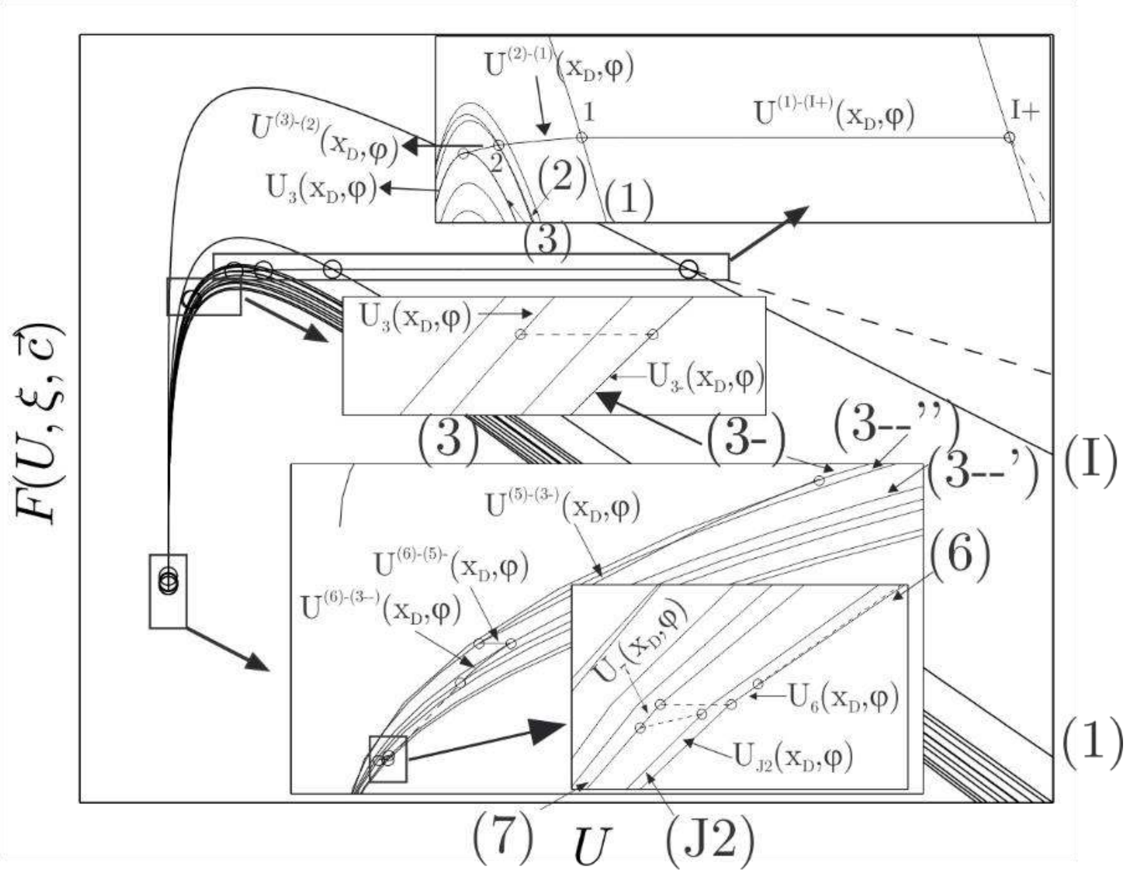

Figure B.5: Solution path of U_V in $F \times U$ plane

$$U_{VI}=\begin{cases}U_{J2}(x_D,\varphi), & x_D<\frac{\varphi-\varphi_{HS}}{V_{pH}^{(2)}}\\ U_7(x_D,\varphi), & \frac{\varphi-\varphi_{HS}}{V_{pH}^{(2)}}<x_D<\frac{\varphi}{V_{(pH)}^{(1)}}\\ U^{(7)-(3---)}(x_D,\varphi), & \frac{\varphi}{V_{(pH)}^{(1)}}<x_D<x_{(3)}^{-}\\ U^{(6)-(3--)}(x_D,\varphi), & x_{(3)}^{-}<x_D<x_{(6)-(5)}^{-(+)}(\varphi)\\ U^{(6)-(5)-}(x_D,\varphi), & x_{(6)-(5)}^{-(+)}(\varphi)<x_D<x_{(6)-(5)}^{-(-)}(\varphi)\\ U_{3-}(x_D,\varphi), & x_{(6)-(5)}^{-(-)}(\varphi)<x_D<x_{(1)}^{-}(\varphi)\\ U_3(x_D,\varphi), & x_{(1)}^{-}(\varphi)<x_D<\frac{\varphi}{\sigma_{(3)}(\vec{\omega}^{(3)},\xi^{(I)})}\\ U^{(3)-(2)}(x_D,\varphi), & \frac{\varphi}{\sigma_{(3)}(\vec{\omega}^{(3)},\xi^{(I)})}<x_D<\frac{\varphi}{\sigma_{(3)}(\vec{\omega}^{(2)},\xi^{(I)})}\\ U^{(2)}, & \frac{\varphi}{\sigma_{(3)}(\vec{\omega}^{(2)},\xi^{(I)})}<x_D<\frac{\varphi}{\sigma_{(2)}(\vec{\omega}^{(2)},\xi^{(I)})}\\ U^{(2)-(1)}(x_D,\varphi), & \frac{\varphi}{\sigma_{(2)}(\vec{\omega}^{(2)},\xi^{(I)})}<x_D<\frac{\varphi}{\sigma_{(2)}(\vec{\omega}^{(1)},\xi^{(I)})}\\ U^{(1)}, & \frac{\varphi}{\sigma_{(2)}(\vec{\omega}^{(1)},\xi^{(I)})}<x_D<\frac{\varphi}{\sigma_{(1)}(\vec{\omega}^{(1)},\xi^{(I)})}\\ U^{(1)-(I+)}(x_D,\varphi), & \frac{\varphi}{\sigma_{(1)}(\vec{\omega}^{(1)},\xi^{(I)})}<x_D<\frac{\varphi}{\sigma_{(1)}(\vec{\omega}^{(I)},\xi^{(I)})}\\ U^{(I+)}, & \frac{\varphi}{\sigma_{(1)}(\vec{\omega}^{(I)},\xi^{(I)})}<x_D<+\infty\\ U^{(I)}, & x_D\to+\infty\end{cases}\tag{B.7}$$

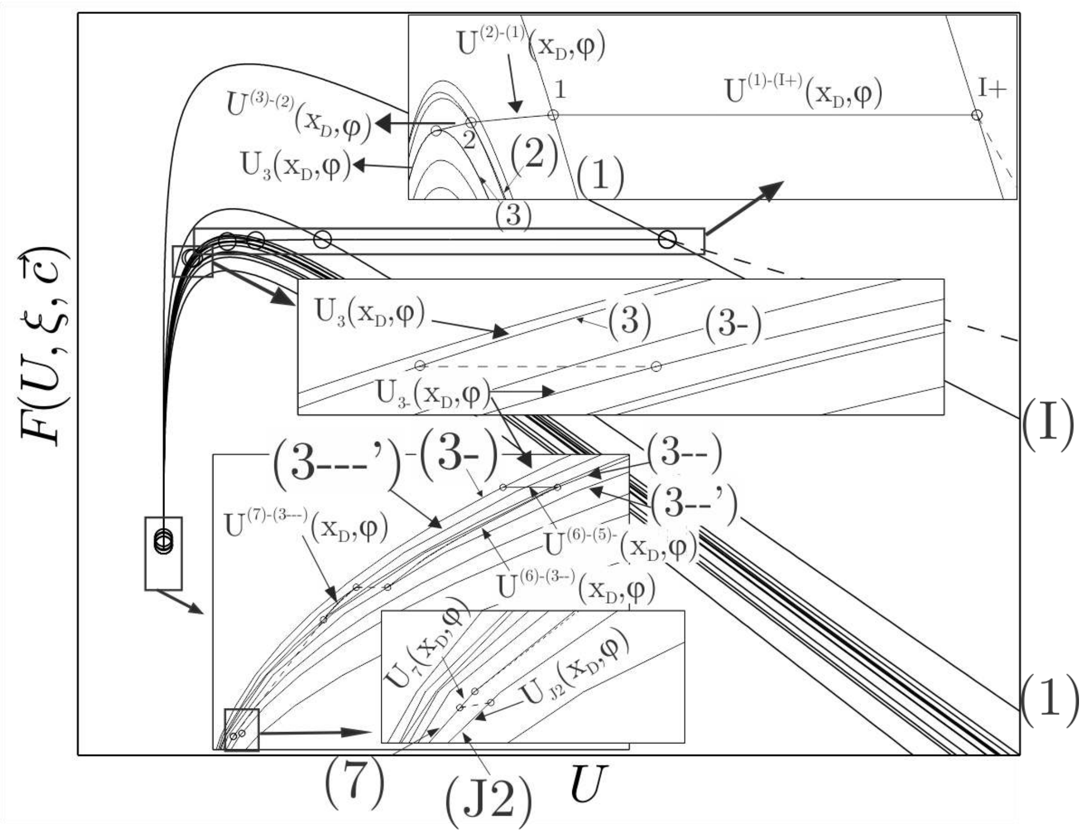

Figure B.6: Solution path of U_{VI} in $F\times U$ plane

$$U_{VII} = \begin{cases} U_{J2}(x_D, \varphi), & x_D < \frac{\varphi - \varphi_{HS}}{V_{pH}^{(2)}} \\ U_7(x_D, \varphi), & \frac{\varphi - \varphi_{HS}}{V_{pH}^{(2)}} < x_D < \frac{\varphi}{V_{(pH)}^{(1)}} \\ U^{(7)-(3---)}(x_D, \varphi), & \frac{\varphi}{V_{(pH)}^{(1)}} < x_D < \frac{\varphi}{\sigma_{pH}(\xi^{(I)})} \\ U_{3---}(x_D, \varphi), & \frac{\varphi}{\sigma_{pH}(\xi^{(I)})} < x_D < x_{(3)}^{-} \\ U_{3--}(x_D, \varphi), & x_{(3)}^{-} < x_D < x_{(6)-(5)}^{-(+)}(\varphi) \\ U^{(6)-(5)-}(x_D, \varphi), & x_{(6)-(5)}^{-(+)}(\varphi) < x_D < x_{(6)-(5)}^{-(-)}(\varphi) \\ U_{3-}(x_D, \varphi), & x_{(6)-(5)}^{-(-)}(\varphi) < x_D < x_{(1)}^{-}(\varphi) \\ U_3(x_D, \varphi), & x_{(1)}^{-}(\varphi) < x_D < \frac{\varphi}{\sigma_{(3)}(\vec{\omega}^{(3)}, \xi^{(I)})} \\ U^{(3)-(2)}(x_D, \varphi), & \frac{\varphi}{\sigma_{(3)}(\vec{\omega}^{(3)}, \xi^{(I)})} < x_D < \frac{\varphi}{\sigma_{(3)}(\vec{\omega}^{(2)}, \xi^{(I)})} \\ U^{(2)}, & \frac{\varphi}{\sigma_{(3)}(\vec{\omega}^{(2)}, \xi^{(I)})} < x_D < \frac{\varphi}{\sigma_{(2)}(\vec{\omega}^{(2)}, \xi^{(I)})} \\ U^{(2)-(1)}(x_D, \varphi), & \frac{\varphi}{\sigma_{(2)}(\vec{\omega}^{(2)}, \xi^{(I)})} < x_D < \frac{\varphi}{\sigma_{(2)}(\vec{\omega}^{(1)}, \xi^{(I)})} \\ U^{(1)}, & \frac{\varphi}{\sigma_{(2)}(\vec{\omega}^{(1)}, \xi^{(I)})} < x_D < \frac{\varphi}{\sigma_{(1)}(\vec{\omega}^{(1)}, \xi^{(I)})} \\ U^{(1)-(I+)}(x_D, \varphi), & \frac{\varphi}{\sigma_{(1)}(\vec{\omega}^{(1)}, \xi^{(I)})} < x_D < \frac{\varphi}{\sigma_{(1)}(\vec{\omega}^{(I)}, \xi^{(I)})} \\ U^{(I+)}, & \frac{\varphi}{\sigma_{(1)}(\vec{\omega}^{(I)}, \xi^{(I)})} < x_D < +\infty \\ U^{(I)}, & x_D \to +\infty \end{cases} \tag{B.8}$$

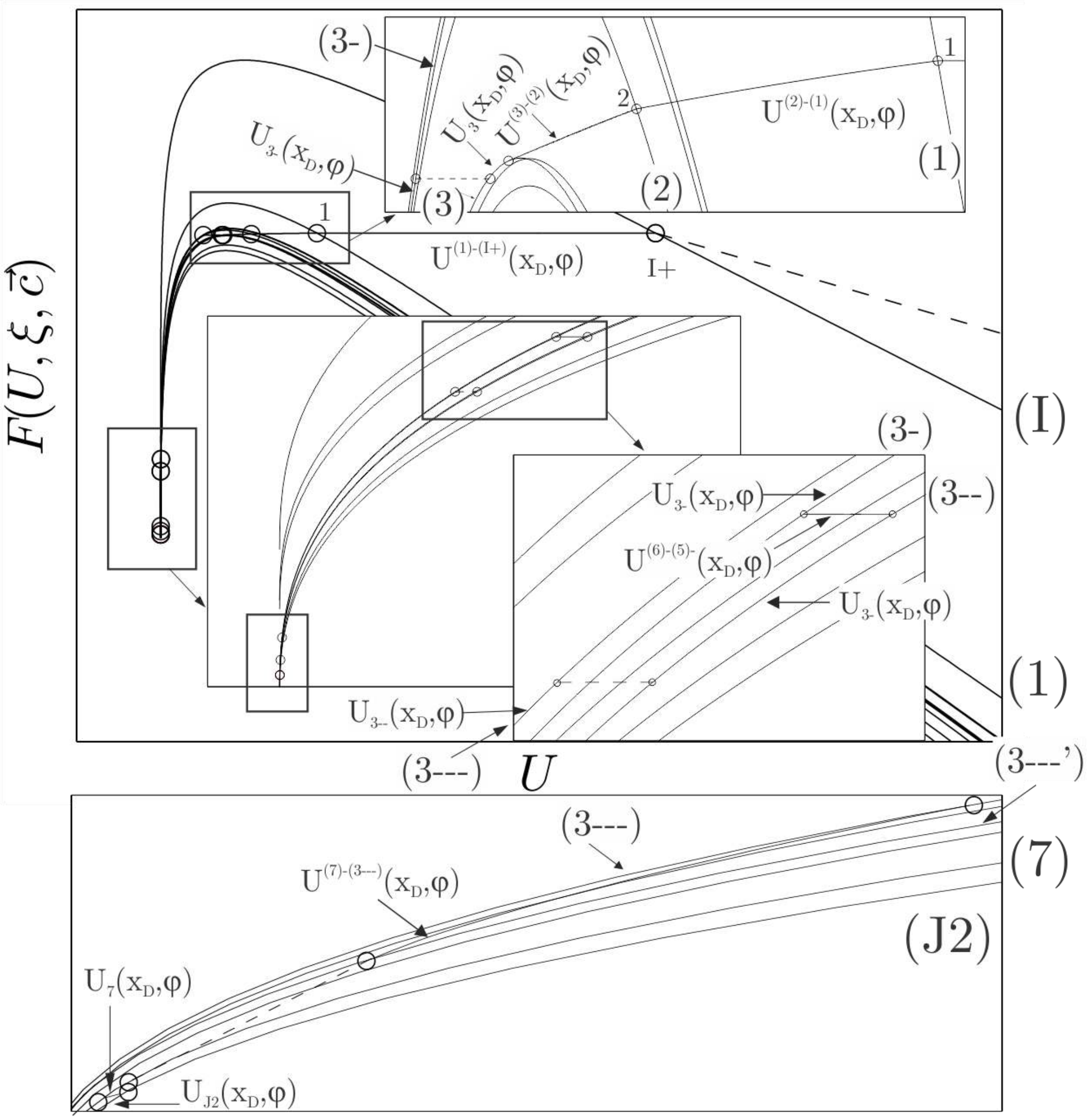

Figure B.7: Solution path of U_{VII} in $F \times U$ plane

$$U_{VIII} = \begin{cases} U_{J2}(x_D,\varphi), & x_D < \frac{\varphi-\varphi_{HS}}{V_{pH}^{(2)}} \\ U_7(x_D,\varphi), & \frac{\varphi-\varphi_{HS}}{V_{pH}^{(2)}} < x_D < \frac{\varphi}{V_{(pH)}^{(1)}} \\ U^{(7)-(3---)}(x_D,\varphi), & \frac{\varphi}{V_{(pH)}^{(1)}} < x_D < \frac{\varphi}{\sigma_{pH}(\xi^{(I)})} \\ U_{3---}(x_D,\varphi), & \frac{\varphi}{\sigma_{pH}(\xi^{(I)})} < x_D < x_{(3)}^{-} \\ U_{3--}(x_D,\varphi), & x_{(3)}^{-} < x_D < x_{(6)-(5)}^{-(+)}(\varphi) \\ U^{(6)-(5)-}(x_D,\varphi), & x_{(6)-(5)}^{-(+)}(\varphi) < x_D < x_{(6)-(5)}^{-(-)}(\varphi) \\ U_{3-}(x_D,\varphi), & x_{(6)-(5)}^{-(-)}(\varphi) < x_D < x_{(3)-(2)}^{-(+)}(\varphi) \\ U^{(3)-(2)-}(x_D,\varphi), & x_{(3)-(2)}^{-(+)}(\varphi) < x_D < x_{(1)}^{--}(\varphi) \\ U^{(3)-(2)}(x_D,\varphi), & x_{(1)}^{--}(\varphi) < x_D < \frac{\varphi}{\sigma_{(3)}(\overrightarrow{\omega}^{(2)},\xi^{(I)})} \\ U^{(2)}, & \frac{\varphi}{\sigma_{(3)}(\overrightarrow{\omega}^{(2)},\xi^{(I)})} < x_D < \frac{\varphi}{\sigma_{(2)}(\overrightarrow{\omega}^{(2)},\xi^{(I)})} \\ U^{(2)-(1)}(x_D,\varphi), & \frac{\varphi}{\sigma_{(2)}(\overrightarrow{\omega}^{(2)},\xi^{(I)})} < x_D < \frac{\varphi}{\sigma_{(2)}(\overrightarrow{\omega}^{(1)},\xi^{(I)})} \\ U^{(1)}, & \frac{\varphi}{\sigma_{(2)}(\overrightarrow{\omega}^{(1)},\xi^{(I)})} < x_D < \frac{\varphi}{\sigma_{(1)}(\overrightarrow{\omega}^{(1)},\xi^{(I)})} \\ U^{(1)-(I+)}(x_D,\varphi), & \frac{\varphi}{\sigma_{(1)}(\overrightarrow{\omega}^{(1)},\xi^{(I)})} < x_D < \frac{\varphi}{\sigma_{(1)}(\overrightarrow{\omega}^{(I)},\xi^{(I)})} \\ U^{(I+)}, & \frac{\varphi}{\sigma_{(1)}(\overrightarrow{\omega}^{(I)},\xi^{(I)})} < x_D < +\infty \\ U^{(I)}, & x_D \to +\infty \end{cases} \tag{B.9}$$

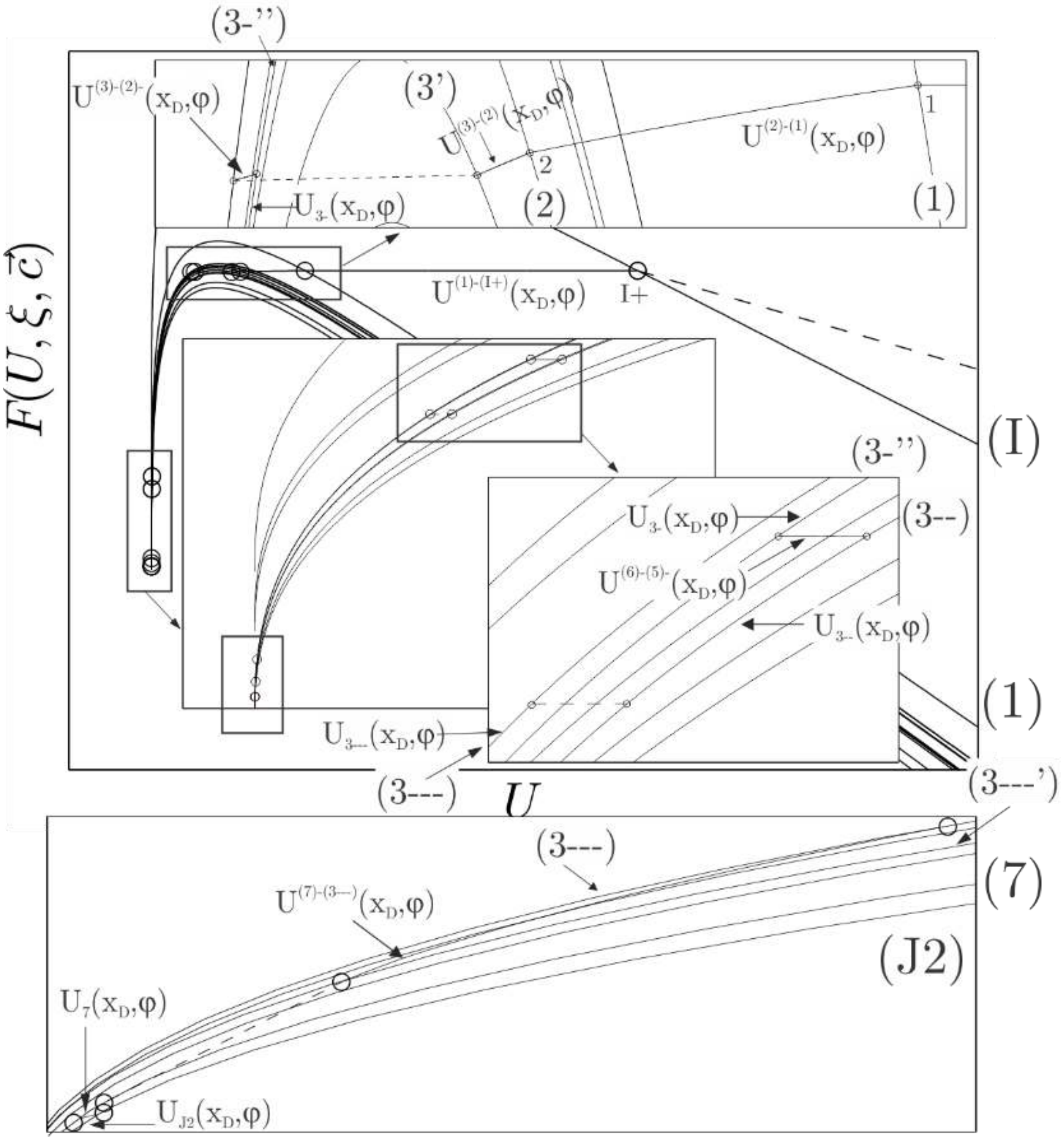

Figure B.8: Solution path of U_{VIII} in $F \times U$ plane

$$U_{IX} = \begin{cases} U_{J2}(x_D, \varphi), & x_D < \frac{\varphi - \varphi_{HS}}{V_{pH}^{(2)}} \\ U_7(x_D, \varphi), & \frac{\varphi - \varphi_{HS}}{V_{pH}^{(2)}} < x_D < \frac{\varphi}{V_{(pH)}^{(1)}} \\ U^{(7)-(3---)}(x_D, \varphi), & \frac{\varphi}{V_{(pH)}^{(1)}} < x_D < \frac{\varphi}{\sigma_{pH}(\xi^{(I)})} \\ U_{3---}(x_D, \varphi), & \frac{\varphi}{\sigma_{pH}(\xi^{(I)})} < x_D < x_{(3)}^{-} \\ U_{3--}(x_D, \varphi), & x_{(3)}^{-} < x_D < x_{(6)-(5)}^{-(+)}(\varphi) \\ U^{(6)-(5)-}(x_D, \varphi), & x_{(6)-(5)}^{-(+)}(\varphi) < x_D < x_{(6)-(5)}^{-(-)}(\varphi) \\ U_{3-}(x_D, \varphi), & x_{(6)-(5)}^{-(-)}(\varphi) < x_D < x_{(3)-(2)}^{-(+)}(\varphi) \\ U^{(3)-(2)-}(x_D, \varphi), & x_{(3)-(2)}^{-(+)}(\varphi) < x_D < x_{(3)-(2)}^{-(-)}(\varphi) \\ U^{(2-)}, & x_{(3)-(2)}^{-(-)}(\varphi) < x_D < x_{(1)}^{--}(\varphi) \\ U^{(2)}, & x_{(1)}^{--}(\varphi) < x_D < \frac{\varphi}{\sigma_{(2)}(\overrightarrow{\omega}^{(2)}, \xi^{(I)})} \\ U^{(2)-(1)}(x_D, \varphi), & \frac{\varphi}{\sigma_{(2)}(\overrightarrow{\omega}^{(2)}, \xi^{(I)})} < x_D < \frac{\varphi}{\sigma_{(2)}(\overrightarrow{\omega}^{(1)}, \xi^{(I)})} \\ U^{(1)}, & \frac{\varphi}{\sigma_{(2)}(\overrightarrow{\omega}^{(1)}, \xi^{(I)})} < x_D < \frac{\varphi}{\sigma_{(1)}(\overrightarrow{\omega}^{(1)}, \xi^{(I)})} \\ U^{(1)-(I+)}(x_D, \varphi), & \frac{\varphi}{\sigma_{(1)}(\overrightarrow{\omega}^{(1)}, \xi^{(I)})} < x_D < \frac{\varphi}{\sigma_{(1)}(\overrightarrow{\omega}^{(I)}, \xi^{(I)})} \\ U^{(I+)}, & \frac{\varphi}{\sigma_{(1)}(\overrightarrow{\omega}^{(I)}, \xi^{(I)})} < x_D < +\infty \\ U^{(I)}, & x_D \to +\infty \end{cases} \tag{B.10}$$

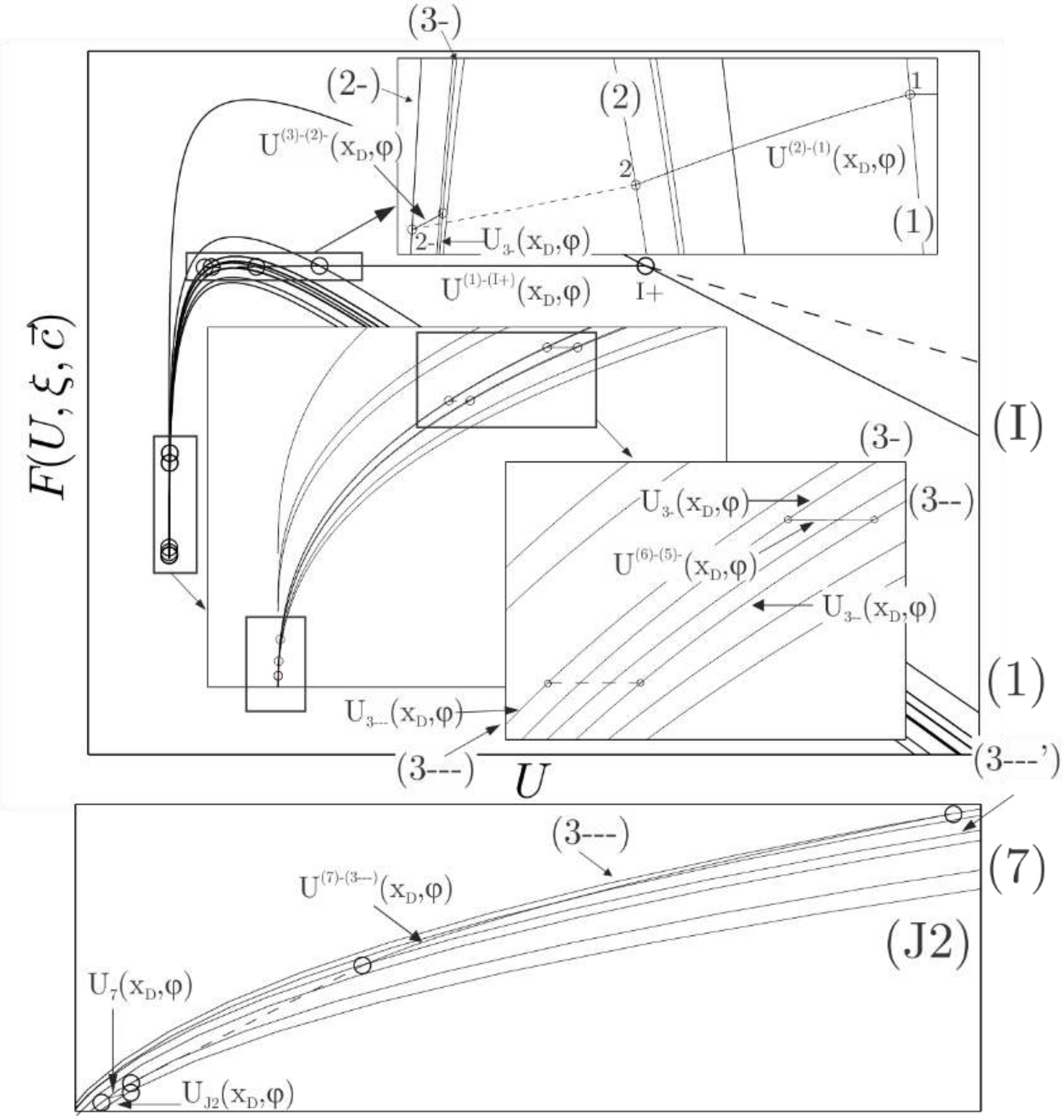

Figure B.9: Solution path of U_{IX} in $F \times U$ plane

$$
U_X = \begin{cases} U_{J2}(x_D,\varphi), & x_D < \frac{\varphi-\varphi_{HS}}{V_{pH}^{(2)}} \\ U_7(x_D,\varphi), & \frac{\varphi-\varphi_{HS}}{V_{pH}^{(2)}} < x_D < \frac{\varphi}{V_{(pH)}^{(1)}} \\ U^{(7)-(3---)}(x_D,\varphi), & \frac{\varphi}{V_{(pH)}^{(1)}} < x_D < \frac{\varphi}{\sigma_{pH}(\xi^{(I)})} \\ U_{3---}(x_D,\varphi), & \frac{\varphi}{\sigma_{pH}(\xi^{(I)})} < x_D < x_{(3)}^{-} \\ U_{3--}(x_D,\varphi), & x_{(3)}^{-} < x_D < x_{(6)-(5)}^{-(+)}(\varphi) \\ U^{(6)-(5)-}(x_D,\varphi), & x_{(6)-(5)}^{-(+)}(\varphi) < x_D < x_{(6)-(5)}^{-(-)}(\varphi) \\ U_{3-}(x_D,\varphi), & x_{(6)-(5)}^{-(-)}(\varphi) < x_D < x_{(3)-(2)}^{-(+)}(\varphi) \\ U^{(3)-(2)-}(x_D,\varphi), & x_{(3)-(2)}^{-(+)}(\varphi) < x_D < x_{(3)-(2)}^{-(-)}(\varphi) \\ U^{(2-)}, & x_{(3)-(2)}^{-(-)}(\varphi) < x_D < x_{(2)-(1)}^{-(+)}(\varphi) \\ U^{(2)-(1)-}, & x_{(2)-(1)}^{-(+)}(\varphi) < x_D < x_{(1)}^{---}(\varphi) \\ U^{(2)-(1)}(x_D,\varphi), & x_{(1)}^{---}(\varphi) < x_D < \frac{\varphi}{\sigma_{(2)}(\vec{\omega}^{(1)},\xi^{(I)})} \\ U^{(1)}, & \frac{\varphi}{\sigma_{(2)}(\vec{\omega}^{(1)},\xi^{(I)})} < x_D < \frac{\varphi}{\sigma_{(1)}(\vec{\omega}^{(1)},\xi^{(I)})} \\ U^{(1)-(I+)}(x_D,\varphi), & \frac{\varphi}{\sigma_{(1)}(\vec{\omega}^{(1)},\xi^{(I)})} < x_D < \frac{\varphi}{\sigma_{(1)}(\vec{\omega}^{(I)},\xi^{(I)})} \\ U^{(I+)}, & \frac{\varphi}{\sigma_{(1)}(\vec{\omega}^{(I)},\xi^{(I)})} < x_D < +\infty \end{cases} \tag{B.11}
$$

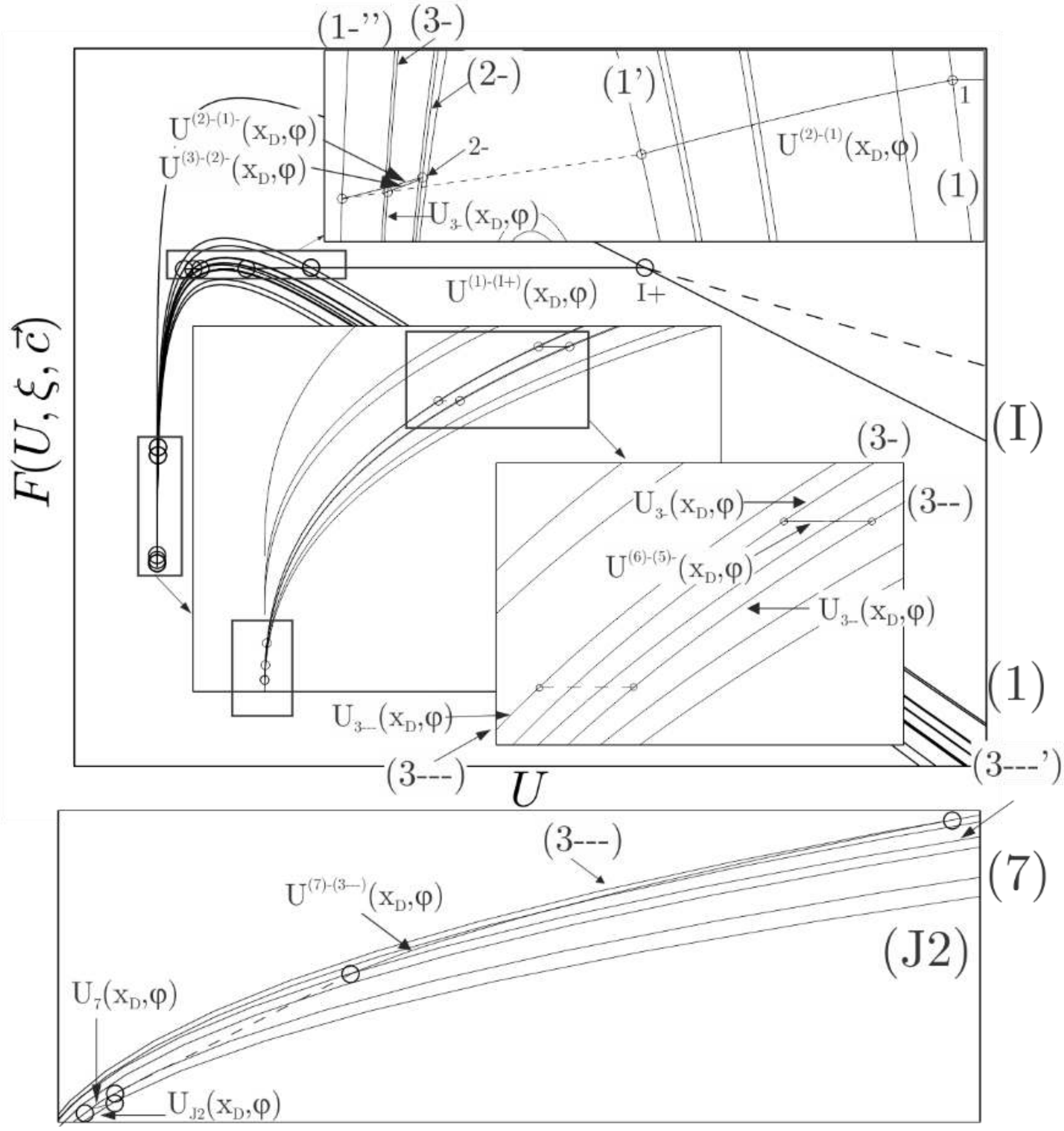

Figure B.10: Solution path of U_X in $F \times U$ plane

$$U_{XI}=\begin{cases} U_{J2}(x_D,\varphi), & x_D<\frac{\varphi-\varphi_{HS}}{V_{pH}^{(2)}} \\ U_7(x_D,\varphi), & \frac{\varphi-\varphi_{HS}}{V_{pH}^{(2)}}<x_D<\frac{\varphi}{V_{(pH)}^{(1)}} \\ U^{(7)-(3---)}(x_D,\varphi), & \frac{\varphi}{V_{(pH)}^{(1)}}<x_D<\frac{\varphi}{\sigma_{pH}(\xi^{(I)})} \\ U_{3---}(x_D,\varphi), & \frac{\varphi}{\sigma_{pH}(\xi^{(I)})}<x_D<x_{(3)}^{-} \\ U_{3--}(x_D,\varphi), & x_{(3)}^{-}<x_D<x_{(6)-(5)}^{-(+)}(\varphi) \\ U^{(6)-(5)-}(x_D,\varphi), & x_{(6)-(5)}^{-(+)}(\varphi)<x_D<x_{(6)-(5)}^{-(-)}(\varphi) \\ U_{3-}(x_D,\varphi), & x_{(6)-(5)}^{-(-)}(\varphi)<x_D<x_{(3)-(2)}^{-(+)}(\varphi) \\ U^{(3)-(2)-}(x_D,\varphi), & x_{(3)-(2)}^{-(+)}(\varphi)<x_D<x_{(3)-(2)}^{-(-)}(\varphi) \\ U^{(2-)}, & x_{(3)-(2)}^{-(-)}(\varphi)<x_D<x_{(2)-(1)}^{-(+)}(\varphi) \\ U^{(2)-(1)-}, & x_{(2)-(1)}^{-(+)}(\varphi)<x_D<x_{(2)-(1)}^{-(-)}(\varphi) \\ U^{(1-)}, & x_{(2)-(1)}^{-(-)}(\varphi)<x_D<x_{(1)}^{---}(\varphi) \\ U^{(1)}, & x_{(1)}^{---}(\varphi)<x_D<\frac{\varphi}{\sigma_{(1)}(\vec{\omega}^{(1)},\xi^{(I)})} \\ U^{(1)-(I+)}(x_D,\varphi), & \frac{\varphi}{\sigma_{(1)}(\vec{\omega}^{(1)},\xi^{(I)})}<x_D<\frac{\varphi}{\sigma_{(1)}(\vec{\omega}^{(I)},\xi^{(I)})} \\ U^{(I+)}, & \frac{\varphi}{\sigma_{(1)}(\vec{\omega}^{(I)},\xi^{(I)})}<x_D<+\infty \\ U^{(I)} & x_D\to+\infty \end{cases} \qquad \text{(B.12)}$$

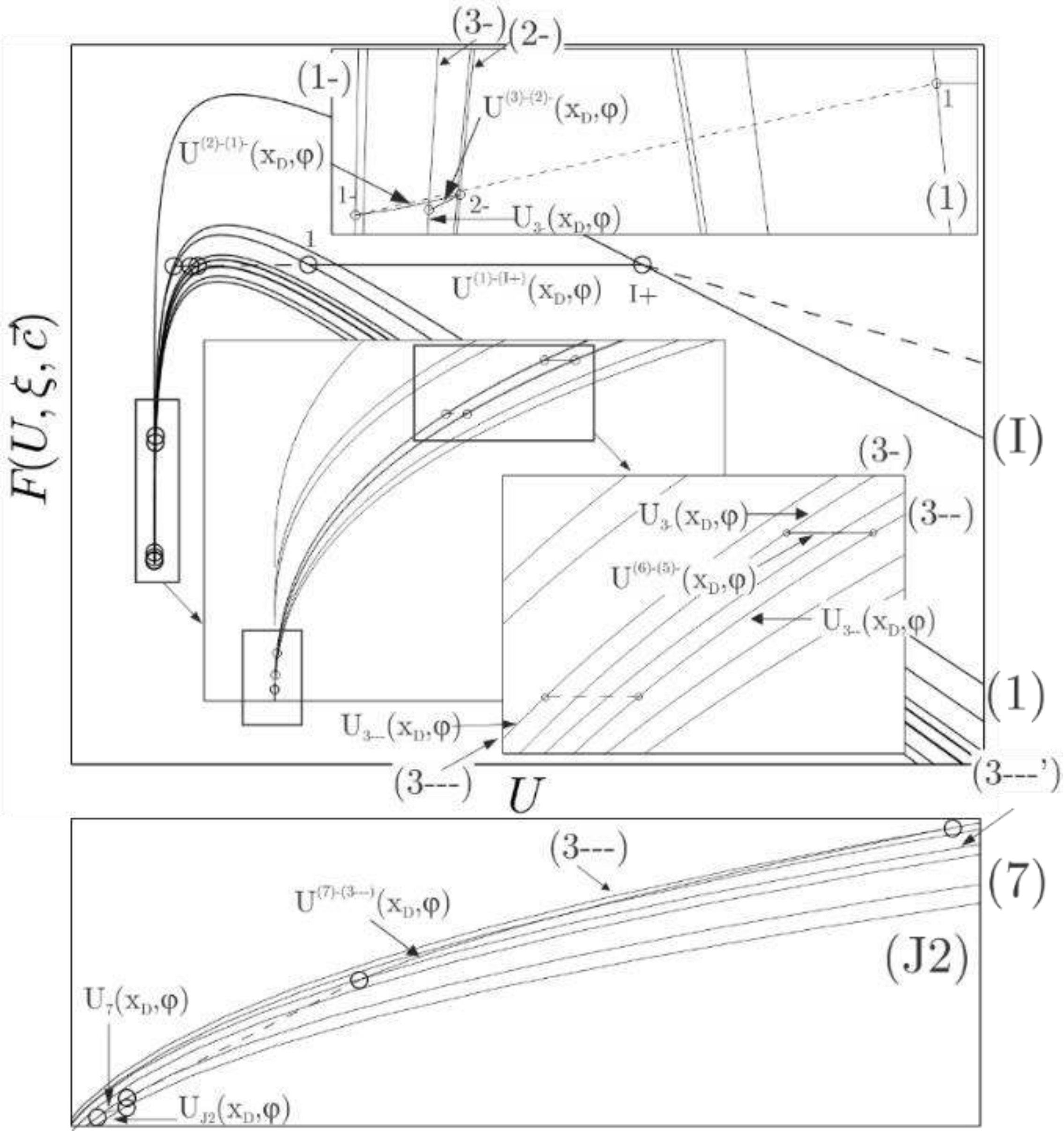

Figure B.11: Solution path of U_{XI} in $F \times U$ plane

$$U_{XII} = \begin{cases} U_{J2}(x_D, \varphi), & x_D < x_{pH}^{-}(\varphi) \\ U^{(7)-(3---)}(x_D, \varphi), & x_{pH}^{-}(\varphi) < x_D < \frac{\varphi}{\sigma_{pH}(\xi^{(I)})} \\ U_{3---}(x_D, \varphi), & \frac{\varphi}{\sigma_{pH}(\xi^{(I)})} < x_D < x_{(3)}^{-} \\ U_{3--}(x_D, \varphi), & x_{(3)}^{-} < x_D < x_{(6)-(5)}^{-(+)}(\varphi) \\ U^{(6)-(5)-}(x_D, \varphi), & x_{(6)-(5)}^{-(+)}(\varphi) < x_D < x_{(6)-(5)}^{-(-)}(\varphi) \\ U_{3-}(x_D, \varphi), & x_{(6)-(5)}^{-(-)}(\varphi) < x_D < x_{(3)-(2)}^{-(+)}(\varphi) \\ U^{(3)-(2)-}(x_D, \varphi), & x_{(3)-(2)}^{-(+)}(\varphi) < x_D < x_{(3)-(2)}^{-(-)}(\varphi) \\ U^{(2-)}, & x_{(3)-(2)}^{-(-)}(\varphi) < x_D < x_{(2)-(1)}^{-(+)}(\varphi) \\ U^{(2)-(1)-}, & x_{(2)-(1)}^{-(+)}(\varphi) < x_D < x_{(2)-(1)}^{-(-)}(\varphi) \\ U^{(1-)}, & x_{(2)-(1)}^{-(-)}(\varphi) < x_D < x_{(1)}^{---}(\varphi) \\ U^{(1)}, & x_{(1)}^{---}(\varphi) < x_D < \frac{\varphi}{\sigma_{(1)}(\vec{\omega}^{(1)}, \xi^{(I)})} \\ U^{(1)-(I+)}(x_D, \varphi), & \frac{\varphi}{\sigma_{(1)}(\vec{\omega}^{(1)}, \xi^{(I)})} < x_D < \frac{\varphi}{\sigma_{(1)}(\vec{\omega}^{(I)}, \xi^{(I)})} \\ U^{(I+)}, & \frac{\varphi}{\sigma_{(1)}(\vec{\omega}^{(I)}, \xi^{(I)})} < x_D < +\infty \\ U^{(I)}, & x_D \to +\infty \end{cases} \tag{B.13}$$

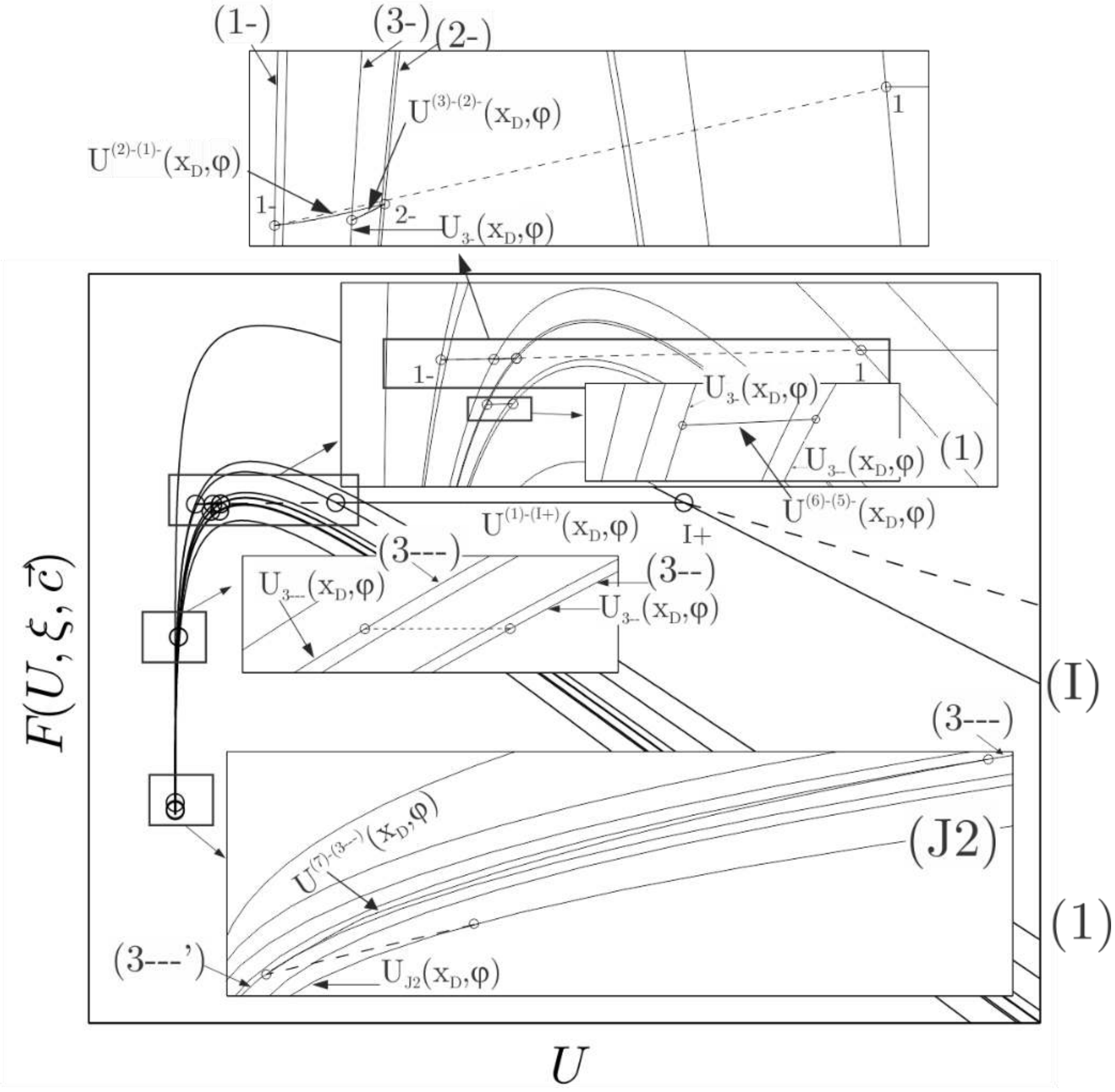

Figure B.12: Solution path of U_{XII} in $F \times U$ plane

$$U_{XIII} = \begin{cases} U_{J2}(x_D, \varphi), & x_D < x_{pH}^{-}(\varphi) \\ U^{(7)-(3---)}(x_D, \varphi), & x_{pH}^{-}(\varphi) < x_D < \frac{\varphi}{\sigma_{pH}(\xi^{(I)})} \\ U_{3---}(x_D, \varphi), & \frac{\varphi}{\sigma_{pH}(\xi^{(I)})} < x_D < x_{(3)}^{-} \\ U_{3--}(x_D, \varphi), & x_{(3)}^{-} < x_D < x_{(6)-(5)}^{-(+)}(\varphi) \\ U^{(6)-(5)-}(x_D, \varphi), & x_{(6)-(5)}^{-(+)}(\varphi) < x_D < x_{(3)-(2)}^{--(+)}(\varphi) \\ U^{(3)-(2)--}(x_D, \varphi), & x_{(3)-(2)}^{--(+)}(\varphi) < x_D < x_{(6)-(5)}^{-(-)}(\varphi) \\ U^{(3)-(2)-}(x_D, \varphi), & x_{(6)-(5)}^{-(-)}(\varphi) < x_D < x_{(3)-(2)}^{--(-)}(\varphi) \\ U^{(2-)}, & x_{(3)-(2)}^{--(-)}(\varphi) < x_D < x_{(2)-(1)}^{-(+)}(\varphi) \\ U^{(2)-(1)-}, & x_{(2)-(1)}^{-(+)}(\varphi) < x_D < x_{(2)-(1)}^{-(-)}(\varphi) \\ U^{(1-)}, & x_{(2)-(1)}^{-(-)}(\varphi) < x_D < x_{(1)}^{---}(\varphi) \\ U^{(1)}, & x_{(1)}^{---}(\varphi) < x_D < \frac{\varphi}{\sigma_{(1)}(\vec{\omega}^{(1)}, \xi^{(I)})} \\ U^{(1)-(I+)}(x_D, \varphi), & \frac{\varphi}{\sigma_{(1)}(\vec{\omega}^{(1)}, \xi^{(I)})} < x_D < \frac{\varphi}{\sigma_{(1)}(\vec{\omega}^{(I)}, \xi^{(I)})} \\ U^{(I+)}, & \frac{\varphi}{\sigma_{(1)}(\vec{\omega}^{(I)}, \xi^{(I)})} < x_D < +\infty \\ U^{(I)} & x_D \to +\infty \end{cases} \qquad \text{(B.14)}$$

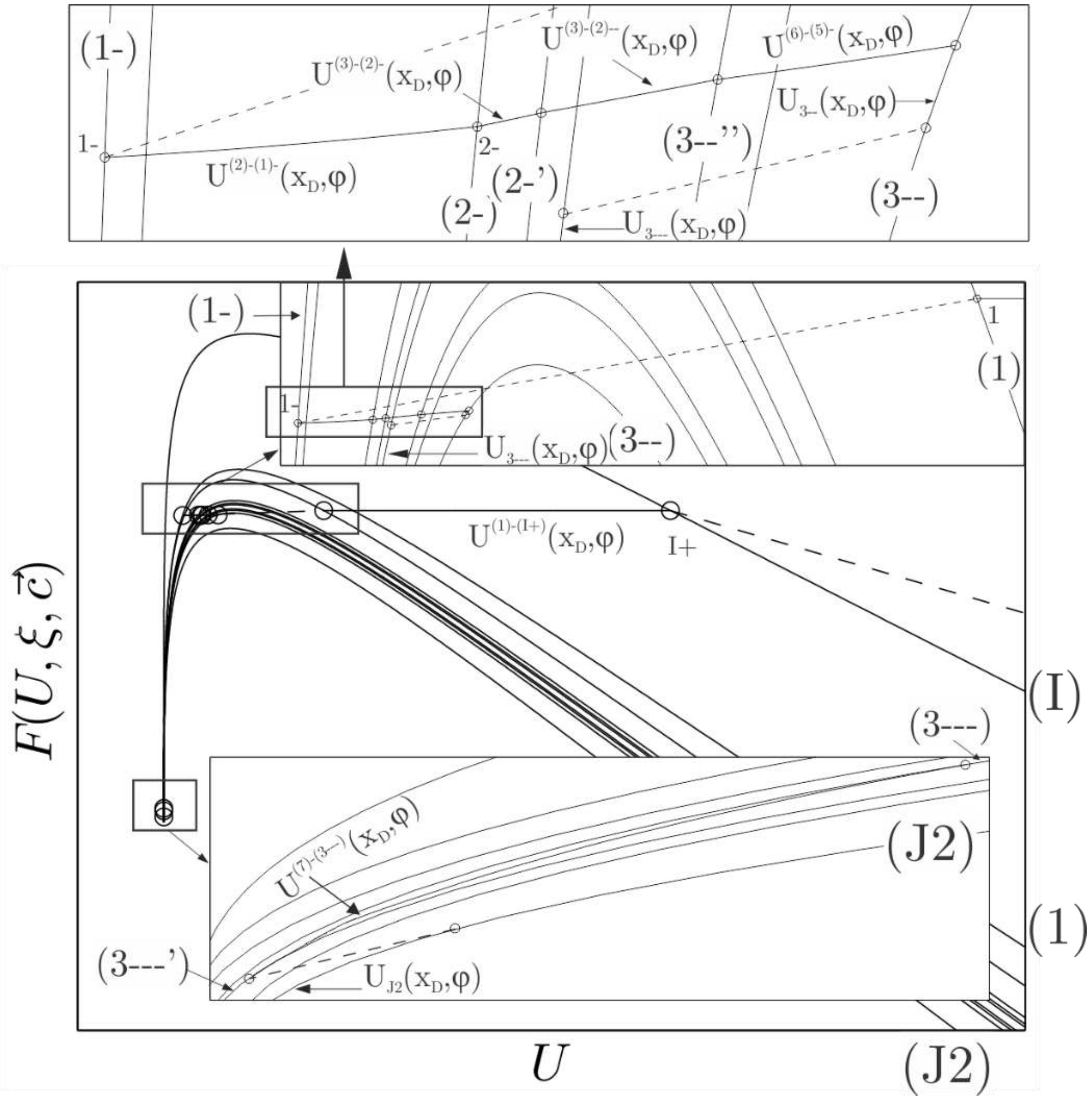

Figure B.13: Solution path of U_{XIII} in $F \times U$ plane

$$U_{XIV} = \begin{cases} U_{J2}(x_D, \varphi), & x_D < x_{pH}^{-}(\varphi) \\ U^{(7)-(3---)}(x_D, \varphi), & x_{pH}^{-}(\varphi) < x_D < \frac{\varphi}{\sigma_{pH}(\xi^{(I)})} \\ U_{3---}(x_D, \varphi), & \frac{\varphi}{\sigma_{pH}(\xi^{(I)})} < x_D < x_{(3)}^{-} \\ U_{3--}(x_D, \varphi), & x_{(3)}^{-} < x_D < x_{(6)-(5)}^{-(+)}(\varphi) \\ U^{(6)-(5)-}(x_D, \varphi), & x_{(6)-(5)}^{-(+)}(\varphi) < x_D < x_{(3)-(2)}^{--(+)}(\varphi) \\ U^{(3)-(2)--}(x_D, \varphi), & x_{(3)-(2)}^{--(+)}(\varphi) < x_D < x_{(3)-(2)}^{--(-)}(\varphi) \\ U^{(6)-(5)--}(x_D, \varphi), & x_{(3)-(2)}^{--(-)}(\varphi) < x_D < x_{(6)-(5)}^{--(-)}(\varphi) \\ U^{(2-)}, & x_{(6)-(5)}^{--(-)}(\varphi) < x_D < x_{(2)-(1)}^{-(+)}(\varphi) \\ \vec{U}^{(2)-(1)-}, & x_{(2)-(1)}^{-(+)}(\varphi) < x_D < x_{(2)-(1)}^{-(-)}(\varphi) \\ U^{(1-)}, & x_{(2)-(1)}^{-(-)}(\varphi) < x_D < x_{(1)}^{---}(\varphi) \\ U^{(1)}, & x_{(1)}^{---}(\varphi) < x_D < \frac{\varphi}{\sigma_{(1)}(\vec{\omega}^{(1)}, \xi^{(I)})} \\ U^{(1)-(I+)}(x_D, \varphi), & \frac{\varphi}{\sigma_{(1)}(\vec{\omega}^{(1)}, \xi^{(I)})} < x_D < \frac{\varphi}{\sigma_{(1)}(\vec{\omega}^{(I)}, \xi^{(I)})} \\ U^{(I+)}, & \frac{\varphi}{\sigma_{(1)}(\vec{\omega}^{(I)}, \xi^{(I)})} < x_D < +\infty \\ U^{(I)}, & x_D \to +\infty \end{cases} \tag{B.15}$$

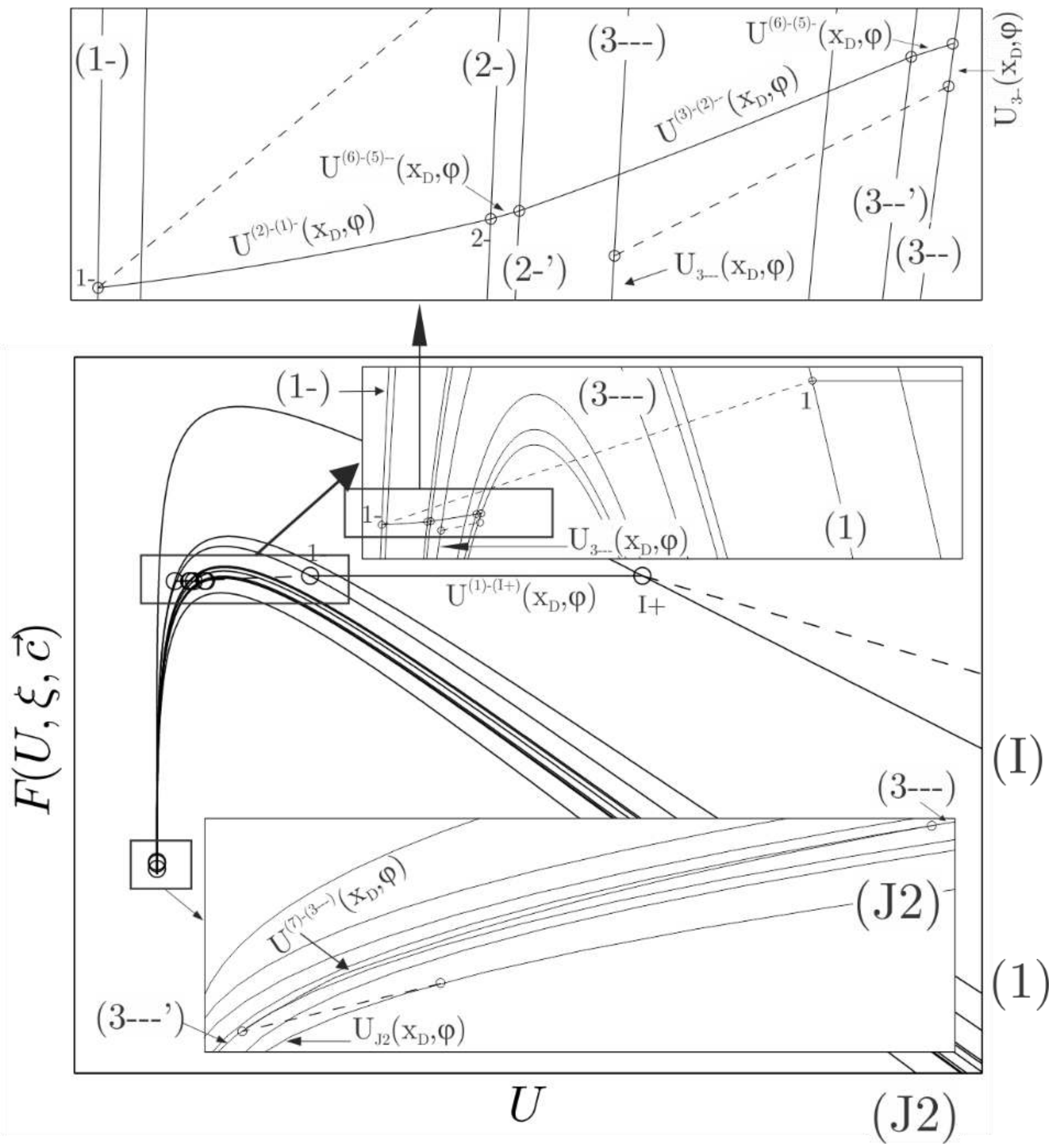

Figure B.14: Solution path of U_{XIV} in $F \times U$ plane

$$U_{XV} = \begin{cases} U_{J2}(x_D, \varphi), & x_D < x_{pH}^{-}(\varphi) \\ U^{(7)-(3---)}(x_D, \varphi), & x_{pH}^{-}(\varphi) < x_D < \frac{\varphi}{\sigma_{pH}(\xi^{(I)})} \\ U_{3---}(x_D, \varphi), & \frac{\varphi}{\sigma_{pH}(\xi^{(I)})} < x_D < x_{(3)}^{-} \\ U_{3--}(x_D, \varphi), & x_{(3)}^{-} < x_D < x_{(3)-(2)}^{--(+)}(\varphi) \\ U^{(3)-(2)---}(x_D, \varphi), & x_{(3)-(2)}^{--(+)}(\varphi) < x_D < x_{(6)-(5)}^{--(+)}(\varphi) \\ U^{(3)-(2)--}(x_D, \varphi), & x_{(6)-(5)}^{--(+)}(\varphi) < x_D < x_{(3)-(2)}^{--(-)}(\varphi) \\ U^{(6)-(5)--}(x_D, \varphi), & x_{(3)-(2)}^{--(-)}(\varphi) < x_D < x_{(6)-(5)}^{--(-)}(\varphi) \\ U^{(2-)}, & x_{(6)-(5)}^{--(-)}(\varphi) < x_D < x_{(2)-(1)}^{-(+)}(\varphi) \\ U^{(2)-(1)-}, & x_{(2)-(1)}^{-(+)}(\varphi) < x_D < x_{(2)-(1)}^{-(-)}(\varphi) \\ U^{(1-)}, & x_{(2)-(1)}^{-(-)}(\varphi) < x_D < x_{(1)}^{---}(\varphi) \\ U^{(1)}, & x_{(1)}^{---}(\varphi) < x_D < \frac{\varphi}{\sigma_{(1)}(\overrightarrow{\omega}^{(1)}, \xi^{(I)})} \\ U^{(1)-(I+)}(x_D, \varphi), & \frac{\varphi}{\sigma_{(1)}(\overrightarrow{\omega}^{(1)}, \xi^{(I)})} < x_D < \frac{\varphi}{\sigma_{(1)}(\overrightarrow{\omega}^{(I)}, \xi^{(I)})} \\ U^{(I+)}, & \frac{\varphi}{\sigma_{(1)}(\overrightarrow{\omega}^{(I)}, \xi^{(I)})} < x_D < +\infty \\ U^{(I)}, & x_D < +\infty \end{cases} \tag{B.16}$$

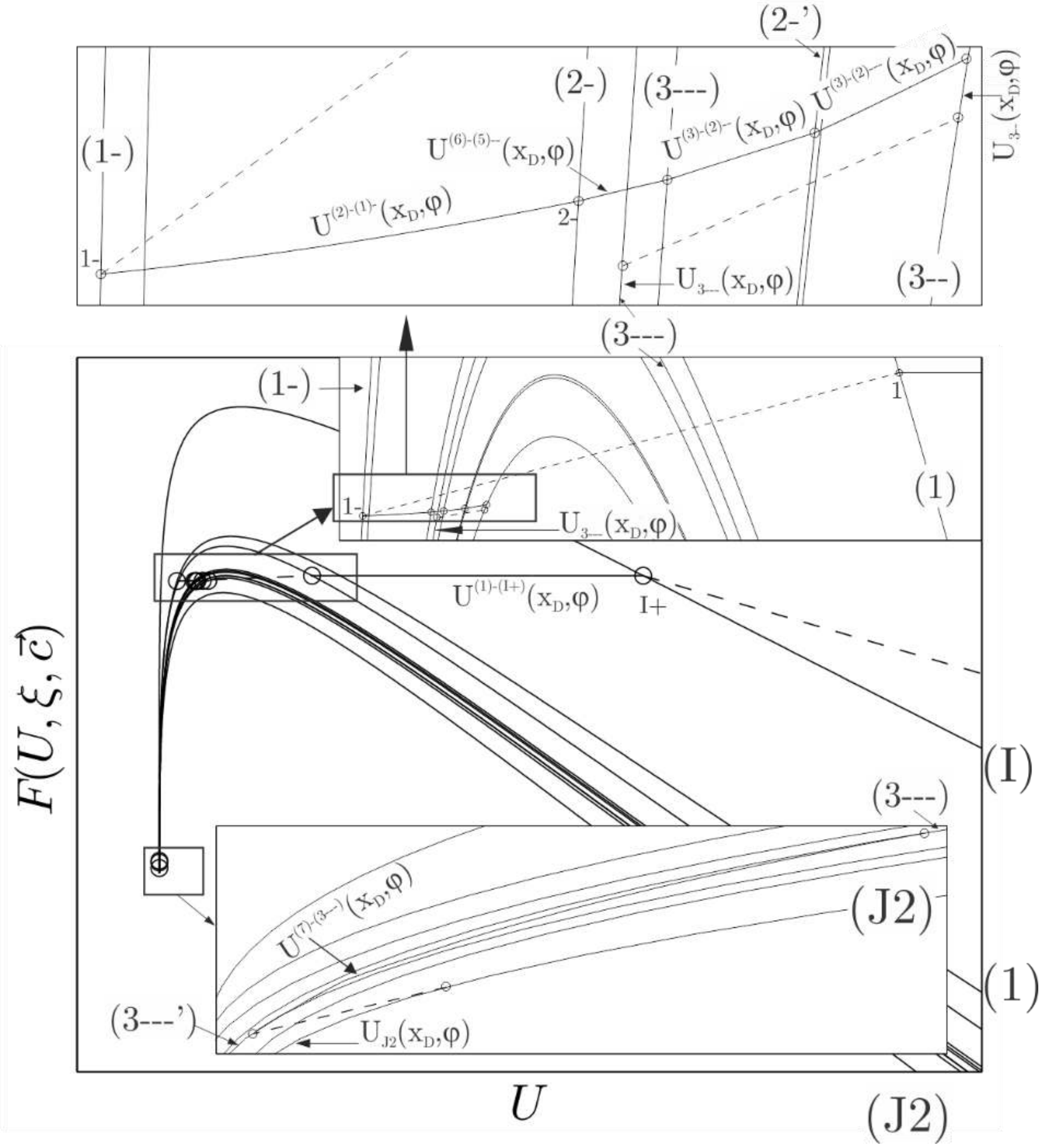

Figure B.15: Solution path of U_{XV} in $F \times U$ plane

$$U_{XVI} = \begin{cases} U_{J2}(x_D, \varphi), & x_D < x_{pH}^{-}(\varphi) \\ U^{(7)-(3---)}(x_D, \varphi), & x_{pH}^{-}(\varphi) < x_D < \frac{\varphi}{\sigma_{pH}(\xi^{(I)})} \\ U_{3---}(x_D, \varphi), & \frac{\varphi}{\sigma_{pH}(\xi^{(I)})} < x_D < x_{(3)}^{-} \\ U_{3--}(x_D, \varphi), & x_{(3)}^{-} < x_D < x_{(3)-(2)}^{--(+)}(\varphi) \\ U^{(3)-(2)---}(x_D, \varphi), & x_{(3)-(2)}^{--(+)}(\varphi) < x_D < x_{(3)-(2)}^{--(-)}(\varphi) \\ U^{(2--)}, & x_{(3)-(2)}^{--(-)}(\varphi) < x_D < x_{(6)-(5)}^{--(+)}(\varphi) \\ U^{(6)-(5)--}(x_D, \varphi), & x_{(6)-(5)}^{--(+)}(\varphi) < x_D < x_{(6)-(5)}^{--(-)}(\varphi) \\ U^{(2-)}, & x_{(6)-(5)}^{--(-)}(\varphi) < x_D < x_{(2)-(1)}^{-(+)}(\varphi) \\ U^{(2)-(1)-}, & x_{(2)-(1)}^{-(+)}(\varphi) < x_D < x_{(2)-(1)}^{-(-)}(\varphi) \\ U^{(1-)}, & x_{(2)-(1)}^{-(-)}(\varphi) < x_D < x_{(1)}^{---}(\varphi) \\ U^{(1)}, & x_{(1)}^{---}(\varphi) < x_D < \frac{\varphi}{\sigma_{(1)}(\vec{\omega}^{(1)}, \xi^{(I)})} \\ U^{(1)-(I+)}(x_D, \varphi), & \frac{\varphi}{\sigma_{(1)}(\vec{\omega}^{(1)}, \xi^{(I)})} < x_D < \frac{\varphi}{\sigma_{(1)}(\vec{\omega}^{(I)}, \xi^{(I)})} \\ U^{(I+)}, & \frac{\varphi}{\sigma_{(1)}(\vec{\omega}^{(I)}, \xi^{(I)})} < x_D < +\infty \\ U^{(I)}, & x_D \to +\infty \end{cases} \tag{B.17}$$

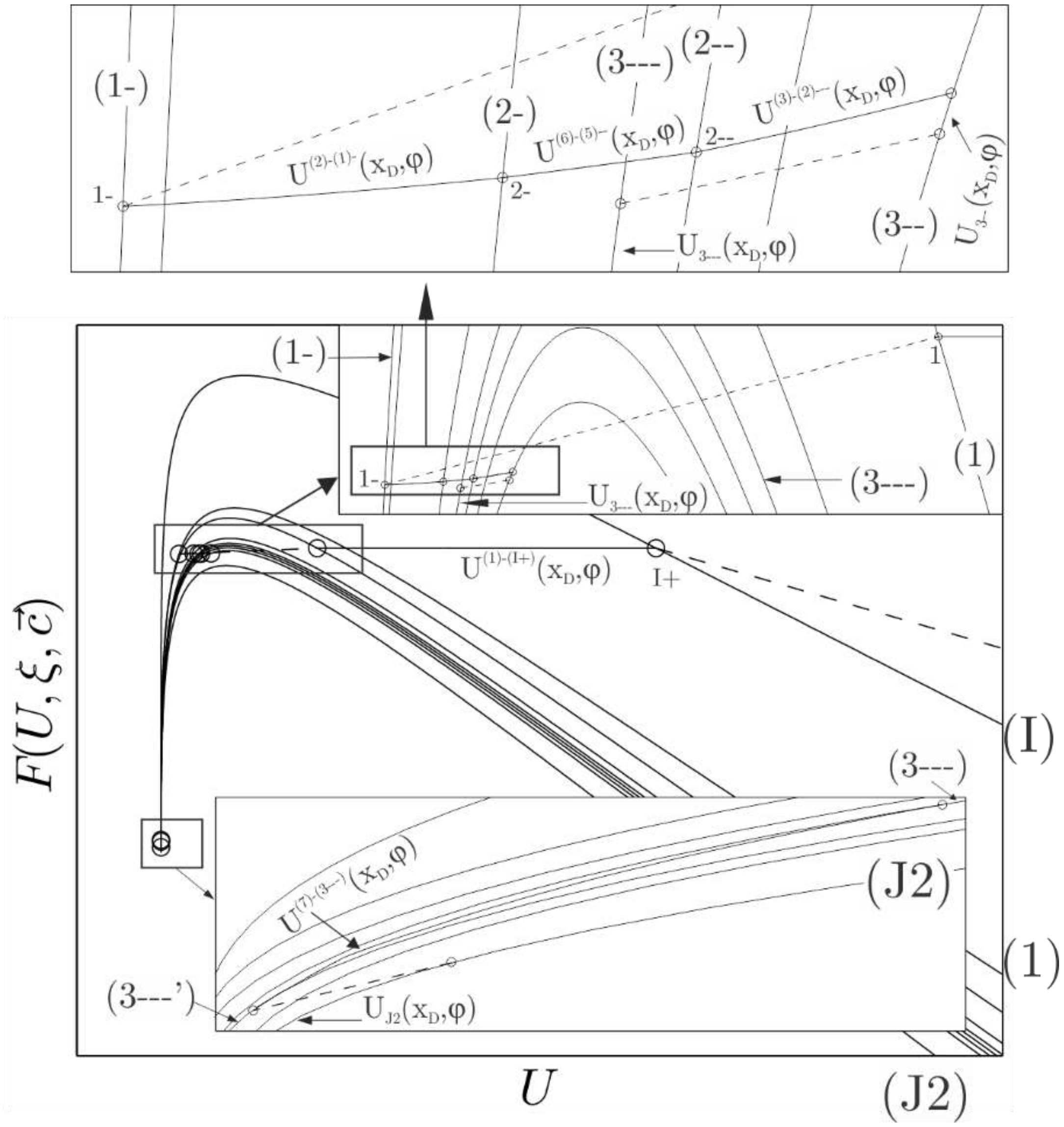

Figure B.16: Solution path of U_{XVI} in $F \times U$ plane

$$U_{XVII}=\begin{cases} U_{J2}(x_D,\varphi), & x_D<x_{pH}^{-}(\varphi)\\ U^{(7)-(3---)}(x_D,\varphi), & x_{pH}^{-}(\varphi)<x_D<\frac{\varphi}{\sigma_{pH}(\xi^{(I)})}\\ U_{3---}(x_D,\varphi), & \frac{\varphi}{\sigma_{pH}(\xi^{(I)})}<x_D<x_{(3)}^{--}\\ U^{(3)-(2)---}(x_D,\varphi), & x_{(3)}^{--}<x_D<x_{(3)-(2)}^{--(-)}(\varphi)\\ U^{(2--)}, & x_{(3)-(2)}^{--(-)}(\varphi)<x_D<x_{(6)-(5)}^{--(+)}(\varphi)\\ U^{(6)-(5)--}(x_D,\varphi), & x_{(6)-(5)}^{--(+)}(\varphi)<x_D<x_{(6)-(5)}^{--(-)}(\varphi)\\ U^{(2-)}, & x_{(6)-(5)}^{--(-)}(\varphi)<x_D<x_{(2)-(1)}^{-(+)}(\varphi)\\ U^{(2)-(1)-}, & x_{(2)-(1)}^{-(+)}(\varphi)<x_D<x_{(2)-(1)}^{-(-)}(\varphi)\\ U^{(1-)}, & x_{(2)-(1)}^{-(-)}(\varphi)<x_D<x_{(1)}^{---}(\varphi)\\ U^{(1)}, & x_{(1)}^{---}(\varphi)<x_D<\frac{\varphi}{\sigma_{(1)}(\vec{\omega}^{(1)},\xi^{(I)})}\\ U^{(1)-(I+)}(x_D,\varphi), & \frac{\varphi}{\sigma_{(1)}(\vec{\omega}^{(1)},\xi^{(I)})}<x_D<\frac{\varphi}{\sigma_{(1)}(\vec{\omega}^{(I)},\xi^{(I)})}\\ U^{(I+)}, & \frac{\varphi}{\sigma_{(1)}(\vec{\omega}^{(I)},\xi^{(I)})}<x_D<+\infty\\ U^{(I)}, & x_D\to+\infty \end{cases} \tag{B.18}$$

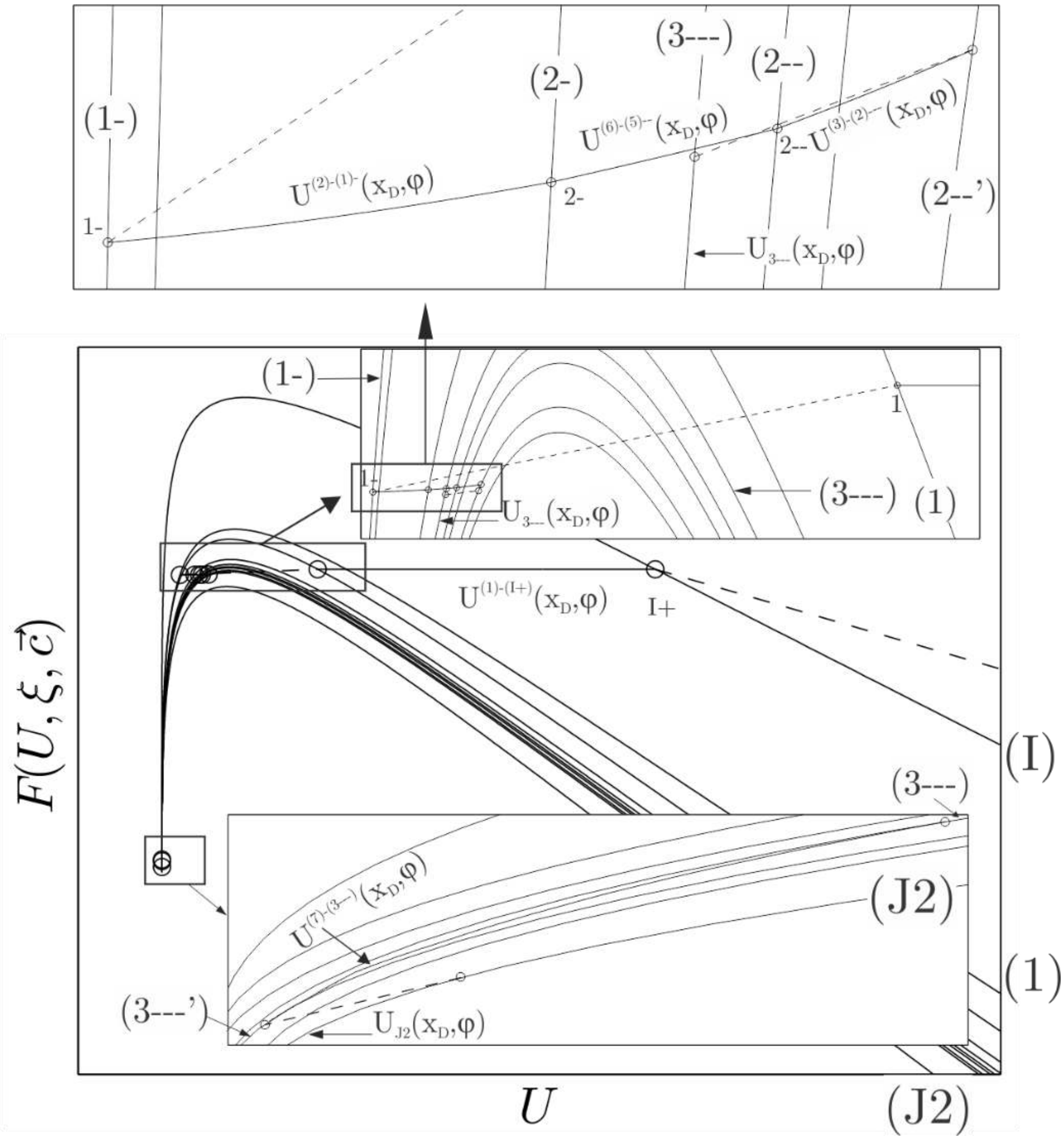

Figure B.17: Solution path of U_{XVII} in $F \times U$ plane

C. Solution in $x_D \times t_D$ plane

The solution in $x_D \times t_D$ plane is also divided in 17 regions:

$$s(x_D, t_D) = \begin{cases} s_I, & t_D < t_{HS} \\ s_{II}, & t_{HS} < t_D < t_A \\ s_{III}, & t_A < t_D < t_B \\ s_{IV}, & t_B < t_D < t_C \\ s_V, & t_C < t_D < t_d \\ s_{VI}, & t_d < t_D < t_E \\ s_{VII}, & t_E < t_D < t_F \\ s_{VIII}, & t_F < t_D < t_G \\ s_{IX}, & t_G < t_D < t_H \\ s_X, & t_H < t_D < t_I \\ s_{XI}, & t_I < t_D < t_{pH} \\ s_{XII}, & t_{pH} < t_D < t_J \\ s_{XIII}, & t_J < t_D < t_K \\ s_{XIV}, & t_K < t_D < t_L \\ s_{XV}, & t_L < t_D < t_M \\ s_{XVI}, & t_M < t_D < t_N \\ s_{XVII}, & t_N < t_D \end{cases} \tag{C.1}$$

The exact expression for each part of the solution is shown in equations (C.2)-(C.18). Water saturation profile, salinity profile, and solution path in $f \times s$ plane are presented in figures (C.1)-(C.51).

The self-similar part of the solution takes place when $t_D < t_{HS}$, solution s_I (Equation C.2).

$$s_I = \begin{cases} s_4(x_D, t_D), & x_D < D^{(1)}_{(pH)} t_D \\ s^{(4)-(3)}(x_D, t_D), & D^{(1)}_{(pH)} t_D < x_D < \lambda_{(pH)}\left(\xi^{(I)}\right) t_D \\ s_3(x_D, t_D), & \lambda_{(pH)}\left(\xi^{(I)}\right) t_D < x_D < \lambda_{(3)}\left(\vec{c}^{(3)}, \xi^{(I)}\right) t_D \\ s^{(3)-(2)}(x_D, t_D), & \lambda_{(3)}\left(\vec{c}^{(3)}, \xi^{(I)}\right) t_D < x_D < \lambda_{(3)}\left(\vec{c}^{(2)}, \xi^{(I)}\right) t_D \\ s^{(2)}, & \lambda_{(3)}\left(\vec{c}^{(2)}, \xi^{(I)}\right) t_D < x_D < \lambda_{(2)}\left(\vec{c}^{(2)}, \xi^{(I)}\right) t_D \\ s^{(2)-(1)}(x_D, t_D), & \lambda_{(2)}\left(\vec{c}^{(2)}, \xi^{(I)}\right) t_D < x_D < \lambda_{(2)}\left(\vec{c}^{(1)}, \xi^{(I)}\right) t_D \\ s^{(1)}, & \lambda_{(2)}\left(\vec{c}^{(1)}, \xi^{(I)}\right) t_D < x_D < \lambda_{(1)}\left(\vec{c}^{(1)}, \xi^{(I)}\right) t_D \\ s^{(1)-(I+)}(x_D, t_D), & \lambda_{(1)}\left(\vec{c}^{(1)}, \xi^{(I)}\right) t_D < x_D < \lambda_{(1)}\left(\vec{c}^{(I)}, \xi^{(I)}\right) t_D \\ s^{(I+)}, & \lambda_{(1)}\left(\vec{c}^{(I)}, \xi^{(I)}\right) t_D < x_D < D_{(s)} t_D \\ s^{(I)}, & x_D > D_{(s)} t_D \end{cases} \tag{C.2}$$

In figures (C.1)-(C.2) it is shown the saturation and salinity profiles. It is possible to note that the pH change plays an important role in water saturation solution. The solution path of s_I is depicted in figure (C.3).

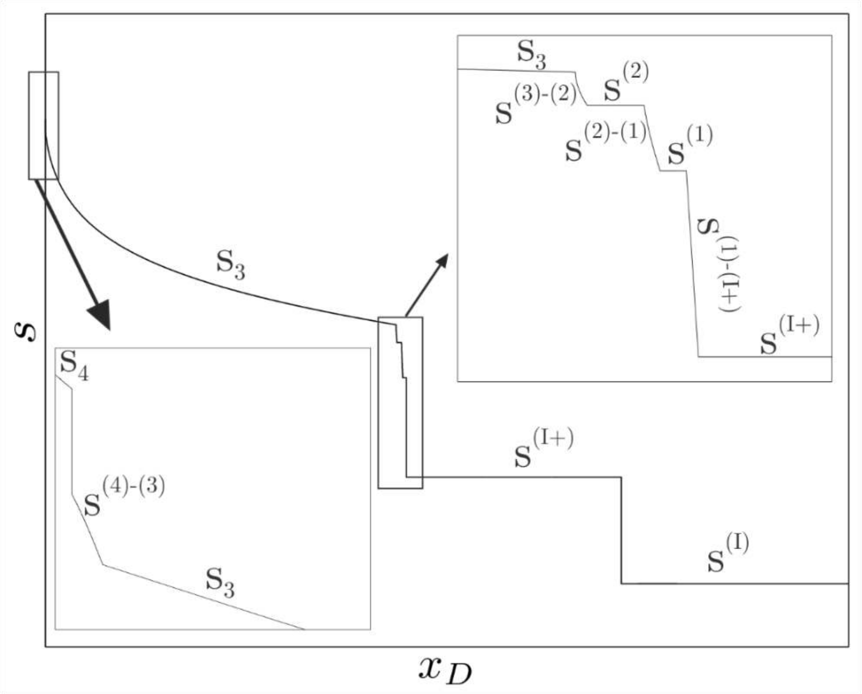

Figure C.1: Water saturation profile for s_I

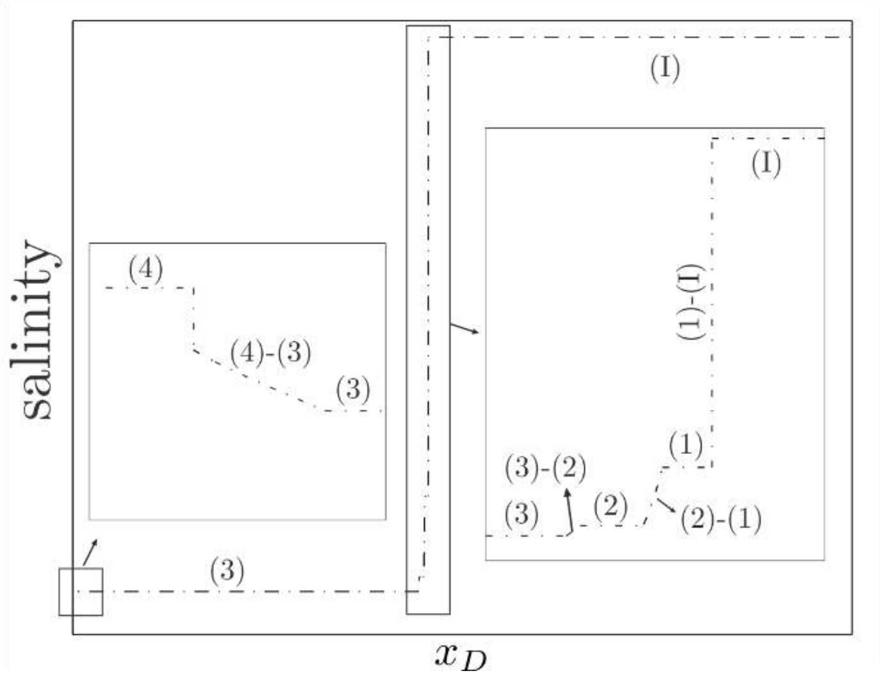

Figure C.2: Salinity profile for $t_D < t_{HS}$

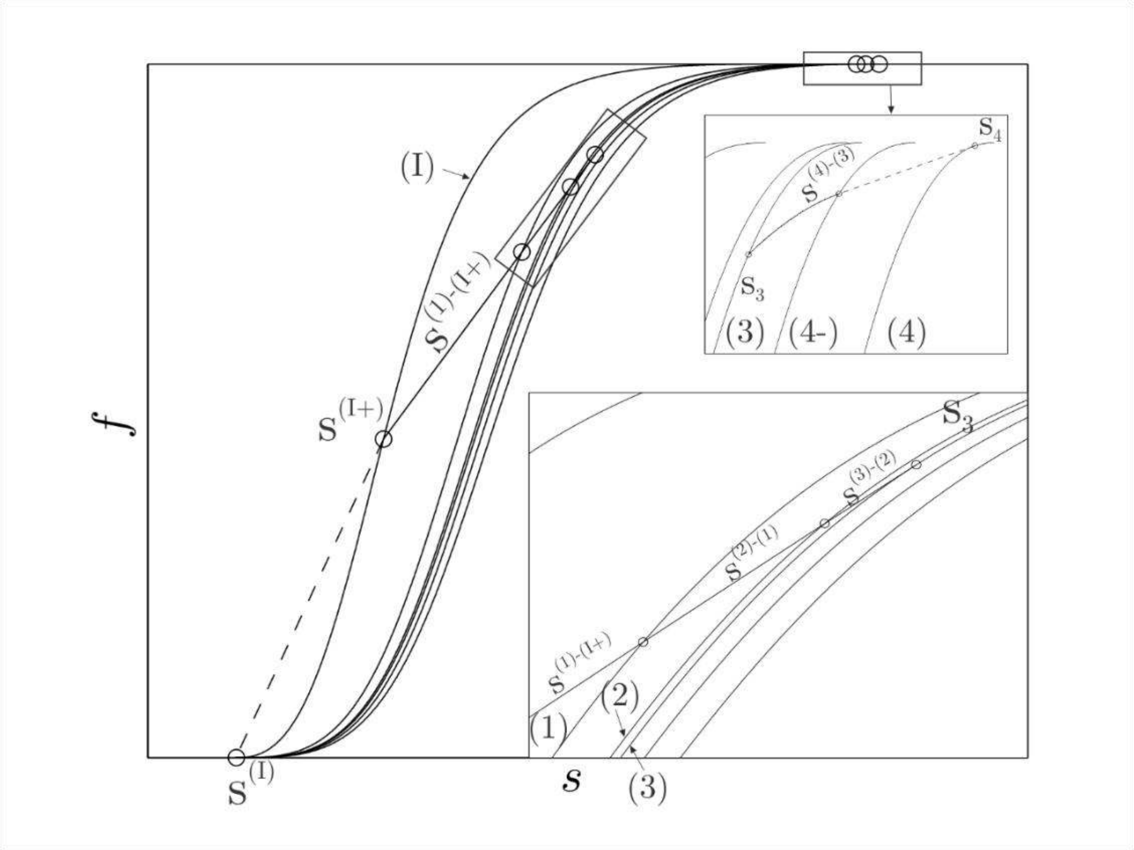

Figure C.3: Solution path of s_I in $f \times s$ plane

Solution s_{II} (Equation C.3) starts at the injection of the seawater drive, when $t_{HS} < t_D < t_A$. The water saturation profile is shown in figure (C.4) and the salinity profile is in figure (C.5). The pH and salinity waves centered in t_{HS} change the saturation (Figure C.4). Note that the decreasing salinity followed by its increase in regions (7), (6) and (6)-(5) (Figure C.5) result in the creation of a small oil bank in saturation solution (saturation s_6 in Figure C.4). The solution path of s_{II} is presented in Figure (C.6).

$$s_{II} = \begin{cases} s_{J2}(x_D, t_D), & x_D < x^S_{HS\,pH}(t_D) \\ s_7(x_D, t_D), & x^S_{HS\,pH}(t_D) < x_D < x^S_{HS\,d}(t_D) \\ s_6(x_D, t_D), & x^S_{HS\,d}(t_D) < x_D < x^R_{HS\,C}(t_D) \\ s^{(6)-(5)}(x_D, t_D), & x^R_{HS\,C}(t_D) < x_D < x^R_{HS\,B}(t_D) \\ s_5(x_D, t_D), & x^R_{HS\,B}(t_D) < x_D < x^S_{HS\,A}(t_D) \\ s_4(x_D, t_D), & x^S_{HS\,A}(t_D) < x_D < D^{(1)}_{(pH)} t_D \\ s^{(4)-(3)}(x_D, t_D), & D^{(1)}_{(pH)} t_D < x_D < \lambda_{(pH)}\left(\xi^{(I)}\right) t_D \\ s_3(x_D, t_D), & \lambda_{(pH)}\left(\xi^{(I)}\right) t_D < x_D < \lambda_{(3)}\left(\vec{c}^{(3)}, \xi^{(I)}\right) t_D \\ s^{(3)-(2)}(x_D, t_D), & \lambda_{(3)}\left(\vec{c}^{(3)}, \xi^{(I)}\right) t_D < x_D < \lambda_{(3)}\left(\vec{c}^{(2)}, \xi^{(I)}\right) t_D \\ s^{(2)}, & \lambda_{(3)}\left(\vec{c}^{(2)}, \xi^{(I)}\right) t_D < x_D < \lambda_{(2)}\left(\vec{c}^{(2)}, \xi^{(I)}\right) t_D \\ s^{(2)-(1)}(x_D, t_D), & \lambda_{(2)}\left(\vec{c}^{(2)}, \xi^{(I)}\right) t_D < x_D < \lambda_{(2)}\left(\vec{c}^{(1)}, \xi^{(I)}\right) t_D \\ s^{(1)}, & \lambda_{(2)}\left(\vec{c}^{(1)}, \xi^{(I)}\right) t_D < x_D < \lambda_{(1)}\left(\vec{c}^{(1)}, \xi^{(I)}\right) t_D \\ s^{(1)-(I+)}(x_D, t_D), & \lambda_{(1)}\left(\vec{c}^{(1)}, \xi^{(I)}\right) t_D < x_D < \lambda_{(1)}\left(\vec{c}^{(I)}, \xi^{(I)}\right) t_D \\ s^{(I+)}, & \lambda_{(1)}\left(\vec{c}^{(I)}, \xi^{(I)}\right) t_D < x_D < D_{(s)} t_D \\ s^{(I)}, & x_D > D_{(s)} t_D \end{cases} \tag{C.3}$$

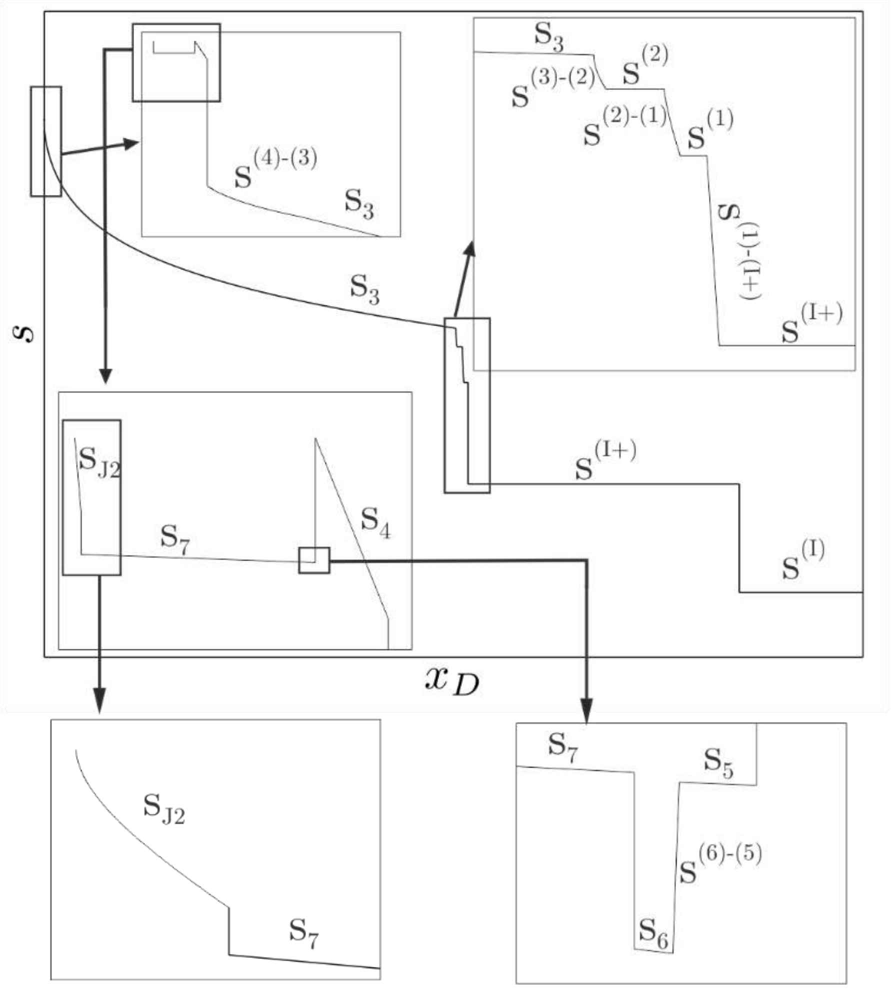

Figure C.4: Water saturation profile for s_{II}

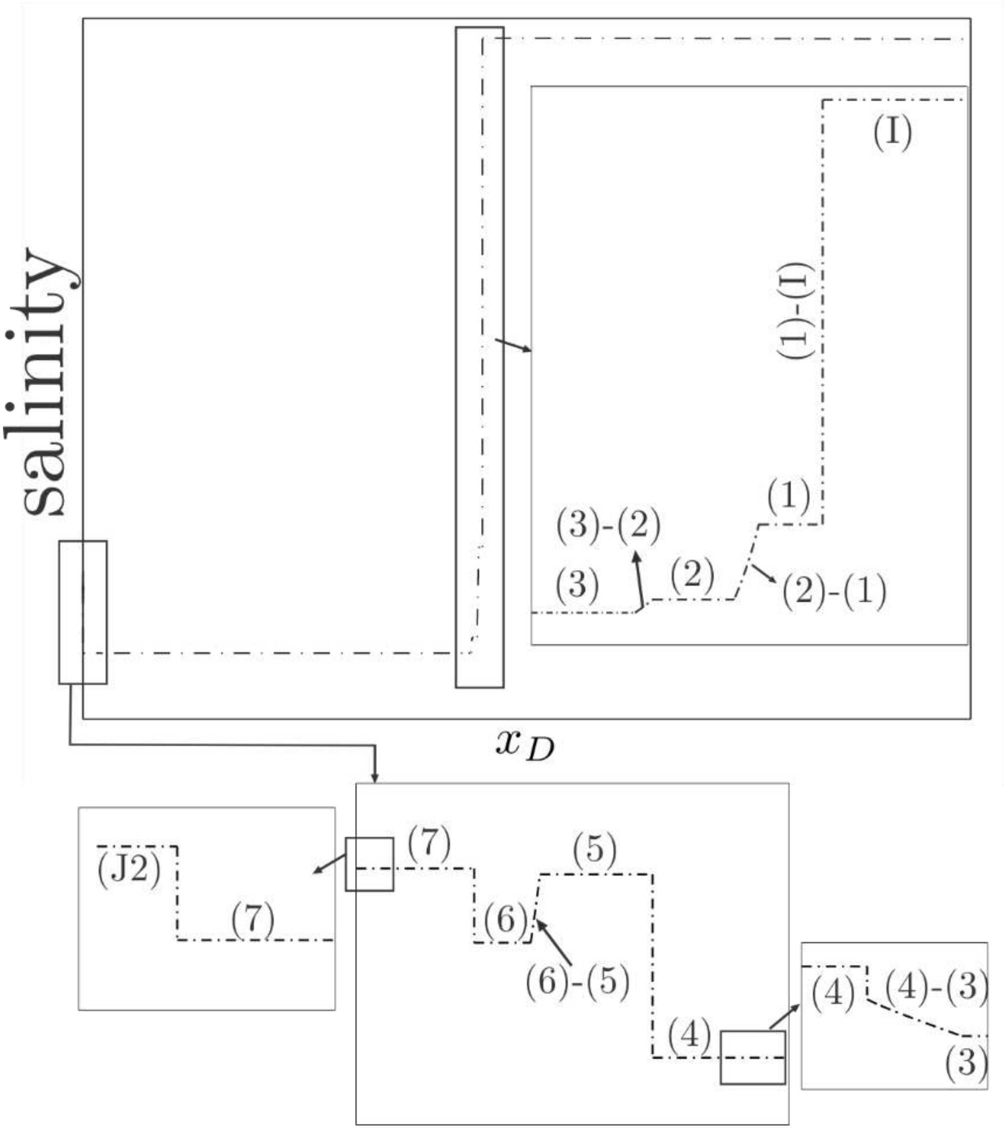

Figure C.5: Salinity profile for $t_{HS} < t_D < t_A$

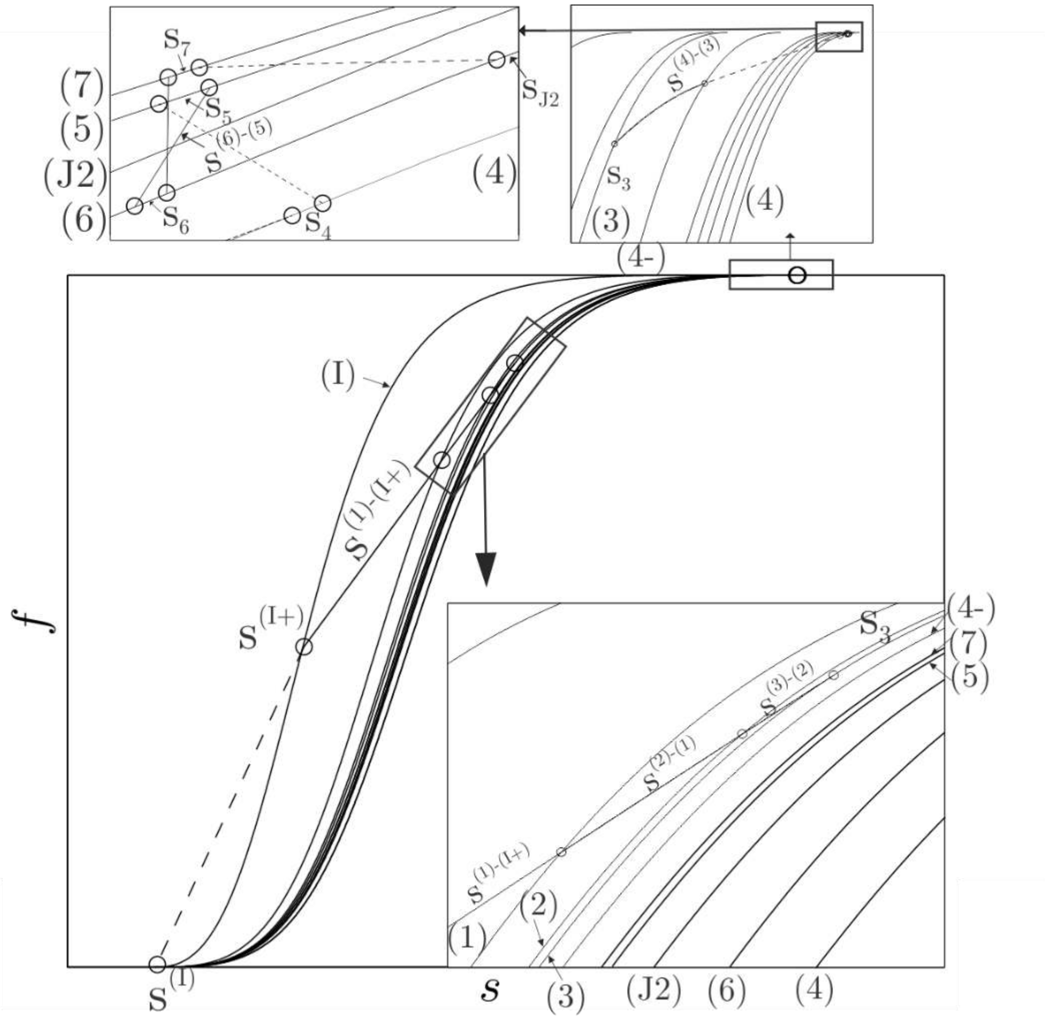

Figure C.6: Solution path of s_{II} in $f \times s$ plane

In solution s_{III} (Equation C.4), when $t_A < t_D < t_B$, the wave $k = 1$ crosses the pH shock from the front of the low salinity slug, and the region of salinity (4) disappears (Figure C.8). Moreover, a new salinity region appears: region (5)-(3-), located between the shock wave $k = 1$ and the last rarefaction wave $k = 2$. The water saturation peak from rarefaction s_4 (see Figure C.4) is no longer present in the solution and a new wave ($s^{(5)-(3)-}$) appears (Figure C.7).

$$s_{III} = \begin{cases} s_{J2}(x_D, t_D), & x_D < x_{HS\,pH}^{S}(t_D) \\ s_7(x_D, t_D), & x_{HS\,pH}^{S}(t_D) < x_D < x_{HS\,d}^{S}(t_D) \\ s_6(x_D, t_D), & x_{HS\,d}^{S}(t_D) < x_D < x_{HS\,C}^{R}(t_D) \\ s^{(6)-(5)}(x_D, t_D), & x_{HS\,C}^{R}(t_D) < x_D < x_{HS\,B}^{R}(t_D) \\ s_5(x_D, t_D), & x_{HS\,B}^{R}(t_D) < x_D < x_{A\,B}^{S}(t_D) \\ s^{(5)-(3-)-}(x_D, t_D), & x_{A\,B}^{S}(t_D) < x_D < x_{A\,F}^{S}(t_D) \\ s^{(4)-(3)}(x_D, t_D), & x_{A\,F}^{S}(t_D) < x_D < \lambda_{(pH)}\left(\xi^{(I)}\right)t_D \\ s_3(x_D, t_D), & \lambda_{(pH)}\left(\xi^{(I)}\right)t_D < x_D < \lambda_{(3)}\left(\vec{c}^{(3)}, \xi^{(I)}\right)t_D \\ s^{(3)-(2)}(x_D, t_D), & \lambda_{(3)}\left(\vec{c}^{(3)}, \xi^{(I)}\right)t_D < x_D < \lambda_{(3)}\left(\vec{c}^{(2)}, \xi^{(I)}\right)t_D \\ s^{(2)}, & \lambda_{(3)}\left(\vec{c}^{(2)}, \xi^{(I)}\right)t_D < x_D < \lambda_{(2)}\left(\vec{c}^{(2)}, \xi^{(I)}\right)t_D \\ s^{(2)-(1)}(x_D, t_D), & \lambda_{(2)}\left(\vec{c}^{(2)}, \xi^{(I)}\right)t_D < x_D < \lambda_{(2)}\left(\vec{c}^{(1)}, \xi^{(I)}\right)t_D \\ s^{(1)}, & \lambda_{(2)}\left(\vec{c}^{(1)}, \xi^{(I)}\right)t_D < x_D < \lambda_{(1)}\left(\vec{c}^{(1)}, \xi^{(I)}\right)t_D \\ s^{(1)-(I+)}(x_D, t_D), & \lambda_{(1)}\left(\vec{c}^{(1)}, \xi^{(I)}\right)t_D < x_D < \lambda_{(1)}\left(\vec{c}^{(I)}, \xi^{(I)}\right)t_D \\ s^{(I+)}, & \lambda_{(1)}\left(\vec{c}^{(I)}, \xi^{(I)}\right)t_D < x_D < D_{(s)}t_D \\ s^{(I)}, & x_D > D_{(s)}t_D \end{cases} \tag{C.4}$$

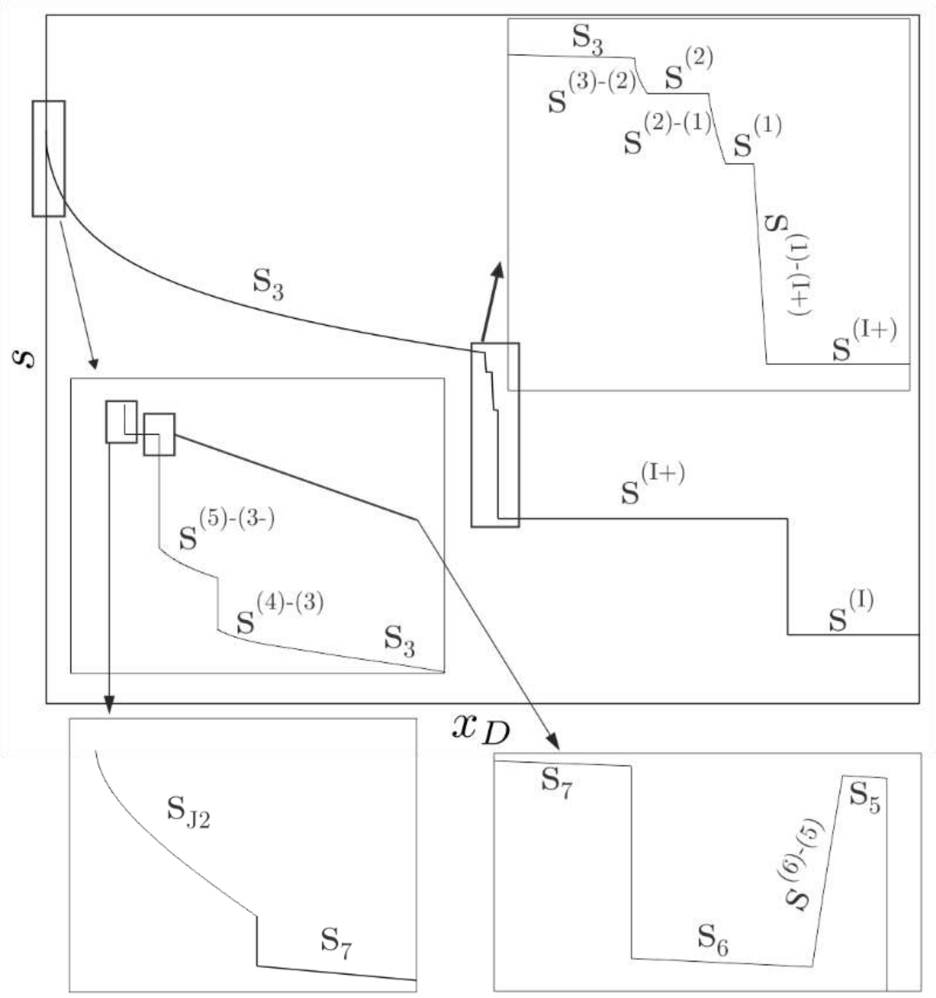

Figure C.7: Water saturation profile for s_{III}

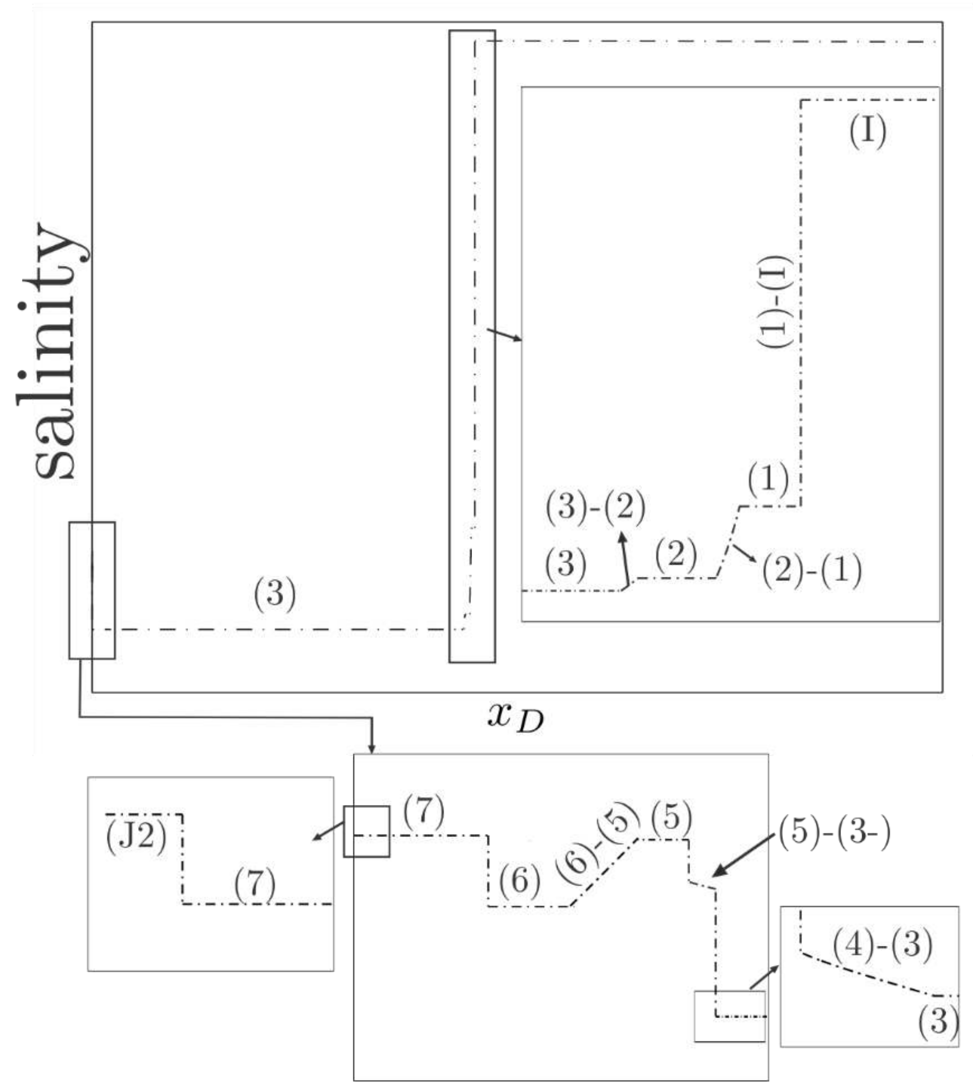

Figure C.8: Water saturation profile for s_{III}

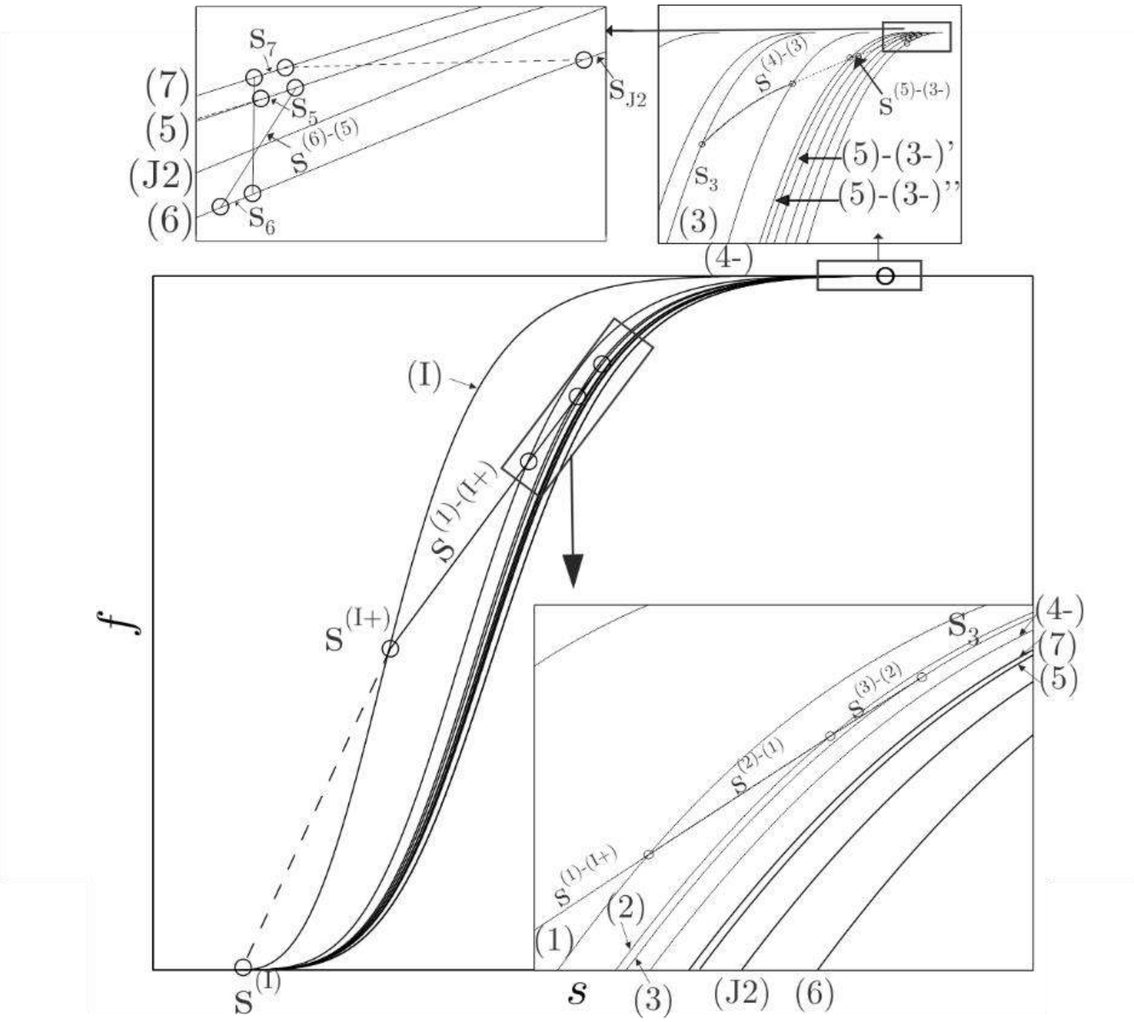

Figure C.9: Solution path of s_{III} in $f \times s$ plane

Solution s_{IV} ($t_B < t_D < t_C$) is characterized by the interaction between the family $k = 2$ rarefaction wave and the pH waves from the front of the slug. The pH shock to a more acidic media changes the adsorption parameters of the cations, and the salinity that increased along x_D for family $k = 2$ starts to decrease (Figure C.11). This behavior impacts water saturation solution: it increases along x_D before the pH shock (saturation wave $s^{(6)-(5)}$ in figure C.10), and decreases after the pH shock (saturation wave $s^{(6)-(5)-}$ in figure C.10). The solution path is presented in figure (C.12).

$$s_{IV} = \begin{cases} s_{J2}(x_D, t_D), & x_D < x^S_{HS\,pH}(t_D) \\ s_7(x_D, t_D), & x^S_{HS\,pH}(t_D) < x_D < x^S_{HS\,d}(t_D) \\ s_6(x_D, t_D), & x^S_{HS\,d}(t_D) < x_D < x^R_{HS\,C}(t_D) \\ s^{(6)-(5)}(x_D, t_D), & x^R_{HS\,C}(t_D) < x_D < x^S_{B\,C}(t_D) \\ s^{(6)-(5)-}(x_D, t_D), & x^S_{B\,C}(t_D) < x_D < x^R_{B\,J}(t_D) \\ s^{(5)-(3-)}(x_D, t_D), & x^R_{B\,J}(t_D) < x_D < x^R_{0\,E}(t_D) \\ s_{3-}(x_D, t_D), & x^R_{0\,E}(t_D) < x_D < x^S_{A\,F}(t_D) \\ s_3(x_D, t_D), & x^S_{A\,F}(t_D) < x_D < \lambda_{(3)}\left(\vec{c}^{(3)}, \xi^{(I)}\right)t_D \\ s^{(3)-(2)}(x_D, t_D), & \lambda_{(3)}\left(\vec{c}^{(3)}, \xi^{(I)}\right)t_D < x_D < \lambda_{(3)}\left(\vec{c}^{(2)}, \xi^{(I)}\right)t_D \\ s^{(2)}, & \lambda_{(3)}\left(\vec{c}^{(2)}, \xi^{(I)}\right)t_D < x_D < \lambda_{(2)}\left(\vec{c}^{(2)}, \xi^{(I)}\right)t_D \\ s^{(2)-(1)}(x_D, t_D), & \lambda_{(2)}\left(\vec{c}^{(2)}, \xi^{(I)}\right)t_D < x_D < \lambda_{(2)}\left(\vec{c}^{(1)}, \xi^{(I)}\right)t_D \\ s^{(1)}, & \lambda_{(2)}\left(\vec{c}^{(1)}, \xi^{(I)}\right)t_D < x_D < \lambda_{(1)}\left(\vec{c}^{(1)}, \xi^{(I)}\right)t_D \\ s^{(1)-(I+)}(x_D, t_D), & \lambda_{(1)}\left(\vec{c}^{(1)}, \xi^{(I)}\right)t_D < x_D < \lambda_{(1)}\left(\vec{c}^{(I)}, \xi^{(I)}\right)t_D \\ s^{(I+)}, & \lambda_{(1)}\left(\vec{c}^{(I)}, \xi^{(I)}\right)t_D < x_D < D_{(s)}t_D \\ s^{(I)}, & x_D > D_{(s)}t_D \end{cases} \tag{C.5}$$

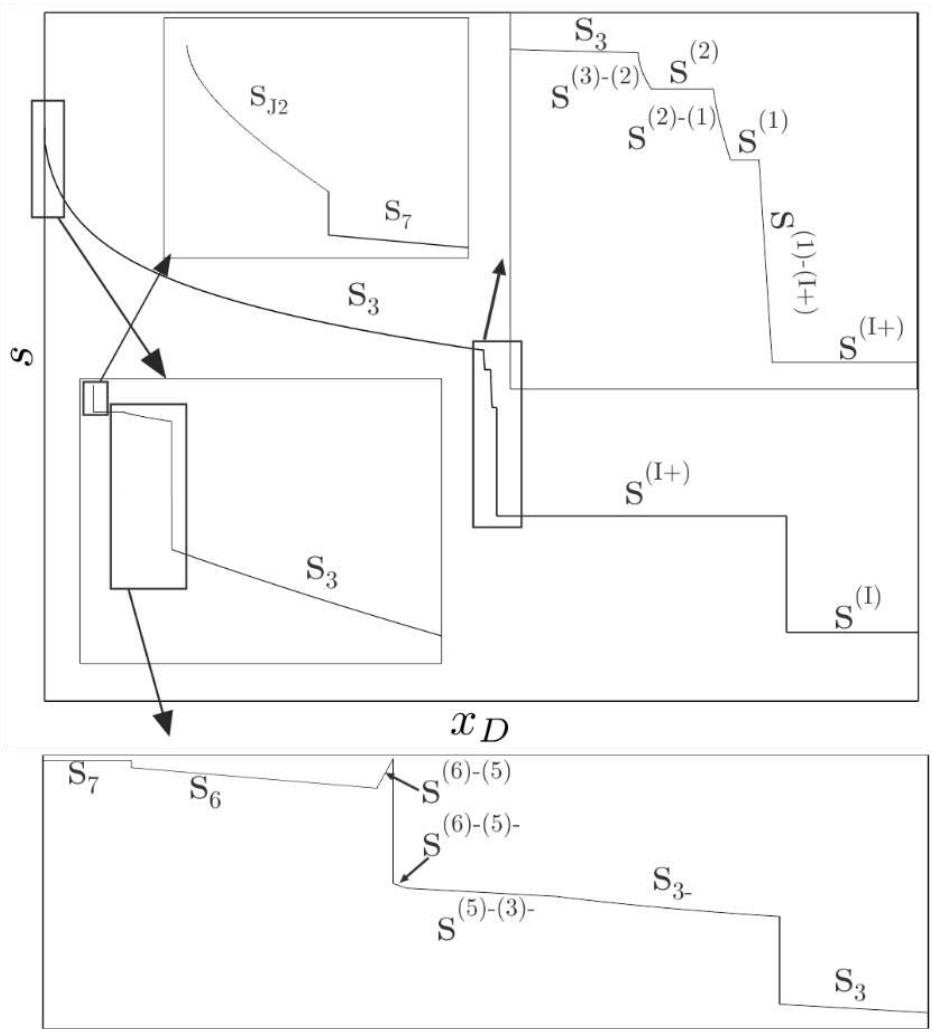

Figure C.10: Water saturation profile for s_{IV}

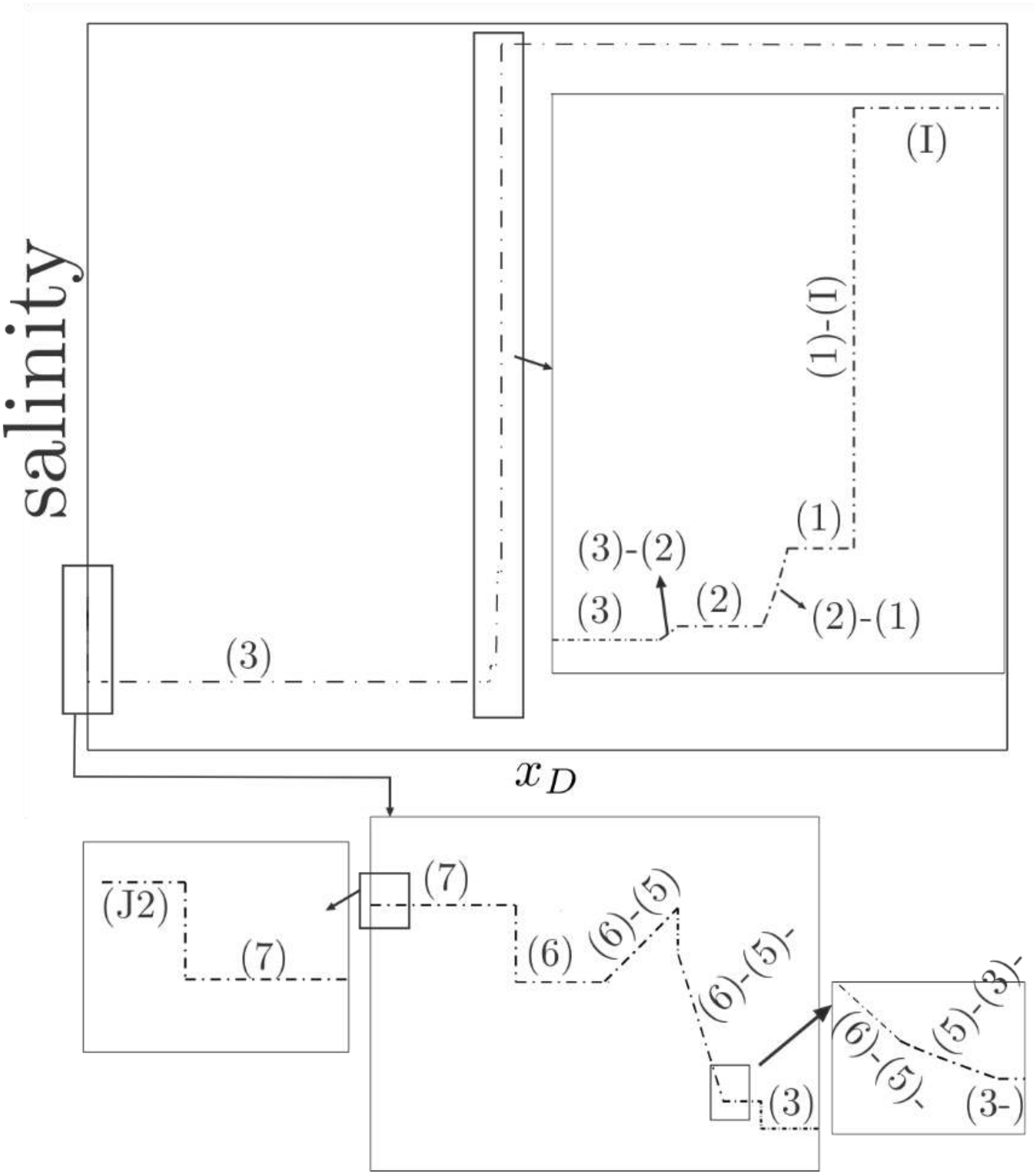

Figure C.11: Salinity profile for $t_B < t_D < t_C$

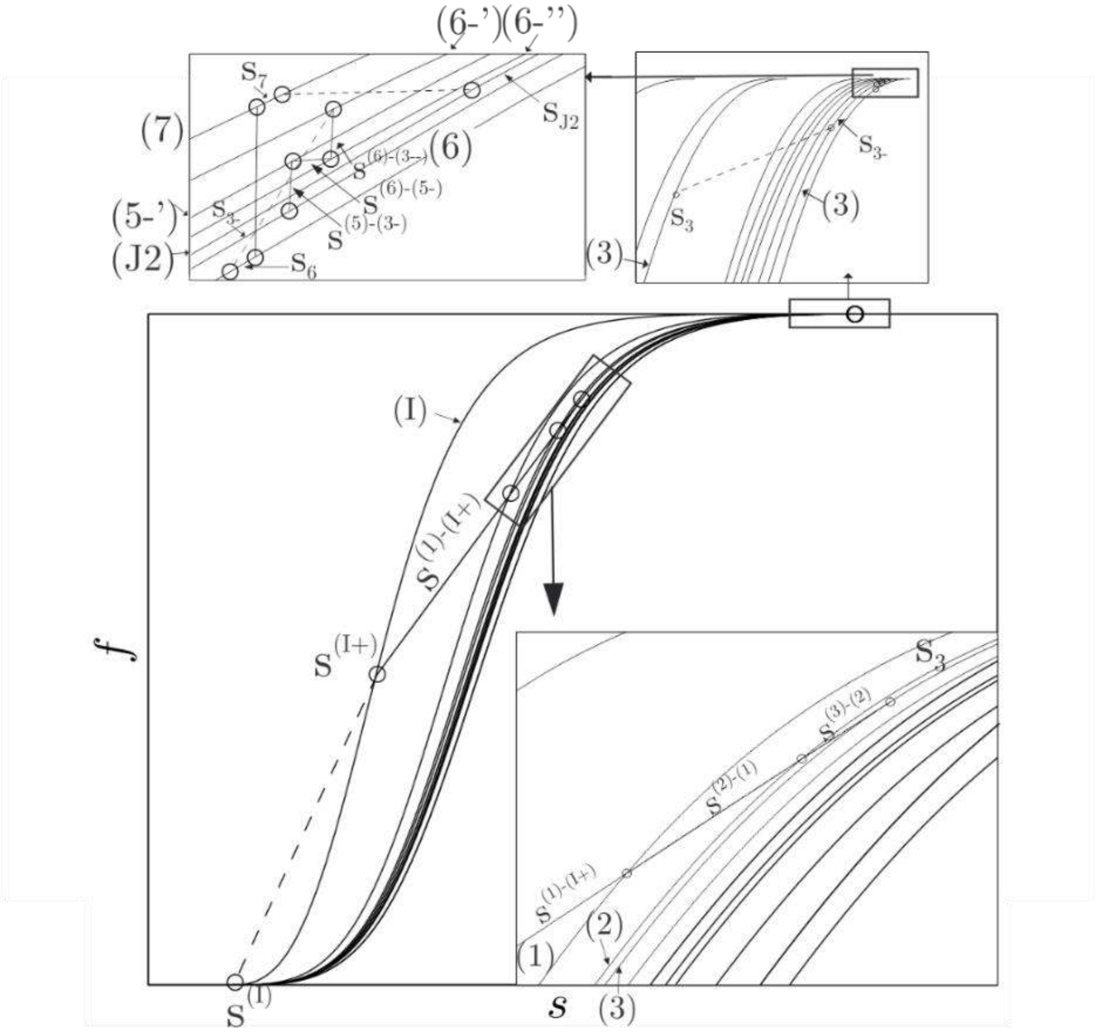

Figure C.12: Solution path of s_{IV} in $f \times s$ plane

In solution s_V ($t_C < t_D < t_d$) family wave $k = 2$ from the rear of the slug interacted with the pH shock from the front and the rarefaction $s^{(6)-(5)-}$ no longer exists in the solution. Besides that, a new salinity rarefaction appears (region (6)-(3--) in figure C.14). In this region the water saturation rarefaction decreases along x_D ($s^{(6)-(3--)}$in figure C.13). The solution path in $f \times s$ plane is presented in figure (C.15).

$$s_V = \begin{cases} s_{J2}(x_D, t_D), & x_D < x^S_{HS\,pH}(t_D) \\ s_7(x_D, t_D), & x^S_{HS\,pH}(t_D) < x_D < x^S_{HS\,d}(t_D) \\ s_6(x_D, t_D), & x^S_{HS\,d}(t_D) < x_D < x^S_{C\,D}(t_D) \\ s^{(6)-(3--)}(x_D, t_D), & x^S_{C\,D}(t_D) < x_D < x^R_{C\,L}(t_D) \\ s^{(6)-(5)-}(x_D, t_D), & x^R_{C\,L}(t_D) < x_D < x^R_{B\,J}(t_D) \\ s^{(5)-(3-)}(x_D, t_D), & x^R_{B\,J}(t_D) < x_D < x^R_{0\,E}(t_D) \\ s_{3-}(x_D, t_D), & x^R_{0\,E}(t_D) < x_D < x^S_{A\,F}(t_D) \\ s_3(x_D, t_D), & x^S_{A\,F}(t_D) < x_D < \lambda_{(3)}\left(\vec{c}^{(3)}, \xi^{(I)}\right)t_D \\ s^{(3)-(2)}(x_D, t_D), & \lambda_{(3)}\left(\vec{c}^{(3)}, \xi^{(I)}\right)t_D < x_D < \lambda_{(3)}\left(\vec{c}^{(2)}, \xi^{(I)}\right)t_D \\ s^{(2)}, & \lambda_{(3)}\left(\vec{c}^{(2)}, \xi^{(I)}\right)t_D < x_D < \lambda_{(2)}\left(\vec{c}^{(2)}, \xi^{(I)}\right)t_D \\ s^{(2)-(1)}(x_D, t_D), & \lambda_{(2)}\left(\vec{c}^{(2)}, \xi^{(I)}\right)t_D < x_D < \lambda_{(2)}\left(\vec{c}^{(1)}, \xi^{(I)}\right)t_D \\ s^{(1)}, & \lambda_{(2)}\left(\vec{c}^{(1)}, \xi^{(I)}\right)t_D < x_D < \lambda_{(1)}\left(\vec{c}^{(1)}, \xi^{(I)}\right)t_D \\ s^{(1)-(I+)}(x_D, t_D), & \lambda_{(1)}\left(\vec{c}^{(1)}, \xi^{(I)}\right)t_D < x_D < \lambda_{(1)}\left(\vec{c}^{(I)}, \xi^{(I)}\right)t_D \\ s^{(I+)}, & \lambda_{(1)}\left(\vec{c}^{(I)}, \xi^{(I)}\right)t_D < x_D < D_{(s)}t_D \\ s^{(I)}, & x_D > D_{(s)}t_D \end{cases} \tag{C.6}$$

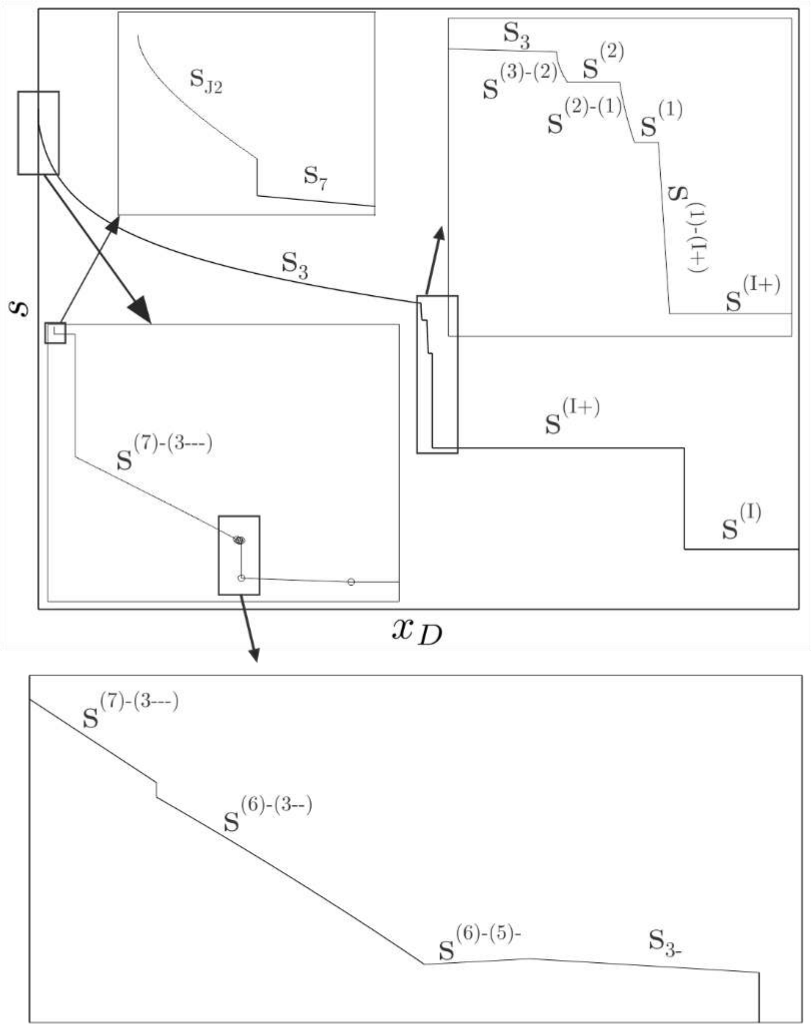

Figure C.13: Water saturation profile for s_V

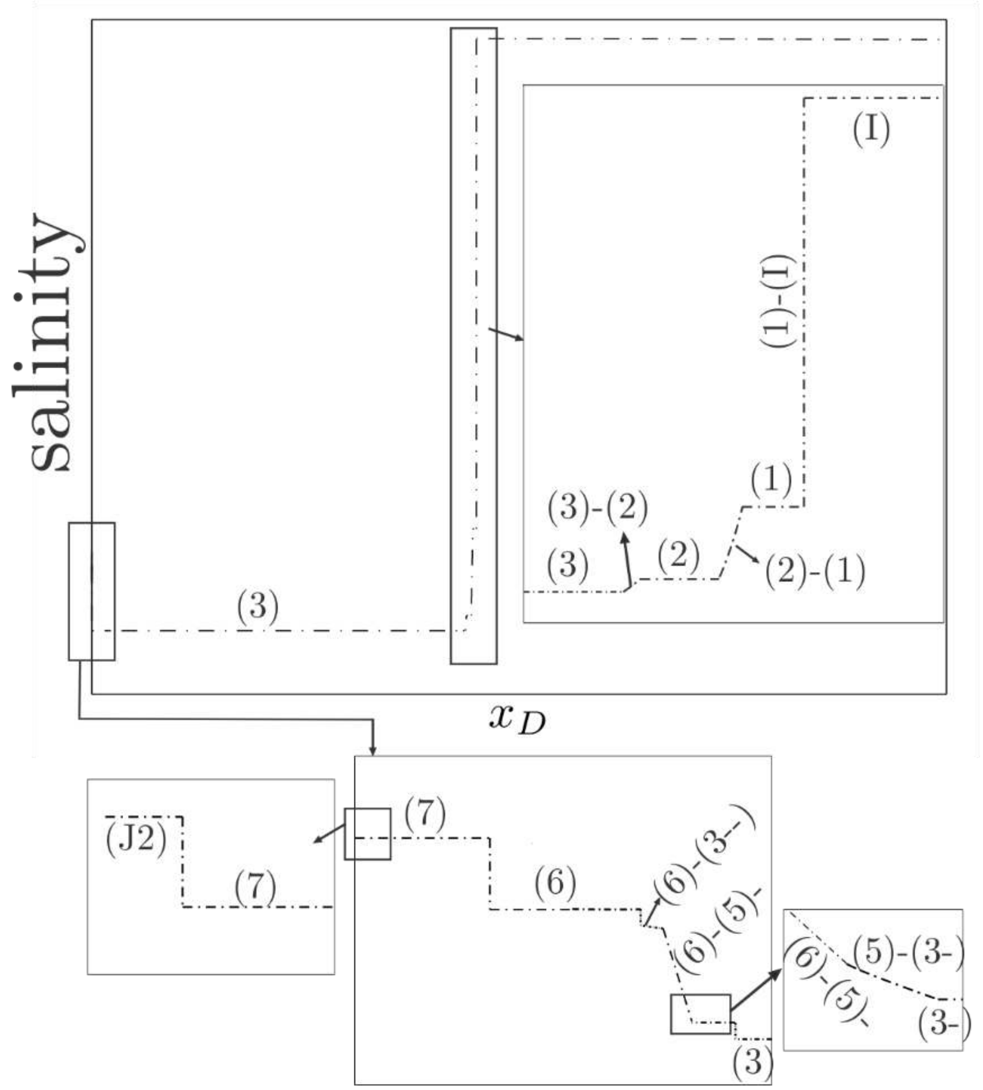

Figure C.14: Salinity profile for $t_C < t_D < t_d$

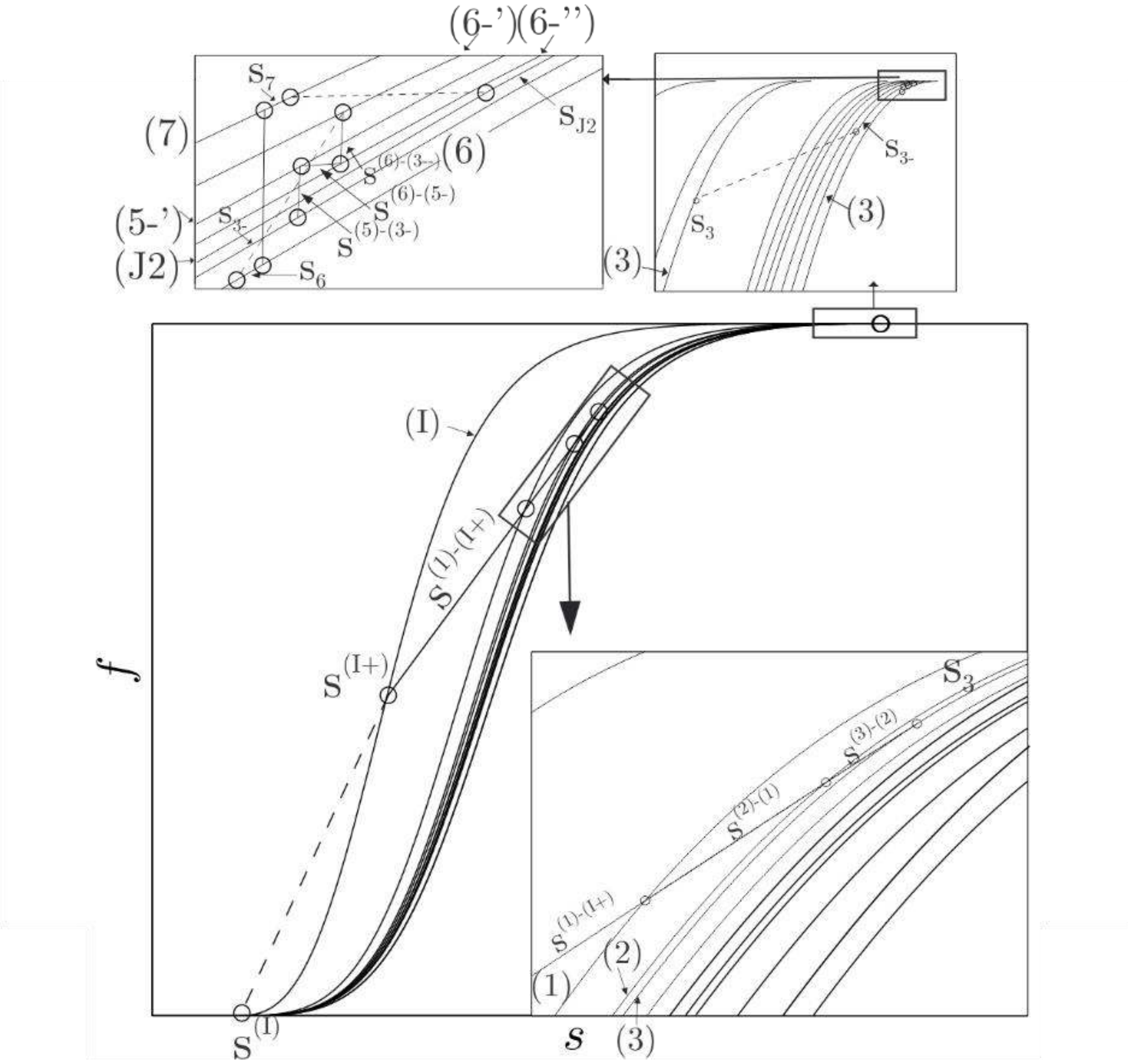

Figure C.15: Solution path of s_V in $f \times s$ plane

Two new features appear in solution s_{VI} ($t_d < t_D < t_E$). The first one is that the family $k = 3$ shock wave crosses the pH shock wave from the front of the slug. As a consequence there is a new pH rarefaction region (7)-(3---) and another rarefaction wave ($s^{(7)-(3---)}$). Moreover, family $k = 2$ rarefaction the located at the rear of the low salinity slug fully interacted with the pH waves from the front and it is located in a region of constant $pH = pH^{(I)}$. The solution path of s_{VI} in $f \times s$ plane is shown in figure (C.18).

$$s_{VI}=\begin{cases} s_{J2}(x_D,t_D), & x_D < x^S_{HS\,pH}(t_D) \\ s_7(x_D,t_D), & x^S_{HS\,pH}(t_D) < x_D < x^S_{d\,pH}(t_D) \\ s^{(7)-(3---)}(x_D,t_D), & x^S_{d\,pH}(t_D) < x_D < x^S_{D\,E}(t_D) \\ s^{(6)-(3--)}(x_D,t_D), & x^S_{D\,E}(t_D) < x_D < x^R_{C\,L}(t_D) \\ s^{(6)-(5)-}(x_D,t_D), & x^R_{C\,L}(t_D) < x_D < x^R_{B\,J}(t_D) \\ s_{3-}(x_D,t_D), & x^R_{B\,J}(t_D) < x_D < x^S_{A\,F}(t_D) \\ s_3(x_D,t_D), & x^S_{A\,F}(t_D) < x_D < \lambda_{(3)}\big(\vec{c}^{(3)},\xi^{(I)}\big)t_D \\ s^{(3)-(2)}(x_D,t_D), & \lambda_{(3)}\big(\vec{c}^{(3)},\xi^{(I)}\big)t_D < x_D < \lambda_{(3)}\big(\vec{c}^{(2)},\xi^{(I)}\big)t_D \\ s^{(2)}, & \lambda_{(3)}\big(\vec{c}^{(2)},\xi^{(I)}\big)t_D < x_D < \lambda_{(2)}\big(\vec{c}^{(2)},\xi^{(I)}\big)t_D \\ s^{(2)-(1)}(x_D,t_D), & \lambda_{(2)}\big(\vec{c}^{(2)},\xi^{(I)}\big)t_D < x_D < \lambda_{(2)}\big(\vec{c}^{(1)},\xi^{(I)}\big)t_D \\ s^{(1)}, & \lambda_{(2)}\big(\vec{c}^{(1)},\xi^{(I)}\big)t_D < x_D < \lambda_{(1)}\big(\vec{c}^{(1)},\xi^{(I)}\big)t_D \\ s^{(1)-(I+)}(x_D,t_D), & \lambda_{(1)}\big(\vec{c}^{(1)},\xi^{(I)}\big)t_D < x_D < \lambda_{(1)}\big(\vec{c}^{(I)},\xi^{(I)}\big)t_D \\ s^{(I+)}, & \lambda_{(1)}\big(\vec{c}^{(I)},\xi^{(I)}\big)t_D < x_D < D_{(s)}t_D \\ s^{(I)}, & x_D > D_{(s)}t_D \end{cases} \tag{C.7}$$

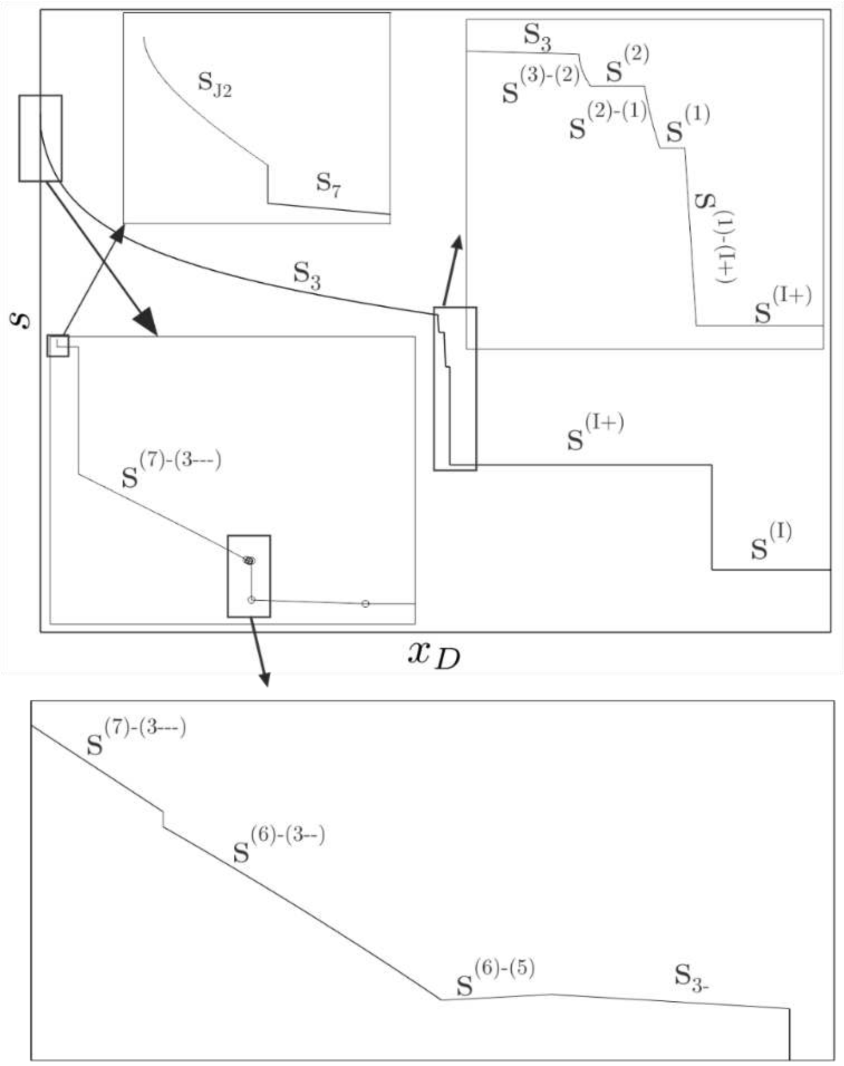

Figure C.16: Water saturation profile for s_{VI}

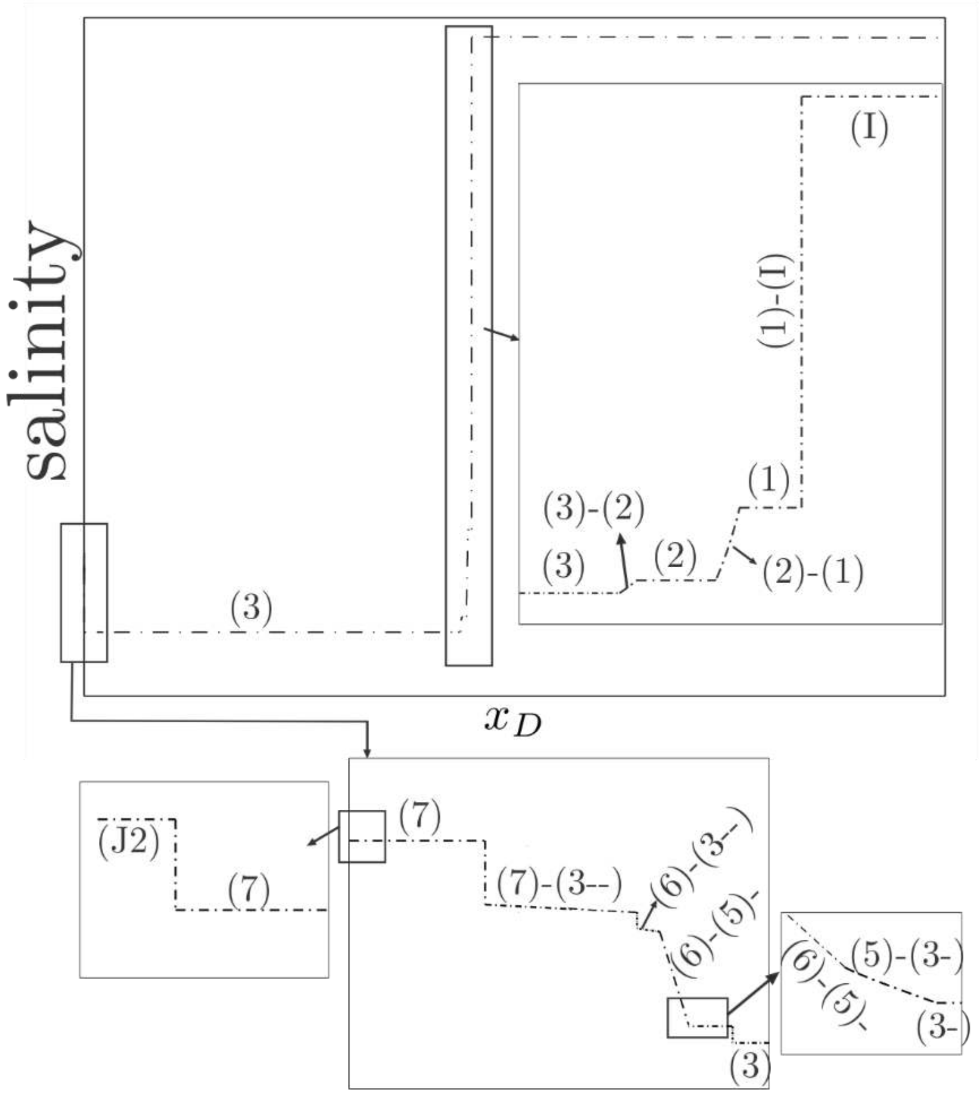

Figure C.17: Salinity profile for $t_d < t_D < t_E$

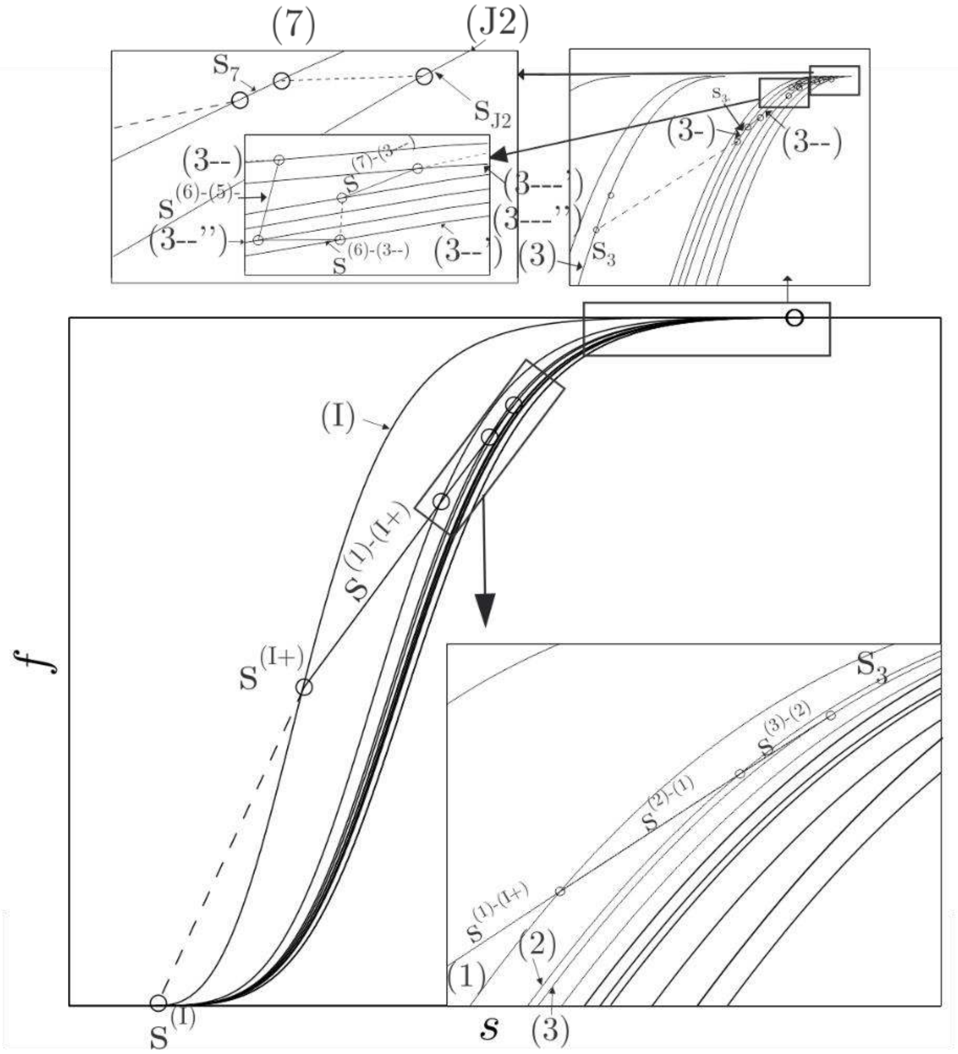

Figure C.18: Solution path of s_{VI} in $f \times s$ plane

Solution s_{VII} (Equation C.8) occurs when $t_E < t_D < t_F$. In this part of the solution the shock wave $k = 3$ from the rear of the low salinity slug has completed its interaction with the pH waves of the front. As a result, two new constant salinity regions (3---) and (3--) appear. Thus, the subsequent saturation rarefactions s_{3---} and s_{3---} take place at constant salinity (see figures C.19 and C.20). Note that the concentration shock from (3---) to (3--) generates a new water bank in saturation solution. In this part of the solution the pH and saturation rarefaction $s^{(6)-(3--)}(x_D, t_D)$ no longer exist. The solution path of s_{VII} is presented in figure (C.21).

$$s_{VII} = \begin{cases} s_{J2}(x_D, t_D), & x_D < x^S_{HS\,pH}(t_D) \\ s_7(x_D, t_D), & x^S_{HS\,pH}(t_D) < x_D < x^S_{d\,pH}(t_D) \\ s^{(7)-(3---)}(x_D, t_D), & x^S_{d\,pH}(t_D) < x_D < x^R_{E\,\infty}(t_D) \\ s_{3---}(x_D, t_D), & x^R_{E\,\infty}(t_D) < x_D < x^S_{E\,N}(t_D) \\ s_{3--}(x_D, t_D), & x^S_{E\,N}(t_D) < x_D < x^R_{C\,L}(t_D) \\ s^{(6)-(5)-}(x_D, t_D), & x^R_{C\,L}(t_D) < x_D < x^R_{B\,J}(t_D) \\ s_{3-}(x_D, t_D), & x^R_{B\,J}(t_D) < x_D < x^S_{A\,F}(t_D) \\ s_3(x_D, t_D), & x^S_{A\,F}(t_D) < x_D < \lambda_{(3)}\left(\vec{c}^{(3)}, \xi^{(I)}\right) t_D \\ s^{(3)-(2)}(x_D, t_D), & \lambda_{(3)}\left(\vec{c}^{(3)}, \xi^{(I)}\right) t_D < x_D < \lambda_{(3)}\left(\vec{c}^{(2)}, \xi^{(I)}\right) t_D \\ s^{(2)}, & \lambda_{(3)}\left(\vec{c}^{(2)}, \xi^{(I)}\right) t_D < x_D < \lambda_{(2)}\left(\vec{c}^{(2)}, \xi^{(I)}\right) t_D \\ s^{(2)-(1)}(x_D, t_D), & \lambda_{(2)}\left(\vec{c}^{(2)}, \xi^{(I)}\right) t_D < x_D < \lambda_{(2)}\left(\vec{c}^{(1)}, \xi^{(I)}\right) t_D \\ s^{(1)}, & \lambda_{(2)}\left(\vec{c}^{(1)}, \xi^{(I)}\right) t_D < x_D < \lambda_{(1)}\left(\vec{c}^{(1)}, \xi^{(I)}\right) t_D \\ s^{(1)-(I+)}(x_D, t_D), & \lambda_{(1)}\left(\vec{c}^{(1)}, \xi^{(I)}\right) t_D < x_D < \lambda_{(1)}\left(\vec{c}^{(I)}, \xi^{(I)}\right) t_D \\ s^{(I+)}, & \lambda_{(1)}\left(\vec{c}^{(I)}, \xi^{(I)}\right) t_D < x_D < D_{(s)} t_D \\ s^{(I)}, & x_D > D_{(s)} t_D \end{cases} \tag{C.8}$$

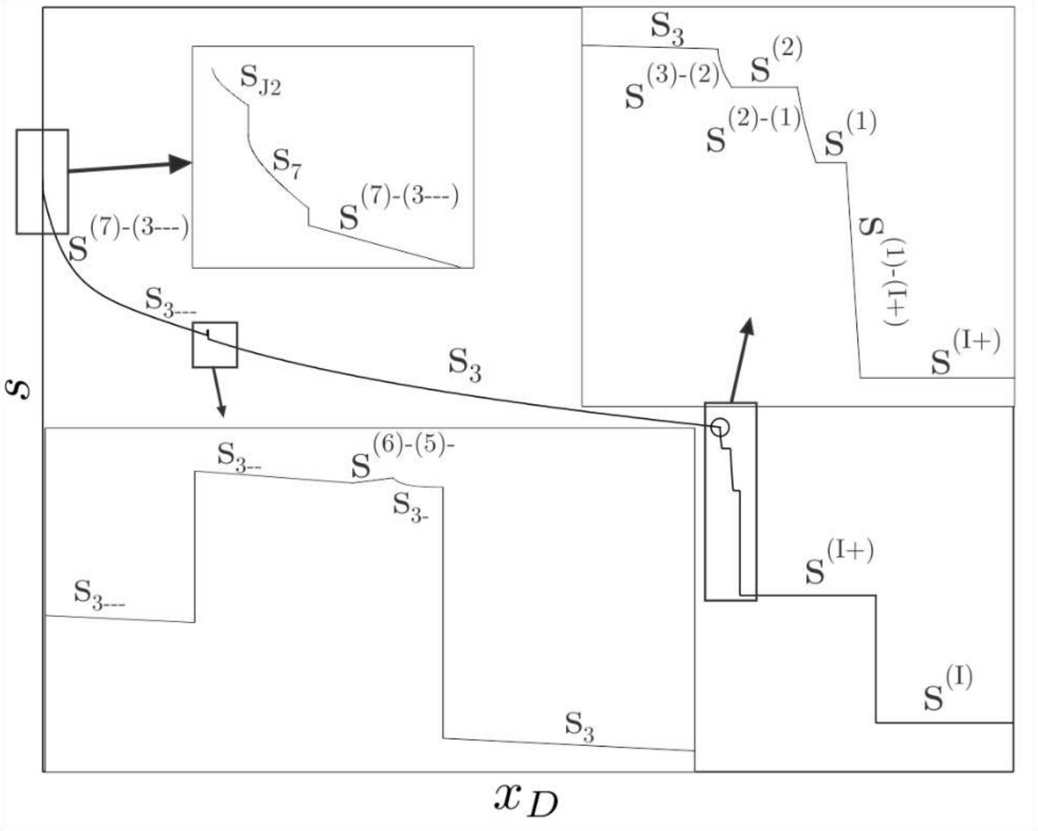

Figure C.19: Water saturation profile for s_{VII}

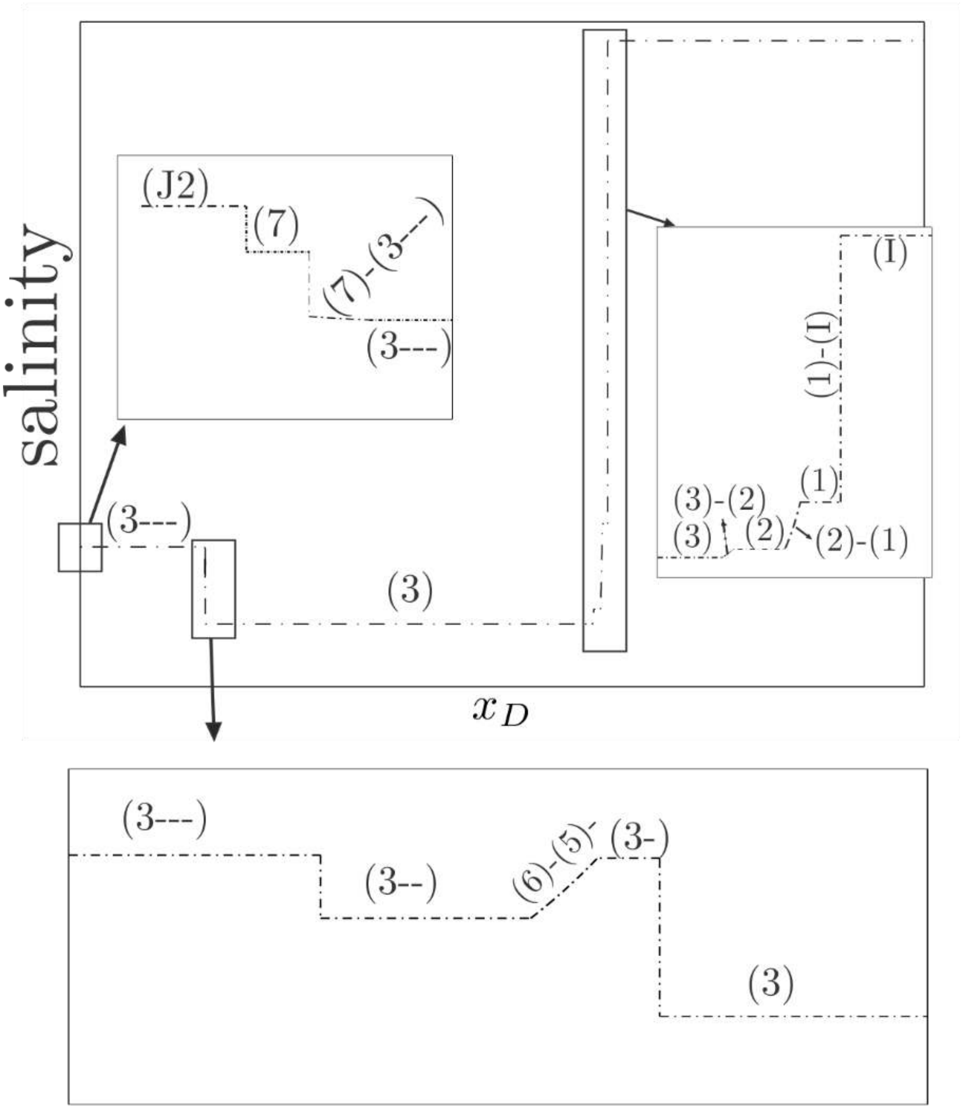

Figure C.20: Salinity profile for $t_E < t_D < t_F$

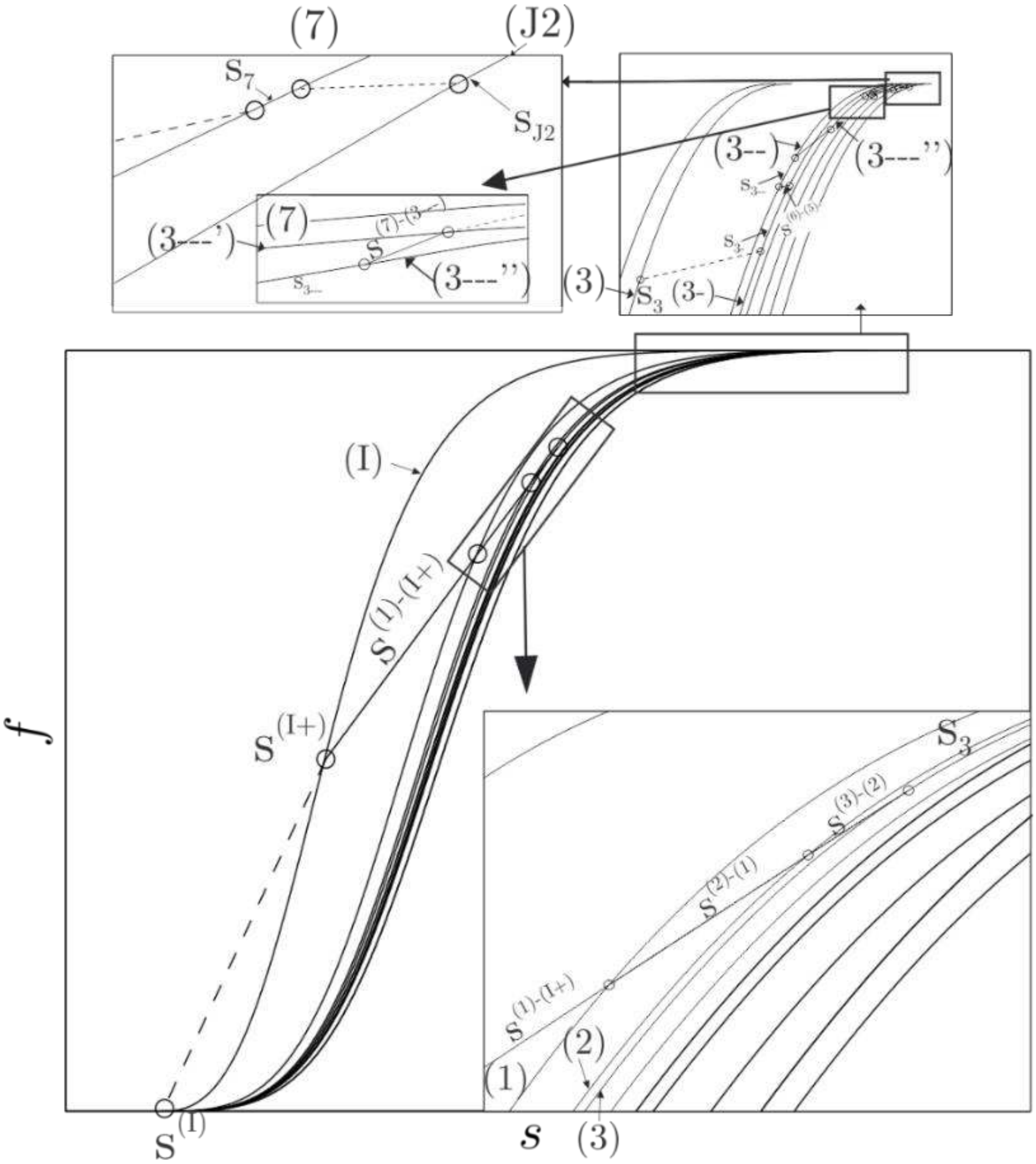

Figure C.21: Solution path of s_{VII} in $f \times s$ plane

Equation (C.9) describes solution s_{VIII} ($t_F < t_D < t_G$), where the first interaction between k-waves starts. The shock $k = 1$ from the rear of the slug is interacting with the rarefaction wave $k = 3$ from the front of the slug. As a result, the constant salinity region (3) no longer appears in the solution, and there is a new salinity region (region (3)-(2)- in figure C.23). Moreover, an oil bank followed by a water bank are created in the central part of the saturation solution (Figure C.22). This feature is a result of the approximation of the waves from the rear and from the front of the low salinity slug. The solution path of s_{VIII} in $f \times s$ plane is presented in figure (C.24).

$$s_{VIII}=\begin{cases} s_{J2}(x_D,t_D), & x_D < x^S_{HS\,pH}(t_D) \\ s_7(x_D,t_D), & x^S_{HS\,pH}(t_D) < x_D < x^S_{d\,pH}(t_D) \\ s^{(7)-(3---)}(x_D,t_D), & x^S_{d\,pH}(t_D) < x_D < x^R_{E\,\infty}(t_D) \\ s_{3---}(x_D,t_D), & x^R_{E\,\infty}(t_D) < x_D < x^S_{E\,N}(t_D) \\ s_{3--}(x_D,t_D), & x^S_{E\,N}(t_D) < x_D < x^R_{C\,L}(t_D) \\ s^{(6)-(5)-}(x_D,t_D), & x^R_{C\,L}(t_D) < x_D < x^R_{B\,J}(t_D) \\ s_{3-}(x_D,t_D), & x^R_{B\,J}(t_D) < x_D < x^R_{F\,J}(t_D) \\ s^{(3)-(2)-}(x_D,t_D), & x^R_{F\,J}(t_D) < x_D < x^S_{F\,G}(t_D) \\ s^{(3)-(2)}(x_D,t_D), & x^S_{F\,G}(t_D) < x_D < \lambda_{(3)}\left(\vec{c}^{(2)},\xi^{(I)}\right)t_D \\ s^{(2)}, & \lambda_{(3)}\left(\vec{c}^{(2)},\xi^{(I)}\right)t_D < x_D < \lambda_{(2)}\left(\vec{c}^{(2)},\xi^{(I)}\right)t_D \\ s^{(2)-(1)}(x_D,t_D), & \lambda_{(2)}\left(\vec{c}^{(2)},\xi^{(I)}\right)t_D < x_D < \lambda_{(2)}\left(\vec{c}^{(1)},\xi^{(I)}\right)t_D \\ s^{(1)}, & \lambda_{(2)}\left(\vec{c}^{(1)},\xi^{(I)}\right)t_D < x_D < \lambda_{(1)}\left(\vec{c}^{(1)},\xi^{(I)}\right)t_D \\ s^{(1)-(I+)}(x_D,t_D), & \lambda_{(1)}\left(\vec{c}^{(1)},\xi^{(I)}\right)t_D < x_D < \lambda_{(1)}\left(\vec{c}^{(I)},\xi^{(I)}\right)t_D \\ s^{(I+)}, & \lambda_{(1)}\left(\vec{c}^{(I)},\xi^{(I)}\right)t_D < x_D < D_{(s)}t_D \\ s^{(I)}, & x_D > D_{(s)}t_D \end{cases} \quad \text{(C.9)}$$

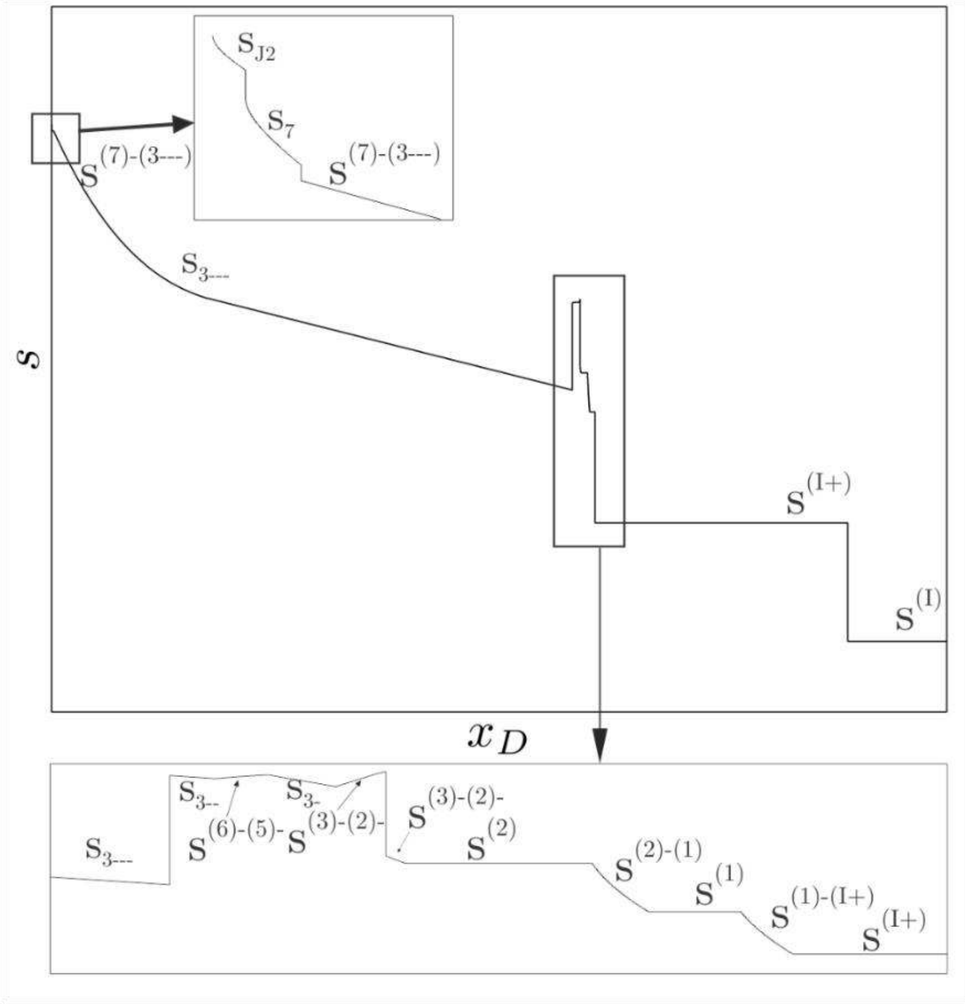

Figure C.22: Water saturation profile for s_{VIII}

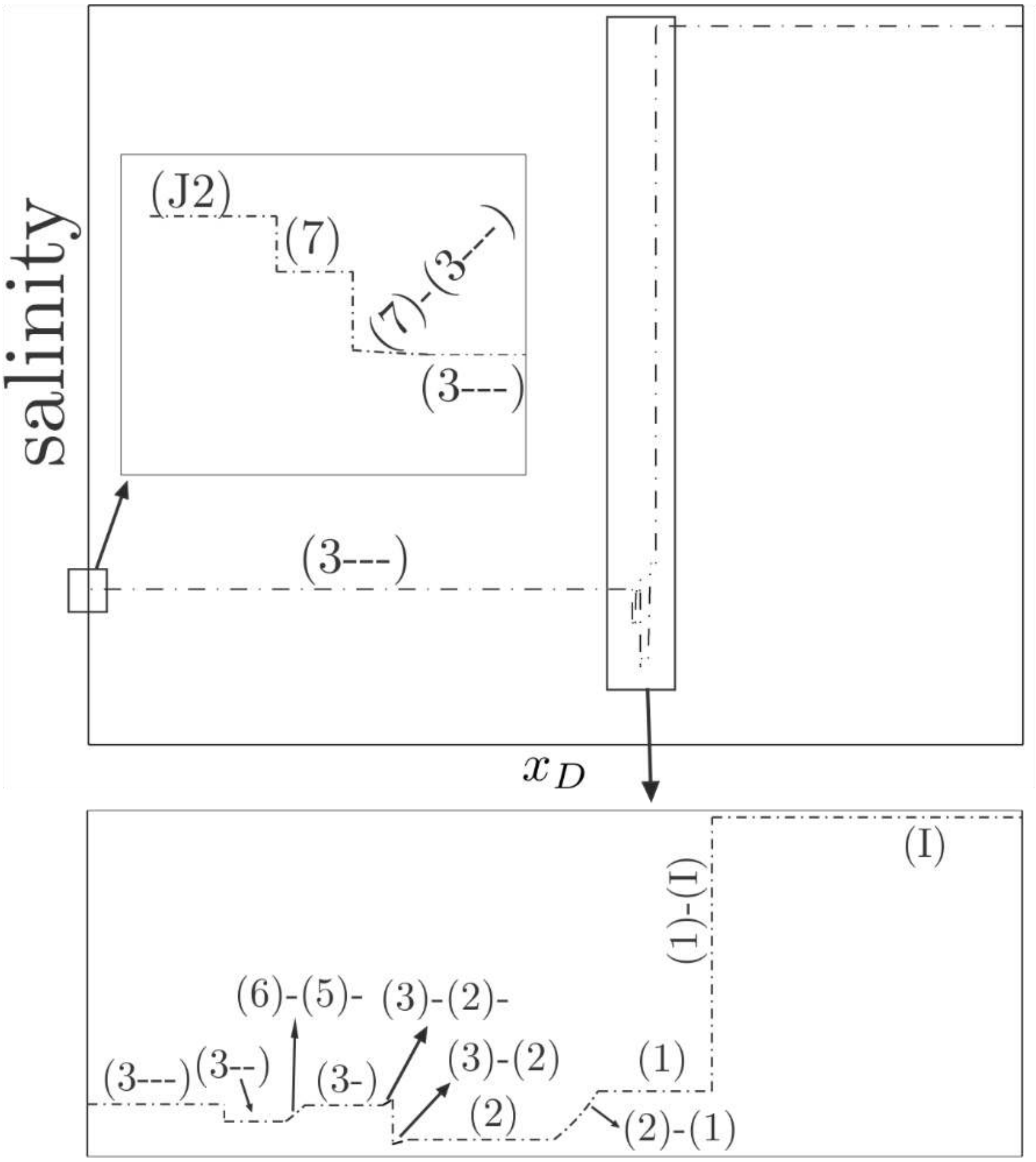

Figure C.23: Salinity profile for $t_F < t_D < t_G$

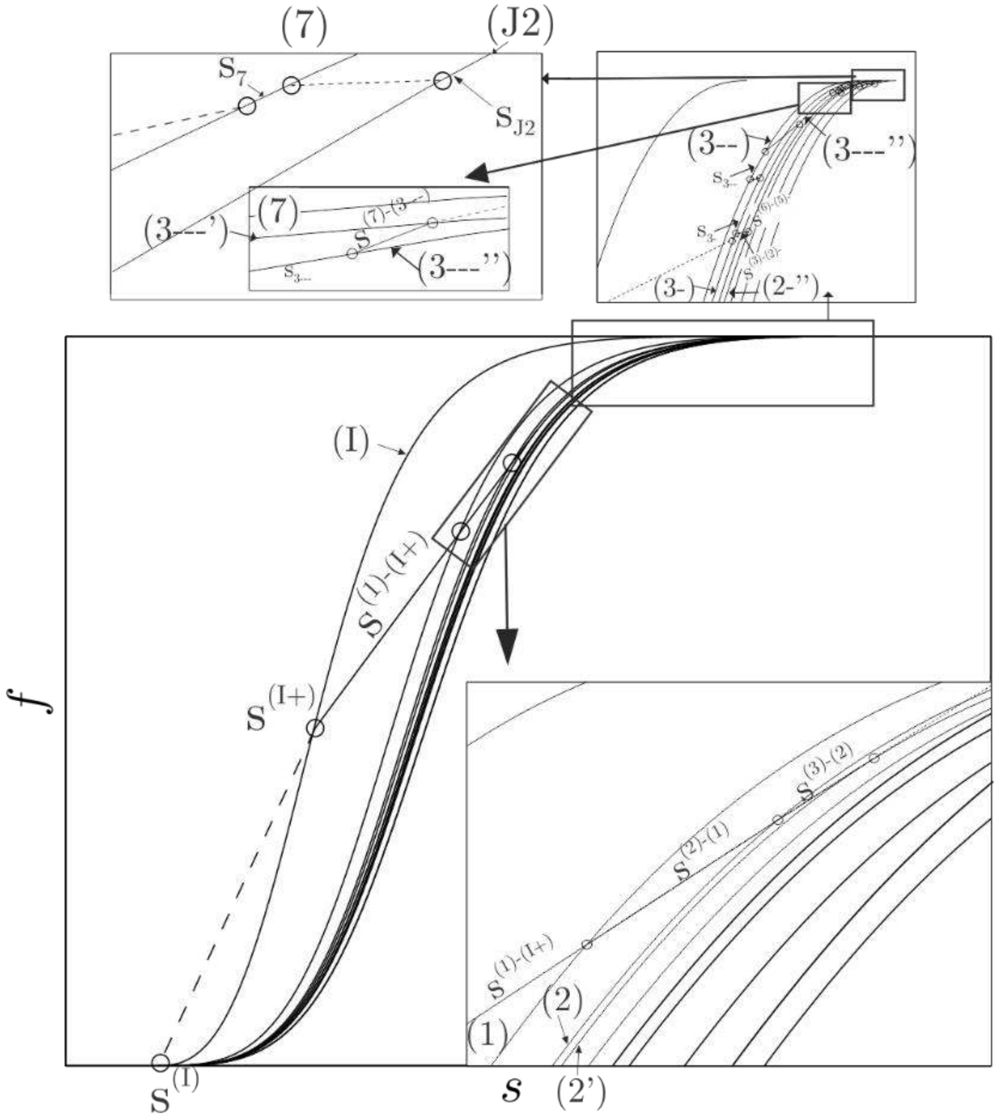

Figure C.24: Solution path of s_{VIII} in $f \times s$ plane

For $t_G < t_D < t_H$ (solution s_{IX}), the interaction between the waves $k = 3$ from the rear and $k = 1$ from the front of the slug is completed. Thus, the salinity region (3)-(2) and its subsequent wave in water saturation solution ($s^{(3)-(2)}$) disappear and a new constant state appears: (2-). As a result, salinity increases in region (3)-(2)- (Figure C.26). The effect in the water saturation solution is the appearance of a small oil bank (in s_{3-}) and a small water bank (in $s^{(2-)}$) (Figure C.25). The solution path of s_{IX} is depicted in figure (C.27).

$$s_{IX}=\begin{cases}s_{J2}(x_D,t_D), & x_D<x^S_{HS\,pH}(t_D)\\ s_7(x_D,t_D), & x^S_{HS\,pH}(t_D)<x_D<x^S_{d\,pH}(t_D)\\ s^{(7)-(3---)}(x_D,t_D), & x^S_{d\,pH}(t_D)<x_D<x^R_{E\,\infty}(t_D)\\ s_{3---}(x_D,t_D), & x^R_{E\,\infty}(t_D)<x_D<x^S_{E\,N}(t_D)\\ s_{3--}(x_D,t_D), & x^S_{E\,N}(t_D)<x_D<x^R_{C\,L}(t_D)\\ s^{(6)-(5)-}(x_D,t_D), & x^R_{C\,L}(t_D)<x_D<x^R_{B\,J}(t_D)\\ s_{3-}(x_D,t_D), & x^R_{B\,J}(t_D)<x_D<x^R_{F\,J}(t_D)\\ s^{(3)-(2)-}(x_D,t_D), & x^R_{F\,J}(t_D)<x_D<x^R_{G\,K}(t_D)\\ s^{(2-)}, & x^R_{G\,K}(t_D)<x_D<x^S_{G\,H}(t_D)\\ s^{(2)}, & x^S_{G\,H}(t_D)<x_D<\lambda_{(2)}\left(\vec{c}^{(2)},\xi^{(I)}\right)t_D\\ s^{(2)-(1)}(x_D,t_D), & \lambda_{(2)}\left(\vec{c}^{(2)},\xi^{(I)}\right)t_D<x_D<\lambda_{(2)}\left(\vec{c}^{(1)},\xi^{(I)}\right)t_D\\ s^{(1)}, & \lambda_{(2)}\left(\vec{c}^{(1)},\xi^{(I)}\right)t_D<x_D<\lambda_{(1)}\left(\vec{c}^{(1)},\xi^{(I)}\right)t_D\\ s^{(1)-(I+)}(x_D,t_D), & \lambda_{(1)}\left(\vec{c}^{(1)},\xi^{(I)}\right)t_D<x_D<\lambda_{(1)}\left(\vec{c}^{(I)},\xi^{(I)}\right)t_D\\ s^{(I+)}, & \lambda_{(1)}\left(\vec{c}^{(I)},\xi^{(I)}\right)t_D<x_D<D_{(s)}t_D\\ s^{(I)}, & x_D>D_{(s)}t_D\end{cases}\tag{C.10}$$

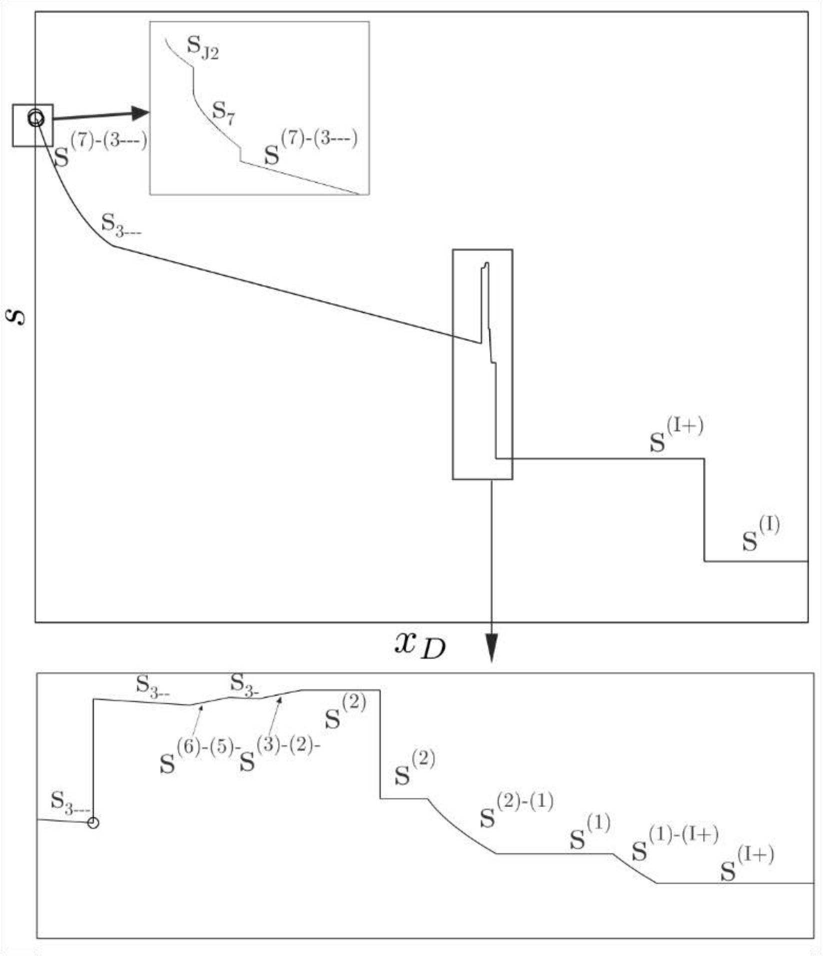

Figure C.25: Water saturation profile for s_{IX}

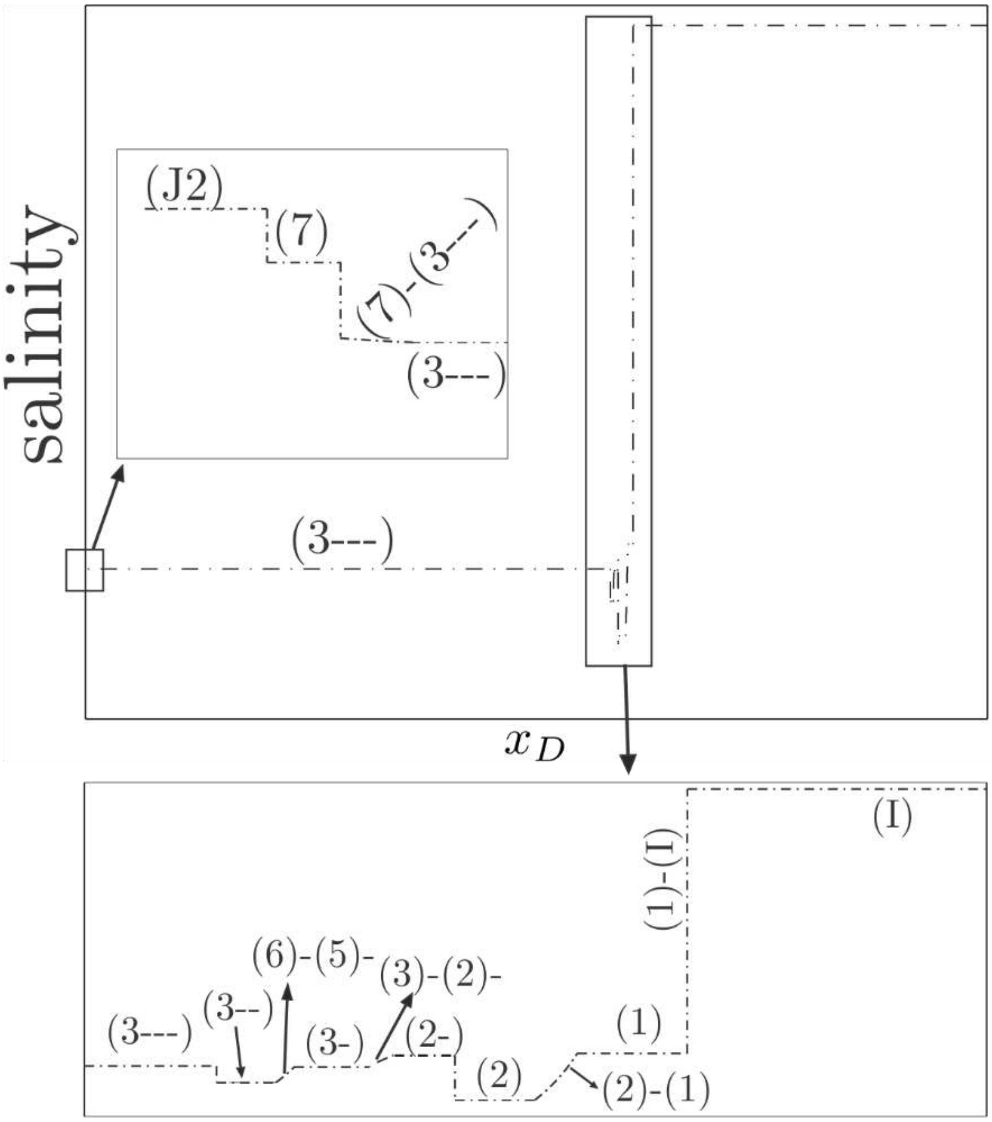

Figure C.26: Salinity profile for $t_G < t_D < t_H$

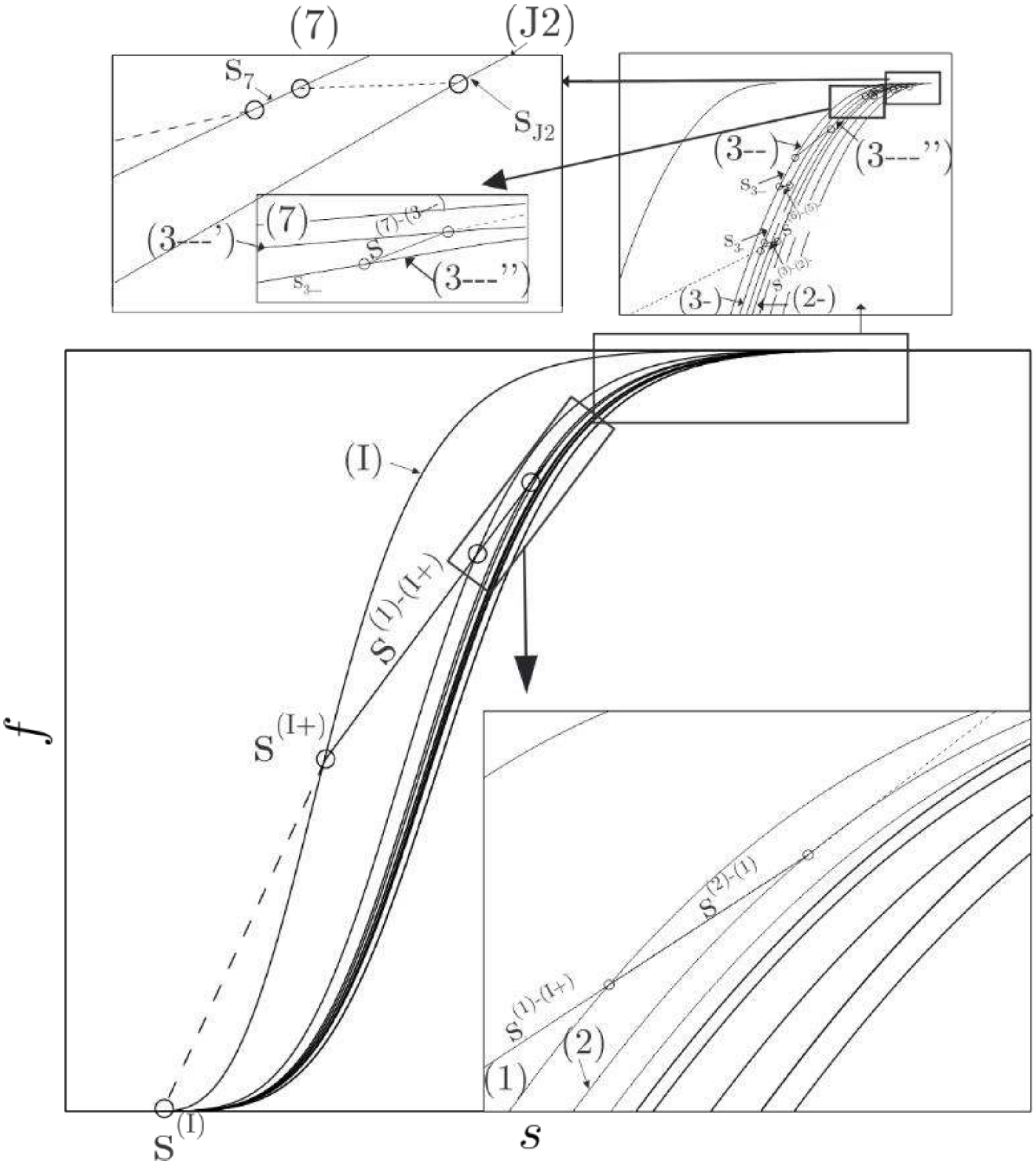

Figure C.27: Solution path of s_{IX} in $f \times s$ plane

In solution s_X $(t_H < t_D < t_I)$, the shock wave $k = 1$ from the rear interacts with the rarefaction wave $k = 2$ from the front of the low salinity slug. Therefore, the constant state (2) no longer appears in salinity and saturation solutions. Note that the increase in salinity in this region results in the appearance of a new small water bank in saturation solution. The solution path of s_X in the $f \times s$ plane is presented in figure (C.30).

$$s_X = \begin{cases} s_{J2}(x_D, t_D), & x_D < x^S_{HS\,pH}(t_D) \\ s_7(x_D, t_D), & x^S_{HS\,pH}(t_D) < x_D < x^S_{d\,pH}(t_D) \\ s^{(7)-(3---)}(x_D, t_D), & x^S_{d\,pH}(t_D) < x_D < x^R_{E\,\infty}(t_D) \\ s_{3---}(x_D, t_D), & x^R_{E\,\infty}(t_D) < x_D < x^S_{E\,N}(t_D) \\ s_{3--}(x_D, t_D), & x^S_{E\,N}(t_D) < x_D < x^R_{C\,L}(t_D) \\ s^{(6)-(5)-}(x_D, t_D), & x^R_{C\,L}(t_D) < x_D < x^R_{B\,J}(t_D) \\ s_{3-}(x_D, t_D), & x^R_{B\,J}(t_D) < x_D < x^R_{F\,J}(t_D) \\ s^{(3)-(2)-}(x_D, t_D), & x^R_{F\,J}(t_D) < x_D < x^R_{G\,K}(t_D) \\ s^{(2-)}, & x^R_{G\,K}(t_D) < x_D < x^R_{H\,\infty}(t_D) \\ s^{(2)-(1)-}(x_D, t_D), & x^R_{H\,\infty}(t_D) < x_D < x^S_{H\,I}(t_D) \\ s^{(2)-(1)}(x_D, t_D), & x^S_{H\,I}(t_D) < x_D < \lambda_{(2)}\left(\vec{c}^{(1)}, \xi^{(I)}\right)t_D \\ s^{(1)}, & \lambda_{(2)}\left(\vec{c}^{(1)}, \xi^{(I)}\right)t_D < x_D < \lambda_{(1)}\left(\vec{c}^{(1)}, \xi^{(I)}\right)t_D \\ s^{(1)-(I+)}(x_D, t_D), & \lambda_{(1)}\left(\vec{c}^{(1)}, \xi^{(I)}\right)t_D < x_D < \lambda_{(1)}\left(\vec{c}^{(I)}, \xi^{(I)}\right)t_D \\ s^{(I+)}, & \lambda_{(1)}\left(\vec{c}^{(I)}, \xi^{(I)}\right)t_D < x_D < D_{(s)}t_D \\ s^{(I)}, & x_D > D_{(s)}t_D \end{cases} \quad \text{(C.11)}$$

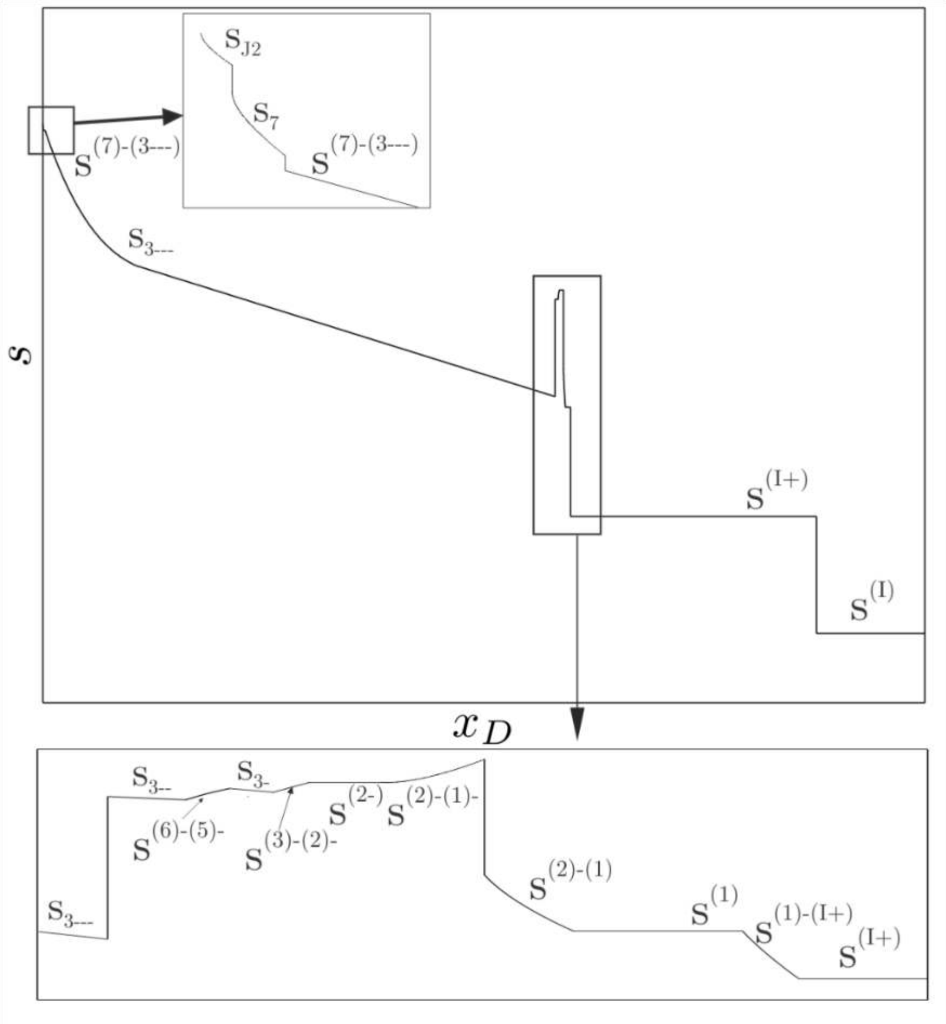

Figure C.28: Water saturation profile for s_X

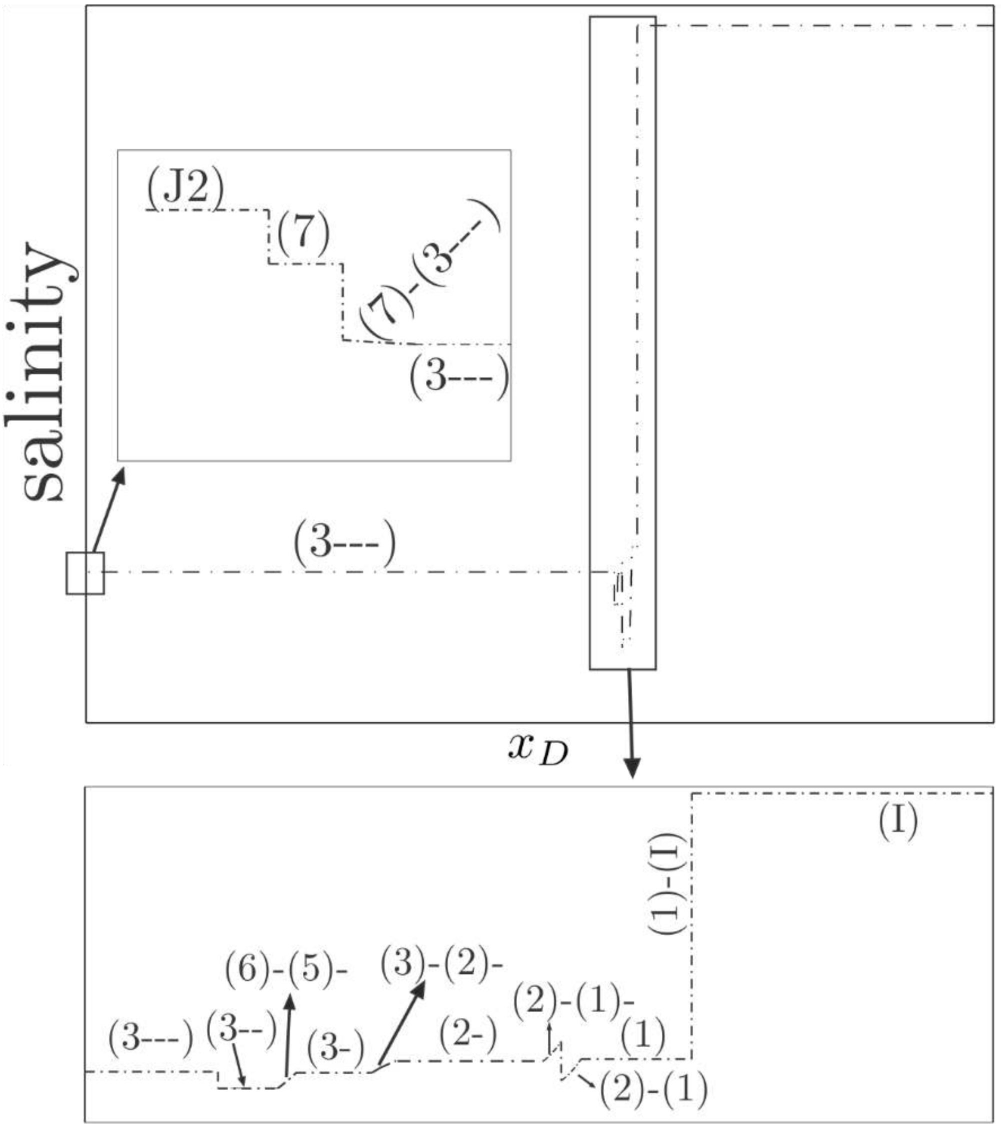

Figure C.29: Salinity profile for $t_H < t_D < t_I$

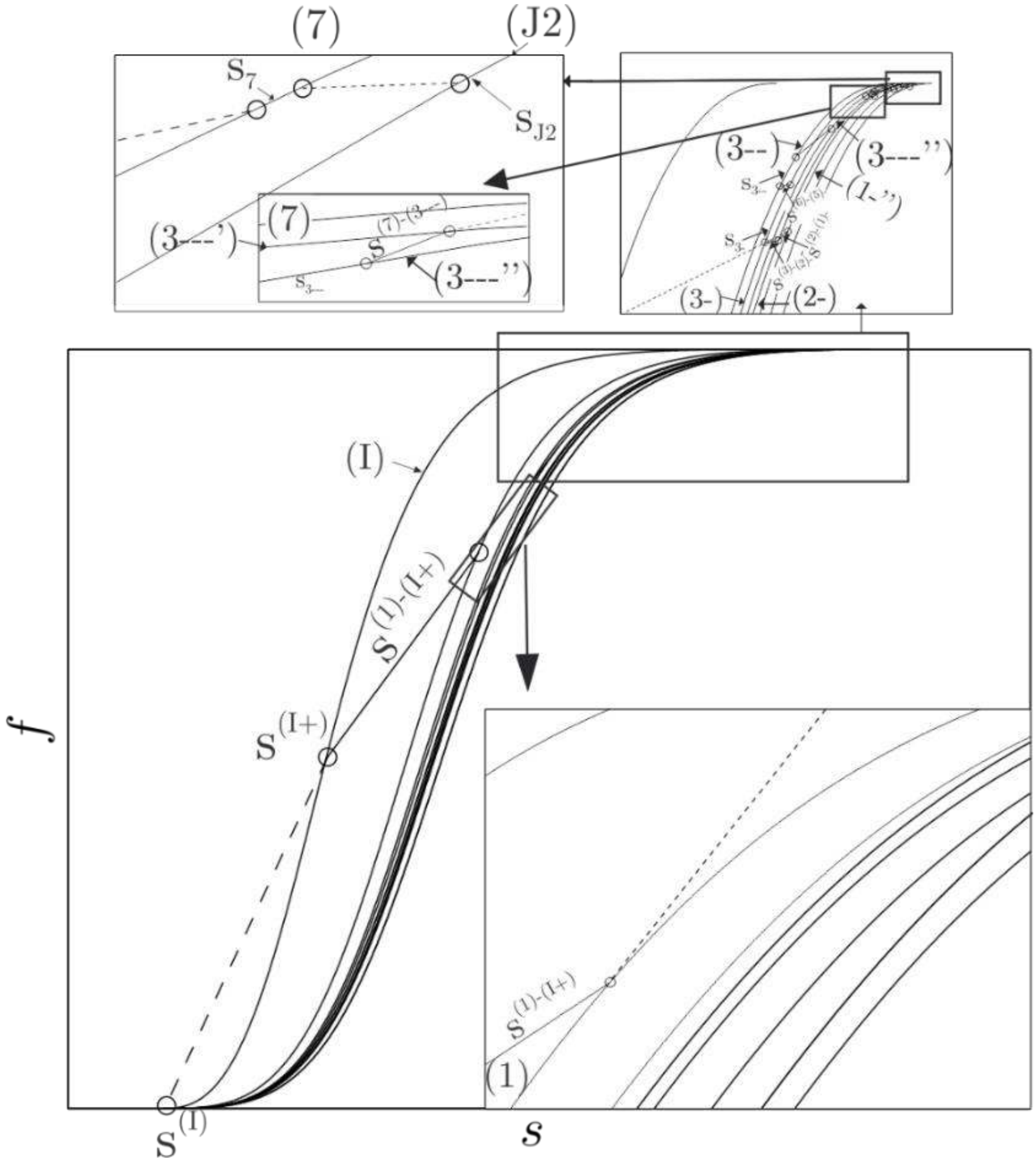

Figure C.30: Solution path of s_X in $f \times s$ plane

In solution s_{XI} ($t_I < t_D < t_{pH}$) the interaction between the waves $k = 1$ from the rear and $k = 2$ from the front ends and the salinity region (2)-(1) (Figure C.32) and its equivalent in saturation solution $s^{(2)-(1)}$ (Figure C.31) no longer exist. On the other hand, the constant state (1-) (and $s^{(1-)}$ in saturation solution) appears in the solution. The solution path of s_{XI} in $f \times s$ plane is shown in figure (C.33).

$$s_{XI} = \begin{cases} s_{J2}(x_D, t_D), & x_D < x^S_{HS\,pH}(t_D) \\ s_7(x_D, t_D), & x^S_{HS\,pH}(t_D) < x_D < x^S_{d\,pH}(t_D) \\ s^{(7)-(3---)}(x_D, t_D), & x^S_{d\,pH}(t_D) < x_D < x^R_{E\,\infty}(t_D) \\ s_{3---}(x_D, t_D), & x^R_{E\,\infty}(t_D) < x_D < x^S_{E\,N}(t_D) \\ s_{3--}(x_D, t_D), & x^S_{E\,N}(t_D) < x_D < x^R_{C\,L}(t_D) \\ s^{(6)-(5)-}(x_D, t_D), & x^R_{C\,L}(t_D) < x_D < x^R_{B\,J}(t_D) \\ s_{3-}(x_D, t_D), & x^R_{B\,J}(t_D) < x_D < x^R_{F\,J}(t_D) \\ s^{(3)-(2)-}(x_D, t_D), & x^R_{F\,J}(t_D) < x_D < x^R_{G\,K}(t_D) \\ s^{(2-)}, & x^R_{G\,K}(t_D) < x_D < x^R_{H\,\infty}(t_D) \\ s^{(2)-(1)-}(x_D, t_D), & x^R_{H\,\infty}(t_D) < x_D < x^R_{I\,\infty}(t_D) \\ s^{(1-)}, & x^R_{I\,\infty}(t_D) < x_D < x^S_{I\,\infty}(t_D) \\ s^{(1)}, & x^S_{I\,\infty}(t_D) < x_D < \lambda_{(1)}\left(\vec{c}^{(1)}, \xi^{(I)}\right)t_D \\ s^{(1)-(I+)}(x_D, t_D), & \lambda_{(1)}\left(\vec{c}^{(1)}, \xi^{(I)}\right)t_D < x_D < \lambda_{(1)}\left(\vec{c}^{(I)}, \xi^{(I)}\right)t_D \\ s^{(I+)}, & \lambda_{(1)}\left(\vec{c}^{(I)}, \xi^{(I)}\right)t_D < x_D < D_{(s)}t_D \\ s^{(I)}, & x_D > D_{(s)}t_D \end{cases} \tag{C.12}$$

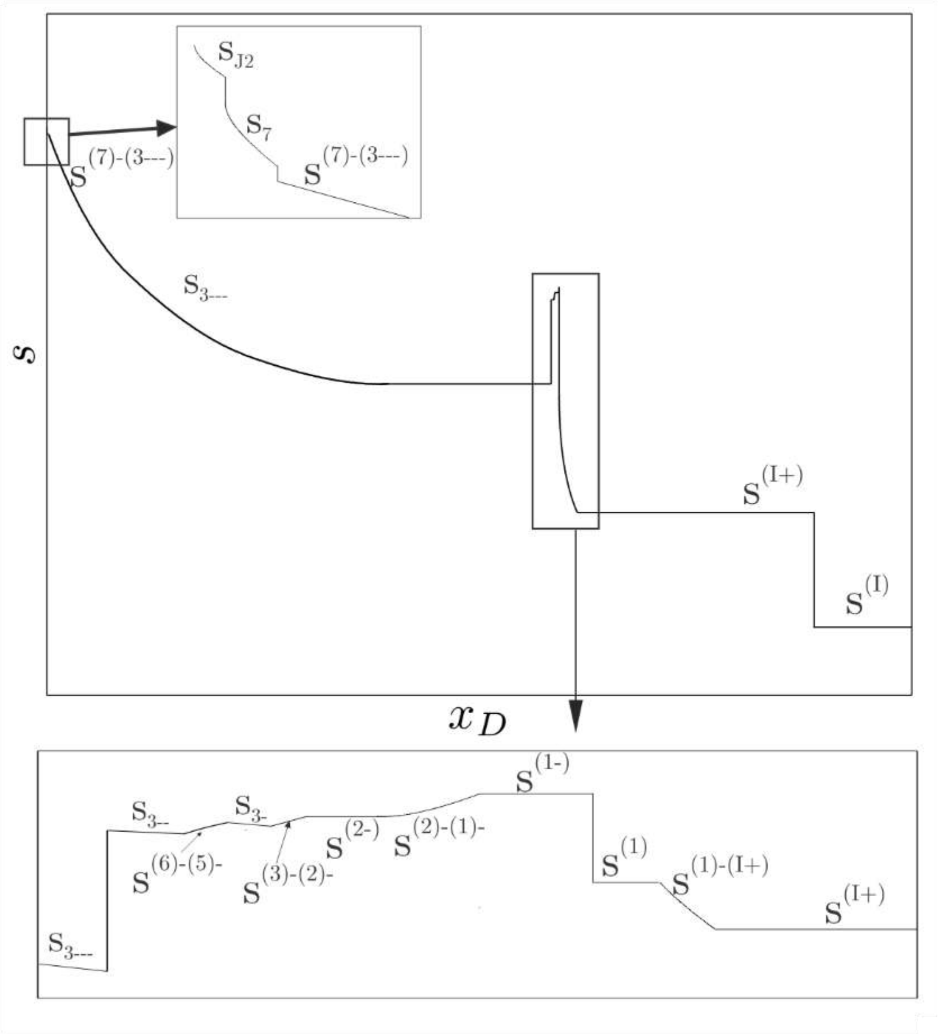

Figure C.31: Water saturation profile for s_{XI}

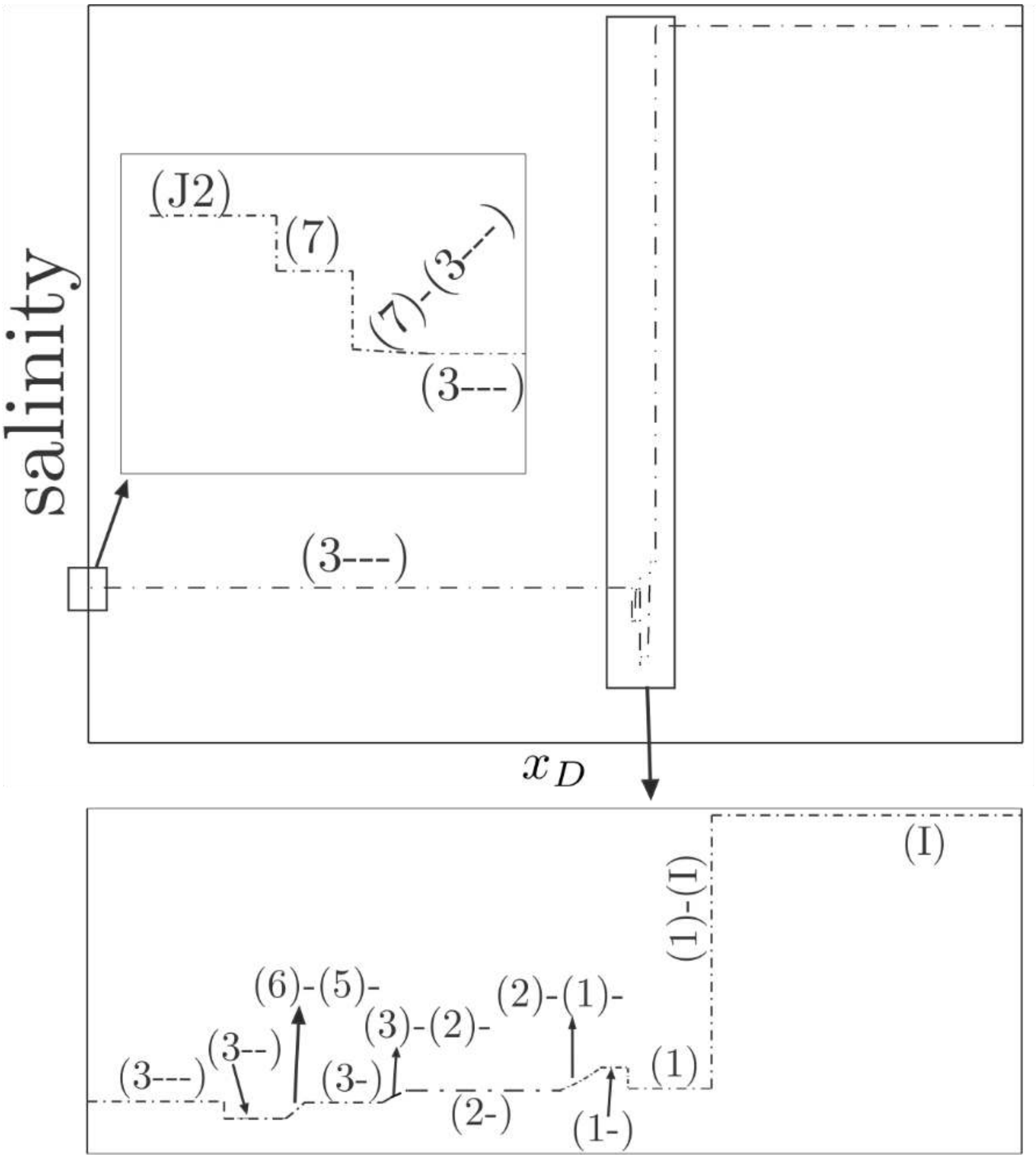

Figure C.32: Salinity profile for $t_I < t_D < t_{pH}$

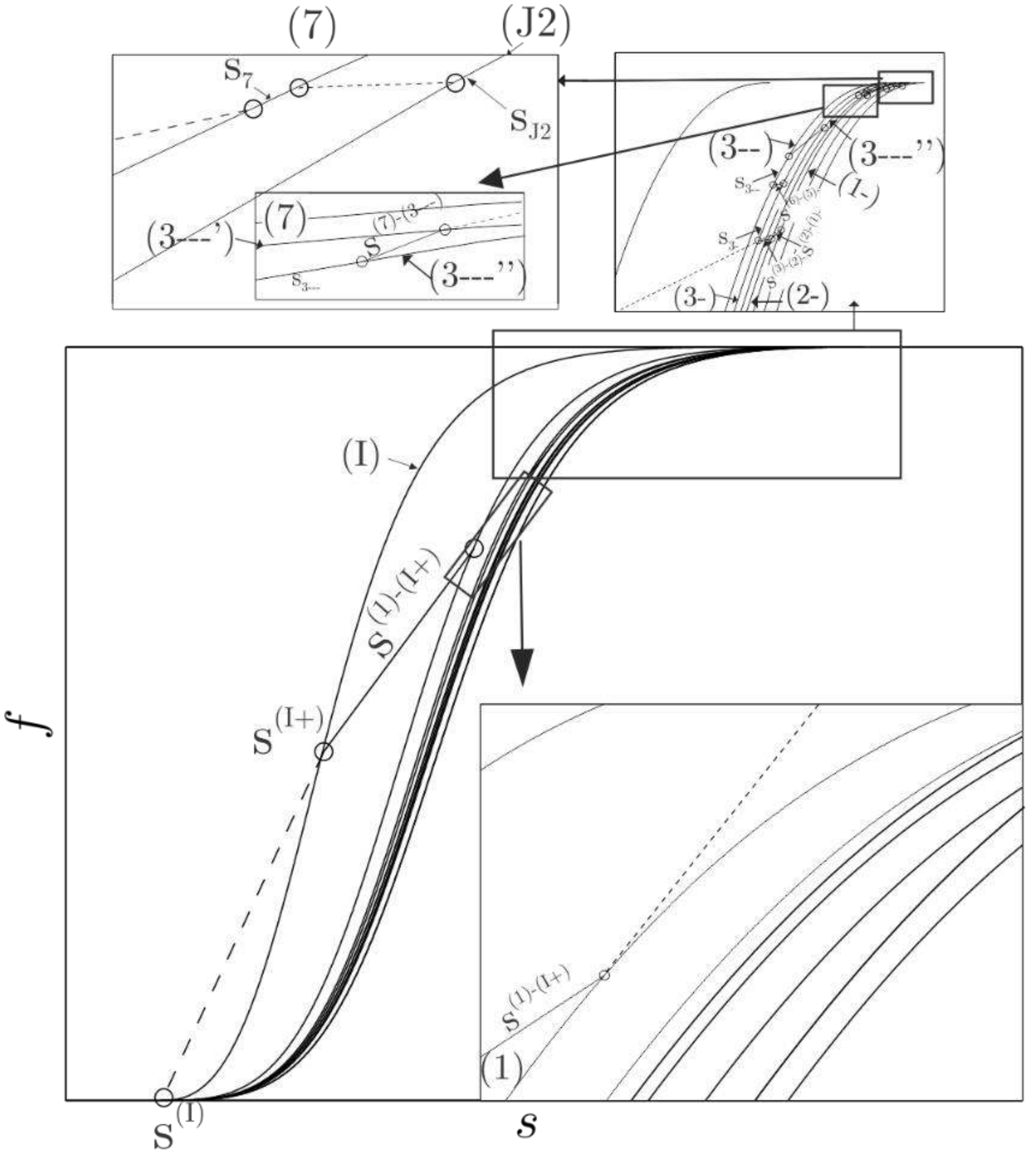

Figure C.33: Solution path of s_{XI} in $f \times s$ plane

The pH waves from the front and from the rear of the slug interact with each other in solution s_{XII} (Equation C.13). The effect of this interaction is the disappearance of region (7) in salinity and saturation solutions (Figures C.34and C.35). The generated wave does not carry the pH effects in the reservoir.

$$s_{XII} = \begin{cases} s_{J2}(x_D, t_D), & x_D < x^S_{pH\,\infty}(t_D) \\ s^{(7)-(3---)}(x_D, t_D), & x^S_{pH\,\infty}(t_D) < x_D < x^R_{E\,\infty}(t_D) \\ s_{3---}(x_D, t_D), & x^R_{E\,\infty}(t_D) < x_D < x^S_{E\,N}(t_D) \\ s_{3--}(x_D, t_D), & x^S_{E\,N}(t_D) < x_D < x^R_{C\,L}(t_D) \\ s^{(6)-(5)-}(x_D, t_D), & x^R_{C\,L}(t_D) < x_D < x^R_{B\,J}(t_D) \\ s_{3-}(x_D, t_D), & x^R_{B\,J}(t_D) < x_D < x^R_{F\,J}(t_D) \\ s^{(3)-(2)-}(x_D, t_D), & x^R_{F\,J}(t_D) < x_D < x^R_{G\,K}(t_D) \\ s^{(2-)}, & x^R_{G\,K}(t_D) < x_D < x^R_{H\,\infty}(t_D) \\ s^{(2)-(1)-}(x_D, t_D), & x^R_{H\,\infty}(t_D) < x_D < x^R_{I\,\infty}(t_D) \\ s^{(1-)}, & x^R_{I\,\infty}(t_D) < x_D < x^S_{I\,\infty}(t_D) \\ s^{(1)}, & x^S_{I\,\infty}(t_D) < x_D < \lambda_{(1)}\left(\vec{c}^{(1)}, \xi^{(I)}\right)t_D \\ s^{(1)-(I+)}(x_D, t_D), & \lambda_{(1)}\left(\vec{c}^{(1)}, \xi^{(I)}\right)t_D < x_D < \lambda_{(1)}\left(\vec{c}^{(I)}, \xi^{(I)}\right)t_D \\ s^{(I+)}, & \lambda_{(1)}\left(\vec{c}^{(I)}, \xi^{(I)}\right)t_D < x_D < D_{(s)}t_D \\ s^{(I)}, & x_D > D_{(s)}t_D \end{cases} \tag{C.13}$$

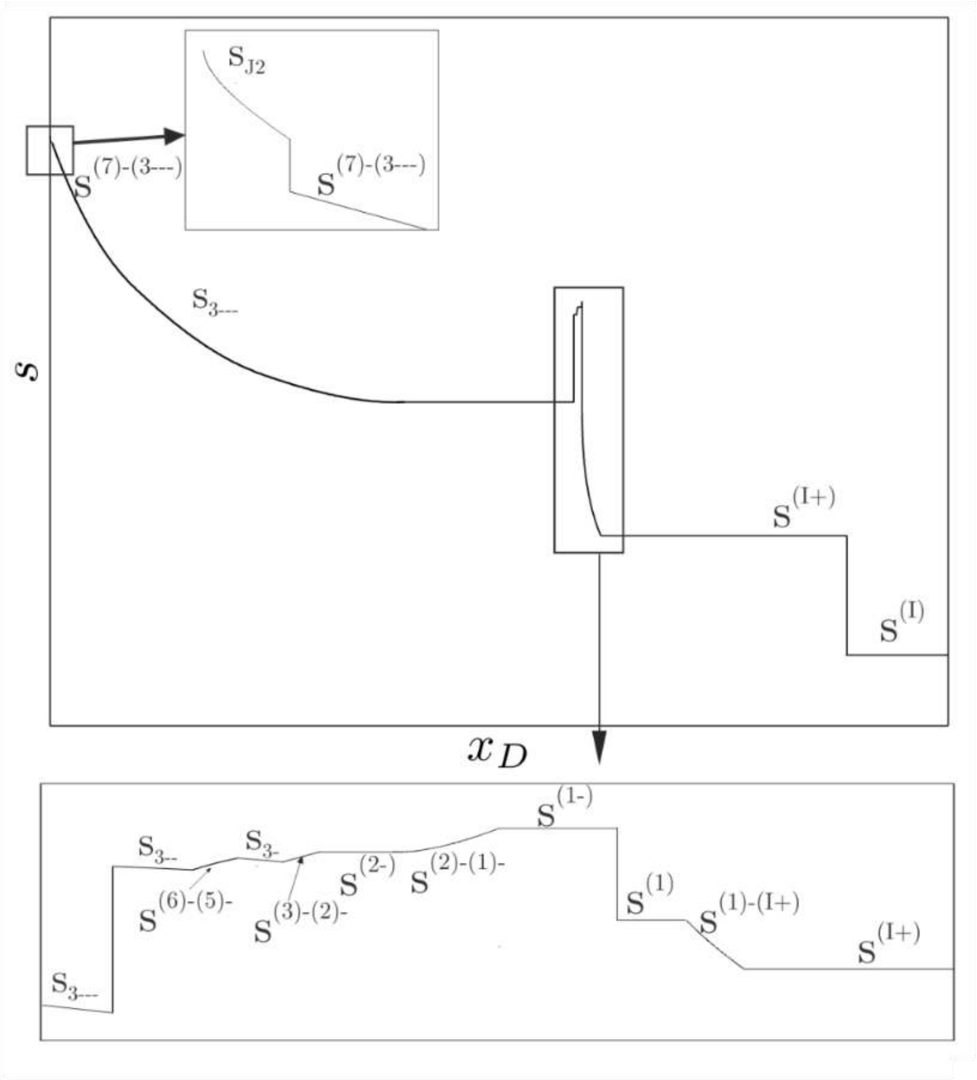

Figure C.34: Water saturation profile for s_{XII}

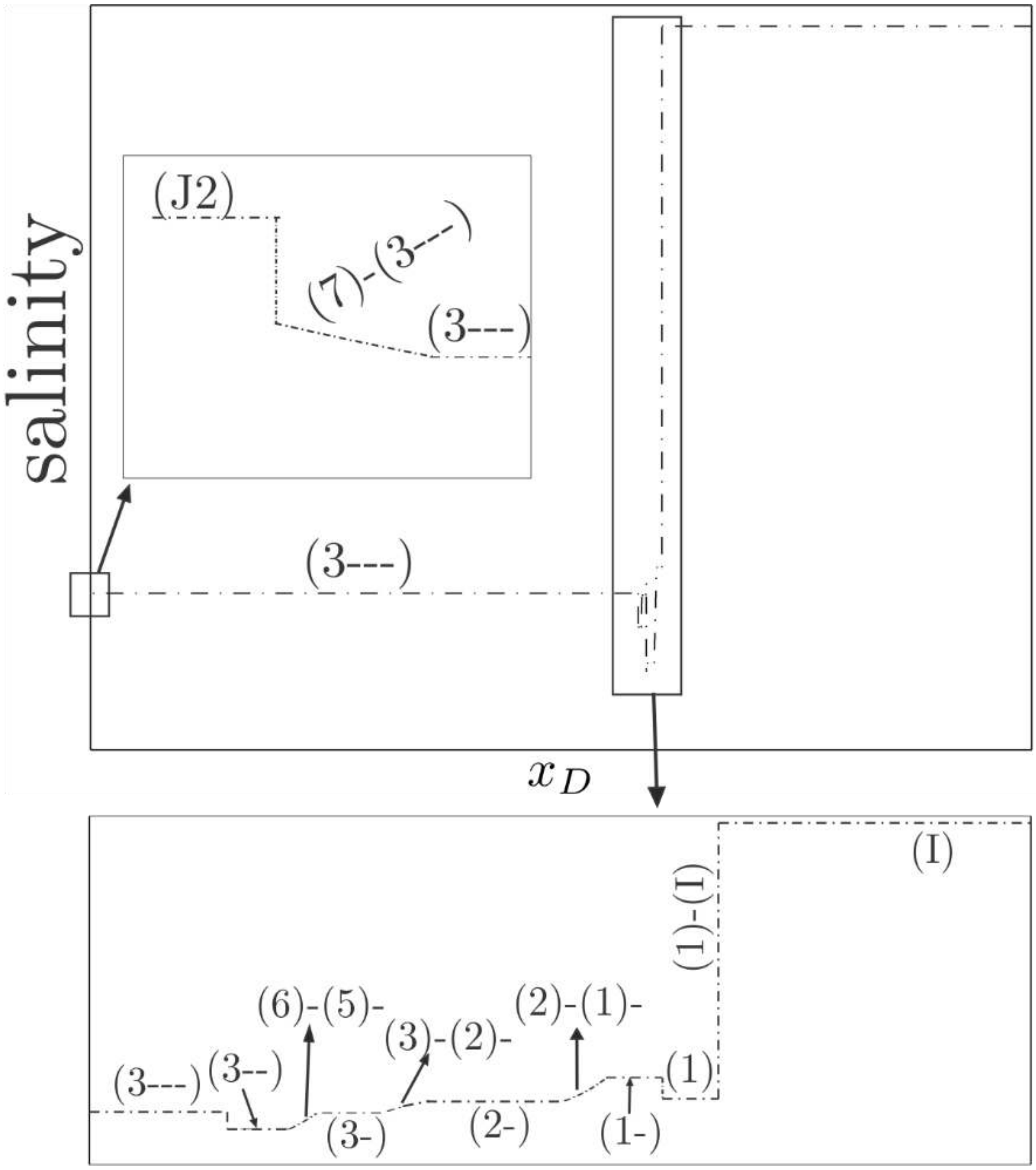

Figure C.35: Salinity profile for $t_{pH} < t_D < t_J$

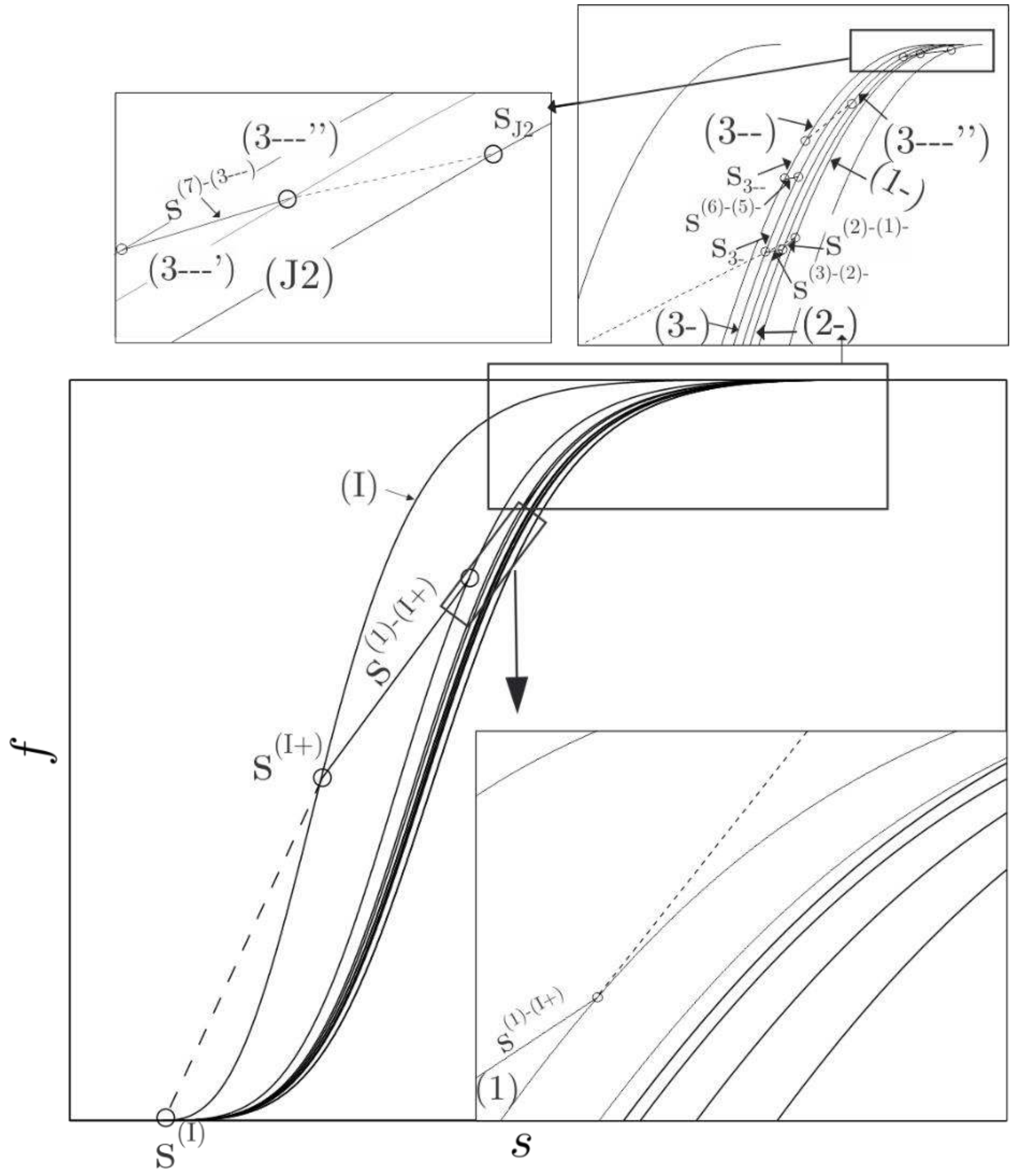

Figure C.36: Solution path of s_{XII} in $f \times s$ plane

In solution s_{XIII} (Equation C.14) the rarefaction wave $k = 2$ from the rear and $k = 3$ from the front of the low salinity slug interact, which leads to the disappearance of region (3-) (Figure C.38) and rarefaction s_{3-} (Figure C.37), and the appearance of the region where these two waves interact: region (3)-(2)— in salinity solution and rarefaction $s^{(3)-(2)--}$ in saturation solution. In the region where the two waves interact there is a slight salinity increase in salinity and thus, a slight increase in water saturation. The solution path of s_{XIII} is displayed in figure (C.39).

$$s_{XIII} = \begin{cases} s_{J2}(x_D, t_D), & x_D < x^S_{pH\,\infty}(t_D) \\ s^{(7)-(3---)}(x_D, t_D), & x^S_{pH\,\infty}(t_D) < x_D < x^R_{E\,\infty}(t_D) \\ s_{3---}(x_D, t_D), & x^R_{E\,\infty}(t_D) < x_D < x^S_{E\,N}(t_D) \\ s_{3--}(x_D, t_D), & x^S_{E\,N}(t_D) < x_D < x^R_{C\,L}(t_D) \\ s^{(6)-(5)-}(x_D, t_D), & x^R_{C\,L}(t_D) < x_D < x^R_{J\,L}(t_D) \\ s^{(3)-(2)--}(x_D, t_D), & x^R_{J\,L}(t_D) < x_D < x^R_{J\,K}(t_D) \\ s^{(3)-(2)-}(x_D, t_D), & x^R_{J\,K}(t_D) < x_D < x^R_{G\,K}(t_D) \\ s^{(2-)}, & x^R_{G\,K}(t_D) < x_D < x^R_{H\,\infty}(t_D) \\ s^{(2)-(1)-}(x_D, t_D), & x^R_{H\,\infty}(t_D) < x_D < x^R_{I\,\infty}(t_D) \\ s^{(1-)}, & x^R_{I\,\infty}(t_D) < x_D < x^S_{I\,\infty}(t_D) \\ s^{(1)}, & x^S_{I\,\infty}(t_D) < x_D < \lambda_{(1)}\left(\vec{c}^{(1)}, \xi^{(I)}\right)t_D \\ s^{(1)-(I+)}(x_D, t_D), & \lambda_{(1)}\left(\vec{c}^{(1)}, \xi^{(I)}\right)t_D < x_D < \lambda_{(1)}\left(\vec{c}^{(I)}, \xi^{(I)}\right)t_D \\ s^{(I+)}, & \lambda_{(1)}\left(\vec{c}^{(I)}, \xi^{(I)}\right)t_D < x_D < D_{(s)}t_D \\ s^{(I)}, & x_D > D_{(s)}t_D \end{cases} \tag{C.14}$$

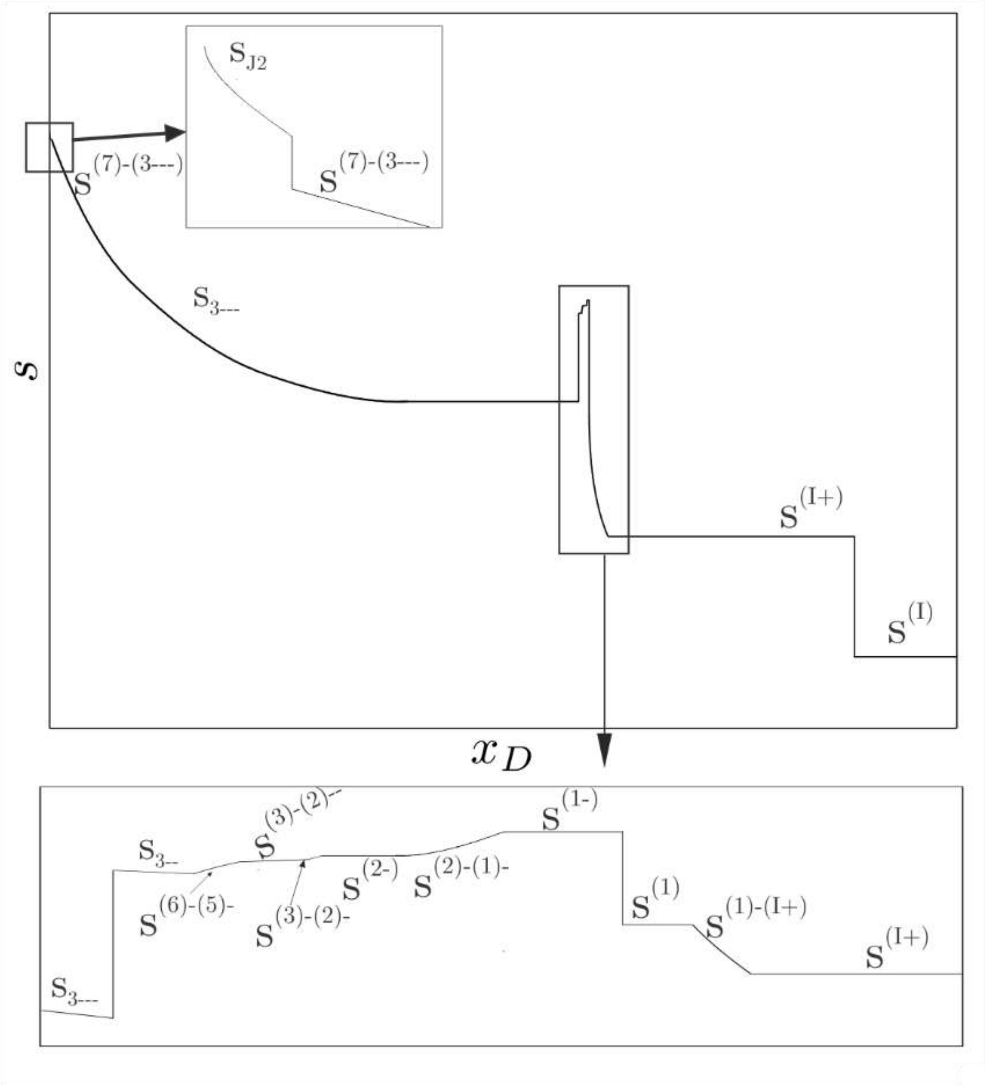

Figure C.37: Water saturation profile for s_{XIII}

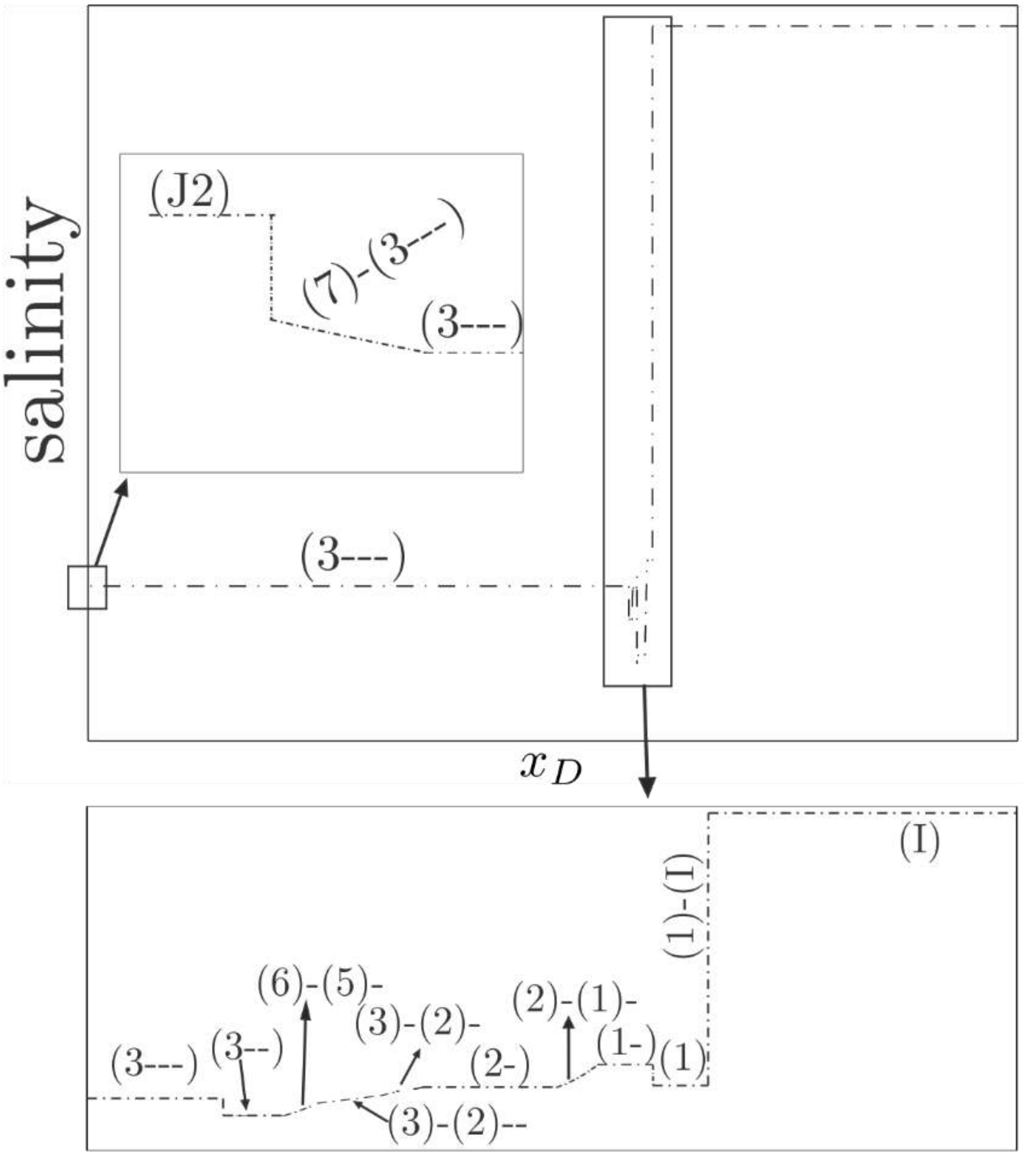

Figure C.38: Salinity profile for $t_J < t_D < t_K$

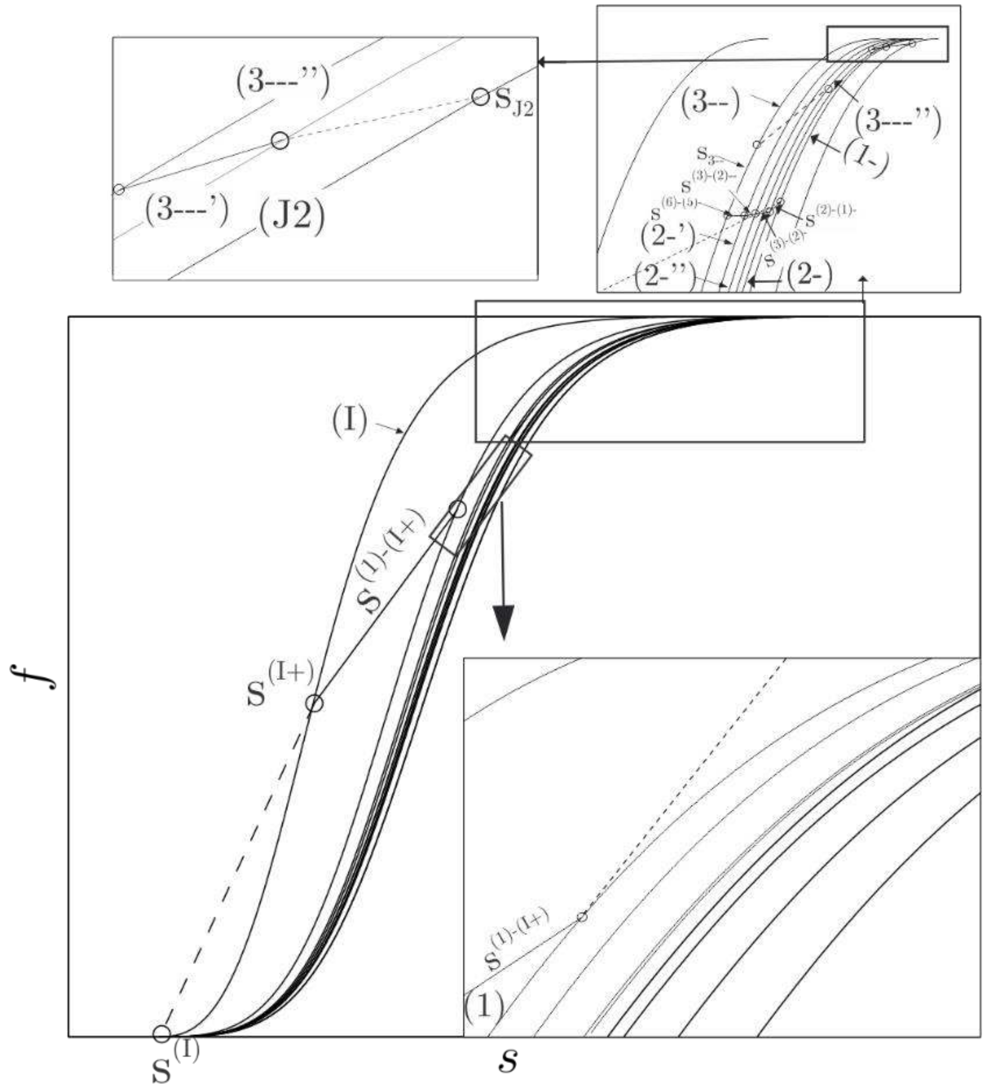

Figure C.39: Solution path of s_{XIII} in $f \times s$ plane

Solution s_{XIV} occurs when $t_K < t_D < t_L$, and its main feature is that part of the rarefaction wave $k = 2$ from the rear of the slug have crossed all the rarefaction $k = 3$ from the front (salinity wave (6)-(5)-- and saturation $s^{(6)-(5)--}$). Moreover, in this solution all characteristics of the rarefaction $k = 3$ are interacting with the wave $k = 2$. As a result, the region (3)-(2)- no longer exists in salinity solution, and the rarefaction $s^{(3)-(2)-}$ disappears in saturation solution. Note that the salinity increase in region (6)-(5)-- resulted in water saturation increase, and the water bank in the central part of saturation solution also increased. The solution path of s_{XIV} in $f \times s$ plane is presented in figure (C.42).

$$s_{XIV}=\begin{cases} s_{J2}(x_D,t_D), & x_D<x^S_{pH\,\infty}(t_D)\\ s^{(7)-(3---)}(x_D,t_D), & x^S_{pH\,\infty}(t_D)<x_D<x^R_{E\,\infty}(t_D)\\ s_{3---}(x_D,t_D), & x^R_{E\,\infty}(t_D)<x_D<x^S_{E\,N}(t_D)\\ s_{3--}(x_D,t_D), & x^S_{E\,N}(t_D)<x_D<x^R_{C\,L}(t_D)\\ s^{(6)-(5)-}(x_D,t_D), & x^R_{C\,L}(t_D)<x_D<x^R_{J\,L}(t_D)\\ s^{(3)-(2)--}(x_D,t_D), & x^R_{J\,L}(t_D)<x_D<x^R_{K\,M}(t_D)\\ s^{(6)-(5)--}(x_D,t_D), & x^R_{K\,M}(t_D)<x_D<x^R_{K\,\infty}(t_D)\\ s^{(2-)}, & x^R_{K\,\infty}(t_D)<x_D<x^R_{H\,\infty}(t_D)\\ s^{(2)-(1)-}(x_D,t_D), & x^R_{H\,\infty}(t_D)<x_D<x^R_{I\,\infty}(t_D)\\ s^{(1-)}, & x^R_{I\,\infty}(t_D)<x_D<x^S_{I\,\infty}(t_D)\\ s^{(1)}, & x^S_{I\,\infty}(t_D)<x_D<\lambda_{(1)}\big(\vec{c}^{(1)},\xi^{(I)}\big)t_D\\ s^{(1)-(I+)}(x_D,t_D), & \lambda_{(1)}\big(\vec{c}^{(1)},\xi^{(I)}\big)t_D<x_D<\lambda_{(1)}\big(\vec{c}^{(I)},\xi^{(I)}\big)t_D\\ s^{(I+)}, & \lambda_{(1)}\big(\vec{c}^{(I)},\xi^{(I)}\big)t_D<x_D<D_{(s)}t_D\\ s^{(I)}, & x_D>D_{(s)}t_D \end{cases} \tag{C.15}$$

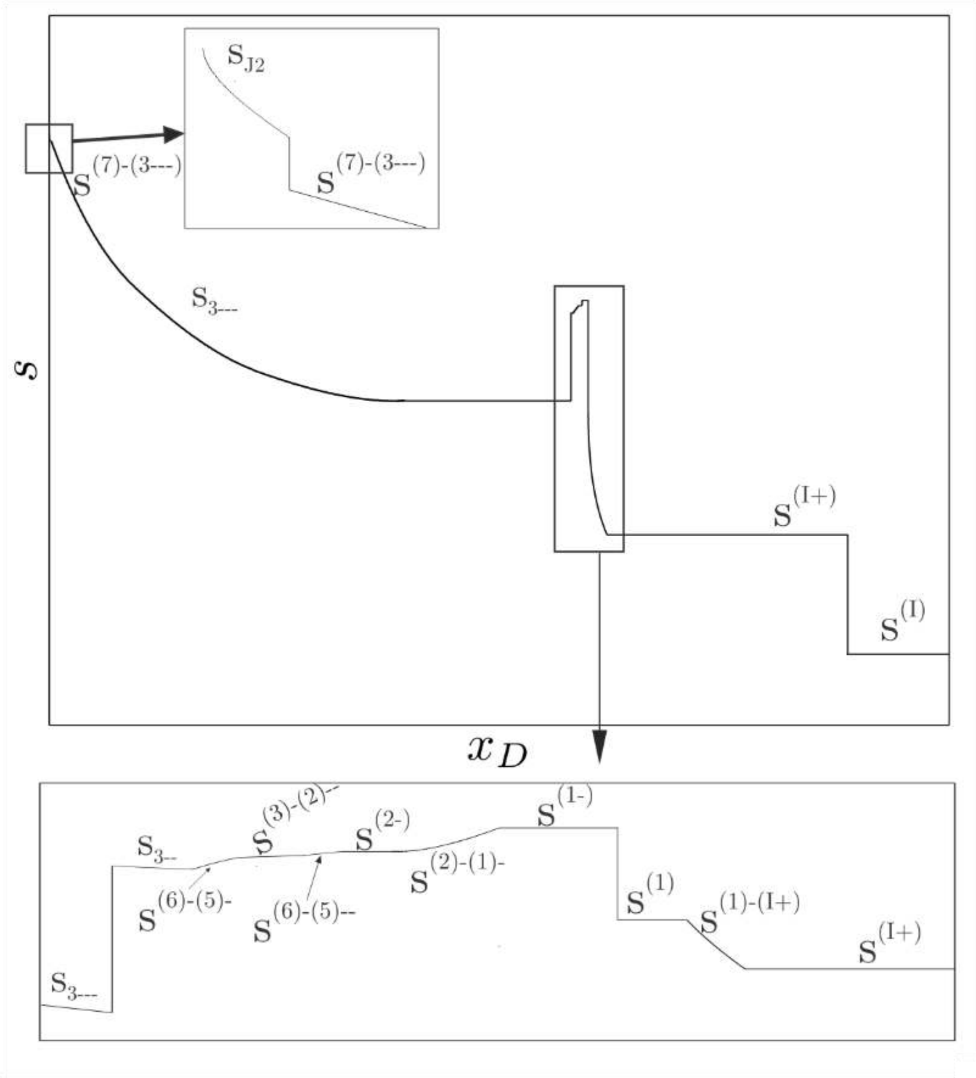

Figure C.40: Water saturation profile for s_{XIV}

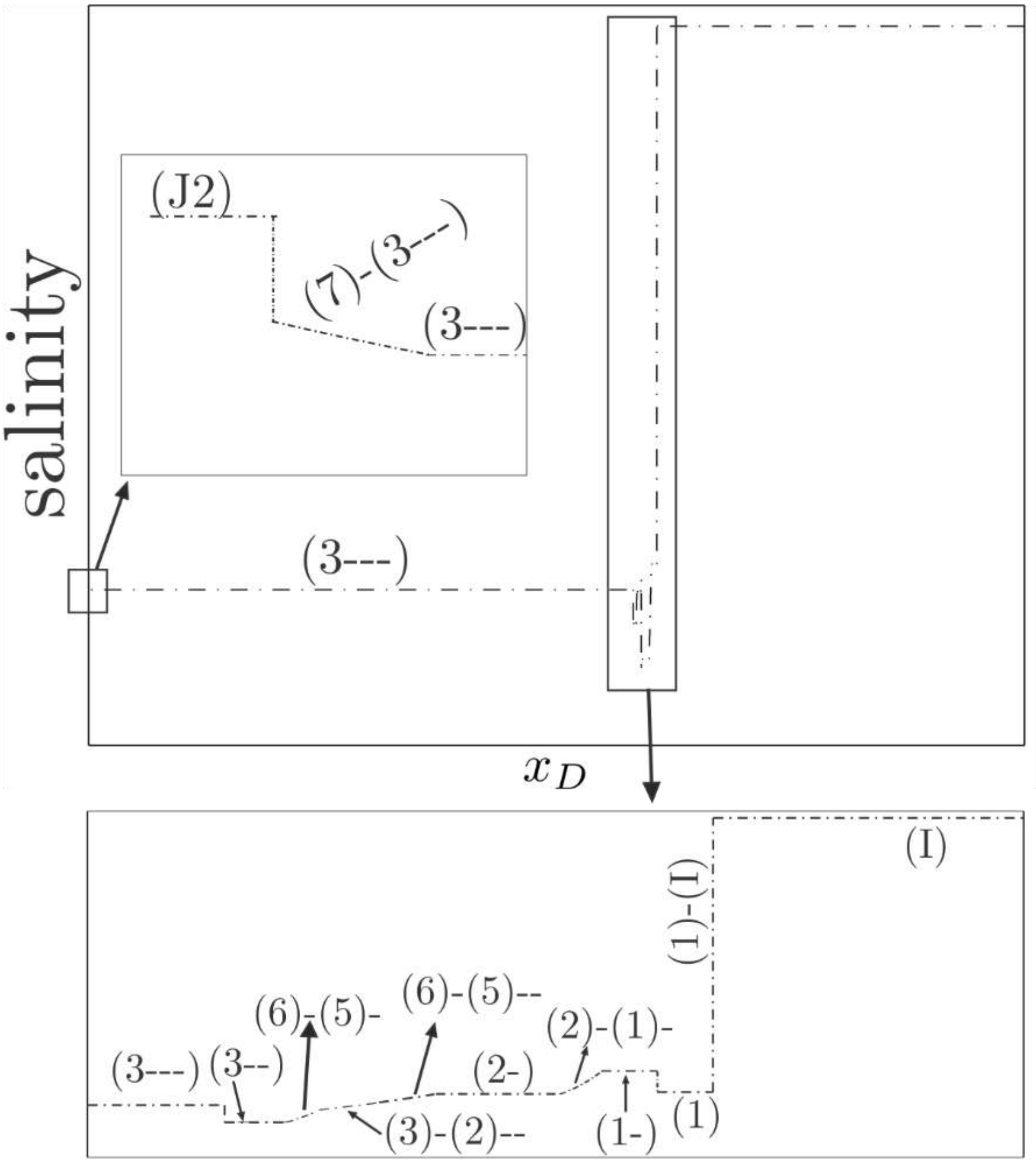

Figure C.41: Salinity profile for $t_K < t_D < t_L$

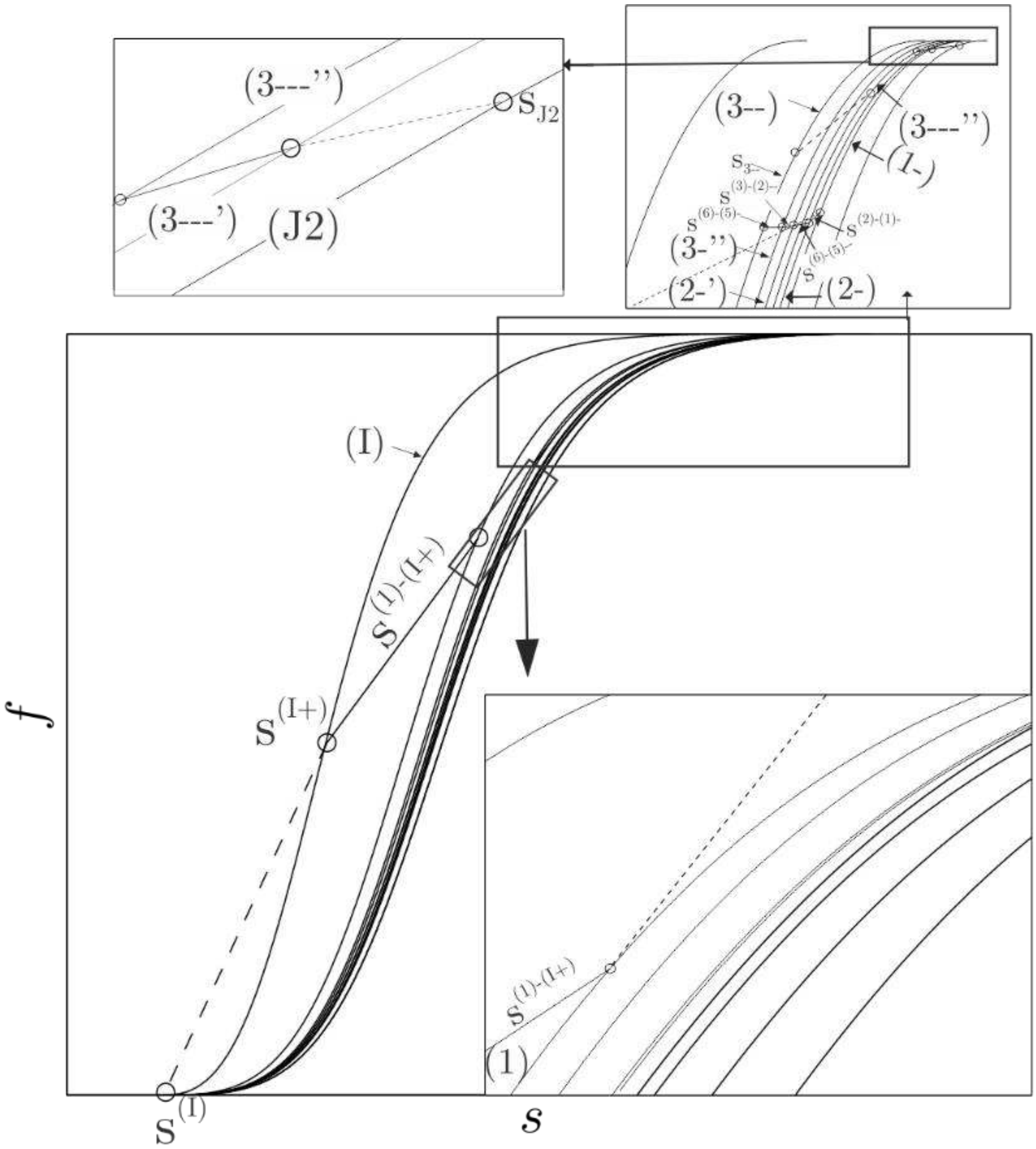

Figure C.42: Solution path of s_{XIV} in $f \times s$ plane

For $t_L < t_D < t_M$ (solution s_{XV}, equation C.16), part of the rarefaction $k = 3$ is separated from the rarefaction $k = 2$, however there is still an interaction region between these two waves. The separated part of the rarefaction $k = 2$ creates a new salinity and water saturation region: (3)-(2)--- and $s^{(3)-(2)---}$. In this region the salinity increases (Figure C.44), as well as the water saturation and a the water bank size. The solution path of s_{XV} in $f \times s$ plane is presented in figure (C.44).

$$s_{XV} = \begin{cases} s_{J2}(x_D, t_D), & x_D < x^S_{pH\,\infty}(t_D) \\ s^{(7)-(3---)}(x_D, t_D), & x^S_{pH\,\infty}(t_D) < x_D < x^R_{E\,\infty}(t_D) \\ s_{3---}(x_D, t_D), & x^R_{E\,\infty}(t_D) < x_D < x^S_{E\,N}(t_D) \\ s_{3--}(x_D, t_D), & x^S_{E\,N}(t_D) < x_D < x^R_{L\,N}(t_D) \\ s^{(3)-(2)---}(x_D, t_D), & x^R_{L\,N}(t_D) < x_D < x^R_{L\,M}(t_D) \\ s^{(3)-(2)--}(x_D, t_D), & x^R_{L\,M}(t_D) < x_D < x^R_{K\,M}(t_D) \\ s^{(6)-(5)--}(x_D, t_D), & x^R_{K\,M}(t_D) < x_D < x^R_{K\,\infty}(t_D) \\ s^{(2-)}, & x^R_{K\,\infty}(t_D) < x_D < x^R_{H\,\infty}(t_D) \\ s^{(2)-(1)-}(x_D, t_D), & x^R_{H\,\infty}(t_D) < x_D < x^R_{I\,\infty}(t_D) \\ s^{(1-)}, & x^R_{I\,\infty}(t_D) < x_D < x^S_{I\,\infty}(t_D) \\ s^{(1)}, & x^S_{I\,\infty}(t_D) < x_D < \lambda_{(1)}\left(\vec{c}^{(1)}, \xi^{(I)}\right)t_D \\ s^{(1)-(I+)}(x_D, t_D), & \lambda_{(1)}\left(\vec{c}^{(1)}, \xi^{(I)}\right)t_D < x_D < \lambda_{(1)}\left(\vec{c}^{(I)}, \xi^{(I)}\right)t_D \\ s^{(I+)}, & \lambda_{(1)}\left(\vec{c}^{(I)}, \xi^{(I)}\right)t_D < x_D < D_{(s)}t_D \\ s^{(I)}, & x_D > D_{(s)}t_D \end{cases} \tag{C.16}$$

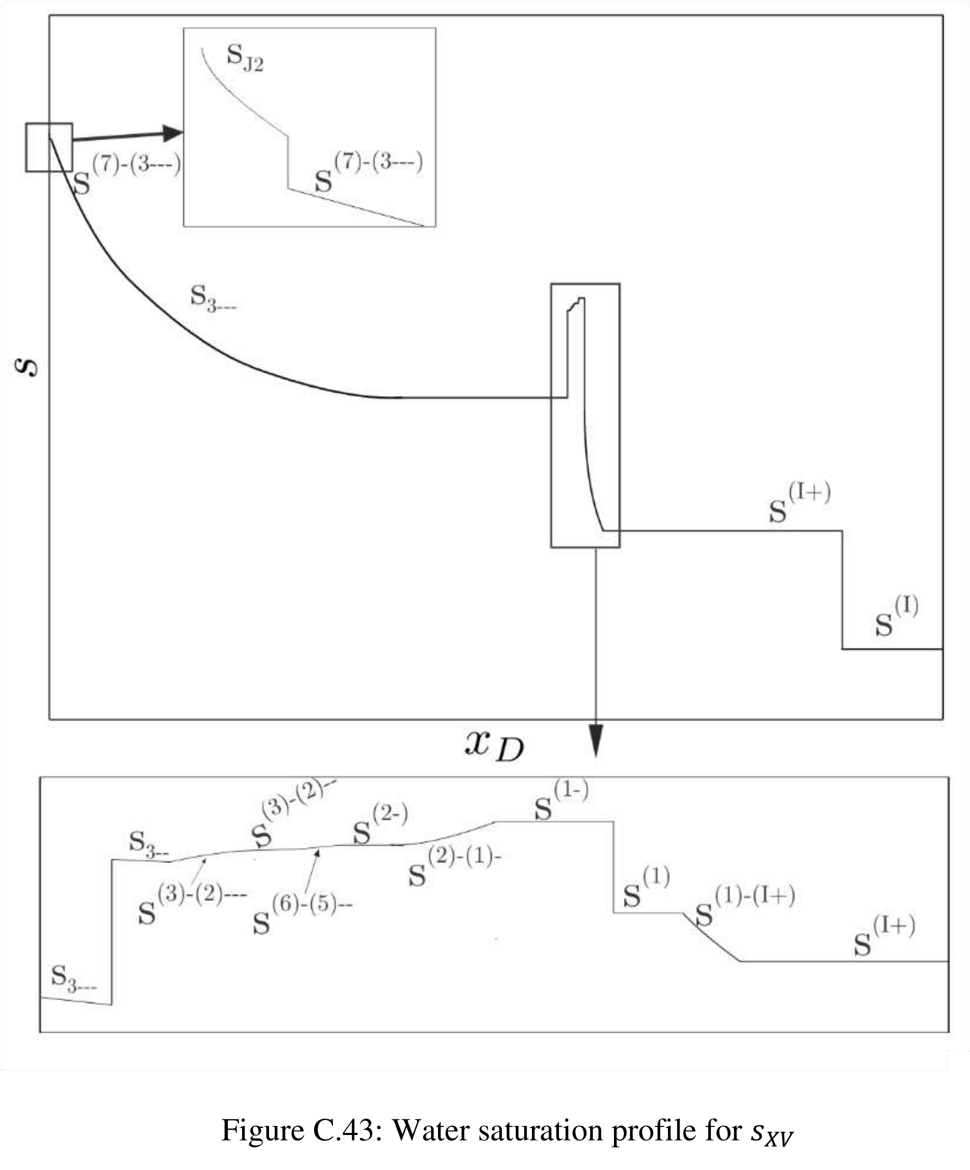

Figure C.43: Water saturation profile for s_{XV}

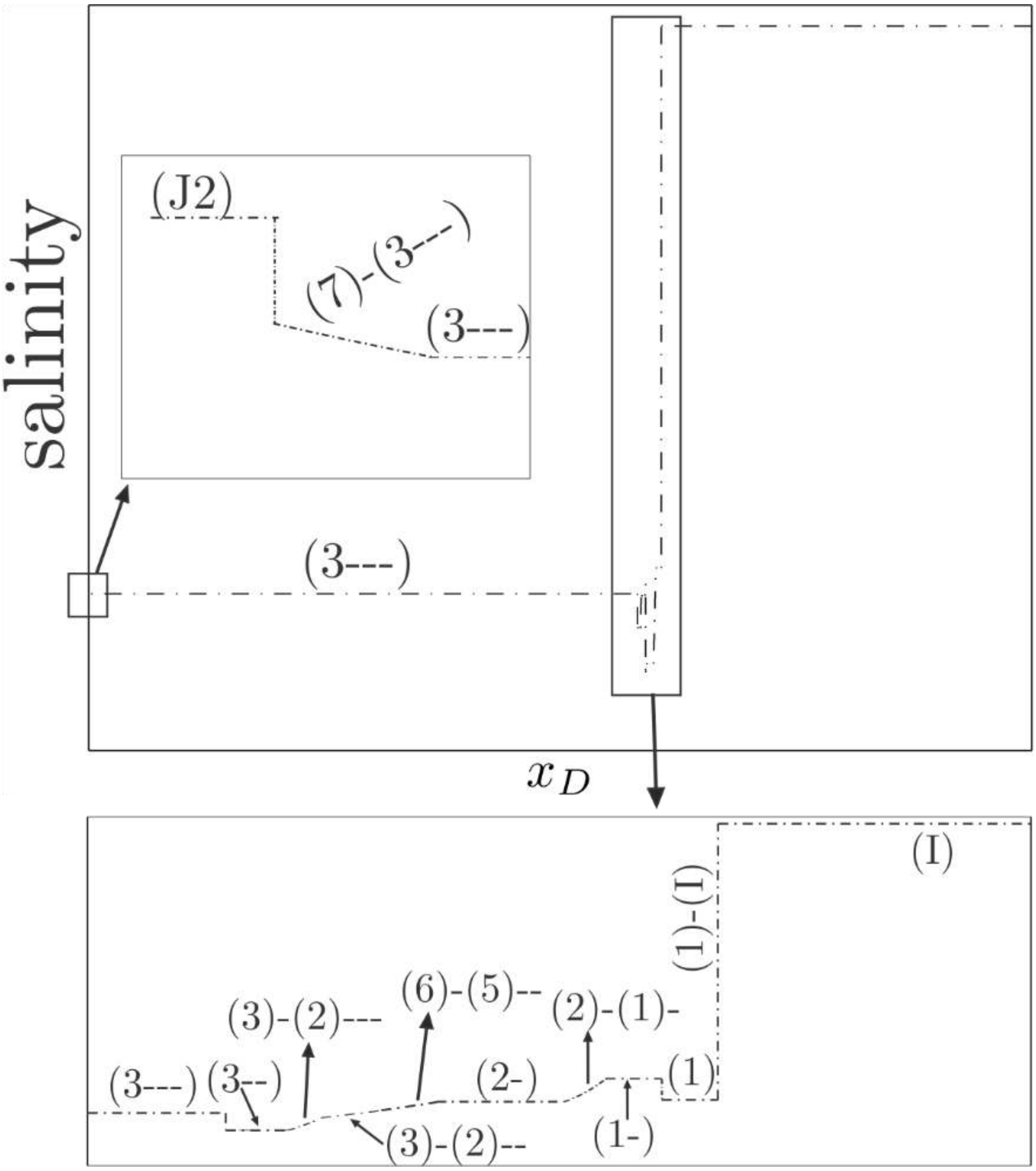

Figure C.44: Salinity profile for $t_L < t_D < t_M$

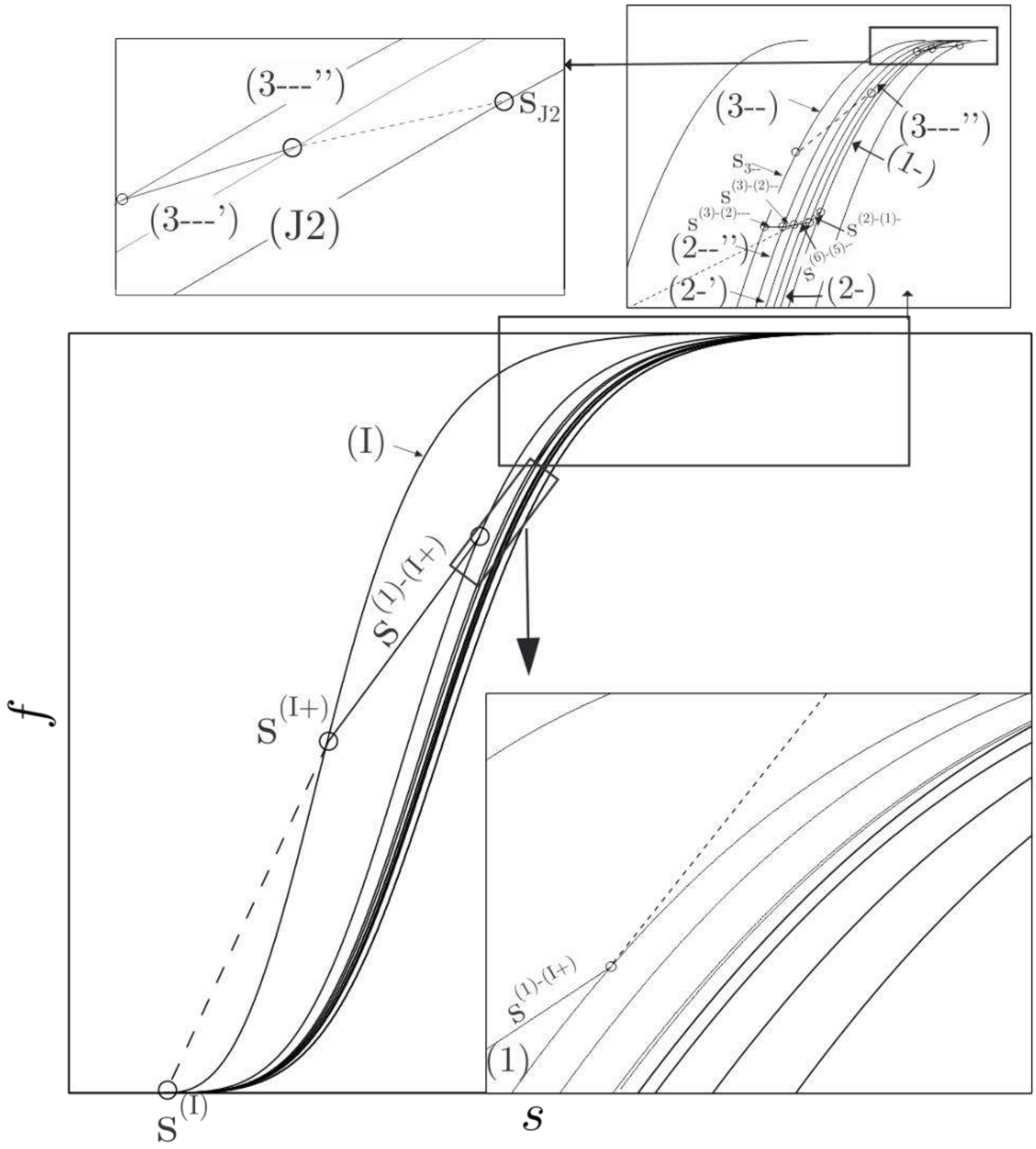

Figure C.45: Solution path of s_{XV} in $f \times s$ plane

Solution s_{XVI} (Equation C.17) takes place in the region $t_M < t_D < t_N$. In this solution, the waves $k = 2$ from the rear and $k = 3$ from the front are completely separated, and therefore the region (3)-(2)-- disappears. Moreover, there is a new constant state (2--) in the solution. The solution path of s_{XVI} in $f \times s$ plane is presented in figure (C.48).

$$s_{XVI} = \begin{cases} s_{J2}(x_D, t_D), & x_D < x^S_{pH\,\infty}(t_D) \\ s^{(7)-(3---)}(x_D, t_D), & x^S_{pH\,\infty}(t_D) < x_D < x^R_{E\,\infty}(t_D) \\ s_{3---}(x_D, t_D), & x^R_{E\,\infty}(t_D) < x_D < x^S_{E\,N}(t_D) \\ s_{3--}(x_D, t_D), & x^S_{E\,N}(t_D) < x_D < x^R_{L\,N}(t_D) \\ s^{(3)-(2)---}(x_D, t_D), & x^R_{L\,N}(t_D) < x_D < x^R_{M\infty}(t_D) \\ s^{(2--)}, & x^R_{M\infty}(t_D) < x_D < x^R_{LM\infty}(t_D) \\ s^{(6)-(5)--}(x_D, t_D), & x^R_{LM\infty}(t_D) < x_D < x^R_{K\,\infty}(t_D) \\ s^{(2-)}, & x^R_{K\,\infty}(t_D) < x_D < x^R_{H\,\infty}(t_D) \\ s^{(2)-(1)-}(x_D, t_D), & x^R_{H\,\infty}(t_D) < x_D < x^R_{I\,\infty}(t_D) \\ s^{(1-)}, & x^R_{I\,\infty}(t_D) < x_D < x^S_{I\,\infty}(t_D) \\ s^{(1)}, & x^S_{I\,\infty}(t_D) < x_D < \lambda_{(1)}\left(\vec{c}^{(1)}, \xi^{(I)}\right)t_D \\ s^{(1)-(I+)}(x_D, t_D), & \lambda_{(1)}\left(\vec{c}^{(1)}, \xi^{(I)}\right)t_D < x_D < \lambda_{(1)}\left(\vec{c}^{(I)}, \xi^{(I)}\right)t_D \\ s^{(I+)}, & \lambda_{(1)}\left(\vec{c}^{(I)}, \xi^{(I)}\right)t_D < x_D < D_{(s)}t_D \\ s^{(I)}, & x_D > D_{(s)}t_D \end{cases} \tag{C.17}$$

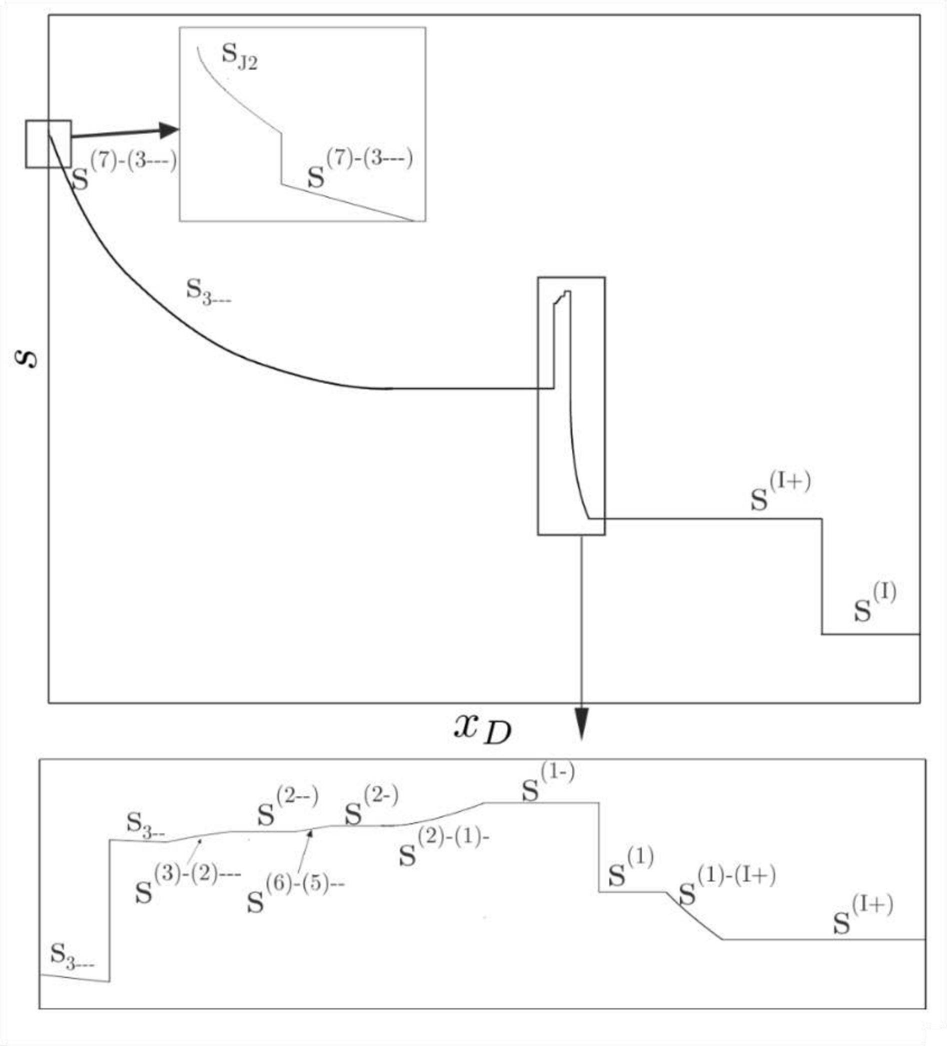

Figure C.46: Water saturation profile for s_{XVI}

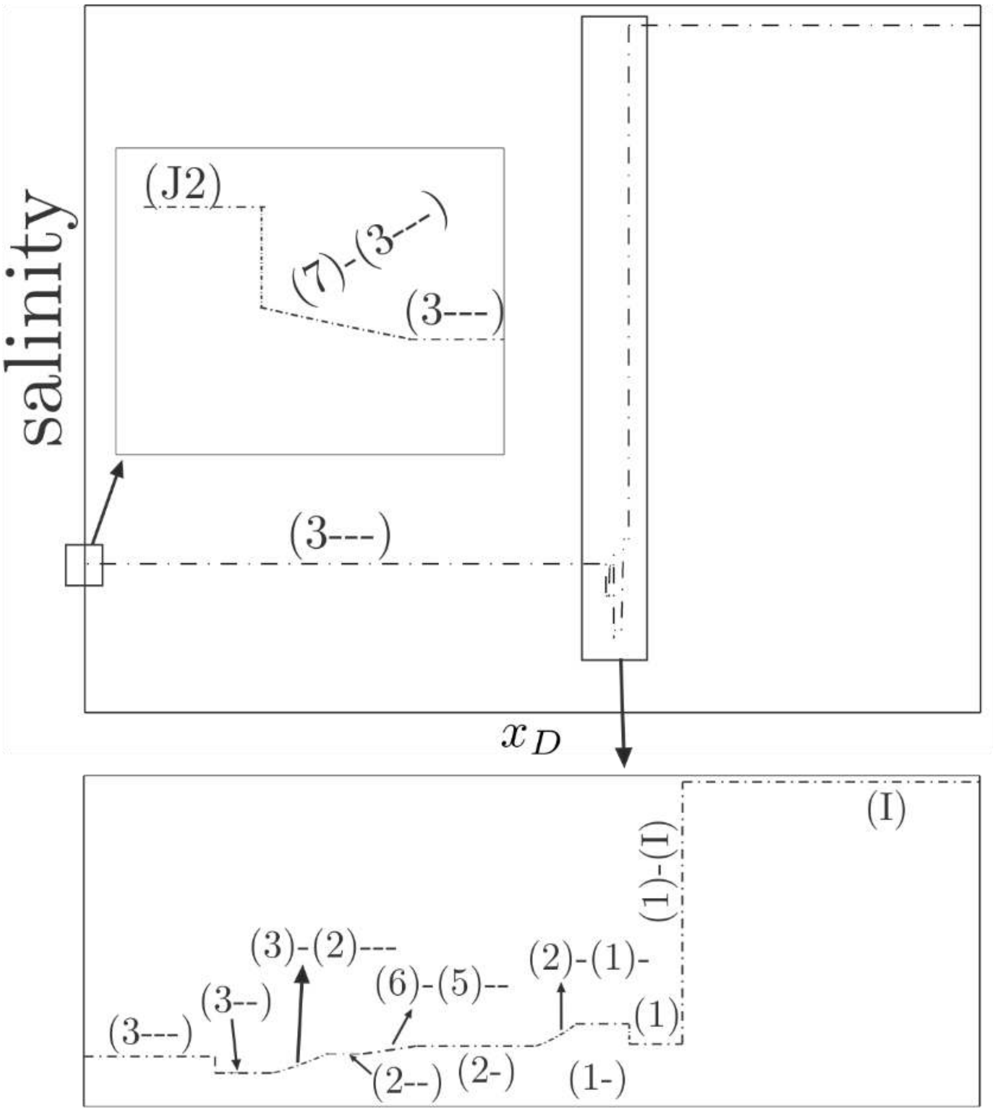

Figure C.47: Salinity profile for $t_M < t_D < t_N$

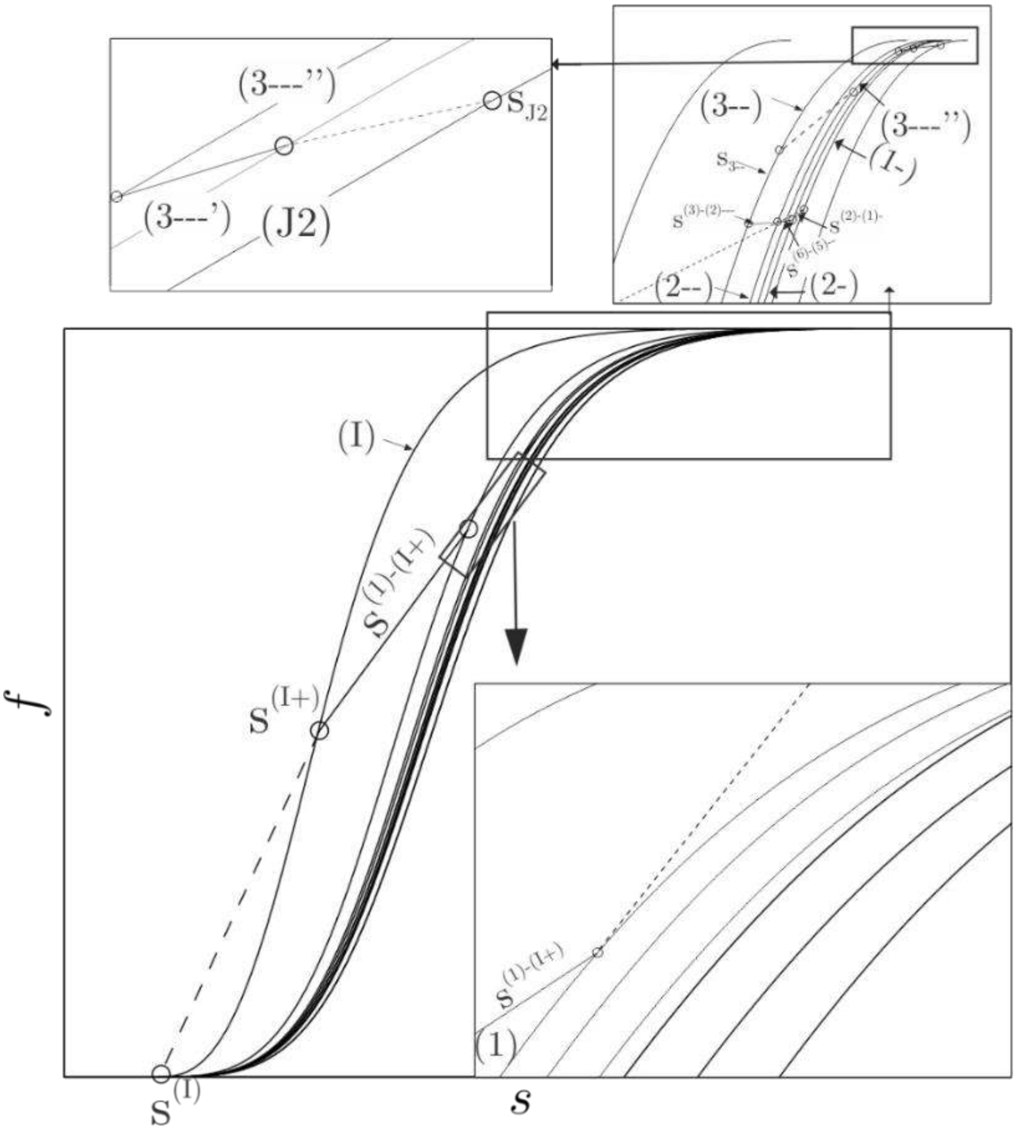

Figure C.48: Solution path of s_{XVI} in $f \times s$ plane

The last solution part is s_{XVII} (Equation C.18), when $t_D > t_N$. In this region the waves $k = 3$ from the front and from the rear of the low salinity slug interact and there is a cancelation between them (waves of the same family). Therefore, both region (3--) (Figure C.50) and rarefaction s_{3--} (Figure C.49) disappear. The solution path of s_{XVII} in $f \times s$ plane is presented in figure (C.51).

$$s_{XVII} = \begin{cases} s_{J2}(x_D, t_D), & x_D < x^S_{pH\,\infty}(t_D) \\ s^{(7)-(3---)}(x_D, t_D), & x^S_{pH\,\infty}(t_D) < x_D < x^R_{E\,\infty}(t_D) \\ s_{3---}(x_D, t_D), & x^R_{E\,\infty}(t_D) < x_D < x^S_{N\,\infty}(t_D) \\ s^{(3)-(2)---}(x_D, t_D), & x^S_{N\,\infty}(t_D) < x_D < x^R_{M\infty}(t_D) \\ s^{(2--)}, & x^R_{M\infty}(t_D) < x_D < x^R_{LM\infty}(t_D) \\ s^{(6)-(5)--}(x_D, t_D), & x^R_{LM\infty}(t_D) < x_D < x^R_{K\,\infty}(t_D) \\ s^{(2-)}, & x^R_{K\,\infty}(t_D) < x_D < x^R_{H\,\infty}(t_D) \\ s^{(2)-(1)-}(x_D, t_D), & x^R_{H\,\infty}(t_D) < x_D < x^R_{I\,\infty}(t_D) \\ s^{(1-)}, & x^R_{I\,\infty}(t_D) < x_D < x^S_{I\,\infty}(t_D) \\ s^{(1)}, & x^S_{I\,\infty}(t_D) < x_D < \lambda_{(1)}\left(\vec{c}^{(1)}, \xi^{(I)}\right)t_D \\ s^{(1)-(I+)}(x_D, t_D), & \lambda_{(1)}\left(\vec{c}^{(1)}, \xi^{(I)}\right)t_D < x_D < \lambda_{(1)}\left(\vec{c}^{(I)}, \xi^{(I)}\right)t_D \\ s^{(I+)}, & \lambda_{(1)}\left(\vec{c}^{(I)}, \xi^{(I)}\right)t_D < x_D < D_{(s)}t_D \\ s^{(I)}, & x_D > D_{(s)}t_D \end{cases} \tag{C.18}$$

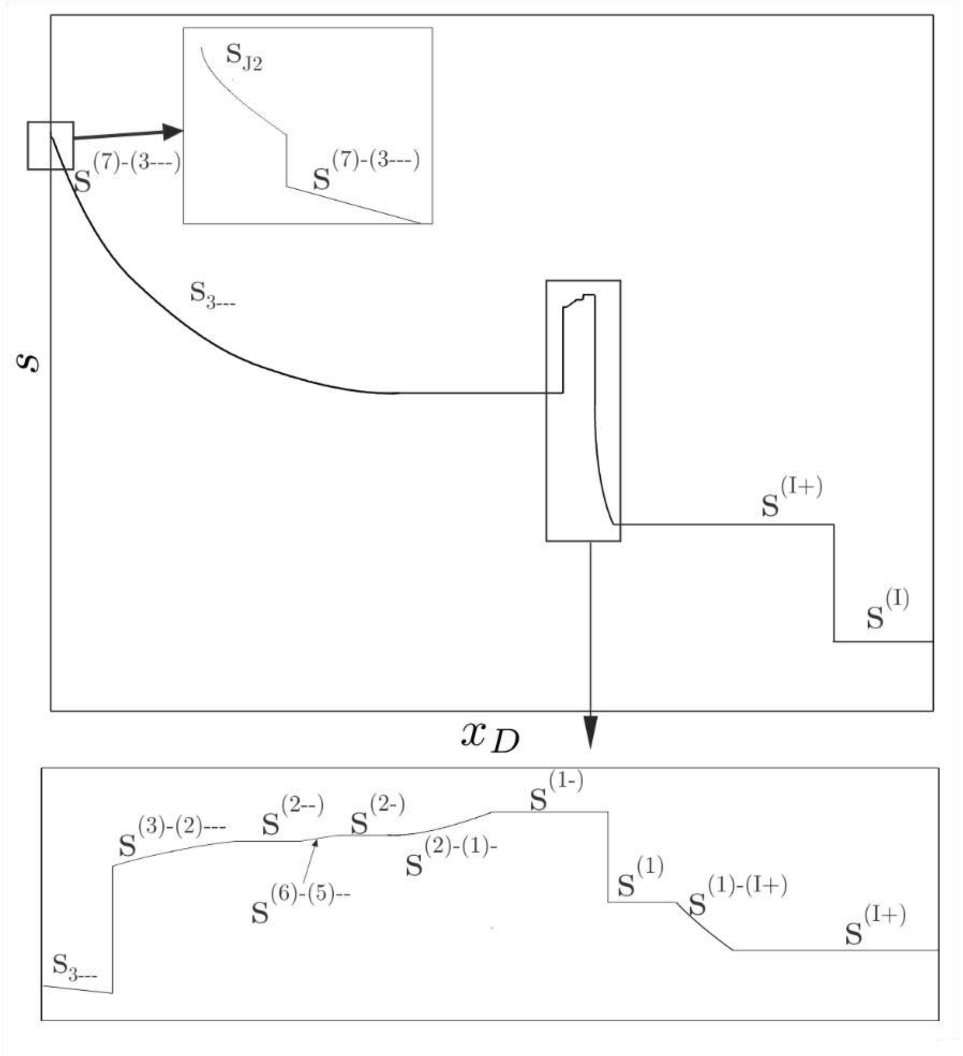

Figure C.49: Water saturation profile for s_{XVII}

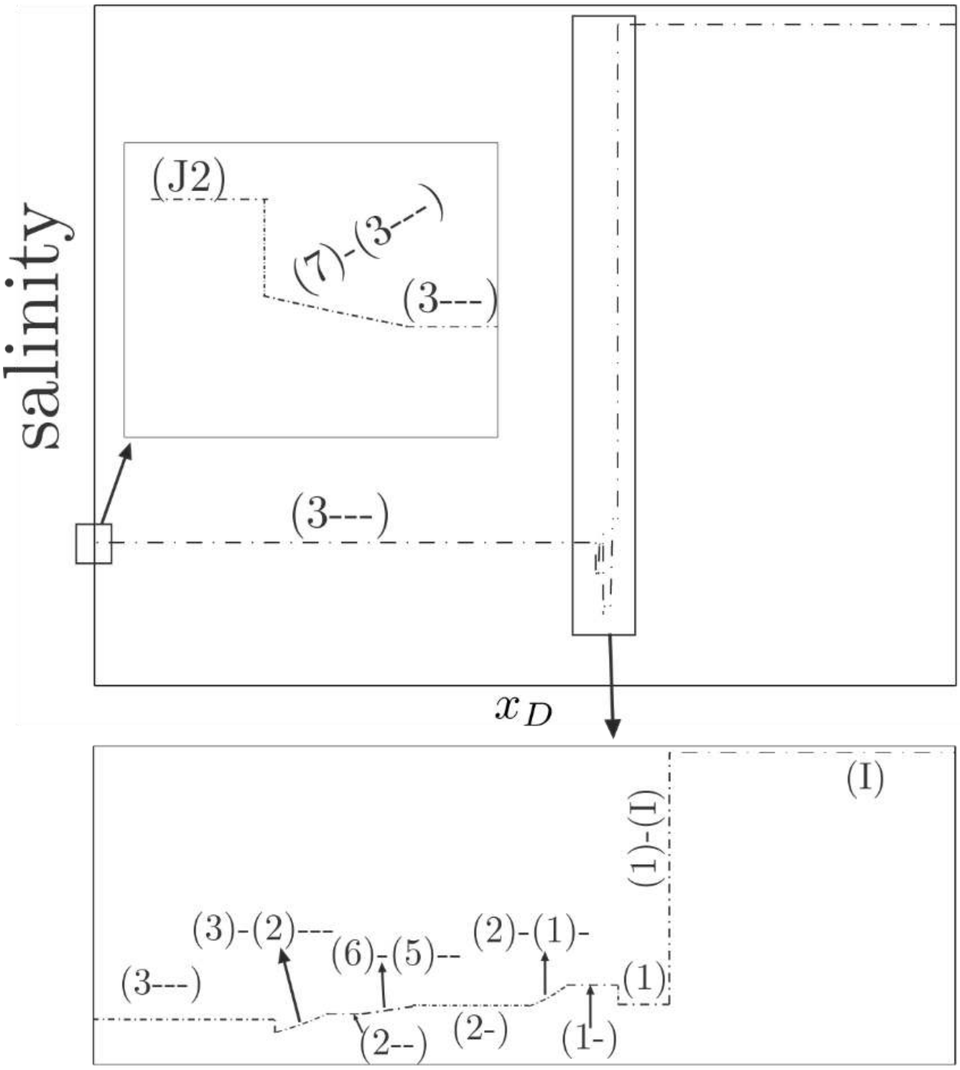

Figure C.50: Salinity profile for $t_D > t_N$

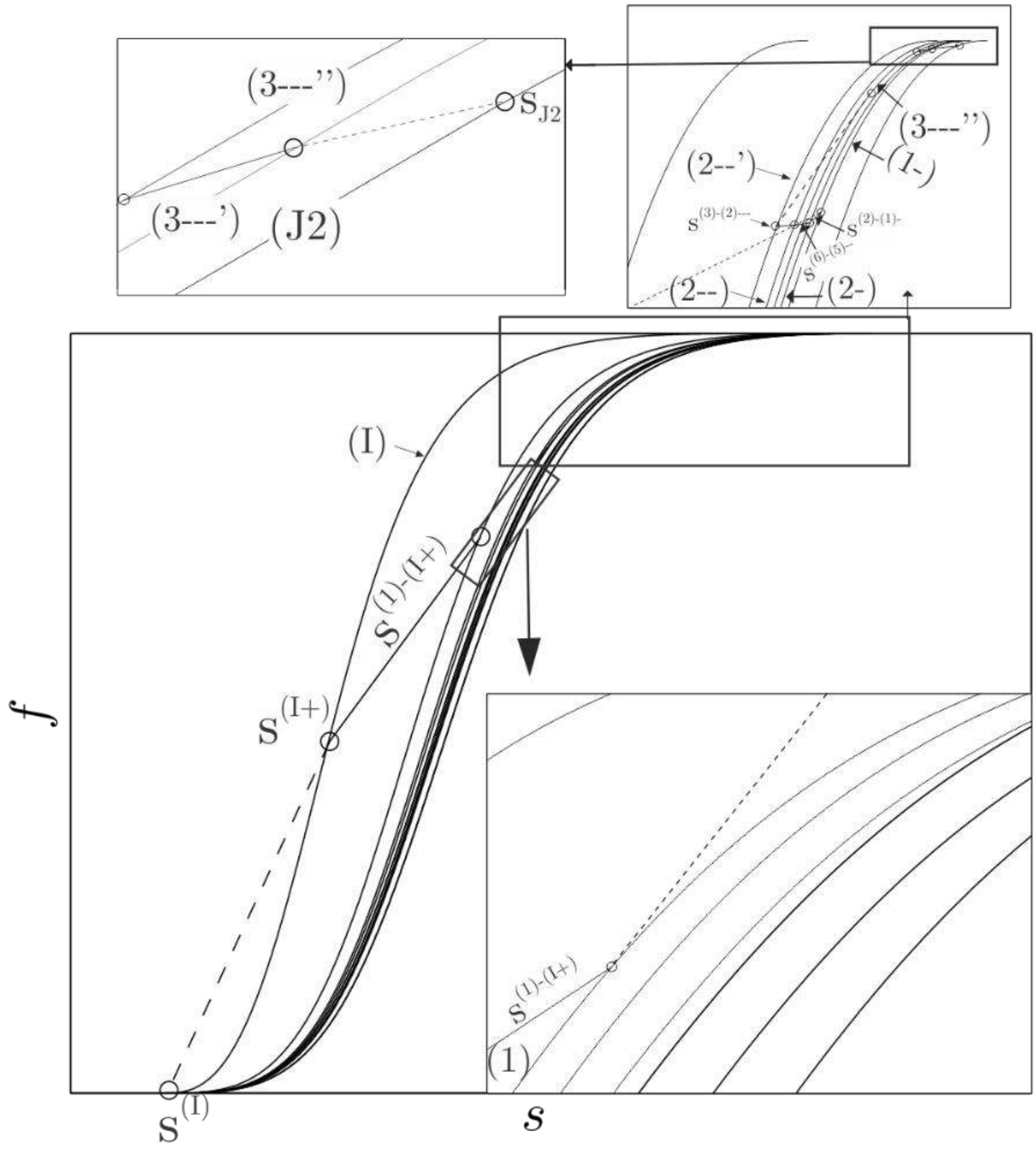

Figure C.51: Solution path of s_{XVII} in $f \times s$ plane

Appendix C – Admissibility and Existence of the Shock Waves of the Low Salinity Problem (Chapter 4)

In this appendix we derive the admissibility and existence of discontinuities in the solution of the low salinity problem. This analysis is divided into two main steps: first we check the discontinuities of the pH problem and auxiliary system, followed by the discontinuities of the original system of conservation laws.

The first step is the evaluation of Lax conditions (Lax, 1975), Oleinik conditions (Oleinik, 1957) and vanishing viscosity (Liu, 1981). Later, we will discuss Oleinik conditions for the original problem of the low salinity waterflooding. Lax condition can be found in Pires *et al.* (2006).

a. Admissibility and existence of discontinuities in the pH problem and auxiliary system

The auxiliary system associated with the problem of low salinity injection is given by:

$$\frac{\partial a_i(\vec{c},\xi)}{\partial \varphi} + \frac{\partial c_i}{\partial x_D} = 0, i = 1,2,\dots,n \tag{C.1}$$

where n is the number of dissolved cations in water.

The pH partial differential equation is:

$$\frac{\partial a_H(\xi)}{\partial \varphi} + \frac{\partial \xi}{\partial x_D} = 0 \tag{C.2}$$

where,

$$\xi = c_H - c_{OH} = c_H - \frac{K_w}{c_H} \tag{C.3}$$

in which K_w is water ionization constant. Cations adsorption isotherm a_i is given by:

$$a_i(\vec{c},\xi) = \frac{\alpha_i(\xi)c_i}{1+\sum_{j=1}^{3}\beta_j(\xi)c_j} \tag{C.4}$$

where α_i and β_i are adsorption parameters that depend on fluid pH.

Hydrogen adsorption isotherm is written as a function of ξ:

$$a_H(\xi) = \frac{\alpha_H\left(\frac{\xi+\sqrt{\xi^2+4K_W}}{2}\right)^{n_H}}{1+\beta_H\left(\frac{\xi+\sqrt{\xi^2+4K_W}}{2}\right)^{m_H}} \tag{C.5}$$

where α_H, β_H, n_H and m_H are constants. Moreover, we consider that $\alpha_H >>> \alpha_i$ and $\beta_H >>> \beta_i$.

In equation (C.4) the adsorption parameters are ordered as:

$$\alpha_1 < \alpha_2 < \cdots < \alpha_n \tag{C.6}$$

$$\beta_1 < \beta_2 < \cdots < \beta_n \tag{C.7}$$

The adsorption order in equations (C.6)-(C.7) results in the following root sequence in the solution of ω^n (Equation 51 in Chapter 4):

$$0 \leq \omega_1 \leq \alpha_1 \leq \omega_2 \leq \alpha_2 \leq \cdots \leq \omega_n \leq \alpha_n \tag{C.8}$$

The slopes of the characteristics of a k-wave family of the auxiliary system (Equation C.1) is given by:

$$\sigma_{(k)}(\omega_k, \xi) = \frac{d\varphi}{dx_D} = \omega_k(\xi) \prod_{j=1}^{n} \frac{\omega_j(\xi)}{\alpha_j(\xi)} \tag{C.9}$$

Due to equation (C.8), the characteristics slopes of the k^{th} family will follow:

$$0 \leq \sigma_{(1)} \leq \sigma_{(2)} \leq \cdots \leq \sigma_{(n)} \tag{C.10}$$

The shock wave of the k^{th}-family is given by:

$$V_{(k)}(\omega_k, \xi) = \omega_k^+(\xi) \prod_{j=1}^{3} \frac{\omega_j^-(\xi)}{\alpha_j(\xi)} = \omega_k^-(\xi) \prod_{j=1}^{3} \frac{\omega_j^+(\xi)}{\alpha_j(\xi)} \tag{C.11}$$

where the superscripts + and – represent the right and left states of the shock. Analogously to the slopes of the characteristics, it follows for the shock waves:

$$0 \leq V_{(1)} \leq V_{(2)} \leq \cdots \leq V_{(n)} \tag{C.12}$$

For the pH problem (Equation C.2) the slope of the characteristics waves is given by:

$$\sigma_{pH} = \frac{d\alpha_H}{d\xi} = \frac{\frac{\alpha_H}{2^{n_H}} n_H \left(\xi + \sqrt{\xi^2 + 4K_w}\right)^{n_H - 1} \left(1 + \frac{\xi}{\sqrt{\xi^2 + 4K_w}}\right)}{1 + \beta_H \left(\frac{\xi + \sqrt{\xi^2 + 4K_w}}{2}\right)^{m_H}} -$$

$$\frac{\frac{\alpha_H \beta_H m_H}{2^{n_H + m_H}} \left(\xi + \sqrt{\xi^2 + 4K_w}\right)^{n_H + m_H - 1} \left(1 + \frac{\xi}{\sqrt{\xi^2 + 4K_w}}\right)}{\left[1 + \beta_H \left(\frac{\xi + \sqrt{\xi^2 + 4K_w}}{2}\right)^{m_H}\right]^2} \tag{C.13}$$

Figure (C.1) presents the slopes of the characteristics as a function of ξ. Note that when $\xi = 0$, the derivative reaches a maximum (which is equivalent to $pH = 7$). Moreover, when $\xi < 0$, $\sigma'_{pH} > 0$, and when $\xi > 0$, $\sigma'_{pH} < 0$.

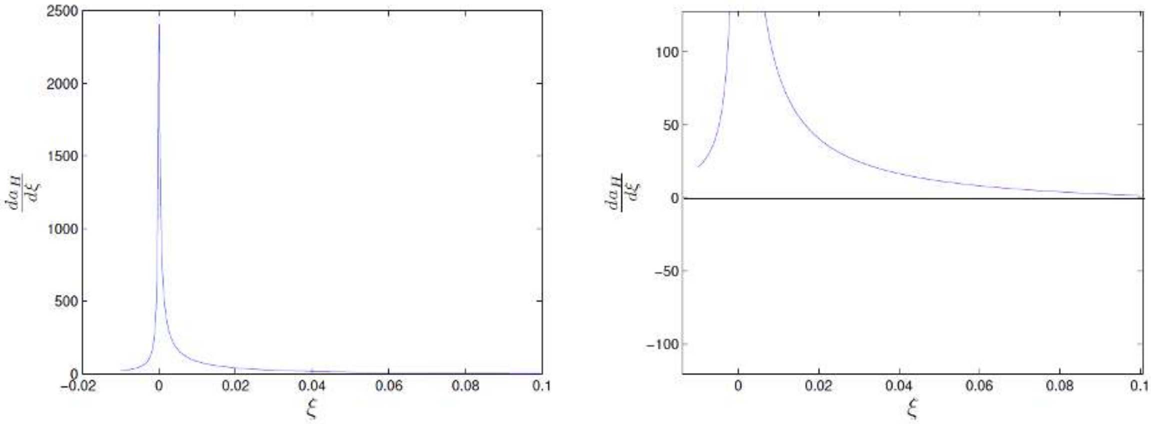

Figure (C.1): Slopes of the characteristics of the pH problem

The characteristic diagram for the solution of the auxiliary system (Equation C.1) for $n = 3$ and containing only shock waves is presented in figure (C.2). It is important to emphasize that $\alpha_H >>> \alpha_i$, $\beta_H >>> \beta_i$, and $V_{pH} >>> V_{(k)}$.

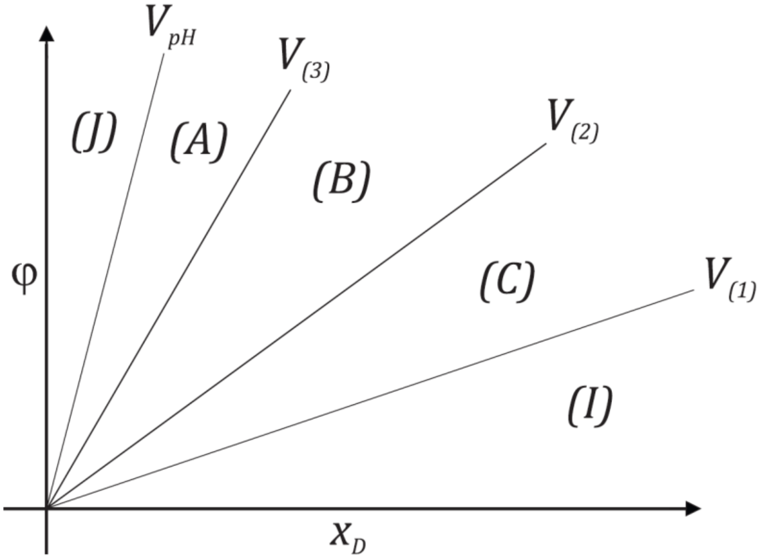

Figure (C.2): Solution of the auxiliary system for $n = 3$ containing only shock waves

i. Lax Condition

The generalized Lax condition for hyperbolic systems of partial differential equations is given by (Lax, 1957):

$$\begin{cases} \lambda_{(\gamma)}\left(\omega_{(\gamma)}^{(-)}\right) \geq D_{(\gamma)} \geq \lambda_{(\gamma)}\left(\omega_{(\gamma)}^{(+)}\right) \\ \lambda_{(\gamma-1)}\left(\omega_{(\gamma)}^{(-)}\right) \leq D_{(\gamma)} \leq \lambda_{(\gamma+1)}\left(\omega_{(\gamma)}^{(+)}\right) \end{cases} \tag{C.14}$$

where $\lambda_{(\gamma)} = \frac{dx_D}{dt_D}$ are the eigenvalues of the system of conservation laws following

$$\lambda_{(1)} < \lambda_{(2)} < \cdots < \lambda_{(n)} \tag{C.15}$$

and $D_{(\gamma)} = \frac{dx_D}{dt_D}$ is the shock slope of family γ.

Lax conditions for the low salinity problem are given by:

$$\begin{cases} \sigma_{(k)}\left(\omega_{(k)}^{(-)}\right) \leq V_{(k)} \leq \ \sigma_{(k)}\left(\omega_{(k)}^{(+)}\right) \\ \sigma_{(k+1)}\left(\omega_{(k)}^{(-)}\right) \geq V_{(k)} \geq \ \sigma_{(k-1)}\left(\omega_{(k)}^{(+)}\right) \end{cases} \tag{C.16}$$

where k is the cation family.

First, we will verify the first condition of equation (C.16) for the discontinuities of the auxiliary system (Equation C.1) and pH problem (Equation C.2).

For the shock $V_{(1)}$ we have:

$$\sigma_{(1)}\left(\omega_{(1)}^{(C)}\right) \leq V_{(1)} \leq \sigma_{(1)}\left(\omega_{(1)}^{(I)}\right) \tag{C.17}$$

From equations (C.9) and (C.11), we obtain:

$$\omega_{(1)}^{(C)} \prod_{j=1}^{n} \frac{\omega_{(j)}^{(C)}}{\alpha_{(j)}} \leq \omega_{(1)}^{+} \prod_{j=1}^{3} \frac{\omega_{(j)}^{-}}{\alpha_{(j)}} = \omega_{(1)}^{-} \prod_{j=1}^{3} \frac{\omega_{(j)}^{+}}{\alpha_{(j)}} \leq \omega_{(1)}^{(I)} \prod_{j=1}^{n} \frac{\omega_{(j)}^{(I)}}{\alpha_{(j)}} \tag{C.18}$$

which leads to:

$$\omega_{(1)}^{(I)} \geq \omega_{(1)}^{(C)} \tag{C.19}$$

for both sides of equation (C.19). Moreover, in region (C) of figure (C.2), $\omega_{(1)}^{(C)} = \omega_{(1)}^{(J)}$, $\omega_{(2)}^{(C)} = \omega_{(1)}^{(I)}$ and $\omega_{(3)}^{(C)} = \omega_{(3)}^{(I)}$.

So, equation (C.19) becomes:

$$\omega_{(1)}^{(I)} \geq \omega_{(1)}^{(J)} \tag{C.20}$$

Now shock $V_{(2)}$ is analyzed. For the first condition of (C.16) we find:

$$\sigma_{(2)}\left(\omega_{(2)}^{(B)}\right) \leq V_{(2)} \leq \sigma_{(2)}\left(\omega_{(2)}^{(C)}\right) \tag{C.21}$$

Applying equations (C.9) and (C.11) in equation (C.21), we obtain:

$$\omega_{(2)}^{(B)} \prod_{j=1}^{n} \frac{\omega_{(j)}^{(B)}}{\alpha_{(j)}} \leq \omega_{(2)}^{+} \prod_{j=1}^{3} \frac{\omega_{(j)}^{-}}{\alpha_{(j)}} = \omega_{(2)}^{-} \prod_{j=1}^{3} \frac{\omega_{(j)}^{+}}{\alpha_{(j)}} \leq \omega_{(2)}^{(C)} \prod_{j=1}^{n} \frac{\omega_{(j)}^{(C)}}{\alpha_{(j)}} \tag{C.22}$$

After some manipulation, both sides of equation (C.22) become

$$\omega_{(2)}^{(C)} \geq \omega_{(2)}^{(B)} \tag{C.23}$$

In region (B) (Figure C.2), $\vec{\omega}^{(B)} = \left[\omega_{(1)}^{(J)}, \omega_{(2)}^{(J)}, \omega_{(3)}^{(I)}\right]$, thus

$$\omega_{(2)}^{(I)} \geq \omega_{(2)}^{(J)} \tag{C.24}$$

The first condition of equation (C.16) for the shock $V_{(3)}$ is:

$$\sigma_{(3)}\left(\omega_{(3)}^{(A)}\right) \leq V_{(3)} \leq \sigma_{(3)}\left(\omega_{(3)}^{(A)}\right) \tag{C.25}$$

Applying equations (C.9) and (C.11) in equation (C.25), we obtain:

$$\omega_{(3)}^{(A)} \prod_{j=1}^{n} \frac{\omega_{(j)}^{(A)}}{\alpha_{(j)}} \leq \omega_{(3)}^{+} \prod_{j=1}^{3} \frac{\omega_{(j)}^{-}}{\alpha_{(j)}} = \omega_{(3)}^{-} \prod_{j=1}^{3} \frac{\omega_{(j)}^{+}}{\alpha_{(j)}} \leq \omega_{(3)}^{(B)} \prod_{j=1}^{n} \frac{\omega_{(j)}^{(B)}}{\alpha_{(j)}} \tag{C.26}$$

In region (A) of the solution of the auxiliary system (Figure C.2) $\vec{\omega}^{(A)} = \left[\omega_{(1)}^{(J)}, \omega_{(2)}^{(J)}, \omega_{(3)}^{(J)}\right]$. Thus, equation (C.26) results in:

$$\omega_{(3)}^{(I)} \geq \omega_{(3)}^{(J)} \tag{C.27}$$

From equations (C.20), (C.24) and (C.27), the first Lax admissibility condition for the auxiliary system is given by:

$$\omega_{(k)}^{(I)} \geq \omega_{(k)}^{(J)} \tag{C.28}$$

Finally, first equation (C.16) for shock V_{pH} leads to:

$$\sigma_{(pH)}\left(\xi^{(J)}\right) \leq V_{pH} \leq \sigma_{(pH)}\left(\xi^{(I)}\right) \tag{C.29}$$

The locus of the shock for the cases $pH^{(J)} < pH^{(I)} < 7$ and $pH^{(I)} > pH^{(J)} > 7$, as well as the waves speed at injection and initial conditions, is presented in figures (C.3) and (C.4), respectively. Dashed lines connecting (I) and (J) are the shock V_{pH}.

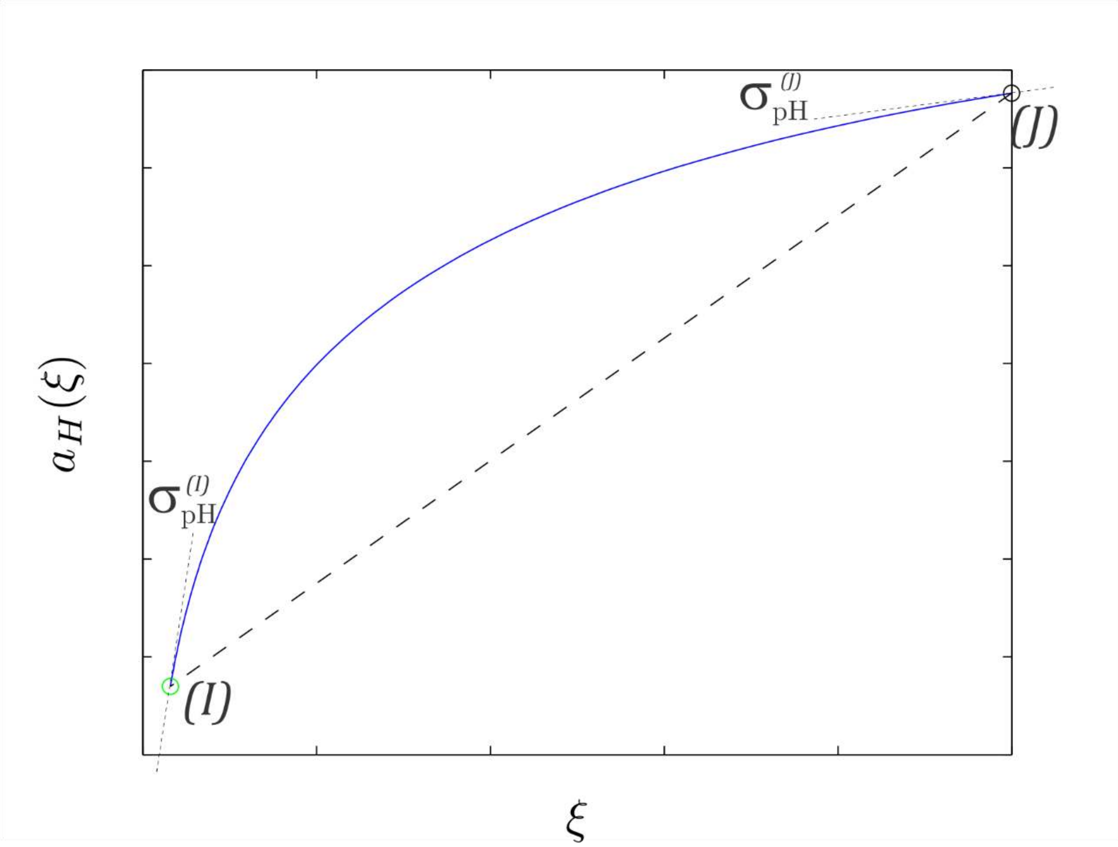

Figure C.3: Lax Condition of the pH problem for $pH^{(J)} < pH^{(I)} < 7$

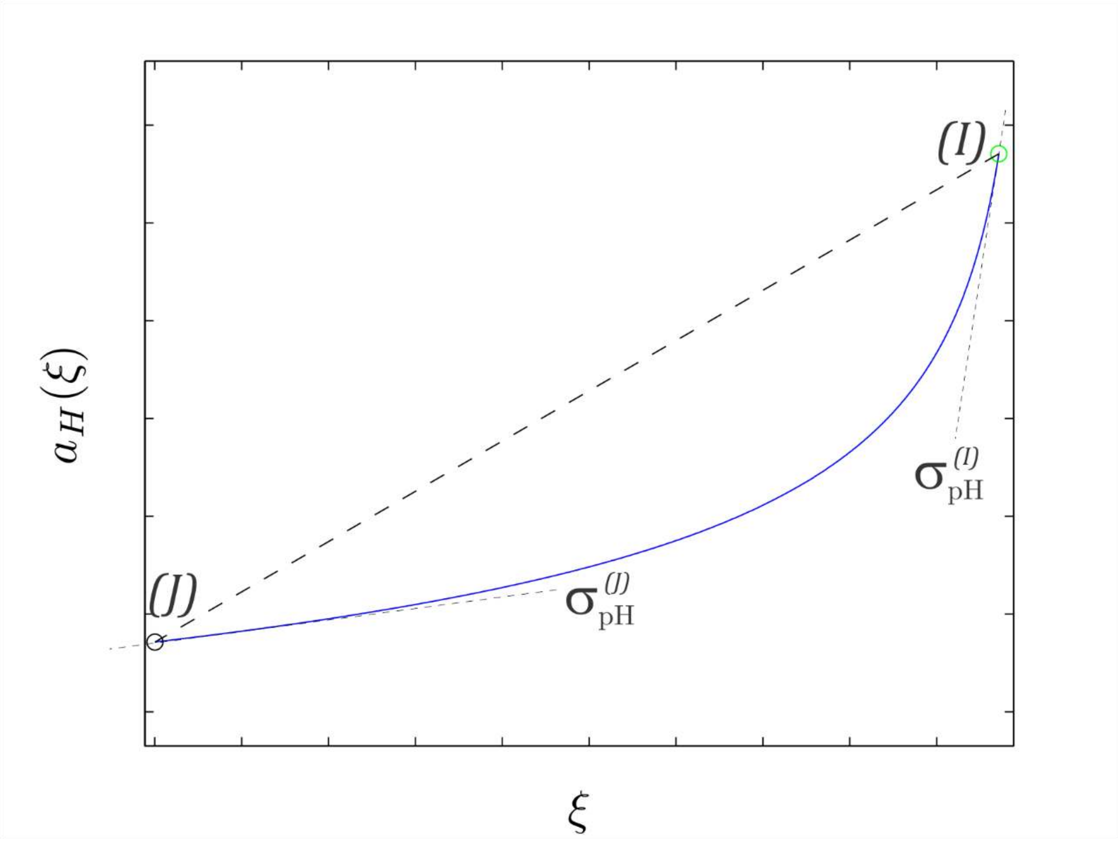

Figure C.4: Lax Condition of the pH problem for $pH^{(I)} > pH^{(J)} > 7$

Comparing the slopes V_{pH}, $\sigma_{pH}\left(\xi^{(I)}\right)$ and $\sigma_{pH}\left(\xi^{(J)}\right)$ in figures (C.3) and (C.4), Lax first condition for pH problem holds if

$$\sigma_{(pH)}\left(\xi^{(J)}\right) \leq V_{pH} \leq \sigma_{(pH)}\left(\xi^{(I)}\right) \tag{C.30}$$

For shock $V_{(1)}$, the second Lax condition for systems is given by:

$$\sigma_{(2)}\left(\omega_{(1)}^{(C)}\right) \geq V_{(1)} \tag{C.31}$$

which leads to:

$$\omega_{(2)}^{(C)} \prod_{j=1}^{n} \frac{\omega_{(j)}^{(C)}}{\alpha_{(j)}} \geq \omega_{(1)}^{(I)} \prod_{j=1}^{3} \frac{\omega_{(j)}^{(I)}}{\alpha_{(j)}} \tag{C.32}$$

From (C.31) it is possible to find:

$$\omega_{(2)}^{(I)} \geq \omega_{(1)}^{(I)} \tag{C.33}$$

For shock $V_{(2)}$ the second condition is given by,

$$\sigma_{(3)}\left(\omega_{(2)}^{(B)}\right) \geq V_{(2)} \tag{C.34}$$

$$V_{(2)} \geq \sigma_{(1)}\left(\omega_{(2)}^{(C)}\right) \tag{C.35}$$

Therefore,

$$\omega_{(3)}^{(B)} \prod_{j=1}^{n} \frac{\omega_{(j)}^{(B)}}{\alpha_{(j)}} \geq \omega_{(2)}^{(C)} \prod_{j=1}^{3} \frac{\omega_{(j)}^{(B)}}{\alpha_{(j)}} \tag{C.36}$$

$$\omega_{(2)}^{(B)} \prod_{j=1}^{n} \frac{\omega_{(j)}^{(C)}}{\alpha_{(j)}} \geq \omega_{(1)}^{(C)} \prod_{j=1}^{3} \frac{\omega_{(j)}^{(C)}}{\alpha_{(j)}} \tag{C.37}$$

Then:

$$\omega_{(3)}^{(I)} \geq \omega_{(2)}^{(I)} \tag{C.38}$$

$$\omega_{(2)}^{(J)} \geq \omega_{(1)}^{(J)} \tag{C.39}$$

Shock relations of the problem for $V_{(3)}$ are:

$$\sigma_{pH}\left(\xi^{(I)}\right) >>> V_{(3)} \tag{C.40}$$

$$V_{(3)} \geq \sigma_{(2)}\left(\omega_{(3)}^{(B)}\right) \tag{C.41}$$

Equation (C.40) always holds because $\sigma_{pH} >>> V_{(k)}$. From equation (C.41) we obtain:

$$\omega_{(3)}^{(J)} \geq \omega_{(2)}^{(J)} \tag{C.42}$$

Finally, for the shock V_{pH} we must have:

$$V_{pH} \geq \sigma_{(3)}\left(\omega_{(3)}^{(A)}\right) \tag{C.43}$$

which is always true because $V_{pH} >>> \sigma_{(k)}$.

Therefore, the second condition of equation (C.16) holds if:

$$\omega_{(k+1)}^{(I)} \geq \omega_{(k)}^{(I)} \tag{C.44}$$

$$\omega_{(k+1)}^{(J)} \geq \omega_{(k)}^{(J)} \tag{C.45}$$

together with equations (C.40) and (C.43).

ii. Oleinik condition

Oleinik condition for a convex flux $f(u)$ is given by:

$$\frac{f(u^{(-)})-f(u)}{u^{(-)}-u} \leq \frac{f(u^{(-)})-f(u^{(+)})}{u^{(-)}-u^{(+)}} \leq \frac{f(u)-f(u^{(+)})}{u-u^{(+)}} \tag{C.46}$$

for $u^{(-)} \leq u \leq u^{(+)}$.

Figure (C.5) presents the hydrogen adsorption isotherm as a function of ξ. The inflexion point ($\xi = 0$) divides the adsorption curve into an acidic ($\xi > 0$), and an alkaline media ($\xi < 0$), and the acidic region is presented in Figure (C.6). It will be considered the case where $7 > pH^{(I)} > pH^{(J)}$ (Figure C.6).

A shock wave will follow Oleinik condition if

$$\frac{a_H(\xi^{(J)})-a_H(\xi^{(-)})}{\xi^{(J)}-\xi^{(-)}} \leq V_{pH} \leq \frac{a_H(\xi^{(+)})-a_H(\xi^{(I)})}{\xi^{(+)}-\xi^{(I)}} \tag{C.47}$$

for all $\xi^{(I)} \leq \xi^{(-)} \leq \xi^{(J)}$, where the shock V_{pH} is given by Rankine-Hugoniot condition:

$$V_{pH} = \frac{a_H(\xi^{(+)})-a_H(\xi^{(-)})}{\xi^{(+)}-\xi^{(-)}} \tag{C.48}$$

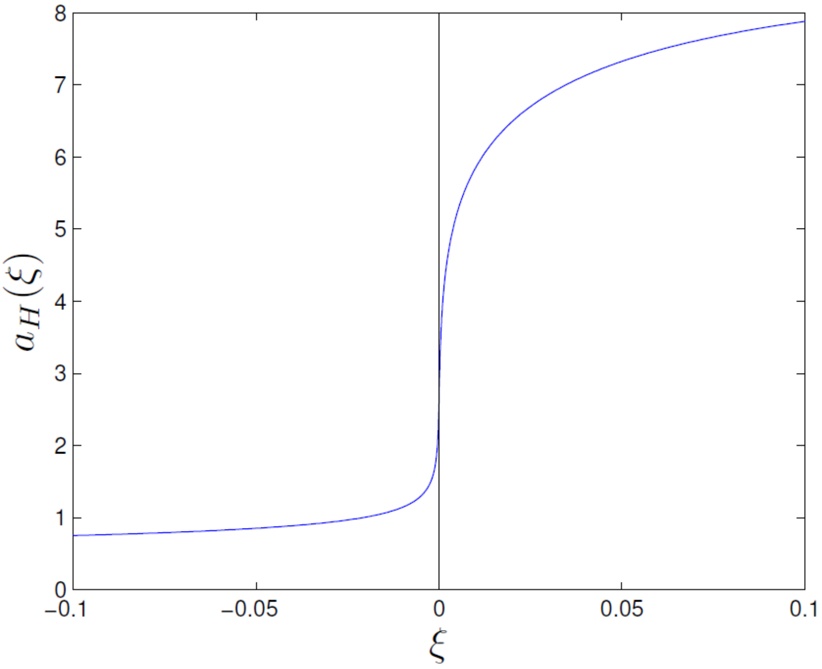

Figure C.5: Hydrogen adsorption isotherm

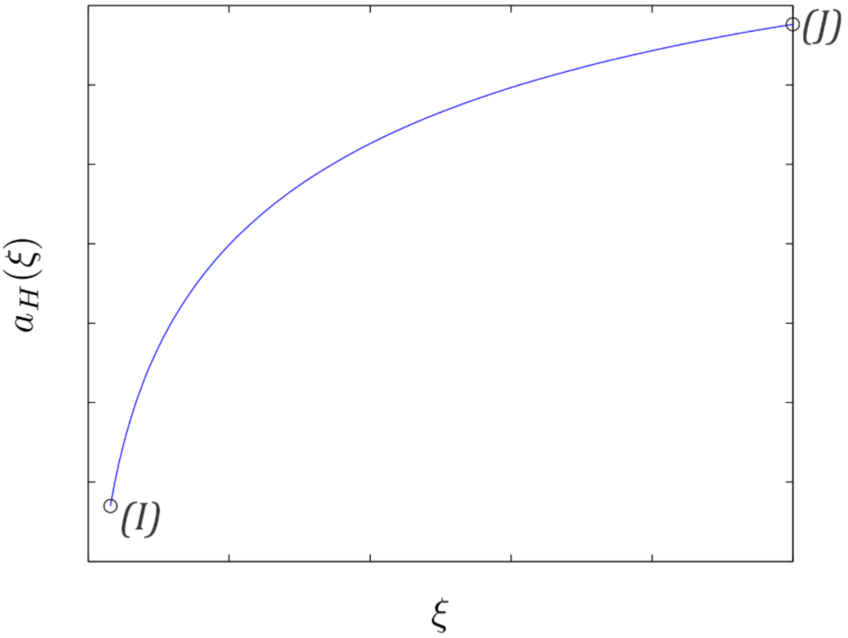

Figure C.6: Hydrogen adsorption isotherm for $7 > pH^{(I)} > pH^{(J)}$

In figure (C.7) we present the locus of the shock for $\xi^{(I)} \leq \xi \leq \xi^{(J)}$, where each dashed line is a shock connecting the left state (J) to a right state $\xi^{(-)}$.

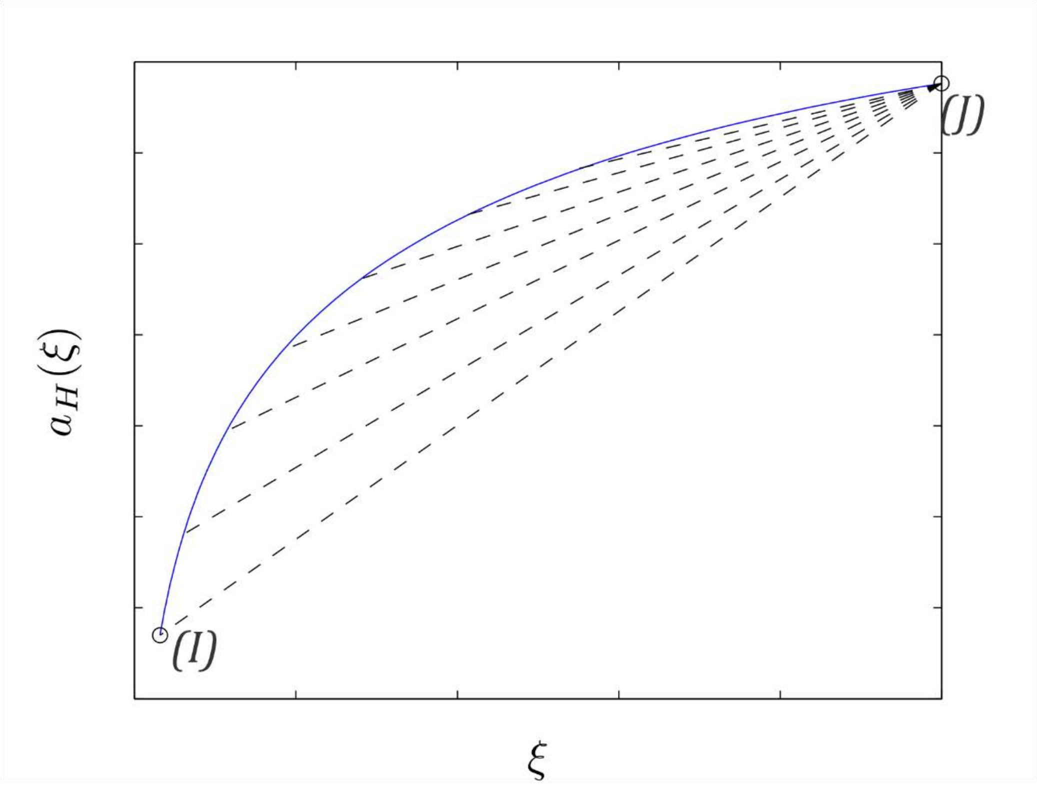

Figure C.7: Shock locus for $7 > pH^{(I)} > pH^{(J)}$

The shock with the greatest slope is the one connecting the states (J) and (I) (Figure C.7), which is the shock that satisfies Oleinik condition (Equation C.47).

We now test Oleinik condition for each shock of the auxiliary system (Equation C.1). The shock velocity $V_{(k)}$ in space ω^n is:

$$V_{(k)} = \omega_{(k)}^{(+)} \prod_{j=1}^{3} \frac{\omega_{(j)}^{(-)}}{\alpha_{(j)}} \tag{C.49}$$

which can be rewritten as

$$V_{(k)} = \frac{\omega_{(k)}^{(+)} \omega_{(k)}^{(-)}}{\alpha_{(k)}} \prod_{\substack{j=1 \\ j\neq k}}^{3} \frac{\omega_{(j)}^{(-)}}{\alpha_{(j)}} \tag{C.50}$$

Oleinik condition for equation (C.50) is given by:

$$\frac{\omega_{(k)}^{(+)} \omega'_{(k)}}{\alpha_{(k)}} \prod_{\substack{j=1 \\ j\neq k}}^{3} \frac{\omega_{(j)}^{(-)}}{\alpha_{(j)}} \geq \frac{\omega_{(k)}^{(+)} \omega_{(k)}^{(-)}}{\alpha_{(k)}} \prod_{\substack{j=1 \\ j\neq k}}^{3} \frac{\omega_{(j)}^{(-)}}{\alpha_{(j)}} \geq \frac{\omega''_{(k)} \omega_{(k)}^{(-)}}{\alpha_{(k)}} \prod_{\substack{j=1 \\ j\neq k}}^{3} \frac{\omega_{(j)}^{(-)}}{\alpha_{(j)}} \tag{C.51}$$

Thus,

$$\omega_{(k)}^{(+)}\omega'_{(k)} \geq \omega_{(k)}^{(+)}\omega_{(k)}^{(-)} \geq \omega''_{(k)}\omega_{(k)}^{(-)} \tag{C.52}$$

For the first inequality we have:

$$\omega'_{(k)} \geq \omega_{(k)}^{(-)} \tag{C.53}$$

and for the second one

$$\omega_{(k)}^{(+)} \geq \omega''_{(k)} \tag{C.54}$$

From equations (C.53) and (C.54) a shock of the auxiliary system is admissible if and only if it connects initial and injection conditions.

iii. Vanishing viscosity criteria for shock stability

In this subsection we apply the vanishing viscosity criteria (Liu, 1981) to analyze the stability of the pH and concentration shock waves of the low salinity waterflooding problem in the auxiliary plane for a two cations system. For this case, the auxiliary system and the pH problem are given by:

$$\begin{cases} \frac{\partial a_1(\vec{c},\xi)}{\partial \varphi} + \frac{\partial c_1}{\partial x_D} = 0 \\ \frac{\partial a_2(\vec{c},\xi)}{\partial \varphi} + \frac{\partial c_2}{\partial x_D} = 0 \end{cases} \tag{C.55}$$

$$\frac{\partial a_H(\xi)}{\partial \varphi} + \frac{\partial \xi}{\partial x_D} = 0 \tag{C.56}$$

Rewriting equations (C.55) and (C.56) in matrix form:

$$\overrightarrow{a_\varphi} + \overrightarrow{y_{x_D}} = \vec{0} \tag{C.57}$$

where,

$$\overrightarrow{a_\varphi} = \frac{\partial}{\partial \varphi}\begin{bmatrix} a_1(\vec{c},\xi) \\ a_2(\vec{c},\xi) \\ a_H(\xi) \end{bmatrix} \tag{C.58}$$

$$\overrightarrow{y_{x_D}} = \frac{\partial}{\partial x_D}\begin{bmatrix} c_1 \\ c_2 \\ \xi \end{bmatrix} \tag{C.59}$$

A viscous system related to equation (C.57) is:

$$\overrightarrow{a_\varphi} + \overrightarrow{y_{x_D}} = \left(\overleftrightarrow{B}(\vec{y},\epsilon)\overrightarrow{y_{x_D}}\right)_{x_D} \tag{C.60}$$

in which ϵ is a viscous dissipation parameter, such that $\overleftrightarrow{B}(\vec{y},\epsilon = 0) = 0$.

Considering the case where $\overleftrightarrow{B} = \overleftrightarrow{I}$, in which $\overleftrightarrow{I}$ is the $(n+1) \times (n+1)$ identity matrix, we have

$$\overleftrightarrow{B}(\vec{y},\epsilon) = \epsilon\overleftrightarrow{I}, \epsilon > 0, \epsilon \in \mathbb{R}_+^* \tag{C.61}$$

Thus, we can rewrite the matrix system in its viscous form as

$$\begin{cases} \frac{\partial a_1(\vec{c},\xi)}{\partial \varphi} + \frac{\partial c_1}{\partial x_D} = \epsilon\frac{\partial^2 c_1}{\partial x_D^2} \\ \frac{\partial a_2(\vec{c},\xi)}{\partial \varphi} + \frac{\partial c_2}{\partial x_D} = \epsilon\frac{\partial^2 c_2}{\partial x_D^2} \\ \frac{\partial a_H(\xi)}{\partial \varphi} + \frac{\partial \xi}{\partial x_D} = \epsilon\frac{\partial^2 \xi}{\partial x_D^2} \end{cases} \tag{C.61}$$

The solution for the system (C.61) is given by a travelling wave type of solution with velocity $\eta = \frac{x_D}{\varphi}$. The travelling wave is defined as:

$$\theta = \frac{x_D - \eta\varphi}{\epsilon} \tag{C.62}$$

We assume that the solution can be written as $\vec{y} = [c_1(\theta), c_2(\theta), \xi(\theta)]$. Thus, rewriting equation (C.61) we find:

$$\frac{\partial a_i(\vec{c},\xi)}{\partial \varphi} = \frac{\partial a_i}{\partial c_1}\frac{dc_1}{d\theta}\frac{\partial \theta}{\partial \varphi} + \frac{\partial a_i}{\partial c_2}\frac{dc_2}{d\theta}\frac{\partial \theta}{\partial \varphi} + \frac{\partial a_i}{\partial \xi}\frac{d\xi}{d\theta}\frac{\partial \theta}{\partial \varphi} \tag{C.63}$$

$$\frac{\partial a_H(\vec{c},\xi)}{\partial \varphi} = \frac{\partial a_H}{\partial \xi}\frac{d\xi}{d\theta} \tag{C.64}$$

From the traveling wave definition, we have

$$\frac{\partial \theta}{\partial \varphi} = -\frac{\eta}{\epsilon} \tag{C.65}$$

Therefore, we can rewrite equations (C.63) and (C.64) as:

$$\frac{\partial a_i(\vec{c},\xi)}{\partial \varphi} = -\frac{\eta}{\epsilon}\left(\frac{\partial a_i}{\partial c_1}\frac{dc_1}{d\theta} + \frac{\partial a_i}{\partial c_2}\frac{dc_2}{d\theta} + \frac{\partial a_i}{\partial \xi}\frac{d\xi}{d\theta}\right) \tag{C.66}$$

$$\frac{\partial a_H(\xi)}{\partial \varphi} = -\frac{\eta}{\epsilon}\frac{\partial a_H}{\partial \xi}\frac{d\xi}{d\theta} \tag{C.67}$$

For the flux and viscous terms, we find:

$$\frac{\partial y_i}{\partial x_D} = \frac{1}{\epsilon}\frac{dy_i}{d\theta} \tag{C.68}$$

$$\frac{\partial^2 y_i}{\partial x_D^2} = \left(\frac{1}{\epsilon}\right)^2 \frac{d^2 y_i}{d\theta^2} \tag{C.69}$$

Applying equations (C.66)-(C.69) in equation (C.61), we obtain:

$$\begin{cases} -\frac{\sigma}{\epsilon}\left(\frac{\partial a_1}{\partial c_1}\frac{dc_1}{d\theta} + \frac{\partial a_1}{\partial c_2}\frac{dc_2}{d\theta} + \frac{\partial a_1}{\partial \xi}\frac{d\xi}{d\theta}\right) + \frac{1}{\epsilon}\frac{dc_1}{d\theta} = \left(\frac{1}{\epsilon}\right)^2 \frac{d^2 c_1}{d\theta^2} \\ -\frac{\sigma}{\epsilon}\left(\frac{\partial a_2}{\partial c_1}\frac{dc_1}{d\theta} + \frac{\partial a_2}{\partial c_2}\frac{dc_2}{d\theta} + \frac{\partial a_1}{\partial \xi}\frac{d\xi}{d\theta}\right) + \frac{1}{\epsilon}\frac{dc_2}{d\theta} = \left(\frac{1}{\epsilon}\right)^2 \frac{d^2 c_2}{d\theta^2} \\ -\frac{\sigma}{\epsilon}\frac{\partial a_H}{\partial \xi}\frac{d\xi}{d\theta} + \frac{1}{\epsilon}\frac{d\xi}{d\theta} = \left(\frac{1}{\epsilon}\right)^2 \frac{d^2 \xi}{d\theta^2} \end{cases} \tag{C.70}$$

From system (C.70) we find:

$$\begin{cases} -\frac{1}{\epsilon}\left[\frac{d^2 c_1}{d\theta^2} - \frac{dc_1}{d\theta} + \eta\left(\frac{\partial a_1}{\partial c_1}\frac{dc_1}{d\theta} + \frac{\partial a_1}{\partial c_2}\frac{dc_2}{d\theta} + \frac{\partial a_1}{\partial \xi}\frac{d\xi}{d\theta}\right)\right] = 0 \\ -\frac{1}{\epsilon}\left[\frac{d^2 c_2}{d\theta^2} - \frac{dc_2}{d\theta} + \eta\left(\frac{\partial a_2}{\partial c_1}\frac{dc_1}{d\theta} + \frac{\partial a_2}{\partial c_2}\frac{dc_2}{d\theta} + \frac{\partial a_2}{\partial \xi}\frac{d\xi}{d\theta}\right)\right] = 0 \\ -\frac{1}{\epsilon}\left[\frac{d^2 \xi}{d\theta^2} - \frac{d\xi}{d\theta} + \eta\frac{\partial a_H}{\partial \xi}\frac{d\xi}{d\theta}\right] = 0 \end{cases} \tag{C.71}$$

Rewriting equation (C.71) in matrix form:

$$-\frac{1}{\epsilon}\begin{pmatrix}\frac{d^2c_1}{d\theta^2}\\ \frac{d^2c_2}{d\theta^2}\\ \frac{d^2\xi}{d\theta^2}\end{pmatrix}-\begin{pmatrix}\frac{dc_1}{d\theta}\\ \frac{dc_2}{d\theta}\\ \frac{d\xi}{d\theta}\end{pmatrix}+\eta\begin{pmatrix}\frac{\partial a_1}{\partial c_1} & \frac{\partial a_1}{\partial c_2} & \frac{\partial a_1}{\partial \xi}\\ \frac{\partial a_2}{\partial c_1} & \frac{\partial a_2}{\partial c_2} & \frac{\partial a_2}{\partial \xi}\\ 0 & 0 & \frac{\partial a_H}{\partial \xi}\end{pmatrix}\begin{pmatrix}\frac{dc_1}{d\theta}\\ \frac{dc_2}{d\theta}\\ \frac{d\xi}{d\theta}\end{pmatrix}=0 \tag{C.72}$$

and

$$\begin{pmatrix}\frac{\partial a_1}{\partial c_1} & \frac{\partial a_1}{\partial c_2} & \frac{\partial a_1}{\partial \xi}\\ \frac{\partial a_2}{\partial c_1} & \frac{\partial a_2}{\partial c_2} & \frac{\partial a_2}{\partial \xi}\\ 0 & 0 & \frac{\partial a_H}{\partial \xi}\end{pmatrix}\begin{pmatrix}\frac{dc_1}{d\theta}\\ \frac{dc_2}{d\theta}\\ \frac{d\xi}{d\theta}\end{pmatrix}=\begin{pmatrix}\frac{da_1}{d\theta}\\ \frac{da_2}{d\theta}\\ \frac{da_H}{d\theta}\end{pmatrix} \tag{C.73}$$

Thus,

$$-\frac{1}{\epsilon}\begin{pmatrix}\frac{d^2c_1}{d\theta^2}\\ \frac{d^2c_2}{d\theta^2}\\ \frac{d^2\xi}{d\theta^2}\end{pmatrix}-\begin{pmatrix}\frac{dc_1}{d\theta}\\ \frac{dc_2}{d\theta}\\ \frac{d\xi}{d\theta}\end{pmatrix}+\eta\begin{pmatrix}\frac{da_1}{d\theta}\\ \frac{da_2}{d\theta}\\ \frac{da_H}{d\theta}\end{pmatrix}=\vec{0} \tag{C.74}$$

Integration of equation (C.74) with respect to θ:

$$-\frac{1}{\epsilon}\begin{pmatrix}\frac{dc_1}{d\theta}\\ \frac{dc_2}{d\theta}\\ \frac{d\xi}{d\theta}\end{pmatrix}-\begin{pmatrix}c_1\\ c_2\\ \xi\end{pmatrix}+\eta\begin{pmatrix}a_1\\ a_2\\ a_H\end{pmatrix}+\begin{pmatrix}W_1\\ W_2\\ W_3\end{pmatrix}=\vec{0} \tag{C.75}$$

where W_1, W_2 and W_3 are integration constants. The conditions to solve the ordinary differential equation (ODE) (C.75) are:

$$\lim_{\theta\to\pm\infty}\left(\frac{dc_1}{d\theta},\frac{dc_2}{d\theta},\frac{d\xi}{d\theta}\right)=(0,0,0) \tag{C.76}$$

$$\lim_{\theta\to+\infty}(c_1,c_2,\xi)=\left(c_1^{(+)},c_2^{(+)},\xi^{(+)}\right) \tag{C.77}$$

$$\lim_{\theta\to-\infty}(c_1,c_2,\xi)=\left(c_1^{(-)},c_2^{(-)},\xi^{(-)}\right) \tag{C.78}$$

Replacing equations (C.76) and (C.78) in equation (C.75), we obtain:

$$-\begin{pmatrix} c_1^{(-)} \\ c_2^{(-)} \\ \xi^{(-)} \end{pmatrix} + \eta \begin{pmatrix} a_1\left(c_1^{(-)}, c_2^{(-)}, \xi^{(-)}\right) \\ a_2\left(c_1^{(-)}, c_2^{(-)}, \xi^{(-)}\right) \\ a_H(\xi^{(-)}) \end{pmatrix} + \begin{pmatrix} W_1 \\ W_2 \\ W_3 \end{pmatrix} = \vec{0} \qquad \text{(C.79)}$$

Therefore, the integration constants are:

$$\begin{pmatrix} W_1 \\ W_2 \\ W_3 \end{pmatrix} = \begin{pmatrix} c_1^{(-)} - \eta a_1\left(c_1^{(-)}, c_2^{(-)}, \xi^{(-)}\right) \\ c_2^{(-)} - \eta a_2\left(c_1^{(-)}, c_2^{(-)}, \xi^{(-)}\right) \\ \xi^{(-)} - \eta a_H\left(\xi^{(-)}\right) \end{pmatrix} \qquad \text{(C.80)}$$

Replacing equation (C.80) in equation (C.75), we find the following system of ODE´s:

$$\begin{pmatrix} \frac{dc_1}{d\theta} \\ \frac{dc_2}{d\theta} \\ \frac{d\xi}{d\theta} \end{pmatrix} - \begin{pmatrix} c_1 \\ c_2 \\ \xi \end{pmatrix} + \eta \begin{pmatrix} a_1 \\ a_2 \\ a_H \end{pmatrix} + \begin{pmatrix} c_1^{(-)} - \eta a_1\left(c_1^{(-)}, c_2^{(-)}, \xi^{(-)}\right) \\ c_2^{(-)} - \eta a_2\left(c_1^{(-)}, c_2^{(-)}, \xi^{(-)}\right) \\ \xi^{(-)} - \eta a_H\left(\xi^{(-)}\right) \end{pmatrix} = \vec{0} \qquad \text{(C.75)}$$

leading to

$$\begin{pmatrix} \frac{dc_1}{d\theta} \\ \frac{dc_2}{d\theta} \\ \frac{d\xi}{d\theta} \end{pmatrix} - \begin{pmatrix} c_1 - c_1^{(-)} \\ c_2 - c_2^{(-)} \\ \xi - \xi^{(-)} \end{pmatrix} + \eta \begin{pmatrix} a_1 - a_1\left(c_1^{(-)}, c_2^{(-)}, \xi^{(-)}\right) \\ a_2 - a_2\left(c_1^{(-)}, c_2^{(-)}, \xi^{(-)}\right) \\ a_H - a_H\left(\xi^{(-)}\right) \end{pmatrix} = \vec{0} \qquad \text{(C.76)}$$

and finally

$$\frac{dc_1}{d\theta} = \left(c_1 - c_1^{(-)}\right) - \eta\left(a_1 - a_1\left(c_1^{(-)}, c_2^{(-)}, \xi^{(-)}\right)\right) = 0 \qquad \text{(C.77)}$$

$$\frac{dc_2}{d\theta} = \left(c_2 - c_2^{(-)}\right) - \eta\left(a_2 - a_2\left(c_1^{(-)}, c_2^{(-)}, \xi^{(-)}\right)\right) = 0 \qquad \text{(C.78)}$$

$$\frac{d\xi}{d\theta} = \left(\xi - \xi^{(-)}\right) - \eta\left(a_H - a_H\left(\xi^{(-)}\right)\right) = 0 \qquad \text{(C.79)}$$

Equations (C.77)-(C.79) are used to find orbits for the stable shock waves of c_1, c_2 and ξ following the vanishing viscosity method.

From equation (C.77), we define a function $H_1(c_1, c_2, \xi)$ such that

$$\frac{dc_1}{d\theta} = \left(c_1 - c_1^{(-)}\right) - \eta\left(a_1 - a_1\left(c_1^{(-)}, c_2^{(-)}, \xi^{(-)}\right)\right) = H_1(c_1, c_2, \xi) \qquad \text{(C.80)}$$

For both $c_1^{(+)} > c_1^{(-)}$ and $c_1^{(+)} < c_1^{(-)}$, a necessary and sufficient condition for a stable orbit is $H_1(c_1, c_2, \xi) \geq 0$. Thus:

$$\left(c_1 - c_1^{(-)}\right) - \eta\left(a_1 - a_1\left(c_1^{(-)}, c_2^{(-)}, \xi^{(-)}\right)\right) \geq 0, \forall c_1 \in \left(c_1^{(-)}, c_1^{(+)}\right) \qquad \text{(C.81)}$$

The velocity of the travelling wave is given by:

$$\eta = \frac{dx_D}{d\varphi} = \frac{c_1^{(-)} - c_1^{(+)}}{a_1\left(c_1^{(-)}, c_2^{(-)}, \xi^{(-)}\right) - a_1\left(c_1^{(+)}, c_2^{(+)}, \xi^{(+)}\right)} \qquad \text{(C.82)}$$

Thus, from equation (C.81), we find:

$$\frac{a_1\left(c_1^{(-)}, c_2^{(-)}, \xi^{(-)}\right) - a_1\left(c_1^{(+)}, c_2^{(+)}, \xi^{(+)}\right)}{c_1^{(-)} - c_1^{(+)}} \geq \frac{a_1\left(c_1^{(-)}, c_2^{(-)}, \xi^{(-)}\right) - a_1}{c_1^{(-)} - c_1}, \forall c_1 \in \left(c_1^{(-)}, c_1^{(+)}\right) \qquad \text{(C.83)}$$

The same procedure is done for the other two ODEs. Thus, shock waves that follow Oleinik condition are shock waves that jump to stable orbits following the vanishing viscosity criteria.

b. Oleinik condition for the original system of conservation laws of low salinity waterflooding problem

In this section we evaluate Oleinik condition for discontinuities in the solution of the system of partial differential equations that model low salinity waterflooding in oil reservoirs for two dissolved cations in injection water ($n = 2$). The system of conservation laws is given by:

$$\begin{cases}\frac{\partial s_w}{\partial t_D}+\frac{\partial f_w(s,\vec{c},\xi)}{\partial x_D}=0\\ \frac{\partial(c_i s_w+a_i(\vec{c},\xi))}{\partial t_D}+\frac{\partial c_i f_w(s,\vec{c},\xi)}{\partial x_D}=0,\ i=1,2\\ \frac{\partial(\xi s_w+a_H(\xi))}{\partial t_D}+\frac{\partial \xi f_w(s,\vec{c},\xi)}{\partial x_D}=0\end{cases} \tag{C.84}$$

The shock waves from the auxiliary system are mapped onto $x_D \times t_D$ plane through the relations (Pires *et al*., 2006):

$$D_{pH}=\frac{f_w^{\pm}}{s_w^{\pm}+V_{pH}} \tag{C.85}$$

$$D_1=\frac{f_w^{\pm}}{s_w^{\pm}+V_1} \tag{C.86}$$

$$D_2=\frac{f_w^{\pm}}{s_w^{\pm}+V_2} \tag{C.87}$$

where V_{pH}, V_1 and V_2 are the pH, $k=1$ family and $k=2$ family shock slopes in $x_D \times \varphi$ plane. In figure (C.8) we present the characteristic diagram of the auxiliary system solution and the velocities of each shock wave.

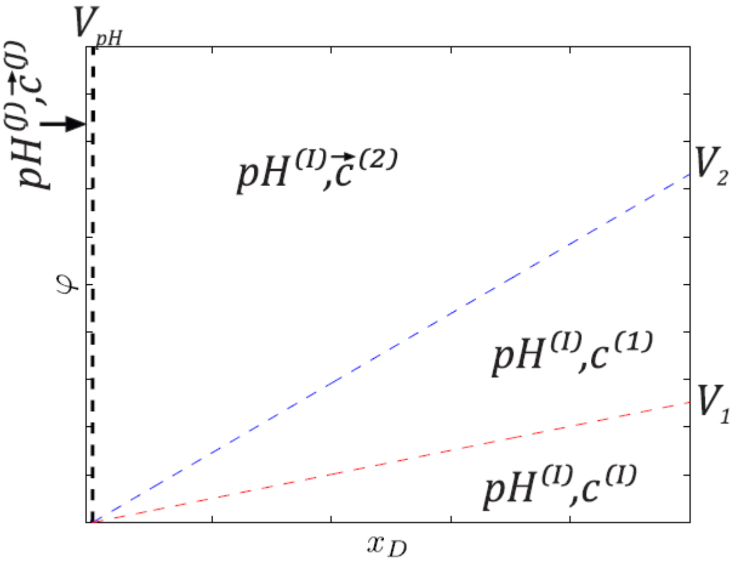

Figure C.8: Characteristic diagram of the auxiliary system solution

For the relative permeability curves, we use Corey's model, which is given by:

$$k_{rw}(s_w, \vec{c}, \xi) = k_{rw}^*(\vec{c}, \xi)\left(\frac{s_w - s_{wi}}{1 - s_{or}(\vec{c}, \xi) - s_{wi}}\right)^{n_w(\vec{c}, \xi)} \quad \text{(C.88)}$$

$$k_{ro}(s_w, \vec{c}, \xi) = k_{ro}^*(\vec{c}, \xi)\left(\frac{1 - s_{or}(\vec{c}, \xi) - s_w}{1 - s_{or}(\vec{c}, \xi) - s_{wi}}\right)^{n_o(\vec{c}, \xi)} \quad \text{(C.89)}$$

where the parameters k_{rw}^*, k_{ro}^*, s_{or}, n_w and n_o are determined through:

$$s_{or}(\vec{c}, \xi) = 10^{-6} S_{al} + 0.225 - 0.0978.pH \quad \text{(C.90)}$$

$$n_w(\vec{c}, \xi) = -10^{-5} S_{al} + 2.8554 + 0.05214.pH \quad \text{(C.91)}$$

$$n_o(\vec{c}, \xi) = 10^{-5} S_{al} + 2.4258 - 0.4873.pH \quad \text{(C.92)}$$

$$k_{rw}^*(\vec{c}, \xi) = 2.10^{-6} S_{al} + 0.3311 - 0.00517.pH \quad \text{(C.93)}$$

$$k_{ro}^*(\vec{c}, \xi) = -2.10^{-6} S_{al} + 05913 + 0.0181.pH \quad \text{(C.94)}$$

Water viscosity μ_w is calculated using the properties of brine in reservoir conditions (McCain Jr., 1991):

$$\mu_B(T) = AT^{-B} \quad \text{(C.95)}$$

$$A = 109.574 - 8.40564\, S_{al} + 0.313314\, S_{al}^2 + 8.72213.10^{-3}\, S_{al}^3 \quad \text{(C.96)}$$

$$B = 1.12166 - 2.63951.10^{-2}\, S_{al} + 6.79461.10^{-3} S_{al}^2 + 5.47119.10^{-5} S_{al}^3 - 1.55586.10^{-6} S_{al}^4 \quad \text{(C.97)}$$

$$\mu_w(T, P) = \mu_B(T)(0.9994 + 4.0295.10^{-5} p + 3.1062.10^{-9} p^2) \quad \text{(C.98)}$$

where μ_B is the viscosity (cP) at atmospheric pressure, T is the temperature (°F), S_{al} is the salinity (TDS).

Water fractional flow curves for the constant concentration states in the solution and the solution path is presented in figure (C.9).

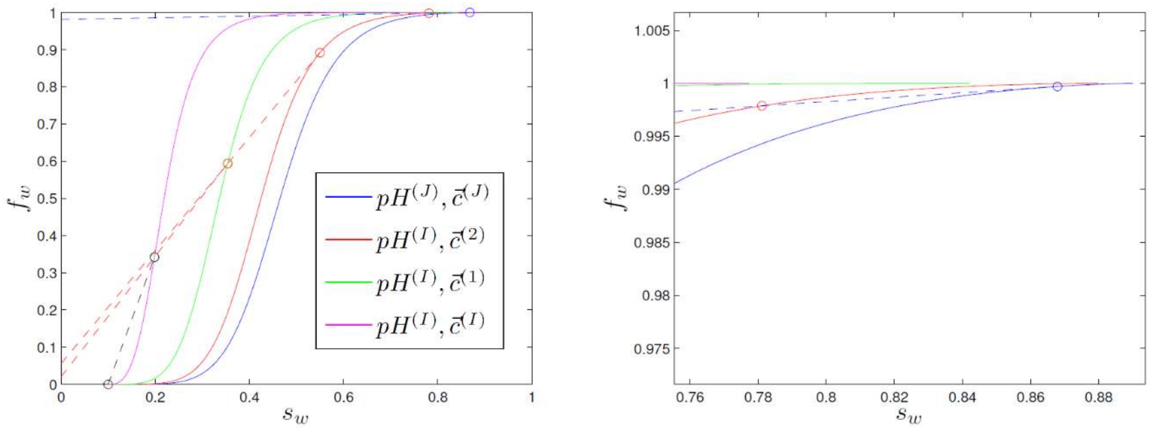

Figure C.9: Water fractional flow curves and solution path for $n = 2$

From now on we analyze Oleinik condition for each shock wave, defined as:

$$\frac{f(u^{(-)})-f(u)}{u^{(-)}-u} \geq \frac{f(u^{(-)})-f(u^{(+)})}{u^{(-)}-u^{(+)}} \tag{C.99}$$

For the pH shock of the auxiliary system solution, Oleinik condition is:

$$\frac{f_w}{s_w+V'_{pH}} \geq \frac{f_w^{(-)}}{s_w^{(-)}+V_{pH}} \tag{C.100}$$

in which V'_{pH} is the shock slope in figure C.7. Each shock V'_{pH} results in a different right state $[c_1, c_2, \xi]$, and therefore, a different fractional flow curve. To verify Oleinik condition, we map all possible V'_{pH} shocks onto $f_w \times s_w$ plane, determining the shocks D'_{pH} in $x_D \times t_D$ plane. Locus of the pH shock in $f_w \times s_w$ plane is presented in figure (C.10), the green points are the s_w shock condition for the shock D_{pH}, and in figure (C.11) we show the velocities D_{pH} as a function of the saturation shock condition.

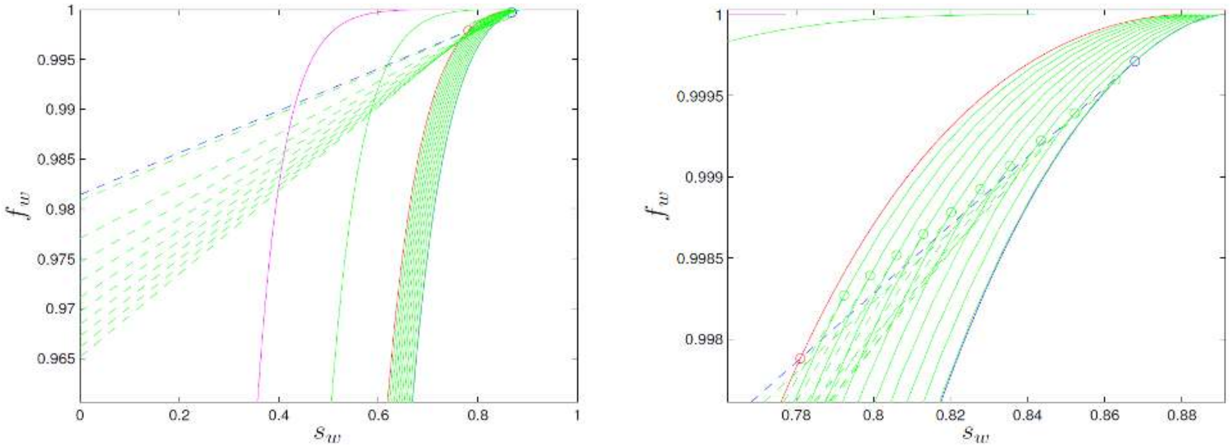

Figure C.10: Locus of pH shock in $f_w \times s_w$ plane

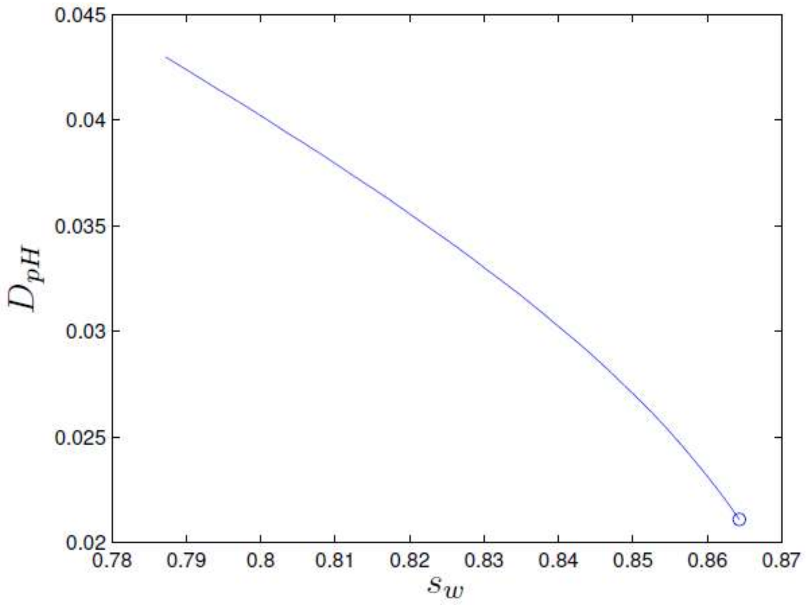

Figure C.11: Velocities of the pH shock

In figure (C.11) the blue point is the velocity of the shock wave that satisfies Oleinik condition in the auxiliary system solution. This is the smallest shock speed, and therefore satisfies Oleinik condition in $x_D \times t_D$ plane.

A similar analysis for the other two shock waves of the auxiliary system was developed. For the shock V_2, $\omega_2^{(J)} \leq \omega_2 \leq \omega_2^{(I)}$, $\omega_1 = \omega_1^{(J)}$ and $\xi^{(I)}$. The concentration locus of the shock is calculated changing ω_2 from the condition (J) to condition (I) and the relation:

$$c_i = \frac{1}{\beta_i(\xi^{(I)})}\frac{\left(\omega_i - \alpha_i(\xi^{(I)})\right)}{\omega_i}\prod_{\substack{j=1\\ j\neq i}}^{2}\frac{\alpha_j(\xi^{(I)})[\omega_j - \alpha_j(\xi^{(I)})]}{\omega_j[\alpha_j(\xi^{(I)}) - \alpha_i(\xi^{(I)})]}, i = 1,2 \qquad \text{(C.101)}$$

The shock velocity V_2' for each point can be determined through the expression:

$$V_2' = \omega_2^{(+)}\prod_{j=1}^{2}\left(\frac{\omega_j^{(-)}}{\alpha_j(\xi^{(I)})}\right), \omega_2^{(J)} \leq \omega_2^{(+)} \leq \omega_2^{(I)} \qquad \text{(C.102)}$$

After the concentration shock condition is calculated, the water fractional flow curves may be determined (Figure C.12). The saturation shock locus is found following the same procedure described for the pH shock (Figure C.12).

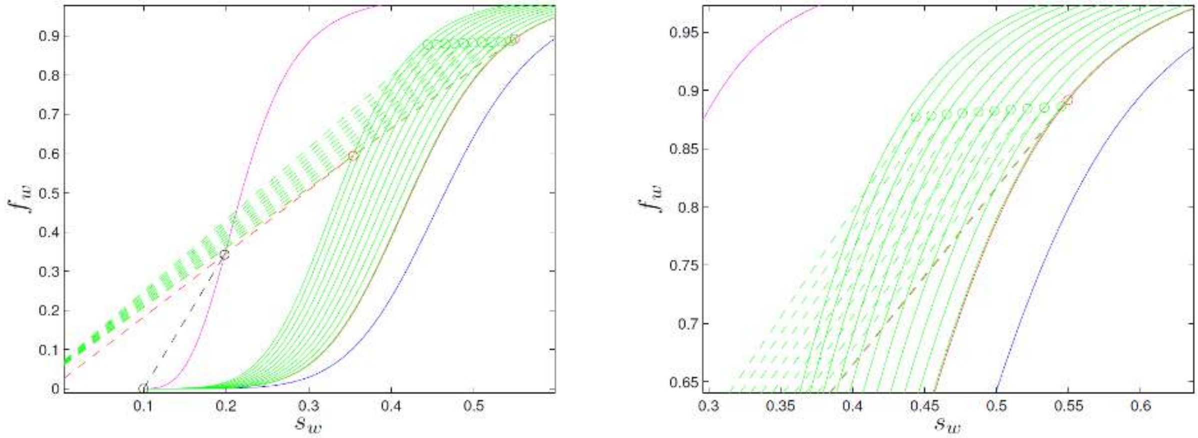

Figure C.12: Locus of ω_2 shock mapped into $f_w \times s_w$ plane

The red point is the saturation shock condition that satisfies Oleinik condition in the auxiliary system solution, also the smallest shock velocity in $x_D \times t_D$ plane.

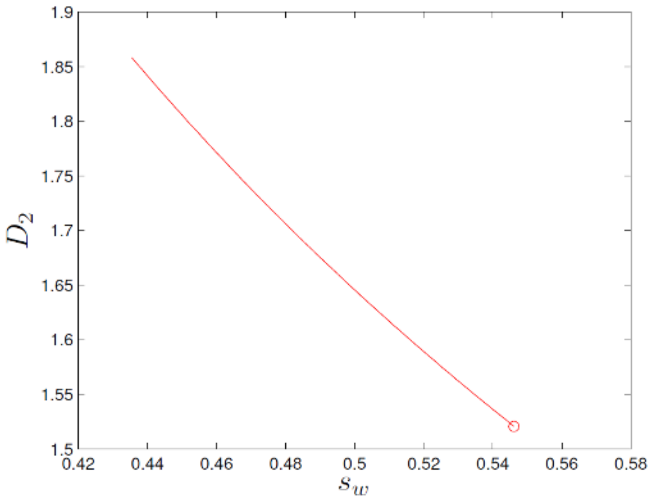

Figure C.13: Velocities of the ω_2 shock locus

Following the same steps for the shock V_1, where $\omega_1^{(J)} \leq \omega_1 \leq \omega_1^{(I)}$, $\omega_2 = \omega_2^{(I)}$ and $\xi^{(I)}$. The fractional flow curves calculated from the concentration locus of shock V_1 are presented in figure (C.14).

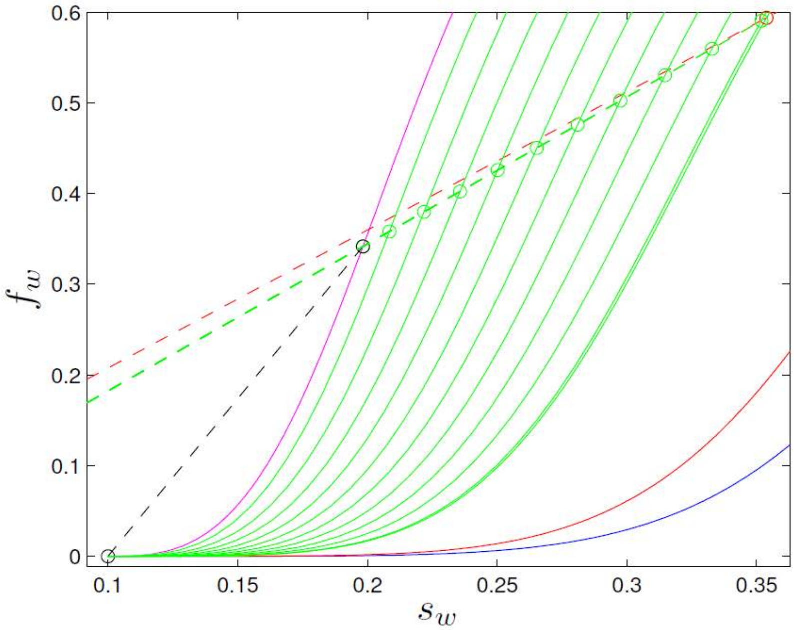

Figure C.14: Locus of ω_1 shock

Figure (C.15) shows the shock velocities for the saturation condition of ω_1 shock. The shock that satisfies Oleinik condition in the auxiliary plane $x_D \times \varphi$ has the lowest velocity in $x_D \times t_D$ plane (red point). Therefore, this shock also satisfies Oleinik condition.

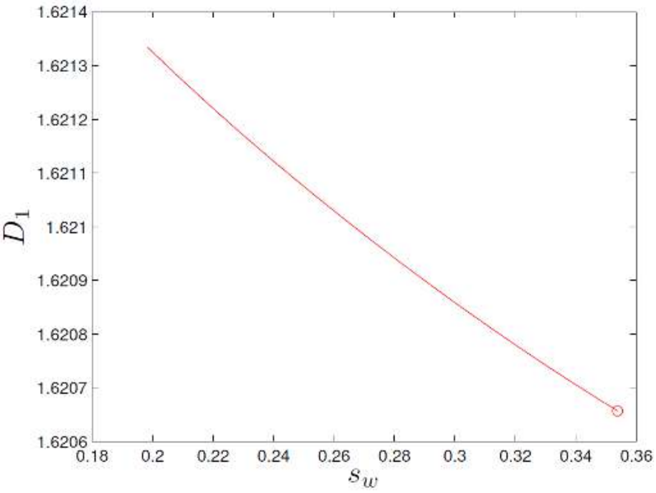

Figure C.15: Velocities of the ω_1 shock

References

Lax, P.D. (1973). Hyperbolic Systems of Conservation Laws and the Mathematical Theory of Shock Waves. SIAM CBMS-NSF Regional Conference Series in Applied Mathematics, vol. 11, Philadelphia, USA

Liu, T. (1981). Admissible Solutions of Hyperbolic Conservation Laws. Memoirs of the American Mathematical Society, vol. 30, n. 240, Providence, USA

Oleinik, O.A. (1957). Discontinuous Solutions of Non-Linear Differential Equations. *Uspekhi Mat. Nauk*, 12(3), pp. 3-73. DOI: 10.1090/trans2/026/05

Pires, A.P., Bedrikovetsky, P.G. & Shapiro, A.A. (2006). A Splitting Technique for Analytical Modelling of Two-Phase Multicomponent Flow in Porous Media. *Journal of Petroleum Science and Engineering*, 51(1-2), pp. 54-67. DOI: 10.1016/j.petrol.2005.11.009